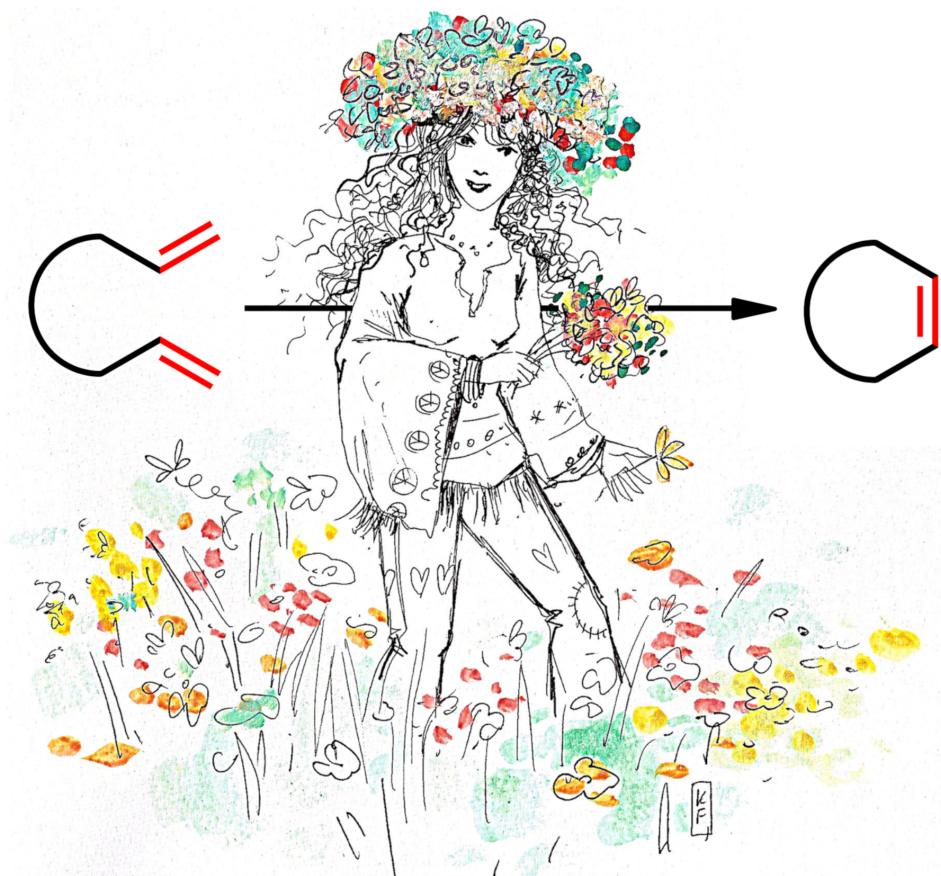




Progress in metathesis chemistry III

Edited by Karol Grela and Anna Kajetanowicz



A green metathesis technology

Imprint

Beilstein Journal of Organic Chemistry

www.bjoc.org

ISSN 1860-5397

Email: journals-support@beilstein-institut.de

The *Beilstein Journal of Organic Chemistry* is published by the Beilstein-Institut zur Förderung der Chemischen Wissenschaften.

Beilstein-Institut zur Förderung der Chemischen Wissenschaften
Trakehner Straße 7–9
60487 Frankfurt am Main
Germany
www.beilstein-institut.de

The copyright to this document as a whole, which is published in the *Beilstein Journal of Organic Chemistry*, is held by the Beilstein-Institut zur Förderung der Chemischen Wissenschaften. The copyright to the individual articles in this document is held by the respective authors, subject to a Creative Commons Attribution license.

The cover image is copyright Katarzyna Czyzyska Golos, Effe.fineart.



Progress in metathesis chemistry

Karol Grela* and Anna Kajetanowicz*

Editorial

Open Access

Address:

Faculty of Chemistry, University of Warsaw, Żwirki i Wigury Street 101, 02-089 Warsaw, Poland

Email:

Karol Grela* - karol.grela@gmail.com; Anna Kajetanowicz* - anna.kajetanowicz@gmail.com

* Corresponding author

Keywords:

metathesis

Beilstein J. Org. Chem. **2019**, *15*, 2765–2766.

doi:10.3762/bjoc.15.267

Received: 14 October 2019

Accepted: 30 October 2019

Published: 15 November 2019

This article is part of the thematic issue "Progress in metathesis chemistry III".

Guest Editors: K. Grela and A. Kajetanowicz

© 2019 Grela and Kajetanowicz; licensee Beilstein-Institut.

License and terms: see end of document.

Ten years have already passed since the publication of the first thematic issue on olefin metathesis in the *Beilstein Journal of Organic Chemistry* [1], and four years ago, the second part of the thematic issue [2] was published. Now we have the true pleasure to introduce the third one.

Researchers who read these three issues, as well as the followers of the excellent blog "All Things Metathesis" [3] know how much great progress has been made over these years. For example, a number of new highly stereoselective Ru and Mo catalysts have been introduced, solving the problem of *E*- and *Z*-selectivity. Some tagged Ru catalysts can be applied in water and even in biological systems, while Mo and W alkylidenes packed into innovative wax pills are now truly user friendly. Olefin metathesis catalysts can work under homo- or heterogeneous conditions, as well as under continuous flow. The stability of Ru–methylidene species (an attribute important for a successful ethenolysis process) has been significantly improved. Importantly, we have observed a growing number of metathesis examples utilizing very low loading (at the single part-per-million level) of catalysts, which is crucial for the application of this reaction in the production of bulk chemicals. At the same time, much effort was invested in understanding

the mechanisms of how new catalysts work and decompose, how macrocycles are formed in ring-closing metathesis, etc. Representative examples of these directions have been the subject of the current, third thematic issue on *Olefin Metathesis*, including highly educative reviews on tandem olefin metathesis–Suzuki–Miyaura cross coupling by Kotha et al. [4], on artificial metalloproteins by Okuda et al. [5], on stereoretentive ruthenium dithiolate catalysts by Mauduit et al. [6], on unsymmetrical NHC ligands by Grisi et al. [7], on polymers by Kudryavtsev [8] and on polyhedral oligomeric silsesquioxanes by Pietraszuk et al. [9]. Finally, Ward and Sabatino wrote a very well-composed review on aqueous olefin metathesis [10]. These tutorials are accompanied by a number of research papers authored by the best experts in the field.

At the same time, the enormous scientific success of this research has – unfortunately – not yet been reflected by a growing number of new industrial openings. No new metathesis-based biorefineries have been built, while the traditional polymer industry seems to prefer ill-defined catalysts, and sadly, no new drugs are being produced by metathesis. On the contrary, Janssen Therapeutics recently announced the discontinuation of the drug Olysio (simeprevir) due to a significant

decline in utilization [11]. It is consoling, however, that most of this lack of development is not due to weaknesses of the technology itself. It can rather be attributed to the less-than-favourable business environment and complicated current World's economy. At the same time, a number of recent acquisitions between catalyst producers makes the society fear that a new monopoly may be formed, with the obvious threats for the end-users.

We are therefore looking forward to the future developments in this field. We stay optimistic as we deeply believe that metathesis promoted by modern, innovative catalysts will not be locked-up as a scientific curiosity with little industrial interest. On the contrary, we anticipate that the field will stay competitive and the forthcoming years will bring an explosion of applications utilizing this excellent (and green!) methodology.

It was a great pleasure for us to serve as editors of this thematic issue. We are very thankful to all authors for their first-class contributions. At the same time, we would like to thank the colleagues at the Beilstein-Institut for their professional support and patience.

Karol Grela and Anna Kajetanowicz

Warsaw, October 2019

ORCID® IDs

Karol Grela - <https://orcid.org/0000-0001-9193-3305>

Anna Kajetanowicz - <https://orcid.org/0000-0003-0315-0998>

References

1. Grela, K. *Beilstein J. Org. Chem.* **2010**, *6*, 1089–1090. doi:10.3762/bjoc.6.124
2. Grela, K. *Beilstein J. Org. Chem.* **2015**, *11*, 1639–1640. doi:10.3762/bjoc.11.179
3. <http://allthingsmetathesis.com/> (accessed Oct 9, 2019).
4. Kotha, S.; Meshram, M.; Chakkapalli, C. *Beilstein J. Org. Chem.* **2018**, *14*, 2468–2481. doi:10.3762/bjoc.14.223
5. Sauer, D. F.; Schiffels, J.; Hayashi, T.; Schwaneberg, U.; Okuda, J. *Beilstein J. Org. Chem.* **2018**, *14*, 2861–2871. doi:10.3762/bjoc.14.265
6. Müller, D. S.; Baslé, O.; Mauduit, M. *Beilstein J. Org. Chem.* **2018**, *14*, 2999–3010. doi:10.3762/bjoc.14.279
7. Paradiso, V.; Costabile, C.; Grisi, F. *Beilstein J. Org. Chem.* **2018**, *14*, 3122–3149. doi:10.3762/bjoc.14.292
8. Gringolts, M. L.; Denisova, Y. I.; Finkelshtein, E. S.; Kudryavtsev, Y. V. *Beilstein J. Org. Chem.* **2019**, *15*, 218–235. doi:10.3762/bjoc.15.21
9. Źak, P.; Pietraszuk, C. *Beilstein J. Org. Chem.* **2019**, *15*, 310–332. doi:10.3762/bjoc.15.28
10. Sabatino, V.; Ward, T. R. *Beilstein J. Org. Chem.* **2019**, *15*, 445–468. doi:10.3762/bjoc.15.39
11. https://professionals.optumrx.com/publications/library/drugwithdrawal_olysio_2018-0420.html (accessed Oct 9, 2019).

License and Terms

This is an Open Access article under the terms of the Creative Commons Attribution License (<http://creativecommons.org/licenses/by/4.0>). Please note that the reuse, redistribution and reproduction in particular requires that the authors and source are credited.

The license is subject to the *Beilstein Journal of Organic Chemistry* terms and conditions: (<https://www.beilstein-journals.org/bjoc>)

The definitive version of this article is the electronic one which can be found at:
doi:10.3762/bjoc.15.267



Non-metal-templated approaches to bis(borane) derivatives of macrocyclic dibrighead diphosphines via alkene metathesis

Tobias Fiedler^{1,2}, Michał Barbasiewicz^{2,3}, Michael Stollenz^{1,4} and John A. Gladysz^{*1,2}

Full Research Paper

Open Access

Address:

¹Department of Chemistry, Texas A&M University, PO Box 30012, College Station, Texas 77842-3012, USA, ²Institut für Organische Chemie and Interdisciplinary Center for Molecular Materials, Friedrich-Alexander-Universität Erlangen-Nürnberg, Henkestraße 42, 91054 Erlangen, Germany, ³Present address: Faculty of Chemistry, University of Warsaw, Pasteura 1, 02-093 Warszawa, Poland and ⁴Present address: Department of Chemistry and Biochemistry, Kennesaw State University, 370 Paulding Building NW, MD#1203, Kennesaw, Georgia 30144, USA

Email:

John A. Gladysz^{*} - gladysz@mail.chem.tamu.edu

* Corresponding author

Keywords:

alkene metathesis; crystal structures; homeomorphic isomerization; hydrogenation; *in/out* isomers; metathesis; phosphine boranes

Beilstein J. Org. Chem. 2018, 14, 2354–2365.

doi:10.3762/bjoc.14.211

Received: 14 June 2018

Accepted: 24 August 2018

Published: 07 September 2018

This article is part of the thematic issue "Progress in metathesis chemistry III".

Guest Editor: K. Grela

© 2018 Fiedler et al.; licensee Beilstein-Institut.

License and terms: see end of document.

Abstract

Two routes to the title compounds are evaluated. First, a ca. 0.01 M CH_2Cl_2 solution of $\text{H}_3\text{B}\cdot\text{P}((\text{CH}_2)_6\text{CH}=\text{CH}_2)_3$ (**1**· BH_3) is treated with 5 mol % of Grubbs' first generation catalyst (0 °C to reflux), followed by H_2 (5 bar) and Wilkinson's catalyst (55 °C). Column chromatography affords $\text{H}_3\text{B}\cdot\text{P}(n\text{-C}_8\text{H}_{17})_3$ (1%), $\text{H}_3\text{B}\cdot\text{P}((\text{CH}_2)_{13}\text{CH}_2)(n\text{-C}_8\text{H}_{17})$ (8%; see text for tie bars that indicate additional phosphorus–carbon linkages, which are coded in the abstract with italics), $\text{H}_3\text{B}\cdot\text{P}((\text{CH}_2)_{13}\text{CH}_2)((\text{CH}_2)_{14})\text{P}((\text{CH}_2)_{13}\text{CH}_2)\cdot\text{BH}_3$ (**6**· 2BH_3 , 10%), *in,out*- $\text{H}_3\text{B}\cdot\text{P}((\text{CH}_2)_{14})_3\text{P}\cdot\text{BH}_3$ (*in,out*-**2**· 2BH_3 , 4%) and the stereoisomer (*in,in/out,out*)-**2**· 2BH_3 (2%). Four of these structures are verified by independent syntheses. Second, 1,14-tetradecanedioic acid is converted (reduction, bromination, Arbuzov reaction, LiAlH_4) to $\text{H}_2\text{P}((\text{CH}_2)_{14})\text{PH}_2$ (**10**; 76% overall yield). The reaction with $\text{H}_3\text{B}\cdot\text{SMe}_2$ gives **10**· 2BH_3 , which is treated with *n*-BuLi (4.4 equiv) and $\text{Br}(\text{CH}_2)_6\text{CH}=\text{CH}_2$ (4.0 equiv) to afford the tetraalkenyl precursor ($\text{H}_2\text{C}=\text{CH}(\text{CH}_2)_6)_2(\text{H}_3\text{B})\text{P}((\text{CH}_2)_{14})\text{P}(\text{BH}_3)((\text{CH}_2)_6\text{CH}=\text{CH}_2)_2$ (**11**· 2BH_3 ; 18%). Alternative approaches to **11**· 2BH_3 (e.g., via **11**) were unsuccessful. An analogous metathesis/hydrogenation/chromatography sequence with **11**· 2BH_3 (0.0010 M in CH_2Cl_2) gives **6**· 2BH_3 (5%), *in,out*-**2**· 2BH_3 (6%), and (*in,in/out,out*)-**2**· 2BH_3 (7%). Despite the doubled yield of **2**· 2BH_3 , the longer synthesis of **11**· 2BH_3 vs **1**· BH_3 renders the two routes a toss-up; neither compares favorably with precious metal templated syntheses.

Introduction

We have found that a variety of metal complexes with *trans*-phosphine ligands of the formula $\text{P}((\text{CH}_2)_m\text{CH}=\text{CH}_2)_3$ (**1**; $m = 4\text{--}14$) undergo threefold interligand ring closing alkene

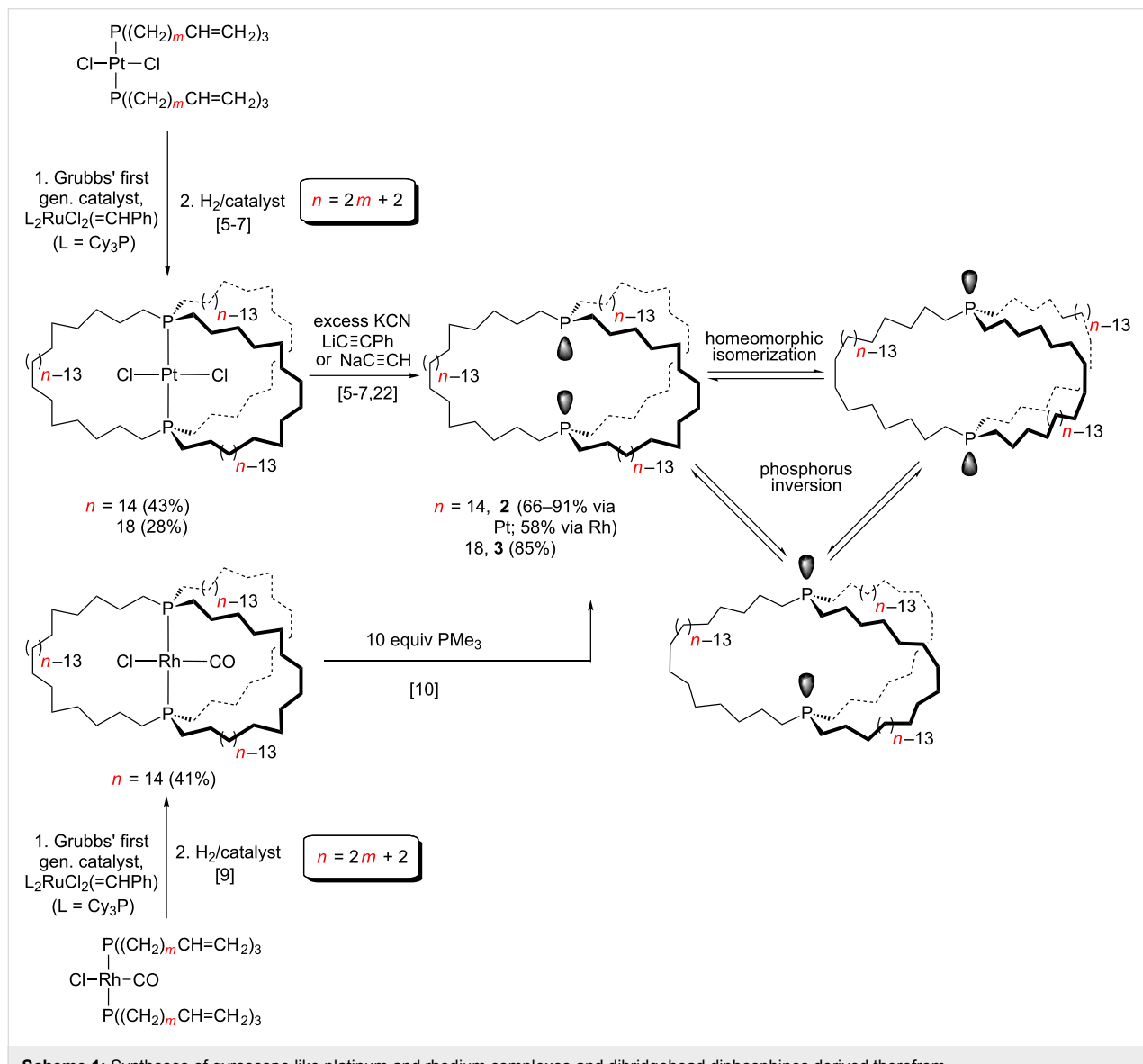
metatheses to give, after hydrogenations, metal complexes of *in,in* isomers of macrocyclic dibrighead diphosphines [1–13]. Representative examples with square planar complexes are

shown in Scheme 1. Analogous sequences with trigonal bipyramidal substrates proceed in somewhat higher overall yields, as analyzed elsewhere [1–4]. Setaka has developed a similar chemistry in which the phosphorus atoms are replaced by silicon and the metal fragment by *p*-phenylene (*p*-C₆H₄) or related aromatic moieties [14–19]. These types of compounds are viewed as promising candidates for molecular gyroscopes [14–21].

We subsequently developed an interest in the free dibridgehead diphosphine ligands P((CH₂)_{*n*}CH=CH₂)₃ (*n* = 14, **2**; 18, **3**), prompted in part by the unexpected discovery of the facile demetalations shown in Scheme 1 [5,6,10,22]. Such compounds were previously known only for much smaller ring sizes (*n* ≤ 4) [23]. These reactions require excesses of certain nucleophiles, and the mechanisms remain under study. The yields are quite good,

but the routes are stoichiometric in precious metals. Although the metals can be recovered as species such as K₂Pt(CN)₄ or RhCl(PMe₃)₃, we have nonetheless sought to develop more economical protocols.

The analogous Fe(CO)₃ adducts are easily prepared [1–4], but in efforts to date it has not been possible to efficiently remove the dibridgehead diphosphine ligands from the low cost iron fragment. Oxidations that lead to the corresponding dibridgehead diphosphine dioxides (O=)P((CH₂)_{*n*}CH=CH₂)₃P(=O) have exhibited promise, but purification has been problematic [24]. Indeed, phosphine oxides are everyday precursors to phosphines, so we have considered various non-metal-templated routes to **2**·2(=O), **3**·2(=O), and related species. However, as described in the discussion section, the yields have not been competitive [25].



Another preliminary point concerns the ability of macrocyclic dibridgehead diphosphorus compounds to exhibit *in/out* isomerism [26]. As shown in Scheme 1, there are three limiting configurations for **2** and **3**: *in,in*, *out,out*, and *in,out* (identical to *out,in*). The first two, as well as the degenerate *in,out* pair, can rapidly interconvert by a process termed homeomorphic isomerization [26,27], which is akin to turning the molecules inside out. Readers are referred to earlier publications in this series for additional details [22,25,28–30]. Interconversions between the *in,in/out,out* and *in,out/out,in* manifolds require phosphorus inversion and temperatures considerably in excess of 100 °C.

In this paper, we describe two non-metal-templated approaches to **2** that are based upon metatheses of phosphine boranes of alkene containing phosphines. The first involves the monophosphorus precursor $\text{H}_3\text{B}\cdot\text{P}((\text{CH}_2)_6\text{CH}=\text{CH}_2)_3$ (**1**· BH_3) [31], and the second a diphosphorus precursor in which one of the methylene chains linking the two phosphorus atoms has already been installed. The advantages and limitations of each are analyzed in detail. Some of the results (Scheme 2) have appeared in the supporting information of a preliminary communication [28], and others in a dissertation [32].

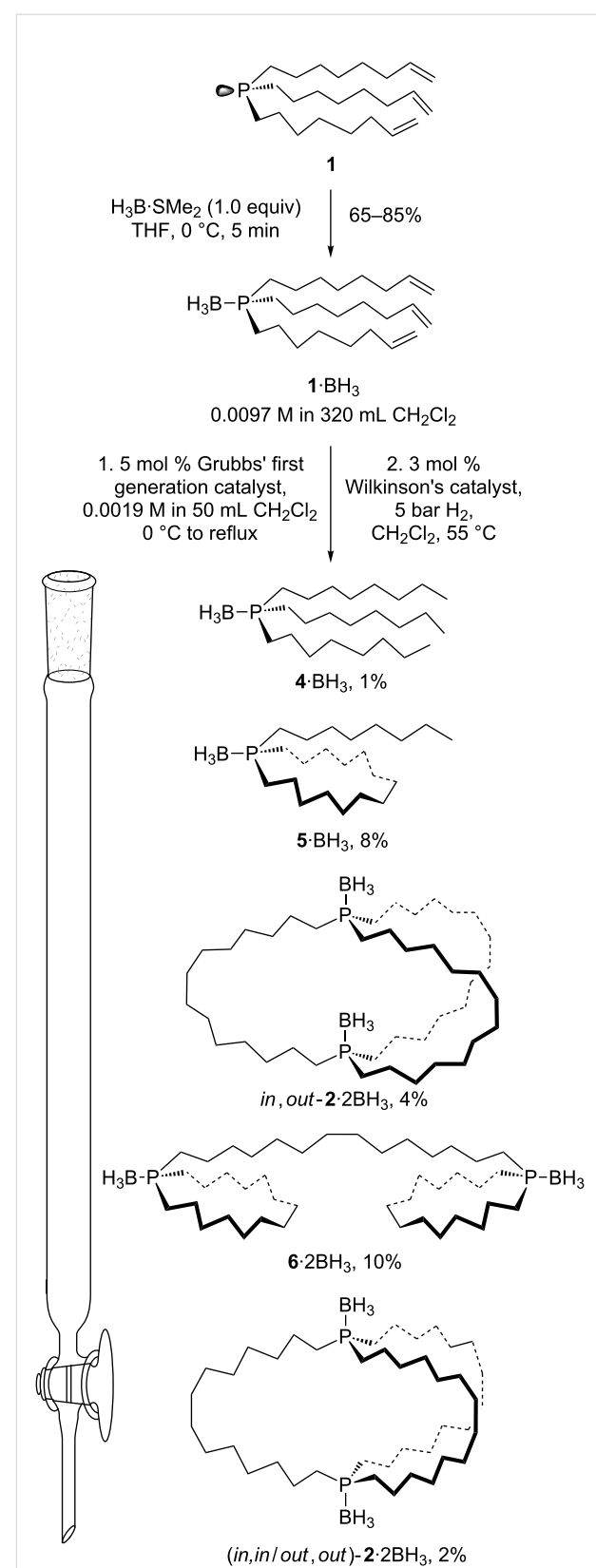
Results

1. Monophosphorus precursors

As reported earlier [31], the alkene containing phosphine $\text{P}((\text{CH}_2)_6\text{CH}=\text{CH}_2)_3$ (**1**) can be prepared in 87% yield from the reaction of PCl_3 and $\text{MgBr}(\text{CH}_2)_6\text{CH}=\text{CH}_2$. Following the addition of $\text{H}_3\text{B}\cdot\text{SMe}_2$, the phosphine borane **1**· BH_3 can be isolated in 65–85% yields [31], as shown in Scheme 2. It is critical to avoid an excess of $\text{H}_3\text{B}\cdot\text{SMe}_2$, as this brings the C=C units into play. In fact, when substoichiometric amounts of $\text{H}_3\text{B}\cdot\text{SMe}_2$ are added to THF solutions of purified **1**· BH_3 , gels immediately form.

A ca. 0.01 M CH_2Cl_2 solution of **1**· BH_3 and a ca. 0.002 M CH_2Cl_2 solution of Grubbs' first generation catalyst (3 mol %) were combined at 0 °C. The mixture was warmed to room temperature, and a second charge of Grubbs' catalyst added (2 mol %). The sample was refluxed, and then filtered through silica gel. The filtrate was concentrated and treated with H_2 (5 bar) and Wilkinson's catalyst (55 °C). The mixture was taken to dryness and the residue tediously chromatographed on a silica gel column. Numerous fractions were collected and analyzed by TLC. The mass recovery from the column was 33% of theory (for complete metathesis).

More than ten mobile products could be discerned, but only five could be isolated in pure form and ultimately identified. These are described in order of elution. Each was analyzed by NMR (^1H , $^{31}\text{P}\{^1\text{H}\}$, $^{13}\text{C}\{^1\text{H}\}$; always CDCl_3) and IR spectroscopy,



Scheme 2: Synthesis and alkene metathesis of the monophosphorus precursor **1**· BH_3 .

mass spectrometry, and microanalysis, as summarized in the experimental section. The $^{13}\text{C}\{^1\text{H}\}$ NMR spectra proved to be most diagnostic of structure, and were analyzed in detail. The $^{31}\text{P}\{^1\text{H}\}$ NMR spectra were all very similar (broad apparent doublets due to phosphorus boron coupling).

First, traces of a colorless oil were obtained. The ^1H NMR spectrum showed a characteristic triplet at 0.83 ppm consistent with a terminal methyl group. The $^{13}\text{C}\{^1\text{H}\}$ NMR spectrum exhibited eight signals, two of which were phosphorus coupled doublets. One of the singlets (14.0 ppm) was typical of a terminal methyl group. Based upon these data, and the integration of the ^1H NMR spectrum, the oil was assigned as the hydrogenated phosphine borane $\text{H}_3\text{B}\cdot\text{P}(n\text{-C}_8\text{H}_{17})_3$ (**4**· BH_3), a known compound [33]. The yield was only 1%.

Next, another colorless oil eluted. The ^1H NMR and $^{13}\text{C}\{^1\text{H}\}$ NMR spectra again exhibited signals characteristic of a methyl group (0.86 ppm, t; 14.0 ppm, s). Integration of the ^1H NMR spectrum established a 14:1 area ratio for the methylene (1.62–1.19 ppm) and methyl signals. The $^{13}\text{C}\{^1\text{H}\}$ NMR spectrum featured one set of seven signals and another set of eight with an intensity ratio of approximately 2:1. The less intense set resembled the signals arising from the *n*-octyl groups in **4**· BH_3 . The more intense set was very similar to the signals arising from the cyclic $\text{H}_3\text{B}\cdot\text{P}(\text{CH}_2)_{13}\text{CH}_2$ substructures of **6**· 2BH_3 (described below) and a phosphine borane $\text{H}_3\text{B}\cdot\text{PPh}((\text{CH}_2)_{13}\text{CH}_2)$ reported earlier [34]. The mass spectrum exhibited an intense ion at m/z 340 (**5** $^+$, 93%), and no ions of higher mass. Hence, the oil was assigned

as the monocyclic intramolecular metathesis product $\text{H}_3\text{B}\cdot\text{P}((\text{CH}_2)_{13}\text{CH}_2)(n\text{-C}_8\text{H}_{17})$ (**5**· BH_3 ; see Scheme 2). The yield was 8%.

The third product was also a colorless oil. The $^{13}\text{C}\{^1\text{H}\}$ NMR spectrum exhibited seven signals, three of which were phosphorus coupled doublets (second spectrum from top, Figure 1). Analogous coupling patterns are found with the free dibridgehead diphosphines **2** and **3** in Scheme 1. No NMR signals diagnostic of methyl groups were present, and further analysis is presented along with that for an isomer below.

A white powder was obtained next. The $^{13}\text{C}\{^1\text{H}\}$ NMR spectrum exhibited fourteen signals, half of which were approximately twice as intense as the others. Two signals of each set exhibited phosphorus coupling. The overall pattern was quite similar to those shown by metal complexes with *cis* or *trans* coordinating diphosphine ligands of the formula $(\text{P}(\text{CH}_2)_{13}\text{CH}_2)((\text{CH}_2)_{14})(\text{P}(\text{CH}_2)_{13}\text{CH}_2)$ (**6**) [6,7,12,13,35]. This suggested the diphosphine borane structure **6**· 2BH_3 (see Scheme 2), which is derived from one metathesis involving alkenyl moieties on different phosphorus atoms, and two metatheses of alkenyl moieties on identical phosphorus atoms. The yield was 10%. The structure has been confirmed by an independent synthesis (detachment of the diphosphine from a platinum complex followed by borane addition) and a crystal structure [6].

Finally, another white powder was obtained. As with the previous oil isolated above, the $^{13}\text{C}\{^1\text{H}\}$ NMR spectrum exhib-

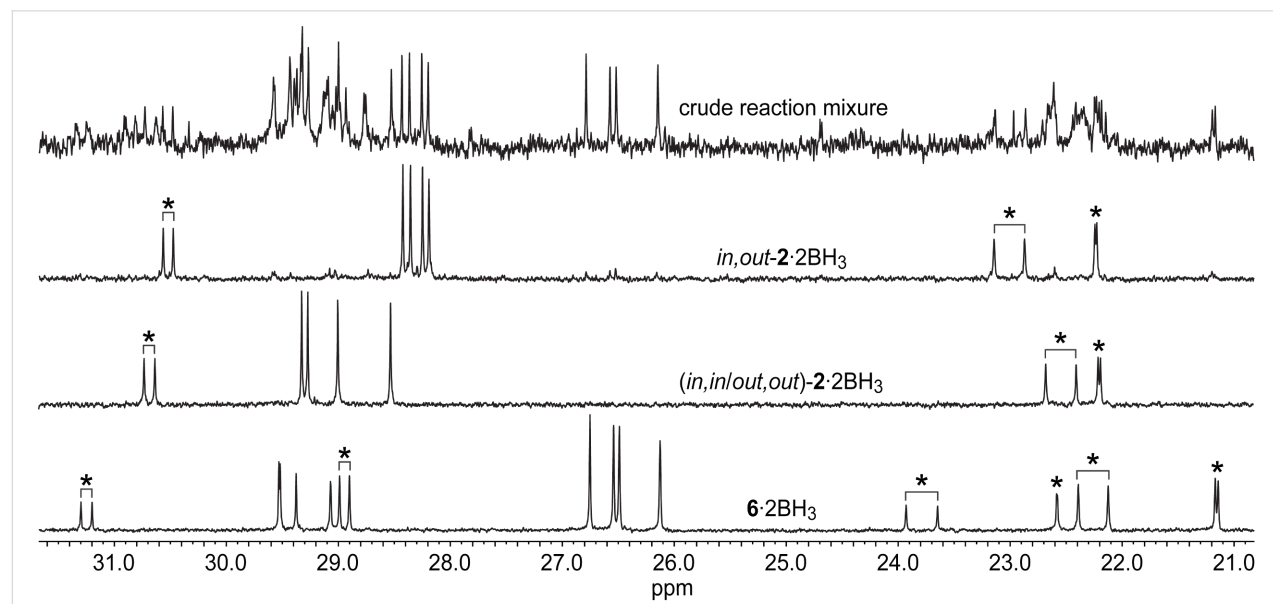


Figure 1: The $^{13}\text{C}\{^1\text{H}\}$ NMR spectra (CDCl_3 , 100 MHz) of *in,out*-**2**· 2BH_3 , (*in,in/out,out*)-**2**· 2BH_3 , **6**· 2BH_3 , and the crude reaction mixture after hydrogenation from Scheme 5 (top); doublets are marked with an asterisk.

ited seven signals, three of which were phosphorus coupled doublets (third spectrum from top, Figure 1). Both spectra were consistent with dibridgehead diphosphine diboranes $\text{H}_3\text{B}\cdot\text{P}((\text{CH}_2)_{14})_3\text{P}\cdot\text{BH}_3$ (**2·2BH₃**) derived from threefold intermolecular metatheses of **1·BH₃**. Based upon independent syntheses from the dibridgehead diphosphines **2** obtained in Scheme 1 [6], they were assigned as *in,out*-**2·2BH₃** (4%) and the stereoisomer (*in,in/out,out*)-**2·2BH₃** (2%), as shown in Scheme 2. The depiction of the latter as an *out,out* (vs *in,in*) isomer in Scheme 2 is arbitrary, but represents the form found in a confirming crystal structure [6].

Parallel reactions were conducted with Grubbs' second generation catalyst and the nitro-Grela catalyst [36]. However, the combined yields of **2** diminished.

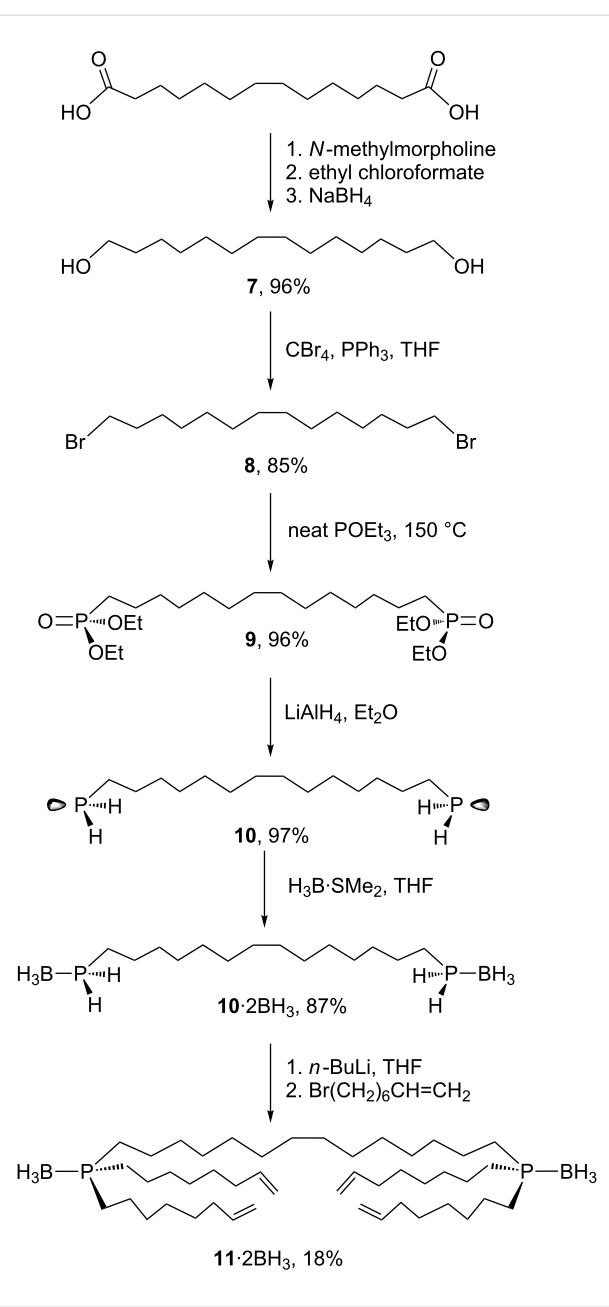
2. Diphosphorus precursors

Since the yields of the cage like diphosphine diboranes **2·2BH₃** in Scheme 2 were – as expected – very low, alternative strategies were considered. The poor mass balance was attributed, at least in part, to the formation of oligomeric products that were retained on the column. Improvements might be expected from precursors in which one of the methylene chains tethering the two phosphorus atoms was pre-formed. Thus, we set out to prepare a tetraalkenyl metathesis precursor as shown in Scheme 3.

The first step, a previously reported reduction of commercial 1,14-tetradecanedioic acid to 1,14-tetradecanediol (**7**) [37], was followed by an Appel reaction to give 1,14-dibromotetradecane (**8**) [38–43]. An Arbuzov reaction then afforded the diphosphonate $(\text{EtO})_2(\text{O}=\text{P}((\text{CH}_2)_{14})\text{P}(\text{O}=\text{O})(\text{OEt})_2$ (**9**) [44]. Subsequent reduction with LiAlH_4 gave the diprimary diphosphine $\text{H}_2\text{P}((\text{CH}_2)_{14})\text{PH}_2$ (**10**) in 76% yield from **7** as a foul smelling white powder.

It has been shown that borane adducts of primary phosphines can be doubly deprotonated, and that the resulting phosphorus dianions can be bis(alkylated) [45–47]. Thus, the diphosphine **10** and $\text{H}_3\text{B}\cdot\text{SMe}_2$ were reacted to give the diphosphine diborane $\text{H}_2(\text{H}_3\text{B})\text{P}((\text{CH}_2)_{14})\text{P}(\text{BH}_3)\text{H}_2$ (**10·2BH₃**) as a white solid in 87% yield. A subsequent reaction with *n*-BuLi (4.4 equiv) and $\text{Br}(\text{CH}_2)_6\text{CH}=\text{CH}_2$ (4.0 equiv) gave the tetraalkenyl target ($\text{H}_2\text{C}=\text{CH}(\text{CH}_2)_6)_2(\text{H}_3\text{B})\text{P}((\text{CH}_2)_{14})\text{P}(\text{BH}_3)((\text{CH}_2)_6\text{CH}=\text{CH}_2)_2$ (**11·2BH₃**), but in only 18% yield.

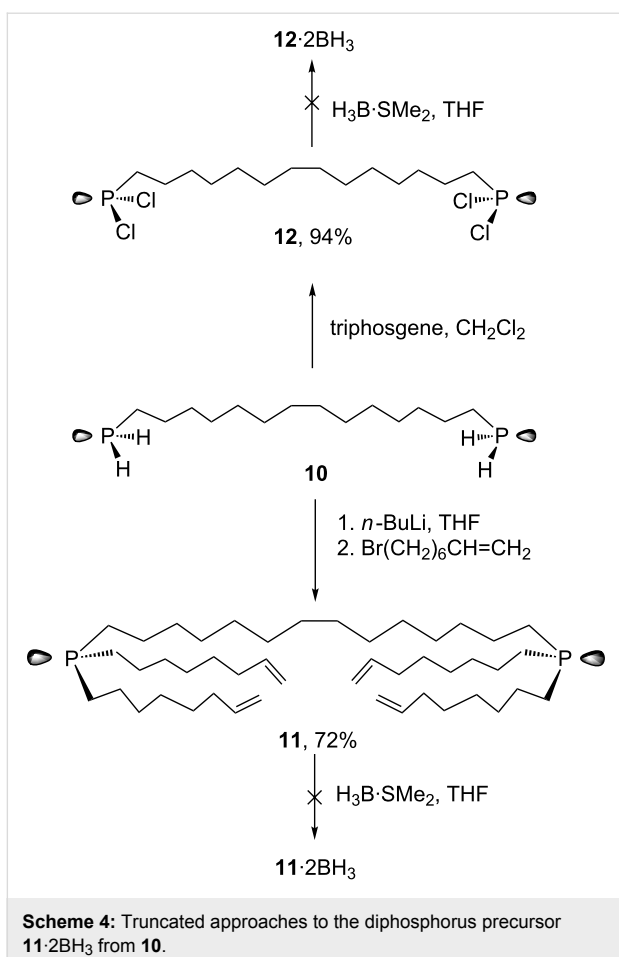
Accordingly, two alternative routes to **11·2BH₃** were considered. The initial step for the first is depicted in Scheme 4. Primary phosphines can be doubly deprotonated, analogously to borane adducts, and the phosphorus dianions subsequently bis(alkylated) [34,48]. Thus, **10** was treated with *n*-BuLi



Scheme 3: Synthesis of the diphosphorus precursor **11·2BH₃**.

(4.1 equiv) and then $\text{Br}(\text{CH}_2)_6\text{CH}=\text{CH}_2$ (4.0 equiv). Work-up gave the target compound $(\text{H}_2\text{C}=\text{CH}(\text{CH}_2)_6)_2\text{P}((\text{CH}_2)_{14})\text{P}((\text{CH}_2)_6\text{CH}=\text{CH}_2)_2$ (**11**) in 72% yield. However, all attempts to convert **11** to **11·2BH₃** gave only traces of the latter. Mainly insoluble material formed, which was presumed to be oligomeric and possibly derived from B–H additions to the alkenyl groups.

In the second approach, **10** was first converted to the tetrachloride $\text{Cl}_2\text{P}((\text{CH}_2)_{14})\text{PCl}_2$ (**12**) in 94% yield using triphosgene, a standard reagent for the chlorination of phos-

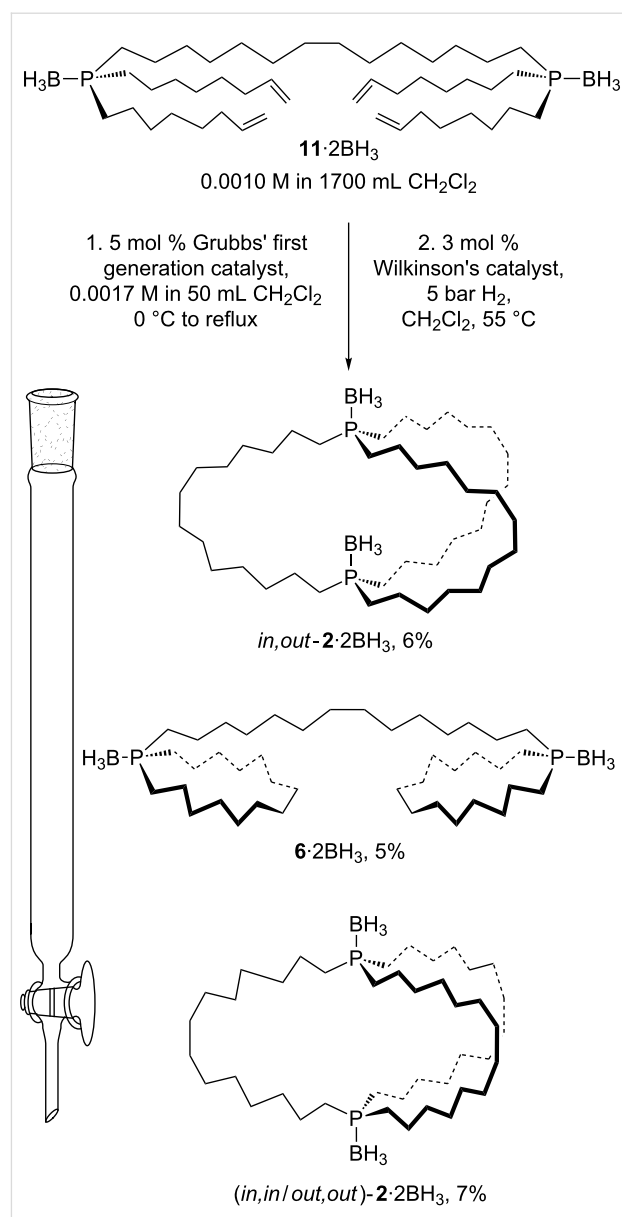


Scheme 4: Truncated approaches to the diphosphorus precursor $11\cdot 2\text{BH}_3$ from **10**.

phorus–hydrogen bonds [49]. Since a direct reaction with an excess of the Grignard reagent $\text{BrMg}(\text{CH}_2)_6\text{CH}=\text{CH}_2$ would give **11**, a dead end, initial conversion to the bis(borane) adduct **12·2BH₃** was envisioned. However, reactions of **12** and $\text{H}_3\text{B}\cdot\text{SMe}_2$ (2.1 equiv) afforded only insoluble material.

Thus, despite the low yield of the final step in Scheme 3, reasonable quantities of the diphosphine borane **11·2BH₃** could be stockpiled. As shown in Scheme 5, **11·2BH₃** was subjected to a metathesis/hydrogenation/column chromatography sequence similar to that for **1·BH₃** in Scheme 2. However, a tenfold higher dilution was used in the metathesis step (0.0010 M as compared to 0.010 M).

Figure 1 shows a $^{13}\text{C}\{^1\text{H}\}$ NMR spectrum of the crude product after hydrogenation stacked above spectra of the three products that could be isolated after the rather tedious column chromatography: the dibridgehead diphosphine borane *in,out*-**2·2BH₃**, its constitutional isomer **6·2BH₃**, and its stereoisomer (*in,in/out,out*)-**2·2BH₃**. It can be inferred from the top spectrum that the three products were the major components and moreover present in approximately equal amounts. However, the isolated



Scheme 5: Alkene metathesis of the diphosphorus precursor $11\cdot 2\text{BH}_3$.

yields were affected by the challenging separation. In particular, *in,out*-**2·2BH₃** and **6·2BH₃** eluted very closely, rendering some mixed fractions unavoidable and lowering the amounts of pure products.

Compared to the metathesis/hydrogenation sequence for **1·BH₃** (Scheme 2) the yields of *in,out*-**2·2BH₃** and (*in,in/out,out*)-**2·2BH₃** (Scheme 5) are higher but still poor. Taking into account the overall yields (three steps from PCl_3 and $\text{BrMg}(\text{CH}_2)_6\text{CH}=\text{CH}_2$ in the first synthesis vs seven steps from 1,14-tetradecanedioic acid in the second), the latter route does not offer any advantage, even if one were to improve the conversion of **10·2BH₃** to **11·2BH₃**.

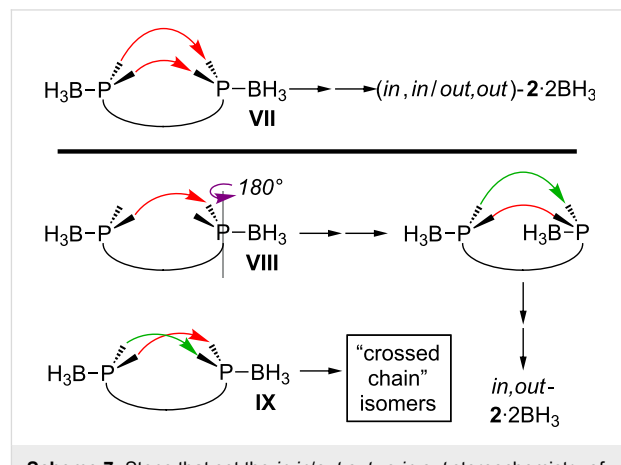
Discussion

As contrasted in Scheme 6, Scheme 2 and Scheme 5 present two conceptually related routes to the isomeric title compound $2\cdot2\text{BH}_3$. In the first, two trialkenylphosphine boranes ($1\cdot\text{BH}_3 = \mathbf{I}$) must undergo metathesis. The first productive step is intermolecular, giving a diphosphorus compound with a $\text{P}(\text{CH}_2)_6\text{CH}=\text{CH}(\text{CH}_2)_6\text{P}$ tether **II** that is positioned for subsequent intramolecular ring closing steps. Those involving alkenyl groups from different phosphorus atoms are productive (leading to $2\cdot2\text{BH}_3$ via hydrogenation of **IIIa**), and those involving groups from the same phosphorus atoms are non-productive (leading to $6\cdot2\text{BH}_3$ via hydrogenation of **IVa**). In the second, the starting material has a preformed $\text{P}(\text{CH}_2)_{14}\text{P}$ tether ($11\cdot2\text{BH}_3 = \mathbf{V}$), and the four alkenyl groups have reactivity options ($\rightarrow \mathbf{IIIb}$ or \mathbf{IVb}) analogous to those of intermediate **II** with the $\text{P}(\text{CH}_2)_6\text{CH}=\text{CH}(\text{CH}_2)_6\text{P}$ tether. Importantly, all of these steps are presumed to be largely under kinetic control, consistent with experience with the types of metatheses in Scheme 1 [1-13,34].

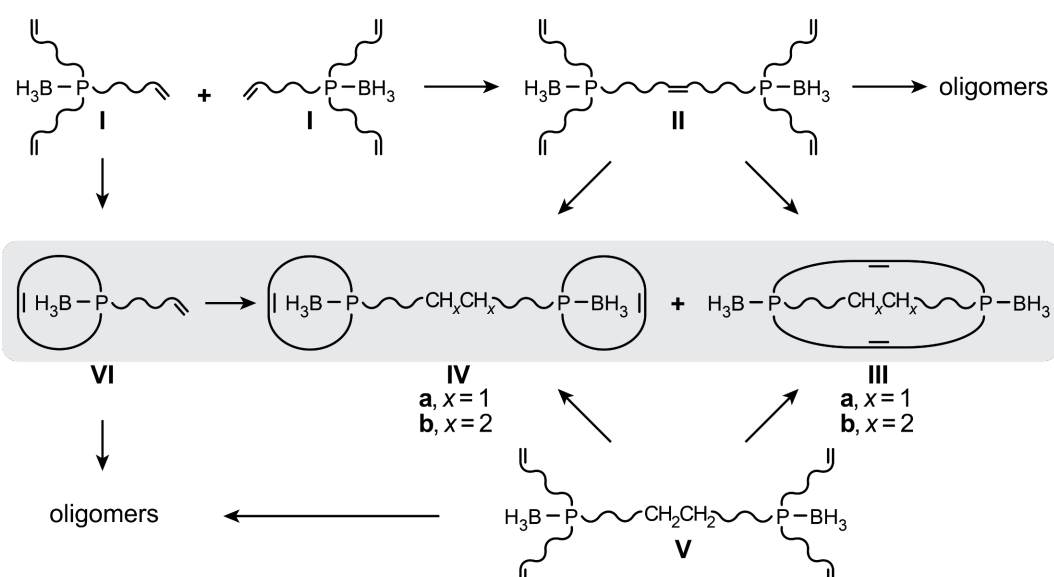
Although the second route intuitively seems more favorable, after the initial intermolecular metathesis of $1\cdot\text{BH}_3$ (**I**), both require an equivalent series of steps to reach (after hydrogenation) $2\cdot2\text{BH}_3$. One reason $1\cdot\text{BH}_3$ is an inferior substrate is that following the initial generation of a $\text{P}(\text{CH}_2)_6\text{CH}=\text{Ru}$ species, two $\text{P}(\text{CH}_2)_6\text{CH}=\text{CH}_2$ moieties remain available for non-productive intramolecular ring closing metathesis (giving **VI**). In contrast, with the analogous intermediate derived from $11\cdot2\text{BH}_3$ (**V**), there is only one $\text{P}(\text{CH}_2)_6\text{CH}=\text{CH}_2$ moiety that can give non-productive chemistry. It is also worth noting that

high dilution provides less of an advantage in Scheme 2, as one wants to favor intermolecular over intramolecular metatheses in the first step. In Scheme 5, one wants to avoid intermolecular metatheses at all stages.

At present, we have no rationale for the *in,out* vs (*in,in/out,out*) isomer ratios for $2\cdot2\text{BH}_3$. However, it is easy to map the sequence leading to each, as shown in Scheme 7. When there is only one tether between the two phosphorus atoms, the phosphorus–boron bonds can be arrayed in an *anti* fashion, as depicted in **VII**. When subsequent metatheses join alkenyl groups in the *syn* positions on each phosphorus atom (front to front and rear to rear), (*in,in/out,out*)- $2\cdot2\text{BH}_3$ must result (as drawn in Scheme 7, the *out,out* isomer would be the kinetic



Scheme 7: Steps that set the *in,in/out,out* vs *in,out* stereochemistry of $2\cdot2\text{BH}_3$ in Scheme 2 and Scheme 5.



Scheme 6: Schematic comparison of the key alkene metathesis steps in Scheme 2 and Scheme 5.

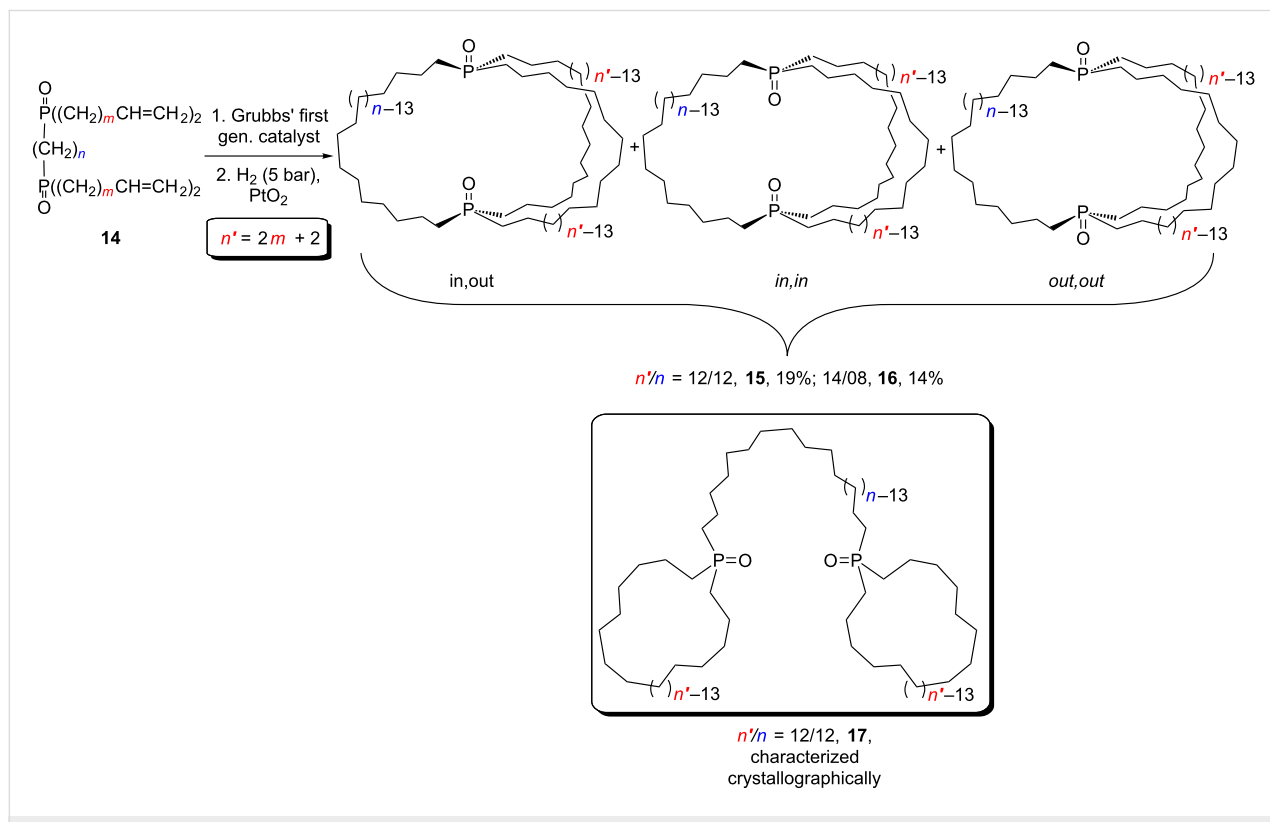
product). When the first metathesis does not join the *syn* positions, as in **VIII** (front to rear), one phosphorus–boron bond must subsequently be rotated by 180° to create a *syn* orientation for the second metathesis.

Of course, if the first metathesis step does not require a *syn* relationship (per **VIII**), the same possibility can be entertained for the second (see **IX**). This would lead to an isomeric bicyclic compound with "crossed chains". We have sought to access such species by conducting metatheses of substrates of the types in Scheme 1 that give thirty-three membered macrocycles ($n = 30$) [7]. However, none have so far been detected. Other types of crossed chain *in/out* isomer systems have in fact been realized [25,30].

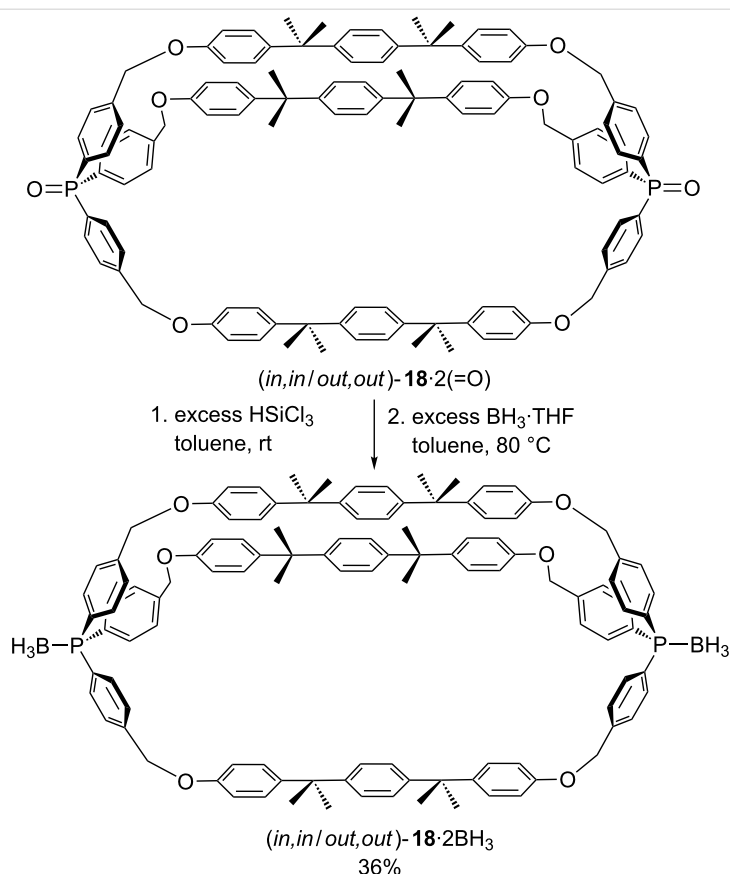
As communicated earlier [28] and will be described more fully in a later paper, both isomers of **2·2BH₃** are easily deprotected to give the respective isomers of the dibridgehead diphosphine **2** in high yields. Since phosphine oxides are also easily converted to phosphines, one could consider parallel approaches to **2** via metatheses of the phosphine oxide (O=)P((CH₂)_mCH=CH₂)₃ (**1**(=O)) or diphosphine dioxide (H₂C=CH(CH₂)₆)₂(O=)P((CH₂)₁₄)P(=O)((CH₂)₆CH=CH₂)₂ (**11·2**(=O)). Given the poor results with **1·BH₃** in Scheme 2, no attempt has been made to explore similar reactions with **1**(=O).

However, as shown in Scheme 8, it has proved possible to synthesize the diphosphine dioxides **14**, in which the two phosphorus atoms are tethered by a methylene chain, in two steps in 66–68% overall yields from diethyl phosphonate ((O=)PH(OEt)₂), Grignard reagents BrMg(CH₂)_mCH=CH₂, base (NaH), and appropriate α,ω -dibromides Br(CH₂)_nBr [25]. Following metathesis and hydrogenation, these afford dibridgehead diphosphine oxides **15** and **16** in 14–19% yields. This is slightly better than the combined yield of *in,out*- and (*in,in*/*out,out*)-**2·2BH₃** in Scheme 5, although the data are not strictly comparable as the ring sizes differ. It has not yet proved possible to efficiently separate the *in/out* isomers of **15** and **16**. However, byproducts derived from metatheses of alkenyl groups on the same phosphorus atom – such as **17** (comparable to **6·2BH₃**) – appear to form in much smaller amounts.

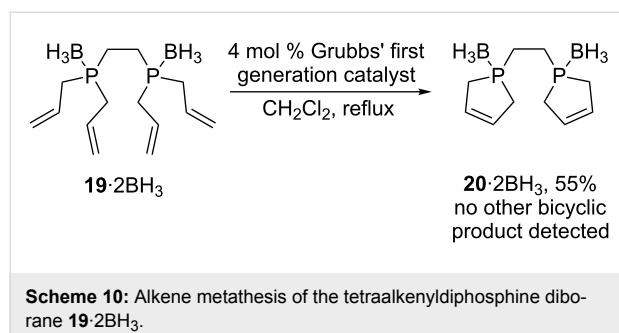
To our knowledge, only one macrocyclic dibridgehead diphosphine diborane has been previously reported, (*in,in*/*out,out*)-**18·2BH₃** in Scheme 9 [50,51]. This features triarylphosphorus bridgeheads and *p*-phenylene containing tethers that are long enough to allow rapid homeomorphic isomerization. The precursor **18·2**(=O) was prepared by a threefold Williamson ether synthesis in surprisingly high yields (61% *in,in*/*out,out* and *in,out* combined) [50,51], likely aided by the geminal dialkyl effect associated with the quaternary centers [52].



Scheme 8: Another non-metal-templated approach to dibridgehead diphosphorus compounds.

**Scheme 9:** Previously synthesized dibridgehead diphosphine boranes.

Finally, it should be noted that a number of alkene containing phosphine boranes have been employed in metathesis reactions [53,54]. In particular, the tetraalkenyl diphosphine borane **19·2BH₃** in Scheme 10 represents a downsized version of **11·2BH₃**. A species analogous to **6·2BH₃**, **20·2BH₃**, is obtained in much higher yield than any of the products in Scheme 5 [53]. Hence, selectivities can strongly depend upon the lengths of the methylene segments in the precursor.

**Scheme 10:** Alkene metathesis of the tetraalkenyldiphosphine dibo-rane **19·2BH₃**.

compounds that employ alkene metathesis. The new approaches (Scheme 2; Scheme 3 and Scheme 5) lack metal templates, which differentiates them from the routes presented in Scheme 1. However, neither is competitive with Scheme 1, despite eliminating the requirement for stoichiometric amounts of precious metals. Furthermore, preassembling a diphosphine borane substrate per Scheme 3 and Scheme 5 is not competitive with the "shotgun" approach in Scheme 2, and both routes require comparably demanding preparative column chromatography. Hence, the most promising direction for future research would seem to be templated syntheses via non-precious metals [55]. This remains an area of ongoing investigation in our laboratory and further results will be reported in due course.

Experimental

General. Reactions (except hydrogenations) were conducted under inert atmospheres using standard Schlenk techniques. All chromatography was carried out under aerobic conditions. Additional data are supplied in Supporting Information File 1.

Conclusion

In conclusion, this work constitutes a further installment in the evolution of synthetic strategies for dibridgehead diphosphorus

Metathesis/hydrogenation of $\text{H}_3\text{B}\cdot\text{P}((\text{CH}_2)_6\text{CH}=\text{CH}_2)_3$

(**1·BH₃**; Scheme 2 [32]). A Schlenk flask was charged with **1·BH₃** (1.177 g, 3.110 mmol) [31] and CH_2Cl_2 (320 mL; the re-

sulting solution was 0.0097 M in **1**·BH₃) and cooled to 0 °C. A solution of Grubbs' first generation catalyst (0.077 g, 0.094 mmol, 3 mol %) in CH₂Cl₂ (50 mL) was added dropwise via syringe with stirring over 1 h. The cooling bath was removed. After 2 h, additional Grubbs' first generation catalyst was added as a solid (0.051 g, 0.062 mmol, 2 mol %). The flask was fitted with a condenser and the mixture was refluxed overnight, cooled to room temperature, and passed through a SiO₂ pad (3 cm), which was rinsed with CH₂Cl₂. The eluate was concentrated to ca. 20 mL by rotary evaporation, and transferred to a Fischer–Porter bottle. Wilkinson's catalyst (0.086 g, 0.093 mmol, 3 mol %) was added, and the bottle was partially evacuated and charged with hydrogen (5 bar). The sample was kept at 55 °C for 60 h. The solvent was removed and the residue was placed at the top of a chromatography column (SiO₂, 3.5 × 36 cm), which was eluted with hexanes/CH₂Cl₂ (3:1 to 1:3 v/v) and then CH₂Cl₂. Fractions were assayed by TLC, combined where appropriate, and slowly evaporated to dryness in a fume hood. Some fractions (0.091 g total out of the recovered mass of 0.344 g) consisted of unidentified and/or impure products, or oligomers and polymers. Products that could be characterized are as follows (in order of elution).

H₃B·P(n-C₈H₁₇)₃ (**4**·BH₃ [33]; 0.007 g, 0.018 mmol, 1%), colorless oil. Anal. calcd for C₂₄H₅₄BP (384.47): C, 74.98; H, 14.16; found: C, 74.93; H, 14.02; ¹H NMR (400 MHz, CDCl₃) δ 1.53–1.37 (m, 12H, CH₂), 1.33–1.30 (m, 6H, CH₂), 1.26–1.23 (m, 24H, CH₂), 0.83 (t, ³J_{HH} = 6.9 Hz, 9H, CH₃), 0.47 and 0.19 (br apparent d, 3H, BH₃); ¹³C{¹H} NMR (101 MHz, CDCl₃) δ 31.7 (s, CH₂), 31.1 (d, J_{CP} = 12.0 Hz, CH₂), 29.0 (s, CH₂), 28.9 (s, CH₂), 22.9 (d, J_{CP} = 34.3 Hz, CH₂), 22.50 (s, CH₂), 22.48 (s, CH₂), 14.0 (s, CH₃); ³¹P{¹H} NMR (162 MHz, CDCl₃) δ 15.9 and 15.5 (br apparent d); IR (oil film): 2926 (s), 2856 (m), 2366 (m), 1463 (m), 1413 (w), 1378 (w), 1135 (w), 1061 (m), 1034 (w), 807 (w), 764 (w), 722 (m) cm⁻¹; MS (EI) [56]: 384 (M⁺, <1%), 370 ([M – BH₃]⁺, 79%).

H₃B·P(CH₂)₁₃CH₂(n-C₈H₁₇)₃ (**5**·BH₃; 0.090 g, 0.25 mmol, 8%), colorless oil. Anal. calcd for C₂₂H₄₈BP (354.40): C, 74.56; H, 13.65; found: C, 74.27; H, 13.52; ¹H NMR (500 MHz, CDCl₃) δ 1.62–1.19 (m, 42H, CH₂), 0.86 (t, 3H, ³J_{HH} = 7.0 Hz, CH₃), 0.48 and 0.26 (br apparent d, 3H, BH₃); ¹³C{¹H} NMR (126 MHz, CDCl₃) δ 31.7 (s, CH₂), 31.2 (d, J_{CP} = 12.6 Hz, CH₂), 29.03 (s, CH₂), 29.01 (s, CH₂), 28.9 (d, J_{CP} = 11.1 Hz, 2CH₂), 26.7 (s, 2CH₂), 26.53 (s, 2CH₂), 26.48 (s, 2CH₂), 26.1 (s, 2CH₂), 23.8 (d, J_{CP} = 35.4 Hz, CH₂), 22.57 (d, J_{CP} = 1.2 Hz, 2CH₂), 22.55 (s, CH₂), 22.3 (d, J_{CP} = 33.6 Hz, CH₂), 21.2 (d, J_{CP} = 3.3 Hz, 2CH₂), 14.0 (s, CH₃); ³¹P{¹H} NMR (202 MHz, CDCl₃) δ 15.6 and 15.2 (br apparent d); IR (oil film): 2926 (s), 2856 (m), 2366 (m), 1459 (m), 1417 (w), 1135 (w), 1061 (m), 791 (w), 722 (m) cm⁻¹; MS (EI) [56]: 678 (M⁺, 9%), 665 ([M – BH₃]⁺, 100%), 652 ([M – 2BH₃ + 1]⁺, 72%).

(EI) [56]: 340 ([M – BH₃]⁺, 93%), 228 ([M – BH₃ – C₈H₁₇ + 1]⁺, 100%).

in,out-H₃B·P((CH₂)₁₄)₃P·BH₃ (*in,out-2*·2BH₃; 0.039 g, 0.057 mmol, 4%), colorless oil. Anal. calcd for C₄₂H₉₀B₂P₂ (678.73): C, 74.32; H, 13.37; found: C, 73.86; H, 13.49; ¹H NMR (500 MHz, CDCl₃) δ 1.56–1.51 (m, 12H, PCH₂), 1.49–1.42 (m, 12H, CH₂), 1.39–1.33 (m, 12H, CH₂), 1.31–1.21 (m, 48H, CH₂), 0.45 and 0.27 (br apparent d, 6H, BH₃); ¹³C{¹H} NMR (126 MHz, CDCl₃) δ 30.5 (d, J_{CP} = 11.3 Hz, CH₂), 28.35 (s, CH₂), 28.28 (s, CH₂), 28.2 (s, CH₂), 28.1 (s, CH₂), 23.0 (d, J_{CP} = 34.3 Hz, CH₂), 22.2 (d, J_{CP} = 1.9 Hz, CH₂); ³¹P{¹H} NMR (202 MHz, CDCl₃) δ 15.6 and 15.4 (br apparent d); IR (oil film): 2926 (s), 2853 (m), 2366 (w), 1459 (w), 1413 (w), 1135 (w), 1061 (m), 803 (w), 722 (w) cm⁻¹; MS (MALDI⁺, THAP) [56]: 651.6 ([M – 2BH₃ + 1]⁺, 100%).

H₃B·P(CH₂)₁₃CH₂(CH₂)₁₄P((CH₂)₁₃CH₂)·BH₃ (6**·2BH₃; 0.101 g, 0.149 mmol, 10%), white solid, mp 96 °C (capillary). Anal. calcd for C₄₂H₉₀B₂P₂ (678.73): C, 74.32; H, 13.37; found: C, 73.92; H, 13.47. The identity of this compound, which has been independently synthesized, has been confirmed crystallographically [6]. ¹H NMR (500 MHz, CDCl₃) δ 1.65–1.14 (br m, 84H, CH₂), 0.49 and 0.26 (br apparent d, 6H, BH₃); ¹³C{¹H} NMR (126 MHz, CDCl₃) δ 31.3 (d, J_{CP} = 12.6 Hz, CH₂), 29.54 (s, CH₂), 29.53 (s, CH₂), 29.4 (s, CH₂), 29.1 (s, CH₂), 29.0 (d, J_{CP} = 11.1 Hz, 2CH₂), 26.8 (s, 2CH₂), 26.6 (s, 2CH₂), 26.5 (s, 2CH₂), 26.1 (s, 2CH₂), 23.8 (d, J_{CP} = 35.3 Hz, CH₂), 22.6 (d, J_{CP} = 1.0 Hz, CH₂), 22.3 (d, J_{CP} = 33.5 Hz, 2CH₂), 21.2 (d, J_{CP} = 3.3 Hz, 2CH₂); ³¹P{¹H} NMR (202 MHz, CDCl₃) δ 15.6 and 15.2 (br apparent d); IR (powder film): 2922 (s), 2853 (m), 2366 (m), 1459 (m), 1417 (w), 1135 (w), 1061 (m), 791 (w), 722 (m) cm⁻¹; MS (EI) [56]: 678 (M⁺, 9%), 665 ([M – BH₃]⁺, 100%), 652 ([M – 2BH₃ + 1]⁺, 72%).**

(in,in/out,out)-H₃B·P((CH₂)₁₄)₃P·BH₃ (*(in,in/out,out)-2*·2BH₃; 0.016 g, 0.024 mmol, 2%), colorless oil that solidified to give a white powder, mp 112 °C. Anal. calcd for C₄₂H₉₀B₂P₂ (678.73): C, 74.32; H, 13.37; found: C, 74.71; H, 13.34; ¹H NMR (500 MHz, CDCl₃) δ 1.55–1.50 (m, 12H, CH₂), 1.47–1.39 (m, 12H, CH₂), 1.37–1.32 (m, 12H, CH₂), 1.29–1.21 (m, 48H, CH₂), 0.38 and 0.26 (br apparent d, 6H, BH₃); ¹³C{¹H} NMR (126 MHz, CDCl₃) δ 30.6 (d, J_{CP} = 12.1 Hz, CH₂), 29.23 (s, CH₂), 29.17 (s, CH₂), 28.9 (s, CH₂), 28.4 (s, CH₂), 22.5 (d, J_{CP} = 34.1 Hz, CH₂), 22.1 (d, J_{CP} = 2.7 Hz, CH₂); ³¹P{¹H} NMR (202 MHz, CDCl₃) δ 14.9 and 14.7 (br apparent d); IR (powder film): 2922 (s), 2853 (s), 2366 (m), 1467 (m), 1413 (w), 1131 (w), 1061 (m), 807 (w), 760 (w), 718 (m) cm⁻¹; MS (MALDI⁺, THAP) [56]: 702.0 ([M + Na]⁺, 98%), 666.0 ([M – BH₃ + 1]⁺, 100%).

Metathesis/hydrogenation of $(H_2C=CH(CH_2)_6)_2(H_3B)P((CH_2)_{14})P(BH_3)((CH_2)_6CH=CH_2)_2$ (11·2BH₃; Scheme 5 [32]). Diphosphine diborane **11·2BH₃** (1.222 g, 1.672 mmol), CH₂Cl₂ (1700 mL; the resulting solution was 0.0010 M in **11·2BH₃**), Grubbs' first generation catalyst (0.069 g, 0.083 mmol, 5 mol %), Wilkinson's catalyst (0.046 g, 0.050 mmol, ca. 3 mol %), and H₂ were combined in a procedure analogous to that used for **1·BH₃**. An identical work-up gave *in,out*-**2·2BH₃** (0.072 g, 0.106 mmol, 6%, minor impurities evident by ¹³C{¹H} NMR), **6·2BH₃** (0.056 g, 0.083 mmol, 5%, minor impurities evident by ¹³C{¹H} NMR), and (*in,in/out,out*)-**2·2BH₃** (0.075 g, 0.111 mmol, 7%), along with several fractions consisting of unidentified and/or impure products, or oligomers and polymers. Spectroscopic data for *in,out*-**2·2BH₃**, (*in,in/out,out*)-**2·2BH₃**, and **6·2BH₃** matched those reported above.

Supporting Information

Supporting Information File 1

Additional experimental data.

[<https://www.beilstein-journals.org/bjoc/content/supplementary/1860-5397-14-211-S1.pdf>]

Acknowledgements

The authors thank the National Science Foundation (CHE-1153085, CHE-1566601) and Deutsche Forschungsgemeinschaft (DFG, GL 300/9-1) for support. As noted above, many of the experiments can be found in the doctoral dissertation of Dr. Tobias Fiedler.

ORCID® IDs

Tobias Fiedler - <https://orcid.org/0000-0001-7169-305X>

Michał Barbasiewicz - <https://orcid.org/0000-0002-0907-7034>

Michael Stollenz - <https://orcid.org/0000-0002-8635-164X>

John A. Gladysz - <https://orcid.org/0000-0002-7012-4872>

References

- Shima, T.; Hampel, F.; Gladysz, J. A. *Angew. Chem., Int. Ed.* **2004**, *43*, 5537–5540. doi:10.1002/anie.200460534
Angew. Chem. **2004**, *116*, 5653–5656. doi:10.1002/ange.200460534
- Lang, G. M.; Shima, T.; Wang, L.; Cluff, K. J.; Skopek, K.; Hampel, F.; Blümel, J.; Gladysz, J. A. *J. Am. Chem. Soc.* **2016**, *138*, 7649–7663. doi:10.1021/jacs.6b03178
- Lang, G. M.; Bhuvanesh, N.; Reibenspies, J. H.; Gladysz, J. A. *Organometallics* **2016**, *35*, 2873–2889. doi:10.1021/acs.organomet.6b00447
- Lang, G. M.; Skaper, D.; Hampel, F.; Gladysz, J. A. *Dalton Trans.* **2016**, *45*, 16190–16204. doi:10.1039/C6DT03258C
- Nawara, A. J.; Shima, T.; Hampel, F.; Gladysz, J. A. *J. Am. Chem. Soc.* **2006**, *128*, 4962–4963. doi:10.1021/ja061044w
- Nawara-Hultsch, A. J.; Stollenz, M.; Barbasiewicz, M.; Szafer, S.; Lis, T.; Hampel, F.; Bhuvanesh, N.; Gladysz, J. A. *Chem. – Eur. J.* **2014**, *20*, 4617–4637. doi:10.1002/chem.201304419
- Kharel, S.; Joshi, H.; Bhuvanesh, N.; Gladysz, J. A. *Organometallics* **2018**, *37*, in press. doi:10.1021/acs.organomet.8b00345
- Wang, L.; Hampel, F.; Gladysz, J. A. *Angew. Chem., Int. Ed.* **2006**, *45*, 4372–4375. doi:10.1002/anie.200601191
Angew. Chem. **2006**, *118*, 4479–4482. doi:10.1002/ange.200601191
- Wang, L.; Shima, T.; Hampel, F.; Gladysz, J. A. *Chem. Commun.* **2006**, *4075–4077*. doi:10.1039/B606728J
- Estrada, A. L.; Jia, T.; Bhuvanesh, N.; Blümel, J.; Gladysz, J. A. *Eur. J. Inorg. Chem.* **2015**, *5318–5321*. doi:10.1002/ejic.201500953
- Hess, G. D.; Hampel, F.; Gladysz, J. A. *Organometallics* **2007**, *26*, 5129–5131. doi:10.1021/om700625u
- Fiedler, T.; Bhuvanesh, N.; Hampel, F.; Reibenspies, J. H.; Gladysz, J. A. *Dalton Trans.* **2016**, *45*, 7131–7147. doi:10.1039/C6DT00692B
- Hess, G. D.; Fiedler, T.; Hampel, F.; Gladysz, J. A. *Inorg. Chem.* **2017**, *56*, 7454–7469. doi:10.1021/acs.inorgchem.7b00909
- Setaka, W.; Yamaguchi, K. *J. Am. Chem. Soc.* **2013**, *135*, 14560–14563. doi:10.1021/ja408405f
and earlier work cited therein.
- Setaka, W.; Inoue, K.; Higa, S.; Yoshigai, S.; Kono, H.; Yamaguchi, K. *J. Org. Chem.* **2014**, *79*, 8288–8295. doi:10.1021/jo501539h
- Setaka, W.; Higa, S.; Yamaguchi, K. *Org. Biomol. Chem.* **2014**, *12*, 3354–3357. doi:10.1039/C4OB00470A
- Shionari, H.; Inagaki, Y.; Yamaguchi, K.; Setaka, W. *Org. Biomol. Chem.* **2015**, *13*, 10511–10516. doi:10.1039/C5OB01644D
- Nishiyama, Y.; Inagaki, Y.; Yamaguchi, K.; Setaka, W. *J. Org. Chem.* **2015**, *80*, 9959–9966. doi:10.1021/acs.joc.5b01489
- Masuda, T.; Arase, J.; Inagaki, Y.; Kawahata, M.; Yamaguchi, K.; Ohhara, T.; Nakao, A.; Momma, H.; Kwon, E.; Setaka, W. *Cryst. Growth Des.* **2016**, *16*, 4392–4401. doi:10.1021/cgd.6b00508
- Kottas, G. S.; Clarke, L. I.; Horinek, D.; Michl, J. *Chem. Rev.* **2005**, *105*, 1281–1376. doi:10.1021/cr0300993
- Vogelsberg, C. S.; Garcia-Garibay, M. A. *Chem. Soc. Rev.* **2012**, *41*, 1892–1910. doi:10.1039/C1CS15197E
- Kharel, S.; Joshi, H.; Bierschenk, S.; Stollenz, M.; Taher, D.; Bhuvanesh, N.; Gladysz, J. A. *J. Am. Chem. Soc.* **2017**, *139*, 2172–2175. doi:10.1021/jacs.6b12788
- Alder, R. W.; Butts, C. P.; Orpen, A. G.; Read, D.; Oliva, J. M. *J. Chem. Soc., Perkin Trans. 2* **2001**, 282–287. doi:10.1039/b008903f
and references cited therein.
- Hilliard, C. R. Diphosphine Dioxide Cages and Hydrogen Peroxide Adducts of Phosphine Oxides: Syntheses and Applications in Surface Science. Ph.D. Thesis, Texas A&M University, College Station, USA, 2013.
- Kharel, S.; Jia, T.; Bhuvanesh, N.; Reibenspies, J. H.; Blümel, J.; Gladysz, J. A. *Chem. – Asian J.* **2018**, *13*, in press. doi:10.1002/asia.201800739
- Alder, R. W.; East, S. P. *Chem. Rev.* **1996**, *96*, 2097–2112. doi:10.1021/cr940246k
- Park, C. H.; Simmons, H. E. *J. Am. Chem. Soc.* **1968**, *90*, 2429–2431. doi:10.1021/ja01011a046

28. Stollenz, M.; Barbasiewicz, M.; Nawara-Hultsch, A. J.; Fiedler, T.; Laddusaw, R. M.; Bhuvanesh, N.; Gladysz, J. A. *Angew. Chem., Int. Ed.* **2011**, *50*, 6647–6651. doi:10.1002/anie.201100893

29. Stollenz, M.; Bhuvanesh, N.; Reibenspies, J. H.; Gladysz, J. A. *Organometallics* **2011**, *30*, 6510–6513. doi:10.1021/om200924g

30. Stollenz, M.; Taher, D.; Bhuvanesh, N.; Reibenspies, J. H.; Baranová, Z.; Gladysz, J. A. *Chem. Commun.* **2015**, *51*, 16053–16056. doi:10.1039/C5CC05620A

31. Nawara-Hultsch, A. J.; Skopek, K.; Shima, T.; Barbasiewicz, M.; Hess, G. D.; Skaper, D.; Gladysz, J. A. *Z. Naturforsch., B: J. Chem. Sci.* **2010**, *65*, 414–424. doi:10.1515/znb-2010-0327

The yield range given for $\mathbf{1}\cdot\text{BH}_3$ reflects the results of repeated preparations since this original report.

32. Fiedler, T. Syntheses of Gyroscope-like Osmium Complexes and Cage-like Diphosphines. Doctoral Thesis, Friedrich-Alexander-University, Erlangen, Germany, 2011.

33. Berthod, M.; Favre-Réguillon, A.; Mohamad, J.; Mignani, G.; Docherty, G.; Lemaire, M. *Synlett* **2007**, 1545–1548. doi:10.1055/s-2007-982536

34. Shima, T.; Bauer, E. B.; Hampel, F.; Gladysz, J. A. *Dalton Trans.* **2004**, 1012–1028. doi:10.1039/b400156g

35. Joshi, H.; Kharel, S.; Ehnbom, A.; Skopek, K.; Hess, G. D.; Fiedler, T.; Hampel, F.; Bhuvanesh, N.; Gladysz, J. A. *J. Am. Chem. Soc.* **2018**, *140*, 8463–8478. doi:10.1021/jacs.8b02846

36. Grela, K.; Harutyunyan, S.; Michrowska, A. *Angew. Chem., Int. Ed.* **2002**, *41*, 4038–4040. doi:10.1002/1521-3773(20021104)41:21<4038::AID-ANIE4038>3.0.CO;2-0

Angew. Chem. **2002**, *114*, 4210–4212. doi:10.1002/1521-3757(20021104)114:21<4210::AID-ANGE4210>3.0.CO;2-J

37. Nguyen, T. B.; Castanet, A.-S.; Nguyen, T.-H.; Nguyen, K. P. P.; Bardeau, J.-F.; Gibaud, A.; Mortier, J. *Tetrahedron* **2006**, *62*, 647–651. doi:10.1016/j.tet.2005.10.003

38. For previous syntheses and characterization of **8**, see references [39–41].

39. Woolford, R. G. *Can. J. Chem.* **1962**, *40*, 1846–1850. doi:10.1139/v62-280

40. Taffa, D.; Kathiresan, M.; Walder, L. *Langmuir* **2009**, *25*, 5371–5379. doi:10.1021/la8038126

See Supporting Information.

41. Matsubara, H.; Tsukida, M.; Ishihara, D.; Kuniyoshi, K.; Ryu, I. *Synlett* **2010**, 2014–2018. doi:10.1055/s-0030-1258482

42. Soomro, S. A.; Benmouna, R.; Berger, R.; Meier, H. *Eur. J. Org. Chem.* **2005**, 3586–3593. doi:10.1002/ejoc.200500185

See for the methodology used to prepare **8**.

43. de Andrade, V. S. C.; de Mattos, M. C. S. *Curr. Org. Synth.* **2015**, *12*, 309–327. doi:10.2174/1570179412666150305231358

44. For a related Arbuzov reaction of **8**, see reference [40].

45. Stranne, R.; Vasse, J.-L.; Moberg, C. *Org. Lett.* **2001**, *3*, 2525–2528. doi:10.1021/o1016193s

46. Staubitz, A.; Robertson, A. P. M.; Sloan, M. E.; Manners, I. *Chem. Rev.* **2010**, *110*, 4023–4078. doi:10.1021/cr100105a (see section 4.2.1.1).

47. Gaumont, A.-C.; Bourumeau, K.; Denis, J.-M.; Guenot, P. *J. Organomet. Chem.* **1994**, *484*, 9–12. doi:10.1016/0022-328X(94)87178-7

48. Pinto, P.; Götz, A. W.; Marconi, G.; Hess, B. A.; Marinetti, A.; Heinemann, F. W.; Zenneck, U. *Organometallics* **2006**, *25*, 2607–2616. doi:10.1021/om050461z

49. Dahlenburg, L.; Kaunert, A. *Eur. J. Inorg. Chem.* **1998**, 885–887. doi:10.1002/(SICI)1099-0682(199807)1998:7<885::AID-EJIC885>3.0.CO;2-6

50. Däbritz, F.; Theumer, G.; Gruner, M.; Bauer, I. *Tetrahedron* **2009**, *65*, 2995–3002. doi:10.1016/j.tet.2009.01.102

51. Bauer, I.; Habicher, W. D. *Collect. Czech. Chem. Commun.* **2004**, *69*, 1195–1230. doi:10.1135/cccc20041195

52. Jung, M. E.; Piuzzi, G. *Chem. Rev.* **2005**, *105*, 1735–1766. doi:10.1021/cr940337h

53. Schuman, M.; Trevitt, M.; Redd, A.; Gouverneur, V. *Angew. Chem., Int. Ed.* **2000**, *39*, 2491–2493. doi:10.1002/1521-3773(20000717)39:14<2491::AID-ANIE2491>3.0.CO;2-H

Angew. Chem. **2000**, *112*, 2604–2607. doi:10.1002/1521-3757(20000717)112:14<2604::AID-ANGE2604>3.0.CO;2-#

54. Wu, X.; O'Brien, P.; Ellwood, S.; Secci, F.; Kelly, B. *Org. Lett.* **2013**, *15*, 192–195. doi:10.1021/o1303253h

55. The NiCl_2 analog of the PtCl_2 adduct of *in,in*-**2** in Scheme 1 is known, but is so far only available from the free dibridgehead diphosphine **2** [22].

56. The most intense peak of the isotope envelope is given; *m/z* (relative intensity, %). THAP = 2,4,6-trihydroxyacetophenone matrix.

License and Terms

This is an Open Access article under the terms of the Creative Commons Attribution License (<http://creativecommons.org/licenses/by/4.0>). Please note that the reuse, redistribution and reproduction in particular requires that the authors and source are credited.

The license is subject to the *Beilstein Journal of Organic Chemistry* terms and conditions: (<https://www.beilstein-journals.org/bjoc>)

The definitive version of this article is the electronic one which can be found at: doi:10.3762/bjoc.14.211



Efficient catalytic alkyne metathesis with a fluoroalkoxy-supported ditungsten(III) complex

Henrike Ehrhorn, Janin Schlösser, Dirk Bockfeld and Matthias Tamm*

Full Research Paper

Open Access

Address:

Institut für Anorganische und Analytische Chemie, Technische Universität Braunschweig, Hagenring 30, 38106 Braunschweig, Germany

Email:

Matthias Tamm* - m.tamm@tu-bs.de

* Corresponding author

Keywords:

alkylidyne complexes; alkyne metathesis; catalysis; terminal alkynes; tungsten

Beilstein J. Org. Chem. 2018, 14, 2425–2434.

doi:10.3762/bjoc.14.220

Received: 25 June 2018

Accepted: 27 August 2018

Published: 18 September 2018

This article is part of the thematic issue "Progress in metathesis chemistry III".

Guest Editor: K. Grela

© 2018 Ehrhorn et al.; licensee Beilstein-Institut.

License and terms: see end of document.

Abstract

The molybdenum and tungsten complexes $M_2(OR)_6$ (**Mo2F6**, $M = Mo$, $R = C(CF_3)_2Me$; **W2F3**, $M = W$, $R = OC(CF_3)Me_2$) were synthesized as bimetallic congeners of the highly active alkyne metathesis catalysts $[MesC\equiv M\{OC(CF_3)_nMe_{3-n}\}]$ (**MoF6**, $M = Mo$, $n = 2$; **WF3**, $M = W$, $n = 1$; $Mes = 2,4,6$ -trimethylphenyl). The corresponding benzylidyne complex $[PhC\equiv W\{OC(CF_3)Me_2\}]$ (**WPhF3**) was prepared by cleaving the $W\equiv W$ bond in **W2F3** with 1-phenyl-1-propyne. The catalytic alkyne metathesis activity of these metal complexes was determined in the self-metathesis, ring-closing alkyne metathesis and cross-metathesis of internal and terminal alkynes, revealing an almost equally high metathesis activity for the bimetallic tungsten complex **W2F3** and the alkylidyne complex **WPhF3**. In contrast, **Mo2F6** displayed no significant activity in alkyne metathesis.

Introduction

While the field of olefin metathesis has seen significant progress in the past decades [1-5], the synthetic potential of alkyne metathesis has been growing only recently [6-11]. Alkyne metathesis represents a transition-metal-catalyzed transformation in which carbon–carbon triple bonds are cleaved and formed under mild conditions via metallacyclobutadiene (MCBD) intermediates [12]. Ongoing progress in the development of highly active homogeneous alkyne metathesis catalysts (Figure 1) has increased the value of this method in natural product and materials chemistry.

The contributions from our group to the development of alkyne metathesis catalysts were initially based on a design strategy inspired by the structure of highly active olefin metathesis catalysts, the Schrock-type molybdenum and tungsten alkylidene complexes [13-15]. Imidazolin-2-iminato ligands were used to modify Schrock-type alkylidyne complexes, resulting in new active alkyne metathesis catalysts such as **I** (Figure 1) [16-20]. Initially, the neopentylidyne tungsten complex was synthesized via the conventional “high-oxidation-state route” developed by R. R. Schrock [16,17,21,22]; later, the “low-oxidation-state

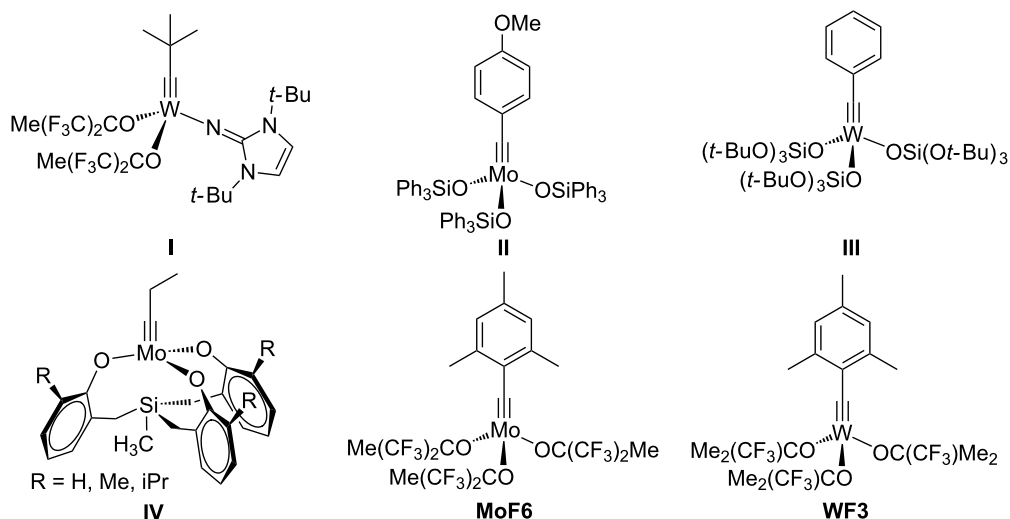


Figure 1: Selected homogeneous catalysts for alkyne metathesis.

route”, starting from $M(CO)_6$ ($M = Mo, W$), was employed, which gave rise to the corresponding molybdenum and tungsten benzylidene complexes [18–20].

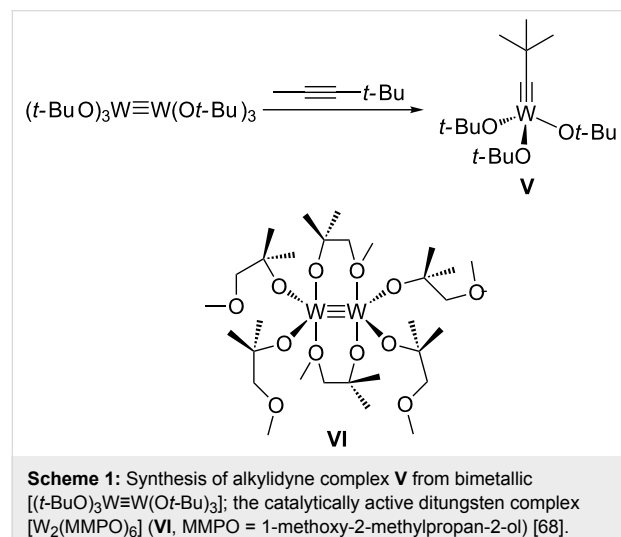
In addition to these, several well-defined alkylidene complexes have been developed and successfully utilized in alkyne metathesis in the past decade. The molybdenum alkylidene complex with triphenylsiloxide ligands (type **II**) introduced by A. Fürstner and co-workers is frequently used in the total synthesis of natural products [23–27]. A unique catalytic reactivity towards conjugated diynes was observed for the tungsten benzylidene complex with $OSi(Ot-Bu)_3$ ligands (type **III**) [28–30]. The catalyst **III**, which is capable of promoting conventional alkyne metathesis [19], also proved to be highly active in the cross metathesis of symmetric 1,3-butadiynes to form unsymmetrically substituted 1,3-butadiynes [30]. W. Zhang and his group introduced several multidentate phenoxide ligands to molybdenum propylidene precursors to form chelate complexes of type **IV** [31–34]. These catalysts were especially successful in the construction of supramolecular materials such as ethynylene-linked polymers [11,35], porous networks [36] and molecular cages [37–43]. Furthermore, living ring-opening alkyne metathesis polymerization (ROAMP) has been intensely studied for different molybdenum alkylidene complexes by the group of F. R. Fischer, who was able to monitor the influence of both the alkylidene moiety as well as the ancillary ligands [44–48].

More recently, we expanded the “low-oxidation-state route” to the synthesis of 2,4,6-trimethylbenzylidene complexes of molybdenum and tungsten [18,49,50], which led to an increased steric demand at the metal center. This proved to be ad-

vantageous for the catalytic activity, since the removal of coordinating solvents like THF or DME was facilitated [49]. The molybdenum 2,4,6-trimethylbenzylidene complex $[MesC\equiv Mo\{OC(CF_3)_2Me\}_3]$ (Figure 1, **MoF6**) represents the first alkyne metathesis catalyst capable of effective and highly selective terminal alkyne metathesis [49,51–53]. Later, a study was conducted to determine the optimum degree of fluorination of the alkoxide ligands for tungsten alkylidene complexes [53,54]. It was found that the tungsten alkylidene complex $[MesC\equiv W\{OC(CF_3)Me_2\}_3]$ (Figure 1, **WF3**) showed excellent catalytic performance not only in the metathesis of internal but also, for the first time with the metal tungsten, terminal alkynes at room temperature [54]. Our studies clearly display a strong dependency of the catalytic alkyne metathesis activity on the metal-alkoxide combination. The electrophilicity of the metal sites can be controlled by the number of fluorine atoms of the ancillary fluoroalkoxide ligands [55–57]. The difference in the optimum degree of fluorination for molybdenum and tungsten is rationalized by the increased intrinsic electrophilicity of tungsten compared to molybdenum [56].

Based on these insights into the structure–activity relationship of alkyne metathesis catalysts, we wanted to establish an alternative and convenient access to highly active catalysts. Herein, we report the systematic study on the metathesis performance of bimetallic hexaalkoxide complexes $M_2(OR)_6$ ($M = Mo$, $R = OC(CF_3)_2Me$, **Mo2F6**; $M = W$, $R = OC(CF_3)Me_2$, **W2F3**), which draw upon the most catalytically active alkylidene complexes **MoF6** and **WF3**. R. R. Schrock synthesized the first alkylidene complex which was able to undergo alkyne metathesis, $[t-BuC\equiv W(Ot-Bu)_3]$ (**V**), originally from $[NEt_4][t-BuC\equiv WCl_4]$ [22,58–61]. Subsequently, he reported a protocol

to synthesize the alkylidyne complex **V** by a stoichiometric alkyne metathesis reaction of the ditungsten complex $[(t\text{-BuO})_3\text{W}\equiv\text{W}(\text{Ot-Bu})_3]$ with $\text{MeC}\equiv\text{C}t\text{-Bu}$ (Scheme 1) [62]. Even though Schrock's catalyst **V** was the most established alkyne metathesis catalyst for many years [63,64], it does not promote terminal alkyne metathesis efficiently and leads to polymerization initiated by intermediate deprotiometallacyclobutadiene species [55,60,61,65–67]. Moreover, the bimetallic $[(t\text{-BuO})_3\text{W}\equiv\text{W}(\text{Ot-Bu})_3]$ complex has not been directly employed in catalytic alkyne metathesis.



Scheme 1: Synthesis of alkylidyne complex **V** from bimetallic $[(t\text{-BuO})_3\text{W}\equiv\text{W}(\text{Ot-Bu})_3]$; the catalytically active ditungsten complex $[\text{W}_2(\text{MMPO})_6]$ (**VI**, MMPO = 1-methoxy-2-methylpropan-2-ol) [68].

A. Mortreux and his group found that the alkyne metathesis selectivity of Schrock's original catalyst **V** can be enhanced by adding an external ligand like quinuclidine to the reaction mix-

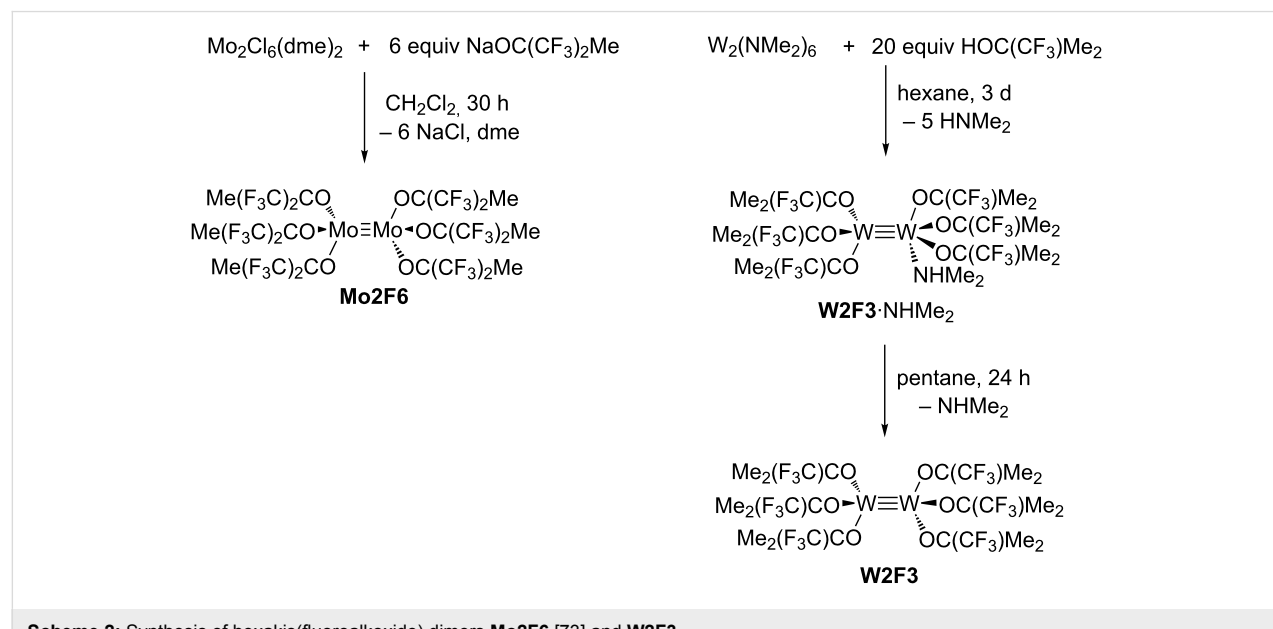
ture [61]. Thereby, the self-metathesis yield of 1-heptyne could be increased to 80% at elevated temperatures. Based on this approach, the dinuclear tungsten complex $[\text{W}_2(\text{MMPO})_6]$ (**VI**, MMPO = 1-methoxy-2-methylpropan-2-ol) was isolated which catalyzed alkyne metathesis of 1-heptyne at elevated temperatures [68] and to date represents the only well-defined ditungsten complex which has been successfully used in alkyne metathesis.

The organometallic chemistry of the M_2X_6 complexes ($\text{X} = \text{R}$ (alkyl), NR_2 , OR) with metal–metal triple bonds ($\text{M} = \text{Mo, W}$) has attracted attention for many years (mainly during the 70s, 80s and 90s) [69]. A plethora of dinuclear compounds has been published [70–78], and detailed studies on their reactivity have been conducted [79–85]. Therefore, the reactivity of ditungsten complexes towards alkynes has been known for quite some time. The metal–metal triple bond of many ditungsten complexes can be cleaved by alkynes in a metathesis-like reaction to form the corresponding alkylidyne complexes [62,86]. Dinuclear $\text{Mo}\equiv\text{Mo}$ complexes, however, have not yet been cleaved efficiently by alkynes [87].

Results and Discussion

Complex synthesis

The dimeric molybdenum complex $[\text{Mo}_2\text{Cl}_6(\text{dme})_2]$ (dme = 1,2-dimethoxyethane) serves as an excellent starting material for compounds of the type Mo_2X_6 ($\text{X} = \text{alkyl, alkoxide}$) [73]. The desired hexakis(fluoroalkoxide) dimer $[\text{Mo}_2\{\text{OC}(\text{CF}_3)_2\text{Me}\}_6]$ (**Mo2F6**) was first isolated by D. Rogers and his group by salt metathesis of $[\text{Mo}_2\text{Cl}_6(\text{dme})_2]$ with 6 equiv of $\text{NaOC}(\text{CF}_3)_2\text{Me}$ (Scheme 2) [73]. This reaction



Scheme 2: Synthesis of hexakis(fluoroalkoxide) dimers **Mo2F6** [73] and **W2F3**.

affords a red, sparingly soluble complex in moderate yield (28%).

The bimetallic tungsten analogue to **WF3**, $[W_2\{OC(CF_3)Me_2\}_6]$ (**W2F3**), can be prepared by the reaction of $[NaW_2Cl_7(THF)_5]$ with 6 equiv of $NaOC(CF_3)Me_2$ [86], but this procedure requires one equivalent of toxic sodium amalgam. Therefore, we decided to attempt the protonolysis of hexakis(dimethylamido)ditungsten $[W_2(NMe_2)_6]$ with the alcohol $HOC(CF_3)Me_2$ [71,88], which has been described very briefly in the literature [89]. $[W_2(NMe_2)_6]$ is easily accessible from WCl_4 and $LiNMe_2$ and has emerged as an important starting material for various dinuclear tungsten compounds [90]. M. H. Chisholm and co-workers used 6 equiv of the free alcohol to exchange the amide ligands and isolated the bis(dimethylamino) adduct of the ditungsten complex [89]. The amine ligands were liberated under reduced pressure and at elevated temperature. However, in our hands, an excess of $HOC(CF_3)Me_2$ was required to drive the reaction to completion and led to the formation of the complex $[W_2\{OC(CF_3)Me_2\}_6(NHMe_2)]$ (**W2F3·NHMe₂**) (Scheme 2). The additional amine ligand stems from the protonolysis reaction of the amide with the fluorinated alcohol. Brown crystals suitable for X-ray diffraction analysis were isolated from a saturated pentane solution at $-40\text{ }^{\circ}\text{C}$. The molecular structure of this complex was established by X-ray diffraction analysis. The ORTEP diagram is shown in Figure 2, and selected bond lengths and angles are displayed in Table 1.

The tungsten–tungsten triple bond of $2.3452(2)\text{ \AA}$ falls in the range of previously reported bond lengths of this type [69]. For example, the $W\equiv W$ distance in $[W_2\{OC(CF_3)_2Me\}_6]$ is $2.309(3)\text{ \AA}$ [78], $2.430(8)\text{ \AA}$ in $[W_2(MMPO)_6]$ [68], and $2.332(1)\text{ \AA}$ in $[W_2(OCHMe_2)_6(py)_2]$ (py = pyridine) [90]. The $W1-N$ bond length of $2.270(3)\text{ \AA}$ is longer compared to the $W-N$ distances in $[W_2(NMe_2)_6]$ ($1.95(2)-1.99(2)\text{ \AA}$) [71] and $[W_2Cl_2(NMe_2)_4]$ ($1.935(8)-1.937(9)\text{ \AA}$) [91]. This is attributed to the neutral nature of the $NHMe_2$ ligand compared to the

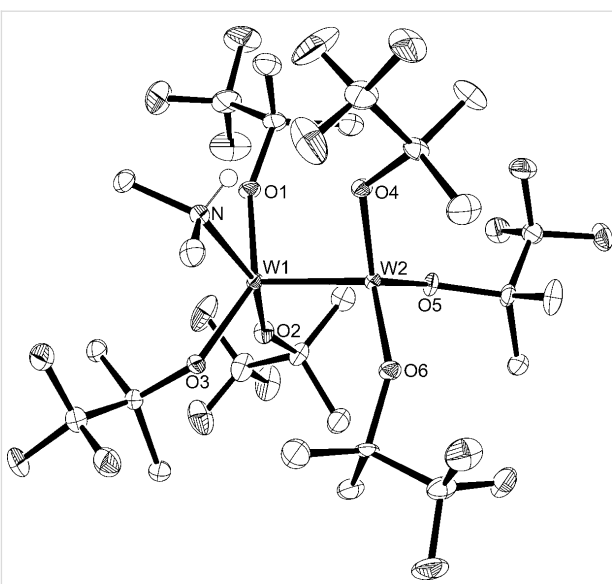


Figure 2: Molecular structure of **W2F3·NHMe₂** with thermal displacement parameters drawn at 50% probability. Hydrogen atoms are omitted for clarity.

negative NMe_2 ligand and indicates a weak bond between the tungsten and the nitrogen atom. Coordination of the $NHMe_2$ ligand to $W1$ affords markedly longer $W1-O$ bonds ($1.905(2)-1.970(2)\text{ \AA}$) than the $W2-O$ bonds ($1.818(2)-1.930(2)\text{ \AA}$). The $W1$ atom is coordinated in an almost square-pyramidal fashion ($\tau_5 = 0.25$) [92] while the $W2$ atom adopts a nearly tetrahedral geometry ($\tau_4 = 0.89$) [93], which is usually observed in $X_3W\equiv WX_3$ complexes [72,83,94]. The coordination of one amine ligand after the protonolysis of the amide ligands in $[W_2(NMe_2)_6]$ has been observed before, e.g., in $[W_2(OAr)_6(HNMe_2)]$ ($Ar = 3,5\text{-dimethylphenoxy}$) [95].

Complex **W2F3·NHMe₂** appeared to be rather unstable especially in hexane and pentane solutions. Over a period of 24 h, a color change from brown to bright red occurred in solution. This observation indicates the loss of the additional amine

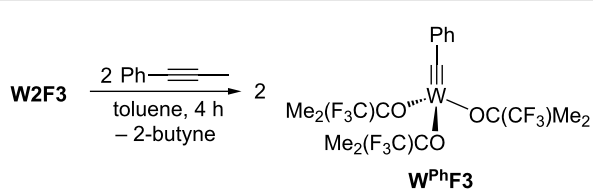
Table 1: Selected bond lengths [\AA] and angles [$^{\circ}$]:

Bond	Bond length [\AA]	Bond angle	Angle [$^{\circ}$]	Bond angle	Angle [$^{\circ}$]
W1-W2	2.3452(2)	O1-W1-O2	93.75(11)	O5-W2-O4	122.91(11)
W1-O1	1.905(2)	O1-W1-O3	145.01(10)	O1-W1-W2	104.75(8)
W1-O2	1.911(3)	O2-W1-O3	91.61(11)	O2-W1-W2	108.97(8)
W1-O3	1.970(2)	O1-W1-N	82.15(11)	O3-W1-W2	106.06(7)
W1-N	2.270(3)	O2-W1-N	159.81(11)	N-W1-W2	91.17(8)
W2-O4	1.930(2)	O3-W1-N	81.06(11)	O4-W2-W1	98.33(7)
W2-O5	1.818(2)	O6-W2-O5	110.53(11)	O5-W2-W1	99.29(7)
W2-O6	1.872(2)	O6-W2-O4	112.06(11)	O6-W2-W1	111.85(8)

ligand, and after recrystallization from pentane at $-25\text{ }^{\circ}\text{C}$, the red complex **W2F3** was isolated. The ^1H NMR spectrum reveals the only expected signal at 1.51 ppm, which is in line with the previously reported values, where **W2F3** had been prepared from $[\text{NaW}_2\text{Cl}_7(\text{THF})_5]$ [86]. The ^{13}C and ^{19}F NMR spectra are also consistent with literature values. Crystals of **W2F3** suitable for X-ray diffraction analysis were obtained upon cooling a saturated pentane solution to $-40\text{ }^{\circ}\text{C}$. Unfortunately, the crystal structure suffers from severe disorder. Each tungsten atom is disordered over four positions, and additionally, the alkoxide ligands are also disordered (for more details, see Supporting Information File 1). Therefore, the crystal structure only confirms the connectivity and does not allow the discussion of bond lengths and angles. This disorder pattern has been reported repeatedly for molybdenum and tungsten hexaalkoxides and silanlates [73,78,83,96–98]. An ORTEP diagram of **W2F3** is displayed in Supporting Information File 1 (Scheme S13).

As stated above, R. R. Schrock could generate alkyne metathesis catalysts of type **V** (Scheme 1) from the corresponding bimetallic complex [62,99]. Thus, we attempted the cleavage of the $\text{M}\equiv\text{M}$ bond of **Mo2F6** and **W2F3** by an alkyne to generate the corresponding benzylidyne complexes. Unfortunately, as reported in the past by Schrock [62,87], we could not achieve the selective cleavage of the triple bond in **Mo2F6** by internal or terminal alkynes to isolate the corresponding alkylidyne complex. In an NMR study on the cleavage of the $\text{Mo}\equiv\text{Mo}$ triple bond, in which **Mo2F6** was treated with two equivalents of 1-phenyl-1-propyne, no signals corresponding to a possible molybdenum alkylidyne complex were detected in the ^1H and ^{19}F NMR spectra over a period of three days.

In contrast, the reaction of the bimetallic tungsten complex **W2F3** with two equivalents of 1-phenyl-1-propyne in toluene afforded the light yellow benzylidyne complex **W^{Ph}F3** (Scheme 3) in satisfactory yield after recrystallization from *n*-pentane. In a metathesis-like reaction, the $\text{W}\equiv\text{W}$ bond is cleaved, with 2-butyne forming as a side product. Following this reaction by ^1H and ^{19}F NMR spectroscopy revealed fast and selective formation of **W^{Ph}F3**, and after 14 minutes, most of the starting material **W2F3** was already consumed, with full



Scheme 3: Preparation of the alkylidyne complex **W^{Ph}F3**.

conversion observed after 28 minutes. Selected ^{19}F NMR spectra can be found in Figure S7 of Supporting Information File 1.

The ^1H NMR spectrum of **W^{Ph}F3** displays two multiplets in the aromatic region for the benzylidyne hydrogen atoms and one singlet for the methyl groups of the trifluoro-*tert*-butoxy ligand at 1.65 ppm. In the ^{13}C NMR spectrum, the signal of the carbyne carbon atom can be found at 266.9 ppm, which is in the range typically observed for $\text{RC}\equiv\text{W}$ moieties [16–18,49,50,54]. The ^{19}F NMR spectrum only exhibits one singlet for the complex with a chemical shift of -82.4 ppm . Crystals suitable for X-ray diffraction analysis were isolated from a saturated pentane solution at $-40\text{ }^{\circ}\text{C}$; again, the crystal structure suffers from crystallographic problems: one alkoxide ligand is refined on two positions, while another one is refined on three positions. The crystal structure, which is displayed in Figure 3, only confirms the connectivity of this molecule, and discussion of any bond length is not meaningful (for more details, see Supporting Information File 1). A similar crystal structure with the 2,4,6-trimethylbenzylidyne moiety at the tungsten atom, which does not exhibit disorder, has been reported previously [54].

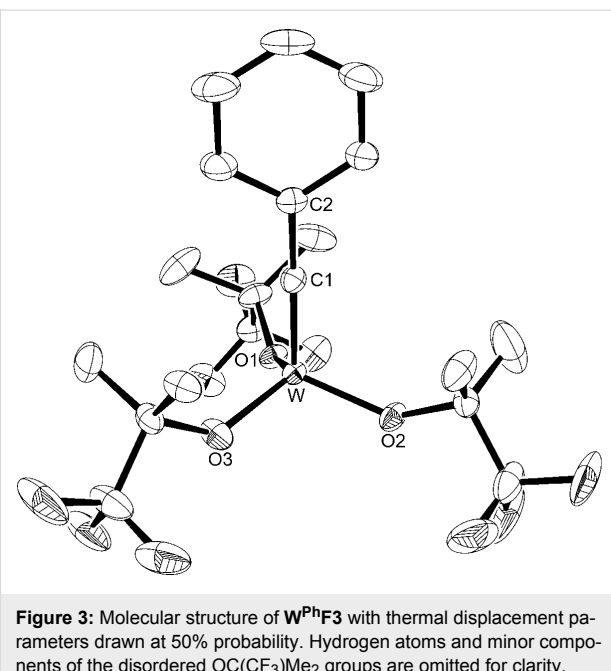


Figure 3: Molecular structure of **W^{Ph}F3** with thermal displacement parameters drawn at 50% probability. Hydrogen atoms and minor components of the disordered $\text{OC}(\text{CF}_3)\text{Me}_2$ groups are omitted for clarity.

Catalytic studies

With the bimetallic complexes **Mo2F6** and **W2F3** and the new alkylidyne complex **W^{Ph}F3** at hand, we aimed at systematically investigating the catalytic activity of those complexes. Even though we failed in selectively cleaving the $\text{Mo}\equiv\text{Mo}$ triple bond, we attempted catalytic alkyne metathesis with **Mo2F6**. Interestingly, a marginal catalytic activity could be detected for complex **Mo2F6**: over the course of four days, the dimolybdenum

dium complex achieved a conversion of 70% in the self-metathesis of the standard substrate 3-pentynyl benzyl ether in toluene in the presence of molecular sieves (MS 5 Å) as 2-butyne scavenger. The conversion versus time diagram (Supporting Information File 1, Figure S8) exhibits a sigmoidal curve progression, which indicates the slow formation of a catalytically active species, presumably an alkylidyne complex, despite our inability to monitor the formation of such a species by NMR spectroscopy. We attribute the poor catalytic performance of **Mo2F6** to the low solubility in all common solvents [73], since most of the compound still remained undissolved in the reaction mixture after four days. However, all efforts to optimize the metathesis conditions and to achieve higher conversions failed. Attempts to increase the solubility of **Mo2F6** in toluene by performing the metathesis reaction at 60 °C led to no detectable conversion of the starting material. Furthermore, catalysis in CH_2Cl_2 afforded even lower conversions compared to toluene, while the metathesis failed completely in diethyl ether.

For the potential tungsten catalysts, toluene solutions of 1-phenyl-1-propyne were treated with **W2F3** (0.5 mol %) and **W^{Ph}F3** (1 mol %) and stirred in the presence of molecular sieves (MS 5 Å) as 2-butyne scavenger and *n*-decane as internal standard at room temperature (Scheme 4). The catalysis was initially monitored over time through gas chromatography, affording the conversion versus time diagram depicted in Figure 4.

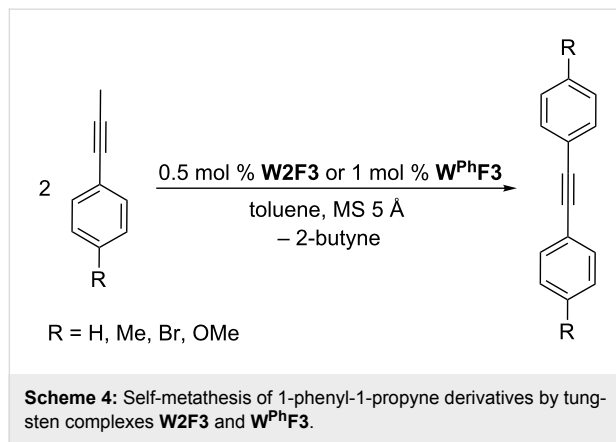


Figure 4 clearly shows that both tungsten complexes are active in the metathesis of 1-phenyl-1-propyne, with the bimetallic compound **W2F3** (grey) showing a slower initiation rate compared to the alkylidyne complex **W^{Ph}F3**. For the bimetallic complex **W2F3**, an additional initiation step is required, in which the $\text{W}\equiv\text{W}$ triple bond is cleaved and catalytically active alkylidyne species are formed. Therefore, the conversion of the substrate with catalyst **W2F3** is significantly slower at the beginning of the reaction. The initial catalyst turnover frequen-

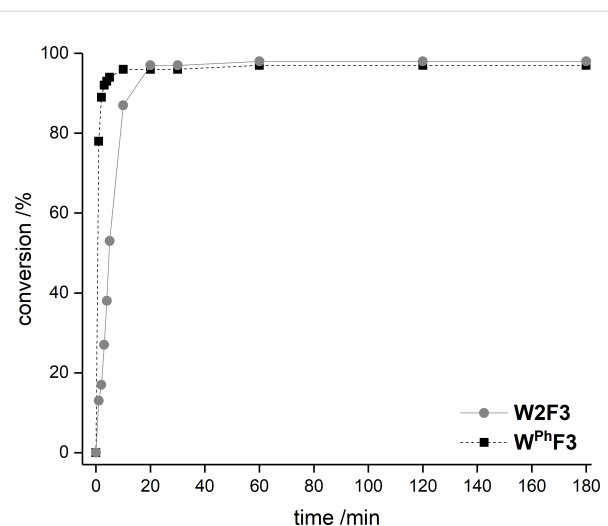


Figure 4: Conversion versus time diagram for the self-metathesis of 1-phenyl-1-propyne catalyzed by 0.5 mol % **W2F3** (grey) and 1 mol % **W^{Ph}F3** (black).

cies were calculated from the conversion of 1-phenyl-1-propyne after one minute (TOF_{1min}). The TOF of the alkylidyne complex **W^{Ph}F3** reaches 78 min^{-1} (1.30 s^{-1}), while **W2F3** has a significantly lower TOF of 13 min^{-1} (0.21 s^{-1}) after one minute; this value is based on the formation of two catalytically active alkylidyne species upon treatment with the alkyne substrate. After 10 minutes, the alkylidyne complex **W^{Ph}F3** has accomplished nearly full conversion and after 20 minutes, catalyst **W2F3** achieves the same conversion of the starting material. The maximum conversion of around 97% is reached for both catalysts within 60 minutes. Accordingly, we aimed at further monitoring the substrate scope of the complexes including the metathesis of terminal alkynes as well as ring-closing alkyne metathesis (RCAM).

Table 2 summarizes the isolated yields for various self-metathesis and RCAM reactions. These findings are in line with our initial results regarding the conversion of 1-phenyl-1-propyne (Table 2, entry 1). Both tungsten complexes afforded excellent yields in the metathesis of different *para*-substituted phenylpropynes (Table 2, entries 2–4). For both catalysts, the yields are identical within the error of the experiment. Furthermore, the well-established substrates 3-pentynyl ($\text{R} = \text{Me}$) and 3-butynyl ($\text{R} = \text{H}$) benzyl ether (Table 2, entry 5) and 3-pentynyl ($\text{R} = \text{Me}$) and 3-butynyl ($\text{R} = \text{H}$) benzyl ester (Table 2, entry 6) afforded good isolated yields. The bimetallic complex **W2F3** is even capable of metathesizing terminal alkynes at room temperature and performs in the same manner as the alkylidyne complex **W^{Ph}F3**. Additional conversion versus time diagrams are displayed in Figures S9 and S10 in Supporting Information File 1. Finally, the ditungsten catalyst

Table 2: Alkyne metathesis of different substrates.^a

Entry	Substrate	Product	Cat.	R	Yield [%]
1			W2F3 W^{Ph}F3		96 95
2			W2F3 W^{Ph}F3		95 96
3			W2F3 W^{Ph}F3		94 97
4			W2F3 W^{Ph}F3		98 97
5			W2F3 W^{Ph}F3	R = Me R = H	96 88 94 88
6			W2F3 W^{Ph}F3	R = Me R = H	93 79 94 72
7			W2F3 W^{Ph}F3		86 84
8			W2F3 W^{Ph}F3		93 96

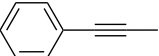
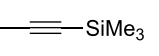
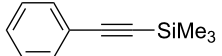
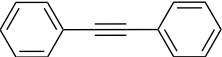
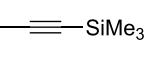
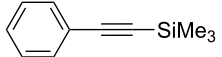
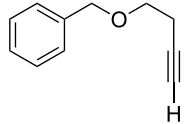
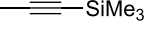
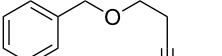
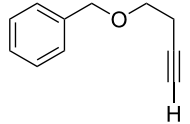
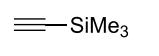
^aSelf-metathesis: substrate (0.5 mmol), catalyst (0.5 mol % **W2F3**; 1 mol % **W^{Ph}F3**), toluene (internal alkynes: 2.5 mL, 200 mM; terminal alkynes: 24 mL, 21 mM), MS 5 Å (500 mg), 25 °C, 2 h. RCAM: substrate (0.5 mmol), catalyst (1 mol % **W2F3**; 2 mol % **W^{Ph}F3**), toluene (24 mL, 21 mM), MS 5 Å (1.0 g), 25 °C, 2 h.

W2F3 was also employed in alkyne cross-metathesis (ACM), a reaction which is of large interest for the application of alkyne metathesis, but often leads to product mixtures. Therefore, (trimethylsilyl)propyne and (trimethylsilyl)acetylene were chosen as reaction partners in ACM, since this reaction proved to be quite efficient in the past [25,54,100]. A toluene solution of both substrates (1:2 ratio, TMS–alkyne in excess) was charged with the catalyst **W2F3** (0.5–1 mol %) in the presence of molecular sieves 5 Å and stirred for two hours at room temperature. The isolated yields of the ACM are summarized in Table 3. The depicted reactions selectively afforded the unsymmetrical alkynes, corroborating that the bimetallic tungsten complex **W2F3** is able to introduce a trimethylsilyl protecting group to alkynes.

Conclusion

Previously, we have reported the optimum level of fluorination in **MoF6** and **WF3** as the most catalytically active alkylidene complexes [54]. Thus, we intended to study the catalytic activity of the well-known bimetallic molybdenum and tungsten complexes bearing the same fluoroalkoxide ligands. Indeed, **W2F3** as the bimetallic analogue to mononuclear **WF3** is highly active in the metathesis of internal and even terminal alkynes and also promotes alkyne cross-metathesis efficiently. The **Mo2F6** complex, however, does not exhibit satisfactory alkyne metathesis activity, which we attribute to its low solubility. Furthermore, the corresponding mononuclear benzylidene complex **W^{Ph}F3** is easily accessible from the dinuclear **W2F3** complex and performs equally well compared to the latter.

Table 3: Alkyne cross metathesis (ACM) with catalyst **W2F3**.^a

Entry	Substrates	Product	Cat.	Yield [%]	
1				0.5 mol %	87
2				1 mol %	82
3				0.5 mol %	93
4				0.5 mol %	92

^aSubstrate (0.5 mmol), TMS-propyne or TMS-acetylene (1 mmol), toluene (internal alkynes: 2.5 mL, terminal alkynes: 24 mL), MS 5 Å (500 mg), 25 °C, 2 h.

The finding that **W2F3** is a highly active alkyne metathesis pre-catalyst and does not have to be converted into an alkylidyne species prior to catalysis could be beneficial for future applications of alkyne metathesis since this protocol represents a convenient approach to alkyne metathesis catalysts in two steps starting from WCl_4 .

Supporting Information

CCDC 1850924–1850926 contain the supplementary crystallographic data for this paper. These data can be obtained free of charge via http://www.ccdc.cam.ac.uk/data_request/cif.

Supporting Information File 1

Experimental section, NMR spectra, catalysis procedure and product characterization, crystallographic details for **W2F3**·(NHMe₂), **W2F3** and **W^{Ph}F3**.

[<https://www.beilstein-journals.org/bjoc/content/supplementary/1860-5397-14-220-S1.pdf>]

Acknowledgements

H.E. wishes to thank the Fonds der Chemischen Industrie (FCI) for a Chemiefonds Fellowship. This work was funded by the Deutsche Forschungsgemeinschaft (DFG) through project TA 189/12-1 (“Mechanistic studies on the catalytic metathesis of internal and terminal alkynes and diynes”). The authors wish to thank Dr. M. Freytag for the crystal structure determination of **W2F3**·(NHMe₂).

ORCID® IDs

Dirk Bockfeld - <https://orcid.org/0000-0003-1084-8577>

Matthias Tamm - <https://orcid.org/0000-0002-5364-0357>

References

- Fürstner, A. *Angew. Chem., Int. Ed.* **2000**, *39*, 3012–3043. doi:10.1002/1521-3773(20000901)39:17<3012::aid-anie3012>3.3.co;2-7
- Connon, S. J.; Blechert, S. *Angew. Chem., Int. Ed.* **2003**, *42*, 1900–1923. doi:10.1002/anie.200200556
- Grela, K. *Olefin Metathesis*; John Wiley & Sons: Hoboken, NJ, U.S.A., 2014. doi:10.1002/9781118711613
- Hoveyda, A. H.; Zhugralin, A. R. *Nature* **2007**, *450*, 243–251. doi:10.1038/nature06351
- Grubbs, R. H.; Wenzel, A. G.; O’Leary, D. J.; Khosravi, E., Eds. *Handbook of Metathesis*; Wiley-VCH Verlag GmbH: Weinheim, Germany, 2015. doi:10.1002/9783527674107
- Fürstner, A.; Davies, P. W. *Chem. Commun.* **2005**, 2307–2320. doi:10.1039/b419143a
- Mortreux, A.; Coutelier, O. *J. Mol. Catal. A: Chem.* **2006**, *254*, 96–104. doi:10.1016/j.molcata.2006.03.054
- Zhang, W.; Moore, J. S. *Adv. Synth. Catal.* **2007**, *349*, 93–120. doi:10.1002/adsc.200600476
- Wu, X.; Tamm, M. *Beilstein J. Org. Chem.* **2011**, *7*, 82–93. doi:10.3762/bjoc.7.12
- Fürstner, A. *Angew. Chem., Int. Ed.* **2013**, *52*, 2794–2819. doi:10.1002/anie.201204513
- Yang, H.; Jin, Y.; Du, Y.; Zhang, W. *J. Mater. Chem. A* **2014**, *2*, 5986–5993. doi:10.1039/c3ta14227b
- Katz, T. J.; McGinnis, J. *J. Am. Chem. Soc.* **1975**, *97*, 1592–1594. doi:10.1021/ja00839a063
- Schrock, R. R.; Hoveyda, A. H. *Angew. Chem., Int. Ed.* **2003**, *42*, 4592–4633. doi:10.1002/anie.200300576
- Schrock, R. R.; Czekelius, C. *Adv. Synth. Catal.* **2007**, *349*, 55–77. doi:10.1002/adsc.200600459
- Cortez, G. A.; Schrock, R. R.; Hoveyda, A. H. *Angew. Chem., Int. Ed.* **2007**, *46*, 4534–4538. doi:10.1002/anie.200605130
- Beer, S.; Hrib, C. G.; Jones, P. G.; Brandhorst, K.; Grunenberg, J.; Tamm, M. *Angew. Chem., Int. Ed.* **2007**, *46*, 8890–8894. doi:10.1002/anie.200703184
- Beer, S.; Brandhorst, K.; Hrib, C. G.; Wu, X.; Haberlag, B.; Grunenberg, J.; Jones, P. G.; Tamm, M. *Organometallics* **2009**, *28*, 1534–1545. doi:10.1021/om801119t

18. Haberlag, B.; Wu, X.; Brandhorst, K.; Grunenberg, J.; Daniiliuc, C. G.; Jones, P. G.; Tamm, M. *Chem. – Eur. J.* **2010**, *16*, 8868–8877. doi:10.1002/chem.201000597
19. Lysenko, S.; Haberlag, B.; Daniiliuc, C. G.; Jones, P. G.; Tamm, M. *ChemCatChem* **2011**, *3*, 115–118. doi:10.1002/cctc.201000355
20. Lysenko, S.; Daniiliuc, C. G.; Jones, P. G.; Tamm, M. *J. Organomet. Chem.* **2013**, *744*, 7–14. doi:10.1016/j.jorgancchem.2013.03.035
21. Clark, D. N.; Schrock, R. R. *J. Am. Chem. Soc.* **1978**, *100*, 6774–6776. doi:10.1021/ja00489a049
22. Schrock, R. R.; Clark, D. N.; Sancho, J.; Wengrovius, J. H.; Rocklage, S. M.; Pedersen, S. F. *Organometallics* **1982**, *1*, 1645–1651. doi:10.1021/om00072a018
23. Heppekausen, J.; Stade, R.; Goddard, R.; Fürstner, A. *J. Am. Chem. Soc.* **2010**, *132*, 11045–11057. doi:10.1021/ja104800w
24. Heppekausen, J.; Stade, R.; Kondoh, A.; Seidel, G.; Goddard, R.; Fürstner, A. *Chem. – Eur. J.* **2012**, *18*, 10281–10299. doi:10.1002/chem.201200621
25. Persich, P.; Llaveria, J.; Lhermet, R.; de Haro, T.; Stade, R.; Kondoh, A.; Fürstner, A. *Chem. – Eur. J.* **2013**, *19*, 13047–13058. doi:10.1002/chem.201302320
26. Willwacher, J.; Heggen, B.; Wirtz, C.; Thiel, W.; Fürstner, A. *Chem. – Eur. J.* **2015**, *21*, 10416–10430. doi:10.1002/chem.201501491
27. Schaubach, S.; Gebauer, K.; Ungeheuer, F.; Hoffmeister, L.; Ilg, M. K.; Wirtz, C.; Fürstner, A. *Chem. – Eur. J.* **2016**, *22*, 8494–8507. doi:10.1002/chem.201601163
28. Lysenko, S.; Volbeda, J.; Jones, P. G.; Tamm, M. *Angew. Chem., Int. Ed.* **2012**, *51*, 6757–6761. doi:10.1002/anie.201202101
29. Li, S. T.; Schnabel, T.; Lysenko, S.; Brandhorst, K.; Tamm, M. *Chem. Commun.* **2013**, *49*, 7189–7191. doi:10.1039/c3cc43108h
30. Tamm, M.; Schnabel, T.; Melcher, D.; Brandhorst, K.; Bockfeld, D. *Chem. – Eur. J.* **2018**, *24*, 9022–9032. doi:10.1002/chem.201801651
31. Jyothish, K.; Zhang, W. *Angew. Chem., Int. Ed.* **2011**, *50*, 3435–3438. doi:10.1002/anie.201007559
32. Jyothish, K.; Wang, Q.; Zhang, W. *Adv. Synth. Catal.* **2012**, *354*, 2073–2078. doi:10.1002/adsc.201200243
33. Yang, H.; Liu, Z.; Zhang, W. *Adv. Synth. Catal.* **2013**, *355*, 885–890. doi:10.1002/adsc.201201105
34. Du, Y.; Yang, H.; Zhu, C.; Ortiz, M.; Okochi, K. D.; Shoemaker, R.; Jin, Y.; Zhang, W. *Chem. – Eur. J.* **2016**, *22*, 7959–7963. doi:10.1002/chem.201505174
35. Hu, K.; Yang, H.; Zhang, W.; Qin, Y. *Chem. Sci.* **2013**, *4*, 3649–3653. doi:10.1039/c3sc51264a
36. Yang, H.; Zhu, Y.; Du, Y.; Tan, D.; Jin, Y.; Zhang, W. *Mater. Chem. Front.* **2017**, *1*, 1369–1372. doi:10.1039/c6qm00359a
37. Zhang, C.; Wang, Q.; Long, H.; Zhang, W. *J. Am. Chem. Soc.* **2011**, *133*, 20995–21001. doi:10.1021/ja210418t
38. Wang, Q.; Zhang, C.; Noll, B. C.; Long, H.; Jin, Y.; Zhang, W. *Angew. Chem., Int. Ed.* **2014**, *53*, 10663–10667. doi:10.1002/anie.201404880
39. Wang, Q.; Yu, C.; Long, H.; Du, Y.; Jin, Y.; Zhang, W. *Angew. Chem., Int. Ed.* **2015**, *54*, 7550–7554. doi:10.1002/anie.201501679
40. Yu, C.; Long, H.; Jin, Y.; Zhang, W. *Org. Lett.* **2016**, *18*, 2946–2949. doi:10.1021/acs.orglett.6b01293
41. Wang, Q.; Yu, C.; Zhang, C.; Long, H.; Azarnoush, S.; Jin, Y.; Zhang, W. *Chem. Sci.* **2016**, *7*, 3370–3376. doi:10.1039/c5sc04977f
42. Ortiz, M.; Cho, S.; Niklas, J.; Kim, S.; Poluektov, O. G.; Zhang, W.; Rumbles, G.; Park, J. *J. Am. Chem. Soc.* **2017**, *139*, 4286–4289. doi:10.1021/jacs.7b00220
43. Ortiz, M.; Yu, C.; Jin, Y.; Zhang, W. *Top. Curr. Chem.* **2017**, *375*, 69. doi:10.1007/s41061-017-0156-1
44. Paley, D. W.; Sedbrook, D. F.; Decatur, J.; Fischer, F. R.; Steigerwald, M. L.; Nuckolls, C. *Angew. Chem., Int. Ed.* **2013**, *52*, 4591–4594. doi:10.1002/anie.201300758
45. Bellone, D. E.; Bours, J.; Menke, E. H.; Fischer, F. R. *J. Am. Chem. Soc.* **2015**, *137*, 850–856. doi:10.1021/ja510919v
46. von Kugelgen, S.; Bellone, D. E.; Cloke, R. R.; Perkins, W. S.; Fischer, F. R. *J. Am. Chem. Soc.* **2016**, *138*, 6234–6239. doi:10.1021/jacs.6b02422
47. von Kugelgen, S.; Sifri, R.; Bellone, D.; Fischer, F. R. *J. Am. Chem. Soc.* **2017**, *139*, 7577–7585. doi:10.1021/jacs.7b02225
48. Jeong, H.; von Kugelgen, S.; Bellone, D.; Fischer, F. R. *J. Am. Chem. Soc.* **2017**, *139*, 15509–15514. doi:10.1021/jacs.7b09390
49. Haberlag, B.; Freytag, M.; Daniiliuc, C. G.; Jones, P. G.; Tamm, M. *Angew. Chem., Int. Ed.* **2012**, *51*, 13019–13022. doi:10.1002/anie.201207772
50. Haberlag, B.; Freytag, M.; Jones, P. G.; Tamm, M. *Adv. Synth. Catal.* **2014**, *356*, 1255–1265. doi:10.1002/adsc.201400051
51. Hötlung, S.; Bittner, C.; Tamm, M.; Dähn, S.; Collatz, J.; Steidle, J. L. M.; Schulz, S. *Org. Lett.* **2015**, *17*, 5004–5007. doi:10.1021/acs.orglett.5b02461
52. Estes, D. P.; Bittner, C.; Árias, Ó.; Casey, M.; Fedorov, A.; Tamm, M.; Copéret, C. *Angew. Chem., Int. Ed.* **2016**, *55*, 13960–13964. doi:10.1002/anie.201605129
53. Estes, D. P.; Gordon, C. P.; Fedorov, A.; Liao, W.-C.; Ehrhorn, H.; Bittner, C.; Zier, M. L.; Bockfeld, D.; Chan, K. W.; Eisenstein, O.; Raynaud, C.; Tamm, M.; Copéret, C. *J. Am. Chem. Soc.* **2017**, *139*, 17597–17607. doi:10.1021/jacs.7b09934
54. Bittner, C.; Ehrhorn, H.; Bockfeld, D.; Brandhorst, K.; Tamm, M. *Organometallics* **2017**, *36*, 3398–3406. doi:10.1021/acs.organomet.7b00519
55. Freudenberg, J. H.; Schrock, R. R.; Churchill, M. R.; Rheingold, A. L.; Ziller, J. W. *Organometallics* **1984**, *3*, 1563–1573. doi:10.1021/om00088a019
56. Buhro, W. E.; Chisholm, M. H. *Adv. Organomet. Chem.* **1987**, *27*, 311–369. doi:10.1016/s0065-3055(08)60030-1
57. Schrock, R. R. *Chem. Rev.* **2002**, *102*, 145–180. doi:10.1021/cr0103726
58. Wengrovius, J. H.; Sancho, J.; Schrock, R. R. *J. Am. Chem. Soc.* **1981**, *103*, 3932–3934. doi:10.1021/ja00403a058
59. Schrock, R. R. *J. Organomet. Chem.* **1986**, *300*, 249–262. doi:10.1016/0022-328x(86)84064-5
60. Bray, A.; Mortreux, A.; Petit, F.; Petit, M.; Szymanska-Buzar, T. *J. Chem. Soc., Chem. Commun.* **1993**, 197–199. doi:10.1039/c39930000197
61. Coutelier, O.; Mortreux, A. *Adv. Synth. Catal.* **2006**, *348*, 2038–2042. doi:10.1002/adsc.200606116
62. Listemann, M. L.; Schrock, R. R. *Organometallics* **1985**, *4*, 74–83. doi:10.1021/om00120a014
63. Fürstner, A.; Seidel, G. *Angew. Chem., Int. Ed.* **1998**, *37*, 1734–1736. doi:10.1002/(sici)1521-3773(19980703)37:12<1734::aid-anie1734>3.0.co;2-6
64. Nicolaou, K. C.; Bulger, P. G.; Sarlah, D. *Angew. Chem., Int. Ed.* **2005**, *44*, 4490–4527. doi:10.1002/anie.200500369

65. McCullough, L. G.; Listemann, M. L.; Schrock, R. R.; Churchill, M. R.; Ziller, J. W. *J. Am. Chem. Soc.* **1983**, *105*, 6729–6730. doi:10.1021/ja00360a040

66. Freudenberger, J. H.; Schrock, R. R. *Organometallics* **1986**, *5*, 1411–1417. doi:10.1021/om00138a019

67. Mortreux, A.; Petit, F.; Petit, M.; Szymanska-Buzar, T. *J. Mol. Catal. A: Chem.* **1995**, *96*, 95–105. doi:10.1016/1381-1169(94)00004-2

68. Coutelier, O.; Nowogrocki, G.; Paul, J.-F.; Mortreux, A. *Adv. Synth. Catal.* **2007**, *349*, 2259–2263. doi:10.1002/adsc.200700104

69. Chisholm, M. H.; Cotton, F. A. *Acc. Chem. Res.* **1978**, *11*, 356–362. doi:10.1021/ar50129a006

70. Chisholm, M. H.; Cotton, F. A.; Frenz, B. A.; Reichert, W. W.; Shive, L. W.; Stults, B. R. *J. Am. Chem. Soc.* **1976**, *98*, 4469–4476. doi:10.1021/ja00431a024

71. Chisholm, M. H.; Cotton, F. A.; Extine, M.; Stults, B. R. *J. Am. Chem. Soc.* **1976**, *98*, 4477–4485. doi:10.1021/ja00431a025

72. Coffindaffer, T. W.; Rothwell, I. P.; Huffmann, J. C. *Inorg. Chem.* **1985**, *24*, 1643–1646. doi:10.1021/ic00205a010

73. Gilbert, T. M.; Landes, A. M.; Rogers, R. D. *Inorg. Chem.* **1992**, *31*, 3438–3444. doi:10.1021/ic00042a020

74. Su, K.; Tilley, T. D. *Chem. Mater.* **1997**, *9*, 588–595. doi:10.1021/cm960413s

75. Chisholm, M. H.; Folting, K.; Wu, D.-D. *Chem. Commun.* **1998**, 379–380. doi:10.1039/a708268a

76. Radius, U.; Attner, J. *Eur. J. Inorg. Chem.* **1998**, 299–303. doi:10.1002/(sici)1099-0682(199803)1998:3<299::aid-ejic299>3.0.co;2-q

77. Budzichowski, T. A.; Chisholm, M. H.; Tiedtke, D. B.; Gruhn, N. E.; Lichtenberger, D. L. *Polyhedron* **1998**, *17*, 705–711. doi:10.1016/s0277-5387(97)00360-4

78. Gilbert, T. M.; Bauer, C. B.; Bond, A. H.; Rogers, R. D. *Polyhedron* **1999**, *18*, 1293–1301. doi:10.1016/s0277-5387(98)00433-1

79. Chetcuti, M. J.; Chisholm, M. H.; Huffman, J. C.; Leonelli, J. *J. Am. Chem. Soc.* **1983**, *105*, 292–293. doi:10.1021/ja00340a025

80. Chisholm, M. H.; Huffman, J. C.; Ratermann, A. L. *Inorg. Chem.* **1983**, *22*, 4100–4105. doi:10.1021/ic00168a055

81. Chisholm, M. H.; Conroy, B. K.; Eichhorn, B. W.; Folting, K.; Hoffman, D. M.; Huffman, J. C.; Marchant, N. S. *Polyhedron* **1987**, *6*, 783–792. doi:10.1016/s0277-5387(00)86884-9

82. Chisholm, M. H.; Eichhorn, B. W.; Folting, K.; Huffman, J. C.; Ontiveros, C. D.; Streib, W. E.; van der Sluys, W. G. *Inorg. Chem.* **1987**, *26*, 3182–3186. doi:10.1021/ic00266a024

83. Chisholm, M. H.; Cook, C. M.; Huffman, J. C.; Streib, W. E. *J. Chem. Soc., Dalton Trans.* **1991**, 929–937. doi:10.1039/dt9910000929

84. Chisholm, M. H.; Huang, J.-H.; Huffman, J. C.; Parkin, I. P. *Inorg. Chem.* **1997**, *36*, 1642–1651. doi:10.1021/ic961429n

85. Budzichowski, T. A.; Chisholm, M. H.; Folting, K.; Huffman, J. C.; Streib, W. E.; Tiedtke, D. B. *Polyhedron* **1998**, *17*, 857–867. doi:10.1016/s0277-5387(97)00290-8

86. Girolami, G. S.; Sattelberger, A. P., Eds. *Inorganic Syntheses: Volume 36*; Inorganic Syntheses; John Wiley & Sons, Inc.: Hoboken, NJ, U.S.A., 2014. doi:10.1002/9781118744994

87. Strutz, H.; Schrock, R. R. *Organometallics* **1984**, *3*, 1600–1601. doi:10.1021/om00088a030

88. Fackler, J. P., Ed. *Inorganic syntheses*; Wiley: New York, NY, U.S.A., 1982; Vol. 21. doi:10.1002/9780470132524

89. Budzichowski, T. A.; Chisholm, M. H.; Tiedtke, D. B.; Huffman, J. C.; Streib, W. E. *Organometallics* **1995**, *14*, 2318–2324. doi:10.1021/om00005a033

90. Akiyama, M.; Chisholm, M. H.; Cotton, F. A.; Extine, M. W.; Haitko, D. A.; Little, D.; Fanwick, P. E. *Inorg. Chem.* **1979**, *18*, 2266–2270. doi:10.1021/ic50198a043

91. Chisholm, M. H.; Cotton, F. A.; Extine, M.; Millar, M.; Stults, B. R. *J. Am. Chem. Soc.* **1976**, *98*, 4486–4491. doi:10.1021/ja00431a026

92. Addison, A. W.; Rao, T. N.; Reedijk, J.; van Rijn, J.; Verschoor, G. C. *J. Chem. Soc., Dalton Trans.* **1984**, 1349–1356. doi:10.1039/dt9840001349

93. Yang, L.; Powell, D. R.; Houser, R. P. *Dalton Trans.* **2007**, 955–964. doi:10.1039/b617136b

94. Chisholm, M. H.; Parkin, I. P.; Huffman, J. C.; Lobkovsky, E. M.; Folting, K. *Polyhedron* **1991**, *10*, 2839–2846. doi:10.1016/s0277-5387(00)86188-4

95. Coffindaffer, T. W.; Niccolai, G. P.; Powell, D.; Rothwell, I. P. *J. Am. Chem. Soc.* **1985**, *107*, 3572–3583. doi:10.1021/ja00298a029

96. Chisholm, M. H.; Folting, K.; Hampden-Smith, M.; Smith, C. A. *Polyhedron* **1987**, *6*, 1747–1755. doi:10.1016/s0277-5387(00)86546-8

97. Cayton, R. H.; Chisholm, M. H. *Inorg. Chem.* **1991**, *30*, 1422–1425. doi:10.1021/c00006a051

98. Chisholm, M. H.; Gallucci, J. C.; Hollandsworth, C. B. *Polyhedron* **2006**, *25*, 827–833. doi:10.1016/j.poly.2005.07.010

99. Schrock, R. R.; Listemann, M. L.; Sturges, L. G. *J. Am. Chem. Soc.* **1982**, *104*, 4291–4293. doi:10.1021/ja00379a061

100. Lhermet, R.; Fürstner, A. *Chem. – Eur. J.* **2014**, *20*, 13188–13193. doi:10.1002/chem.201404166

License and Terms

This is an Open Access article under the terms of the Creative Commons Attribution License (<http://creativecommons.org/licenses/by/4.0>). Please note that the reuse, redistribution and reproduction in particular requires that the authors and source are credited.

The license is subject to the *Beilstein Journal of Organic Chemistry* terms and conditions: (<https://www.beilstein-journals.org/bjoc>)

The definitive version of this article is the electronic one which can be found at:

[doi:10.3762/bjoc.14.220](https://doi.org/10.3762/bjoc.14.220)



Synergistic approach to polycycles through Suzuki–Miyaura cross coupling and metathesis as key steps

Sambasivarao Kotha*, Milind Meshram and Chandravathi Chakkapalli

Review

Open Access

Address:

Department of Chemistry, Indian Institute of Technology Bombay, Powai, Mumbai-400 076, India, Fax: +91(22)-2576 7152

Beilstein J. Org. Chem. **2018**, *14*, 2468–2481.

doi:10.3762/bjoc.14.223

Email:

Sambasivarao Kotha* - srk@chem.iitb.ac.in

Received: 29 May 2018

Accepted: 28 August 2018

Published: 21 September 2018

* Corresponding author

This article is part of the thematic issue "Progress in metathesis chemistry III".

Keywords:

Claisen rearrangement; Diels–Alder reaction; metathesis; polycycles; Suzuki–Miyaura cross coupling

Guest Editor: K. Grela

© 2018 Kotha et al.; licensee Beilstein-Institut.

License and terms: see end of document.

Abstract

This account provides an overview of recent work, including our own contribution dealing with Suzuki–Miyaura cross coupling in combination with metathesis (or vice-versa). Several cyclophanes, polycycles, macrocycles, spirocycles, stilbenes, biaryls, and heterocycles have been synthesized by employing a combination of Suzuki cross-coupling and metathesis. Various popular reactions such as Diels–Alder reaction, Claisen rearrangement, cross-metathesis, and cross-alkyne metathesis are used. The synergistic combination of these powerful reactions is found to be useful for the construction of complex targets and fulfill synthetic brevity.

Introduction

Transition-metal catalysts are used in metathesis and cross-coupling reactions. Such advances have opened the door for efficient construction of C–C bonds in organic synthesis. These catalysts tolerate diverse functional groups and the reaction occurs under mild reaction conditions. Among different metathetic processes, ring-closing metathesis (RCM) [1–6] is of a greater interest than cross-metathesis (CM). It is a widely used protocol for the synthesis of unsaturated cyclic systems [7]. Palladium-catalyzed Suzuki–Miyaura (SM) cross-coupling reaction is also considered as one of the most versatile methods for C–C bond formation [8–12]. Application of a wide range of

organometallic reagents (e.g., organoboron reagents) are possible due to their commercial availability. Owing to the mild reaction conditions and ease of handling of organoboron reagents [13–17] have propelled the growth of the SM cross coupling. A synergistic combination of these two elegant methods (i.e., SM coupling and metathesis) [18] was found to increase the synthetic efficiency of complex targets (e.g., macrocycles [19–22], oligomers [23,24], polycyclic ethers [25], heterocycles [26], nonbenzenoid aromatics [27], and spirocycles [28,29]) by decreasing the number of steps. Different metathesis catalysts used in this study are shown in Figure 1.

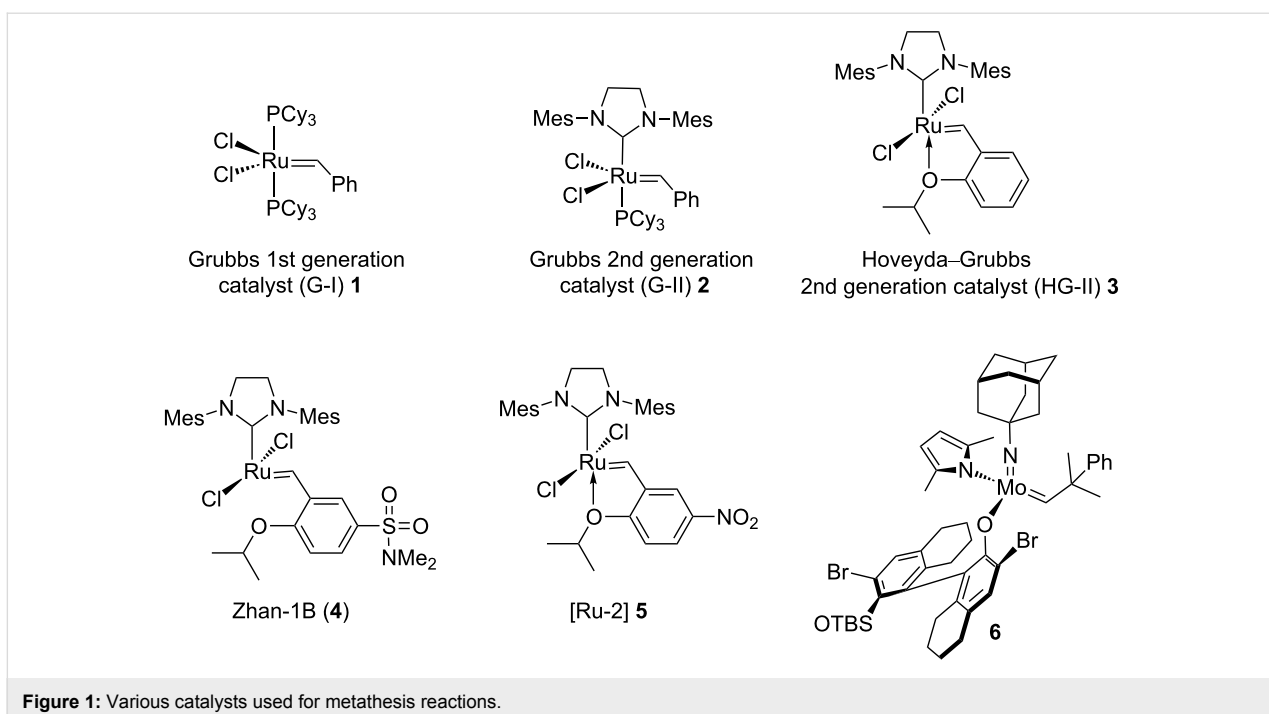


Figure 1: Various catalysts used for metathesis reactions.

Review

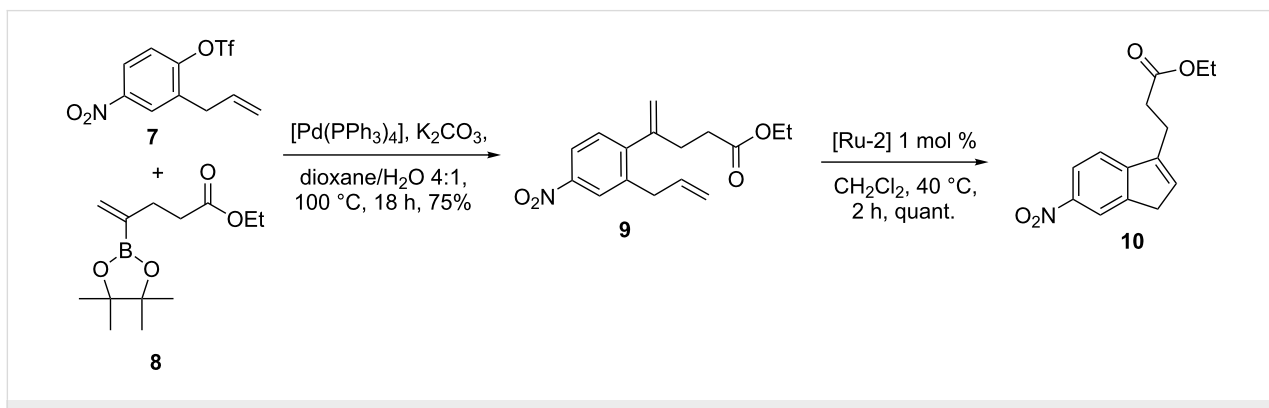
Annulation

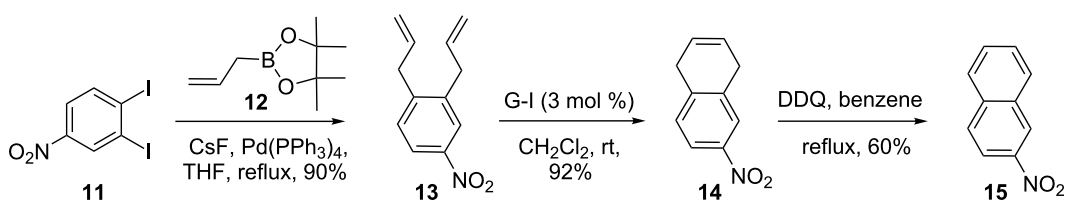
Grela and co-workers [30] demonstrated a useful protocol to build indene derivatives by employing SM coupling and RCM in sequence. To this end, the SM coupling of triflate **7** was accomplished by using pinacol boronic ester **8** in the presence of a palladium catalyst to give the cross-coupling product **9** (75%). Later on, exposure of the diolefinic precursor **9** to [Ru-2] catalyst **5** gave the ring-closure product **10** in quantitative yield (Scheme 1).

A sequential usage of SM cross coupling and RCM was responsible to construct various naphthalene derivatives such as **15** [31]. The SM coupling product 3,4-diallylbenzene derivative **13** (90%) was obtained from diiodobenzene **11** using allylboronate

ester **12** via a SM-type allylation sequence [32]. Next, compound **13** was exposed to Grubbs 1st generation (G-I) catalyst **1** to effect the ring-closure to produce tetrahydronaphthalene derivative **14** (92%). Subsequently, aromatization of compound **14** was accomplished with 2,3-dichloro-5,6-dicyano-1,4-benzoquinone (DDQ) to generate nitronaphthalene **15** (60%, Scheme 2).

Due to their useful biological activity and intricate structural features of angucyclines such as **16–19** (Figure 2), several approaches have been reported for their assembly. In this context, de Koning and co-workers [33] demonstrated an efficient route for the construction of the benz[a]anthracene structural unit by employing SM cross coupling followed by RCM sequence. Treatment of the bromonaphthalene derivative **20** with

Scheme 1: SM coupling and RCM protocol to substituted indene derivative **10**.



Scheme 2: Synthesis of polycycles via SM and RCM approach.

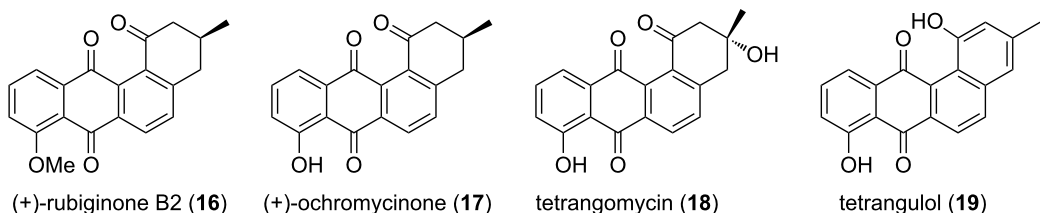


Figure 2: Various angucyclines.

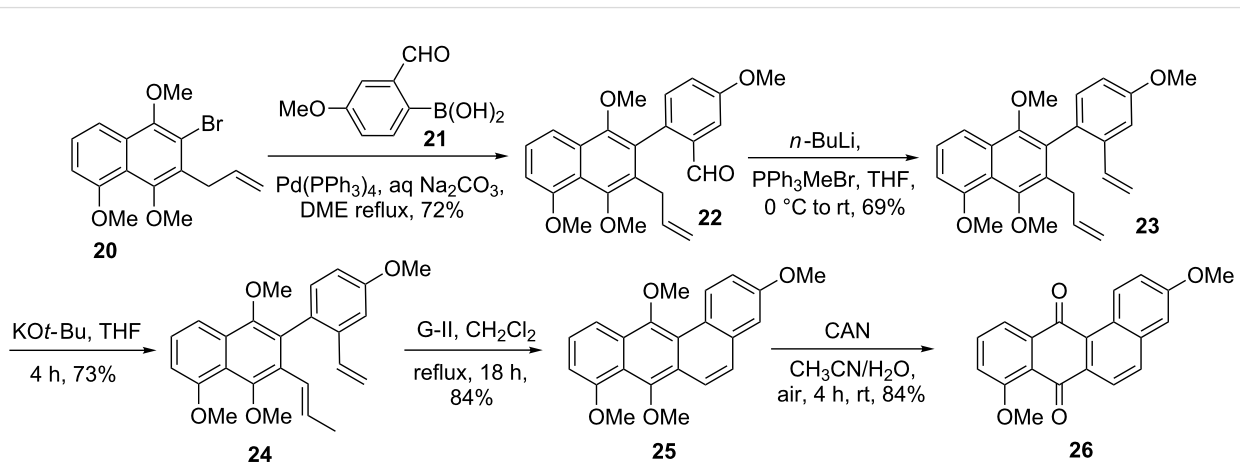
(2-formyl-4-methoxyphenyl)boronic acid (**21**) in the presence of a palladium catalyst generated the cross-coupling product **22** (72%). Next, aldehyde **22** was subjected to Wittig olefination to provide the corresponding alkene **23** (69%), which on subsequent treatment with $KOt\text{-}Bu$ in THF gave the isomerized product **24** (73%). Later, RCM of isomerized olefin **24** with the help of G-II catalyst offered the ring-closure product **25** (84%). Finally, CAN oxidation gave the desired tetracyclic compound **26** in 84% yield (Scheme 3).

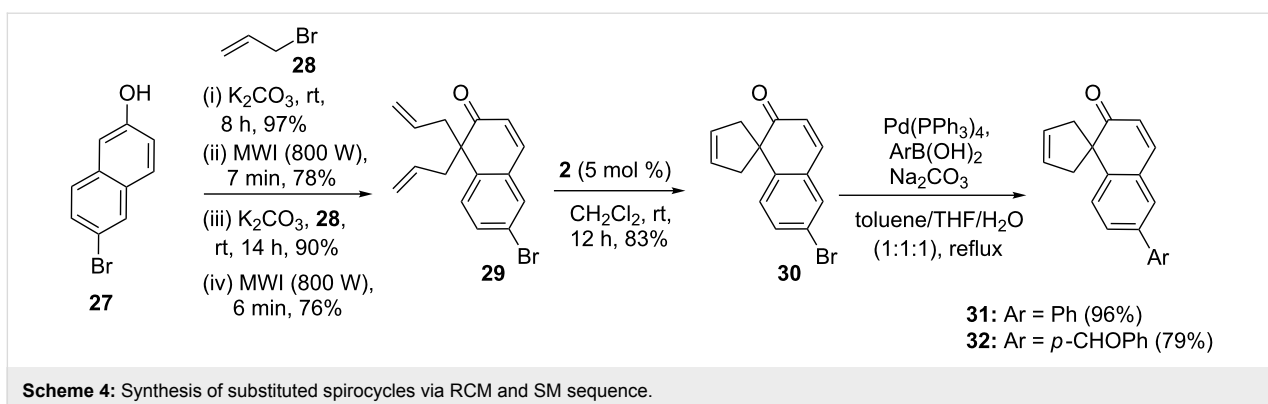
Spirocycles

In another event, an efficient approach to spirocyclopentane derivatives has been described, where the combination of RCM and SM coupling was employed [34]. In this respect, the key

building block **29** was derived by employing a sequential *O*-allylation and CR, then again *O*-allylation, and CR [35] starting with a commercially available 6-bromo-2-naphthol (**27**). Subsequently, the diallyl derivative **29** was exposed to G-II catalyst **2** to deliver a ring-closure product **30** (83%). Finally, the spiro compound **30** was subjected to the SM coupling using two different boronic acids to produce the aryl substituted spiro compounds such as **31** (96%) and **32** (79%) (Scheme 4).

Along similar lines, we have also demonstrated the synthesis of bis-spirocycles such as **37** by adopting a double RCM sequence followed by SM coupling [36]. The key precursor **34** was assembled from a commercially available tetralone **33** via

Scheme 3: SM coupling and RCM protocol to the benz[a]anthracene skeleton **26**.

**Scheme 4:** Synthesis of substituted spirocycles via RCM and SM sequence.

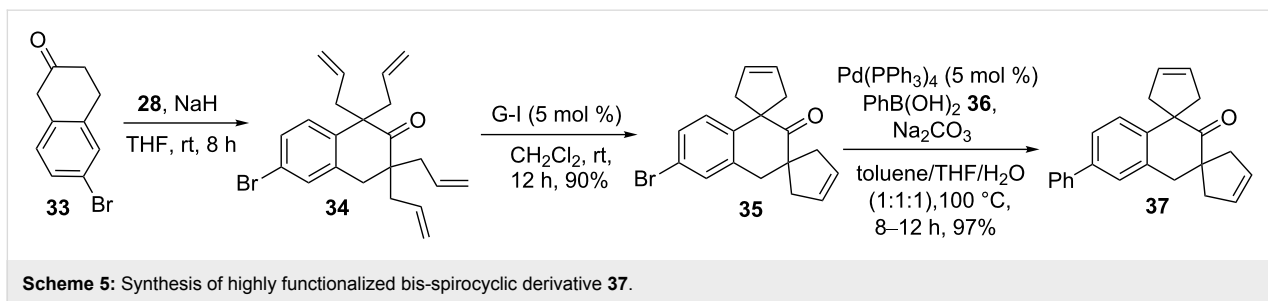
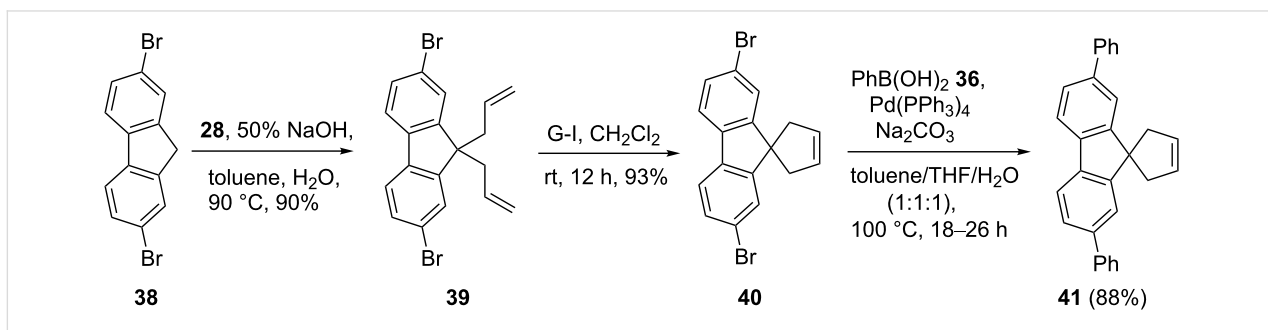
tetraallylation sequence. Then, tetraallyl derivative **34** was subjected to RCM with the aid of the G-I catalyst **1** to furnish the bis-spirocyclic compound **35** (90%). Next, the cyclized product **35** was subjected to SM coupling using phenylboronic acid (**36**) to afford the cross-coupling product **37** (97%, Scheme 5).

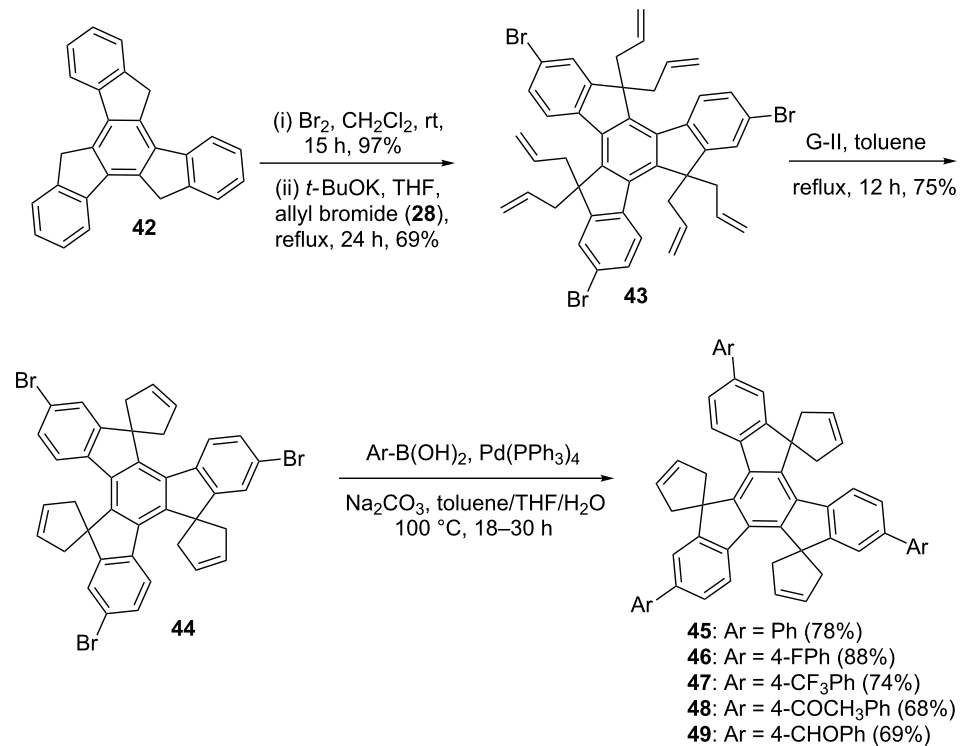
In another instance, a simple synthetic approach to spiro-fluorene derivative **41** was described involving a serial usage of RCM and SM coupling [37]. To this end, bromofluorene **38** was reacted with allyl bromide (**28**) in the presence of 50% NaOH to deliver the expected 9,9'-diallylfluorene derivative **39** (90%). Next, diallyl compound **39** was subjected to RCM with the aid of the G-I catalyst **1** to furnish a ring-closure product, spirofluorene derivative **40** (93%). Later, the dibromide **40** was subjected to SM coupling in the presence of phenylboronic acid (**36**) to generate the new spirofluorene **41** (88%, Scheme 6).

Interestingly, highly substituted truxene derivatives **45–49** were also synthesized by applying the RCM and SM coupling protocol (Scheme 7).

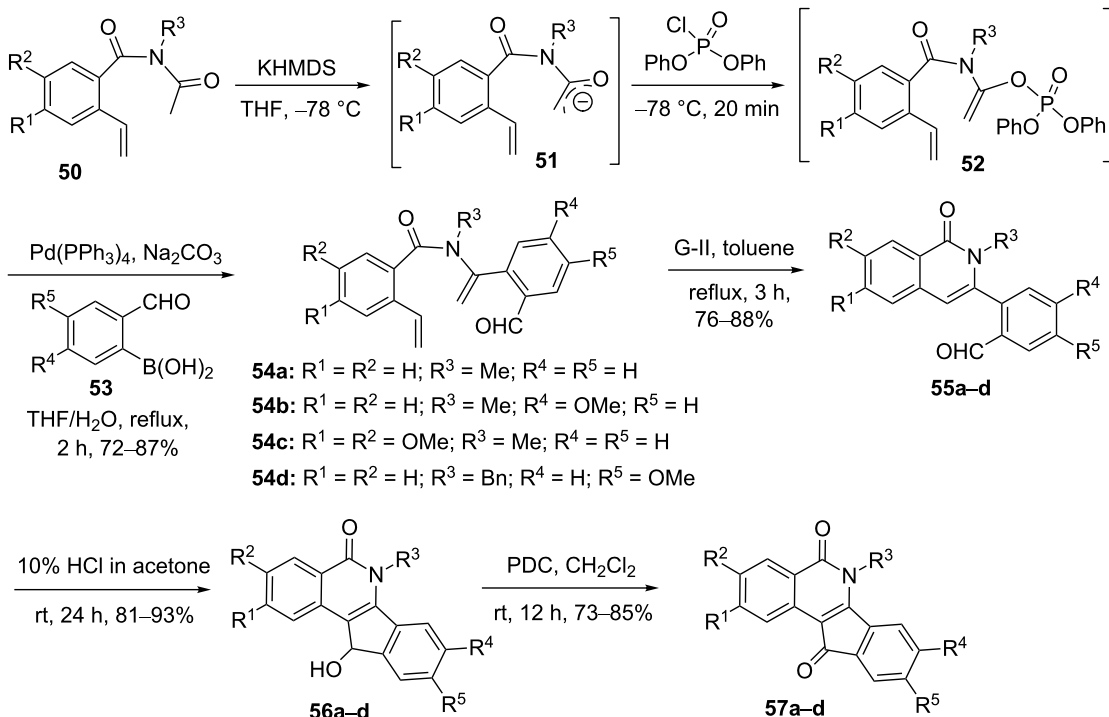
Heterocycles

Couture and co-workers [38] demonstrated an elegant approach to highly substituted isoquinolones (e.g., **57a–d**, Scheme 8) by employing a SM coupling followed by RCM. To this end, they started with *o*-vinylbenzoic acid and it was transformed to the benzamide derivatives **50** by employing a four-step synthetic sequence. Later, compound **50** was treated with KHMDS in THF at -78°C to produce enolate **51**. Further, it was reacted with diphenyl chlorophosphate to generate vinyl phosphate **52**, which was subjected to SM coupling in the presence of different 2-formylboronic acids **53** with the aid of the $\text{Pd}(\text{PPh}_3)_4$ catalyst to provide the respective coupling products **54a–d**

**Scheme 5:** Synthesis of highly functionalized bis-spirocyclic derivative **37**.**Scheme 6:** Synthesis of spirofluorene derivatives via RCM and SM coupling sequence.



Scheme 7: Synthesis of truxene derivatives via RCM and SM coupling.



Scheme 8: Synthesis of substituted isoquinoline derivative via SM and RCM protocol.

(72–87%). Next, exposure of the diolefins **54a–d** to G-II catalyst **2** delivered ring-closure products, iso-quinolones **55a–d** (76–88%). Finally, the cyclized products **55a–d** were converted into the corresponding indeno[1,2-*c*]isoquinolin-5,11-diones **57a–d** (73–85%) through cyclization with the aid of HCl followed by pyridinium dichromate (PDC) oxidation (Scheme 8).

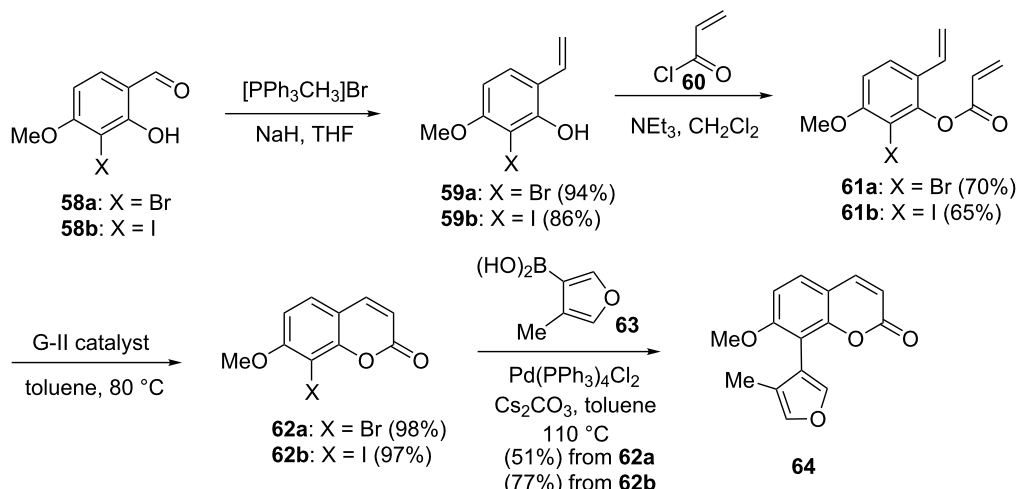
Schmidt and co-workers [39] described an efficient route involving RCM and SM coupling towards the synthesis of 8-aryl-substituted coumarin **64**, a natural product isolated from the plant *Galipea panamensis*. To this end, aldehydes **58a,b** were subjected to a Wittig olefination followed by condensation with acryloyl chloride (**60**) to generate the corresponding diolefinic substrates such as **61a** (70%) and **61b** (65%). Later, these diolefins **61a,b** were subjected to RCM with the aid of G-II catalyst **2** to furnish the respective ring-closure products **62a** (98%) and **62b** (97%). Finally, SM coupling of 8-halo-7-methoxycoumarins **62a,b** with (4-methylfuran-3-yl)boronic acid (**63**) delivered the cross-coupling product **64** (Scheme 9).

In another event, Magnier and co-workers [40] described a simple synthetic route to sulfoximines by adopting SM coupling and RCM as key steps. In this respect, SM coupling of sulfoximine **65** with potassium vinyltrifluoroborate (**66**) in the

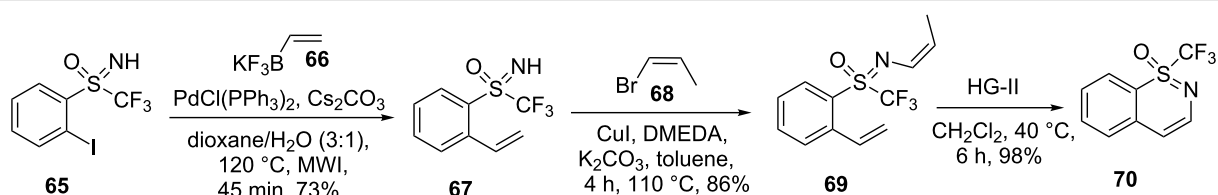
presence of a palladium catalyst produced vinyl sulfoximine derivative **67** (73%). Next, *N*-alkenylation of sulfoximine **67** was accomplished with *Z*-vinyl bromide (**68**) to generate diolefinic substrate **69** (86%). Finally, diolefin **69** was exposed to Hoveyda–Grubbs 2nd generation catalyst (HG-II) **3** to deliver the cyclic sulfoximine **70** in 98% yield (Scheme 10).

Additionally, we also demonstrated a sequential usage of SM coupling and the RCM protocol to construct 1-benzazepine derivative **75** [41]. To this end, iodoacetanilide **71** was subjected to SM coupling in the presence of allylboronate ester **12** to give *ortho*-allylacetanilide (**72**), which was further modified by *N*-allylation with allyl bromide (**28**) to offer a mixture of diallyl compound **73a** (82%) and isomerized product **73b** (8%). Next, exposure of the diallyl derivative **73a** to G-II catalyst **2** yielded the cyclized product **74** (72%). Eventually, hydrogenation of the RCM product **74** was achieved with H_2 , Pd/C conditions to give the saturated 2,3,4,5-tetrahydro-1-benzazepine **75** in 81% yield (Scheme 11).

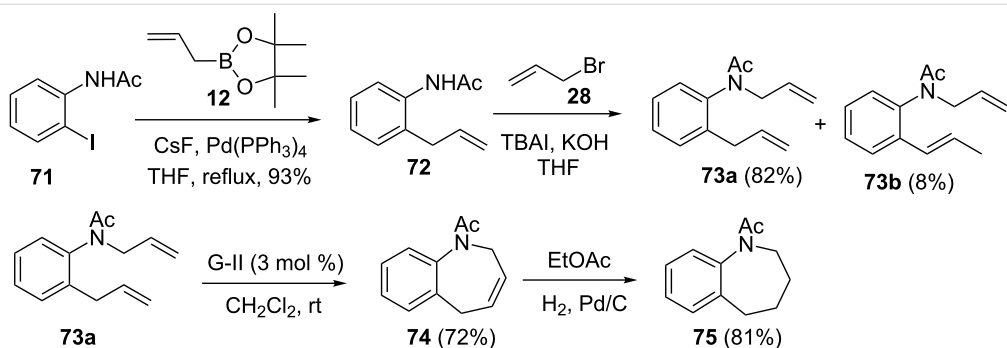
Naphthoxepine derivatives play an important role as cosmetics and as pharmaceutical ingredients. Therefore, we conceived a simple approach, where the SM coupling and RCM were employed as critical steps [42,43]. Our journey begin with *O*-allyl-



Scheme 9: Synthesis to 8-aryl substituted coumarin **64** via RCM and SM sequence.



Scheme 10: Synthesis of cyclic sulfoximine **70** via SM and RCM as key steps.

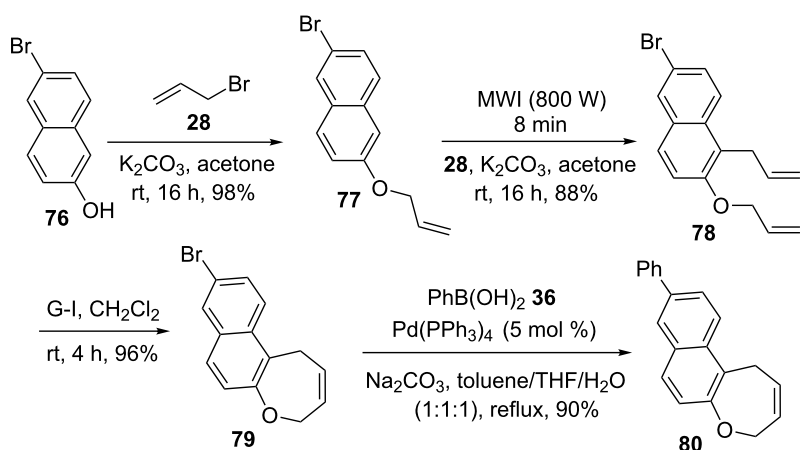


Scheme 11: Synthesis of 1-benzazepine derivative 75 via SM and RCM as key steps.

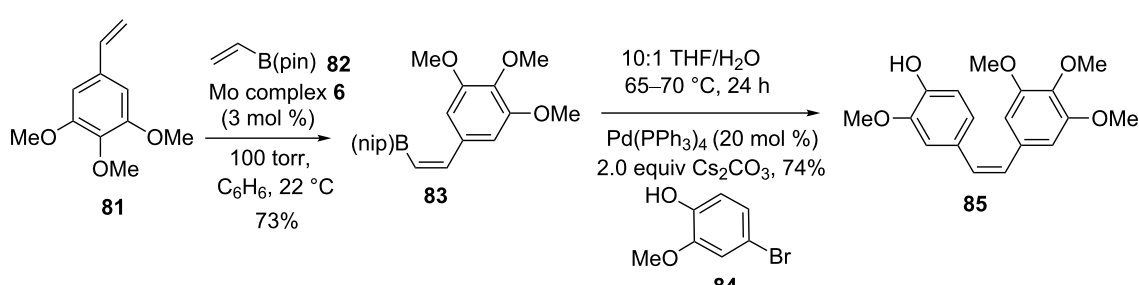
lation of β -naphthol 76 by using allyl bromide (28) to give *O*-allyl derivative 77. Then, Claisen rearrangement (CR) of 77 under microwave irradiation (MWI) conditions on a silica gel support followed by *O*-allylation of the resulting CR product furnished diallyl compound 78. Treatment of diallyl compound 78 with G-I catalyst 1 delivered the expected naphthoxepine derivative 79 (96%). Next, Suzuki coupling of 79 with diverse arylboronic acids (e.g., phenylboronic acid (36)) gave a highly substituted naphthoxepine derivative 80 (90%) (Scheme 12).

Stilbene derivatives

Hoveyda and co-workers [44] reported the synthesis of *Z*-(pinacolato)allylboron and *Z*-(pinacolato)alkenylboron derivatives via CM by using Mo complex 6. In this regard, they assembled stilbene derivative 85 as an antitumor agent by a two-step strategy that involve catalytic CM and SM coupling. To this end, the *Z*-selective CM of a styrene derivative (e.g., 81) with vinyl-B(pin) 82 was realized in the presence of Mo complex 6 to provide a highly substituted vinyl-B(pin) 83 (73%) with



Scheme 12: Synthesis of naphthoxepine derivative 79 via RCM followed by SM coupling.

Scheme 13: Sequential CM and SM coupling approach to *Z*-stilbene derivative 85.

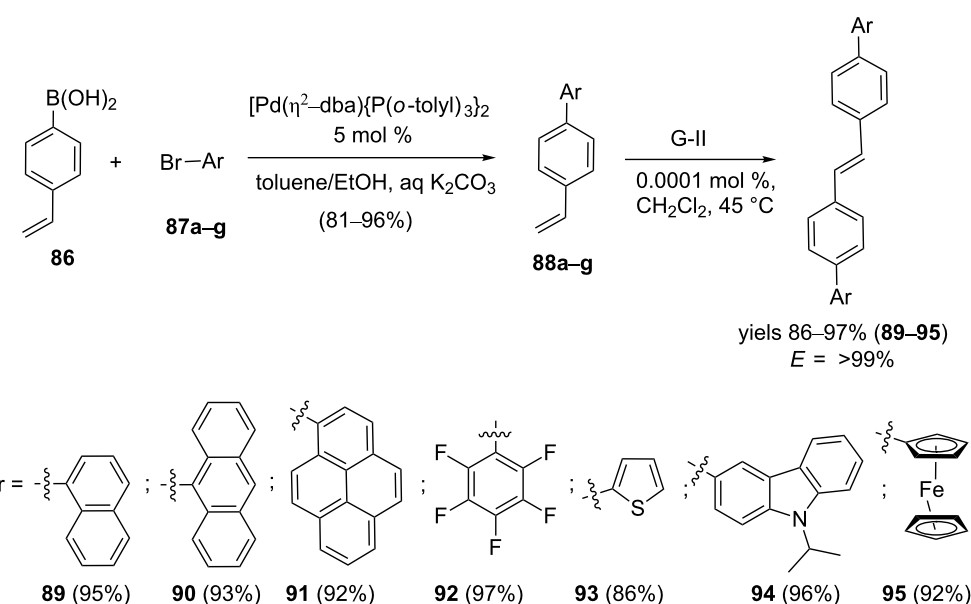
excellent selectivity (96:4 *Z:E*). Further, vinylboron compound **83** was subjected to SM coupling with a suitable partner (e.g., **84**) to afford the stilbene derivative **85** (96:4 *Z:E*) in 74% yield (Scheme 13).

Majchrzak and co-workers [45] demonstrated a synergistic approach involving SM cross coupling and CM to synthesize various substituted *trans*-stilbene derivatives **89–95** stereoselectively. In this context, 4-vinylphenylboronic acid (**86**) was subjected to SM coupling using diverse bromoarenes **87a–g** in the presence of $[\text{Pd}(\eta^2\text{-dba})\{\text{P}(o\text{-tolyl})_3\}_2]$ catalyst to obtain the cross-coupling products **88a–g** (81–96%). Finally, exposure of olefins **88a–g** to G-II catalyst **2** in CH_2Cl_2 led to the formation of the respective *trans*-stilbene derivatives **89–95** in high yields

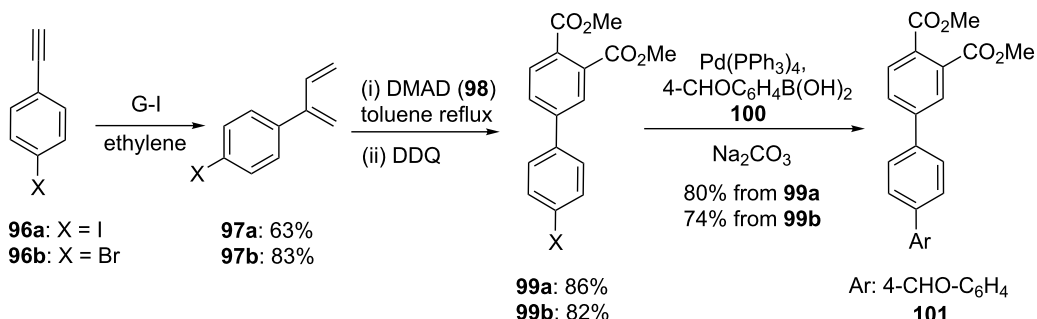
(Scheme 14). It is worth mentioning that the loading of only 0.0001 mol % catalyst can effect a CM in an efficient manner.

Biaryl derivatives

In view of the interesting properties of biaryl derivatives, we have identified a three-step sequence, which involve cross-alkyne metathesis (CEM), DA reaction followed by SM coupling [46]. To this end, acetylene derivatives **96a,b** were subjected to CEM with G-I catalyst **1** under ethylene, which resulted in the formation of the dienes **97a** (63%) and **97b** (83%, Scheme 15). Further, treatment of dienes **97a,b** with dimethyl acetylenedicarboxylate (**98**) separately delivered the corresponding cycloadducts. Subsequently, aromatization was achieved by using DDQ to give biaryl products **99a,b**.



Scheme 14: Synthesis of substituted *trans*-stilbene derivatives via SM coupling and RCM.



Scheme 15: Synthesis of biaryl derivatives via sequential EM, DA followed by SM coupling.

Further, aryl halides **99a,b** were subjected to SM coupling by employing various boronic acids (e.g., 4-formylphenylboronic acid (**100**) to produce biaryl derivative **101** (80% from **99a** and 74% from **99b**).

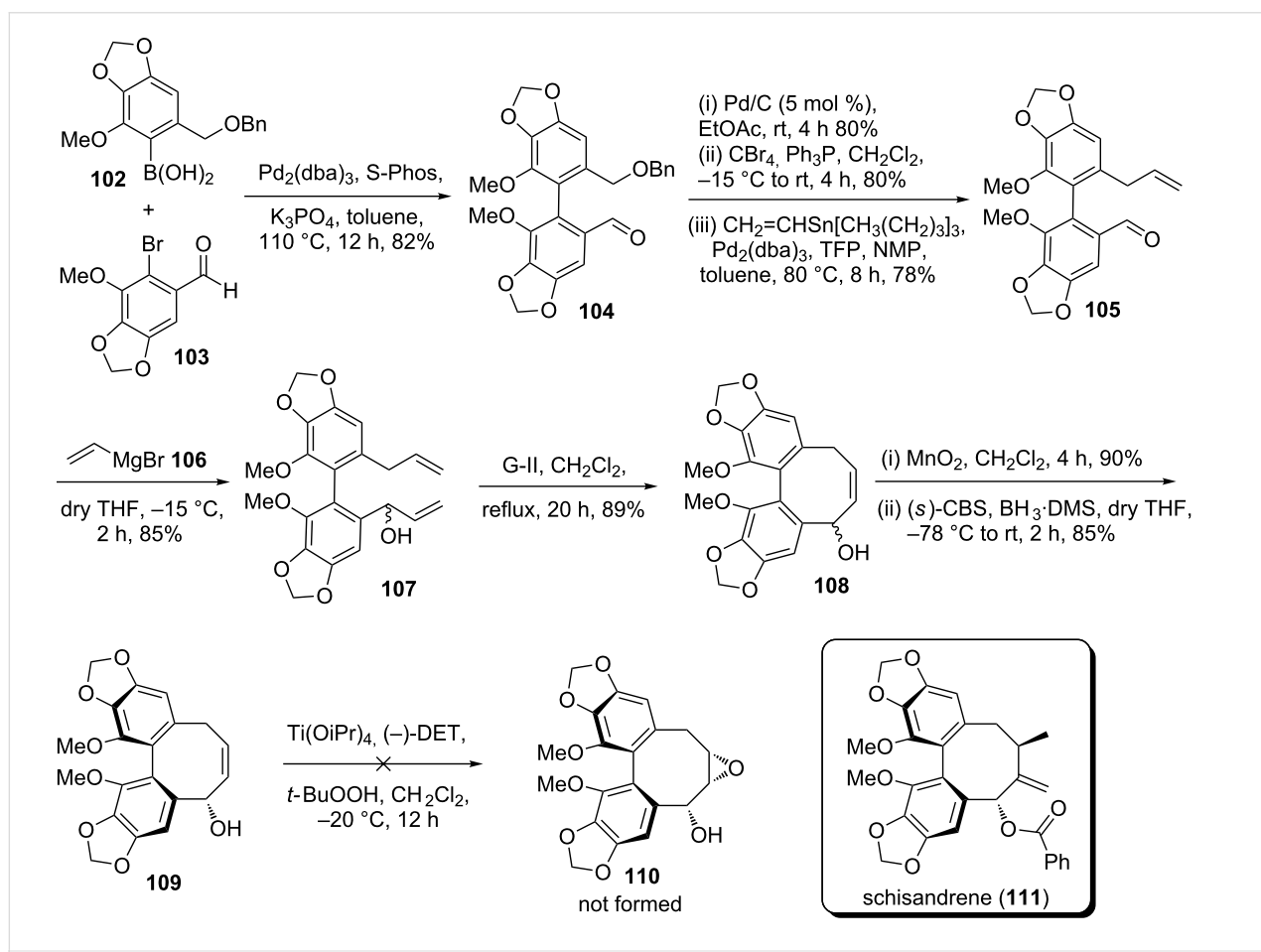
Very recently, Suresh Babu and co-workers [47] demonstrated a new route to construct the dibenzocyclooctadiene lignan core of the natural product schisandrene via SM coupling and RCM as key steps. In this context, the SM reaction of boronic acid **102** with bromoaldehyde **103** in the presence of $\text{Pd}_2(\text{dba})_3$ and the S-Phos ligand provided the cross-coupling product **104** (82%). Later, it was transformed into the allyl substrate **105** by following a three-step sequence. Afterwards, the aldehyde **105** was treated with vinylmagnesium bromide (**106**) to furnish diallyl derivative **107** (85%). Next, diolefinic substrate **107** was exposed to G-II catalyst **2** to furnish the ring-closure product **108** (89%). Then, MnO_2 oxidation of compound **108** offered the keto derivative in 90% yield. Corey–Bakshi–Shibata (CBS) reduction of the resulting keto derivative produced the hydroxy compound **109** (85%, ee 98%). Eventually, hydroxy olefin **109** was subjected to Sharpless asymmetric epoxidation to generate

the corresponding epoxide **110**. Unfortunately, generation of epoxide was not realized (Scheme 16).

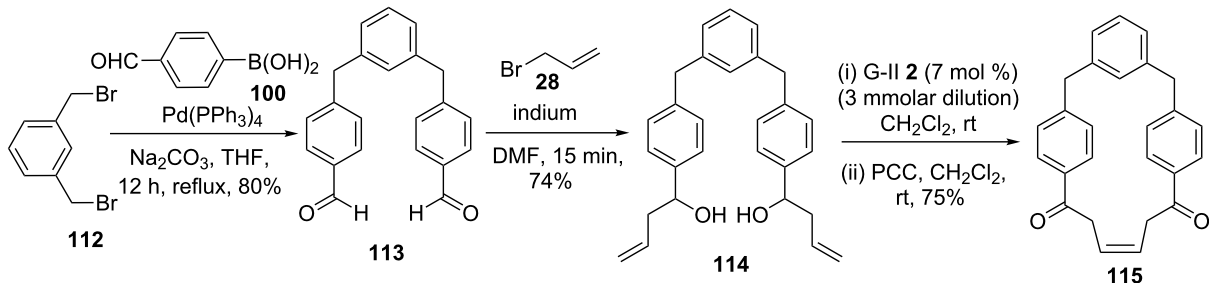
Macrocycles

To develop new synthetic strategies to various cyclophanes, we conceived a sequential usage of the SM coupling and RCM as key steps [48,49]. In this context, the required dialdehyde **113** (80%) was prepared via a SM coupling of the dibromo compound **112** with 4-formylphenylboronic acid (**100**). Treatment of dialdehyde **113** with allyl bromide (**28**) in the presence of indium powder furnished the RCM precursor **114**. Under the influence of the G-II catalyst **2** RCM of diolefinic compound **114** was realized. Then, the cyclized product was subjected to the oxidation sequence with pyridinium chlorochromate (PCC) to generate cyclophane derivative **115** in 75% yield (Scheme 17).

Similarly, treatment of dialdehyde **113** with a freshly prepared Grignard reagent derived from 4-bromobut-1-ene (**116**) afforded dialkenyl substrate **117**, which was subjected to RCM with the aid of G-II catalyst **2** to produce a mixture of products



Scheme 16: Synthesis of the dibenzocyclooctadiene core of schisandrene.



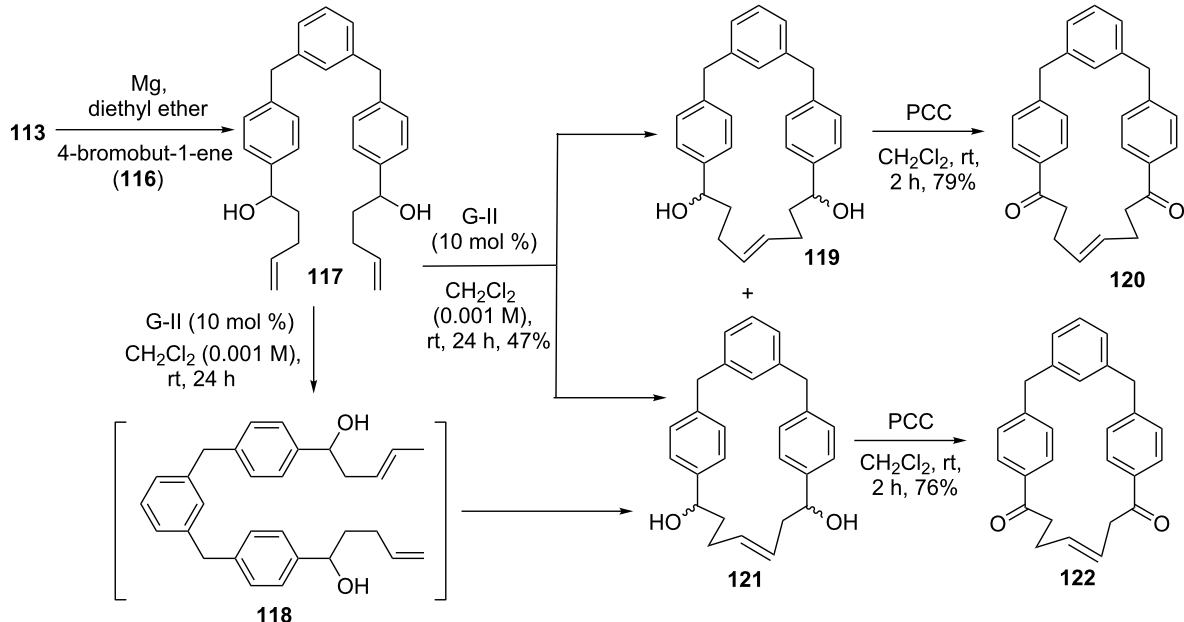
Scheme 17: Synthesis of cyclophane 115 via SM coupling and RCM as key steps.

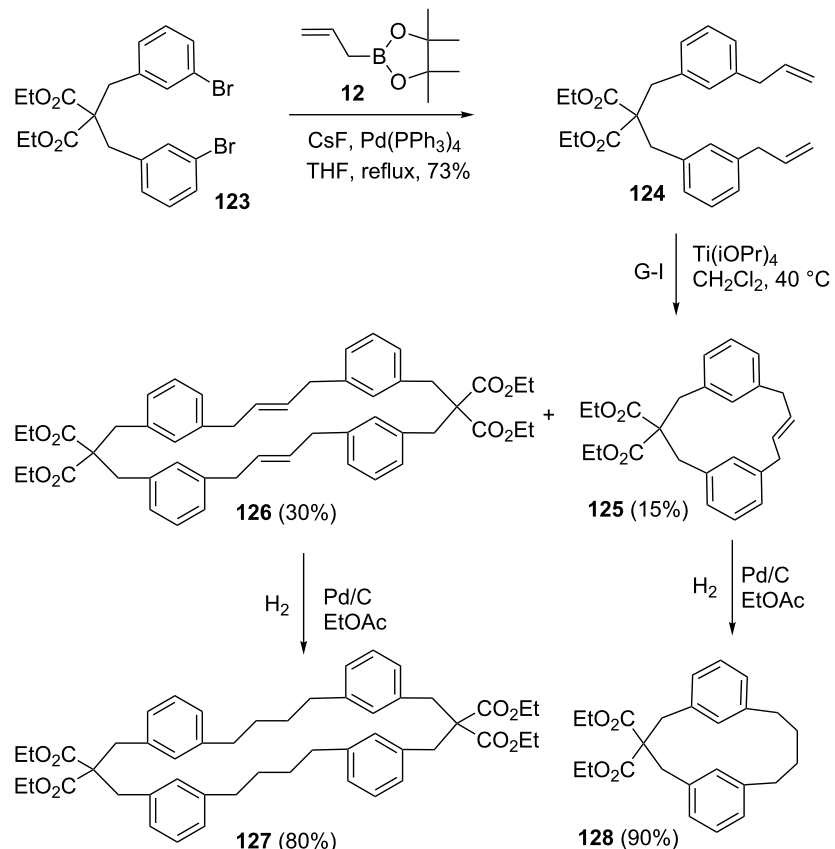
119 and **121** in combined 47% yield. It should be noted that the resulting product **121** was obtained through isomerization of the terminal double bond followed by RCM. Later, oxidation of diols **119** and **121** was accomplished with PCC to provide the corresponding diones **120** (79%) and **122** (76%) with *trans* geometry. The stereochemistry was confirmed on the basis of the coupling constant (*J* = 15.0 Hz, ¹H NMR spectrum) of the olefinic protons (Scheme 18).

A variety of macrocycles were synthesized through SM cross coupling followed by RCM as key steps [50]. To this end, dibromo compound **123** was subjected to dialylation by using allylboronate ester **12** to form the diallyl derivative **124** (73%). Treatment of compound **124** with G-I catalyst **1** gave unsaturated dimer **126** (30%) and monomer **125** (15%). Subsequently,

hydrogenation of compounds **126** and **125** was accomplished with H₂ under Pd/C catalysis conditions to afford the respective saturated macrocyclic products **127** (80%) and **128** (90%). Since the small ring cyclophane is highly strained, compound **125** was formed as a minor product (Scheme 19).

Recently, Li et al. [51] disclosed an elegant synthesis of MK-6325 (**141**) through a sequential usage of RCM and SM coupling as key steps. In this respect, the required RCM precursor **130** was derived from **129** by employing a six-step synthesis sequence. Next, the alkene derivative **130** was subjected to RCM under the influence of Zhan-1B catalyst **4** to deliver the cyclized product **131** (91%). Later, TFA-mediated deprotection of cyclized product **131** gave amine **132** (97%). Treatment of chloro derivative **132** with boronate ester **133** provided the SM

Scheme 18: Synthesis of cyclophane **120** and **122** via SM coupling and RCM as key steps.



Scheme 19: Synthesis of cyclophanes via SM and RCM.

coupling precursor **134** (77%). Later, an intramolecular SM coupling of Bpin derivative **134** was realized in the presence of a Pd(OAc)₂ catalyst with the aid of the ligand cataCXium A (**135**) to generate the macrocyclic product **136**. Eventually, synthesis of MK-6325 (**141**) was achieved by adopting saponification followed by amidation (Scheme 20).

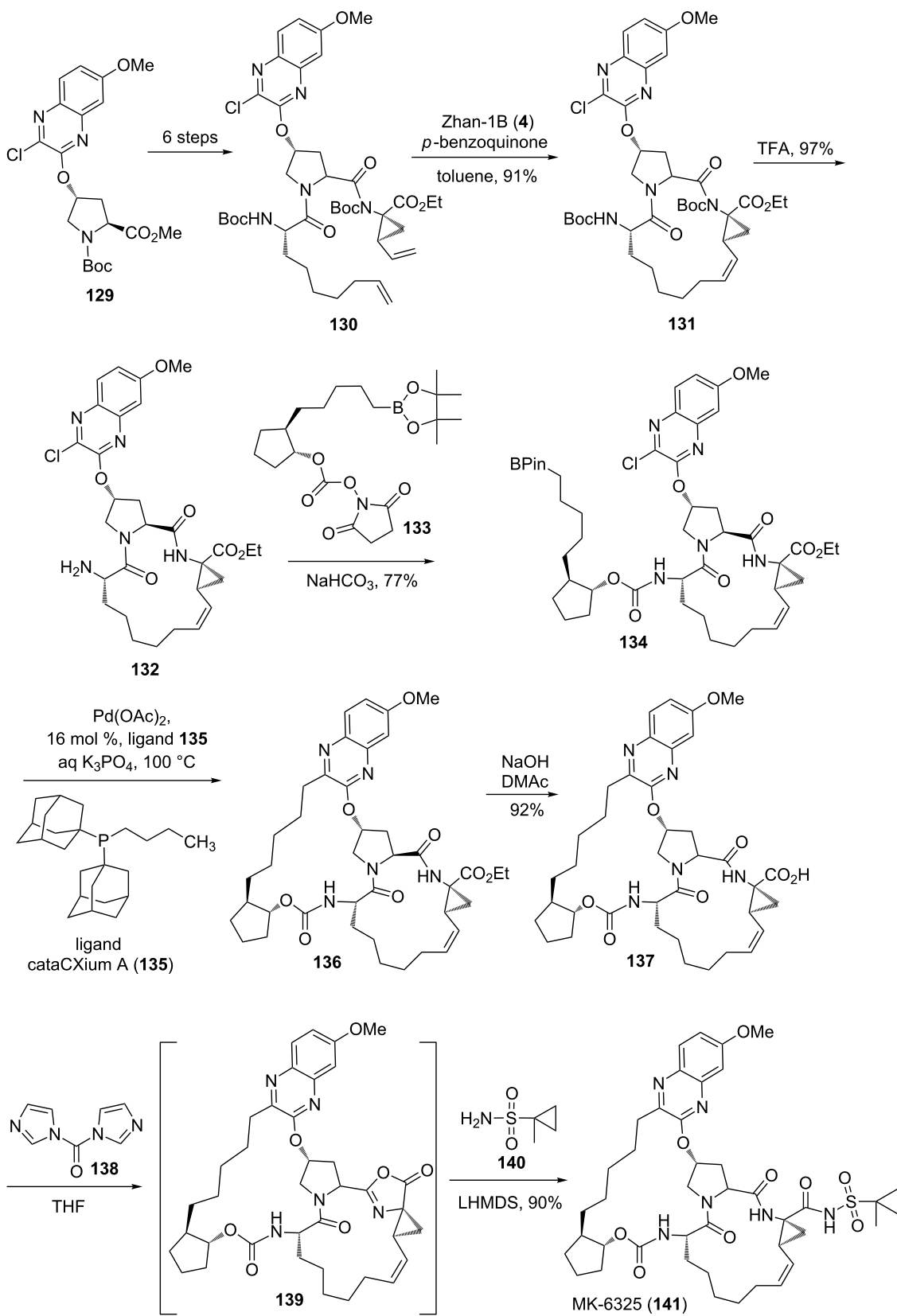
Conclusion

In this review, we have summarized various approaches to a wide range of carbocycles and heterocycles that deals with a strategic utilization of SM coupling and metathesis as key steps. Interestingly, application of these two powerful methods in combination for a C–C bond formation process shorten the synthesis sequence for the assembly of the target molecules and thus enhances the ease of preparation of various functional molecules. These processes are considered as “green” because of atom economy and synthetic brevity [52] involved in these reactions [12,53,54]. Additionally, several methods are available to remove palladium and ruthenium impurities in minor amounts from the reaction mixture. This aspect is also important in the pharmaceutical industry [4,55].

Biography of the Authors



Sambasivarao Kotha graduated with M.Sc. degree in Chemistry from the University of Hyderabad and obtained his Ph.D. in Organic Chemistry from the University of Hyderabad in 1985. Later, he moved to UMIST Manchester, UK and the University of Wisconsin, USA as a research associate. Subsequently, he was appointed as a visiting scientist at Cornell University and as a research chemist at Hoechst Celanese Texas prior to joining IIT Bombay in 1994 as an assistant professor.



Scheme 20: Synthesis of MK-6325 (141) via RCM and SM coupling.

Later, in 2001, he was promoted to Professor. He has published 250 publications in peer-reviewed journals and elected fellow of various academies (FNASc, FASc, FRSC and FNA). He was also associated with editorial advisory boards of several journals. His research interests include: organic synthesis, green chemistry, development of new synthetic methods for unusual amino acids, peptide modifications, cross-coupling reactions, and metathesis. Currently, he occupies the Pramod Chaudhari Chair Professor in Green Chemistry.



Milind P. Meshram was born in Amravati, Maharashtra, India. He obtained his M.Sc. degree in Chemistry from the Amravati University. He joined the Department of Chemistry, IIT Bombay in 2007 and graduated with Ph.D. degree in 2014 (Organic Chemistry) under the supervision of Prof. S. Kotha. Later, he worked with Prof. Dr. Van der Eycken as a Post-Doctoral Fellow at the KU Leuven, Belgium under the EMINTE programme. During post-doctoral work his research work was related to organic synthesis under microwave reaction conditions. Presently, he is Research Associate with Prof. S. Kotha. His research interests include various transition-metal-catalyzed reactions and their applications in organic synthesis.



Chandravathi Chakkapalli obtained her B.Sc. and M.Sc. in Chemistry from Andhra University, Andhra Pradesh, India. She completed her Ph.D. under the supervision of Dr. J. S. Yadav

from IICT, Hyderabad in 2016. Her research interests are in the area of organic synthesis and green chemistry.

Acknowledgements

We thank the Council of Scientific and Industrial Research (CSIR), New Delhi [02(0272)/16/EMR-II] for the financial support. SK thanks the Department of Science and Technology (DST), New Delhi for the award of a J. C. Bose fellowship (SR/S2/JCB-33/2010), and Praj Industries, Pune for the Pramod Chaudhari Chair Professorship (Green Chemistry).

ORCID® IDs

Milind Meshram - <https://orcid.org/0000-0002-8922-4363>

References

1. Grubbs, R. H.; Wenzel, A. G.; O'Leary, D. J.; Khosravi, E. *Handbook of Metathesis*; Wiley-VCH: Weinheim, Germany, 2015; Vol. 1. doi:10.1002/9783527674107
2. Ogbu, O. M.; Warner, N. C.; O'Leary, D. J.; Grubbs, R. H. *Chem. Soc. Rev.* **2018**, *47*, 4510–4544. doi:10.1039/c8cs00027a
3. Kotha, S.; Lahiri, K. *Synlett* **2007**, 2767–2784. doi:10.1055/s-2007-990954
4. Kotha, S.; Dipak, M. K. *Tetrahedron* **2012**, *68*, 397–421. doi:10.1016/j.tet.2011.10.018
5. Kotha, S.; Sreenivasachary, N. *Indian J. Chem.* **2001**, *40B*, 763–780.
6. Kotha, S.; Misra, S.; Sreevani, G.; Babu, B. *Curr. Org. Chem.* **2013**, *17*, 2776–2795. doi:10.2174/13852728113179990118
7. Carey, F. A.; Sunburg, R. J. *Reactions Involving Transition Metals. Advanced Organic Chemistry: Reaction and Synthesis*, 5th ed.; Springer: New York, NY, U.S.A., 2007. doi:10.1007/978-0-387-71481-3
8. Suzuki, A.; Miyaura, N.; Yamada, K. *Tetrahedron Lett.* **1979**, *20*, 3437–3440. doi:10.1016/s0040-4039(01)95429-2
9. Miyaura, N.; Suzuki, A. *J. Chem. Soc., Chem. Commun.* **1979**, 866–867. doi:10.1039/c39790000866
10. Miyaura, N.; Suzuki, A. *Chem. Rev.* **1995**, *95*, 2457–2483. doi:10.1021/cr00039a007
11. Kotha, S.; Lahiri, K.; Kashinath, D. *Tetrahedron* **2002**, *58*, 9633–9695. doi:10.1016/s0040-4020(02)01188-2
12. Chatterjee, A.; Ward, T. R. *Catal. Lett.* **2016**, *146*, 820–840. doi:10.1007/s10562-016-1707-8
13. Lennox, A. J. J.; Lloyd-Jones, G. C. *Chem. Soc. Rev.* **2014**, *43*, 412–443. doi:10.1039/c3cs60197h
14. Molander, G. A. *J. Org. Chem.* **2015**, *80*, 7837–7848. doi:10.1021/acs.joc.5b00981
15. Hall, D. G., Ed. *Boronic Acids*, 2nd ed.; Wiley-VCH Verlag GmbH: Weinheim, Germany, 2011. doi:10.1002/9783527639328
16. Hemelaere, R.; Carreaux, F.; Carboni, B. *J. Org. Chem.* **2013**, *78*, 6786–6792. doi:10.1021/jo400872x
17. Topolovčan, N.; Panov, I.; Kotora, M. *Org. Lett.* **2016**, *18*, 3634–3637. doi:10.1021/acs.orglett.6b01682
18. Kotha, S.; Mandal, K. *Chem. – Asian J.* **2009**, *4*, 354–362. doi:10.1002/asia.200800244
19. Moulin, E.; Nevado, C.; Gagnepain, J.; Kelter, G.; Fiebig, H.-H.; Fürstner, A. *Tetrahedron* **2010**, *66*, 6421–6428. doi:10.1016/j.tet.2010.05.043
20. Liao, L.; Zhou, J.; Xu, Z.; Ye, T. *Angew. Chem., Int. Ed.* **2016**, *55*, 13263–13266. doi:10.1002/anie.201606679

21. Reck, L. M.; Haberhauer, G.; Lüning, U. *Eur. J. Org. Chem.* **2016**, 1119–1131. doi:10.1002/ejoc.201501289

22. Sakamoto, K.; Hakamata, A.; Tsuda, M.; Fuwa, H. *Angew. Chem., Int. Ed.* **2018**, 57, 3801–3805. doi:10.1002/anie.201800507

23. Inoue, M.; Komori, T.; Iwanaga, T.; Toyota, S. *Chem. Lett.* **2017**, 46, 1836–1838. doi:10.1246/cl.170884

24. Kuttner, J. R.; Hilt, G. *Macromolecules* **2014**, 47, 5532–5541. doi:10.1021/ma5012446

25. Sasaki, M.; Ishikawa, M.; Fuwa, H.; Tachibana, K. *Tetrahedron* **2002**, 58, 1889–1911. doi:10.1016/s0040-4020(02)00045-5

26. Essig, S.; Schmalzbauer, B.; Bretzke, S.; Scherer, O.; Koeberle, A.; Werz, O.; Müller, R.; Menche, D. *J. Org. Chem.* **2016**, 81, 1333–1357. doi:10.1021/acs.joc.5b02844

27. Arican, D.; Braukmüller, S.; Brückner, R. *Chem. – Eur. J.* **2017**, 23, 4537–4541. doi:10.1002/chem.201700622

28. Maitra, S.; Bodugam, M.; Javed, S.; Hanson, P. R. *Org. Lett.* **2016**, 18, 3094–3097. doi:10.1021/acs.orglett.6b01248

29. Kotha, S.; Panguluri, N. R.; Ali, R. *Eur. J. Org. Chem.* **2017**, 5316–5342. doi:10.1002/ejoc.201700439

30. Jana, A.; Misztal, K.; Źak, A.; Grela, K. *J. Org. Chem.* **2017**, 82, 4226–4234. doi:10.1021/acs.joc.7b00200

31. Kotha, S.; Shah, V. R.; Mandal, K. *Adv. Synth. Catal.* **2007**, 349, 1159–1172. doi:10.1002/adsc.200600469

32. Kotha, S.; Behera, M.; Shah, V. R. *Synlett* **2005**, 1877–1880. doi:10.1055/s-2005-871569

33. Johnson, M. M.; Ngwira, K. J.; Rousseau, A. L.; Lemmerer, A.; de Koning, C. B. *Tetrahedron* **2018**, 74, 12–18. doi:10.1016/j.tet.2017.11.023

34. Kotha, S.; Ali, R.; Srinivas, V.; Krishna, N. G. *Tetrahedron* **2015**, 71, 129–138. doi:10.1016/j.tet.2014.11.024

35. Kotha, S.; Mandal, K. *Tetrahedron Lett.* **2004**, 45, 1391–1394. doi:10.1016/j.tetlet.2003.12.075

36. Kotha, S.; Ali, R. *Turk. J. Chem.* **2015**, 39, 1190–1198. doi:10.3906/kim-1502-116

37. Ali, R. Diversity oriented approach to spirocycles and heterocycles via olefin metathesis, cycloaddition reaction, Fischer indolization, and Suzuki–Miyaura cross-coupling reaction as key steps. Ph.D. Thesis, IIT, Bombay, India, 2015.

38. Lebrun, S.; Couture, A.; Deniau, E.; Grandclaudon, P. *Tetrahedron Lett.* **2011**, 52, 1481–1484. doi:10.1016/j.tetlet.2011.01.113

39. Schmidt, B.; Krehl, S.; Kelling, A.; Schilde, U. *J. Org. Chem.* **2012**, 77, 2360–2367. doi:10.1021/jo2026564

40. Barthelemy, A.-L.; Prieto, A.; Diter, P.; Hannedouche, J.; Toffano, M.; Anselmi, E.; Magnier, E. *Eur. J. Org. Chem.* **2018**, 3764–3770. doi:10.1002/ejoc.201800324

41. Kotha, S.; Shah, V. R. *Eur. J. Org. Chem.* **2008**, 1054–1064. doi:10.1002/ejoc.200700921

42. Kotha, S.; Mandal, K.; Tiwari, A.; Mobin, S. M. *Chem. – Eur. J.* **2006**, 12, 8024–8038. doi:10.1002/chem.200600540

43. Kotha, S.; Srinivas, V.; Krishna, N. G. *Heterocycles* **2012**, 86, 1555–1563. doi:10.3987/com-12-s(n)89

44. Kiesewetter, E. T.; O'Brien, R. V.; Yu, E. C.; Meek, S. J.; Schrock, R. R.; Hoveyda, A. H. *J. Am. Chem. Soc.* **2013**, 135, 6026–6029. doi:10.1021/ja403188t

45. Majchrzak, M.; Wilkowski, G.; Kubicki, M. *Eur. J. Org. Chem.* **2017**, 4291–4299. doi:10.1002/ejoc.201700602

46. Kotha, S.; Seema, V. *Synlett* **2011**, 2329–2334. doi:10.1055/s-0030-1260315

47. Venkanna, A.; Poornima, B.; Siva, B.; Babu, B. H.; Babu, K. S. *Synlett* **2018**, 29, 908–911. doi:10.1055/s-0036-1591539

48. Kotha, S.; Mandal, K.; Arora, K. K.; Pedireddi, V. R. *Adv. Synth. Catal.* **2005**, 347, 1215–1218. doi:10.1002/adsc.200404373

49. Kotha, S.; Mandal, K. *Eur. J. Org. Chem.* **2006**, 5387–5393. doi:10.1002/ejoc.200600549

50. Kotha, S.; Chavan, A. S.; Shaikh, M. *J. Org. Chem.* **2012**, 77, 482–489. doi:10.1021/jo2020714

51. Li, H.; Scott, J. P.; Chen, C.-y.; Journet, M.; Belyk, K.; Balsells, J.; Kosjek, B.; Baxter, C. A.; Stewart, G. W.; Wise, C.; Alam, M.; Song, Z. J.; Tan, L. *Org. Lett.* **2015**, 17, 1533–1536. doi:10.1021/acs.orglett.5b00418

52. Hudlicky, T.; Reed, J. W. *The Way of Synthesis*; Wiley-VCH: Weinheim, Germany, 2007; p 98.

53. Hughes, D.; Wheeler, P.; Ene, D. *Org. Process Res. Dev.* **2017**, 21, 1938–1962. doi:10.1021/acs.oprd.7b00319

54. Náray-Szabó, G.; Mika, L. T. *Green Chem.* **2018**, 20, 2171–2191. doi:10.1039/c8gc00514a

55. Szczepaniak, G.; Ruszczyńska, A.; Kosiński, K.; Bulska, E.; Grela, K. *Green Chem.* **2018**, 20, 1280–1289. doi:10.1039/c7gc03324a

License and Terms

This is an Open Access article under the terms of the Creative Commons Attribution License (<http://creativecommons.org/licenses/by/4.0>). Please note that the reuse, redistribution and reproduction in particular requires that the authors and source are credited.

The license is subject to the *Beilstein Journal of Organic Chemistry* terms and conditions: (<https://www.beilstein-journals.org/bjoc>)

The definitive version of this article is the electronic one which can be found at:

[doi:10.3762/bjoc.14.223](https://doi.org/10.3762/bjoc.14.223)



Design and synthesis of C_3 -symmetric molecules bearing propellane moieties via cyclotrimerization and a ring-closing metathesis sequence

Sambasivarao Kotha *§, Saidulu Todeti and Vikas R. Aswar

Full Research Paper

Open Access

Address:

Department of Chemistry, Indian Institute of Technology Bombay,
Powai, Mumbai-400076, India

Email:

Sambasivarao Kotha * - srk@chem.iitb.ac.in

* Corresponding author

§ Fax: +91(22)-2572 7152

Keywords:

cyclotrimerization; Diels–Alder; propellane; ring-closing metathesis

Beilstein J. Org. Chem. **2018**, *14*, 2537–2544.

doi:10.3762/bjoc.14.230

Received: 18 June 2018

Accepted: 14 September 2018

Published: 01 October 2018

This article is part of the thematic issue "Progress in metathesis chemistry III".

Guest Editor: K. Grela

© 2018 Kotha et al.; licensee Beilstein-Institut.

License and terms: see end of document.

Abstract

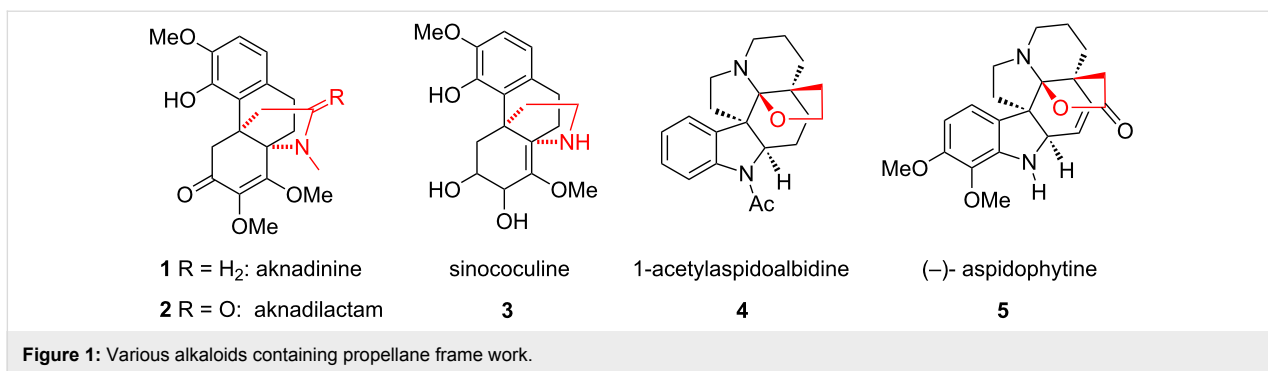
We have developed an efficient synthetic strategy to assemble C_3 -symmetric molecules containing propellane moieties as end groups and a benzene ring as a central core. The synthesis of these C_3 -symmetric molecules involves simple starting materials. Our approach to C_3 -symmetric compounds relies on a Diels–Alder reaction, cyclotrimerization and ring-closing metathesis as key steps.

Introduction

In 1966 Ginsburg coined the word “propellane” [1,2] and Wiberg reviewed various aspects of medium and small ring propellanes [3,4]. Propellanes consist of tricyclic compounds where three rings are conjoined by a common C–C bond [1,5,6]. Heterocyclic systems contain a heteroatom (e.g., oxygen, nitrogen, and sulfur, etc.) along with carbon atoms. The name of a heterocyclic propellane may be organized by prefixing aza, oxa, etc.

Among various propellanes, nitrogen-containing compounds occupy a special place because they are present as core structural units in bioactive natural products and pharmaceuticals.

Some of these propellanes exhibit interesting properties like antibiotic, antifungal, anticancer, platelet-activating factor antagonistic and antibacterial activities. The propellane skeleton is present in many alkaloids such as aknadinine (**1**), aknadilactam (**2**), and the known morphinan alkaloid sinocouline (**3**), which was identified as a bioactive component from *S. japonica* [7]. In 1963 Brown et al. isolated 1-acetyl-aspidoalbidine (**4**) from *Vallesia dichotoma* [8] and subsequently, Djerassi proposed its structure [9]. Another alkaloid (–)-aspidophytine (**5**) differs from 1-acetylaspidoalbidine (**4**) only in the degree of unsaturation and the substitution pattern on the aromatic ring (Figure 1).



The design of propellanes demands unique synthetic methods and these include: manganese or palladium-catalyzed transformations [10], the Diels–Alder (DA) reaction [11,12], and rearrangement of spiro-ketones, nucleophilic substitutions of alkenes, and photochemical addition reactions. Multicomponent reactions (MCRs) are also used for the synthesis of hetero-propellanes [13,14]. Recently, heterocyclic propellanes have been reviewed [15,16]. Our group also developed simple synthetic approaches to propellanes via ring-closing metathesis (RCM) as a key step [17,18].

The development of new synthetic strategies to C_3 -symmetric molecules bearing propellane moieties from commercially available starting materials is worthy of systematic investigation. To this end, our efforts are directed to design star-shaped molecules that involve a wide range of structural variations. To the best of our knowledge there are no synthetic reports available for C_3 -symmetric molecules bearing propellane moieties. As part of our major program aimed at designing star-shaped C_3 -symmetric molecules [19–30], here, we conceived new strategies to N-containing star-shaped molecules. Such star-shaped molecules are generally used in organic light-emitting diodes (OLEDs) [31–33], organic photovoltaics (OPVs) [34], organic field-effect transistors (OFETs) [35,36], and other optoelectronic devices. Our approach to C_3 -symmetric molecules containing propellane moieties involve DA reaction [37], cyclotrimerization [19] and RCM [38–41] as key steps.

Results and Discussion

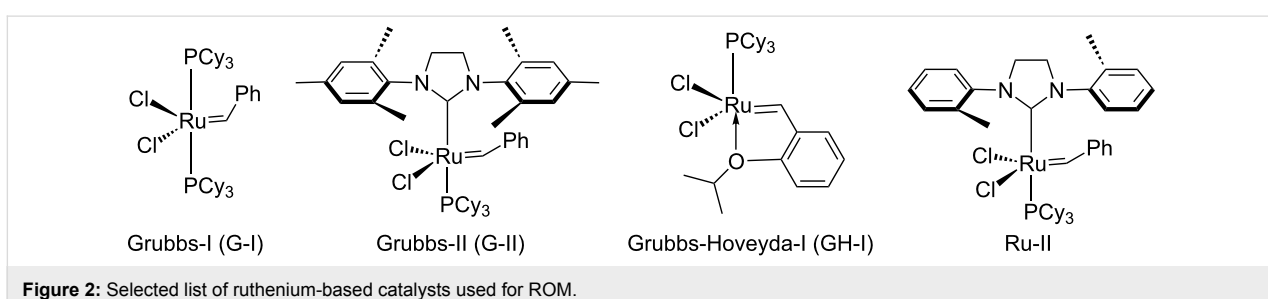
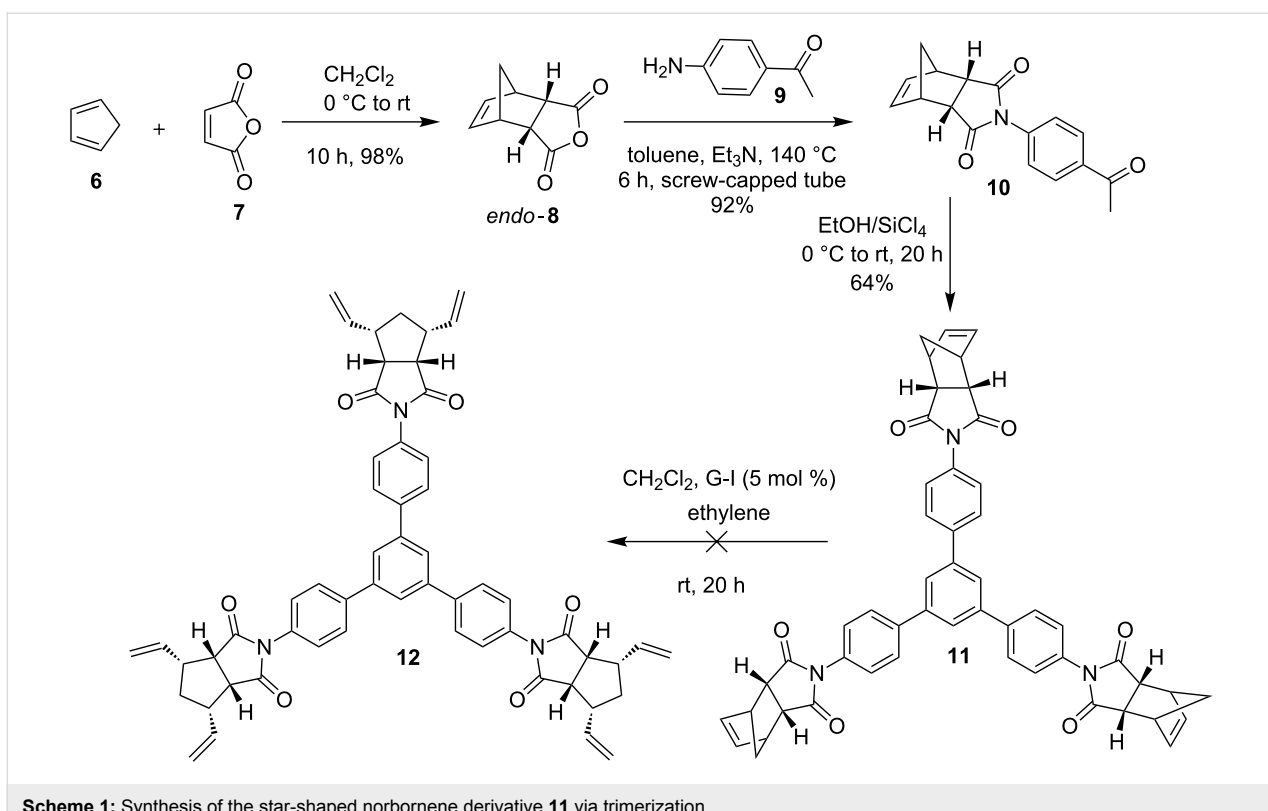
The synthesis of propellane-bearing C_3 -symmetric derivatives starts with commercially available dicyclopentadiene and maleic anhydride (7). Here, we used a DA reaction of freshly cracked cyclopentadiene (6) and maleic anhydride (7) to obtain the *endo*-DA adduct 8 [42] in 98% yield. Next, this cyclo-adduct 8 was treated with commercially available 4-aminoacetophenone (9) in the presence of triethylamine (Et_3N) in toluene at 140 °C to obtain the acetophenone derivative 10 in excellent yield (92%) [43]. Later, the acetophenone derivative 10 was subjected to trimerization reaction under ethanol/silicon

tetrachloride (EtOH/SiCl_4) conditions to deliver the trimerized product 11 (64%). Having the trimerized product 11, we attempted to open the norbornene system due to the fact that not all norbornene rings open up during RCM to generate propellane derivative. After allylation, RCM is not a clean reaction and it gave a mixture of the C_3 -symmetrical compounds. Therefore it is desirable to open the norbornene double bond before the trimerization sequence. To this end, the trimerized product 11 was treated with Grubbs first generation (G-I) catalyst in CH_2Cl_2 under ethylene atmosphere but, we were unable to get the ring-opened product 12 (Scheme 1).

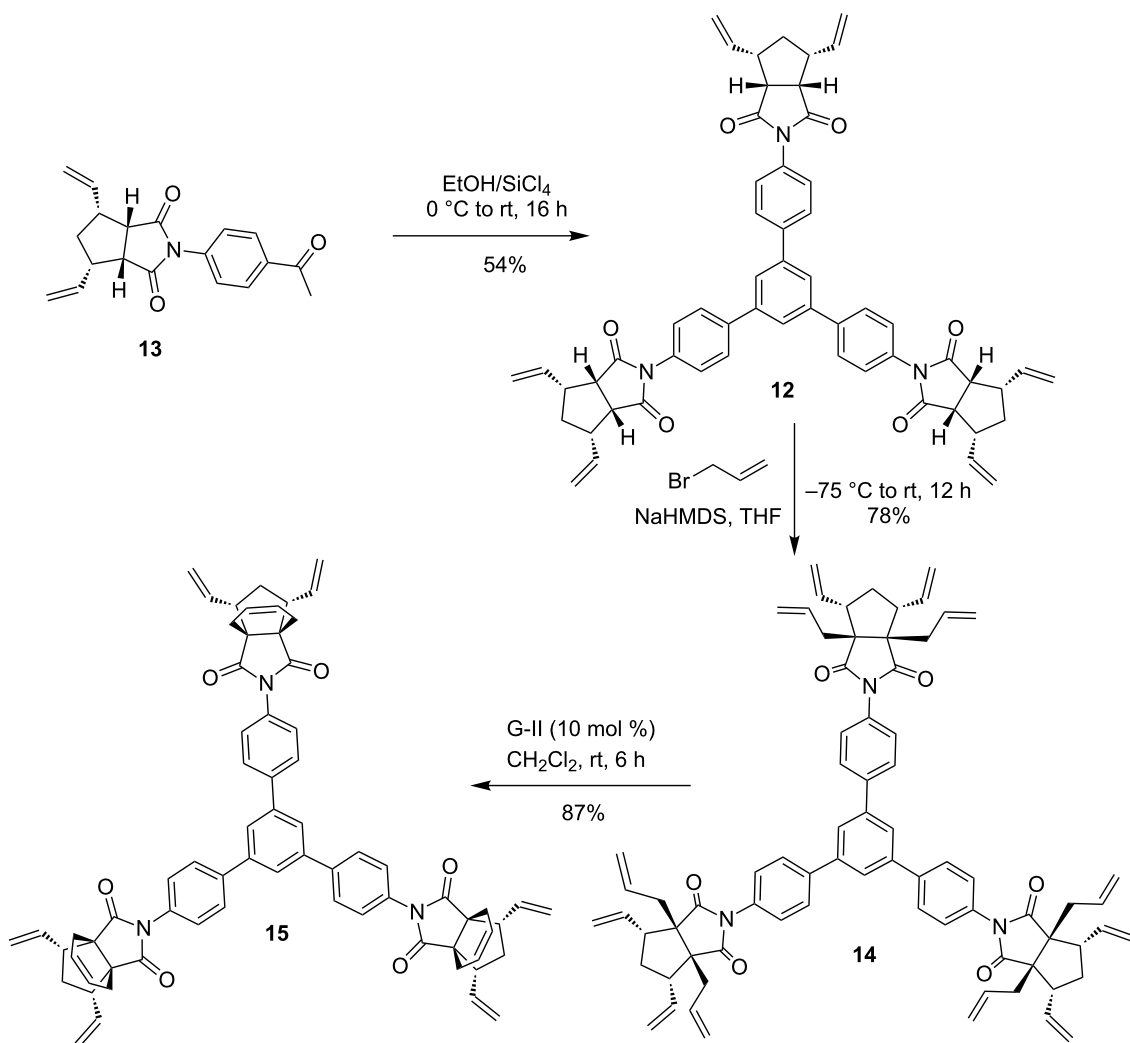
Later, we considered an alternate route to synthesize compound 12. In this regard, we employed different ruthenium-based catalysts (Figure 2) and reaction conditions to obtain the ring-opening metathesis (ROM) product 13 from norbornene derivative 10. Under these conditions the starting material was not consumed completely. After some experimentation, we found that G-I catalyst (5 mol %) in CH_2Cl_2 is suitable to generate the ROM product 13 in 56% yield (Table 1).

Having the ROM product 13 in hand, it was subjected to trimerization in the presence of EtOH/SiCl_4 at 0 °C to room temperature to afford the trimerized product 12 in 54% yield. Next, the C_3 -symmetric product 12 was reacted with allyl bromide in the presence of sodium bis(trimethylsilyl)amide (NaHMDS , 1 M solution in THF) at –75 °C to deliver the RCM precursor 14 in good yield (78%). The hexaallyl derivative 14 was subjected to RCM in the presence of Grubbs second generation (G-II) catalyst in CH_2Cl_2 under nitrogen to give the propellane moiety bearing C_3 -symmetric product 15 in good yield (87%). Its structure was established on the basis of NMR spectral data, and its molecular formula was confirmed by HRMS data (Scheme 2).

Along similar lines, we expanded the scope of this strategy. To this end, commercially available anthracene (16) was reacted with maleic anhydride (7) in a screw-capped tube at 150 °C in *o*-xylene to obtain the DA adduct 17 in 94% yield [44,45].

**Table 1:** Different conditions attempted to obtain the ROM product **13**.

entry	catalyst	mol %	solvent	temp	time (h)	yield (%)
1	G-I	5 or 10	CH ₂ Cl ₂	rt	48	56
2	G-I	5 or 10	CH ₂ Cl ₂	reflux	32	48
4	G-II	5 or 10	toluene	rt	46	24
5	G-II	5	toluene	reflux	43	20
6	Ru-II	5 or 10	CH ₂ Cl ₂	rt	48	52
7	GH-I	5 or 10	CH ₂ Cl ₂	rt	40	53
8	GH-I	5 or 10	CH ₂ Cl ₂	reflux	40	50



Scheme 2: Synthesis of the C_3 -symmetric molecule **15** bearing propellane moieties via trimerization and RCM.

Later, the DA adduct **17** was treated with 4-aminoacetophenone (**9**) in the presence of Et_3N in toluene at 140°C to deliver the acetophenone derivative **18** (91% yield) and it was subjected to trimerization in the presence of $\text{EtOH}/\text{SiCl}_4$ at 0°C to rt to obtain the trimerized product **19** in 64% yield. Afterwards, the trimerized product **19** was treated with allyl bromide to accomplish C -allylation in the presence of NaHMDS (1 M solution in THF) at -75°C to deliver the hexaallyl derivative **20** in 84% yield. Then, RCM in the presence of G-II catalyst in CH_2Cl_2 under nitrogen atmosphere gave the propellane moieties bearing C_3 -symmetric product **21** in good yield (91%). Its structure was established with the help of ^1H NMR, ^{13}C NMR spectral data and was further supported by HRMS details (Scheme 3).

Conclusion

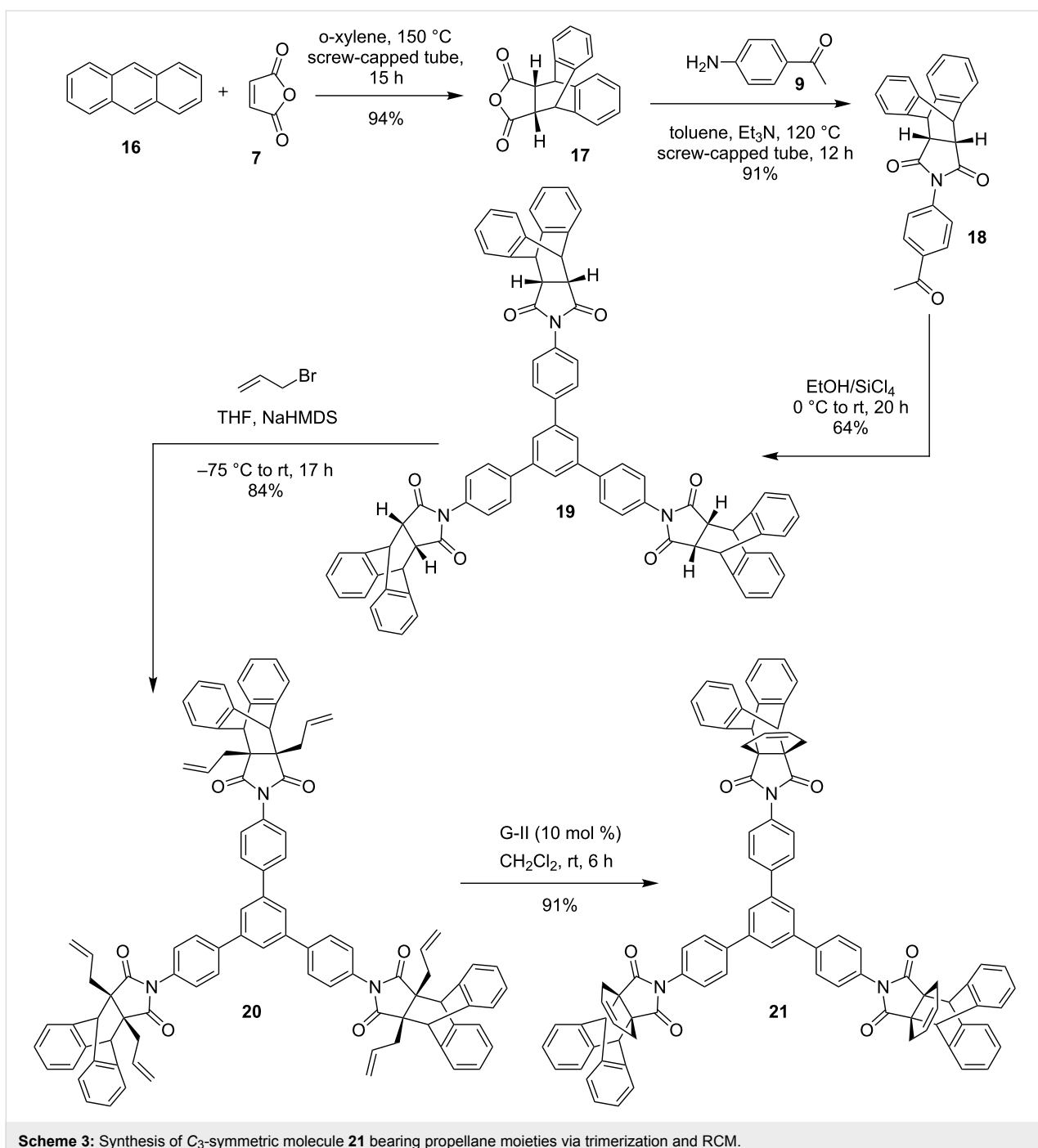
We have demonstrated a simple synthetic methodology to C_3 -symmetric star-shaped molecules containing propellane

moieties at the periphery which may be useful for material science applications. Here, we have prepared DA adducts **8** and **17** from commercially available maleic anhydride (**7**), which was further utilized for trimerization and RCM sequence. We have successfully synthesized C_3 -symmetric molecules **15** and **21** bearing propellane moieties by employing RCM in the presence of 2nd generation (G-II) catalyst.

Experimental

General information

Some of these reactions were carried out in screw-capped tubes and other reactions under nitrogen or argon and ethylene atmosphere in oven-dried glassware. Air- and moisture-sensitive reactions were performed in degassed solvents. Transfer of moisture-sensitive materials were carried out using standard syringe–septum techniques. All the commercial grade reagents were used without any purification until otherwise specified.



Melting points were recorded on a Veego or Büchi melting point apparatus and are uncorrected. NMR Spectra were generally recorded on Bruker (Avance 400 or Avance III 500) spectrometers operated at 400 or 500 MHz for ^1H and 100 or 125.7 MHz for ^{13}C nuclei. NMR Samples were generally made in chloroform-*d* solvent, and chemical shifts (δ values) are reported in parts per million (ppm). Coupling constants (J values) were reported in hertz (Hz). HRMS measurements were carried out using a Bruker (Maxis Impact) spectrometer. IR spectra

were recorded on a Nicolet Impact-400 or Cary 630 FTIR spectrometer.

Synthesis of norbornene-based trimerized product **11**

To a solution of norbornene derivative **10** (500 mg, 1.77 mmol) in EtOH (8 mL), silicon tetrachloride (SiCl_4 , 0.61 mL, 5.36 mmol) was added dropwise at $0\text{ }^\circ\text{C}$ and the reaction mixture was stirred for 10–15 min at the same temperature. Later,

the reaction mixture was stirred at room temperature for 20 h. After completion of the reaction (TLC monitoring), the reaction mixture was quenched with sat. aq NH_4Cl . Thereafter, the reaction mixture was diluted with EtOAc (10 mL) washed with water and brine (2×10 mL). Then, the aqueous layer was extracted with EtOAc (3×10 mL) and the combined organic layers were dried over Na_2SO_4 . The solvent was removed under reduced pressure and the crude product was purified by silica gel column chromatography (65% $\text{EtOAc}/\text{petroleum ether}$) to afford the trimerized product **11** (321 mg, 64%) as a colourless solid. $R_f = 0.54$ (4:6 $\text{EtOAc}/\text{petroleum ether}$); mp 203–206 °C; ^1H NMR (400 MHz, CDCl_3) δ 7.68 (d, $J = 5.2$ Hz, 6H), 7.66 (s, 3H), 7.24 (d, $J = 2.4$ Hz, 6H), 6.28 (s, 6H), 3.51–3.44 (m, 12H), 1.79 (d, $J = 8.8$ Hz, 3H), 1.61 (d, $J = 8.8$ Hz, 3H) ppm; ^{13}C NMR (125 MHz, CDCl_3) δ 177.0, 141.8, 141.3, 134.8, 131.4, 128.2, 127.2, 125.7, 52.4, 46.0, 45.7 ppm; HRMS (ESI, Q-ToF) m/z : [M + Na]⁺ calcd for $\text{C}_{57}\text{H}_{51}\text{N}_3\text{O}_6\cdot\text{Na}$, 896.3670; found; 896.3678; IR (neat) $\tilde{\nu}_{\text{max}}$: 2342, 1709, 1512, 1183, 919, 736 cm^{-1} .

Synthesis of ring open metathesis (ROM) product **13**

The solution of compound **10** (500 mg, 1.76 mmol) in dry CH_2Cl_2 (25 mL) was degasified by ethylene and G-I (5 mol %) was added to the reaction mixture at rt. Further, the reaction mixture was stirred for 48 h under ethylene atmosphere at rt. After completion of the reaction (TLC monitoring), the solvent was removed under reduced pressure. Later, the crude product was purified by silica gel column chromatography (30% $\text{EtOAc}/\text{petroleum ether}$) to obtain the ROM product **13** as a colourless solid (310 mg, 56%); $R_f = 0.68$ (4:6 $\text{EtOAc}/\text{petroleum ether}$); mp 143–145 °C; ^1H NMR (400 MHz, CDCl_3) δ 8.03 (d, $J = 8.4$ Hz, 2H), 7.40 (d, $J = 8.4$ Hz, 2H), 6.12–6.03 (m, 2H), 5.20–5.15 (m, 4H), 3.43 (q, $J = 2.0$ Hz, 2H), 3.08–3.00 (m, 2H), 2.60 (s, 3H), 2.08–2.02 (m, 1H), 1.57 (t, $J = 6.4$ Hz, 1H) ppm; ^{13}C NMR (100 MHz, CDCl_3) δ 197.2, 175.4, 136.7, 136.2, 136.1, 129.2, 126.5, 116.3, 49.1, 46.4, 35.4, 26.8 ppm; HRMS (ESI, Q-ToF) m/z : [M + Na]⁺ calcd for $\text{C}_{19}\text{H}_{19}\text{NO}_3\cdot\text{Na}$, 332.1257; found, 332.1254; IR (neat) $\tilde{\nu}_{\text{max}}$: 2325, 1671, 1263, 746 cm^{-1} .

Synthesis of trimerized compound **12**

Based on the earlier procedure of trimerization, compound **13** (500 mg, 1.61 mmol) was treated with SiCl_4 (0.55 mL, 4.84 mmol) in the presence of EtOH (8 mL) for 16 h to afford trimerized product **12** after silica gel column chromatography (60% $\text{EtOAc}/\text{petroleum ether}$) as a colourless solid (254 mg, 54%); mp 152–154 °C; $R_f = 0.55$ (5:5 $\text{EtOAc}/\text{petroleum ether}$); ^1H NMR (400 MHz, CDCl_3) δ 7.72 (d, $J = 8.0$ Hz, 6H), 7.70 (s, 3H), 7.37 (d, $J = 8.4$ Hz, 6H), 6.15–6.07 (m, 6H), 5.19 (q, $J = 8.4$ Hz, 12H), 3.43 (dd, $J_1 = 2.0$ Hz, $J_2 = 2.0$ Hz, 6H),

3.07–2.99 (m, 6H), 2.04 (q, $J = 6.8$ Hz, 3H), 1.58 (q, $J = 13.2$ Hz, 3H) ppm; ^{13}C NMR (100 MHz, CDCl_3) δ 175.7, 141.7, 141.1, 136.4, 131.4, 128.1, 126.9, 125.6, 116.1, 49.1, 46.3, 35.5 ppm; HRMS (ESI, Q-ToF) m/z : [M + Na]⁺ calcd for $\text{C}_{57}\text{H}_{51}\text{N}_3\text{O}_6\cdot\text{Na}$, 896.3670; found; 896.3678; IR (neat) $\tilde{\nu}_{\text{max}}$: 2342, 1709, 1512, 1183, 919, 736 cm^{-1} .

Synthesis of trimerized product **19**

Based on the earlier procedure of trimerization, compound **18** (500 mg, 1.27 mmol) was treated with SiCl_4 (0.43 mL, 3.83 mmol) in the presence of EtOH (8 mL) for 20 h to give the trimerized product **19** after silica gel (100–200 mesh) column chromatography (50% $\text{EtOAc}/\text{petroleum ether}$) as a colourless solid (324 mg, 64%); $R_f = 0.61$ (4:6 $\text{EtOAc}/\text{petroleum ether}$); mp 224–226 °C; ^1H NMR (500 MHz, CDCl_3) δ 7.56 (s, 3H), 7.51 (d, $J = 8.0$ Hz, 6H), 7.43 (d, $J = 3.0$ Hz, 6H), 7.37 (d, $J = 3.0$ Hz, 6H), 7.24–7.22 (m, 12H), 6.62 (d, $J = 8.5$ Hz, 6H), 4.92 (s, 6H), 3.41 (s, 6H) ppm; ^{13}C NMR (125 MHz, CDCl_3) δ 176.3, 141.5, 141.4, 138.9, 128.2, 127.4, 127.1, 127.0, 125.3, 124.5, 47.2, 46.1 ppm; HRMS (ESI, Q-ToF) m/z : [M + Na]⁺ calcd for $\text{C}_{78}\text{H}_{51}\text{N}_3\text{O}_6\cdot\text{Na}$, 1148.3670; found, 1148.3672; IR (neat) $\tilde{\nu}_{\text{max}}$: 2318, 1266, 745, 707 cm^{-1} .

Synthesis of hexaallyl derivative **14**

To the solution of compound **12** (200 mg, 0.22 mmol) in anhydrous THF (15 mL) was added NaHMDS (2 mL of 1 M solution in THF , 1.93 mmol) at -75 °C and the reaction mixture was stirred for 30 min under nitrogen atmosphere. Then allyl bromide (0.11 mL, 1.60 mmol) was added to the reaction mixture and stirred for 2 h at -75 °C. Later, the reaction mixture was stirred to room temperature for 10 h. After completion of the reaction (TLC monitoring), the reaction mixture was quenched with 1 M aq HCl solution, and the aqueous layer was extracted by EtOAc (3×10 mL). Then the organic fraction was washed with brine solution, dried over Na_2SO_4 and concentrated. The crude residue was purified by silica gel column chromatography (10% $\text{EtOAc}/\text{petroleum ether}$) to afford hexaallyl derivative **14** as a colourless solid (199 mg, 78%); $R_f = 0.60$ (3:7 $\text{EtOAc}/\text{petroleum ether}$); mp 204–206 °C; ^1H NMR (500 MHz, CDCl_3) δ 7.71 (d, $J = 5.5$ Hz, 6H), 7.69 (s, 3H), 7.33 (d, $J = 8.5$ Hz, 6H), 6.08–5.96 (m, 12H), 5.28–5.13 (m, 24H), 2.77–2.66 (m, 18H), 2.04–2.00 (m, 3H), 1.65 (q, $J = 12.5$ Hz, 3H) ppm; ^{13}C NMR (125 MHz, CDCl_3) δ 178.2, 141.9, 141.3, 136.5, 132.8, 131.5, 128.1, 127.1, 125.7, 120.3, 117.1, 59.9, 51.2, 36.6, 35.1 ppm; HRMS (ESI, Q-ToF) m/z : [M + Na]⁺ calcd for $\text{C}_{75}\text{H}_{75}\text{N}_3\text{O}_6\cdot\text{Na}$, 1136.5548; found, 1136.5544; IR (neat) $\tilde{\nu}_{\text{max}}$: 2345, 1671, 1263, 746 cm^{-1} .

Synthesis of hexaallyl product **20**

Based on the earlier procedure of allylation, compound **19** (336 mg, 0.29 mmol) was treated with NaHMDS (2.3 mL of

1 M solution in THF, 2.39 mmol) and allyl bromide (0.14 mL, 1.93 mmol) for 17 h to deliver hexaallyl product **20** after silica gel column chromatography (20% EtOAc/petroleum ether) as a colourless solid (345 mg, 84%); R_f = 0.83 (2:8 EtOAc/petroleum ether); mp 195–197 °C; ^1H NMR (400 MHz, CDCl_3) δ 7.57 (s, 3H), 7.51 (d, J = 8.8 Hz, 6H), 7.40 (q, J = 3.2 Hz, 6H), 7.32 (q, J = 3.2 Hz, 6H), 7.24–7.20 (m, 12H), 6.58 (d, J = 8.0 Hz, 6H), 6.33–6.23 (m, 6H), 5.20 (dd, J_1 = 11.6 Hz, J_2 = 17.2 Hz, 12H), 4.68 (s, 6H), 2.45 (dd, J_1 = 5.6 Hz, J_2 = 5.6 Hz, 6H), 2.16 (q, J = 8.8 Hz, 6H) ppm; ^{13}C NMR (100 MHz, CDCl_3) δ 178.5, 141.7, 141.4, 139.9, 139.4, 133.6, 131.0, 128.1, 127.2, 127.1, 126.7, 126.5, 125.6, 125.3, 119.4, 55.7, 51.6, 37.3 ppm; HRMS (ESI, Q-ToF) m/z : [M + Na]⁺ calcd for $\text{C}_{96}\text{H}_{75}\text{N}_3\text{O}_6\text{Na}$, 1388.5548; found, 1389.5585; IR (neat) $\tilde{\nu}_{\text{max}}$: 2925, 2335, 1706, 1461, 1376, 1273, 741 cm^{-1} .

General procedure for ring-closing metathesis (RCM)

The solution of hexaallyl derivatives **14** or **20** in dry CH_2Cl_2 (20 mL) was degassed by nitrogen and G-II (10 mol %) was added to the reaction mixture. Further, the reaction mixture was stirred for 6 h under nitrogen atmosphere at room temperature. After completion of the reaction (TLC monitoring), the solvent was removed under reduced pressure. The crude product was purified by silica gel column chromatography (EtOAc/petroleum ether) to afford the propellane bearing C_3 -symmetric products **15** or **21**.

Synthesis of RCM derivative **15**

Colourless solid, 87% (121 mg, starting with 150 mg of hexaallyl compound **14**); R_f = 0.60 (3:7 EtOAc/petroleum ether); mp 272–275 °C; ^1H NMR (400 MHz, CDCl_3) δ 7.71 (d, J = 2.0 Hz, 6H), 7.69 (s, 3H), 7.35 (d, J = 8.4 Hz, 6H), 6.08–5.99 (m, 12H), 5.18–5.14 (m, 12H), 2.76 (dd, J_1 = 4.0 Hz, J_2 = 3.2 Hz, 6H), 2.67–2.61 (m, 6H), 2.23 (dd, J_1 = 2.0 Hz, J_2 = 2.0 Hz, 6H), 2.04–1.98 (m, 3H), 1.58 (q, J = 12.8, 3H) ppm; ^{13}C NMR (100 MHz, CDCl_3) δ 178.2, 141.8, 141.2, 136.2, 131.6, 128.5, 128.1, 126.9, 125.7, 116.4, 58.7, 53.3, 35.7, 30.9 ppm; HRMS (ESI, Q-ToF) m/z : [M + Na]⁺ calcd for $\text{C}_{69}\text{H}_{63}\text{N}_3\text{O}_6\text{Na}$, 1052.4609; found, 1052.4617; IR (neat) $\tilde{\nu}_{\text{max}}$: 2305, 1651, 1363, 844 cm^{-1} .

Synthesis of RCM derivative **21**

Colourless solid, 91% (258 mg, starting with 300 mg of hexaallyl product **20**); R_f = 0.75 (3:7 EtOAc/petroleum ether); mp 264–267 °C; ^1H NMR (400 MHz, CDCl_3) δ 7.56 (s, 3H), 7.49 (d, J = 6.8 Hz, 6H), 7.43 (d, J = 2.4 Hz, 6H), 7.34 (d, J = 2.4 Hz, 6H), 7.25–7.23 (m, 12H), 6.57 (d, J = 7.6 Hz, 6H), 5.83 (s, 6H), 4.47 (s, 6H), 2.90 (d, J = 14.4 Hz, 6H), 1.80 (d, J = 14.8 Hz, 6H) ppm; ^{13}C NMR (100 MHz, CDCl_3) δ 180.0, 141.6, 141.4, 140.4, 140.2, 131.2, 128.0, 127.9, 127.2, 127.1,

127.0, 126.5, 125.6, 125.2, 57.4, 51.5, 30.2 ppm; HRMS (ESI, Q-ToF) m/z : [M + K]⁺ calcd for $\text{C}_{90}\text{H}_{63}\text{N}_3\text{O}_6\text{K}$, 1320.4348; found, 1320.4344; IR (neat) $\tilde{\nu}_{\text{max}}$: 2328, 1708, 1383, 837, 690 cm^{-1} .

Supporting Information

Supporting Information File 1

Copies of ^1H , ^{13}C NMR and HRMS spectra of new compounds.

[<https://www.beilstein-journals.org/bjoc/content/supplementary/1860-5397-14-230-S1.pdf>]

Acknowledgements

We thank the Department of Science and Technology (DST), New Delhi, India, for financial support and IIT Bombay, for recording spectral data. S.K. thanks the Department of Science and Technology for the award of a J. C. Bose fellowship (SR/S2/JCB-33/2010), Praj industries, Pune for Pramod Chaudhari Chair Professorship (Green Chemistry) and CSIR (02(0272)/16/EMR-II). S.T. thanks the IIT Bombay for the award of a research fellowship. V.R.A. thanks the CSIR-New Delhi and IIT Bombay for the award of a research fellowship.

ORCID® IDs

Sambasivarao Kotha - <https://orcid.org/0000-0002-7173-0233>

Saidulu Todeti - <https://orcid.org/0000-0001-5244-7558>

Vikas R. Aswar - <https://orcid.org/0000-0002-2932-1815>

References

- Altman, J.; Babad, E.; Itzchaki, J.; Ginsburg, D. *Tetrahedron* **1966**, *22*, 279–304. doi:10.1016/S0040-4020(01)82189-X
- Ginsburg, D. *Acc. Chem. Res.* **1969**, *2*, 121–128. doi:10.1021/ar50016a005
- Wiberg, K. B. *Acc. Chem. Res.* **1984**, *17*, 379–386. doi:10.1021/ar00107a001
- Wiberg, K. B. *Acc. Chem. Res.* **1996**, *29*, 229–234. doi:10.1021/ar950207a
- Weber, R. W.; Cook, J. M. *Can. J. Chem.* **1978**, *56*, 189–192. doi:10.1139/v78-030
- Schneider, L. M.; Schmiedel, V. M.; Pecchioli, T.; Lenz, D.; Merten, C.; Christmann, M. *Org. Lett.* **2017**, *19*, 2310–2313. doi:10.1021/acs.orglett.7b00836
- Carroll, A. R.; Arumugan, T.; Redburn, J.; Ngo, A.; Guymer, G. P.; Forster, P. I.; Quinn, R. J. *J. Nat. Prod.* **2010**, *73*, 988–991. doi:10.1021/np100009j
- Brown, K., Jr.; Budzikiewicz, H.; Djerassi, C. *Tetrahedron Lett.* **1963**, *4*, 1731–1736. doi:10.1016/S0040-4039(01)90904-9
- Walser, A.; Djerassi, C. *Helv. Chim. Acta* **1965**, *48*, 391–404. doi:10.1002/hlca.19650480220
- Asahi, K.; Nishino, H. *Tetrahedron* **2008**, *64*, 1620–1634. doi:10.1016/j.tet.2007.12.017

11. Diels, O.; Alder, K. *Chem. Ber.* **1929**, *62*, 2081–2087. doi:10.1002/cber.19290620829

12. Diels, O.; Alder, K. *Justus Liebigs Ann. Chem.* **1931**, *486*, 191–202. doi:10.1002/jlac.19314860110

13. Yamamoto, N.; Fujii, H.; Nemoto, T.; Nakajima, R.; Momen, S.; Izumimoto, N.; Hasebe, K.; Mochizuki, H.; Nagase, H. *Bioorg. Med. Chem. Lett.* **2011**, *21*, 4104–4107. doi:10.1016/j.bmcl.2011.04.147

14. Alizadeh, A.; Bayat, F.; Sadeghi, V. *Lett. Org. Chem.* **2015**, *12*, 153–158. doi:10.2174/1570178612666150108003359

15. Pihko, A. J.; Koskinen, A. M. *Tetrahedron* **2005**, *61*, 8769–8807. doi:10.1016/j.tet.2005.06.013

16. Yavari, I.; Khajeh-Khezri, A. *Mol. Diversity* **2017**, *21*, 849–854. doi:10.1007/s11030-017-9761-8

17. Kotha, S.; Chinnam, A. K.; Tiwari, A. *Beilstein J. Org. Chem.* **2013**, *9*, 2709–2714. doi:10.3762/bjoc.9.307

18. Kotha, S.; Manivannan, E.; Ganesh, T.; Sreenivasachary, N.; Deb, A. *Synlett* **1999**, 1618–1620. doi:10.1055/s-1999-2896

19. Kotha, S.; Chakraborty, K.; Brahmachary, E. *Synlett* **1999**, 1621–1623. doi:10.1055/s-1999-2895

20. Dash, B. P.; Satapathy, R.; Maguire, J. A.; Hosmane, N. S. *Org. Lett.* **2008**, *10*, 2247–2250. doi:10.1021/o18005248

21. Dash, B. P.; Satapathy, R.; Gaillard, E. R.; Maguire, J. A.; Hosmane, N. S. *J. Am. Chem. Soc.* **2010**, *132*, 6578–6587. doi:10.1021/ja101845m

22. Kashiki, T.; Kohara, M.; Osaka, I.; Miyazaki, E.; Takimiya, K. *J. Org. Chem.* **2011**, *76*, 4061–4070. doi:10.1021/jo2005044

23. Mbyas Saroukou, M. S.; Skalski, T.; Skene, W. G.; Lubell, W. D. *Tetrahedron* **2014**, *70*, 450–458. doi:10.1016/j.tet.2013.11.043

24. Dash, J.; Trawny, D.; Rabe, J. P.; Reissig, H.-U. *Synlett* **2015**, *26*, 1486–1489. doi:10.1055/s-0034-1380716

25. Preis, E.; Dong, W.; Brunklaus, G.; Scherf, U. *J. Mater. Chem.* **2015**, *3*, 1582–1587. doi:10.1039/C4TC02664K

26. Shah, S. R.; Thakore, R. R.; Vyas, T. A.; Sridhar, B. *Synlett* **2016**, *27*, 294–300. doi:10.1055/s-0035-1560576

27. Kotha, S.; Todeti, S.; Gopal, M. B.; Datta, A. *ACS Omega* **2017**, *2*, 6291–6297. doi:10.1021/acsomega.7b00941

28. Kotha, S.; Todeti, S.; Das, T.; Datta, A. *ChemistrySelect* **2018**, *3*, 136–141. doi:10.1002/slct.201702675

29. Kotha, S.; Todeti, S.; Das, T.; Datta, A. *Tetrahedron Lett.* **2018**, *59*, 1023–1027. doi:10.1016/j.tetlet.2018.01.084

30. Thallapally, P. K.; Chakraborty, K.; Carrell, H. L.; Kotha, S.; Desiraju, G. R. *Tetrahedron* **2000**, *56*, 6721–6728. doi:10.1016/S0040-4020(00)00493-2

31. Justin Thomas, K. R.; Lin, J. T.; Tao, Y.-T.; Ko, C.-W. *Chem. Mater.* **2002**, *14*, 1354–1361. doi:10.1021/cm010976q

32. Shirota, Y. *J. Mater. Chem.* **2000**, *10*, 1–25. doi:10.1039/A908130E

33. Kimura, M.; Kuwano, S.; Sawaki, Y.; Fujikawa, H.; Noda, K.; Taga, Y.; Takagi, K. *J. Mater. Chem.* **2005**, *15*, 2393–2398. doi:10.1039/b502268a

34. Yu, G.; Gao, J.; Hummelen, J. C.; Wudl, F.; Heeger, A. J. *Science* **1995**, *270*, 1789–1791. doi:10.1126/science.270.5243.1789

35. Hoang, M. H.; Cho, M. J.; Kim, D. C.; Kim, K. H.; Shin, J. W.; Cho, M. Y.; Joo, J.-s.; Choi, D. H. *Org. Electron.* **2009**, *10*, 607–617. doi:10.1016/j.orgel.2009.02.021

36. Ponomarenko, S. A.; Kirchmeyer, S.; Elschner, A.; Huisman, B.-H.; Karbach, A.; Drechsler, D. *Adv. Funct. Mater.* **2003**, *13*, 591–596. doi:10.1002/adfm.200304363

37. Fringuelli, F.; Taticchi, A. *Dienes in the Diels–Alder Reaction*; Wiley: New York, 1990.

38. Shafi, S.; Kędziora, M.; Grela, K. *Synlett* **2011**, 124–128. doi:10.1055/s-0030-1259083

39. Grubbs, R. H.; O’Leary, D. J. *Handbook of Metathesis, Application in Organic Synthesis*, 2nd ed.; Wiley-VCH: Weinheim, Germany, 2015.

40. Kotha, S.; Aswar, V. R. *Org. Lett.* **2016**, *18*, 1808–1811. doi:10.1021/acs.orglett.6b00537

41. Kotha, S.; Shah, V. R.; Mandal, K. *Adv. Synth. Catal.* **2007**, *349*, 1159–1172. doi:10.1002/adsc.200600469

42. Kiriazis, A.; af Gennäs, G. B.; Talman, V.; Ekokoski, E.; Ruotsalainen, T.; Kylälahti, I.; Rüffer, T.; Wissel, G.; Xhaard, H.; Lang, H.; Tuominen, R. K.; Yli-Kauhaluoma, J. *Tetrahedron* **2011**, *67*, 8665–8670. doi:10.1016/j.tet.2011.09.044

43. Kocyigit, U. M.; Budak, Y.; Gürdere, M. B.; Tekin, Ş.; Köprülü, T. K.; Ertürk, F.; Özcan, K.; Gülcin, İ.; Ceylan, M. *Bioorg. Chem.* **2017**, *70*, 118–125. doi:10.1016/j.bioorg.2016.12.001

44. Marsh, B. J.; Adams, H.; Barker, M. D.; Kutama, I. U.; Jones, S. *Org. Lett.* **2014**, *16*, 3780–3783. doi:10.1021/o15016702

45. Obermayer, D.; Znidar, D.; Glotz, G.; Stadler, A.; Dallinger, D.; Kappe, C. O. *J. Org. Chem.* **2016**, *81*, 11788–11801. doi:10.1021/acs.joc.6b02242

License and Terms

This is an Open Access article under the terms of the Creative Commons Attribution License (<http://creativecommons.org/licenses/by/4.0>). Please note that the reuse, redistribution and reproduction in particular requires that the authors and source are credited.

The license is subject to the *Beilstein Journal of Organic Chemistry* terms and conditions: (<https://www.beilstein-journals.org/bjoc>)

The definitive version of this article is the electronic one which can be found at:
doi:10.3762/bjoc.14.230



Ring-opening metathesis of some strained bicyclic systems; stereocontrolled access to diolefinated saturated heterocycles with multiple stereogenic centers

Zsanett Benke¹, Melinda Nonn^{1,2}, Márton Kardos¹, Santos Fustero³ and Loránd Kiss^{*1}

Full Research Paper

Open Access

Address:

¹Institute of Pharmaceutical Chemistry, University of Szeged, Eötvös u. 6, H-6720 Szeged, Hungary, ²MTA-SZTE Stereochemistry Research Group, Hungarian Academy of Sciences, Eötvös u. 6, H-6720 Szeged, Hungary and ³Departamento de Química Orgánica, Facultad de Farmacia, Universidad de Valencia, Av. Vicente Andrés Estellés, s/n 46100 Valencia, Spain

Email:

Loránd Kiss* - kiss.lorand@pharm.u-szeged.hu

* Corresponding author

Keywords:

functionalization; heterocycles; metathesis; ring opening; stereogenic centers

Beilstein J. Org. Chem. **2018**, *14*, 2698–2707.

doi:10.3762/bjoc.14.247

Received: 31 July 2018

Accepted: 10 October 2018

Published: 24 October 2018

This article is part of the thematic issue "Progress in metathesis chemistry III".

Guest Editor: K. Grela

© 2018 Benke et al.; licensee Beilstein-Institut.

License and terms: see end of document.

Abstract

Ring-opening metathesis (ROM) of various unsaturated, constrained bicyclic ring systems has been investigated with the use of commercial ruthenium-based catalysts. Starting from various cyclodienes, the corresponding derived bicyclic lactone, lactam, and isoxazoline derivatives were submitted to ROM under ethenolysis. These functionalized, strained bicyclic systems afforded novel highly-functionalized diolefinated heterocyclic scaffolds in ROM reactions with stereocontrol, through the conservation of the configuration of the stereogenic centers of the starting compounds.

Introduction

Metathesis reactions, among them ring-opening metathesis (ROM), have received a great deal of attention in synthetic organic chemistry, affording access to various highly functionalized, alkenylated molecular entities [1-10].

Highly functionalized three-dimensional organic scaffolds with multiple stereogenic centers as small molecular entities represent an important segment of organic and pharmaceutical chemistry. Therefore, selective syntheses with stereocontrol of such

scaffolds [11,12], such as highly-functionalized olefinated derivatives [13], are of main importance and a major challenge in synthetic organic chemistry. Thus, ring-opening metathesis is a powerful and widely applied methodology for the synthesis of such derivatives, including alkenylated molecular scaffolds with multiple stereogenic centers [14-16] and references cited therein. Diversity-oriented synthesis (DOS), with the aim of the preparation of structurally diverse elements of small molecules, has become increasingly important in drug research, and well

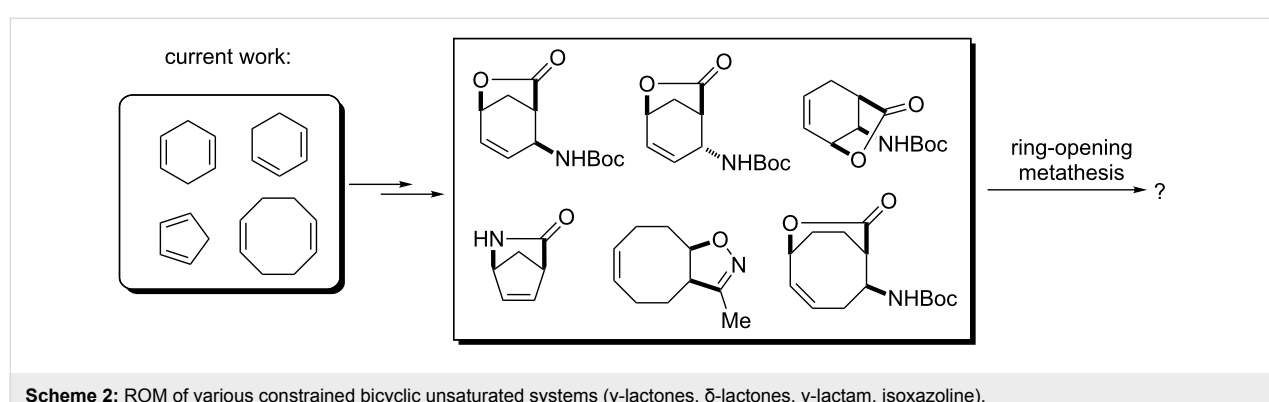
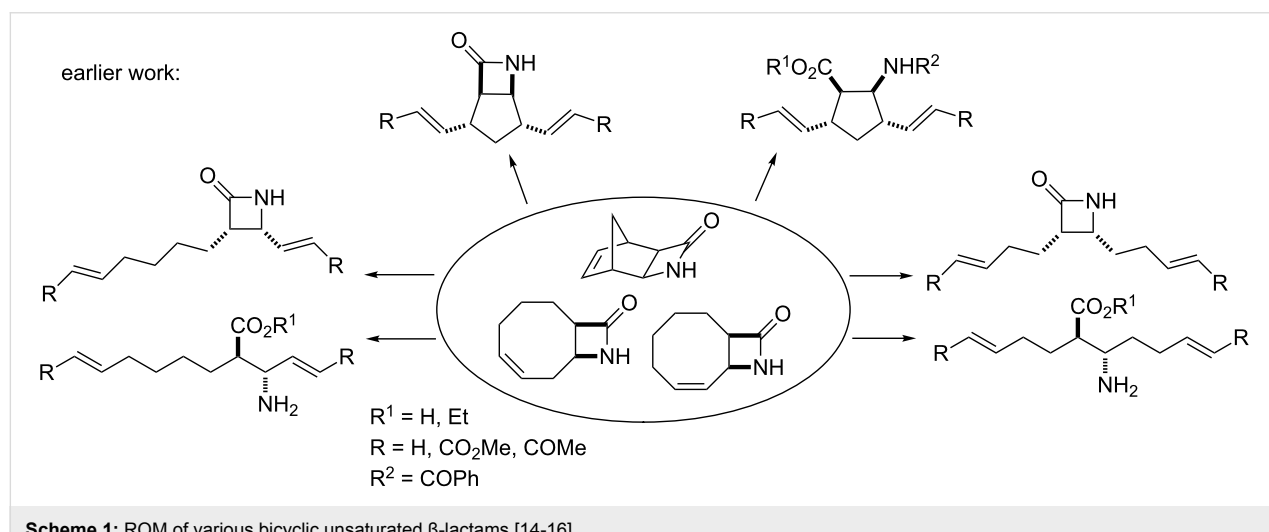
recognized as a common approach to generate molecular libraries. Results with respect to the various strategies utilized in DOS with special focus on selective and stereocontrolled methods have been published [17–20]. The major features of these studies are the use of readily available and easily accessible starting materials towards the construction of diverse and complex scaffolds and the application of the resulting compound collections in drug discovery.

Since their ring C–C double bond offers a number of possible chemical transformations, cyclic dienes with different ring sizes might be considered to be important starting materials for the generation of structurally diverse molecules. Among the large number of possible transformations, the ring olefinic bond of alicyclic dienes may lead to valuable β -lactams [21–23] or γ -lactams [24], shown to be highly important precursors for the access of various structures (e.g., amino acids, azido esters, hydroxylated amino esters, fluorinated amino esters, etc.) with various functional groups as well as stereochemical and skeletal diversity [21–23].

Results and Discussion

Recently, we have demonstrated the high utility of various constrained cyclic dienes, such as norbornadiene as well as 1,5- and 1,3-cyclooctadienes in the context of their applicability towards the access of diverse, highly functionalized olefinated molecules [14–16]. The corresponding β -lactams derived from cyclo-dienes were used as starting substances for further functionalization with ROM. We have described a stereocontrolled synthetic route to access difunctionalized cyclic β -amino acid derivatives [14] and β -lactams [15,16] based on ring-opening metathesis (ROM) through ethenolysis of the structurally restricted cycloalkene β -amino acids or unsaturated bicyclic β -lactams, followed by cross-coupling metathesis (CM) of the newly created C–C double bonds (Scheme 1).

Our current goal was to expand the study of the ROM protocol of functionalized strained ring systems to the investigation of functionalized derivatives such as bicyclic lactones, γ -lactams or isoxazolines, derived from various cyclodienes and to evaluate their chemical behavior under Ru-catalyzed ring-opening conditions (Scheme 2).



First, the ring opening of racemic bicyclic γ -lactone (\pm) -3 (derived from cyclodiene **1** via β -lactam (\pm) -2) [25] was investigated. Ring opening was performed in ethylene atmosphere at 20 °C in the presence of four commercially available Ru-based catalysts (5 mol %, Figure 1). Note that based on our earlier results [15], bicyclic unsaturated lactam (\pm) -2 bearing the azetidinone ring fused with a six-membered ring system thus possessing ring strain, did not afford any ROM products. Inter-

estingly, lactone (\pm) -3 in the presence of second generation catalysts (G-2 and HG-2) provided the corresponding ring-opened compound (\pm) -5 albeit with modest yields (Scheme 3, Table 1).

In the presence of G-2 and HG-2 catalysts, bicyclic lactone (\pm) -4 a stereoisomer of (\pm) -3 furnished olefinated γ -lactone (\pm) -6 similar to (\pm) -5 (Scheme 3, Table 2). Unfortunately, ROM

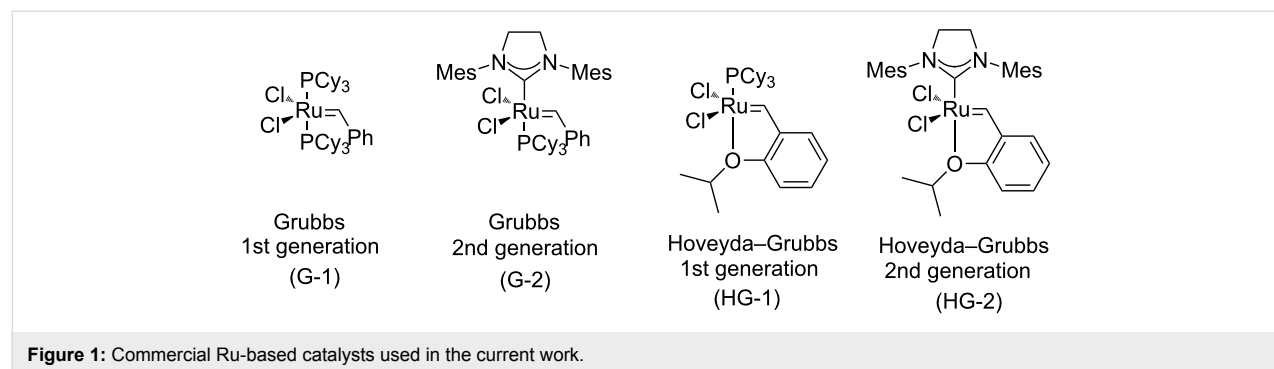
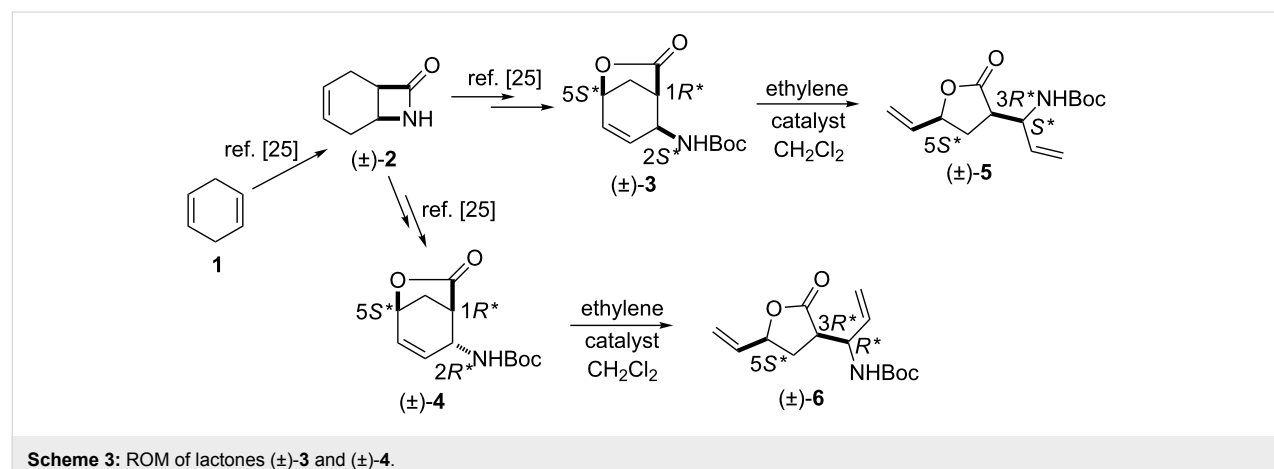


Figure 1: Commercial Ru-based catalysts used in the current work.



Scheme 3: ROM of lactones (\pm) -3 and (\pm) -4.

Table 1: Isolated yields for compound (\pm) -5 formed in the ring-opening reaction of lactone (\pm) -3 with ethylene in ROM reactions with various catalysts.

catalyst	G-1 catalyst	G-2 catalyst	HG-1 catalyst	HG-2 catalyst
product				
(\pm) -5	0%	21%	0%	25%

Table 2: Isolated yields for compound (\pm) -6 formed in the ring-opening reaction of lactone (\pm) -4 with ethylene in ROM reactions with various catalysts.

catalyst	G-1 catalyst	G-2 catalyst	HG-1 catalyst	HG-2 catalyst
product				
(\pm) -6	0%	26%	traces	36%

reactions, however, took place with total conversions, they were always accompanied by the formation of a significant amount of polymeric materials (ROMP) responsible for the observed modest yields of these reactions. Noteworthy, neither the variation of the catalyst loading (amount or in portion) nor the substrate concentration (in 5, 10, 20 or 30 mL of solvent) had any significant influence on the yield of the products.

Next, racemic lactone (\pm) -9 (synthesized from 1,3-cyclohexadiene (7) through lactam (\pm) -8) [26] was subjected to ring-opening reactions with all four catalysts.

It should be noted again, that based on our earlier findings [15], bicyclic lactam (\pm) -8 did not provide any ring-opened product, while bicyclic lactone (\pm) -9 could be opened with G-2 and HG-2 catalysts (5 mol %) affording olefinated amino lactone (\pm) -10 at 20 °C. Notably, the yield of the transformation with catalyst HG-2 to obtain lactone derivative (\pm) -10 was twice as high as in the case of G-2 (Scheme 4, Table 3).

From the above comparative results it may be assumed that unsaturated bicyclic β -lactams (\pm) -2 and (\pm) -8, bearing the fused four-membered and six-membered ring system, have a lower ring strain than bicyclic, unsaturated γ -lactones (\pm) -3, (\pm) -4 and (\pm) -9. Because of their higher constraint, the latter compounds underwent ring opening providing the corresponding monocyclic, dialkenylated amino lactones, albeit with modest yields (Scheme 5); (for relevant literature date for the ROM for various cyclic systems with ring strain see ref. [27-29].

We continued our ring-opening investigations with other model derivatives possessing a larger ring system. According to results published previously [15] and in contrast with bicyclic cyclo-

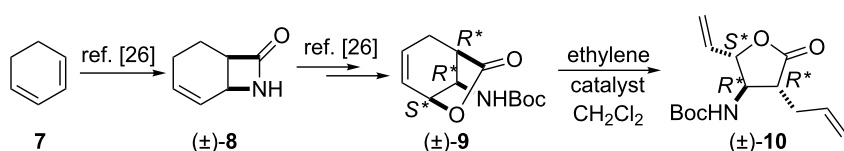
hexene-fused lactams (\pm) -2 and (\pm) -8, lactam (\pm) -12 [30], derived from 1,5-cyclooctadiene, afforded the corresponding dialkenylated ring-opened product under ROM protocol.

The isolated yields of (\pm) -15 were higher than those of the analogous cyclohexene systems in the presence of both G-2 and HG-2 catalysts because of the higher ring strain of the eight-membered framework. Bicyclic, unsaturated bridged lactone (\pm) -14 (derived from (\pm) -12) underwent ring-opening not only with second generation catalysts but also with HG-1 (5 mol %), leading at 20 °C to δ -lactone derivative (\pm) -15 although with low yield (Scheme 6, Table 4). In continuation, we selected a cyclooctene-fused system, namely isoxazoline (\pm) -16 which, in turn, was accessed through nitrile–oxide dipolar cycloaddition, by using nitroethane, DMAP and Boc_2O .

Ring opening proved to be successful with second generation catalysts, yielding the corresponding diolefinated isoxazoline (\pm) -17 (Scheme 6).

Our studies were continued with the ROM reactions of conformationally restricted γ -lactam (\pm) -18 (Vince's lactam) as model compound [24]. The ring opening in ethylene atmosphere of bridged pyrrolidinone (\pm) -18 took place at 20 °C and afforded the corresponding divinylated lactam (\pm) -19 [31,32]. Somewhat surprisingly, in contrast to model derivatives used previously, the highest yield (70%) was attained with first generation catalyst HG-1 (5 mol %). In the presence of the second generation catalysts, in turn, the ring-opened pyrrolidinone derivative (\pm) -19 could be isolated only in low yields (Scheme 7, Table 5).

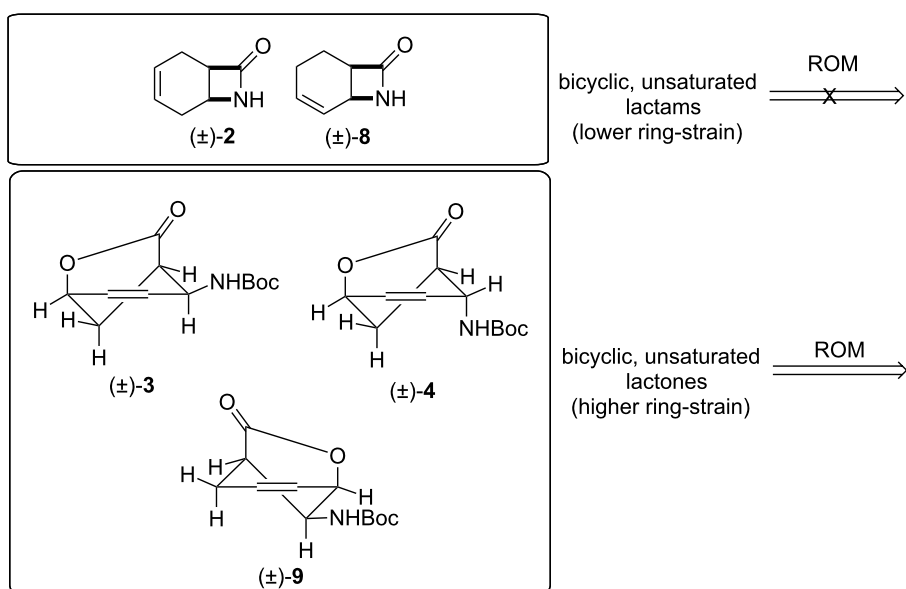
As observed, the ROM reactions of the investigated unsaturated cyclic substrates (namely (\pm) -3, (\pm) -4, (\pm) -9, (\pm) -14,



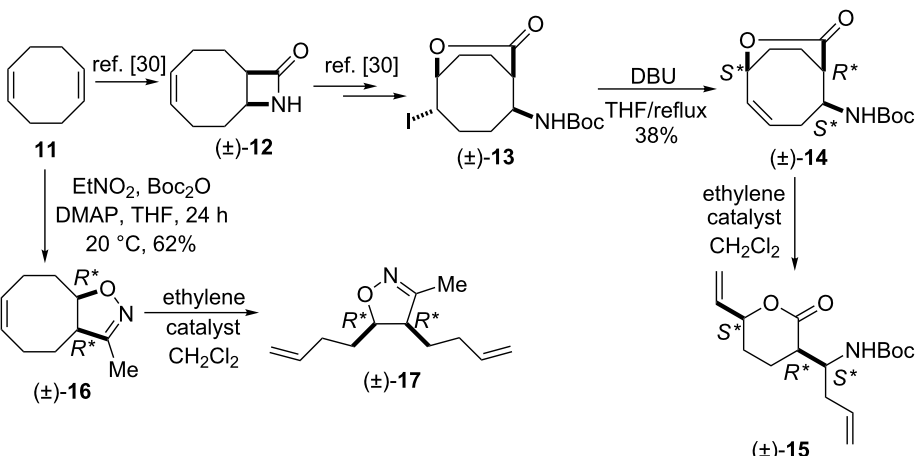
Scheme 4: ROM of lactones (\pm) -9.

Table 3: Isolated yields for compound (\pm) -10 formed in the ring-opening reaction of lactone (\pm) -9 with ethylene in ROM reactions with various catalysts.

catalyst	G-1 catalyst	G-2 catalyst	HG-1 catalyst	HG-2 catalyst
product				
(\pm) -10	0%	16%	traces	35%



Scheme 5: ROM of structurally constrained bicyclic lactones and lactams.



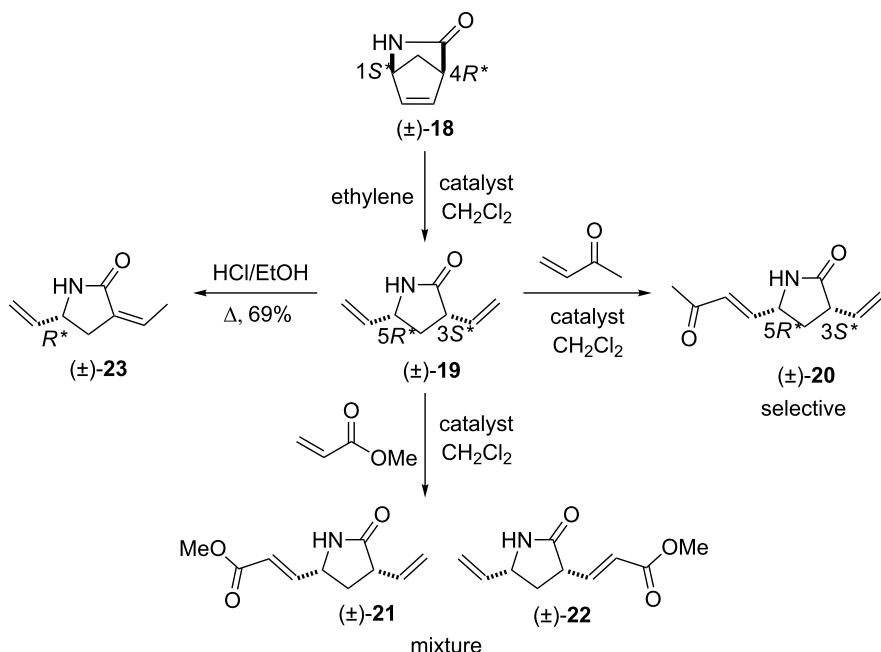
Scheme 6: ROM of bridged lactone (±)-14 and cyclooctene-fused isoxazoline (±)-16.

Table 4: Isolated yields for compounds formed in the ring-opening reaction of lactone (±)-14 and isoxazoline (±)-16 with ethylene in ROM reactions with various catalysts.

catalyst	G-1 catalyst	G-2 catalyst	HG-1 catalyst	HG-2 catalyst
product				
(±)-15	0%	52%	11%	59%
(±)-17	38%	–	–	0%

(±)-16 and (±)-18) gave different results in view of the used Ru-based catalyst, which allowed us to conclude that all these transformations are highly substrate and catalyst dependent, the

nature of the structure of the cyclic starting material determining the outcome of the transformations. It is well known that the prediction of the behavior of the catalyst efficiency is a



Scheme 7: ROM and transformations of lactam (±)-18.

Table 5: Isolated yields for compound (±)-19 formed in the ring-opening reaction of lactam (±)-18 with ethylene in ROM reactions with various catalysts.

catalyst	G-1 catalyst	G-2 catalyst	HG-1 catalyst	HG-2 catalyst
product				
(±)-19	9%	29%	70%	15%

rather difficult task. Metathesis reactions are known to be often catalyst or substrate dependent. Electronic or steric factors, and chelation effects may contribute to the outcome of metathesis in view of the yield. Moreover, possible H-bonding interactions in the intermediate phase between the catalyst chlorine and the substrate may be responsible for the accomplishments of the reactions, which were deeply investigated and discussed in the literature [33–37] and see references therein. In our case it was observed that the imidazole carbene-based catalysts (G-2 and HG-2) were effective in case of bridged lactones with a six-membered ring part in their framework, with O-functionalities (±)-3, (±)-4, (±)-9 and (±)-14. In case of isoxazoline-fused derivative (±)-16 G-1 gave the best result, while in case of lactam (±)-18 HG-1 was the most efficient. The observed results regarding the current ROM processes were somewhat surprising, the overall comparison of these experimental investigations in the ROM may depend strongly on the structure of the substrates.

The valuable dialkenylated compounds (lactones, lactams, isoxazolines) with multiple stereogenic centers thus synthesized can be considered interesting scaffolds for further transformations in view of the access of novel three-dimensional functionalized scaffolds through cross-metathesis (CM). An illustrative example is shown on Scheme 7. Divinylated γ -lactam (±)-19 selected as a model compound was first subjected to CM with methyl acrylate. When the reaction was performed in the presence of Ru-based catalysts, in CH_2Cl_2 , either at reflux temperature or at 20 °C, it gave a mixture of monometathesised products ((±)-21 and (±)-22) after 6 h together with a large amount of polymeric materials.

The products could not be separated by means of chromatography. Interestingly, however, the CM of (±)-19 with methyl vinyl ketone induced by G-2, HG-1 or HG-2, afforded a single derivative, monometathesised compound (±)-20 bearing the oxo group closest to the amide N-atom (Scheme 7, Table 6). Com-

Table 6: Isolated yields for compound (\pm) -20 formed in the reaction of lactam (\pm) -19 in CM reactions with various catalysts.

catalyst	G-1 catalyst	G-2 catalyst	HG-1 catalyst	HG-2 catalyst
product				
(\pm) -20	0%	5%	19%	28%

ound (\pm) -20 was formed in low yields and *E*-selectively with the chemodiscrimination of the olefinic bonds. The observed low yields for the formation of (\pm) -20 might be explained by stereoelectronic factors. The coordinating ability of both the O- and N-atom of the amide with the Ru atom in the metalla-cyclobutane intermediate may reduce the reactivity of the olefinic bonds. Furthermore, the chelating ability of the amide heteroatoms is also assumed to be responsible for the chemodiscrimination of the vinyl groups. Namely, the chelating five-membered structure **T1** is more favored than **T2** and, therefore, the vinyl group closest to the ring N-atom becomes more reactive in cross-metathesis (Figure 2).

catalysts. The bicyclic systems, derived from various cyclodienes, such as lactone, lactam or isoxazoline derivatives, were investigated under ROM through ethenolysis, which afforded novel dialkenylated scaffolds formed under stereocontrol with the conservation of the configuration of the stereogenic centers. The resulting diolefinated aminolactones, isoxazolines or lactam derivatives with multiple stereogenic centers might be considered to be interesting highly-functionalized three-dimensional compounds for further derivatizations. Extensions of the ROM of various bicyclic, conformationally restricted derivatives are currently being studied by our group.

Experimental

General procedure for the ring-opening metathesis

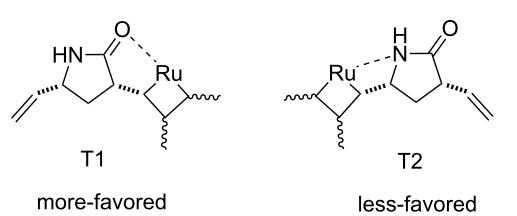
To a solution of bicyclic olefin derivative (150 mg) in anhydrous CH_2Cl_2 (20 mL) the catalyst (5 mol %) was added (see Tables) and the mixture was stirred at 20 °C in the presence of an ethylene atmosphere for the time indicated in the text (monitored by TLC). After completion of the reaction, the mixture was concentrated under vacuum and purified by column chromatography on silica gel (*n*-hexane/EtOAc).

General procedure for cross-metathesis

To a solution of γ -lactam derivative (80 mg) in anhydrous CH_2Cl_2 (15 mL), catalyst (5 mol %, see Table) and methyl vinyl ketone or methyl acrylate (4 equiv) were added and the mixture was stirred for the time and temperature indicated in text. After completion of the reaction (monitored by TLC), the mixture was concentrated under vacuum and the residue was purified by column chromatography on silica gel (*n*-hexane/EtOAc).

General procedure for the nitrile–oxide cycloaddition

To a solution of 1,5-cyclooctadiene (1.5 mmol) in THF (20 mL), EtNO_2 (5 equiv), DMAP (0.3 mmol, 20 mol %) and Boc_2O (4.5 mmol, 3 equiv) were added and the mixture was stirred at 20 °C for 24 h. The reaction mixture was then diluted with H_2O (30 mL) and extracted with EtOAc (3 × 15 mL). The

**Figure 2:** Chelate intermediates in CM of (\pm) -19.

Similar chemodiscriminations of C–C double bonds were previously observed in the transformation of various alkenylated lactams or amino esters [16]. Lactams are known to be useful precursors for the preparation of amino acids and amino esters [21,22]. When compound (\pm) -19 was subjected to either acid-catalyzed hydrolysis or ethanolysis at reflux, it furnished a pyrrolidinone derivative identified as (\pm) -23, instead of the expected product (amino acids or amino ester) formed via the opening of the heteroring, (Scheme 7). The process involves isomerization through olefin bond migration proceeding *Z*-selectively.

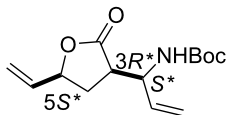
Conclusion

The ring-opening metathesis (ROM) of some ring-constrained, unsaturated bicyclic frameworks has been studied in the presence of commercially available ruthenium-based

combined organic layer was washed with brine (2×20 mL), dried (Na_2SO_4) and concentrated under vacuum. The crude residue was purified by column chromatography on silica gel (*n*-hexane/EtOAc).

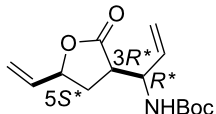
Characterization of the synthesized substances

tert-Butyl ((S^{*})-1-((3R^{*},5S^{*})-2-oxo-5-vinyltetrahydrofuran-3-yl)allyl)carbamate ((\pm)-5).



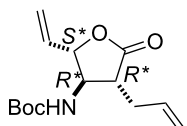
Yellow oil; yield 25%; R_f 0.70 (*n*-hexane/EtOAc 2:1); ^1H NMR (CDCl_3 , 400 MHz) δ 1.41 (s, 9H, *t*-Bu), 1.82–1.88 (m, 1H, CH_2), 2.40–2.47 (m, 1H, CH_2), 2.98–3.06 (m, 1H, H-3), 4.33–4.39 (m, 1H, CHN), 4.78–4.84 (m, 1H, H-5), 5.23–5.32 (m, 4H, CH=), 5.66–5.82 (m, 3H, CH= and NH); ^{13}C NMR (CDCl_3 , 100 MHz) δ 29.0, 29.7, 44.7, 52.5, 79.4, 80.1, 118.7, 119.3, 134.8, 135.1, 155.1, 174.2; MS (ESI, pos) (*m/z*): 288 [M + 1], 168 [M – Boc]; anal. calcd for $\text{C}_{14}\text{H}_{21}\text{NO}_4$: C, 62.90; H, 7.92; N, 5.24; found, C, 62.59; H, 7.60; N, 4.86.

tert-Butyl ((R^{*})-1-((3R^{*},5S^{*})-2-oxo-5-vinyltetrahydrofuran-3-yl)allyl)carbamate ((\pm)-6).



Yellow oil; yield 36%; R_f 0.72 (*n*-hexane/EtOAc 2:1); ^1H NMR (CDCl_3 , 400 MHz) δ 1.47 (s, 9H, *t*-Bu), 1.94–1.99 (m, 1H, CH_2), 2.46–2.51 (m, 1H, CH_2), 3.00–3.09 (m, 1H, H-3), 4.48–4.54 (m, 1H, CHN), 4.73–4.85 (m, 2H, H-5 and NH), 5.27–5.33 (m, 3H, CH=), 5.40–5.46 (m, 1H, CH=), 5.77–6.01 (m, 2H, CH=); ^{13}C NMR (CDCl_3 , 100 MHz) δ 28.9, 29.4, 45.7, 52.0, 79.0, 80.1, 116.8, 118.6, 135.2, 135.7, 155.6, 175.7; MS (ESI, pos) (*m/z*): 288 [M + 1], 168 [M – Boc]; anal. calcd for $\text{C}_{14}\text{H}_{21}\text{NO}_4$: C, 62.90; H, 7.92; N, 5.24; found, C, 62.59; H, 8.30; N, 4.87.

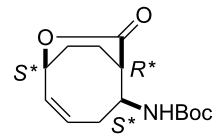
tert-Butyl ((2S^{*},3R^{*},4R^{*})-4-allyl-5-oxo-2-vinyltetrahydrofuran-3-yl)carbamate ((\pm)-10).



Yellow oil; yield 35%; R_f 0.70 (*n*-hexane/EtOAc 2:1); ^1H NMR (CDCl_3 , 400 MHz) δ 1.48 (s, 9H, *t*-Bu), 2.42–2.49 (m, 1H,

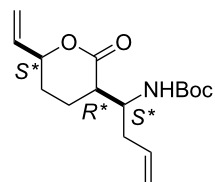
CH_2), 2.53–2.58 (m, 1H, CH_2), 2.61–2.67 (m, 1H, H-4), 3.91–3.97 (m, 1H, H-3), 4.52–4.62 (m, 2H, H-2 and NH), 5.06–5.12 (m, 2H, CH=), 5.33–5.38 (m, 1H, CH=), 5.42–5.48 (m, 1H, CH=), 5.75–5.85 (m, 2H, CH=); ^{13}C NMR (CDCl_3 , 100 MHz) δ 18.9, 22.7, 29.4, 45.7, 57.3, 82.4, 118.8, 119.4, 133.1, 133.2, 154.7, 174.3; MS (ESI, pos) (*m/z*): 288 [M + 1], 168 [M – Boc]; anal. calcd for $\text{C}_{14}\text{H}_{21}\text{NO}_4$: C, 62.90; H, 7.92; N, 5.24; found, C, 62.59; H, 7.60; N, 4.86.

tert-Butyl ((1R^{*},2S^{*},6S^{*},Z)-8-oxo-7-oxabicyclo[4.2.2]dec-4-en-2-yl)carbamate ((\pm)-14).

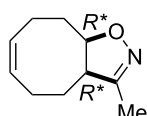


White solid; yield 38%; mp 101–102 °C; R_f = 0.50 (*n*-hexane/EtOAc 2:1); ^1H NMR (CDCl_3 , 400 MHz) δ 1.40 (s, 9H, *t*-Bu), 1.68–1.75 (m, 1H, CH_2), 1.83–1.99 (m, 2H, CH_2), 2.28–2.35 (m, 2H, CH_2), 1.42–1.50 (m, 1H, CH_2), 3.02–3.06 (m, 1H, H-1), 3.90–3.99 (m, 1H, H-2), 5.00–5.08 (brs, 1H, NH), 5.10–5.15 (m, 1H, H-6), 5.47–5.53 (m, 1H, H-4), 5.83–5.92 (m, 1H, H-5); ^{13}C NMR (CDCl_3 , 100 MHz) δ 21.4, 25.3, 28.4, 46.8, 55.6, 78.7, 79.8, 125.9, 129.0, 154.6, 173.0; MS (ESI, pos) (*m/z*): 288 [M + 1], 168 [M – Boc]; anal. calcd for $\text{C}_{14}\text{H}_{21}\text{NO}_4$: C, 62.90; H, 7.92; N, 5.24; found, C, 63.22; H, 7.59; N, 4.88.

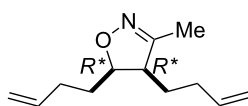
tert-Butyl ((S^{*})-1-((3R^{*},6S^{*})-2-oxo-6-vinyltetrahydro-2H-pyran-3-yl)but-3-en-1-yl)carbamate ((\pm)-15).



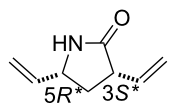
White solid; yield 59%; mp 64–65 °C; R_f 0.65 (*n*-hexane/EtOAc 2:1); ^1H NMR (CDCl_3 , 400 MHz) δ 1.42 (s, 9H, *t*-Bu), 1.67–1.74 (m, 2H, CH_2), 1.93–2.02 (m, 2H, CH_2), 2.32–2.42 (m, 2H, CH_2), 2.74–2.81 (m, 1H, H-3), 3.78–3.85 (m, 1H, CHN), 4.81–4.86 (m, 1H, CH=), 5.13–5.10 (m, 2H, CH=), 5.25–5.35 (m, 2H, CH=), 5.38 (brs, 1H, NH), 5.69–5.80 (m, 2H, CH=); ^{13}C NMR (CDCl_3 , 100 MHz) δ 20.5, 26.3, 27.0, 35.0, 44.0, 51.1, 78.4, 79.2, 117.4, 117.5, 135.5, 135.7, 155.6, 172.8; MS (ESI, pos) (*m/z*): 296 [M + 1]; anal. calcd for $\text{C}_{16}\text{H}_{25}\text{NO}_4$: C, 65.06; H, 8.53; N, 4.74; found, C, 64.69; H, 8.19; N, 4.39.

(3a*R*^{*,9a*R*^{*,*Z*})-3-Methyl-3a,4,5,8,9,9a-hexahydrocycloocta[d]isoxazole ((\pm)-16).}

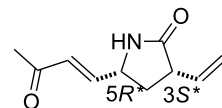
Yellow oil; yield: 62%; R_f 0.37 (*n*-hexane/EtOAc 4:1); ^1H NMR (CDCl_3 , 400 MHz) δ 1.80–1.87 (m, 2H, H-4), 1.95 (s, 3H, CH_3), 2.02–2.19 (m, 3H, H-5, H-8), 2.21–2.36 (m, 1H, H-8), 2.4–2.54 (m, 1H, H-9), 2.97–3.06 (q, 1H, $J^1 = 8.64$ Hz, $J^2 = 8.46$ Hz, $J^3 = 8.64$ Hz, H-3a), 4.37–4.45 (m, 1H, H-9a), 5.55–5.64 (m, 1H, H-6), 5.65–5.73 (m, 1H, H-7); ^{13}C NMR (DMSO, 125 MHz) δ 12.3, 24.4, 24.7, 25.1, 28.5, 51.0, 83.9, 129.0, 130.7, 160.9; anal. calcd for $\text{C}_{10}\text{H}_{15}\text{NO}$: C, 72.69; H, 9.15; N, 8.48; found, C, 72.38; H, 8.80; N, 8.11.

(4*R*^{*,5*R*^{*,*Z*})-4,5-Di(but-3-enyl)-3-methyl-4,5-dihydroisoxazole ((\pm)-17).}

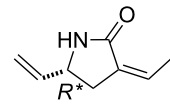
Yellow oil; yield 38%; $R_f = 0.57$ (*n*-hexane/EtOAc 4:1); ^1H NMR (CDCl_3 , 400 MHz) δ 1.51–1.74 (m, 4H, CH_2), 2.00 (s, 3H, CH_3), 2.08–2.19 (m, 3H, CH_2), 2.39–2.48 (m, 1H, CH_2), 2.97–3.05 (m, 1H, H-4), 4.46–4.52 (m, 1H, H-5), 5.02–5.16 (m, 4H, $\text{CH} =$), 5.68–5.79 (m, 2H, $\text{CH} =$); ^{13}C NMR (DMSO, 125 MHz) δ 12.6, 24.5, 27.6, 30.7, 32.0, 51.0, 81.7, 115.6, 115.8, 138.4, 138.6, 159.8; anal. calcd for $\text{C}_{12}\text{H}_{19}\text{NO}$: C, 74.57; H, 9.91; N, 7.25; found, C, 74.20; H, 9.65; N, 6.86.

(3*S*^{*,5*R*^{*,*Z*})-3,5-Divinylpyrrolidin-2-one ((\pm)-19).}

White solid; yield 70%; mp 67–68 °C; $R_f = 0.40$ (*n*-hexane/EtOAc 1:2); ^1H NMR (CDCl_3 , 400 MHz) δ 1.65–1.72 (m, 1H, CH_2), 2.47–2.53 (m, 1H, CH_2), 3.09–3.18 (m, 1H, H-3), 4.05–4.13 (m, 1H, H-5), 5.13–5.25 (m, 4H, $\text{CH} =$), 5.74–5.81 (m, 1H, $\text{CH} =$), 5.84–5.92 (m, 1H, $\text{CH} =$), 6.00 (brs, 1H, NH); ^{13}C NMR (CDCl_3 , 100 MHz) δ 34.9, 46.0, 55.2, 116.8, 117.7, 135.0, 138.5, 177.4; MS (ESI, pos) (m/z): 138 [M + 1]; anal. calcd for $\text{C}_8\text{H}_{11}\text{NO}$: C, 70.04; H, 8.08; N, 10.21; found, C, 69.69; H, 7.81; N, 9.86.

(3*S*^{*,5*R*^{*,*Z*})-5-((*E*)-3-Oxobut-1-en-1-yl)-3-vinylpyrrolidin-2-one ((\pm)-20).}

White solid; yield 28%; mp 58–89 °C; $R_f = 0.45$ (*n*-hexane/EtOAc 1:2); ^1H NMR (CDCl_3 , 400 MHz) δ 1.75–1.82 (m, 1H, CH_2), 2.36 (s, 3H, CH_3), 2.53–2.62 (m, 1H, CH_2), 3.27–3.35 (m, 1H, H-3), 4.29–4.37 (m, 1H, H-5), 5.27–5.35 (m, 2H, $\text{CH} =$), 5.88–5.97 (m, 1H, $\text{CH} =$), 6.20–6.27 (d, $J = 16.1$ Hz, 1H, $\text{CH} =$), 6.51 (brs, 1H, NH), 6.60–6.68 (dd, $J = 16.2$ Hz, $J = 6.6$ Hz, 1H, $\text{CH} =$); ^{13}C NMR (CDCl_3 , 100 MHz) δ 27.6, 34.1, 45.7, 53.4, 118.2, 130.5, 134.3, 145.3, 177.7, 197.7; MS (ESI, pos) (m/z): 181 [M + 1]; anal. calcd for $\text{C}_{10}\text{H}_{13}\text{NO}_2$: C, 67.02; H, 7.31; N, 7.82; found, C, 67.33; H, 7.01; N, 7.52.

(*R*^{*,*Z*}-3-Ethylidene-5-vinylpyrrolidin-2-one ((\pm)-23).

White solid; yield 69%; mp 49–50 °C; $R_f = 0.35$ (*n*-hexane/EtOAc 1:2); ^1H NMR (CDCl_3 , 400 MHz) δ 1.77 (d, $J = 6.9$ Hz, 3H, CH_3), 2.45–2.51 (m, 1H, CH_2), 2.98–3.04 (m, 1H, CH_2), 4.19–4.28 (m, 1H, H-5), 5.02–5.08 (d, $J = 10.1$ Hz, 1H, $\text{CH} =$), 5.20–5.27 (d, $J = 16.6$ Hz, 1H, $\text{CH} =$), 5.78–5.88 (m, 1H, $\text{CH} =$), 6.48–6.54 (m, 1H, $\text{CH} =$), 7.51 (brs, 1H, NH); ^{13}C NMR (CDCl_3 , 100 MHz) δ 14.8, 31.2, 53.9, 115.6, 128.6, 131.5, 139.2, 171.5; MS (ESI, pos) (m/z): 138 [M + 1]; anal. calcd for $\text{C}_8\text{H}_{11}\text{NO}$: C, 70.04; H, 8.08; N, 10.21; found, C, 69.70; H, 7.80; N, 9.84.

Supporting Information**Supporting Information File 1**

Copies of NMR spectra.

[<https://www.beilstein-journals.org/bjoc/content/supplementary/1860-5397-14-247-S1.pdf>]

Acknowledgments

We are grateful to the Hungarian Research Foundation (NKFIH No. K 119282) for financial support. The financial support of the GINOP-2.3.2-15-2016-00038 project is also acknowledged. This research was supported by the EU-funded Hungarian grant EFOP-3.6.1-16-2016-00008.

ORCID® IDs

Santos Fustero - <https://orcid.org/0000-0002-7575-9439>

References

1. Hoveyda, A. H.; Zhugralin, A. R. *Nature* **2007**, *450*, 243–251. doi:10.1038/nature06351
2. Bidange, J.; Fischmeister, C.; Bruneau, C. *Chem. – Eur. J.* **2016**, *22*, 12226–12244. doi:10.1002/chem.201601052
3. Trnka, T. M.; Grubbs, R. H. *Acc. Chem. Res.* **2001**, *34*, 18–29. doi:10.1021/ar000114f
4. Sánchez-Roselló, M.; Miró, J.; del Pozo, C. *Synthesis* **2017**, *49*, 2787–2802. doi:10.1055/s-0036-1589497
5. Meek, S. J.; O'Brien, R. V.; Llaveria, J.; Schrock, R. R.; Hoveyda, A. H. *Nature* **2011**, *461*–466. doi:10.1038/nature09957
6. Fustero, S.; Simón-Fuentes, A.; Barrio, P.; Haufe, G. *Chem. Rev.* **2015**, *115*, 871–930. doi:10.1021/cr500182a
7. Kress, S.; Blechert, S. *Chem. Soc. Rev.* **2012**, *41*, 4389–4408. doi:10.1039/c2cs15348c
8. Higman, C. S.; Lummiss, J. A. M.; Fogg, D. E. *Angew. Chem., Int. Ed.* **2016**, *55*, 3552–3565. doi:10.1002/anie.201506846
9. Prunet, J. *Eur. J. Org. Chem.* **2011**, 3634–3647. doi:10.1002/ejoc.201100442
10. Hughes, D. L. *Org. Process Res. Dev.* **2016**, *20*, 1008–1015. doi:10.1021/acs.oprd.6b00167
11. Garcia-Castro, M.; Zimmermann, S.; Sankar, M. G.; Kumar, K. *Angew. Chem., Int. Ed.* **2016**, *55*, 7586–7605. doi:10.1002/anie.201508818
12. Hung, A. W.; Ramek, A.; Wang, Y.; Kaya, T.; Wilson, J. A.; Clemons, P. A.; Young, D. W. *Proc. Natl. Acad. Sci. U. S. A.* **2011**, *108*, 6799–6804. doi:10.1073/pnas.1015271108
13. Foley, D. J.; Doveston, R. G.; Churcher, I.; Nelson, A.; Marsden, S. P. *Chem. Commun.* **2015**, *51*, 11174–11177. doi:10.1039/C5CC03002A
14. Kiss, L.; Kardos, M.; Forró, E.; Fülöp, F. *Eur. J. Org. Chem.* **2015**, 1283–1289. doi:10.1002/ejoc.201403493
15. Kardos, M.; Kiss, L.; Fülöp, F. *Asian J. Org. Chem.* **2015**, *4*, 1155–1159. doi:10.1002/ajoc.201500286
16. Kardos, M.; Kiss, L.; Haukka, M.; Fustero, S.; Fülöp, F. *Eur. J. Org. Chem.* **2017**, 1894–1901. doi:10.1002/ejoc.201700064
17. Spandl, R. J.; Díaz-Gavilán, M.; O'Connel, K. M. G.; Thomas, G. L.; Spring, D. R. *Chem. Rec.* **2008**, *8*, 129–142. doi:10.1002/tcr.20144
18. O' Connor, C. J.; Beckmann, H. S. G.; Spring, D. R. *Chem. Soc. Rev.* **2012**, *41*, 4444–4456. doi:10.1039/c2cs35023h
19. Sen, S.; Prabhu, G.; Bathula, C.; Hati, S. *Synthesis* **2014**, *46*, 2099–2121. doi:10.1055/s-0033-1341247
20. Collins, S.; Bartlett, S.; Nie, F.; Sore, H. F.; Spring, D. R. *Synthesis* **2016**, *48*, 1457–1473. doi:10.1055/s-0035-1561414
21. Kiss, L.; Fülöp, F. *Chem. Rev.* **2014**, *114*, 1116–1169. doi:10.1021/cr300454h
22. Kiss, L.; Mándity, I. M.; Fülöp, F. *Amino Acids* **2017**, *49*, 1441–1455. doi:10.1007/s00726-017-2439-9
23. Kiss, L.; Fülöp, F. *Chem. Rec.* **2018**, *18*, 266–281. doi:10.1002/tcr.201700038
24. Singh, R.; Vince, R. *Chem. Rev.* **2012**, *112*, 4642–4686. doi:10.1021/cr2004822
25. Kiss, L.; Forró, E.; Fustero, S.; Fülöp, F. *Eur. J. Org. Chem.* **2011**, 4993–5001. doi:10.1002/ejoc.201100583
26. Kiss, L.; Forró, E.; Fustero, S.; Fülöp, F. *Org. Biomol. Chem.* **2011**, *9*, 6528–6534. doi:10.1039/c1ob05648d
27. Grubbs, R. H.; Khosravi, E., Eds. *Handbook of Metathesis*; 2004; Vol. 3.
28. Ofstead, E. A.; Calderon, N. *Makromol. Chem.* **1972**, *154*, 21–34. doi:10.1002/macp.1972.021540102
29. Tuba, R.; Balogh, J.; Hlil, A.; Barlög, M.; Al-Hashimi, M.; Bazzi, H. S. *ACS Sustainable Chem. Eng.* **2016**, *4*, 6090–6094. doi:10.1021/acssuschemeng.6b01496
30. Palkó, M.; Benedek, G.; Forró, F.; Wéber, E.; Hänninen, M.; Sillanpää, R.; Fülöp, F. *Tetrahedron: Asymmetry* **2010**, *21*, 957–961. doi:10.1016/j.tetasy.2010.05.003
31. Arjona, O.; Csáky, A. G.; León, V.; Medel, R.; Plumet, J. *Tetrahedron Lett.* **2004**, *45*, 565–567. doi:10.1016/j.tetlet.2003.10.197
32. Arjona, O.; Cabas, M. J.; Nieto-Rubio, J.; Querejeta, A. *Heterocycles* **2006**, *68*, 2079–2086. doi:10.3987/COM-06-10825
33. Ogba, O. M.; Warner, N. C.; O'Leary, D. J.; Grubbs, R. H. *Chem. Soc. Rev.* **2018**, *47*, 4510–4544. doi:10.1039/C8CS00027A
34. Chatterjee, A. K.; Choi, T.-L.; Sanders, D. P.; Grubbs, R. H. *J. Am. Chem. Soc.* **2003**, *125*, 11360–11370. doi:10.1021/ja0214882
35. Grela, K., Ed. *Olefin metathesis; Theory and practice*; John Wiley & Sons, Inc.: Hoboken, New Jersey, 2014. doi:10.1002/9781118711613
36. Kotha, S.; Dipak, M. K. *Tetrahedron* **2012**, *68*, 397–421. doi:10.1016/j.tet.2011.10.018
37. Hamad, F. B.; Sun, T.; Xiao, S.; Verpoort, F. *Coord. Chem. Rev.* **2013**, *257*, 2274–2292. doi:10.1016/j.ccr.2013.04.015

License and Terms

This is an Open Access article under the terms of the Creative Commons Attribution License (<http://creativecommons.org/licenses/by/4.0>). Please note that the reuse, redistribution and reproduction in particular requires that the authors and source are credited.

The license is subject to the *Beilstein Journal of Organic Chemistry* terms and conditions: (<https://www.beilstein-journals.org/bjoc>)

The definitive version of this article is the electronic one which can be found at:

doi:10.3762/bjoc.14.247



Domino ring-opening–ring-closing enyne metathesis vs enyne metathesis of norbornene derivatives with alkynyl side chains. Construction of condensed polycarbocycles

Ritabrata Datta and Subrata Ghosh*

Full Research Paper

Open Access

Address:

School of Chemical Sciences, Indian Association for the Cultivation of Science, Jadavpur, Kolkata 700 032, India

Beilstein J. Org. Chem. **2018**, *14*, 2708–2714.

doi:10.3762/bjoc.14.248

Email:

Subrata Ghosh* - ocsg@iacs.res.in

Received: 12 August 2018

Accepted: 10 October 2018

Published: 25 October 2018

* Corresponding author

This article is part of the thematic issue "Progress in metathesis chemistry III".

Keywords:

Diels–Alder reaction; domino process; enyne metathesis; natural products; polycarbocycles

Guest Editor: K. Grela

© 2018 Datta and Ghosh; licensee Beilstein-Institut.

License and terms: see end of document.

Abstract

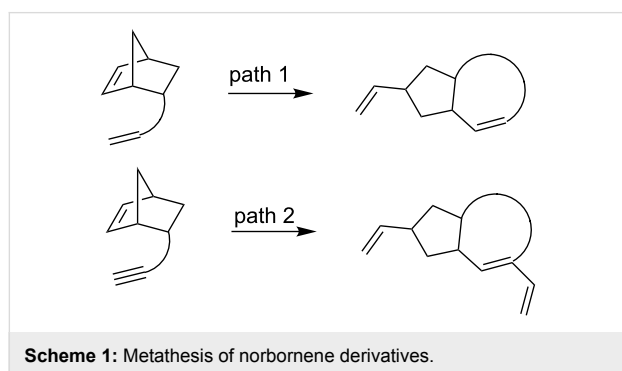
The metathesis of norbornene derivatives with alkynyl side-chain with Grubbs' ruthenium alkylidene as catalyst has been investigated with the objective of constructing condensed polycyclic structures. This investigation demonstrated that the generally observed domino reaction course involving a ring-opening metathesis of the norbornene unit and a ring-closing enyne metathesis is influenced to a great extent by the nature of the functional group and the substrate structure and may follow a different reaction course than what is usually observed. In cases where ROM–RCEYM occurred, the resulting 1,3-diene reacts *in situ* with the dienophile to provide condensed tetracyclic systems.

Introduction

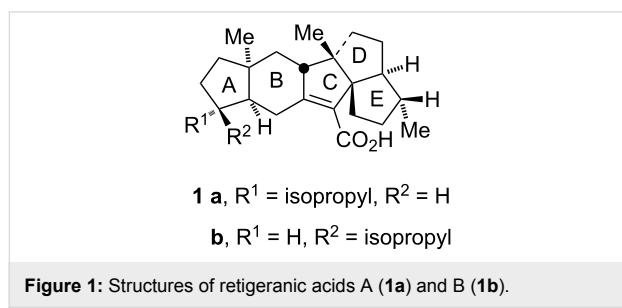
The metathesis of norbornene derivatives having an alkene side-chain on the norbornene nucleus with Grubbs' ruthenium catalysts has been extensively investigated. Generally the reaction proceeds through a domino process involving a ring opening of the norbornene nucleus and ring closing with the alkene side chains to produce ring rearrangement products (path 1, Scheme 1) [1–4]. This protocol has been employed by several groups [5–22] as well as by our group [23–33] for the synthesis of a variety of complex ring systems such as condensed,

bridged and spirocycles difficult to obtain otherwise. On the contrary, the domino process involving a ring-opening metathesis (ROM) followed by a ring-closing enyne metathesis (RCEYM) [34–37] of norbornene derivatives with a suitably located alkynyl side-chain on the nucleus (path 2, Scheme 1) to form carbocycles has been less explored. The greatest advantage of this protocol lies in its potential in increasing the molecular complexity through Diels–Alder reaction of the resulting ring system. Domino metathesis of oxa- and aza-norbornenes

with alkyne side chains [38–40] as well as norbornene derivatives having ether linked alkynes [41,42] in combination with Diels–Alder reaction of the resulting 1,3-dienes have been investigated to construct polycycles with heteroatoms. In spite of the great potential little attention has been paid [43] for exploring its application in the synthesis of complex carbocyclic ring systems, backbones of innumerable natural products.

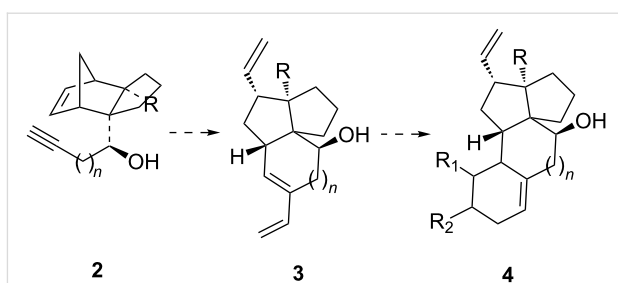


We undertook a program for the synthesis of condensed polycyclic scaffolds using a metathesis of norbornene derivatives with suitably located alkynyl side-chains as the key step. The structurally unique sesterterpenes retigeranic acid A (**1a**) and retigeranic acid B (**1b**, Figure 1) are representative examples of such complex polycyclic structures [44–47]. We speculated that domino ROM–RCEYM of the norbornene derivative **2** would provide the tricyclic 1,3-diene **3** which on Diels–Alder reaction with a dienophile would enable access to condensed polycyclic structures **4** (Scheme 2). Thus an appropriately chosen norbornene derivative and a dienophile may provide the B/C/D/E ring system of retigeranic acids. Herein we describe the results of metathesis of norbornene derivatives **2** with alkynyl side-chains.



Results and Discussion

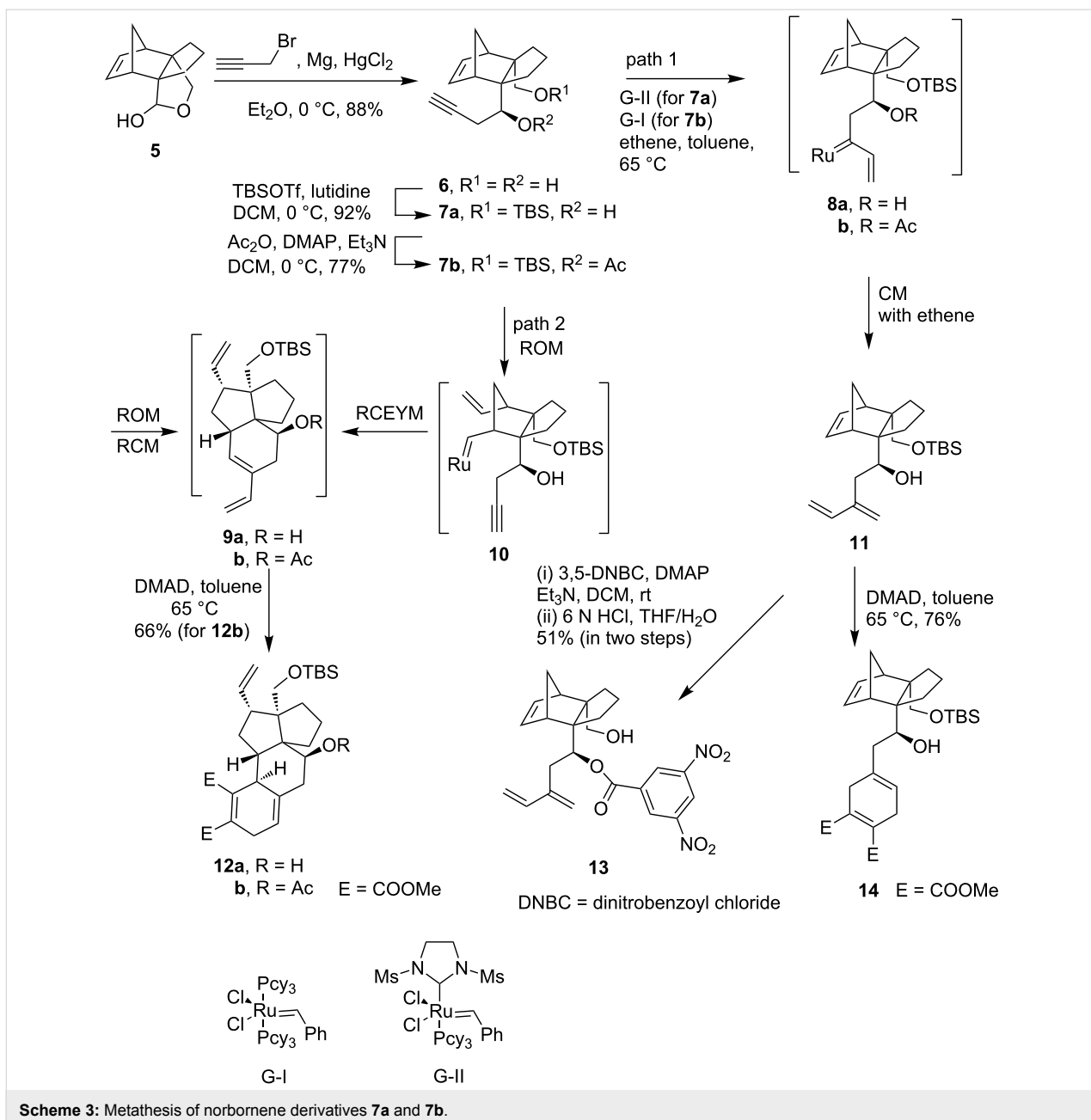
Initially Grubbs' 1st generation catalyst (G-I) was used for metathesis of norbornene derivatives **2**. In case G-I failed to accomplish metathesis in the desired direction, 2nd generation catalyst (G-II) was used. The norbornene derivative **7a** was first chosen for investigating ROM–RCEYM. Compound **7a** was



Scheme 2: Synthesis plan.

prepared in the following way (Scheme 3). Reaction of the known lactol **5** [33] with propargyl magnesium bromide afforded the diol **6** in 88% yield (For detailed experimental procedures and characterization data see Supporting Information File 1). The stereochemical orientation of the secondary hydroxy group was determined through X-ray crystal structure of a compound derived from it in a subsequent step. The primary hydroxy group in the diol **6** was then selectively protected to provide the silyl ether **7a** in 92% yield. Two different paths can be invoked for metathesis of compound **7a**. Metathesis initiation may occur by attack of the ruthenium alkylidene at the alkyne unit to produce the more substituted vinyl alkylidene intermediate **8a** which may undergo concomitant ROM–RCM with the norbornene nucleus to provide the triene **9a** (path 1).

Alternatively the metathesis initiation may occur initially at the norbornene double bond to provide the ring-opened ruthenium alkylidene intermediate **10** (path 2). The latter then undergoes RCEYM to provide the tricycle **9a**. With this background a solution of the compound **7a** in toluene under ethylene atmosphere was heated at 65 °C with Grubbs 1st generation catalyst (G-I). Compound **7a** was found to be inert even after a prolonged reaction time. However, with G-II as the catalyst the metathesis went smoothly. Without isolation, the metathesis product was treated in situ with dimethyl acetylenedicarboxylate (DMAD). In case the Diels–Alder reaction would take place through the triene **9a** the tetracyclic structure **12a** would be formed. However, ^{13}C NMR spectra of the product revealed the presence of eight methylene carbon signals at δ 28.6, 28.9, 30.9, 33.5, 36.7, 41.1, 45.7 and 68.8, one more aliphatic methylene unit than what the structure **12a** requires (see Supporting Information File 1). This indicates that the metathesis product is not **9a**. The structure of the metathesis product was finally settled by X-ray crystal structure (Figure 2) [48] (see Supporting Information File 2) of the 3,5-dinitrobenzoate derivative **13**, mp 171–172 °C, prepared in two steps (51%) from the metathesis product on reaction with 3,5-dinitrobenzoyl chloride (DNBC) followed by acid-induced desilylation. Thus compound **7b** on metathesis produced exclusively triene **11** and accordingly the structure of the Diels–Alder adduct is **14**. The for-



mation of triene **11** could be attributed to cross metathesis of the ruthenium alkylidene **8a** with ethylene. No product arising out of ROM of norbornene derivative **7a** was formed. It is worth mentioning that Spandl et al. [43] reported the metathesis of norbornene derivatives with an alkynyl side chain affording the major product arising from domino ROM–RCEYM while the enyne metathesis product was observed only in very low yield.

In order to realize our objective and to find out if the free hydroxy group has any influence on the outcome of the metathesis, the hydroxy group in compound **7a** was protected to provide the acetate derivative **7b**. The metathesis of compound

7b with G-I as the catalyst proceeded smoothly and the resulting product without isolation was allowed to react with DMAD to produce the tetracycle **12b** in overall 66% yield. The structure of compound **12b** was established through analysis of its NMR spectra. Isolation of **12b** dictated that metathesis of **7b** proceeded through the formation of the triene **9b**. Stereochemical assignment to the adduct follows from addition of the dienophile from the least hindered face (opposite to CH_2OTBS group) of the diene. Thus unlike metathesis of **7a**, metathesis of its acetate analogue **7b** occurred through a domino ROM–RCEYM process. Addition of the Ru-carbene **10** arising from ring opening of norbornene unit in **7b** could add to the

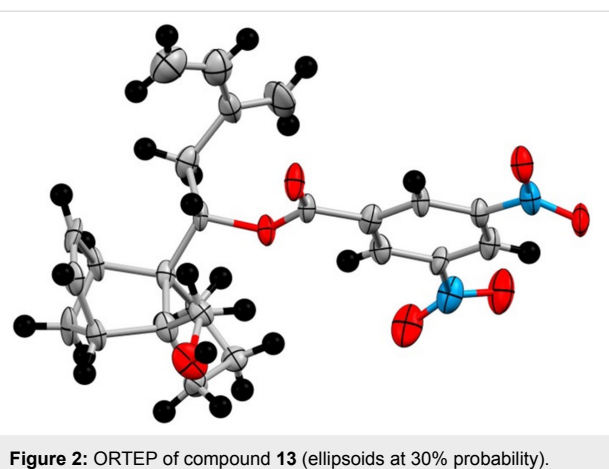


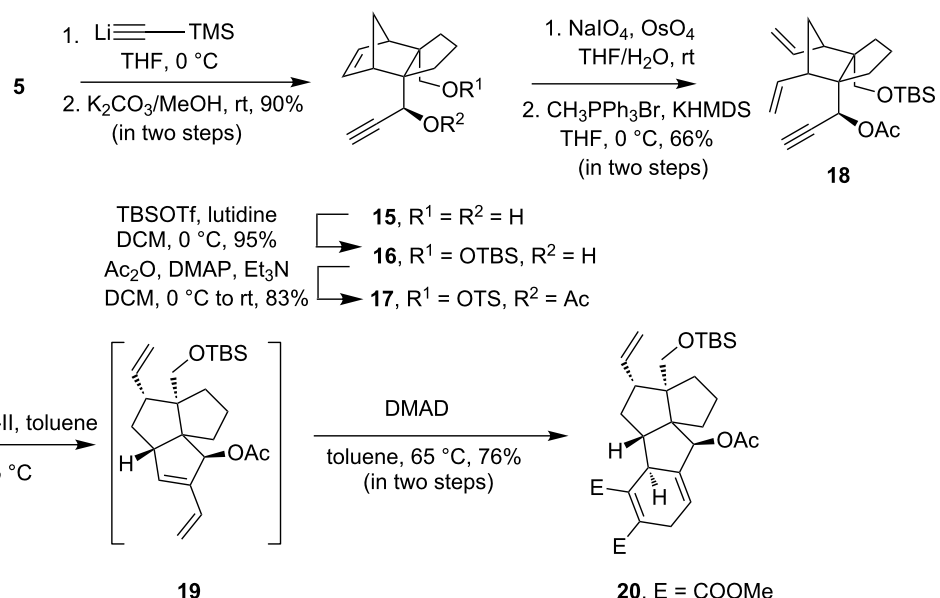
Figure 2: ORTEP of compound 13 (ellipsoids at 30% probability).

acetylenic unit of another molecule of **7b** leading to copolymerization. However, this process generally does not take place under such low molar concentration of the substrate [38–43]. We also did not isolate any copolymerization product. This may be attributed to the much faster rate of addition of the Ru-carbene **10** to the yne unit intramolecularly resulting in ring closure rather than intermolecular addition to an acetylenic unit of another molecule of **7b**. It may be noted that changing the functional group from hydroxy to acetate the metathesis followed a different reaction course.

In order to construct a polycyclic structure analogous to the B/C/D/E ring of retigeranic acids, the norbornene derivative **16** was chosen. Addition of lithium (trimethylsilyl)acetylide to the lactol **5** followed by desilylation by using methanolic K_2CO_3

afforded diol **15** (Scheme 4). The primary hydroxy group in compound **15** was selectively protected to produce the silyl ether **16** in 95% yield. The attempted metathesis of compound **16** with G-I or G-II catalyst under the conditions used for the metathesis of **7a** led to a complete recovery of **16**. Since metathesis of the acetate derivative **7b** proceeded smoothly in the desired direction, we chose to use the acetate **17** for metathesis. The acetate **17** also remained inert when subjected to metathesis conditions with G-I as well as with G-II. Neither ring opening of the norbornene nucleus nor cross metathesis of the alkyne with ethylene did occur. To have an understanding about the inertness of **17** towards metathesis we decided to prepare the ring-opened product **18** using an alternative path. The double bond in the norbornene nucleus in compound **17** was cleaved in the traditional way by treatment with $OsO_4/NaIO_4$ and the resulting dialdehyde on Wittig reaction provided the diene **18** in 66% yield in two steps. Amazingly when compound **18** was treated with G-I or G-II as catalyst, the metathesis was found to take place. After disappearance of the starting material (TLC), the reaction mixture was allowed to react with DMAD. The product obtained in 76% yield was assigned the structure **20** based on spectral data. Isolation of **20** indicates that metathesis of **18** proceeded through RCEYM to produce the triene **19**. The latter then after in situ Diels–Alder reaction with DMAD delivered the product **20**. The tetracyclic compound **20** represents the B/C/D/E tetracyclic core structure of retigeranic acids.

Based on the above observations a mechanistic rationale regarding the metathesis of norbornene derivatives with an alkynyl side chain may be postulated (Figure 3). Possibly the



Scheme 4: Metathesis of the norbornene derivative **17**.

metathesis is initiated at the acetylenic unit to form the ruthenium alkylidene such as **8**. In case of **8a** the ruthenium alkylidene is stabilized by formation of the chelate **21** ($R = H$) which prohibits intramolecular addition of the ruthenium alkylidene to form ruthena cyclobutane **22**. The alkylidene **21** then undergoes cross metathesis with ethylene to form the product **11**. The ruthenium alkylidene **8b** possibly fails to form chelate **21** ($R = Ac$) due to the electron deficient nature of the OAc group. It forms intramolecularly the ruthena cyclobutane **22** which undergoes ring opening to give rise to the triene **9b**. That the metathesis does not proceed through path 2 (Scheme 3) involving ROM–RCM is indicated by failure of the norbornene derivative **17** to undergo ROM. Steric shielding of the acetylenic unit in **17** inhibits metathesis initiation at the acetylenic unit. The norbornene derivative **17** just remains inert under metathesis conditions. Thus metathesis in these examples proceeds through path 1 (Scheme 3).

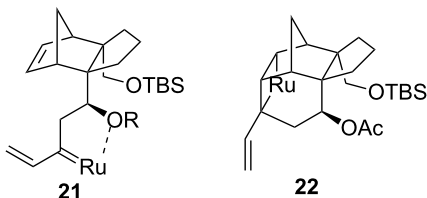


Figure 3: Probable metathesis intermediates.

Conclusion

In conclusion we have developed a protocol for the synthesis of condensed polycycles from metathesis of norbornene derivatives with alkynyl side-chain. This investigation demonstrated that domino metathesis of norbornene derivatives with alkynyl side-chain requires metathesis initiation at the acetylene unit. Further, the nature of functional groups as well as the substrate structure play a significant role in determining the metathesis reaction course.

Experimental

General experimental methods are similar as described in [49]

Synthesis of triene **11.** A solution of the silyl ether **7a** (120 mg, 0.35 mmol) in degassed toluene (7 mL) with Grubbs' catalyst G-II (30 mg, 0.035 mmol) was heated at 65 °C for 6 h under a positive pressure of ethylene atmosphere. After completion (TLC) of the reaction toluene was removed under vacuo. The residual mass was purified by column chromatography (7% EA/PE) to afford diene **11** (89 mg, 69%) as an oil; ^1H NMR (500 MHz) δ 6.42 (dd, $J = 11, 17.5$ Hz, 1H), 6.12 (s, 2H), 5.28 (d, $J = 17.5$ Hz, 1H), 5.15 (d, $J = 29$ Hz, 2H), 5.04 (d, $J = 11$ Hz, 1H), 3.98 (s, 1H), 3.63 (d, $J = 10$ Hz, 1H), 3.56 (s, 2H), 2.53 (s, 1H), 2.45–2.42 (m, 1H), 2.36–2.22 (m, 3H),

1.95–1.92 (m, 1H), 1.82–1.74 (m, 3H), 1.47–1.38 (m, 2H), 1.33–1.28 (m, 1H), 0.89 (s, 9H), 0.07 (s, 6H); ^{13}C NMR (125 MHz) δ 144.3, 139.8, 136.4, 136.1, 117.0, 113.1, 71.9, 68.6, 63.4, 61.2, 52.2, 52.0, 45.8, 36.8, 36.0, 33.8, 28.8, 26.0 ($\times 3$), 18.4, –5.4, –5.6; HRMS–ESI m/z : [M + Na] $^+$ calcd for $\text{C}_{23}\text{H}_{38}\text{O}_2\text{SiNa}$ 397.2539; found, 397.2537.

Diels–Alder reaction of diene **11. Synthesis of adduct **14**.** A mixture of the diene **11** (40 mg, 0.11 mmol) and dimethyl acetylenedicarboxylate (0.02 mL, 0.16 mmol) in toluene (5 mL) was heated at 65 °C for 2 h. The solvent was removed under reduced pressure and was purified by column chromatography (12% EA/PE) to afford the Diels–Alder adduct **14** (42 mg, 76%) as an oil; ^1H NMR (500 MHz) δ 6.12–6.11 (m, 2H), 5.52 (s, 1H), 4.26 (s, 1H), 3.89–3.88 (m, 1H), 3.78 (s, 3H), 3.76 (s, 3H), 3.60–3.52 (m, 3H), 3.05–2.97 (m, 3H), 2.45 (s, 1H), 2.32 (s, 1H), 2.18–2.17 (m, 3H), 1.93–1.89 (m, 1H), 1.83–1.78 (m, 2H), 1.75–1.68 (m, 2H), 1.48–1.41 (m, 1H), 1.39–1.33 (m, 2H), 0.88 (s, 9H), 0.08 (s, 6H); ^{13}C NMR (75 MHz) δ 169.0, 168.7, 136.4, 135.8, 133.6, 132.4, 132.2, 117.9, 72.0, 68.8, 63.1, 61.2, 52.3 ($\times 2$), 52.1 ($\times 2$), 45.7, 41.1, 36.8, 33.6, 30.9, 28.9, 28.6, 26.0 ($\times 3$), 18.4, –5.4, –5.6; IR: 2952, 1728, 1471 cm^{-1} ; HRMS–ESI m/z : [M + Na] $^+$ calcd for $\text{C}_{29}\text{H}_{44}\text{O}_6\text{SiNa}$ 539.2805; found, 539.2802.

Synthesis of tetracycle **12b.** A solution of the norbornene derivative **7b** (70 mg, 0.18 mmol) in degassed toluene (6 mL) was heated with Grubbs' catalyst G-I (15 mg, 0.018 mmol) under ethylene atmosphere at 65 °C for 12 h. After completion (TLC) of the metathesis reaction, dimethyl acetylenedicarboxylate (0.04 mL, 0.27 mmol) was added to the reaction mixture. The reaction mixture was then heated for 12 h till the Diels–Alder reaction of the diene **9b** generated in situ was complete. The solvent was removed under vacuo and the product was purified by column chromatography (15% EA/PE) to afford the tetracycle **12b** (66 mg, 66%) as a colorless oil; ^1H NMR (300 MHz) δ 5.99–5.87 (m, 1H), 5.63–5.57 (m, 1H), 5.35–5.34 (m, 1H), 4.99–4.94 (m, 2H), 3.74 (s, 3H), 3.73 (s, 3H), 3.58–3.48 (m, 2H), 3.25–3.16 (m, 2H), 3.10–3.07 (m, 1H), 2.85–2.75 (m, 1H), 2.14–2.07 (m, 2H), 2.04 (s, 3H), 2.02–1.85 (m, 2H), 1.69–1.59 (m, 4H), 1.53–1.25 (m, 3H), 0.94 (s, 9H), 0.02 (s, 3H), –0.03 (s, 3H); ^{13}C NMR (75 MHz) δ 170.1, 169.3, 168.7, 139.5, 136.9, 134.0, 132.5, 115.9, 115.0, 73.4, 65.1, 60.6, 57.6, 56.2, 53.1, 52.4, 52.1, 40.9, 37.6, 36.2, 34.9, 34.7, 28.2, 26.2 ($\times 3$), 22.1, 21.8, 17.9, –5.8, –6.1; IR: 2950, 1737, 1434, 1249 cm^{-1} ; HRMS–ESI m/z : [M + Na] $^+$ calcd for $\text{C}_{31}\text{H}_{46}\text{O}_7\text{SiNa}$ 581.2911; found, 581.2914.

Synthesis of the tetracycle **20.** The dienyne **18** (100 mg, 0.25 mmol) in degassed anhydrous toluene (7 mL) was treated with Grubbs' catalyst G-II (22 mg, 0.025 mmol) at 65 °C for

5 h. On completion of the reaction (TLC), dimethyl acetylenedicarboxylate (0.06 mL, 0.37 mmol) was added to the resulting reaction mixture. The mixture was heated at 65 °C for 8 h. Removal of the solvent under *vacuo* followed by column chromatography (15% EA/PE) afforded the Diels–Alder adduct **20** (102 mg, 76%) as a colorless oil; ^1H NMR (300 MHz) δ 6.06–6.02 (m, 1H), 6.00–5.94 (m, 1H), 5.24–5.21 (m, 1H), 5.03–4.95 (m, 2H), 3.80 (s, 3H), 3.75 (s, 3H), 3.53 (s, 2H), 3.19–3.11 (m, 1H), 3.09–3.02 (m, 1H), 3.00–2.86 (m, 1H), 2.43–2.34 (m, 1H), 2.14 (s, 3H), 2.08–1.98 (m, 2H), 1.96–1.78 (m, 2H), 1.55–1.50 (m, 2H), 1.46–1.41 (m, 1H), 1.34–1.25 (m, 1H), 1.12–0.99 (m, 1H), 0.91 (s, 9H), 0.04 (s, 3H), 0.02 (s, 3H); ^{13}C NMR (75 MHz) δ 170.0, 169.0, 167.5, 140.1, 139.3, 139.2, 129.0, 115.3, 109.8, 74.4, 65.6, 62.3, 58.1, 56.7, 54.7, 52.4, 52.3, 41.9, 40.1, 35.9, 35.6, 27.6, 26.2 (\times 3), 22.9, 21.1, 18.2, −5.8, −5.9; IR: 2950, 1731, 1434, 1257 cm^{-1} ; HRMS–ESI m/z : [M + Na] $^+$ calcd for $\text{C}_{30}\text{H}_{44}\text{O}_7\text{SiNa}$ 567.2754; found, 567.2756.

Supporting Information

Supporting Information File 1

Experimental and analytical data.

[<https://www.beilstein-journals.org/bjoc/content/supplementary/1860-5397-14-248-S1.pdf>]

Supporting Information File 2

Crystallographic information for compound **13**.

[<https://www.beilstein-journals.org/bjoc/content/supplementary/1860-5397-14-248-S2.cif>]

Acknowledgements

SG is grateful to Indian National Science Academy, New Delhi for financial support through INSA Senior Scientist program. We are grateful to DST, Government of India for financial support for National Single Crystal Diffractometer facility at the Department of Inorganic Chemistry of this institute. We sincerely thank Mr. Mukesh Choudhary of Institute of Chemical Technology, Mumbai for carrying out some preliminary experiments.

ORCID® IDs

Subrata Ghosh - <https://orcid.org/0000-0003-4564-4435>

References

1. Arjona, O.; Csáký, A. G.; Plumet, J. *Eur. J. Org. Chem.* **2003**, 611–622. doi:10.1002/ejoc.200390100
2. Holub, N.; Blechert, S. *Chem. – Asian J.* **2007**, 2, 1064–1082. doi:10.1002/asia.200700072
3. Bose, S.; Ghosh, S. *Proc. Indian Natl. Sci. Acad.* **2014**, 80, 37–54. doi:10.16943/ptinsa/2014/v80i1/55085
4. Kotha, S.; Meshram, M.; Khedkar, P.; Banerjee, S.; Deodhar, D. *Beilstein J. Org. Chem.* **2015**, 11, 1833–1864. doi:10.3762/bjoc.11.199
5. Stille, J. R.; Santarsiero, B. D.; Grubbs, R. H. *J. Org. Chem.* **1990**, 55, 843–862. doi:10.1021/jo00290a013
6. Zuercher, W. J.; Hashimoto, M.; Grubbs, R. H. *J. Am. Chem. Soc.* **1996**, 118, 6634–6640. doi:10.1021/ja9606743
7. Stragies, R.; Blechert, S. *Synlett* **1998**, 169–170. doi:10.1055/s-1998-1592
8. Arjona, O.; Csáký, A. G.; Murcia, M. C.; Plumet, J. *Tetrahedron Lett.* **2000**, 41, 9777–9779. doi:10.1016/S0040-4039(00)01721-4
9. Weatherhead, G. S.; Ford, J. G.; Alexanian, E. J.; Schrock, R. R.; Hoveyda, A. H. *J. Am. Chem. Soc.* **2000**, 122, 1828–1829. doi:10.1021/ja993681a
10. Arjona, O.; Csáký, A. G.; Medel, R.; Plumet, J. *J. Org. Chem.* **2002**, 67, 1380–1383. doi:10.1021/jo016000e
11. Sakurai, H.; Daiko, T.; Hirao, T. *Science* **2003**, 301, 1878. doi:10.1126/science.1088290
12. Arjona, O.; Csáký, A. G.; León, V.; Medel, R.; Plumet, J. *Tetrahedron Lett.* **2004**, 45, 565–567. doi:10.1016/j.tetlet.2003.10.197
13. Holtsclaw, J.; Koreeda, M. *Org. Lett.* **2004**, 6, 3719–3722. doi:10.1021/o10486501
14. Funel, J.-A.; Prunet, J. *Synlett* **2005**, 235–238. doi:10.1055/s-2004-837200
15. Chandler, C. L.; Phillips, A. J. *Org. Lett.* **2005**, 7, 3493–3495. doi:10.1021/o1051199t
16. Maechling, S.; Norman, S. E.; McKendrick, J. E.; Basra, S.; Köppner, K.; Blechert, S. *Tetrahedron Lett.* **2006**, 47, 189–192. doi:10.1016/j.tetlet.2005.10.155
17. Hart, A. C.; Phillips, A. J. *J. Am. Chem. Soc.* **2006**, 128, 1094–1095. doi:10.1021/ja057899a
18. Phillips, A. J.; Hart, A. C.; Henderson, J. A. *Tetrahedron Lett.* **2006**, 47, 3743–3745. doi:10.1016/j.tetlet.2006.03.124
19. Calvet, G.; Blanchard, N.; Koulikovsky, C. *Org. Lett.* **2007**, 9, 1485–1488. doi:10.1021/o10702066
20. Henderson, J. A.; Phillips, A. J. *Angew. Chem., Int. Ed.* **2008**, 47, 8499–8501. doi:10.1002/anie.200803593
21. Nguyen, N. N. M.; Leclère, M.; Stogatis, N.; Fallis, A. G. *Org. Lett.* **2010**, 12, 1684–1687. doi:10.1021/o100150f
22. Lam, J. K.; Pham, H. V.; Houk, K. N.; Vanderwal, C. D. *J. Am. Chem. Soc.* **2013**, 135, 17585–17594. doi:10.1021/ja409618p
23. Malik, C. K.; Ghosh, S. *Org. Lett.* **2007**, 9, 2537–2540. doi:10.1021/o1070906a
24. Maity, S.; Ghosh, S. *Tetrahedron Lett.* **2008**, 49, 1133–1136. doi:10.1016/j.tetlet.2007.12.064
25. Mondal, S.; Malik, C. K.; Ghosh, S. *Tetrahedron Lett.* **2008**, 49, 5649–5651. doi:10.1016/j.tetlet.2008.07.083
26. Malik, C. K.; Yadav, R. N.; Drew, M. G. B.; Ghosh, S. *J. Org. Chem.* **2009**, 74, 1957–1963. doi:10.1021/jo802077t
27. Malik, C. K.; Hossain, M. F.; Ghosh, S. *Tetrahedron Lett.* **2009**, 50, 3063–3066. doi:10.1016/j.tetlet.2009.04.033
28. Mondal, S.; Yadav, R. N.; Ghosh, S. *Tetrahedron Lett.* **2009**, 50, 5277–5279. doi:10.1016/j.tetlet.2009.07.012
29. Maity, S.; Ghosh, S. *Tetrahedron* **2009**, 65, 9202–9210. doi:10.1016/j.tet.2009.09.029
30. Matcha, K.; Maity, S.; Malik, C. K.; Ghosh, S. *Tetrahedron Lett.* **2010**, 51, 2754–2757. doi:10.1016/j.tetlet.2010.03.074
31. Yadav, R. N.; Mondal, S.; Ghosh, S. *Tetrahedron Lett.* **2011**, 52, 1942–1945. doi:10.1016/j.tetlet.2011.02.054

32. Bose, S.; Ghosh, M.; Ghosh, S. *J. Org. Chem.* **2012**, *77*, 6345–6350.
doi:10.1021/jo300945b

33. Datta, R.; Bose, S.; Viththlbhai, P. B.; Ghosh, S. *Tetrahedron Lett.* **2014**, *55*, 3538–3540. doi:10.1016/j.tetlet.2014.04.091

34. Villar, H.; Frings, M.; Bolm, C. *Chem. Soc. Rev.* **2007**, *36*, 55–66.
doi:10.1039/B508899M

35. Diver, S. T.; Giessert, A. *J. Chem. Rev.* **2004**, *104*, 1317–1382.
doi:10.1021/cr020009e

36. Mori, M. *Adv. Synth. Catal.* **2007**, *349*, 121–135.
doi:10.1002/adsc.200600484

37. Mori, M. *Materials* **2010**, *3*, 2087–2140. doi:10.3390/ma3032087

38. Banti, D.; North, M. *Adv. Synth. Catal.* **2002**, *344*, 694–704.

39. Banti, D.; Groaz, E.; North, M. *Tetrahedron* **2004**, *60*, 8043–8052.
doi:10.1016/j.tet.2004.06.114

40. Groaz, E.; Banti, D.; North, M. *Eur. J. Org. Chem.* **2007**, 3727–3745.
doi:10.1002/ejoc.200700291

41. Kotha, S.; Ravikumar, O. *Tetrahedron Lett.* **2014**, *55*, 5781–5784.
doi:10.1016/j.tetlet.2014.08.108

42. Kotha, S.; Ravikumar, O. *Eur. J. Org. Chem.* **2014**, 5582–5590.
doi:10.1002/ejoc.201402273

43. Spandl, R. J.; Rudyk, H.; Spring, D. R. *Chem. Commun.* **2008**,
3001–3003. doi:10.1039/B807278G

44. Breitler, S.; Han, Y.; Corey, E. J. *Org. Lett.* **2017**, *19*, 6686–6687.
doi:10.1021/acs.orglett.7b03412

45. Wright, J.; Drtina, G. J.; Roberts, R. A.; Paquette, L. A.
J. Am. Chem. Soc. **1988**, *110*, 5806–5817. doi:10.1021/ja00225a036

46. Wender, P. A.; Singh, S. K. *Tetrahedron Lett.* **1990**, *31*, 2517–2520.
doi:10.1016/0040-4039(90)80114-2

47. Hudlicky, T.; Fleming, A.; Radescu, L. *J. Am. Chem. Soc.* **1989**, *111*,
6691–6707. doi:10.1021/ja00199a032

48. CCDC 1847091 contains supplementary crystallographic data for the
compound **13**. These data can be obtained free of charge from The
Cambridge Crystallographic Data Centre via
http://www.ccdc.cam.ac.uk/data_request/cif.

49. Datta, R.; Ghosh, S. *J. Org. Chem.* **2017**, *82*, 7675–7682.
doi:10.1021/acs.joc.7b01179

License and Terms

This is an Open Access article under the terms of the
Creative Commons Attribution License
(<http://creativecommons.org/licenses/by/4.0>). Please note
that the reuse, redistribution and reproduction in particular
requires that the authors and source are credited.

The license is subject to the *Beilstein Journal of Organic
Chemistry* terms and conditions:
(<https://www.beilstein-journals.org/bjoc>)

The definitive version of this article is the electronic one
which can be found at:
[doi:10.3762/bjoc.14.248](https://doi.org/10.3762/bjoc.14.248)



Synthesis of a tyrosinase inhibitor by consecutive ethenolysis and cross-metathesis of crude cashew nutshell liquid

Jacqueline Pollini, Valentina Bragoni and Lukas J. Gooßen*

Full Research Paper

Open Access

Address:

Lehrstuhl für Organische Chemie I, Ruhr-Universität Bochum,
ZEMOS, Universitätsstraße 150, 44801 Bochum, Germany

Email:

Lukas J. Gooßen* - lukas.goossen@ruhr-uni-bochum.de

* Corresponding author

Keywords:

cashew nutshell liquid; cross-metathesis; renewable feedstock;
sustainable chemistry; tyrosinase inhibitor

Beilstein J. Org. Chem. **2018**, *14*, 2737–2744.

doi:10.3762/bjoc.14.252

Received: 29 August 2018

Accepted: 19 October 2018

Published: 31 October 2018

This article is part of the thematic issue "Progress in metathesis chemistry III".

Guest Editor: K. Grela

© 2018 Pollini et al.; licensee Beilstein-Institut.

License and terms: see end of document.

Abstract

A convenient and sustainable three-step synthesis of the tyrosinase inhibitor 2-hydroxy-6-tridecylbenzoic acid was developed that starts directly from the anacardic acid component of natural cashew nutshell liquid (CNSL). Natural CNSL contains 60–70% of anacardic acid as a mixture of several double bond isomers. The anacardic acid component was converted into a uniform starting material by ethenolysis of the entire mixture and subsequent selective precipitation of 6-(ω -nonenyl)salicylic acid from cold pentane. The olefinic side chain of this intermediate was elongated by its cross-metathesis with 1-hexene using a first generation Hoveyda–Grubbs catalyst, which was reused as precatalyst in a subsequent hydrogenation step. Overall, the target compound was obtained in an overall yield of 61% based on the unsaturated anacardic acid content and 34% based on the crude CNSL.

Introduction

Cashew nutshell liquid (Scheme 1) is an ideal renewable feedstock. This non-edible industrial waste product, derived from the cashew nut processing, is abundant available and cheap [1–3]. The annual production of cashew nuts with shell reached 4.9 million tons in 2016 [4], leading to an estimated CNSL production of 1.2 million tons per year [5]. CNSL is a mixture of phenolic compounds such as anacardic acid (**1**), cardol and cardanol, each bearing a C-15 side chain in *meta*-position to the hydroxy group with a varying degree of unsaturation [6].

CNSL exhibits a broad range of biological properties and industrial applications, for instance in surfactants, plasticizers, resins, soft materials and diverse medical applications [7]. Isolated via cold-press or solvent extraction processes, it contains predominantly anacardic acid (**1**). Upon distillation or any other thermal treatment, anacardic acid is known to decarboxylate easily with formation of technical cashew nutshell liquid (tCNSL), which consists mainly of cardanol. Due to this industrial processing method, the main focus in research aiming at the chemi-

cal valorization and modification of CNSL is on cardanol-derived products [8–10]. These include aromatic amines as polymers [11,12], cardanol-based phosphates as modifiers for epoxy resins [13], cardanol grafted natural rubber as rubber plasticizers [14], amine-based surfactants [15] and phenol/cardanol-formaldehyde based adhesives [16].

The chemical valorization of anacardic acid (**1**) is even more attractive, because it contains an additional functional group. However, the separation and purification of this CNSL component without decarboxylation is laborious and relies on wasteful and tedious processes such as fractionate precipitation or column chromatography [6,17]. A limited number of derivatizations of anacardic acid are reported by now, including the synthesis of lactones [18–20], sulfonamides [21] or hydrazones [22], typically bioactive compounds though with low commercial value. However, several studies suggest that anacardic acid and its derivatives display a broad range of biological activities such as antimicrobial [23], antioxidant [24], molluscicidal [25] and antiplaque [26]. Ginkgolic acids, structurally closely related analogues of anacardic acid, have been reported to exhibit tyrosinase inhibitory activity [27]. We herein report a concise synthesis of the most potent tyrosinase inhibitor among them, the ginkgolic acid (13:0), starting from crude CNSL (Scheme 1, left).

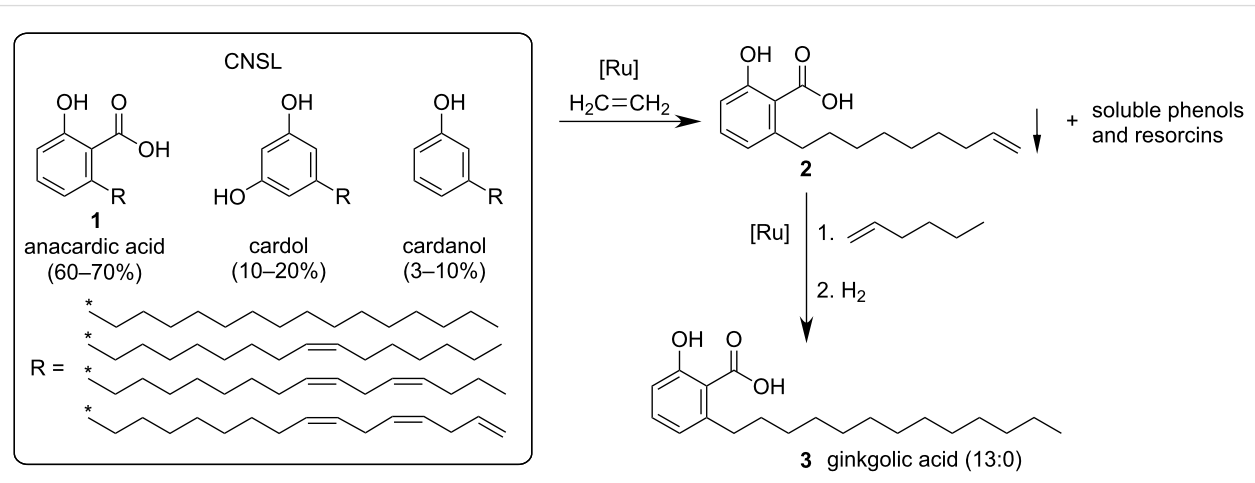
Tyrosinase is an enzyme [28] which is responsible for browning of fruits and vegetables as well as skin pigmentation [29]. Furthermore, it is linked to several neurodegenerative diseases [30]. Therefore, the study and development of tyrosinase inhibitors from renewable resources is of particular interest for research and industry [31,32]. Fu et al. investigated naturally occurring ginkgolic acids which they selectively synthesized from 2,6-dihydroxybenzoic acid (**4**), and found that the tride-

canyl substituted derivative ginkgolic acid (13:0, **3**) exhibits the most promising inhibitory activity.

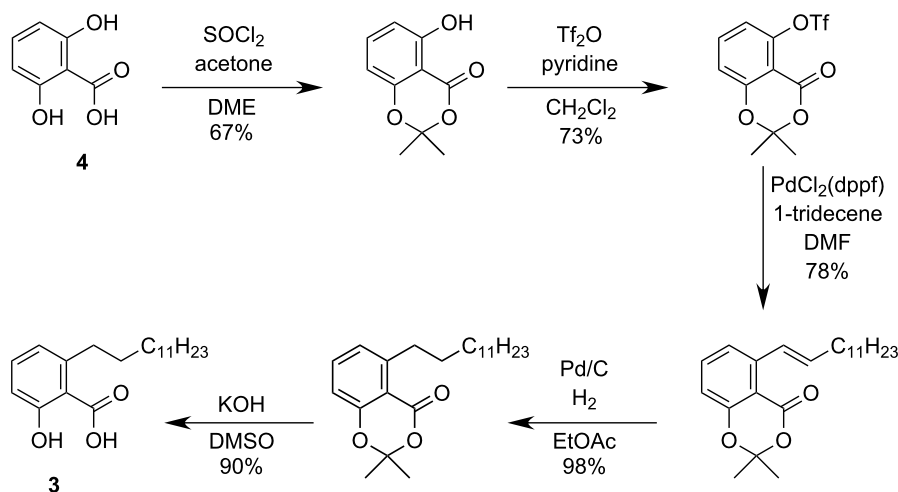
While this modular approach is very appealing for drug-discovery, the use of expensive γ -resorcyclic acid as the substrate basis and the low overall yield over several reaction steps are certainly drawbacks for larger scale production (Scheme 2) [27].

Due to the structural similarity of ginkgolic and anacardic acids, we believed that a particularly desirable synthesis of 2-hydroxy-6-tridecylbenzoic acid (**3**) would involve CNSL as the substrate basis. However, the functionalization of the anacardic acid component of CNSL presents several challenges. Since CNSL consists of a mixture of acids, phenols and resorcinols with saturated and unsaturated side chains, it seemed to be impossible to derive a single product with a shorter side chain via a cross-metathesis with a short olefin, since inevitable, an inseparable mixture of many compounds would result. It is, thus, necessary to converge as many components as possible into one single compound.

Based on concepts that we had previously utilized for the chemical modification of the cardanol component, we first investigated strategies based on cross-metathesis of CNSL with ethylene [33–35]. Each unsaturated double bond isomer has the first double bond located at the C-8 position, so that no matter how many other double-bonds are present, the unsaturated side chains of all arenes will be shortened to ω -nonenyl groups if ethylene is added in excess. The main difficulty is that thermal purification of CNSL would inevitably lead to decarboxylation, and that unpurified CNSL, as it is obtained in an extraction process, contains a wealth of side components, many of which act as catalyst poisons.



Scheme 1: Targeted conversion of CNSL into a tyrosinase inhibitor.

**Scheme 2:** Previous synthesis of 2-hydroxy-6-tridecylbenzoic acid by Fu et al.

However, if an enetholysis could be conducted with crude CNSL, it would lead to the shortened derivatives of all unsaturated components. We reasoned that it might be possible to selectively precipitate the 2-hydroxy-6-(non-8-enyl)benzoic acid (**2**) from this product mixture and use this as a substrate for a consecutive cross-metathesis with 1-hexene followed by a hydrogenation and thus, selectively obtain the target product 2-hydroxy-6-tridecylbenzoic acid (**3**).

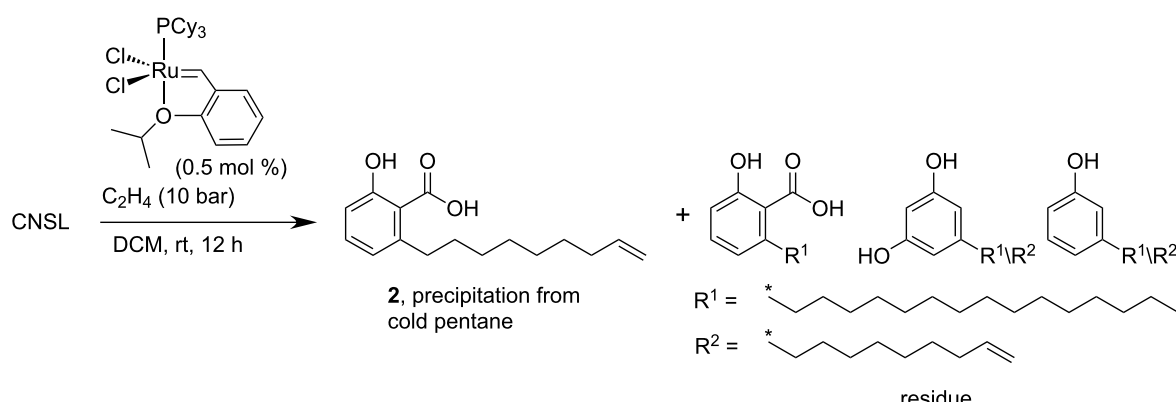
Results and Discussion

Ethenolysis of crude CNSL

After thorough optimization, we found that natural CNSL, a highly viscous brown oil, obtained by ether extraction of cashew nutshell shells, undergoes smooth enetholysis only in dichloromethane as the solvent (Scheme 3). Using more sus-

tainable solvents or no solvent at all, the reaction gave almost no turnover, regardless of the ruthenium catalyst employed. However, as a 1.1 M solution in dichloromethane, the unsaturated components of CNSL were converted in high yields at 10 bar of ethylene in the presence of 0.5 mol % of the first generation Hoveyda–Grubbs catalyst **Ru-1**.

The resulting mixture was filtered through celite, and the dichloromethane solvent was removed in *vacuo*. After addition of pentane, the mixture was chilled causing selective precipitation of the desired product **2** as a colorless solid in an amount that is equivalent to 80% of the anacardic acid content or 84% of the unsaturated anacardic acid. Anacardic acid makes up for ca. 70% of the CNSL, so that the yield is 56% based on the entire CNSL. We were pleased to find that the saturated

**Scheme 3:** Ethenolysis of the crude CNSL.

C15-anacardic acid stays in solution along with cardanol and cardol derivatives. This residue may be utilized for chemical valorization after purification via distillation. This ethenolysis/purification sequence was successfully performed on multi-gram scales, yielding up to 16 g product in a single run.

One-pot cross-metathesis/hydrogenation

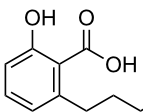
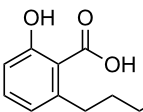
We next sought for suitable conditions that would allow the cross-metathesis of **2** with 1-hexene to give 2-hydroxy-6-(tridec-8-enyl)benzoic acid (**5**). When performing the hexenolysis of **2** with 7 equivalents of 1-hexene using 1 mol % of **Ru-1** in dichloromethane at rt, the desired product was obtained only in unsatisfactory yield after 12 h (Table 1, entry 1). High amounts of starting material were detected in the reaction mixture which points towards either a low conversion or an unfavorable position of the metathesis reaction equilibrium. We tested several methods to shift the equilibrium by purging the ethylene byproduct from the reaction mixture with inert gas, but finally found that the best yields were obtained when allowing the ethylene to slowly evaporate from the reaction mixture via

an oil bubbler. This way, the yield was improved to 53% (Table 1, entry 2).

The yield was further improved by raising the reaction temperature to 60 °C (Table 1, entry 3). Now, only 3% starting material **2** was detected, but unwanted homocoupling of **2** (product **6**, see Supporting Information File 1) became a major side reaction.

We tested several solvents including sustainable solvents like dimethyl carbonate and *p*-cymene. Unfortunately, this led to a decreased conversion and just 44–47% yield of the desired product. The use of the halogenated solvent dichloromethane was still most efficient. Comparative tests with varying amounts of 1-hexene revealed that an excess of 7 equivalents was optimal. With a smaller amount the yield was decreased (Table 1, entry 9 and 10), while a higher excess leads to decreased conversion. This can be explained by the undesired homocoupling of 1-hexene as a side reaction, which delivers the less active 5-decene (**7**, see Supporting Information File 1). In

Table 1: Cross-metathesis of 2-hydroxy-6-(non-8-enyl)benzoic acid (**2**) with 1-hexene.^a

 2		Ru-cat		 5		
entry	catalyst	solvent	1-hexene [equiv]	time	conversion [%]	5 [%] ^b
1 ^c	Ru-1	DCM	7	12 h	35	33
2 ^d	Ru-1	DCM	7	12 h	55	53
3	Ru-1	DCM	7	12 h	97	73
4	Ru-1	<i>p</i> -cymene	7	12 h	28	3
5	Ru-1	DMC	7	12 h	66	44
6	Ru-1	Me-THF	7	12 h	64	47
7	Ru-1	acetone	7	12 h	76	59
8	Ru-1	THF	7	12 h	51	42
9	Ru-1	DCM	5	12 h	94	69
10	Ru-1	DCM	3	12 h	81	65
11	Ru-1	DCM	7	6 h	96	74
12	Ru-2	DCM	7	6 h	98	72
13	Ru-3	DCM	7	6 h	98	65
14	Ru-4	DCM	7	6 h	98	56
15	Ru-5	DCM	7	6 h	93	55
16	Ru-6	DCM	7	6 h	46	27
17	Ru-7	DCM	7	6 h	98	45
18 ^e	Ru-1	DCM	7	6 h	97	76 (72) ^f

^aReaction conditions: 0.5 mmol **2**, given equiv 1-hexene, 1 mol % Ru-cat, 60 °C, given time, open system via oil bubbler, ^bYields determined by GC using *n*-tetradecane as internal standard. ^crt, closed system; ^drt; ^e2 mol % Ru-cat; ^fisolated yield.

principle, these internal olefins can still undergo metathesis albeit with less activity, depending on the catalyst. It was possible to reduce the time of the reaction to 6 h with almost the same yield (Table 1, entry 11).

We investigated various ruthenium catalysts in search for the optimal performance (Figure 1). The second generation Hoveyda–Grubbs catalyst previously used to change the olefinic side chain of cardanol via cross-metathesis [36], only reached a yield of 45% (Table 1, entry 17). Several modified second generation catalysts were tested, reaching yields of up to 72% of the desired product (Table 1, entry 12). However, the first generation Hoveyda–Grubbs catalyst **Ru-1**, which was reported in literature to be highly efficient for the ethenolysis of several CNSL components [35], showed the best activity. Increasing the catalyst loading to 2% gave only insignificantly better yields (Table 1, entry 18).

It is known that ruthenium metathesis catalysts can be transformed *in situ* into an active hydrogenation catalyst [37,38]. We, thus added charcoal and methanol to the crude reaction mixture of the cross-metathesis and stirred the reaction for additional 2 h under 5 bar of hydrogen. This way, the products were fully hydrogenated in quantitative yield. We were pleased to find that the desired product **3** could easily be purified by frac-

tionate precipitation from cold pentane. The one-pot cross-methathesis/hydrogenation was successfully scaled up to multi-gram (8 mmol) scale yielding 72% of the hydrogenated product **3**. Combined with the ethenolysis/precipitation step, the entire sequence afforded 61% overall yield based on unsaturated anacardic acids present in the CNSL (Scheme 4).

Conclusion

In conclusion, a straightforward sequence of an ethenolysis, cross-metathesis and hydrogenation was developed for the synthesis of the tyrosinase inhibitor **3** from the non-edible waste product CNSL. The key step to this process is the ethenolysis of crude CNSL followed by a selective precipitation of 2-hydroxy-6-(non-8-enyl)benzoic acid (**2**), which transforms the complex substrate mixture into a single, pure compound. The subsequent hexenolysis can be combined with an hydrogenation to an efficient one-step process to obtain the target molecule 2-hydroxy-6-tridecylbenzoic acid (**3**). Interestingly, it is a first-generation Hoveyda–Grubbs catalyst **Ru-1** that is most efficient for both metathesis steps.

Experimental

General methods

All reactions were performed in oven-dried glassware containing a Teflon-coated stirring bar and dry septum under argon at-

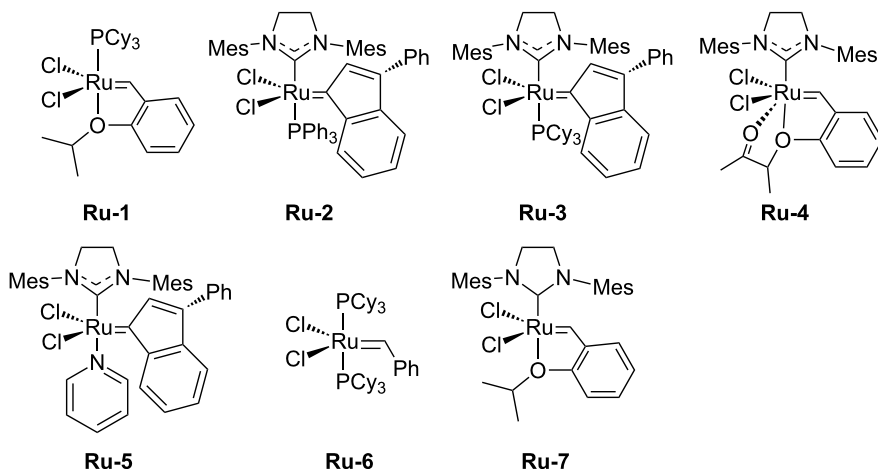
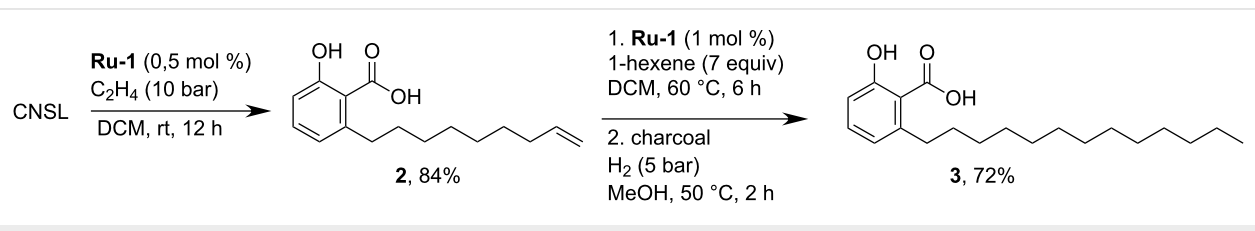


Figure 1: State-of-the-art metathesis catalysts.



Scheme 4: Overall process in a preparative scale.

mosphere. All optimization reactions were monitored by GC using *n*-tetradecane as internal standard. Products were silylated in GC vials with *N*-methyl-*N*-(trimethylsilyl)trifluoroacetamide. Response factors of the products with regard to *n*-tetradecane were obtained experimentally by analyzing known quantities of the substances. GC analyses were carried out using an HP-5 capillary column (phenyl methyl siloxane, 30 m × 320 × 0.25, 100/2.3-30-300/3) and a time program beginning with 2 min at 60 °C, heating rate 30 °C/min, 3 min at 300 °C. NMR spectra were measured at ambient temperature using CDCl₃ as solvent, with proton, and carbon resonances at 300 MHz/400 MHz and 75 MHz, respectively. All NMR data are reported in ppm relative to the solvent signal. CHN-elemental analyses were performed with a Hanau Elemental Analyzer vario Micro cube.

Commercial substrates were used as received unless otherwise stated. All solvents and liquid reactants were degassed with Argon for 15 min prior to use. Ethylene was purchased from Air Liquide GmbH (purity 99,95%). All catalysts were donated by Umicore.

Preparation of CNSL

Cashew nutshell liquid was extracted following the procedure described in the reference [34]: Cashew nutshells (500 g), collected from Naliendele in Mtwara, Tanzania, were comminuted into \approx 1 mm small particles which were then treated by Soxhlet extraction with Et₂O (500 mL) at 50 °C for 6 h. Removal of the solvent in vacuo resulted in a highly viscous brown oil (160 g, 32 wt %). The CNSL was used without further purification.

Synthesis of 2-hydroxy-6-(non-8-enyl)benzoic acid (2) via ethenolysis of CNSL

A 1 L Parr autoclave was charged with the metathesis catalyst **Ru-1** (330 mg, 0.55 mmol), CNSL (37.7 g, 110 mmol) and DCM (100 mL) under ethylene atmosphere. The system was evacuated and backfilled with ethylene (5 bar) three times and finally pressurized to 10 bar. The mixture was stirred at 500 rpm at room temperature for 12 h. After the reaction time, the reaction mixture was filtered through celite and the filter cake was washed with DCM (2 × 10 mL). The solvent was removed in vacuo and the residue was dissolved in pentane (50 mL) and stored in the freezer until precipitation of the solid. The precipitate was filtered and washed with cold pentane (2 × 20 mL) yielding the product 2-hydroxy-6-(non-8-enyl)benzoic acid (2) as colorless solid (16.2 g, 84%). CHN-elemental analysis calcd for C₁₆H₂₂O₃: C, 73.25; H, 8.45; found: C, 73.55; H, 8.53; ¹H NMR (300 MHz, CDCl₃) δ 10.98 (br. s., 1H), 7.38 (dd, *J* = 8.4, 7.5 Hz, 1H), 6.89 (dd, *J* = 8.3, 1.3 Hz, 1H), 6.79 (dd, *J* = 7.5, 1.3 Hz, 1H), 5.82 (ddt, *J* = 17.0,

10.2, 6.7, 6.7 Hz, 1H), 5.03 (q, *J* = 1.7 Hz, 1H), 4.89–4.99 (m, 1H), 2.94–3.05 (m, 2H), 2.00–2.10 (m, 2H), 1.56–1.68 (m, 2H), 1.29–1.44 (m, 8H) ppm; ¹³C NMR (75 MHz, CDCl₃) δ 176.1, 163.7, 147.8, 139.2, 135.5, 122.8, 115.9, 114.1, 110.3, 36.4, 33.8, 31.9, 29.7, 29.3, 29.1, 28.9 ppm. The analytical data matched those reported in the literature [38].

Optimization of the reaction conditions for the synthesis of 2-hydroxy-6-(tridec-8-enyl)benzoic acid (5)

An oven-dried 20 mL vial was charged with **Ru-1** (3 mg, 5.00 μmol), **2** (131 mg, 0.5 mmol) and closed with a crimp cap. The vial was evacuated and backfilled three times with argon. 1-Hexene (3.50 mmol, 0.45 mL) and DCM (1 mL) were added simultaneously via syringe under an argon atmosphere. The continuous elimination of formed ethylene was performed by connecting the reaction vessel via an open system to an oil bubbler. The resulting mixture was stirred at 60 °C for 6 h. After the reaction was complete, the mixture was filtered through celite and the filter cake was washed with DCM (2 × 5 mL). The solvent was removed in vacuo and the residue was dissolved in pentane (5 mL) and stored in the freezer until precipitation of the solid. Product **5** was isolated as colorless solid (120 mg, 72%). CHN-elemental analysis calcd for C₂₀H₃₀O₃: C, 75.43; H, 9.50; found: C, 75.43; H, 9.36; ¹H NMR (400 MHz, CDCl₃) δ 11.00 (s, 1H), 7.38 (t, *J* = 7.9 Hz, 1H), 6.86–6.91 (m, 1H), 6.76–6.82 (m, 1H), 5.33–5.44 (m, 2H), 2.95–3.03 (m, 2H), 1.92–2.08 (m, 4H), 1.56–1.66 (m, 2H), 1.25–1.43 (m, 12H), 0.86–0.92 (m, 3H) ppm; ¹³C NMR (75 MHz, CDCl₃) δ 175.9, 163.7, 147.8, 135.5, 130.4, 130.3, 129.9, 129.8, 122.8, 115.9, 110.3, 36.5, 32.6, 32.3, 32, 31.8, 29.8, 29.6, 29.3, 29.1, 26.9, 22.3, 22.2, 14 ppm. The analytical data matched those reported in the literature [39].

One-pot synthesis of 2-hydroxy-6-tridecylbenzoic acid (3)

An oven-dried 20 mL vial was charged with **Ru-1** (3 mg, 5.00 μmol), **2** (131 mg, 0.50 mmol) and closed with a crimp cap. The vial was evacuated and backfilled three times with argon. 1-Hexene (3.50 mmol, 0.45 mL) and DCM (1 mL) were added simultaneously via syringe under an argon atmosphere. The continuous elimination of formed ethylene was performed by connecting the reaction vessel via an open system to an oil bubbler. The resulting mixture was stirred at 60 °C for 6 h. After the reaction was complete, methanol (0.5 mL) and activated charcoal (20.0 mg) were added. The vial was closed with a septum cap, penetrated with a cannula for pressure equilibration and placed into an autoclave. The system was purged twice with H₂ (5 bar) and finally pressurized to 5 bar. The resulting mixture was stirred for 3 h at 50 °C. After cooling down to room temperature, the pressure was slowly released under con-

stant stirring at 300 rpm. The reaction mixture was filtered through celite and the filter cake was washed with DCM (2×5 mL). The solvent was removed in vacuo and the residue was dissolved in pentane (5 mL) and stored in the freezer until precipitation of the solid. The precipitate was filtered and washed with cold pentane (2×5 mL), yielding the product **3** as colorless solid (120 mg, 72%). CHN-elemental analysis calcd for $C_{20}H_{32}O_3$: C, 74.9; H, 10.1; found: C, 74.8; H, 9.8; 1H NMR (300 MHz, $CDCl_3$) δ 10.98 (s, 1H), 7.38 (dd, $J = 8.3, 7.6$ Hz, 1H), 6.89 (dd, $J = 8.3, 1.2$ Hz, 1H), 6.79 (dd, $J = 7.5, 1.1$ Hz, 1H), 2.92–3.06 (m, 2H), 1.54–1.70 (m, 2H), 1.21–1.44 (m, 20H), 0.84–0.93 (m, 3H) ppm; ^{13}C NMR (75 MHz, $CDCl_3$) δ 176.1, 163.6, 147.9, 135.5, 130.3, 122.8, 115.9, 110.4, 36.5, 32.0, 31.9, 29.8, 29.69, 29.68, 29.65, 29.6, 29.5, 29.4, 29.3, 22.7, 22.2, 14.1 ppm. The analytical data matched those reported in the literature [40].

Supporting Information

Supporting Information File 1

Additional screening and NMR spectra.

[<https://www.beilstein-journals.org/bjoc/content/supplementary/1860-5397-14-252-S1.pdf>]

Acknowledgements

The authors acknowledge Matthias W. Pankau for helpful discussion and corrections and the Deutsche Bundesstiftung Umwelt (fellowship to J.P.), the Deutsche Forschungsgemeinschaft (Collaborative Research Centre SFB/TRR 88 ‘3MET’ and Cluster of Excellence RESOLV, EXC 1069) for the financial support and Umicore for provision of the catalysts.

ORCID® IDs

Lukas J. Gooßen - <https://orcid.org/0000-0002-2547-3037>

References

1. Balachandran, V. S.; Jadhav, S. R.; Vemula, P. K.; John, G. *Chem. Soc. Rev.* **2013**, *42*, 427–438. doi:10.1039/C2CS35344J
2. Tyman, J. H. P.; Morris, L. J. *J. Chromatogr. A* **1967**, *27*, 287–288. doi:10.1016/S0021-9673(01)85871-4
3. Gandhi, T. S.; Dholakiya, B. Z.; Patel, M. R. *Pol. J. Chem. Technol.* **2013**, *15*, 24–27.
4. “FAOSTAT”. <http://faostat3.fao.org/home/E> (accessed Aug 1, 2018).
5. Sood, S. K.; Tyman, J. H. P.; Durrani, A.; Johnson, R. A. *Lipids* **1986**, *21*, 241–246. doi:10.1007/BF02534830
6. Paramashivappa, R.; Phani Kumar, P.; Vithayathil, P. J.; Srinivasa Rao, A. *J. Agric. Food Chem.* **2001**, *49*, 2548–2551. doi:10.1021/jf001222j
7. Anilkumar, P., Ed. *Cashew Nut Shell Liquid*; Springer International Publishing: Cham, 2017. doi:10.1007/978-3-319-47455-7
8. Phani Kumar, P.; Paramashivappa, R.; Vithayathil, P. J.; Subba Rao, P. V.; Srinivasa Rao, A. *J. Agric. Food Chem.* **2002**, *50*, 4705–4708. doi:10.1021/jf020224w
9. Balcar, H.; Žilková, N.; Kubů, M.; Polášek, M.; Zedník, J. *Catal. Today* **2018**, *304*, 127–134. doi:10.1016/j.cattod.2017.09.049
10. Shinde, T.; Varga, V.; Polášek, M.; Horáček, M.; Žilková, N.; Balcar, H. *Appl. Catal., A* **2014**, *478*, 138–145. doi:10.1016/j.apcata.2014.03.036
11. Froidevaux, V.; Negrell, C.; Caillol, S.; Pascault, J.-P.; Boutevin, B. *Chem. Rev.* **2016**, *116*, 14181–14224. doi:10.1021/acs.chemrev.6b00486
12. Darroman, E.; Bonnot, L.; Auvergne, R.; Boutevin, B.; Caillol, S. *Eur. J. Lipid Sci. Technol.* **2015**, *117*, 178–189. doi:10.1002/ejlt.201400248
13. Wang, X.; Zhou, S.; Guo, W.-W.; Wang, P.-L.; Xing, W.; Song, L.; Hu, Y. *ACS Sustainable Chem. Eng.* **2017**, *5*, 3409–3416. doi:10.1021/acssuschemeng.7b00062
14. Mohapatra, S.; Nando, G. B. *RSC Adv.* **2014**, *4*, 15406–15418. doi:10.1039/C3RA46061D
15. Bragoni, V.; Rit, R. K.; Kirchmann, R.; Trita, A. S.; Gooßen, L. J. *Green Chem.* **2018**, *20*, 3210–3213. doi:10.1039/C8GC01686K
16. Varghese, L. A.; Thachil, E. T. *J. Adhes. Sci. Technol.* **2004**, *18*, 1217–1224. doi:10.1163/1568561041588174
17. Nagabhushana, K. S.; Ravindranath, B. *J. Agric. Food Chem.* **1995**, *43*, 2381–2383. doi:10.1021/jf00057a012
18. Mgaya, J. E.; Mubofu, E. B.; Mgani, Q. A.; Cordes, D. B.; Slawin, A. M.; Cole-Hamilton, D. J. *Eur. J. Lipid Sci. Technol.* **2015**, *117*, 190–199. doi:10.1002/ejlt.201400268
19. Logrado, L. P. L.; Santos, C. O.; Romeiro, L. A. S.; Costa, A. M.; Ferreira, J. R. O.; Cavalcanti, B. C.; de Moraes, O. M.; Costa-Lotufo, L. V.; Pessoa, C.; dos Santos, M. L. *Eur. J. Med. Chem.* **2010**, *45*, 3480–3489. doi:10.1016/j.ejmech.2010.05.015
20. Logrado, L. P. L.; Silveira, D.; Romeiro, L. A. S.; de Moraes, M. O.; Cavalcanti, B. C.; Costa-Lotufo, L. V.; do Ó. Pessoa, C.; dos Santos, M. L. *J. Braz. Chem. Soc.* **2005**, *16*, 1217–1225. doi:10.1590/S0103-50532005000700020
21. Reddy, N. S.; Rao, A. S.; Chari, M. A.; Kumar, V. R.; Jyothy, V.; Himabindu, V. *J. Chem. Sci.* **2012**, *124*, 723–730. doi:10.1007/s12039-012-0253-1
22. Swamy, B. N.; Suma, T. K.; Rao, G. V.; Reddy, G. C. *Eur. J. Med. Chem.* **2007**, *42*, 420–424. doi:10.1016/j.ejmech.2006.09.009
23. Rambabu, N.; Dubey, P. K.; Ram, B.; Balram, B. *Asian J. Chem.* **2016**, *28*, 175–180. doi:10.14233/ajchem.2016.19310
24. Maia, F. J. N.; Ribeiro, V. G. P.; Lomonaco, D.; Luna, F. M. T.; Mazzetto, S. E. *Ind. Crops Prod.* **2012**, *36*, 271–275. doi:10.1016/j.indcrop.2011.10.019
25. Sullivan, J. T.; Richards, C. S.; Lloyd, H. A.; Krishna, G. *Planta Med.* **1982**, *44*, 175–177. doi:10.1055/s-2007-971434
26. Muroi, H.; Kubo, I. *J. Agric. Food Chem.* **1993**, *41*, 1780–1783. doi:10.1021/jf00034a049
27. Fu, Y.; Hong, S.; Li, D.; Liu, S. *J. Agric. Food Chem.* **2013**, *61*, 5347–5352. doi:10.1021/jf4012642
28. Wilcox, D. E.; Porras, A. G.; Hwang, Y. T.; Lerch, K.; Winkler, M. E.; Solomon, E. I. *J. Am. Chem. Soc.* **1985**, *107*, 4015–4027. doi:10.1021/ja00299a043
29. del Marmol, V.; Beermann, F. *FEBS Lett.* **1996**, *381*, 165–168. doi:10.1016/0014-5793(96)00109-3
30. Asanuma, M.; Miyazaki, I.; Ogawa, N. *Neurotoxic. Res.* **2003**, *5*, 165–176. doi:10.1007/BF03033137

31. Kubo, I.; Kinst-Hori, I. *J. Agric. Food Chem.* **1998**, *46*, 5338–5341.
doi:10.1021/jf980226+
32. Fais, A.; Corda, M.; Era, B.; Fadda, M. B.; Matos, M. J.; Quezada q, E.; Santana, L.; Picciau, C.; Podda, G.; Delogu, G. *Molecules* **2009**, *14*, 2514–2520. doi:10.3390/molecules14072514
33. Baader, S.; Ohlmann, D. M.; Gooßen, L. J. *Chem. – Eur. J.* **2013**, *19*, 9807–9810. doi:10.1002/chem.201301336
34. Baader, S.; Podsiadly, P. E.; Cole-Hamilton, D. J.; Goossen, L. J. *Green Chem.* **2014**, *16*, 4885–4890. doi:10.1039/C4GC01269K
35. Julis, J.; Bartlett, S. A.; Baader, S.; Beresford, N.; Routledge, E. J.; Cazin, C. S. J.; Cole-Hamilton, D. J. *Green Chem.* **2014**, *16*, 2846–2856. doi:10.1039/C4GC00111G
36. Mgaya, J. E.; Bartlett, S. A.; Mubofu, E. B.; Mgani, Q. A.; Slawin, A. M. Z.; Pogorzelec, P. J.; Cole-Hamilton, D. J. *ChemCatChem* **2016**, *8*, 751–757. doi:10.1002/cctc.201501110
37. Drouin, S. D.; Zamanian, F.; Fogg, D. E. *Organometallics* **2001**, *20*, 5495–5497. doi:10.1021/om010747d
38. Louie, J.; Bielawski, C. W.; Grubbs, R. H. *J. Am. Chem. Soc.* **2001**, *123*, 11312–11313. doi:10.1021/ja016431e
39. Zehnter, R.; Gerlach, H. *Liebigs Ann.* **1995**, 2209–2220.
doi:10.1002/jlac.1995199512307
40. Itokawa, H.; Totsuka, N.; Nakahara, K.; Takeya, K.; Lepoittevin, J.-P.; Asakawa, Y. *Chem. Pharm. Bull.* **1987**, *35*, 3016–3020.
doi:10.1248/cpb.35.3016

License and Terms

This is an Open Access article under the terms of the Creative Commons Attribution License (<http://creativecommons.org/licenses/by/4.0>). Please note that the reuse, redistribution and reproduction in particular requires that the authors and source are credited.

The license is subject to the *Beilstein Journal of Organic Chemistry* terms and conditions:
(<https://www.beilstein-journals.org/bjoc>)

The definitive version of this article is the electronic one which can be found at:
doi:10.3762/bjoc.14.252



Olefin metathesis catalysts embedded in β -barrel proteins: creating artificial metalloproteins for olefin metathesis

Daniel F. Sauer^{*1}, Johannes Schiffels², Takashi Hayashi³, Ulrich Schwaneberg² and Jun Okuda^{*1}

Review

Open Access

Address:

¹Institute of Inorganic Chemistry, RWTH Aachen University, Landoltweg 1, 52074 Aachen, Germany, ²Institute of Biotechnology, RWTH Aachen University, Woringerweg 3, 52074 Aachen, Germany and ³Department of Applied Chemistry, Graduate School of Engineering, Osaka University, 2-1 Yamadaoka, Suita 565-0871, Japan

Email:

Daniel F. Sauer* - daniel.sauer@ac.rwth-aachen.de; Jun Okuda* - jun.okuda@ac.rwth-aachen.de

* Corresponding author

Keywords:

artificial metalloprotein; β -barrel protein; metathese; olefin metathesis; ruthenium

Beilstein J. Org. Chem. **2018**, *14*, 2861–2871.

doi:10.3762/bjoc.14.265

Received: 31 August 2018

Accepted: 26 October 2018

Published: 19 November 2018

This article is part of the thematic issue "Progress in metathesis chemistry III" and is dedicated to the memory of Professor Willi Keim.

Guest Editors: K. Grela and A. Kajetanowicz

© 2018 Sauer et al.; licensee Beilstein-Institut.

License and terms: see end of document.

Abstract

This review summarizes the recent progress of Grubbs–Hoveyda (GH) type olefin metathesis catalysts incorporated into the robust fold of β -barrel proteins. Anchoring strategies are discussed and challenges and opportunities in this emerging field are shown from simple small-molecule transformations over ring-opening metathesis polymerizations to *in vivo* olefin metathesis.

Introduction

Olefin metathesis constitutes the rearrangement of C=C double bonds in the presence of transition metal catalysts based on V, Mo, W, Re, Ru, and Os together with alkylating co-catalysts. This transformation is widely used in organic synthesis as well as in polymerization of various unsaturated monomers [1]. According to the Chauvin mechanism, the catalytically active species are Schrock-type carbenes or alkylidenes [2]. Olefin metathesis greatly profited from the isolation of structurally well-defined metal alkylidene complexes [3,4]. The best studied

and most commonly employed catalysts are based on Mo, W, and Ru [1].

Initially, these complexes were considered to be sensitive towards air and moisture. Nevertheless, adding Ru, Os and Ir salts to an aqueous solution or emulsion of a norbornene derivative led to ring-opening metathesis polymerization to give the corresponding polymer [5,6]. Through modification of the first coordination sphere by adding an *N*-heterocyclic carbene

(NHC) ligand and a chelating styrene to the so-called Grubbs 1st generation catalyst, the relatively air- and moisture-stable Grubbs–Hoveyda type (GH-type) catalysts were obtained [7]. These catalysts do not only show stability towards moisture, but can also be directly used in water, allowing to perform olefin metathesis reactions in aqueous solutions [8,9].

Olefin metathesis is not known in biological systems and therefore can be regarded as bio-orthogonal. The group of Davis utilized the olefin metathesis reaction to perform post-experimental protein modifications [10–12]. For example, a single cysteine mutant of subtilisin from *Bacillus licheniformis* (SBL-S156C) was modified via sulfide bond formation with allyl cysteine displaying an allyl function on the protein surface. This allyl group was modified with a GH-type catalyst and carbohydrate or small polyethylene glycol (PEG) groups were attached [11]. As another strategy to modify a protein surface with olefin metathesis, Isarov and Pokorski introduced a Grubbs 3rd generation catalyst on the surface of lysozyme and performed ring-opening metathesis polymerization (ROMP) on the protein surface employing a PEGylated norbornene derivative as substrate [13]. This led to proteins modified with PEG chains. These two examples illustrate the potential applications of olefin metathesis in protein modification. Further applications would be the implementation of olefin metathesis into natural metabolic pathways to allow synthesis of fine chemicals [14]. Also, a targeted reaction in a certain environment within a living cell with a precise release or activation of the catalyst would enable new ways of drug delivery. The challenge to overcome this regard is the deactivation of the catalyst inside the cells and the transport within organisms without triggering or activating a response of the corresponding target [15]. Additionally, the (kinetic) stability of the catalysts in aqueous solutions needs to be improved for this purpose. For application in organic synthesis

in aqueous environments, water solubility is also essential [16–18].

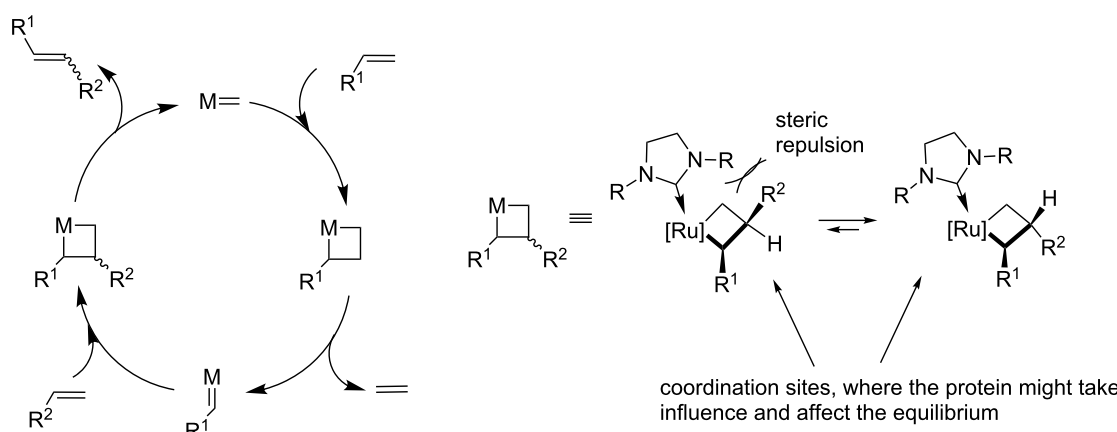
A promising approach is the embedment of the GH-type catalyst into well-defined protein scaffolds [19]. The combination of an engineered protein with a synthetic metal catalyst leads to artificial metalloproteins [20–23]. In the case of a metathesis catalyst, so-called artificial metathases are obtained, which could open new areas of biological applications [19]. The protein as second coordination sphere might take influence on the formation of the metallacyclobutane that was initially postulated by Chauvin [2]. The formation of the *E* or the *Z* product is dependent on the orientation of the R groups in this step of the catalytic cycle (Scheme 1).

In this short review, we focus on the status of embedding the GH-type catalyst into β -barrel proteins and show their application in various reactions using benchmark substrates. These transformations include all three fundamental olefin metathesis reactions: ring-opening metathesis polymerization (ROMP), ring-closing metathesis (RCM) as well as cross metathesis (CM) (Scheme 2).

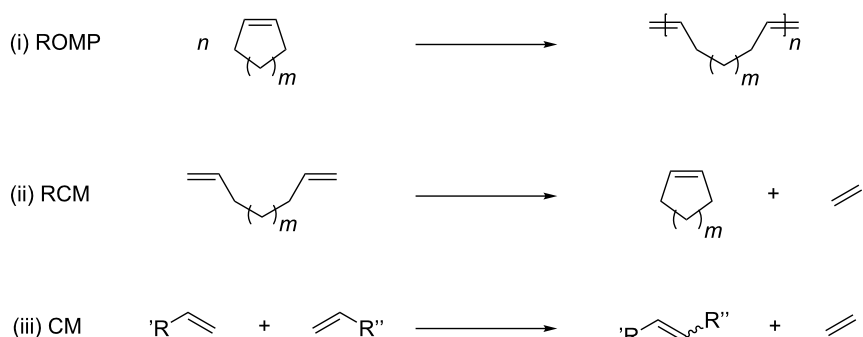
Review

Artificial metathases – anchoring approaches

Metalloproteins that contain one or more metal ions such as Mg, Ca, Mn, Fe, Ni, Co, Cu, Zn etc. within a protein are abundant in nature [24]. As metalloenzymes, these metalloproteins are capable of catalyzing various important reactions in biosynthesis and key steps in cellular energy metabolism. The embedded metal ion mainly acts as a Lewis acid catalyst or redox catalyst. Various metalloenzymes have been applied in laboratory-scale reactions and a few metalloenzymes such as nitrile



Scheme 1: Left: Mechanism of the olefin metathesis reaction postulated by Chauvin [2]. Right: Potential influence of the protein as second coordination sphere in the transition state that lead to different metathesis products.



Scheme 2: (i) Ring-opening metathesis polymerization (ROMP), (ii) ring-closing metathesis (RCM) and (iii) cross metathesis (CM).

hydratase (cobalt(III) in the active site) for the production of acrylamide have found application in industry [25]. Notably, however, the reaction scope of natural enzymes is quite limited. Apart from engineering natural enzymes, the approach of connecting abiotic co-factors (such as organometallic complexes) to natural or re-engineered protein scaffolds offers an attractive combination of both, broad reaction scope of chemical transformations as well as control of selectivity and specificity as found in natural enzymes. These so-called artificial metalloproteins or metalloenzymes offer two ways of fine-tuning activity and selectivity: As chemical means, the metal site can be adjusted and fine-tuned through modification of the ligands surrounding the metal. As biotechnological means, the protein cavity acting as second coordination sphere can be optimized to tune specificity as well as stereo- and regioselectivity. The extensive literature of artificial metalloproteins has been summarized in various comprehensive reviews [20–22].

One of the challenges to overcome in the construction of artificial metalloproteins is to find a method to incorporate a synthetic metal complex into a protein scaffold [26]. The common strategies are shown in Figure 1.

In Figure 1, the three commonly utilized methods to incorporate a synthetic cofactor are shown. Strategies utilized are supramolecular, dative and covalent anchoring. Supramolecular anchoring was pioneered by Wilson and Whitesides in 1978 [27]. They made use of the high affinity of (strept)avidin (Sav) to biotin that represents one of the strongest supramolecular interactions found in nature with a dissociation constant of approximately $K_d \approx 10^{-15} \text{ M}$ [28]. Initially, an achiral Wilkinson-type catalyst was attached to perform hydrogenation [27]. Nowadays, a broad variety of artificial metalloproteins based on this technology has been established [20,29]. Dative anchoring offers the possibility to liberate the active site from the protein easier as compared to supramolecular anchoring. However, the design of catalysts capable of undergoing dative anchoring is usually based on interactions of inhibitors with the active site of the protein. This makes the catalyst design challenging and the application is limited. Covalent anchoring of an organometallic complex offers the precise positioning of a catalyst within a protein scaffold. Formation of the covalent bond between cofactor and protein ensures an irreversible binding of the active site (i.e., the metal complex). This approach is highly versatile, because it is not necessary to have or to design inter-

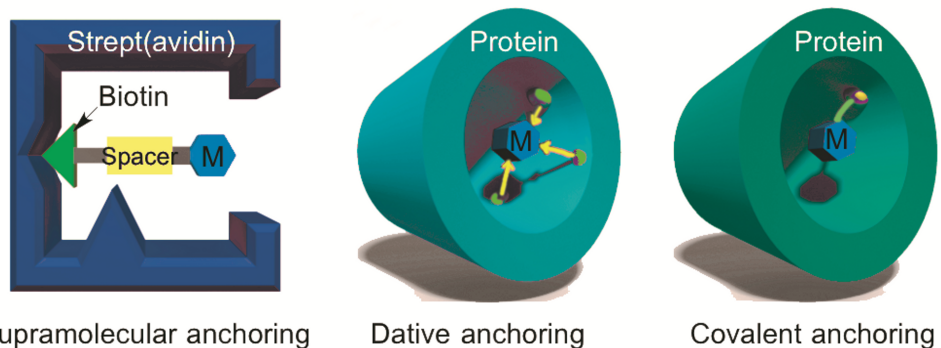


Figure 1: Common anchoring strategies for metal-complex or metal ion incorporation into protein scaffolds.

actions that are required for non-covalent anchoring, e.g., supramolecular or dative anchoring.

All three anchoring approaches – supramolecular, dative and covalent – have been utilized to construct artificial metalloproteins capable of catalyzing olefin metathesis reactions [19]. To date, eight artificial metathases have been reported. Among them, β -barrel proteins play a central role as protein scaffolds.

β -Barrel proteins

Proteins are constructed from two major secondary structural elements, namely α -helices and β -sheets. Notably, the latter are generally regarded to be more rigid than disordered or α -helix structures [30,31]. β -Barrels are structural motifs found in numerous proteins in which (mostly) antiparallel β -strands twist and coil to form closed, quasi-cylindrical structures held together by a network of hydrogen bonds [32]. Characterized by an amphiphilic nature with either hydrophobic “barrel” interiors and hydrophilic surfaces (as in globulins, carriers of hydrophobic molecules and fluorescent proteins) or hydrophilic cores and hydrophobic surfaces (as in membrane-bound β -barrels like porins and channel proteins), they can be present as minor motifs or even dominate the overall protein structure [33,34].

Small β -barrels such as lipocalins (i.e., transporters of small hydrophobic molecules that play vital roles in many biological processes [35]) or heme-containing nitrophorins/nitrobindins of the all- β -barrel type (involved in NO transport, storage and sensing as well as heme metabolism [36]) usually constitute eight to ten antiparallel β -strands and tightly packed hydrophobic or hydrophilic barrel interiors [37]. Membrane-bound β -barrels are confined to mitochondrial and chloroplast membranes and the outer membranes of Gram-negative bacteria [38]. They constitute up to 24 strands, require sophisticated assembly machineries for membrane integration [39] and are usually “plugged” by hydrophilic loops and helices that either ensure the binding of small molecules, or their (energy-dependent) transport across the outer membrane. TIM-barrels (named after triosephosphate isomerase, TIM), in turn, contain both α - and β -structures, i.e., a β -barrel structure (eight strands) enclosed by a series of eight α -helices. The TIM-barrel represents a very common – yet evolutionarily diverse – protein structure [40].

While following very similar structural patterns, β -barrel and TIM-barrel proteins occupy a tremendous sequence space and are highly versatile in terms of metabolic functions, binding properties, transport and catalytic activities. The compact barrel structure can be regarded as a prototype of stable protein scaf-

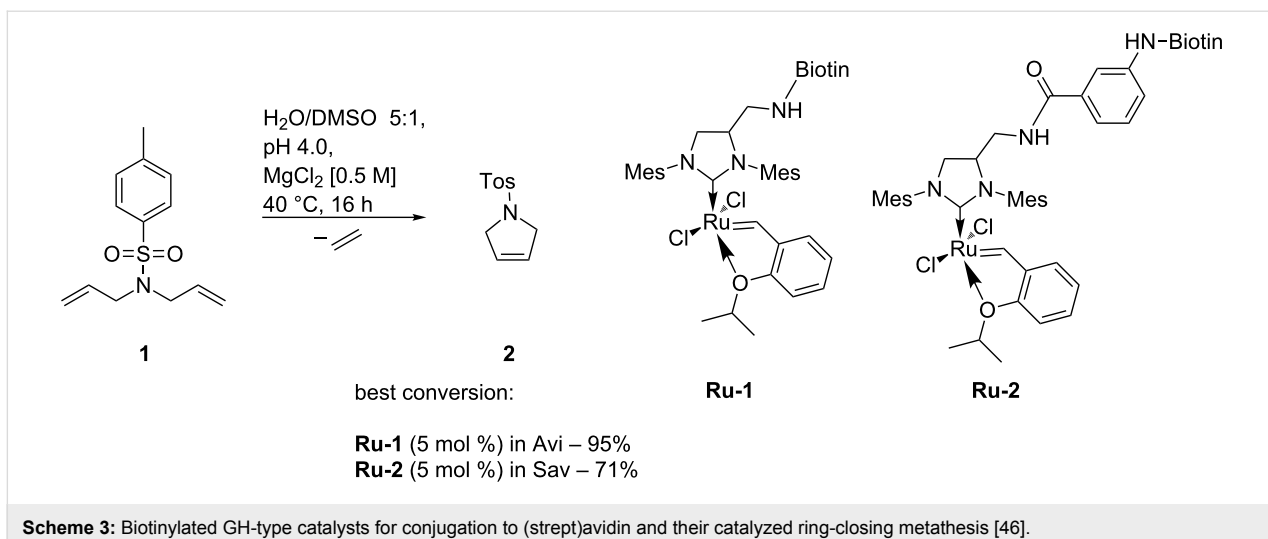
folds/motifs exhibiting stabilities against a wide range of external influences including high salt concentrations, high temperatures and organic solvents [41–45]. These properties make them excellent scaffolds for the construction of artificial metalloenzymes, which is achieved by removing the native cofactors or the cork/plug domains to reveal otherwise occupied pockets or pores that can then be loaded with artificial catalysts.

Artificial metathases within β -barrel proteins (Strept)Avidin

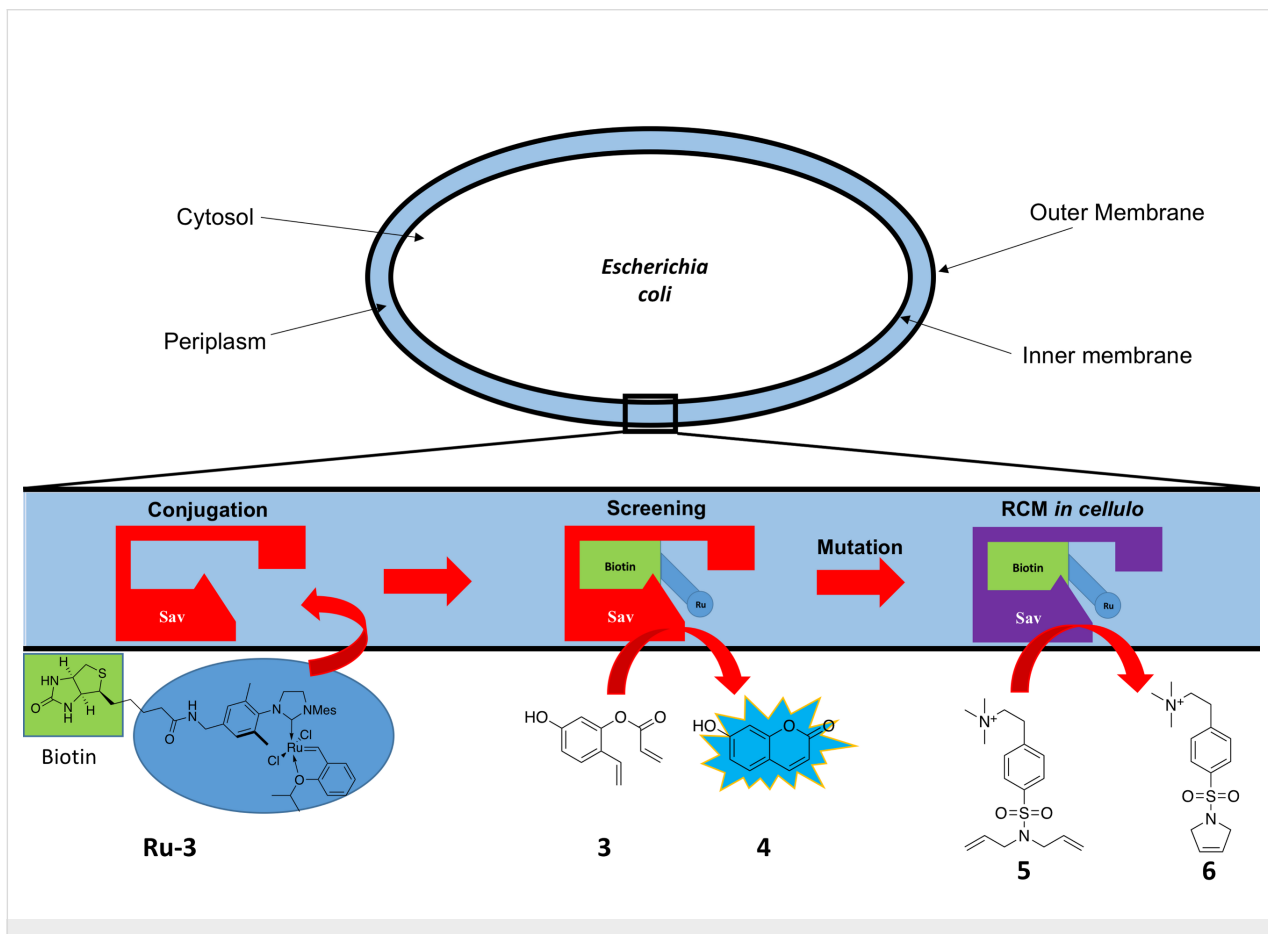
Artificial metalloproteins for olefin metathesis based on the supramolecular anchoring approach were synthesized by Ward [29]. A GH-type second generation olefin metathesis catalyst was modified at the periphery of an NHC ligand with a biotin moiety [46]. The small β -barrel protein avidin (Avi) or streptavidin (Sav) was incubated with the catalyst to give the artificial metalloprotein. This (strept)avidin-based catalyst was tested in the RCM reaction of *N,N*-diallyl-4-toluenesulfonamide (**1**) in aqueous buffer solution [46]. Conversions up to 95% with Avi as a protein scaffold were achieved (catalyst loading of 5 mol %). This was the first example describing olefin metathesis performed within a protein cavity. During this study, already a hint at the importance of the spacer length became apparent. A short spacer between the GH-type catalyst (**Ru-1**) and the biotin moiety did not lead to a successful conversion of the substrate. Elongation of the spacer (**Ru-2**) and therefore moving the active site slightly out of the protein cavity led to improved conversion (Scheme 3) [46].

The combination of the GH-type catalyst and (strept)avidin was further developed in a system that performs RCM reactions within a whole cell [47,48]. The scaffold protein Sav was produced into the periplasm of *Escherichia coli* (*E. coli*) [47]. The recombinant cells were incubated with a biotinylated GH-type catalyst **Ru-3** that reaches the target protein via diffusion through the outer membrane (Scheme 4). Characterization of this whole-cell system included ICP analysis. Whole-cells containing Sav showed an approximately three-fold increase in ruthenium content as compared to cells lacking the Sav variant (80,000 Ru atoms per cell and 29,000 Ru atoms per cell, respectively) [47].

This system was subjected to directed evolution. The twenty amino acid positions closest to the active site were saturated, and the best mutant formed the starting variant for the next iterative round. As screening substrate, the pre-fluorescent styrene derivative **3** was used. Following RCM, the fluorescent molecule umbelliferone (**4**) was generated. In total, five rounds of directed evolution were performed, yielding the mutant Sav_K121R_N49K_A119G_T114Q_V47A (Sav_Mut) [47].



Scheme 3: Biotinylated GH-type catalysts for conjugation to (strept)avidin and their catalyzed ring-closing metathesis [46].



Scheme 4: Whole-cell artificial metathases designed by Ward et al. [47].

As a rescreening, the RCM reaction of a water-soluble, charged diallylamine **5** was performed. Cells harboring the Sav_WT, Sav_Mut and no Sav were tested. Whole-cell Sav_WT and Sav_Mut reached both a turnover number per cell TON(per cell) of about 300,000. Cells without Sav reached

TON(per cell) \approx 20,000. The small difference between Sav_WT and the mutant Sav_Mut is explained by electrostatic repulsion of the positively charged substrate and the arginine at position 121. Another round of site-saturation mutagenesis yielded the variant Sav_R121L_N49K_A119G_T114Q_V47A

(Sav_Mut2), which exhibited an improved activity of TON(per cell) \approx 500,000 compared to Sav_WT [47]. This is the first example of a whole-cell metathesis biohybrid catalyst, opening up new possibilities to utilize olefins in biological systems in the context of artificial metabolism [14].

Nitrobindin

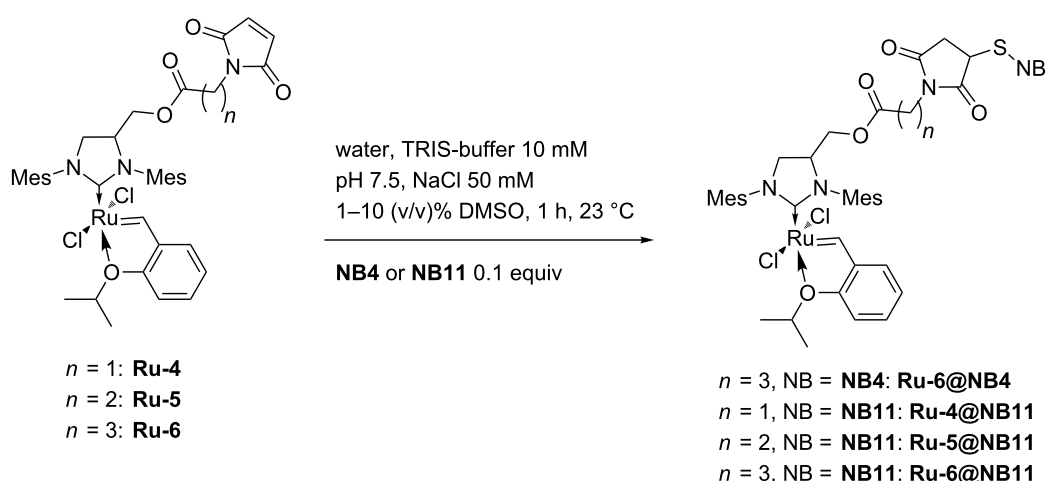
Nitrobindin (NB) is a small, soluble β -barrel protein with a molecular weight of 19 kDa [49]. NB wild-type has 10 β -strands and contains a heme as a prosthetic group [49]. Upon modification of the axial histidine that coordinates the heme, the robust β -barrel structure with a relatively small cavity is retained [50].

Further mutations within the cavity of NB provide a hydrophobic cavity. Several studies reported on the utilization of NB as scaffold for incorporated metal complexes, including the work of Hayashi et al. capitalizing on the polymerization of phenylacetylene [50,51], the Diels–Alder reaction [52,53], and hydrogen evolution [54]. Further, Lewis et al. employed the NB scaffold for epoxidation of styrene and other olefins [55]. In all studies, the catalyst incorporated into the NB scaffold showed increased activity as compared to the protein-free catalyst under similar conditions.

Engineered variants of NB were used to construct artificial metathesases [56]. The cavity of NB was enlarged by introducing five mutations compared to the NB wild-type. Two histidines were substituted by leucine or alanine. Furthermore, a cysteine was introduced allowing covalent anchoring, and the two methionines inside the cavity were substituted by leucines. This yielded the two mutants **NB4** (leucine for histidine; mutations in comparison to NB wild-type: M75L/H76L/Q96C/

M148L/H158L) and **NB11** (alanine for histidine; mutations in comparison to NB wild-type: M75L/H76L/Q96C/M148L/H158A) [56]. Notably, the introduced mutations further affected the cavity size of the proteins. **NB4** has a cavity volume of 855 \AA^3 and **NB11** has an enlarged volume of 1161 \AA^3 [52,56]. These two mutants were tested for the construction of artificial metathesases. As catalyst, GH-type catalysts with different spacer lengths were investigated, including methylene (**Ru-4**), ethylene (**Ru-5**) to a propylene (**Ru-6**) spacers [56]. Thereby, it was aimed to locate the active center properly within the protein cavity. The challenge in the conjugation of the GH-type catalyst into narrow protein cavities is to overcome the space demand of the bulky NHC ligand. The conjugation was performed via maleimide-thiol “click” reaction under slightly basic (pH 7.5) conditions. Within the small cavity of **NB4**, only the GH-type catalyst **Ru-6** with the longest spacer was able to undergo conjugation; however, the conjugational yield was very low (25%). Within the bigger cavity of **NB11**, all three catalysts **Ru-4/5/6** were able to undergo conjugation, and gradually increasing conjugation yields by elongation of the spacer was observed (from 29% for **Ru-4** up to 89% for **Ru-6**; Scheme 5) [56].

These artificial metalloproteins were purified and characterized by different analytical methods [56]. Structural integrity of the β -barrel fold was confirmed by CD spectroscopy. ICP–OES was used to determine the metal content. A little less than one metal center per protein molecule was found to be present. Additional absorption bands in the UV–vis spectra around $\lambda = 380$ nm indicated the presence of the GH-type catalyst. Finally, the peak for the biohybrid conjugate was observed in ESI–TOF–MS suggesting successful covalent anchoring.



Scheme 5: Coupling of GH-type catalysts **Ru-4/5/6** to **NB4** or **NB11**.

Beside ring-closing metathesis (RCM) of 2,2-diallylpropane-1,3-diol to yield the corresponding cyclopentane derivative, the synthesized biohybrid catalysts were tested in the ring-opening metathesis polymerization of a 7-oxanorbornene derivative **7** (Table 1) [56].

Table 1: Ring-opening metathesis polymerization (ROMP) of oxanorbornene **7** catalyzed by artificial metathesases based on NB.

Entry	Catalyst	Conversion ^a [%]	cis/trans ^a	TON
1 ^{b,c}	Ru-4/5/6	<5	n.d.	n.d.
2	Ru-6@NB4	10	40:60	1100
3	Ru-4@NB11	<5	n.d.	n.d.
4	Ru-5@NB11	18	43:57	2000
5	Ru-6@NB11	78	43:57	9700

^aDetermined by ¹H NMR spectroscopy in CDCl₃; ^bcontaining 10% (v/v) THF; ^ccatalyst loading: 0.01 mol %.

With a catalyst loading as low as 0.01 mol %, no activity of the protein-free catalysts **Ru-4/5/6** was detected (Table 1, entry 1) [56]. In turn, the catalysts immobilized within the protein cavity showed activity. Within the small cavity of **NB4**, moderate conversions up to 10% were obtained, and activity was only observed when **Ru-6** (longest spacer) was incorporated (Table 1, entry 2) [56]. By contrast, within the larger cavity of **NB11**, all catalysts **Ru-4/5/6** showed activity (Table 1, entries 3–5). Again, **Ru-6** (longest spacer) was most effective among the catalysts, and up to 78% conversion (corresponds to a TON = 9700; Table 1, entry 5) were achieved with the corresponding **Ru-6@NB11** [56]. The corresponding polymer had a molecular weight of $M_n = 180,000$ g/mol and a narrow molecular weight distribution (PDI = 1.05), suggesting the living nature of the ROMP even within the protein scaffold. Neither regioselectivity (*cis/trans*) nor tacticity were affected [56].

The transmembrane protein FhuA

The β -barrel proteins introduced for the construction of artificial metathesases up to this point are relatively small and soluble proteins. As introduced *vide supra*, membrane-spanning porins and transporters of the all- β -barrel type, which are found in cellular outer membranes, constitute substantially larger “barrel” interiors and were thus utilized as scaffolds to house bulky GH-type catalysts.

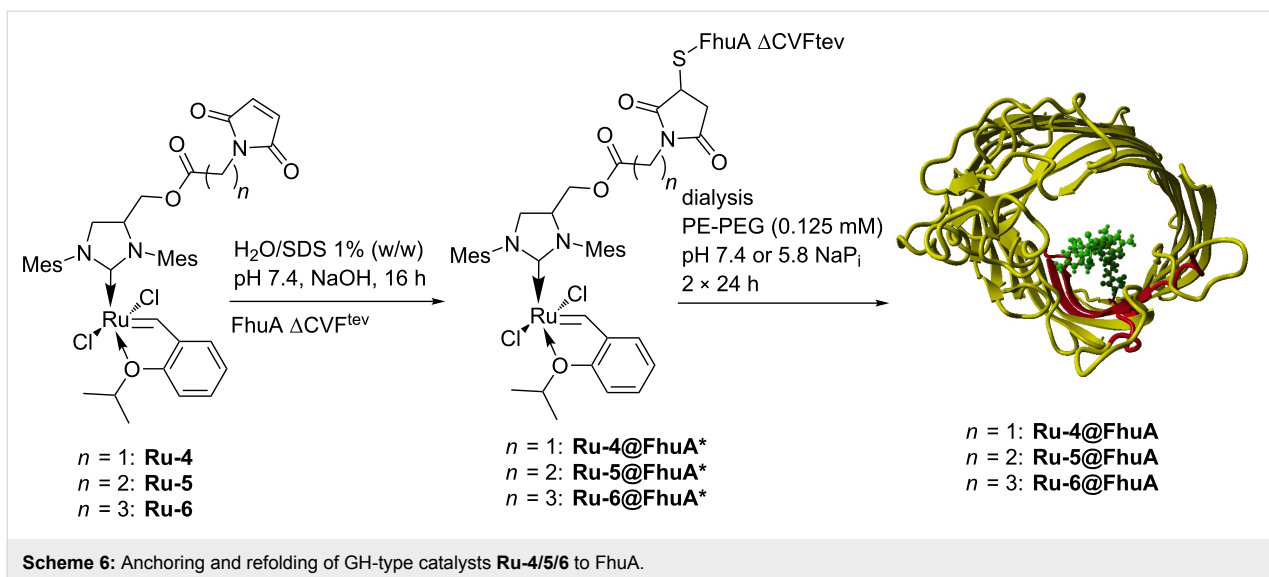
Ferric hydroxamate uptake protein component A (FhuA) is naturally located in the outer membrane of *E. coli*, where it is

involved in cellular iron import. It has a robust β -barrel structure consisting of 22 antiparallel β -strands [57]. By genetic engineering, Braun and co-workers modified this transporter and removed the cork domain that is responsible for the iron transport [58]. This generated an “empty” barrel offering sufficient space to incorporate bulky organometallic catalysts. The variant lacking the cork domain is termed FhuA Δ 1-159 (amino acids from 1 to 159 are deleted compared to the wild-type protein). For covalent anchoring, a cysteine residue was introduced at position 545 [59]. This position is suggested to be in a conformationally stable environment within the β -barrel structure. Additionally, mutation N548V was introduced to enable access of the metal catalyst to position C545. Furthermore, E501 was substituted by phenylalanine to prevent coordination of the Glu side chain to the metal site and deactivation of the catalyst. Two specific TEV (Tobacco Etch Virus protease) cleavage sites were further introduced into loops 7 and 8 to facilitate MALDI-TOF-MS analysis. The final mutant utilized for the construction of artificial metathesases is termed FhuA Δ 1-159_C545_V548_F501_tev (FhuA Δ CVF^{tev}) [59]. Conjugation was performed with GH-type catalysts **Ru-4/5/6** in the presence of SDS (Scheme 6).

Utilization of SDS as detergent resulted in partial denaturation of the FhuA – called unfolded FhuA – and facilitates the access of the GH-type catalysts to the cysteine C545 [59]. The resulting biohybrid catalysts **Ru-4/5/6@FhuA*** were washed repeatedly to remove unbound catalyst. The protein structure was restored (“renaturation”) leading to the refolded biohybrid catalysts **Ru-4/5/6@FhuA** (Scheme 6) which were tested in the ROMP of oxanorbornene **7** (Table 2) [59,60].

The biohybrid catalysts **Ru-4/5/6@FhuA*** in SDS solution showed activities comparable to the protein-free catalyst (Table 2, entries 1–4) [59,60]. Under slightly basic conditions (pH 7.4), 90% conversion was achieved (Table 1, entry 1). Under slightly acidic conditions (pH 5.8), full conversion was observed with the metal complex coupled to the fully unfolded protein (Table 2, entries 2–4) [59,60]. This effect was attributed to the pH and was investigated in detail [61].

After refolding, the activity decreased (Table 2, entries 5–8) [59,60]. This may be related to the steric demand of the refolded β -barrel structure that fully surrounds the metal site. Additionally, the activity of catalyst **Ru-6@FhuA** with the shorter linker increased (Table 2, entry 6 compared to entries 7 and 8) [60]. The restricted movement of the catalyst with shorter spacer within the channel seems advantageous for the turnover. Additionally, a few potentially coordinating residues (glutamic acid and tyrosine) are further away from the active site when the shorter spacer is utilized [60].

Scheme 6: Anchoring and refolding of GH-type catalysts **Ru-4/5/6** to FhuA.Table 2: ROMP of substrate **7** catalyzed by **Ru-4/5/6@FhuA**.

Entry ^a	Catalyst	Detergent	pH	Conv. ^b [%]	TON	<i>cis/trans</i> ^b
1	Ru-4@FhuA*	SDS ^c	7.4	90	900	60/40
2	Ru-4@FhuA*	SDS ^c	5.8	99	990	61/39
3	Ru-5@FhuA*	SDS ^c	5.8	99	990	60/40
4	Ru-6@FhuA*	SDS ^c	5.8	99	990	60/40
5	Ru-4@FhuA	PE-PEG ^d	7.4	7	94	57/43
6	Ru-4@FhuA	PE-PEG ^d	5.8	41	555	58/42
7	Ru-5@FhuA	PE-PEG ^d	5.8	24	325	56/44
8	Ru-6@FhuA	PE-PEG ^d	5.8	37	365	56/44

^aConditions: Protein concentrations determined with BCA assay and catalyst loading determined with ThioGlo titration (approx. 0.09 mM);

^bdetermined by ¹H NMR spectroscopy in CDCl₃; ^ccontaining 1% (w/w) SDS; ^d[PE-PEG] = 0.125 mM.

Structural expansions of β -barrel proteins

Comparing the activities of biohybrid catalysts based on the small β -barrel proteins NB and Sav with the large membrane protein FhuA reveals striking differences. Interestingly, much higher activities were observed when the catalysts were incorporated into the cavities of small β -barrel proteins. For the ROMP reaction, no change in regioselectivity was observed in both proteins. Within FhuA, the activity significantly dropped. This observation suggests that a particular fine-tuning is required to optimally utilize the combination of the metal catalyst with the spacing unit and the protein's precise 3D-structure that forms the second coordination sphere of the metal ion. The active site needs to be situated in the protein cavity to sense the

protein environment. The cavities of NB and Sav are too small to fully surround the bulky catalysts. Methods have been developed to enlarge the cavity or to introduce additional structural motifs to improve the protein–metal interaction. In case of NB4, two additional β -sheets were introduced to give a variant comprising 12 β -sheets, denoted expanded NB (NB4exp) [62]. These two additional β -sheets increased the cavity volume from 855 Å³ to 1399 Å³ (Figure 2) [62].

NB4exp was subjected to conjugation of catalysts **Ru-4/5/6**. Indeed, all catalysts underwent covalent anchoring with high conjugational yield (confirmed via ICP–OES and ESIMS) [62]. Upon catalysis, **Ru-5@NB4exp** as well as **Ru-6@NB4exp**

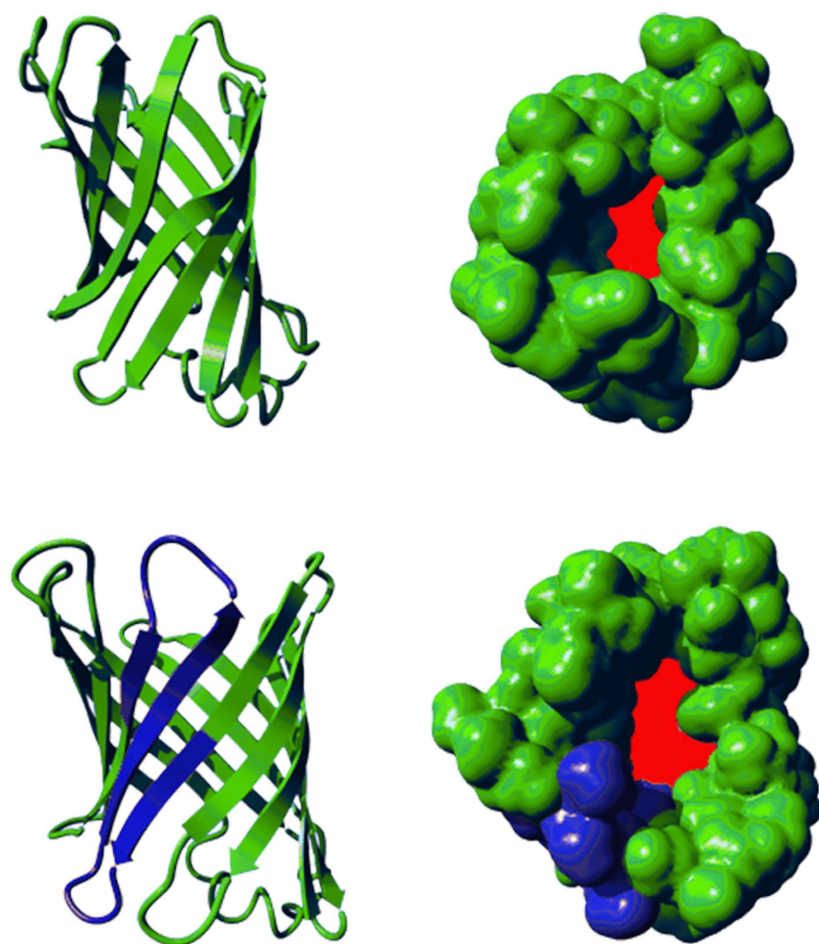


Figure 2: Top: NB4 (PDB 3WJB); bottom: NB4exp. Highlighted in blue are the additional two β -sheets. Highlighted in red is the diameter of the cavity.

showed high activity in the ROMP of norbornene **7** with TONs up to 10,000. For the catalyst **Ru-4** with the short linker, the activity of **Ru-4@NB4exp** dropped to TON = 3,000, even though the conjugation was almost quantitative [62]. However, this “influence” on the activity could not be transferred to the regio- and stereoselectivity of the polymer microstructure. Apart from ROMP, the artificial metathesases based on **NB4exp** were capable of catalyzing both CM and RCM. This makes **NB4exp** based biohybrid catalysts the first artificial metathesases to catalyze all basic metathesis reactions [62].

For the artificial metathesase based on Sav, additional structural motifs – α -helices – were introduced into the loops. These loops are supposed to embed the active site. However, in first ring-closing metathesis reactions, the influence of the newly introduced α -helices was negligible [63].

Conclusion

In this review, we discussed the combination of GH-type catalysts and β -barrel proteins to construct artificial metathesases.

The β -barrel motif offers a robust, well-defined but easily modifiable second coordination sphere. This makes the artificial metathesases applicable in all basic metathesis reactions. The channel provided by β -barrel proteins is a potentially useful feature to immobilize the GH-type complex within the protein. So far, no advantage has been drawn out of this feature. Strategies to enlarge small cavities of small β -barrel proteins likely will lead to more selective artificial metathesases. Directed evolution may open new opportunities for catalyst optimization [64].

Acknowledgements

We gratefully acknowledge the financial support by the Deutsche Forschungsgemeinschaft (DFG) through the International Research Training Group “Selectivity in Chemo- and Biocatalysis” (SeleCa), the Bundesministerium für Bildung und Forschung (BMBF) (FKZ: 031B0297), the Japan Society for the Promotion of Science (JSPS) through the Japanese-German Graduate Externship Program on Environmentally Benign Bio- and Chemical Processes, and JSPS KAKENHI Grant Number JP15H05804.

ORCID® iDs

Daniel F. Sauer - <https://orcid.org/0000-0002-6629-3323>
 Jun Okuda - <https://orcid.org/0000-0002-1636-5464>

References

- Grubbs, R. H. *Handbook of Metathesis*; Wiley-VCH: Weinheim, Germany, 2003. doi:10.1002/9783527619481
- Hérisson, J.-L.; Chauvin, Y. *Makromol. Chem.* **1971**, *141*, 161–176. doi:10.1002/macp.1971.021410112
- Schrock, R. R. *Acc. Chem. Res.* **1990**, *23*, 158–165. doi:10.1021/ar00173a007
- Nguyen, S. T.; Johnson, L. K.; Grubbs, R. H.; Ziller, J. W. *J. Am. Chem. Soc.* **1992**, *114*, 3974–3975. doi:10.1021/ja00036a053
- Hillmyer, M. A.; Lepetit, C.; McGrath, D. V.; Novak, B. M.; Grubbs, R. H. *Macromolecules* **1992**, *25*, 3345–3350. doi:10.1021/ma00039a004
- Feast, W. J.; Harrison, D. B. *Polym. Bull.* **1991**, *25*, 343–350. doi:10.1007/bf00316904
- Garber, S. B.; Kingsbury, J. S.; Gray, B. L.; Hoveyda, A. H. *J. Am. Chem. Soc.* **2000**, *122*, 8168–8179. doi:10.1021/ja001179g
- Hong, S. H.; Grubbs, R. H. *J. Am. Chem. Soc.* **2006**, *128*, 3508–3509. doi:10.1021/ja058451c
- Jordan, J. P.; Grubbs, R. H. *Angew. Chem., Int. Ed.* **2007**, *46*, 5152–5155. doi:10.1002/anie.200701258
- Lin, Y. A.; Chalker, J. M.; Floyd, N.; Bernardes, G. J. L.; Davis, B. G. *J. Am. Chem. Soc.* **2008**, *130*, 9642–9643. doi:10.1021/ja0826168
- Chalker, J. M.; Lin, Y. A.; Bourtouira, O.; Davis, B. G. *Chem. Commun.* **2009**, 3714–3716. doi:10.1039/b908004j
- Lin, Y. A.; Chalker, J. M.; Davis, B. G. *J. Am. Chem. Soc.* **2010**, *132*, 16805–16811. doi:10.1021/ja104994d
- Isarov, S. A.; Pokorski, J. K. *ACS Macro Lett.* **2015**, *4*, 969–973. doi:10.1021/acsmacrolett.5b00497
- Jeschek, M.; Panke, S.; Ward, T. R. *Trends Biotechnol.* **2018**, *36*, 60–72. doi:10.1016/j.tibtech.2017.10.003
- Wilson, Y. M.; Dürrenberger, M.; Nogueira, E. S.; Ward, T. R. *J. Am. Chem. Soc.* **2014**, *136*, 8928–8932. doi:10.1021/ja500613n
- Lipshutz, B. H.; Ghorai, S. *Olefin Metathesis*; John Wiley & Sons, Inc.: New York, NY, U.S.A., 2014; pp 515–521. doi:10.1002/9781118711613.ch21
- Gawin, R.; Czarnecka, P.; Grela, K. *Tetrahedron* **2010**, *66*, 1051–1056. doi:10.1016/j.tet.2009.11.009
- Skowerski, K.; Szczepaniak, G.; Wierzbicka, C.; Gulański, Ł.; Bieniek, M.; Grela, K. *Catal. Sci. Technol.* **2012**, *2*, 2424–2427. doi:10.1039/c2cy20320k
- Sauer, D. F.; Gotzen, S.; Okuda, J. *Org. Biomol. Chem.* **2016**, *14*, 9174–9183. doi:10.1039/c6ob01475e
- Schwizer, F.; Okamoto, Y.; Heinisch, T.; Gu, Y.; Pellizzoni, M. M.; Lebrun, V.; Reuter, R.; Köhler, V.; Lewis, J. C.; Ward, T. R. *Chem. Rev.* **2018**, *118*, 142–231. doi:10.1021/acs.chemrev.7b00014
- Lewis, J. C. *ACS Catal.* **2013**, *3*, 2954–2975. doi:10.1021/cs400806a
- Bos, J.; Roelfes, G. *Curr. Opin. Chem. Biol.* **2014**, *19*, 135–143. doi:10.1016/j.cbpa.2014.02.002
- Hoarau, M.; Hureau, C.; Gras, E.; Faller, P. *Coord. Chem. Rev.* **2016**, *308*, 445–459. doi:10.1016/j.ccr.2015.05.011
- Smith, G. M. *The Nature of Enzymes*. In *Biotechnology Set*; Rehm, H.-J.; Reed, G., Eds.; Wiley-VCH Verlag GmbH: Weinheim, Germany, 2008; pp 4–72. doi:10.1002/9783527620999.ch1
- Faber, K.; Fessner, W. D.; Turner, N. J., Eds. *Biocatalysis in Organic Synthesis*; Georg Thieme Verlag: Stuttgart, Germany, 2015. doi:10.1055/b-003-125813
- Steinreiber, J.; Ward, T. R. *Coord. Chem. Rev.* **2008**, *252*, 751–766. doi:10.1016/j.ccr.2007.09.016
- Wilson, M. E.; Whitesides, G. M. *J. Am. Chem. Soc.* **1978**, *100*, 306–307. doi:10.1021/ja00469a064
- Green, N. M. *Adv. Protein Chem.* **1975**, *29*, 85–133. doi:10.1016/s0065-3233(08)60411-8
- Ward, T. R. *Acc. Chem. Res.* **2011**, *44*, 47–57. doi:10.1021/ar100099u
- Perticaroli, S.; Nickels, J. D.; Ehlers, G.; O'Neill, H.; Zhang, Q.; Sokolov, A. P. *Soft Matter* **2013**, *9*, 9548–9556. doi:10.1039/c3sm50807b
- Perticaroli, S.; Nickels, J. D.; Ehlers, G.; Sokolov, A. P. *Biophys. J.* **2014**, *106*, 2667–2674. doi:10.1016/j.bpj.2014.05.009
- Fairman, J. W.; Noinaj, N.; Buchanan, S. K. *Curr. Opin. Struct. Biol.* **2011**, *21*, 523–531. doi:10.1016/j.sbi.2011.05.005
- Murzin, A. G.; Lesk, A. M.; Chothia, C. *J. Mol. Biol.* **1994**, *236*, 1369–1381. doi:10.1016/0022-2836(94)90064-7
- Murzin, A. G.; Lesk, A. M.; Chothia, C. *J. Mol. Biol.* **1994**, *236*, 1382–1400. doi:10.1016/0022-2836(94)90065-5
- Flower, D. R.; North, A. C. T.; Attwood, T. K. *Protein Sci.* **1993**, *2*, 753–761. doi:10.1002/pro.5560020507
- De Simone, G.; Ascenzi, P.; di Masi, A.; Polticelli, F. *Biomol. Concepts* **2017**, *8*, 105–118. doi:10.1515/bmc-2017-0013
- Youkharijache, P.; Veretnik, S.; Li, Q.; Stanek, K. A.; Mura, C.; Bourne, P. E. *bioRxiv, Bioinf.* **2018**. doi:10.1101/140376
- Wimley, W. C. *Curr. Opin. Struct. Biol.* **2003**, *13*, 404–411. doi:10.1016/s0959-440x(03)00099-x
- Noinaj, N.; Gumbart, J. C.; Buchanan, S. K. *Nat. Rev. Microbiol.* **2017**, *15*, 197–204. doi:10.1038/nrmicro.2016.191
- Wierenga, R. K. *FEBS Lett.* **2001**, *492*, 193–198. doi:10.1016/s0014-5793(01)02236-0
- Hsu, S.-T. D.; Blaser, G.; Jackson, S. E. *Chem. Soc. Rev.* **2009**, *38*, 2951–2965. doi:10.1039/b908170b
- Höcker, B.; Jürgens, C.; Wilmanns, M.; Sterner, R. *Curr. Opin. Biotechnol.* **2001**, *12*, 376–381. doi:10.1016/s0958-1669(00)00230-5
- Tenne, S.-J.; Schwanenberg, U. *Int. J. Mol. Sci.* **2012**, *13*, 2459–2471. doi:10.3390/ijms13022459
- Chamoli, S.; Kumar, P.; Navani, N. K.; Verma, A. K. *Int. J. Biol. Macromol.* **2016**, *85*, 425–433. doi:10.1016/j.ijbiomac.2016.01.001
- Deep, K.; Poddar, A.; Das, S. K. *Appl. Biochem. Biotechnol.* **2016**, *178*, 695–709. doi:10.1007/s12010-015-1903-9
- Lo, C.; Ringenberg, M. R.; Gnandt, D.; Wilson, Y.; Ward, T. R. *Chem. Commun.* **2011**, *47*, 12065–12067. doi:10.1039/c1cc15004a
- Jeschek, M.; Reuter, R.; Heinisch, T.; Trindler, C.; Klehr, J.; Panke, S.; Ward, T. R. *Nature* **2016**, *537*, 661–665. doi:10.1038/nature19114
- Mallin, H.; Hestericová, M.; Reuter, R.; Ward, T. R. *Nat. Protoc.* **2016**, *11*, 835–852. doi:10.1038/nprot.2016.019
- Bianchetti, C. M.; Blouin, G. C.; Bitto, E.; Olson, J. S.; Phillips, G. N., Jr. *Proteins: Struct., Funct., Bioinf.* **2010**, *78*, 917–931. doi:10.1002/prot.22617
- Onoda, A.; Fukumoto, K.; Arlt, M.; Bocola, M.; Schwanenberg, U.; Hayashi, T. *Chem. Commun.* **2012**, *48*, 9756–9758. doi:10.1039/c2cc35165j
- Fukumoto, K.; Onoda, A.; Mizohata, E.; Bocola, M.; Inoue, T.; Schwanenberg, U.; Hayashi, T. *ChemCatChem* **2014**, *6*, 1123. doi:10.1002/cctc.201402206

52. Himiyama, T.; Sauer, D. F.; Onoda, A.; Spaniol, T. P.; Okuda, J.; Hayashi, T. *J. Inorg. Biochem.* **2016**, *158*, 55–61. doi:10.1016/j.jinorgbio.2015.12.026

53. Himiyama, T.; Taniguchi, N.; Kato, S.; Onoda, A.; Hayashi, T. *Angew. Chem., Int. Ed.* **2017**, *56*, 13618–13622. doi:10.1002/anie.201704524

54. Onoda, A.; Kihara, Y.; Fukumoto, K.; Sano, Y.; Hayashi, T. *ACS Catal.* **2014**, *4*, 2645–2648. doi:10.1021/cs500392e

55. Zhang, C.; Srivastava, P.; Ellis-Guardiola, K.; Lewis, J. C. *Tetrahedron* **2014**, *70*, 4245–4249. doi:10.1016/j.tet.2014.03.008

56. Sauer, D. F.; Himiyama, T.; Tachikawa, K.; Fukumoto, K.; Onoda, A.; Mizohata, E.; Inoue, T.; Bocola, M.; Schwaneberg, U.; Hayashi, T.; Okuda, J. *ACS Catal.* **2015**, *5*, 7519–7522. doi:10.1021/acscatal.5b01792

57. Boulanger, P.; le Maire, M.; Bonhivers, M.; Dubois, S.; Desmadril, M.; Letellier, L. *Biochemistry* **1996**, *35*, 14216–14224. doi:10.1021/bi9608673

58. Braun, M.; Killmann, H.; Maier, E.; Benz, R.; Braun, V. *Eur. J. Biochem.* **2002**, *269*, 4948–4959. doi:10.1046/j.1432-1033.2002.03195.x

59. Philippart, F.; Arlt, M.; Gotzen, S.; Tenne, S.-J.; Bocola, M.; Chen, H.-H.; Zhu, L.; Schwaneberg, U.; Okuda, J. *Chem. – Eur. J.* **2013**, *19*, 13865–13871. doi:10.1002/chem.201301515

60. Sauer, D. F.; Bocola, M.; Broglia, C.; Arlt, M.; Zhu, L.-L.; Brocker, M.; Schwaneberg, U.; Okuda, J. *Chem. – Asian J.* **2015**, *10*, 177–182. doi:10.1002/asia.201403005

61. Matsuo, T.; Yoshida, T.; Fujii, A.; Kawahara, K.; Hirota, S. *Organometallics* **2013**, *32*, 5313–5319. doi:10.1021/om4005302

62. Grimm, A. R.; Sauer, D. F.; Davari, M. D.; Zhu, L.; Bocola, M.; Kato, S.; Onoda, A.; Hayashi, T.; Okuda, J.; Schwaneberg, U. *ACS Catal.* **2018**, *8*, 3358–3364. doi:10.1021/acscatal.7b03652

63. Pellizzoni, M. M.; Schwizer, F.; Wood, C. W.; Sabatino, V.; Cotelle, Y.; Matile, S.; Woolfson, D. N.; Ward, T. R. *ACS Catal.* **2018**, *8*, 1476–1484. doi:10.1021/acscatal.7b03773

64. Arnold, F. H. *Angew. Chem., Int. Ed.* **2018**, *57*, 4143–4148. doi:10.1002/anie.201708408

License and Terms

This is an Open Access article under the terms of the Creative Commons Attribution License (<http://creativecommons.org/licenses/by/4.0>). Please note that the reuse, redistribution and reproduction in particular requires that the authors and source are credited.

The license is subject to the *Beilstein Journal of Organic Chemistry* terms and conditions: (<https://www.beilstein-journals.org/bjoc>)

The definitive version of this article is the electronic one which can be found at:
[doi:10.3762/bjoc.14.265](https://doi.org/10.3762/bjoc.14.265)



The influence of the cationic carbenes on the initiation kinetics of ruthenium-based metathesis catalysts; a DFT study

Magdalena Jawiczuk, Angelika Janaszkiewicz and Bartosz Trzaskowski*

Full Research Paper

Open Access

Address:
Centre of New Technologies, University of Warsaw, Banacha 2c,
02-097 Warszawa, Poland

Beilstein J. Org. Chem. **2018**, *14*, 2872–2880.
doi:10.3762/bjoc.14.266

Email:
Bartosz Trzaskowski* - b.trzaskowski@cent.uw.edu.pl

Received: 16 August 2018
Accepted: 01 November 2018
Published: 20 November 2018

* Corresponding author

This article is part of the thematic issue "Progress in metathesis chemistry III"

Keywords:
catalysts; cationic carbenes; DFT; initiation; metathesis

Associate Editor: P. Schreiner

© 2018 Jawiczuk et al.; licensee Beilstein-Institut.
License and terms: see end of document.

Abstract

Cationic carbenes are a relatively new and rare group of ancillary ligands, which have shown their superior activity in a number of challenging catalytic reactions. In ruthenium-based metathesis catalysis they are often used as ammonium tags, to provide water-soluble, environment-friendly catalysts. In this work we performed computational studies on three cationic carbenes with the formal positive charge located at different distances from the carbene carbon. We show that the predicted initiation rates of Grubbs, indenylidene, and Hoveyda–Grubbs-like complexes incorporating these carbenes show little variance and are similar to initiation rates of standard Grubbs, indenylidene, and Hoveyda–Grubbs catalysts. In all investigated cases the partial charge of the carbene carbon atom is similar, resulting in comparable C_{carbene}–Ru bond strengths and Ru–P/O dissociation Gibbs free energies.

Introduction

The isolation of the first stable N-heterocyclic carbene (NHC) by Arduengo [1] was a milestone in organic chemistry which allowed for thorough and systematic studies on all aspects of NHC chemistry in the past 25 years [2–7]. It was soon realized that NHCs are a very useful class of ligands for transition metal catalysis as both their steric and electronic properties can be easily controlled and tuned to obtain very efficient and specific

catalysts. One of the most successful uses of NHCs in catalysis is the olefin metathesis, which nowadays became one of the most commonly used tool in modern synthesis [8–10]. The vast popularity of metathesis results from the high stabilities and efficiencies of Ruthenium catalysts stabilised by NHC moieties. In this class of compounds NHC ligands, with the poor π -acceptor and strong σ -donor properties, stabilize the 14-elec-

tron ruthenium active species during the catalytic cycle [11,12]. Today there are hundreds of examples of second generation Grubbs and Hoveyda–Grubbs catalyst derivatives bearing different NHCs to form specialized catalysts for metathesis [13,14].

An interesting attempt to further modify the electronic properties of NHCs is to introduce a charged moiety to form either anionic or cationic carbenes [15–18]. Cationic ligands with a positive charge close to the coordinating atom are relatively rare, as their coordination ability of transition metals, bearing also a formal positive charge, is weakened. Nevertheless, stable metal complexes with cationic ligands have been synthesized and used in catalysis [19–21]. With respect to olefin metathesis cationic carbenes have been introduced as early as in 2007, where Grubbs described the first ammonium-tagged Hoveyda-type catalyst [22]. The goal of that study was to develop systems that are active and stable in water and, therefore, environmentally-friendly. The idea of incorporating a quaternary ammonium moiety into the imidazole part of the carbene was later expanded by several other groups, including a number of new water-soluble catalysts synthesized by Skowerski et al. [23,24]. In the meantime Schanz and co-workers synthesized also Hoveyda-like complexes with ammonium groups introduced into the aryl rings of the NHC ligands [25]. Most of these complexes showed good efficiency in selected metathesis reactions.

Interestingly in all reported cases of ammonium tagged Ru–alkylidene metathesis catalysts the ammonium tag is relatively far from the carbene carbon atom chelating the ruthenium core. The reason behind such design was likely the low probability of the ammonium tag influencing the ruthenium core and therefore, having a potential negative effect on the efficiency and reaction rate of the catalyst as well as the ease of synthesis. In 2013 Kośnik and Grela performed a study to check the influence of the length of the spacer between the NHC ligand and the onium tag, by synthesizing the tag with an eight $-(\text{CH}_2)-$ linker [26]. The authors concluded that the extension of the linker does not affect the efficiency of the catalyst in model metathesis reactions in comparison to Skowerski's complexes with only one $-\text{CH}_2-$ unit. Curiously, carbenes with the cationic group even closer to the imidazole moiety (with no spacer) or incorporated into the imidazole core have been synthesized only very recently and examples of their transition metal complexes are scarce. In 2013 Ganter described a cationic NHC with a fused pyridinium moiety and the formal +1 charge just one bond away from the imidazole core [27]. In 2017 César synthesized a cationic imidazolylidene NHC with an ammonium tag attached directly to the imidazole core [28]. Finally, in the same year Ganter described a triazoliumylidene with the

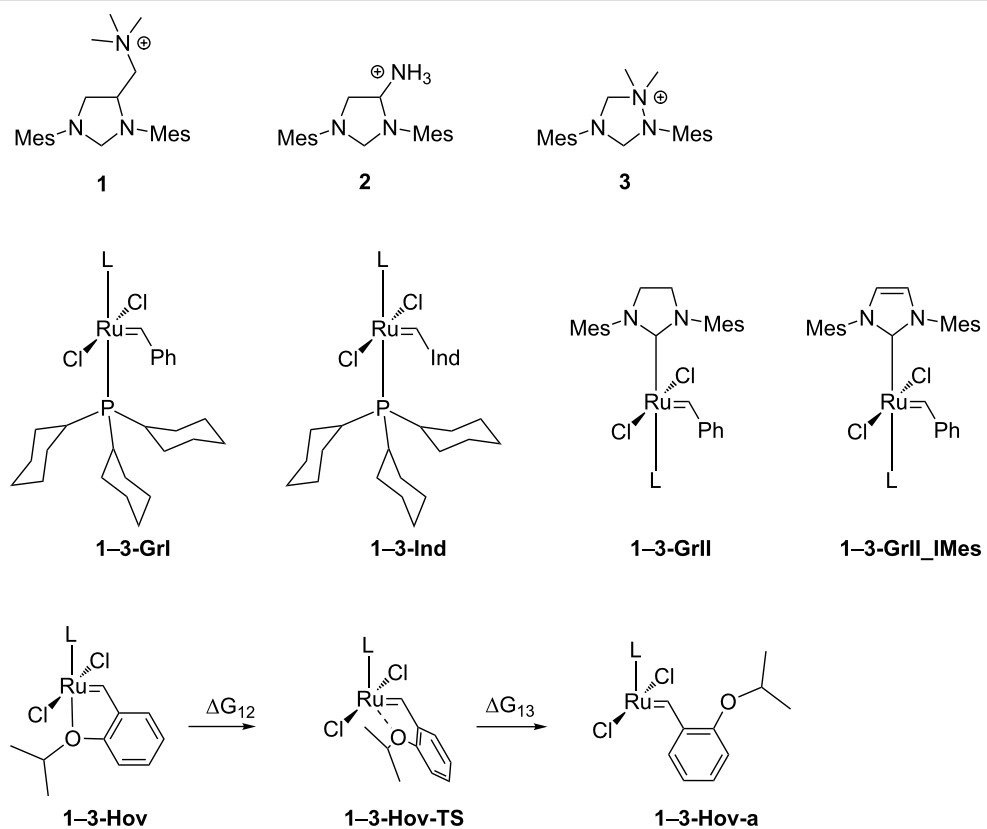
formal +1 charge incorporated into the five-membered ring [29]. Several complexes formed by these carbenes have been also described, however, no ruthenium complexes with such carbenes have been synthesized.

In this work we have performed a systematic study of three cationic carbenes with the formal +1 charge located at different distances from the carbene carbon atom using a computational approach (Scheme 1). We considered the impact of the positive charge on the electronic properties of carbenes, but also on the properties and initiation rates of the most important ruthenium-based metathesis catalysts, including Grubbs, indenylidene, and Hoveyda–Grubbs complexes, as well as carbene dimerization. We also considered two different solvents: dichloromethane, which is a standard solvent for performing metathesis reactions and water, which is commonly used in the case of ammonium-tagged metathesis catalysts.

Results and Discussion

Computational benchmarks

The M06 method has become the method of choice for obtaining accurate energies for ruthenium metathesis for a number of groups investigating this class of catalysts [30–44]. Since the M06 functional already includes some medium-range dispersion it is usually used without additional corrections to better describe dispersion interactions. The commonly used D3 semi-empirical correction for density functionals has been, however, derived also for the M06 functional and shown to improve results for many organic reactions when calculating the differences in relative energies [45,46]. Others have, however, pointed out that M06-D3 may overestimate the effect of dispersion due to double-counting of these effects [47]. To resolve this issue we performed benchmark calculations for standard metathesis catalyst **GrI**, as well as newly developed catalyst featuring a labile carbodicarbene ligand (as a model of **1–3-GrII**) [48]. In the case of **GrI** we found the Gibbs free energy of initiation in the M06 method equal to 20.4 kcal/mol, in perfect agreement with the experimental value of 19.88 kcal/mol [21]. The addition of the D3 dispersion correction increases this value to 29.2 kcal/mol. For the carbodicarbene catalyst the experimental value is 23.5 kcal/mol [48] and we found the value of 23.9 kcal/mol, using M06-D3 approach. Previously we have shown that the addition of D3 correction gives very good agreement with the experimental data for **Hov** and Hoveyda-like systems as well as for investigations of carbenes dimerization [38,49]. As a result we decided to use the M06-D3 functional in calculations of Gibbs free energies all system apart from 1st generation Grubbs and indenylidene-like complexes, for which we used pure M06. Results for all systems and both M06 and M06-D3 methods are listed in Supporting Information File 1.



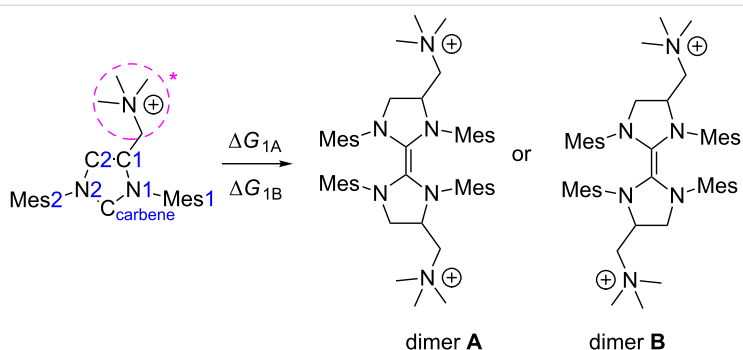
Scheme 1: NHC's and their ruthenium complexes studied in this work; L = carbene **1**, **2** or **3**.

Dimerization

The tendency of selected NHC to dimerize is a well-known and interesting phenomenon, despite its very limited impact on their propensity to form transition metal complexes (Scheme 2) [50]. Many works have been devoted to the study of carbene dimerization and present evidence that mechanism of monomer–dimer equilibrium depends on the balance between the electronic and steric properties of NHCs [49,51–54]. In general, all unsaturated carbenes have strong preference for the monomeric form due to the electronic effect. On the other hand saturated carbenes prefer the dimeric form if either their side-

groups are relatively small (e.g., methyl or ethyl) or if the carbenes are asymmetric [55,56]. Unfortunately the subtle Wanzlick equilibrium between many saturated carbenes may easily shift to either the dimeric or monomeric form with a small structural change and it is not a trivial task to predict the more stable form of the carbene based solely on its structural features.

Since all investigated carbenes are asymmetric we considered the possibility of formation of two different dimers, marked **A** (symmetric) and **B** (asymmetric), respectively (Table 1).



Scheme 2: Schematic representation of carbene dimerization and atom numbering scheme used throughout this work.

Table 1: Calculated dimerization energies (ΔG_1) in CH_2Cl_2 for carbenes **1** and **2** and the $\text{C}_{\text{carbene}}\text{—C'}_{\text{carbene}}$ bond lengths of all corresponding dimers.

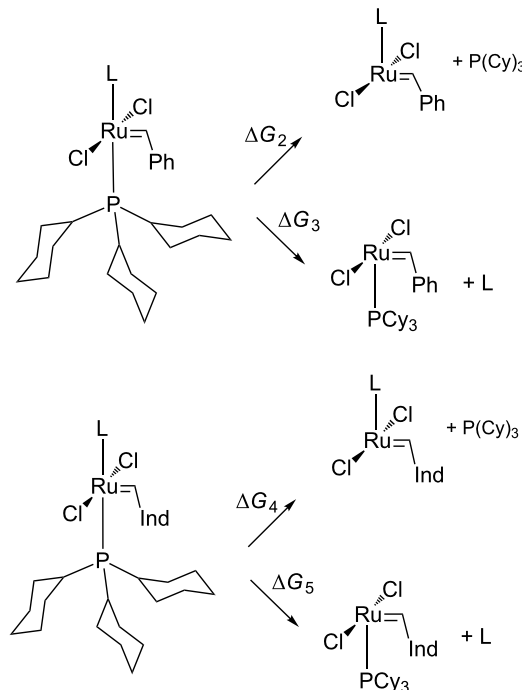
structure	ΔG_1 [kcal/mol]	$\text{C}_{\text{carbene}}\text{—C'}_{\text{carbene}}$ [Å]
1A	-9.4	1.362
1B	-9.0	1.361
2A	-10.3	1.362
2B	-10.0	1.359
3A	—	1.365
3B	—	1.365

Results obtained for carbenes **1** and **2** suggest a strong preference for both systems to dimerize, with a slightly lower Gibbs free energy difference for the symmetric dimer **A**. In the case of carbene **3**, the Gibbs free energy of dimerization could not be estimated due to instability of the monomer during geometry optimization. Thus, the results indicate higher stability of dimers for all examined NHC, which are in agreement with previous literature reports for asymmetrical N-heterocyclic carbenes, as well as accurate DLPNO-CCSD(T) calculations (see Supporting Information File 1) [49,55]. The change of the solvent from CH_2Cl_2 to water only slightly altered the calculated dimerization energies and also indicated higher stabilities of dimers on solution (see Supporting Information File 1).

First generation Grubbs and M1 indenylidene catalyst

In the next step of the study we performed a computational investigation of possible pathways of the initiation of cationic ruthenium catalyst based on the commonly used 1st generation Grubbs catalyst (**GrI**) and **M1** indenylidene catalyst (**Ind**). New complexes were formed by replacing one PCy_3 phosphine ligand with the cationic NHC **1–3** (Scheme 1). We considered

only the dissociative mechanism of initiation, in agreement with the numerous reports on the initiation of Grubbs catalyst [57], but we also considered the possibility of cationic carbene dissociation as the first step of the metathesis catalytic cycle (Scheme 3).



Scheme 3: Dissociative mechanism of initiation for Grubbs-like **1–3-GrI** and **M1** indenylidene type complexes **1–3-Ind**; L = carbene **1**, **2** or **3**.

The results of the computational study are presented in Table 2 and show that in all cases the energy barriers for the dissociation of phosphine ligand (ΔG_2) are 0.4–3.1 kcal/mol lower com-

Table 2: The comparison of dissociation energies ΔG_2 – ΔG_5 and structural parameters of investigated compounds.

complex	ΔG_2 [kcal/mol]	ΔG_3 [kcal/mol]	Ru—P [Å]	$\text{Ru—C}_{\text{carbene}}$ [Å]
1-GrI	20.9	24.0	2.464	2.056
2-GrI	23.3	23.7	2.478	2.036
3-GrI	18.7	—	2.466	2.056
GrI^a exp.	19.88	—	2.435	2.397
GrI calculated	18.9	18.9	2.440	2.434

complex	ΔG_4 [kcal/mol]	ΔG_5 [kcal/mol]	Ru—P [Å]	$\text{Ru—C}_{\text{carbene}}$ [Å]
1-Ind	18.7	25.6	2.470	2.073
2-Ind	16.7	22.5	2.487	2.056
3-Ind	21.9	—	2.478	2.084
Ind^b exp.	21	—	2.410	2.415

^aSee ref. [58]; ^bSee refs. [59,60].

pared to carbene dissociation (ΔG_3). We can speculate that the positive charge of carbenes **1–3** lowers the Ru–C bond strength, making it easier to dissociate than for neutral carbenes. Interestingly, the estimate of the Gibbs free energy of initiation for complex **3-GrI** suggest faster activation than first generation Grubbs catalysts, for which the experimental value of ΔG_2 was found at 19.88 kcal/mol [58].

Similarly, in the case of indenylidene complexes (**1–3-Ind**) the dissociation of phosphine is also preferred over the loss of the cationic carbene. For this series of complexes **3-Ind** displays the activation Gibbs free energy ΔG_4 (21.9 kcal/mol) very similar to **Ind**, for which it was experimentally determined at 21 kcal/mol [60]. Both **2-Ind** and **1-Ind** show, however, longer Ru–P bonds and lower estimates of activation Gibbs free energies, suggesting their relatively fast activation during the catalytic cycle. The estimates of free energies in water follow exactly the same trends, although are always a few kcal/mol lower, indicating that in this solvent Grubbs-like complexes may initiate faster (see Supporting Information File 1).

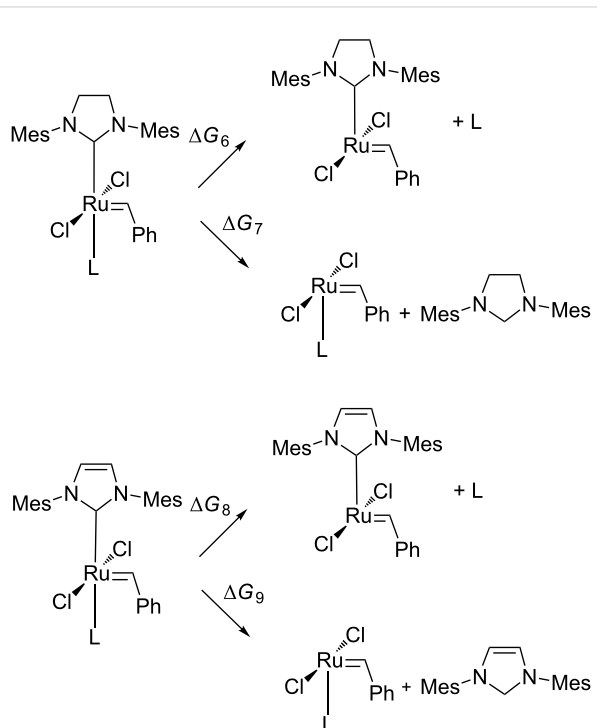
It is worth mentioning that for the 1st generation Grubbs complexes the DLPNO-CCSD(T) results give consistently Gibbs free energy value which are 8–12 kcal/mol higher than those obtained using DFT approach. This is also true for **GrI** for which the computational DLPNO-CCSD(T) method gives the 28.1 kcal/mol value, almost 9 kcal/mol higher than the experimental value. Clearly, DLPNO-CCSD(T) overestimates ΔG values for this series, though it gives very consistent results with the DFT method for other studied systems, described later. At this point we cannot provide any explanation of this discrepancy.

Second generation Grubbs catalyst

Second generation Grubbs complexes featuring either SIMes (1,3-bis(2,4,6-trimethylphenyl)-4,5-dihydroimidazol-2-ylidene) or IMes (1,3-bis(2,4,6-trimethylphenyl)imidazol-2-ylidene) ligands are another class of important ruthenium-based metathesis catalysts, where the initiation relies on phosphine dissociation. The experimental values for PCy_3 dissociation for these catalysts are 23.0 ± 0.4 and 24 ± 1 kcal/mol for SIMes-containing and IMes-containing systems, respectively [57]. Recently Grubbs synthesized and described also a novel metathesis catalyst featuring a labile carbodicarbene ligand replacing PCy_3 [48]. Inspired by these results we decided to design similar systems with either SIMes or IMes and cationic carbenes.

For all systems **1–3-GrII** and **1–3-GrII_IMes** the energy barriers of initiation are relatively high (30–40 kcal/mol, Scheme 4), indicating that these complexes are completely unsuitable for olefin metathesis. Precatalysts with unsaturated

NHC ligands are estimated to have slightly lower Gibbs free energy barriers than saturated ones by ca. 3–5 kcal/mol (Table 3). Interestingly, the free energies in water are 3–12 kcal/mol lower indicating that **1-GrII** and **2-GrII** may act as very slow metathesis catalysts (see Supporting Information File 1).



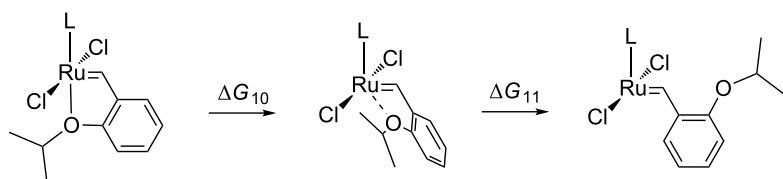
Scheme 4: Dissociative mechanism of initiation of 2nd generation Grubbs-like saturated **1–3-GrII** and unsaturated **1–3-GrII_IMes** complexes; L = carbene **1**, **2** or **3**.

Hoveyda–Grubbs catalysts

In the last step of our study we also designed Hoveyda-like precatalyst **1–3-Hov** with new cationic carbenes replacing SIMes (see Scheme 1). In our investigation we only considered the dissociative mechanism, which was shown to be the most feasible for medium and large-sized olefins (Scheme 5) [61,62]. Results presented in Table 4 suggest that the incorporation of cationic NHC increases the Gibbs free energy (ΔG_{10}) barriers by ca. 4–6 kcal/mol with respect to the standard Hoveyda–Grubbs catalyst (**Hov**) [63]. Given the accuracy of our computational methods, estimated at around 1–2 kcal/mol, we can expect that cationic Hoveyda-type catalysts are only slightly slower than the Hoveyda–Grubbs catalyst. This result is in agreement with experimental reports on various onium tag-modified systems [23,24] showing moderate activities of these systems in model CM reactions. For this group of catalysts the results in water are virtually identical to those in CH_2Cl_2 (see Supporting Information File 1).

Table 3: The comparison of Gibbs free energies ΔG_6 – ΔG_9 and structural parameters of investigated compounds.

complex	ΔG_6 [kcal/mol]	ΔG_7 [kcal/mol]	Ru–C [Å]	Ru–C _{carbene} [Å]
1-GrII	38.0	38.5	2.118	2.109
2-GrII	35.5	37.0	2.134	2.078
3-GrII	–	40.1	2.115	2.098
complex	ΔG_8 [kcal/mol]	ΔG_9 [kcal/mol]	Ru–C [Å]	Ru–C _{carbene} [Å]
1-GrII_IMes	33.3	35.5	2.130	2.102
2-GrII_IMes	30.9	34.1	2.141	2.066
3-GrII_IMes	–	36.7	2.122	2.079

**Scheme 5:** Dissociative mechanism of activation for complexes **1–3-Hov**; L = carbene **1**, **2** or **3**.**Table 4:** The comparison of Gibbs free energies ΔG_{10} and ΔG_{11} and selected structural parameters of **Hov** and **1–3-Hov** catalysts.

complex	ΔG_{10} [kcal/mol]	ΔG_{11} [kcal/mol]	Ru–C _{carbene} [Å]	Ru–C _{Ar} [Å]	Ru–O1 [Å]
1-Hov	24.5	14.2	1.944	1.839	2.299
2-Hov	26.3	15.3	1.930	1.842	2.296
3-Hov	24.9	16.4	1.925	1.843	2.277
Hov^a X-ray	19–20	–	1.979(1)	1.829(1)	2.256(1)

^aSee ref. [64].

Surprisingly the differences in ΔG s for **1–3-Hov** as well as all other candidates for catalysts are relatively small and close to the computational accuracy of our protocol. To justify the lack of influence of the position of the quaternary amine on the Gibbs free energies of initiation we decided to perform a

detailed analysis of partial charges of these systems, as well as complexes **1–3-GrI** (Table 5). Interestingly both natural partial charges and Mulliken partial charges (Table S8 in Supporting Information File 1) show no meaningful differences for the C_{carbene} atom. This result has important consequences concern-

Table 5: Natural partial charges distribution in carbenes of **1–3-Hov** and **1–3-GrI**.

atom	1-Hov	2-Hov	3-Hov	Hov	1-GrI	2-GrI	3-GrI	GrII
C _{carbene}	0.49	0.46	0.47	0.49	0.41	0.38	0.40	0.41
N1	-0.51	-0.53	-0.32	-0.49	-0.50	-0.52	-0.31	-0.48
N2	-0.48	-0.48	-0.50	-0.49	-0.47	-0.47	-0.49	-0.48
C1	0.15	0.42	–	0.22	0.15	0.42	–	0.22
C2	0.24	0.25	0.49	0.22	0.24	0.25	0.49	0.22
Mes1	0.24	0.27	0.31	0.23	0.24	0.28	0.32	0.24
Mes2	0.26	0.27	0.28	0.24	0.25	0.27	0.28	0.22
N*	0.94	0.55	0.51	–	0.94	0.54	0.50	–
Ru1	0.31	0.33	0.32	0.31	0.14	0.15	0.13	0.14

ing the strength of the Ru–C_{carbene} bond which is at least partially driven by the electrostatic interaction between Ru and C_{carbene} atoms. As a result the similar partial charge of C_{carbene} in **1–3–Hov** translates into similar bond strength of the Ru–C_{carbene} bond. This, in turn, has an impact on the Ru–O1 bond strengths due to the well-known *trans* effect which shows that there is a balance between the strength/bond length of the opposite bonds of the ruthenium center [38–41,65]. As a result the Ru–O1 bond strength in **1–3–Hov** is very similar, resulting in similar Gibbs free energies of initiation. The same argument can be made for **1–3–GrI** which also shows very similar natural partial charges on C_{carbene} atoms, resulting in very similar rates of initiation. It is interesting to note that the excess positive charge is located mostly on the –CH₂N(CH₃)₃⁺ group in the case of **1–GrI** and **1–Hov**, but in the case of **2–3–GrI** and **2–3–Hov** it gets distributed over the imidazole core and mesityl groups. A similar feature has been observed by us earlier in carbene dimers formation, where mesityl groups, which usually act as weakly electron-donating moieties, could also accommodate a substantial amount of excess negative or positive charge [49].

Conclusion

Despite hundreds of examples of ruthenium-based olefin metathesis catalysts synthesized up to date the rational design of new catalysts remains a non-trivial task. To gain general insight into the structure–activity relationship for this class of compounds we computationally investigated three different carbenes bearing a formal +1 charge, in form of quaternary amine, and their impact on the activation rates of olefin metathesis catalysts. We predict that these carbenes are likely to dimerize, similarly to other asymmetric carbenes synthesized earlier. We also demonstrate that most of the examined complexes, derivatives of Grubbs and Hoveyda–Grubbs catalysts **1–3–GrI**, **1–3–Ind** and **1–3–Hov** have initiation Gibbs free energy values in the range of standard metathesis catalysts, like **GrI**, **Ind** and Hoveyda–Grubbs and are likely an interesting alternative for them. On the other hand ruthenium complexes with two carbenes are predicted to have relatively high initiation energies. Our partial charges analysis reveals that the location of the quaternary amine and its distance from the carbene carbon atom has little influence on the electronic features of the crucial parts of the catalyst and, therefore, little influence on the initiation rates of catalyst bearing these moieties. The excess positive charge of the quaternary ammonium is, in most cases, distributed over the imidazole core and mesityl groups and does not affect the ruthenium core nor the ruthenium–C_{carbene} bond.

Experimental

We used density functional theory (DFT) using a computational protocol similar to our previous studies. We have used

all-atom models for all studied catalysts. Starting models for carbenes and precatalyst were prepared on the basis of available CSD crystal structures of a Grubbs and Hoveyda–Grubbs precatalysts (refcodes: ABEJUM01, GUBQUP, ZETLOZ and LOVPAP) [58,59,64,66]. In the geometry optimization step we used the M06 density functional with the 6-31G** basis set for C, N, O, Cl and H atoms, while the Ru atom, which was described by the Los Alamos angular momentum projected effective core potential (ECP) using the double- ζ contraction of valence functions (denoted as LACVP**). The choice of the M06 functional was made due to its very good performance in accurate description of ruthenium-based catalysts, giving accurate energies for a number of Grubbs and Hoveyda systems [31,67]. Since the M06 functional has already medium-range dispersion implemented, M06-D3 may overestimate the effect of dispersion due to double-counting of these effects [47]. On the other hand the addition of D3 correction to M06 was shown to improve the results for many organic reactions when calculating the differences in relative energies, therefore we decided to use it in this investigation [31,67,68]. To assess the need to use the D3 correction we have performed additional benchmark calculations for selected ruthenium catalysts and compared them with the experimental data. Based on these results we decided to use the D3 correction in the estimation of all Gibbs free energies apart from the Grubbs-like systems, where the D3 correction was omitted.

In all calculations we have used the standard energy convergence criterion of 5×10^{-5} Hartree. For each structure frequencies were calculated to verify the nature of each stationary point (zero imaginary frequencies for minima and one imaginary frequency for transition states). In the second step we performed solvation energy calculations using the Poisson–Boltzmann self-consistent polarizable continuum method as implemented in Jaguar v.7.9 (Schrodinger, 2013) to represent dichloromethane, using the dielectric constant of 8.93 and the effective radius 2.33 Å. The solvation calculations were performed using the M06-D3/LACVP** level of theory and the gas-phase optimized structures. We also used the same polarizable continuum method to estimate the solvation energies in water (dielectric constant of 80.73 and the effective radius 1.40 Å) and these results are presented in Supporting Information File 1. For all stationary points we have also performed single-point energy calculations with the valence polarized basis set denoted as LACV3P++**. Free energies discussed in this work for stationary points are calculated as the sum of electronic energy (from single-point LACV3P++** calculations), solvation energy, zero-point energy correction, thermal correction to enthalpy, and the negative product of temperature and entropy (at 298 K). All final estimates of Gibbs free energies include the counterpoise correction [69].

To further validate our results we used the very accurate, single-point DLPNO-CCSD(T) calculations using the DFT-optimized geometries and the def2-svp basis set using Orca v4.0.0.1 program [70,71]. Complete DLPNO-CCSD(T) results are presented in Supporting Information File 1.

Supporting Information

Supporting Information File 1

Mulliken partial charges, energy values and Cartesian coordinates for all investigated systems.

[<https://www.beilstein-journals.org/bjoc/content/supplementary/1860-5397-14-266-S1.pdf>]

Acknowledgements

This work was supported by National Science Centre grant UMO-2016/22/E/ST4/00573.

ORCID® iDs

Bartosz Trzaskowski - <https://orcid.org/0000-0003-2385-1476>

References

1. Arduengo, A. J., III; Harlow, R. L.; Kline, M. *J. Am. Chem. Soc.* **1991**, *113*, 361–363. doi:10.1021/ja00001a054
2. Herrmann, W. A.; Köcher, C. *Angew. Chem., Int. Ed. Engl.* **1997**, *36*, 2162–2187. doi:10.1002/anie.199721621
3. Díez-González, S.; Marion, N.; Nolan, S. P. *Chem. Rev.* **2009**, *109*, 3612–3676. doi:10.1021/cr900074m
4. Hopkinson, M. N.; Richter, C.; Schedler, M.; Glorius, F. *Nature* **2014**, *510*, 485–496. doi:10.1038/nature13384
5. Hahn, E. F.; Jahnke, M. C. *Angew. Chem., Int. Ed.* **2008**, *47*, 3122–3172. doi:10.1002/anie.200703883
6. Benhamou, L.; Chardon, E.; Lavigne, G.; Bellemin-Laponnaz, S.; César, V. *Chem. Rev.* **2011**, *111*, 2705–2733. doi:10.1021/cr100328e
7. Dröge, T.; Glorius, F. *Angew. Chem., Int. Ed.* **2010**, *49*, 6940–6952. doi:10.1002/anie.201001865
8. Grubbs, R. H.; Chang, S. *Tetrahedron* **1998**, *54*, 4413–4450. doi:10.1016/s0040-4020(97)10427-6
9. Fürstner, A. *Angew. Chem., Int. Ed.* **2000**, *39*, 3012–3043. doi:10.1002/1521-3773(20000901)39:17<3012::aid-anie3012>3.0.co;2-g
10. Schrock, R. R.; Hoveyda, A. H. *Angew. Chem., Int. Ed.* **2003**, *42*, 4592–4633. doi:10.1002/anie.200300576
11. Vougioukalakis, G. C.; Grubbs, R. H. *Chem. Rev.* **2010**, *110*, 1746–1787. doi:10.1021/cr9002424
12. Samołłowicz, C.; Bieniek, M.; Grela, K. *Chem. Rev.* **2009**, *109*, 3708–3742. doi:10.1021/cr800524f
13. Grela, K. *Olefin Metathesis: Theory and Practice*; John Wiley & Sons, Inc.: Hoboken, 2014. doi:10.1002/9781118711613
14. Grubbs, R. H.; Wenzel, A. G.; O’Leary, D. J.; Khosravi, E. *Handbook of Metathesis*, 2nd ed.; Wiley-VCH: Weinheim, 2015; Vol. 1–3.
15. Nasr, A.; Winkler, A.; Tamm, M. *Coord. Chem. Rev.* **2016**, *316*, 68–124. doi:10.1016/j.ccr.2016.02.011
16. Jana, A.; Grela, K. *Chem. Commun.* **2018**, *54*, 122–139. doi:10.1039/c7cc06535c
17. Hildebrandt, B.; Ganter, C. *J. Organomet. Chem.* **2012**, *717*, 83–87. doi:10.1016/j.jorganchem.2012.07.014
18. Iglesias-Sigüenza, J.; Izquierdo, C.; Díez, E.; Fernández, R.; Lassaletta, J. M. *Dalton Trans.* **2018**, *47*, 5196–5206. doi:10.1039/c8dt00213d
19. Periana, R. A.; Taube, D. J.; Gamble, S.; Taube, H.; Satoh, T.; Fujii, H. *Science* **1998**, *280*, 560–564. doi:10.1126/science.280.5363.560
20. Ahlquist, M.; Periana, R. A.; Goddard, W. A., III. *Chem. Commun.* **2009**, *0*, 2373–2375. doi:10.1039/b821854d
21. Carreras, J.; Patil, M.; Thiel, W.; Alcarazo, M. *J. Am. Chem. Soc.* **2012**, *134*, 16753–16758. doi:10.1021/ja306947m
22. Jordan, J. P.; Grubbs, R. H. *Angew. Chem., Int. Ed.* **2007**, *46*, 5152–5155. doi:10.1002/anie.200701258
23. Skowerski, K.; Szczepaniak, G.; Wierzbicka, C.; Gułajski, Ł.; Bieniek, M.; Grela, K. *Catal. Sci. Technol.* **2012**, *2*, 2424–2427. doi:10.1039/c2cy20320k
24. Skowerski, K.; Wierzbicka, C.; Szczepaniak, G.; Gułajski, Ł.; Bieniek, M.; Grela, K. *Green Chem.* **2012**, *14*, 3264–3268. doi:10.1039/c2gc36015b
25. Balof, S. L.; P’Pool, S. J.; Berger, N. J.; Valente, E. J.; Shiller, A. M.; Schanz, H.-J. *Dalton Trans.* **2008**, *0*, 5791–5799. doi:10.1039/b809793c
26. Kośnik, W.; Grela, K. *Dalton Trans.* **2013**, *42*, 7463–7467. doi:10.1039/c3dt33010a
27. Buhl, H.; Ganter, C. *Chem. Commun.* **2013**, *49*, 5417–5419. doi:10.1039/c3cc42547a
28. Ruamps, M.; Lujan, N.; César, V. *Organometallics* **2017**, *36*, 1049–1055. doi:10.1021/acs.organomet.7b00017
29. Hölzel, T.; Otto, M.; Buhl, H.; Ganter, C. *Organometallics* **2017**, *36*, 4443–4450. doi:10.1021/acs.organomet.7b00670
30. Stewart, I. C.; Benitez, D.; O’Leary, D. J.; Tkatchouk, E.; Day, M. W.; Goddard, W. A., III; Grubbs, R. H. *J. Am. Chem. Soc.* **2009**, *131*, 1931–1938. doi:10.1021/ja8078913
31. Benitez, D.; Tkatchouk, E.; Goddard, W. A., III. *Organometallics* **2009**, *28*, 2643–2645. doi:10.1021/om900041j
32. Nelson, J. W.; Grundy, L. M.; Dang, Y.; Wang, Z.-X.; Wang, X. *Organometallics* **2014**, *33*, 4290–4294. doi:10.1021/om500612r
33. Ashworth, I. W.; Hillier, I. H.; Nelson, D. J.; Percy, J. M.; Vincent, M. A. *ACS Catal.* **2013**, *3*, 1929–1939. doi:10.1021/cs400164w
34. Engle, K. M.; Lu, G.; Luo, S.-X.; Henling, L. M.; Takase, M. K.; Liu, P.; Houk, K. N.; Grubbs, R. H. *J. Am. Chem. Soc.* **2015**, *137*, 5782–5792. doi:10.1021/jacs.5b01144
35. Luo, S.-X.; Engle, K. M.; Dong, X.; Hejl, A.; Takase, M. K.; Henling, L. M.; Liu, P.; Houk, K. N.; Grubbs, R. H. *ACS Catal.* **2018**, *8*, 4600–4611. doi:10.1021/acscatal.8b00843
36. Trzaskowski, B.; Grela, K. *Organometallics* **2013**, *32*, 3625–3630. doi:10.1021/om400233s
37. Pazio, A.; Woźniak, K.; Grela, K.; Trzaskowski, B. *Organometallics* **2015**, *34*, 563–570. doi:10.1021/om5006462
38. Pazio, A.; Woźniak, K.; Grela, K.; Trzaskowski, B. *Dalton Trans.* **2015**, *44*, 20021–20026. doi:10.1039/c5dt03446a
39. Trzaskowski, B.; Ostrowska, K. *RSC Adv.* **2016**, *6*, 21423–21429. doi:10.1039/c6ra01194b
40. Trzaskowski, B.; Grela, K. *Catal. Commun.* **2016**, *86*, 133–138. doi:10.1016/j.catcom.2016.08.025
41. Trzaskowski, B.; Ostrowska, K. *Catal. Commun.* **2017**, *91*, 43–47. doi:10.1016/j.catcom.2016.12.014
42. Trzaskowski, B.; Goddard, W. A.; Grela, K. *Mol. Catal.* **2017**, *433*, 313–320. doi:10.1016/j.mcat.2016.12.018

43. Zhao, Y.; Truhlar, D. G. *Theor. Chem. Acc.* **2008**, *120*, 215–241. doi:10.1007/s00214-007-0310-x

44. Zhao, Y.; Truhlar, D. G. *Chem. Phys. Lett.* **2011**, *502*, 1–13. doi:10.1016/j.cplett.2010.11.060

45. Grimme, S.; Antony, J.; Ehrlich, S.; Krieg, H. *J. Chem. Phys.* **2010**, *132*, 154104. doi:10.1063/1.3382344

46. Luo, S.; Zhao, Y.; Truhlar, D. G. *Phys. Chem. Chem. Phys.* **2011**, *13*, 13683–13689. doi:10.1039/c1cp20834a

47. Goerigk, L. *J. Phys. Chem. Lett.* **2015**, *6*, 3891–3896. doi:10.1021/acs.jpclett.5b01591

48. Liberman-Martin, A. L.; Grubbs, R. H. *Organometallics* **2017**, *36*, 4091–4094. doi:10.1021/acs.organomet.7b00615

49. Młodzikowska, K.; Rajkiewicz, A. A.; Grela, K.; Trzaskowski, B. *New J. Chem.* **2018**, *42*, 6183–6190. doi:10.1039/c8nj00296g

50. Wanzlick, H.-W.; Schikora, E. *Angew. Chem.* **1960**, *72*, 494. doi:10.1002/ange.19600721409

51. Poater, A.; Ragone, F.; Giudice, S.; Costabile, C.; Dorta, R.; Nolan, S. P.; Cavallo, L. *Organometallics* **2008**, *27*, 2679–2681. doi:10.1021/om8001119

52. Alder, R. W.; Blake, M. E.; Chaker, L.; Harvey, J. N.; Paolini, F.; Schütz, J. *Angew. Chem., Int. Ed.* **2004**, *43*, 5896–5911. doi:10.1002/anie.200400654

53. Lemal, D. M.; Lovald, R. A.; Kawano, K. I. *J. Am. Chem. Soc.* **1964**, *86*, 2518–2519. doi:10.1021/ja01066a044

54. Arduengo, A. J., III; Dias, H. V. R.; Harlow, R. L.; Kline, M. *J. Am. Chem. Soc.* **1992**, *114*, 5530–5534. doi:10.1021/ja00040a007

55. Çetinkaya, B.; Demir, S.; Özdemir, I.; Toupet, L.; Sémeril, D.; Bruneau, C.; Dixneuf, P. H. *Chem. – Eur. J.* **2003**, *9*, 2323–2330. doi:10.1002/chem.200204533

56. Abialimov, O.; Kędziora, M.; Malińska, M.; Woźniak, K.; Grela, K. *Organometallics* **2014**, *33*, 2160–2171. doi:10.1021/om4009197

57. Sanford, M. S.; Love, J. A.; Grubbs, R. H. *J. Am. Chem. Soc.* **2001**, *123*, 6543–6554. doi:10.1021/ja010624k

58. Huang, J.; Stevens, E. D.; Nolan, S. P.; Petersen, J. L. *J. Am. Chem. Soc.* **1999**, *121*, 2674–2678. doi:10.1021/ja9831352

59. Yu, B.; Xie, Y.; Hamad, F. B.; Leus, K.; Lyapkov, A. A.; Van Hecke, K.; Verpoort, F. *New J. Chem.* **2015**, *39*, 1858–1867. doi:10.1039/c4nj02034k

60. Urbina-Blanco, C. A.; Poater, A.; Lebl, T.; Manzini, S.; Slawin, A. M. Z.; Cavallo, L.; Nolan, S. P. *J. Am. Chem. Soc.* **2013**, *135*, 7073–7079. doi:10.1021/ja402700p

61. Thiel, V.; Hendann, M.; Wannowius, K.-J.; Plenio, H. *J. Am. Chem. Soc.* **2012**, *134*, 1104–1114. doi:10.1021/ja208967h

62. Vorfalt, T.; Wannowius, K.-J.; Plenio, H. *Angew. Chem., Int. Ed.* **2010**, *49*, 5533–5536. doi:10.1002/anie.201000581

63. Scholl, M.; Trnka, T. M.; Morgan, J. P.; Grubbs, R. H. *Tetrahedron Lett.* **1999**, *40*, 2247–2250. doi:10.1016/s0040-4039(99)00217-8

64. Barbasiewicz, M.; Bieniek, M.; Michrowska, A.; Szadkowska, A.; Makal, A.; Woźniak, K.; Grela, K. *Adv. Synth. Catal.* **2007**, *349*, 193–203. doi:10.1002/adsc.200600478

65. Appleton, T. G.; Clark, H. C.; Manzer, L. E. *Coord. Chem. Rev.* **1973**, *10*, 335–422. doi:10.1016/s0010-8545(00)80238-6

66. Schwab, P.; France, M. B.; Ziller, J. W.; Grubbs, R. H. *Angew. Chem., Int. Ed. Engl.* **1995**, *34*, 2039–2041. doi:10.1002/anie.199520391

67. Benitez, D.; Tkatchouk, E.; Goddard, W. A., III. *Chem. Commun.* **2008**, *6194*–6196. doi:10.1039/b815665d

68. Minenkov, Y.; Occhipinti, G.; Jensen, V. R. *Organometallics* **2013**, *32*, 2099–2111. doi:10.1021/om301192a

License and Terms

This is an Open Access article under the terms of the Creative Commons Attribution License (<http://creativecommons.org/licenses/by/4.0>). Please note that the reuse, redistribution and reproduction in particular requires that the authors and source are credited.

The license is subject to the *Beilstein Journal of Organic Chemistry* terms and conditions: (<https://www.beilstein-journals.org/bjoc>)

The definitive version of this article is the electronic one which can be found at:
doi:10.3762/bjoc.14.266



MoO₃ on zeolites MCM-22, MCM-56 and 2D-MFI as catalysts for 1-octene metathesis

Hynek Balcar*, Martin Kubů, Naděžda Žilková and Mariya Shamzhy

Full Research Paper

Open Access

Address:

J. Heyrovský Institute of Physical Chemistry of the Czech Academy of Sciences, v.v.i., Dolejškova 3, 182 23 Prague 8, Czech Republic

Beilstein J. Org. Chem. **2018**, *14*, 2931–2939.

doi:10.3762/bjoc.14.272

Email:

Hynek Balcar* - hynek.balcar@jh-inst.cas.cz

Received: 30 August 2018

Accepted: 15 November 2018

Published: 27 November 2018

* Corresponding author

This article is part of the thematic issue "Progress in metathesis chemistry III".

Keywords:

metathesis; molybdenum oxide; 1-octene; thermal spreading; zeolites

Guest Editors: K. Grela and A. Kajetanowicz

© 2018 Balcar et al.; licensee Beilstein-Institut.

License and terms: see end of document.

Abstract

Highly active olefin metathesis catalysts were prepared by thermal spreading MoO₃ and/or MoO₂(acac)₂ on MWW zeolites (MCM-22, delaminated MCM-56) and on two-dimensional MFI (all in NH₄⁺ form). The catalysts' activities were tested in the metathesis of neat 1-octene (as an example of a longer chain olefin) at 40 °C. Catalysts with 6 wt % or 5 wt % of Mo were used. The acidic character of the supports had an important effect on both the catalyst activity and selectivity. The catalyst activity increases in the order 6MoO₃/HZSM-5(25) (Si/Al = 25) << 6MoO₂(acac)₂/MCM-22(70) < 6MoO₃/2D-MFI(26) < 6MoO₃/MCM-56(13) < 6MoO₃/MCM-22(28) reflecting both the enhancing effect of the supports' acidity and accessibility of the catalytic species on the surface. On the other hand the supports' acidity decreases the selectivity to the main metathesis product C14 due to an acid-catalyzed double bond isomerization (followed by cross metathesis) and oligomerization. 6MoO₃/2D-MFI(26) with a lower concentration of the acidic centres resulting in catalysts of moderate activity but with the highest selectivity.

Introduction

Molybdenum oxide on silica, alumina or silica-alumina belongs to the well-known and long-time used metathesis catalysts [1]. Albeit typical ill-defined catalysts they are still popular as relatively cheap catalysts finding industrial applications especially in the treatment of low olefins [2-5]. Their catalytic activity depends on many factors, especially on Mo loading, support acidity, and pre-reaction activations. Surface isolated MoO₄

tetrahedra were proved as the main precursors of the catalytic species [6,7], thus the perfect dispersion of MoO₃ on the surface is a crucial precondition for a high catalytic activity. The mechanisms of transformation of these precursors to the surface Mo carbenes as real catalytically active species has been suggested [6,7]. The replacement of ordinary silicas for mesoporous molecular sieves SBA-15 or MCM-41 increased the

catalyst activity substantially, which allowed performing the metathesis of long chain olefins under mild reaction conditions [8–10]. The positive effect of these supports on the catalyst activity was ascribed to their high surface areas enhancing the spreading of MoO_3 molecules on the surface and large pores increasing the substrates/products transport rate.

Microporous zeolites like HZSM-5 impregnated by ammonium heptamolybdate solutions were used for the metathesis of low olefins (ethylene, propylene, butenes) [11–13]. In the case of bulkier substrates they suffer, however, of micropore size limitations. To overcome these limitations a decrease in crystal size and the application of two-dimensional zeolites can be used [14–17]. Two dimensional 2D-MFI and MWW delaminated zeolite MCM-56, which have been prepared recently [18–21], represent two types of these materials, which exhibit relatively high surface areas and high accessibility of catalytic sites on the surface as well [22]. Therefore, we supported MoO_3 and/or $\text{MoO}_2(\text{acac})_2$ on (i) 2D-MFI (and ordinary HZSM-5 for comparison) and similarly on (ii) MCM-56 and its 3D analogue MCM-22 (both in NH_4^+ form) and examined their activity in the metathesis of neat 1-octene (Scheme 1) under ambient pressure and 40 °C. According to our best knowledge, none of these materials have been tested as supports for MoO_3 based catalysts for metathesis of higher alkenes up to now. MoO_x on MCM-22 combined with $\gamma\text{-Al}_2\text{O}_3$ was used in cross metathesis of 2-butene and ethylene in a stream (125 °C, 1 MPa) [23]. MCM-22, and MCM-56 were also used as supports for Hoveyda–Grubbs type hybrid catalysts active in metathesis of long-chain unsaturated esters [24].

Results and Discussion

Catalyst preparation and characterization

XRD patterns and texture properties (Table 1, Figure 1 A,B,C,D) of prepared MCM-22, MCM-56 and 2D-MFI zeolites proved a high quality of these supports. For catalyst labelling following the mode has been adopted: $x\text{ MoO}_3/\text{MCM-22}(y)$, where x = Mo concentration in wt % Mo, y = Si/Al molar ratio. After spreading Mo compounds over the support surface areas (S_{BET} , S_{ext}) as well as void volumes (V) decreased. Similar reduction of these quantities has been already observed earlier [9,10,24]. For $x\text{ MoO}_3/\text{MCM-22}(28)$, XRD patterns of catalysts are similar to those of their parents approximately up to $x = 6$ wt % of Mo (0.9 Mo atoms per nm^2). At higher Mo concentrations signals of crystalline MoO_3 appeared (marked with * in Figure 1 A,B,D). It suggests 6 wt % of Mo being the

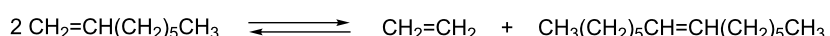
optimal Mo loading. On the other hand, $x\text{ MoO}_3/\text{MCM-22}(70)$ catalyst with $x = 6$ wt % Mo exhibited slight MoO_3 signals, when prepared from MoO_3 probably due to the lower surface area (especially external one) comparing with MCM-22(28). However, when $\text{MoO}_2(\text{acac})_2$ was used as a source of Mo, catalysts with 6 wt % (and lower) content of Mo did not exhibit any MoO_3 signals. It is consistent with the previous observation that $\text{MoO}_2(\text{acac})_2$ provided better catalyst than MoO_3 [9]. XRD patterns of $6\text{MoO}_3/\text{MCM-56}(13)$ and $6\text{MoO}_3/2\text{D-MFI}(26)$ indicated also a good MoO_3 spreading, contrary to $6\text{MoO}_3/\text{HZSM-5}(25)$ where MoO_3 signals were clearly visible, probably as a result of lower external surface area.

Table 1: Texture properties of catalysts and corresponding supports.

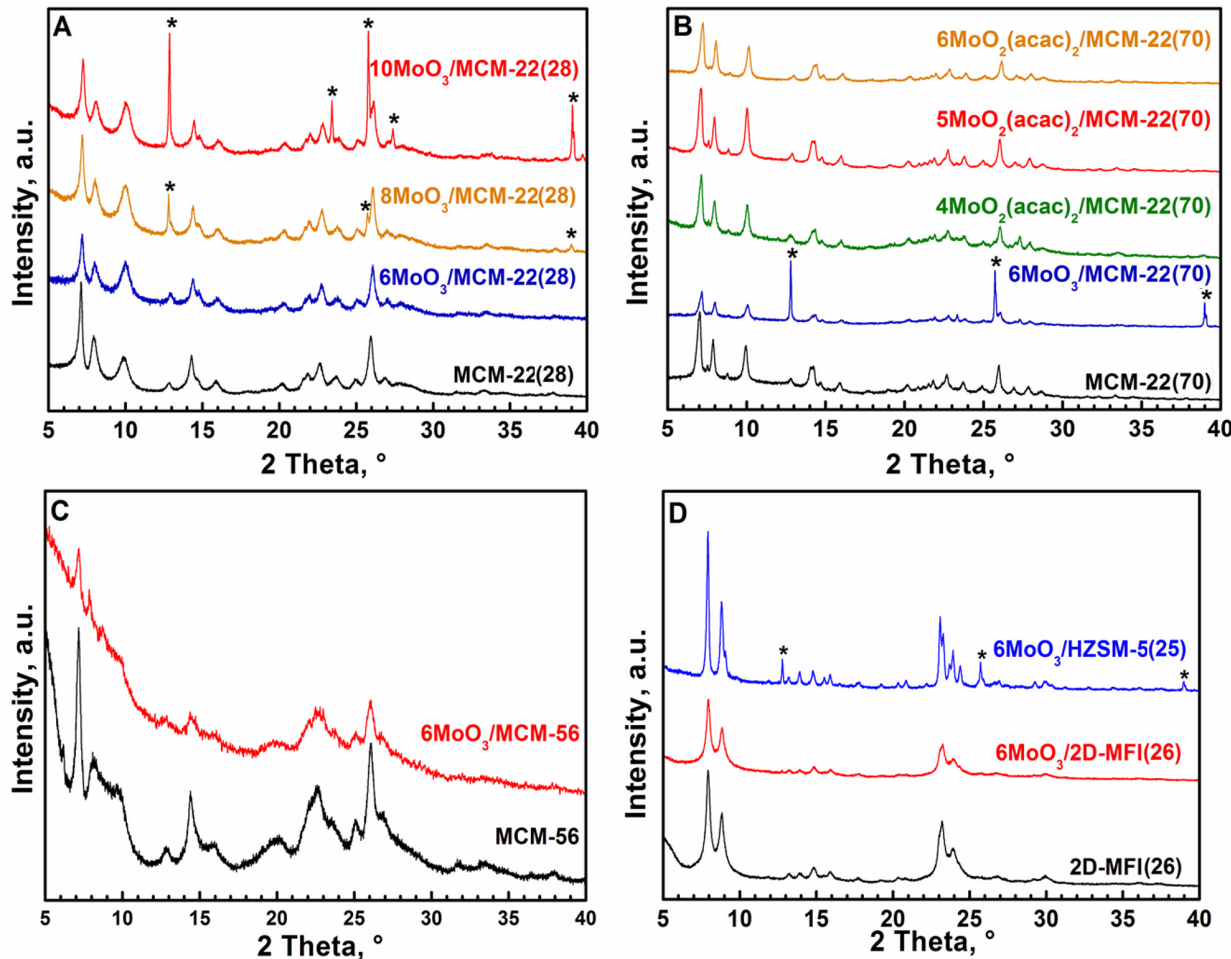
catalyst	S_{BET} (m^2/g)	S_{ext} (m^2/g)	V (cm^3/g)
1 MCM-22(28)	455	119	0.59
2 $6\text{MoO}_3/\text{MCM-22}(28)$	423	119	0.38
3 $6\text{MoO}_2(\text{acac})_2/\text{MCM-22}(28)$	426	94	0.57
4 MCM-22(70)	421	58	0.29
5 $6\text{MoO}_3/\text{MCM-22}(70)$	180	39	0.25
6 $6\text{MoO}_2(\text{acac})_2/\text{MCM-22}(70)$	355	41	0.24
7 2D-MFI(26)	565	343	0.61
8 $6\text{MoO}_3/2\text{D-MFI}(26)$	478	221	0.57
9 MCM-56(13)	469	164	0.57
10 $6\text{MoO}_3/\text{MCM-56}(13)$	269	129	0.55
11 HZSM-5(25)	410	44	0.23
12 $6\text{MoO}_3/\text{HZSM-5}(25)$	388	38	0.23

S_{BET} = BET area, V = total void volume ($p/p_0 = 0.95$), S_{ext} = external surface (from t -plot).

Contrary to the all-siliceous mesoporous sieves (like SBA-15) which are neutral, zeolites are acidic and their acidity (both Brønsted and Lewis-type) plays an important role for catalysis. The acid site concentrations of zeolitic supports and the corresponding catalysts measured using FTIR spectroscopy of adsorbed pyridine are shown in Table 2, while the relevant IR spectra are shown in Supporting Information File 1 (Figures S1–S5). It is seen that all supports contained both Brønsted and Lewis acid sites of various strength. MCM-22(28) and MCM-56(13) exhibited the highest concentrations of acid sites (both Brønsted and Lewis) in accord with their highest Al concentrations. The acid sites concentrations of MCM-22(70) and 2D-MFI(26) were lower and close to each other. The Brønsted acid site concentration of HZSM-5(25) was as high as that of



Scheme 1: 1-Octene metathesis reaction.

Figure 1: A,B,C,D: XRD patterns of parent supports and catalysts used. Asterisk marks MoO_3 .Table 2: Acid site concentrations in catalysts and corresponding supports.^a

sample	c(B) ^b , mmol/g				c(L) ^c , mmol/g			
	150 °C	250 °C	350 °C	450 °C	150 °C	250 °C	350 °C	450 °C
MCM-22(70)	0.11	0.12	0.09	0.02	0.06	0.04	0.03	0.03
6MoO ₃ /MCM-22(70)	0.02	0.01	–	–	0.10	0.01	0.01	–
6MoO ₂ (acac) ₂ /MCM-22(70)	0.06	0.06	0.05	0.02	0.16	0.07	0.04	0.03
MCM-22(28)	0.29	0.32	0.30	0.19	0.13	0.09	0.08	0.06
6MoO ₃ /MCM-22(28)	0.07	0.09	0.07	0.04	0.31	0.10	0.03	0.01
6MoO ₂ (acac) ₂ / MCM-22(28)	0.09	0.07	0.05	0.02	0.23	0.08	0.03	0.01
2D-MFI(26)	0.13	0.13	0.08	0.02	0.07	0.07	0.06	0.04
6MoO ₃ /2D-MFI(26)	0.06	0.04	0.03	0.01	0.10	0.03	0.01	–
HZSM-5(25)	0.29	0.28	0.22	0.07	0.04	0.03	0.02	0.02
6MoO ₃ /HZSM-5(25)	0.14	0.12	0.09	0.03	0.17	0.07	0.04	0.04
MCM-56(13)	0.23	0.17	0.13	0.04	0.18	0.12	0.09	0.08
MoO ₃ /MCM-56(13)	0.04	0.03	0.01	–	0.17	0.06	0.03	0.02

^aDetermined by FTIR. ^bBrønsted acid site. ^cLewis acid site.

MCM-22(28), however, its Lewis acid site concentration was significantly lower. After supporting Mo compounds the concentrations of Brønsted acid sites decreased significantly which may indicate that MoO_x species reacted predominantly with Brønsted acid sites of the supports. It is manifested by intensity decrease of the band in the region $3609\text{--}3625\text{ cm}^{-1}$, ascribed to OH vibration in the Si–O(H)–Al acid site (see Supporting Information File 1, Figures S1–S5) [25]. On the other hand, the concentrations of Lewis acid sites in the catalysts was slightly higher compared to the parent supports. It may be explained by the formation of some amount of Mo in a lower oxidation state which has been already described for siliceous supports (MCM-41, SBA-15) [9,26].

Catalytic activity

MCM-22-based catalysts

Na^+ forms of zeolites turned out to be unsuitable supports for metathesis catalysts. For example, by supporting MoO_3 on MCM-22(28) in Na^+ form (6 wt % of Mo) we obtained material providing only 0.5% 1-octene conversion in 19 h (1-octene/Mo = 320, $t = 40\text{ }^\circ\text{C}$). Therefore, we converted Na^+ forms to NH_4^+ forms, which were used for supporting Mo compounds by thermal spreading method.

The time development of 1-octene conversion over $6\text{MoO}_3/\text{MCM-22(28)}$ is shown in Figure 2. The GC chromatogram of the final product is shown in Figure S6 (in Supporting Information File 1). It is seen that in addition to the main metathesis product (7-tetradecene), alkenes from C13 to C9 are present in considerable amounts. It is a consequence of the 1-octene double bond isomerization followed by cross metathesis. Moreover, a certain amount of oligomers (mainly dimers) were also observed in the reaction mixtures. Both isomerization and oligomerization are due to the acidic character of the support (vide infra). In addition to the total conversion of 1-octene (K_{tot}), the conversion to all metathesis products (K_{met}), and the conversion to tetradecene (K_{C14}) calculated according to the following equations are plotted in Figure 2.

$$K_{\text{tot}} = \frac{(2\sum m_i/M_i + 2m_d/M_d + 3m_t/M_t)}{(2\sum m_i/M_i + 2m_d/M_d + 3m_t/M_t + m_{\text{C8}}/M_{\text{C8}})}$$

$$K_{\text{met}} = \frac{(2\sum m_i/M_i)}{(2\sum m_i/M_i + 2m_d/M_d + 3m_t/M_t + m_{\text{C8}}/M_{\text{C8}})}$$

$$K_{\text{C14}} = \frac{(2m_{\text{C14}}/M_{\text{C14}})}{(2\sum m_i/M_i + 2m_d/M_d + 3m_t/M_t + m_{\text{C8}}/M_{\text{C8}})}$$

where m_i and M_i ($i = 9\text{--}14$) are weight amounts and molecular weights of alkenes from C9 to C14; m_d , m_t and M_d , M_t are weight amounts and molecular weights of octene dimers and

trimers, respectively; m_{C8} is weight amount of octene (all isomers) and M_{C8} is the molecular weight of octene.

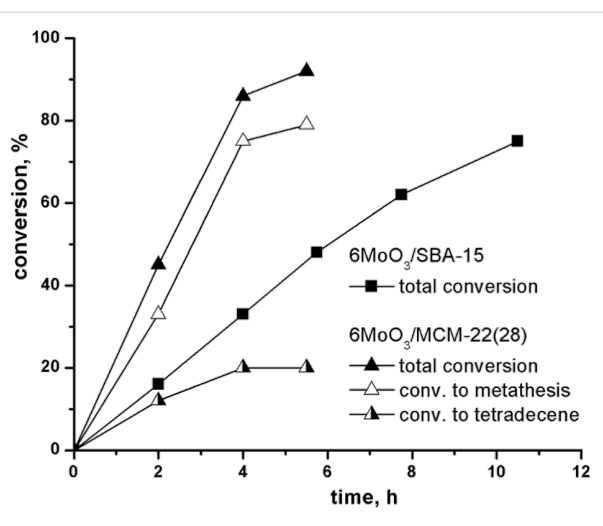


Figure 2: Conversion vs time curves for 1-octene metathesis over $6\text{MoO}_3/\text{MCM-22(28)}$ and $6\text{MoO}_3/\text{SBA-15}$. Neat 1-octene, 1-octene/Mo = 320, $t = 40\text{ }^\circ\text{C}$.

For comparison, the conversion curve over $6\text{MoO}_3/\text{SBA-15}$ is added in Figure 2. $6\text{MoO}_3/\text{SBA-15}$ was prepared from all-siliceous SBA-15 ($S_{\text{BET}} = 877\text{ m}^2/\text{g}$, $V = 1.07\text{ cm}^3/\text{g}$, pore diameter $D = 6.4\text{ nm}$) and it is known as a very active and selective catalyst [9,10]. Under reaction conditions applied the selectivity to tetradecene was about 98% during the whole experiment, and therefore only K_{tot} is plotted in Figure 2 in this case.

Both K_{tot} and K_{met} for $6\text{MoO}_3/\text{MCM-22(28)}$ were significantly higher than the total conversion for $6\text{MoO}_3/\text{SBA-15}$ (Figure 2). Conversions to oligomers ($K_{\text{ol}} = K_{\text{tot}} - K_{\text{met}}$) were about 12% (at 2 h) and practically did not change in the further course of the reaction. However, the conversions to tetradecene were rather low (maximum conversion about 20% was achieved). Higher catalytic activity of molybdenum oxide on zeolitic support in metathesis may be ascribed to the higher acidity of supports. The enhancing effect of Brønsted acidity on the catalytic activity has been already described [6] and it assumed that most of Mo active species in zeolite-based catalysts are formed by reacting molybdenum oxide with Si–O(H)–Al groups [12,27]. Similarly, Lim et al. showed recently [28], that Brønsted acid sites improve dispersion of molybdenum oxide on the surface. Moreover, for related system based on tungsten oxide in zeolite, it was suggested using high resolution STEM that Brønsted acid sites in proximity to metathesis active sites facilitate olefin adsorption and metallocycle formation [29]. Such mechanism may be effective also for Mo catalysts. The decrease in the selectivity due to isomerization and/or oligomerization seems to be an unavoidable cost for this activity enhancement.

It is known for molybdenum oxide catalysts, that with increasing Mo loading the catalytic activities increase up to maximum value [6,10]. At higher loadings the molybdenum oxide spreading on the surface became imperfect and catalytically inactive bulk MoO_3 appears. The effect of increasing Mo loading on catalyst activity for MCM-22(28)-based catalyst is shown in Table 3.

For $8\text{MoO}_3/\text{MCM-22(28)}$ XRD pattern shows a small amount of bulk MoO_3 (marked with asterisk in Figure 1A). In accord with this, the conversions fell down in comparison with $6\text{MoO}_3/\text{MCM-22(28)}$, the selectivity, however, slightly increased: the amount of oligomers was reduced and the selectivity to the tetradecene approximately doubled. It suggests that more acid sites were covered by MoO_x species and oligomerization and isomerization ability of catalysts decreased. However, further increase in the Mo loading to 10 wt % in $10\text{MoO}_3/\text{MCM-22(28)}$ led nearly to the lost of catalytic activity, which is explained by deposition of Mo in the catalytically inactive bulk MoO_3 . Correspondingly, very intensive diffraction lines of the

bulk MoO_3 appeared in the XRD pattern of $10\text{MoO}_3/\text{MCM-22(28)}$ (see Figure 1A).

To reduce isomerization and oligomerization ability of MCM-22-based catalysts we prepared zeolite with $\text{Si}/\text{Al} = 70$ (and therefore with lower acidity – *vide supra*): MCM-22(70). The results showing the catalytic behavior of the prepared MCM-22(70)-based catalysts $6\text{MoO}_2(\text{acac})_2/\text{MCM-22(70)}$, $5\text{MoO}_2(\text{acac})_2/\text{MCM-22(70)}$, and $4\text{MoO}_2(\text{acac})_2/\text{MCM-22(70)}$ are collected in Table 4.

XRD pattern of $6\text{MoO}_3/\text{MCM-22(70)}$ exhibited some amount of bulk MoO_3 (Figure 1B). Evidently on this less acidic support the MoO_3 spreading is not perfect, which explains its negligible activity in metathesis reaction. However, using bis(acetylacetone) complex $\text{MoO}_2(\text{acac})_2$ as a source of Mo we obtained $6\text{MoO}_2(\text{acac})_2/\text{MCM-22(70)}$, $5\text{MoO}_2(\text{acac})_2/\text{MCM-22(70)}$, and $4\text{MoO}_2(\text{acac})_2/\text{MCM-22(70)}$ exhibiting no signals of bulk MoO_3 in XRD pattern (Figure 1B) and showing a mild metathesis activity. The highest conversion $K_{\text{tot}} = 35\%$ (after

Table 3: The effect of Mo loading on catalyst activity in 1-octene metathesis.^a

catalyst	reaction time, h	K_{tot} , %	K_{met} , %	K_{ol} , %	K_{C14} , %
$6\text{MoO}_3/\text{MCM-22(28)}$	2	45	33	12	12
	4	86	75	11	20
	6	92	79	13	20
$8\text{MoO}_3/\text{MCM-22(28)}$	2	21	15	6	10
	4	41	35	6	18
	6.5	58	51	7	25
	22	85	77	8	36
$10\text{MoO}_3/\text{MCM-22(28)}$	2	2.6	0.6	2	0.6
	4	3.4	0.7	2.7	0.7
	6	4	1	3	1

^a50 mg Catalyst, 1.5 mL 1-octene, 40 °C.

Table 4: 1-Octene metathesis over MCM-22(70)-based catalysts.^a

catalyst	reaction time, h	K_{tot} , %	K_{met} , %	K_{ol} , %	K_{C14} , %
$6\text{MoO}_3/\text{MCM-22(70)}$	2	2	–	–	–
	4.5	3	–	–	–
	6	2	–	–	–
$6\text{MoO}_2(\text{acac})_2/\text{MCM-22(70)}$	2	8	7.5	0.5	5
	4	9	8	1	6
	22	11.5	10.5	1	7
$5\text{MoO}_2(\text{acac})_2/\text{MCM-22(70)}$	2.3	8	7	1	5
	3.3	11	10	1	7
	20	35	32	3	17
$4\text{MoO}_2(\text{acac})_2/\text{MCM-22(70)}$	2	11	11	0	10
	4	16	15	1	14
	21	16	15	1	14

^a50 mg Catalyst, 1.5 mL 1-octene, 40 °C.

20 h) was achieved over $5\text{MoO}_2(\text{acac})_2/\text{MCM-22}(70)$. Oligomerization activity of all these catalysts was considerably lower in comparison with that of $6\text{MoO}_3/\text{MCM-22}(28)$ ($K_{\text{ol}} = 1\%$ only). However, the isomerization was not suppressed and conversion to tetradecene K_{C14} was low.

MCM-56-based catalysts

Conversion curves for the 1-octene metathesis over $6\text{MoO}_3/\text{MCM-56}(13)$ under standard conditions are displayed in Figure 3. In spite of the 2D character of support the conversions over $6\text{MoO}_3/\text{MCM-56}(13)$ were significantly lower in comparison with $6\text{MoO}_3/\text{MCM-22}(28)$: the initial reaction rate (calculated at reaction time = 2 h) being about a half of the initial reaction rate over $6\text{MoO}_3/\text{MCM-22}(28)$. On the other hand the extent of oligomerization was practically the same (for final product the oligomerization selectivity was 14%) and the extent of cross metathesis was even higher (the selectivity to tetradecene was only 15%). The crystals of MCM-22 (see SEM image in Supporting Information File 1, Figure S7) consist of very thin platelets and therefore a great amounts of 12-membered ring cups of MWW structure are on crystal exterior [18]. These cups as we assume host MoO_x species. Although MCM-56(13) as 2D zeolite consists of very thin layers, these layers may be curled and packed, which prevents the access of substrate molecules to the most of 12MR cups (for MCM-56(13) morphology see Supporting Information File 1, Figure S8). This may explain the lower activity of $6\text{MoO}_3/\text{MCM-56}(13)$ compared with $6\text{MoO}_3/\text{MCM-22}(28)$. Similarly, a higher activity of MCM-22 in comparison with MCM-56 has been observed in toluene disproportionation [18] and also for RCM of citronelene over immobilized Ru catalysts the activity of catalyst based on MCM-56 was not higher than that based on MCM-22 [24].

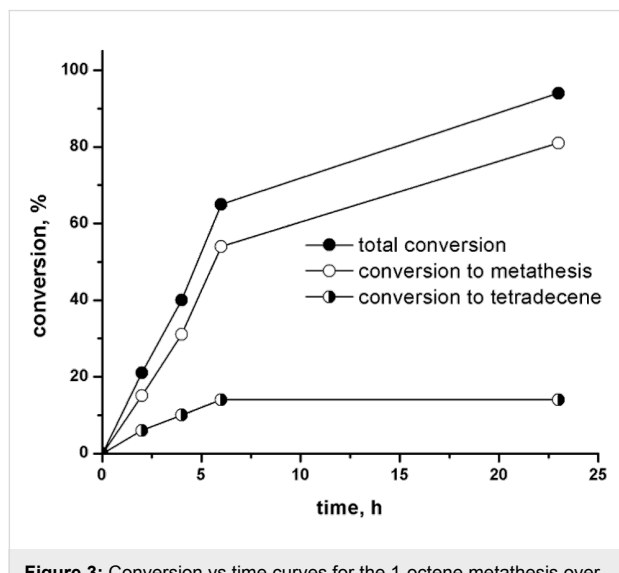


Figure 3: Conversion vs time curves for the 1-octene metathesis over $6\text{MoO}_3/\text{MCM-56}(13)$. Neat 1-octene, $1\text{-octene}/\text{Mo} = 320$, $t = 40\text{ }^{\circ}\text{C}$.

MFI-based catalysts

The comparison of conversion curves for 1-octene over $6\text{MoO}_3/2\text{D-MFI}(26)$ and $6\text{MoO}_3/\text{HZSM-5}(25)$ under standard conditions is given in Figure 4. It is seen that $6\text{MoO}_3/\text{HZSM-5}(25)$ exhibited only negligible activity ($K_{\text{tot}} = K_{\text{met}} = 3\%$ after 20 h) in accord with poor MoO_3 spreading (see Figure 1D). Despite the high acidity of the support, a poor accessibility of relevant surface OH groups during the thermal spreading process and a poor accessibility of possible active sites by substrate molecule during metathesis may cause $6\text{MoO}_3/\text{HZSM-5}(25)$ to be practically inactive. On the other hand, over $6\text{MoO}_3/2\text{D-MFI}(26)$ about 90% conversion was achieved for the same reaction time (20 h). The initial reaction rate over $6\text{MoO}_3/2\text{D-MFI}(26)$ was only slightly lower than that over $6\text{MoO}_3/\text{MCM-56}(13)$ and about one half of that over $6\text{MoO}_3/\text{MCM-22}(28)$. Contrary to $6\text{MoO}_3/\text{MCM-22}(28)$ the oligomerization activity of $6\text{MoO}_3/2\text{D-MFI}(26)$ was reduced (K_{ol} was from 1% to 5%) and the selectivity to tetradecene was higher (for final conversions $K_{\text{C14}}/K_{\text{met}} = 0.41$ and 0.25 for $6\text{MoO}_3/2\text{D-MFI}(26)$ and $6\text{MoO}_3/\text{MCM-22}(28)$, respectively). Lower acidity of $6\text{MoO}_3/2\text{D-MFI}(26)$ may explain the lower extent of oligomerization and isomerization reactions and increased tetradecene selectivity. Lower acidity may also bring about the reduced activity as compared with $6\text{MoO}_3/\text{MCM-22}(28)$; however, different structures of MCM-22 and MFI do not allow simple comparison.

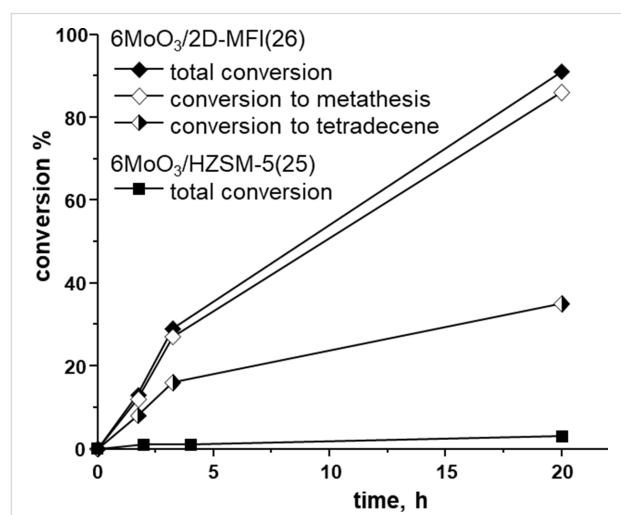


Figure 4: Conversion vs time curves for 1-octene metathesis over $6\text{MoO}_3/2\text{D-MFI}(26)$ and $6\text{MoO}_3/\text{HZSM-5}(25)$. Neat 1-octene, $1\text{-octene}/\text{Mo} = 320$, $t = 40\text{ }^{\circ}\text{C}$.

The accompanying oligomerization activity

The experiments with Mo-free zeolites (Figure 5a,b) confirmed that the oligomerization activity was connected with the support itself. In these “blank” experiments the reaction conditions, as well as pretreatment mode were the same as for Mo oxide cata-

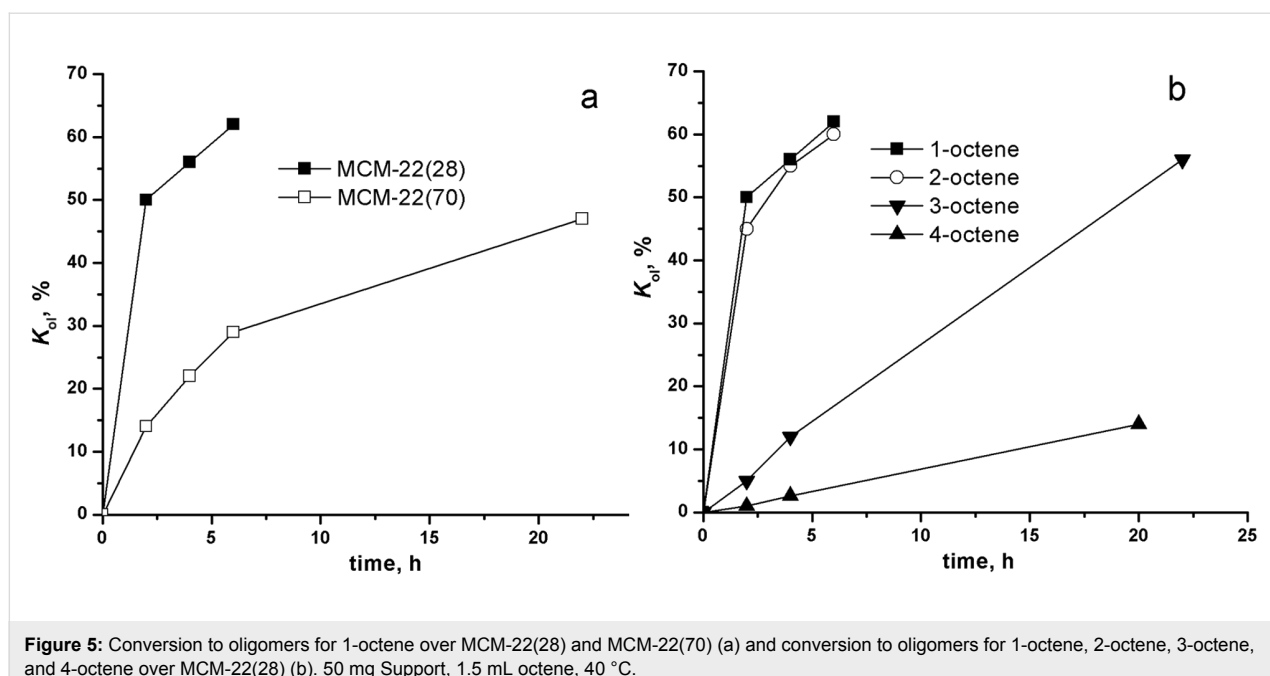


Figure 5: Conversion to oligomers for 1-octene over MCM-22(28) and MCM-22(70) (a) and conversion to oligomers for 1-octene, 2-octene, 3-octene, and 4-octene over MCM-22(28) (b). 50 mg Support, 1.5 mL octene, 40 °C.

lysts. No metathesis products were observed, only 1-octene oligomerization and double bond isomerization occurred. Figure 5a shows 1-octene oligomerization over MCM-22(28) and MCM-22(70). Families of dimers and trimers (in weight ratio dimers/trimers approximately 20:1 for the final conversions) were detected, isolation and characterization of individual dimers/trimer was not possible. It was visible from GC, that isomerization of starting 1-octene also occurred, however, the exact quantification was not possible. The oligomerization rate was higher for MCM-22(28) in accord with its higher acidity as compared with MCM-22(70). The extent of oligomerization in these blank experiments is several times higher than that achieved over metathesis catalysts: it may be due to the partial capping of support acid sites with Mo species catalysts and also due the parallel consumption of 1-octene in metathesis.

Figure 5b shows oligomerization of 1-octene, 2-octene (*cis* + *trans*), 3-octene (*trans*), and 4-octene (*trans*) over MCM-22(28). It is seen that the initial reaction rate decreases in the order 1-octene \approx 2-octene $>$ 3-octene $>$ 4-octene. The low-temperature oligomerization of alkenes over zeolite was studied as concerns industrially important low alkenes oligomerization and lower reactivity of internal alkenes in comparison with 1-alkenes was also recognized [30,31]. The reduced activity of 3- and 4-octenes in oligomerization might explain the fact, that in our metathesis experiments the accompanying oligomerization occurred practically only in the beginning of the reaction. In later stages when most of 1-octene was isomerized to 3- and 4-octenes only little increase in oligomer amounts was observed.

Conclusion

3D and 2D zeolites of MWW (MCM-22 and MCM-56) and MFI topologies were used for the first time as supports for the preparation of highly active molybdenum oxide metathesis catalysts. The catalysts, prepared by thermal spreading of MoO_3 and/or $\text{MoO}_2(\text{acac})_2$ on these supports in NH_4^+ forms (6 wt % and/or 5 wt % of Mo) were tested in neat 1-octene metathesis under mild conditions (batch reactor, atmospheric pressure, 40 °C).

The catalyst activity (expressed as K_{tot} values at the reaction time = 2 h) decreased in the order $6\text{MoO}_3/\text{MCM-22(28)} > 6\text{MoO}_3/\text{MCM-56(13)} > 6\text{MoO}_3/\text{2D-MFI(26)} > 6\text{MoO}_2(\text{acac})_2/\text{MCM-22(70)} >> 6\text{MoO}_3/\text{HZSM-5(25)}$. This activity order reflects two effects enhancing the activity: (i) support acidity and (ii) structure characteristics ensuring good accessibility of active species by substrate molecules. The most active $6\text{MoO}_3/\text{MCM-22(28)}$ exhibited a significantly higher activity than that of a similar catalyst supported on siliceous mesoporous molecular sieve SBA-15.

Due to the catalyst acidity accompanying reactions occurred: (i) 1-octene double bond isomerization followed by cross metathesis and (ii) 1-octene oligomerization (mainly dimerization). The extent of these reactions depends strongly on the support acidity. Highly acidic supports MCM-22(28) and MCM-56(13) delivered a catalyst of rather low selectivity (up to 14% conversion to oligomers, 15–20% conversion to tetradecene at about $K_{\text{tot}} = 90\%$). Less acidic supports – MCM-22(70) and 2D-MFI(26) gave rise catalysts of significantly higher selec-

tivity: conversion to oligomers was reduced to 1%, double bond isomerization and cross metathesis proceeded in less extent, so selectivity to tetradecene increased (e.g., for 2D-MFI(26) to 35% at $K_{\text{tot}} = 90\%$).

It is seen that for the metathesis of longer chain hydrocarbons like 1-octene, supports ensuring a good access of bulkier substrate to the active centers are necessary. The acidity of the support increases the catalyst activity, however, simultaneously with decrease of the catalyst selectivity. 2D-MFI(26) due to its moderate acidity and 2D character results in catalysts of moderate activity but of the highest selectivity.

With the described catalysts 1-octene was converted into a mixture of higher olefins: in addition to tetradecene as a homometathesis product, olefins of 9–13 C atoms from cross metathesis and C16 dimers were formed in various extent. Therefore, the described catalysts may find application especially if a mixture of higher olefins is desired, for example in the preparation of detergents, lubricants etc.

Experimental

Catalyst preparation and characterization

The zeolite supports MCM-22 and MCM-56 were prepared according to [32,33], 2D-MFI was synthesized according to [21]. HZSM-5 (CBV 5524) was purchased from Zeolyst. Na^+ forms of zeolites were converted to NH_4^+ form by three-fold treatment with 1.0 M NH_4NO_3 solution at room temperature for 3 h. The supports were characterized by XRD (Bruker AXS D8 Advance diffractometer with a graphite monochromator and a Vantec-1 position sensitive detector using $\text{Cu K}\alpha$ radiation in Bragg–Brentano geometry) and by N_2 adsorption (77 K, Micromeritics GEMINI II 2370 volumetric Surface Area Analyzer). Molybdenum(VI) oxide (Sigma-Aldrich) and bis(acetylacetone)dioxomolybdenum(VI) (Aldrich) as sources of Mo oxide species were used for catalyst preparation using the thermal spreading method (500 °C, 8 h). SEM images were recorded using a JEOL JSM-5500LV microscope.

The concentrations of Lewis ($c\text{L}$) and Brønsted ($c\text{B}$) acid sites were determined by FTIR spectroscopy of adsorbed pyridine (Py) using a Nicolet 6700 with a transmission MCT/B detector. The zeolites were pressed into self-supporting wafers with a density of 8.0–12 $\text{mg}\cdot\text{cm}^{-2}$ and activated in situ at $T = 450$ °C and $p = 5\cdot10^{-5}$ torr for 4 h. Pyridine adsorption was carried out at 150 °C and a partial pressure of 3.5 torr for 20 min followed by desorption for 20 min at 150, 250, 350 or 450 °C. Before adsorption, pyridine was degassed by freeze–pump–thaw cycles. All spectra were recorded with a resolution of 4 cm^{-1} by collecting 128 scans for a single spectrum at room temperature.

The spectra were recalculated using a wafer density of 10 $\text{mg}\cdot\text{cm}^{-2}$. $c\text{L}$ and $c\text{B}$ were evaluated from the integral intensities of bands at 1454 cm^{-1} ($c\text{L}$) and 1545 cm^{-1} ($c\text{B}$) using extinction coefficients, $\epsilon(\text{L})=2.22\text{ cm}\cdot\text{mmol}^{-1}$ and $\epsilon(\text{B})=1.67\text{ cm}\cdot\text{mmol}^{-1}$ [34].

For elemental analysis ICP OES (iCAP 7000, Thermo Scientific) was used. About 50 mg of the catalyst was digested in a mixture of HF, HCl, and HNO_3 (1:2:2). The samples were placed in a Berghof microwave in a closed vessel at $T = 140$ °C for 35 min. Saturated solution of H_3BO_3 was then added for complexation of the excess of HF. After digestion solutions under analysis were collected in 250 mL flasks and diluted with ultra pure water.

Catalytic experiments

Catalytic experiments were carried out in an argon atmosphere using a vacuum argon line. 1-Octene (Aldrich, 98%) was passed through alumina and stored with Na. The content of water in 1-octene was about 5 ppm. 2-Octene (Alfa-Aesar, 98%), *trans*-3-octene (Alfa-Aesar, 97%) and *trans*-4-octene (Aldrich) were purified in a similar way. In a typical experiment 50 mg of catalyst (6 wt % of Mo) was used. Before reaction catalyst was pretreated in vacuo at 500 °C for 30 min. After cooling to 40 °C, the reactor was filled with Ar and neat 1-octene (1-octene/Mo ratio = 320) was added under stirring. The reaction progress was followed by GC analysis of reaction mixture samples taken at given intervals. Individual compounds were identified by GC/MS. A high-resolution gas chromatograph Agilent 6890 with a DB-5 column (length: 50 m, inner diameter: 320 μm , stationary phase thickness: 1 μm), equipped with a 7683 Automatic Liquid Sampler and a FID detector and GC/MS (ThermoFinnigan, FOCUS DSQ II single Quadrupole) were used. Conversions were calculated from the mass balance.

Supporting Information

Supporting Information File 1

IR spectra of catalysts, GC of reaction products, and SEM images of catalysts.

[<https://www.beilstein-journals.org/bjoc/content/supplementary/1860-5397-14-272-S1.pdf>]

Acknowledgements

The authors thank J. Přech (J. Heyrovský Institute) for the preparation of MFI support samples, and Valeryia Kasneryk (J. Heyrovský Institute) for the SEM images. Financial support from the Grant Agency of the Czech Republic (project No. 17-01440S) is gratefully acknowledged.

References

- Ivin, K. J.; Mol, J. C. Applications of the Olefin Metathesis Reaction. *Olefin Metathesis and Metathesis Polymerization*, 2nd ed.; Academic Press: London, 1997; pp 397–410. doi:10.1016/b978-012377045-5/50018-5
- Hahn, T.; Bentrup, U.; Armbrüster, M.; Kondratenko, E. V.; Linke, D. *ChemCatChem* 2014, 6, 1664–1672. doi:10.1002/cctc.201400040
- Zhang, D.; Li, X.; Liu, S.; Huang, S.; Zhu, X.; Chen, F.; Xie, S.; Xu, L. *Appl. Catal., A* 2012, 439–440, 171–178. doi:10.1016/j.apcata.2012.07.002
- Hahn, T.; Kondratenko, E. V.; Linke, D. *Chem. Commun.* 2014, 50, 9060–9063. doi:10.1039/c4cc01827c
- Gholampour, N.; Yusubov, M.; Verpoort, F. *Catal. Rev.: Sci. Eng.* 2016, 58, 113–156. doi:10.1080/01614940.2015.1100871
- Lwin, S.; Wachs, I. E. *ACS Catal.* 2014, 4, 2505–2520. doi:10.1021/cs500528h
- Amakawa, K.; Kröhnert, J.; Wrabetz, S.; Frank, B.; Hemmann, F.; Jäger, C.; Schlögl, R.; Trunschke, A. *ChemCatChem* 2015, 7, 4059–4065. doi:10.1002/cctc.201500725
- Balcar, H.; Čejka, J. *Coord. Chem. Rev.* 2013, 257, 3107–3124. doi:10.1016/j.ccr.2013.07.026
- Balcar, H.; Mishra, D.; Marceau, E.; Carrier, X.; Žilková, N.; Bastl, Z. *Appl. Catal., A* 2009, 359, 129–135. doi:10.1016/j.apcata.2009.02.037
- Topka, P.; Balcar, H.; Rathouský, J.; Žilková, N.; Verpoort, F.; Čejka, J. *Microporous Mesoporous Mater.* 2006, 96, 44–54. doi:10.1016/j.micromeso.2006.06.016
- Lin, B.; Zhang, Q.; Wang, Y. *Ind. Eng. Chem. Res.* 2009, 48, 10788–10795. doi:10.1021/ie901227p
- Handzlik, J. *J. Mol. Catal. A: Chem.* 2010, 316, 106–111. doi:10.1016/j.molcata.2009.10.007
- Li, X.; Zhang, W.; Liu, S.; Han, X.; Xu, L.; Bao, X. *J. Mol. Catal. A: Chem.* 2006, 250, 94–99. doi:10.1016/j.molcata.2006.01.046
- Díaz, U.; Corma, A. *Dalton Trans.* 2014, 43, 10292–10316. doi:10.1039/c3dt53181c
- Roth, W. J.; Nachtigall, P.; Morris, R. E.; Čejka, J. *Chem. Rev.* 2014, 114, 4807–4837. doi:10.1021/cr400600f
- Wei, R.; Yang, H.; Scott, J. A.; Aguey-Zinsou, K.-F.; Zhang, D. *Mater. Today Chem.* 2018, 8, 1–12. doi:10.1016/j.mtchem.2018.01.002
- Opanasenko, M. V.; Roth, W. J.; Čejka, J. *Catal. Sci. Technol.* 2016, 6, 2467–2484. doi:10.1039/c5cy02079d
- Juttu, G. G.; Lobo, R. F. *Microporous Mesoporous Mater.* 2000, 40, 9–23. doi:10.1016/s1387-1811(00)00233-x
- Roth, W. J.; Čejka, J.; Millini, R.; Montanari, E.; Gil, B.; Kubu, M. *Chem. Mater.* 2015, 27, 4620–4629. doi:10.1021/acs.chemmater.5b01030
- Leonowicz, M. E.; Lawton, J. A.; Lawton, S. L.; Rubin, M. K. *Science* 1994, 264, 1910–1913. doi:10.1126/science.264.5167.1910
- Choi, M.; Na, K.; Kim, J.; Sakamoto, Y.; Terasaki, O.; Ryoo, R. *Nature* 2009, 461, 246–249. doi:10.1038/nature08288
- Přech, J.; Pizarro, P.; Serrano, D. P.; Čejka, J. *Chem. Soc. Rev.* 2018, 47, 8263–8306. doi:10.1039/c8cs00370j
- Liu, S.; Li, X.; Xin, W.; Xie, S.; Zeng, P.; Zhang, L.; Xu, L. *J. Nat. Gas Chem.* 2010, 19, 482–486. doi:10.1016/s1003-9953(09)60095-5
- Balcar, H.; Žilková, N.; Kubu, M.; Mazur, M.; Bastl, Z.; Čejka, J. *Beilstein J. Org. Chem.* 2015, 11, 2087–2096. doi:10.3762/bjoc.11.225
- Bordiga, S.; Lamberti, C.; Bonino, F.; Travert, A.; Thibault-Starzyk, F. *Chem. Soc. Rev.* 2015, 44, 7262–7341. doi:10.1039/c5cs00396b
- Topka, P. Molybdenum oxide supported on mesoporous molecular sieves – new catalysts for alkene metathesis and alkyne polymerization. Ph.D. Thesis, Charles University, Prague, 2008.
- Handzlik, J.; Ogonowski, J.; Stoch, J.; Mikolajczyk, M.; Michorczyk, P. *Appl. Catal., A* 2006, 312, 213–219. doi:10.1016/j.apcata.2006.07.002
- Lim, T. H.; Nam, K.; Song, I. K.; Lee, K.-Y.; Kim, D. H. *Appl. Catal., A* 2018, 552, 11–20. doi:10.1016/j.apcata.2017.12.021
- Zhao, P.; Ye, L.; Sun, Z.; Lo, B. T. W.; Woodcock, H.; Huang, C.; Tang, C.; Kirkland, A. I.; Mei, D.; Edman Tsang, S. C. *J. Am. Chem. Soc.* 2018, 140, 6661–6667. doi:10.1021/jacs.8b03012
- Knifton, J. F.; Sanderson, J. R.; Dai, P. E. *Catal. Lett.* 1994, 28, 223–230. doi:10.1007/bf00806051
- O'Connor, C. T.; Kojima, M. *Catal. Today* 1990, 6, 329–349. doi:10.1016/0920-5861(90)85008-c
- Kresge, C. T.; Roth, W. J.; Simmons, K. G.; Vartuli, J. C. Crystalline oxide material. U.S. Patent 5,229,341, June 20, 1993.
- Fung, A. S.; Lawton, S. L.; Roth, W. J. Synthetic layered MCM-56, its synthesis and use. U. S. Patent 5,362,697, Nov 8, 1994.
- Emeis, C. A. *J. Catal.* 1993, 141, 347–354. doi:10.1006/jcat.1993.1145

License and Terms

This is an Open Access article under the terms of the Creative Commons Attribution License (<http://creativecommons.org/licenses/by/4.0>). Please note that the reuse, redistribution and reproduction in particular requires that the authors and source are credited.

The license is subject to the *Beilstein Journal of Organic Chemistry* terms and conditions: (<https://www.beilstein-journals.org/bjoc>)

The definitive version of this article is the electronic one which can be found at:
doi:10.3762/bjoc.14.272



Stereodivergent approach in the protected glycal synthesis of L-vancosamine, L-saccharosamine, L-daunosamine and L-ristosamine involving a ring-closing metathesis step

Pierre-Antoine Nocquet¹, Aurélie Macé¹, Frédéric Legros², Jacques Lebreton³,
Gilles Dujardin², Sylvain Collet³, Arnaud Martel², Bertrand Carboni¹
and François Carreaux^{*1}

Full Research Paper

Open Access

Address:

¹Univ Rennes, CNRS, ISCR (Institut des Sciences Chimiques de Rennes), UMR 6226, 263 avenue du Général Leclerc, Campus de Beaulieu, F-35000 Rennes, France, ²Institut des Molécules et Matériaux du Mans, UMR 6283 CNRS-Université du Maine, avenue Olivier Messiaen, 72085 Cedex Le Mans, France and ³Chimie Et Interdisciplinarité: Synthèse, Analyse, Modélisation (CEISAM), UMR 6230 CNRS-Université de Nantes, 2 chemin de la Houssinière, 44322 Cedex Nantes, France

Email:

François Carreaux* - francois.carreaux@univ-rennes1.fr

* Corresponding author

Keywords:

3-amino glycals; diastereoselective additions to aldehydes; pluramycins; ring-closing metathesis; vinyl ethers

Beilstein J. Org. Chem. **2018**, *14*, 2949–2955.

doi:10.3762/bjoc.14.274

Received: 04 September 2018

Accepted: 15 November 2018

Published: 29 November 2018

This article is part of the thematic issue "Progress in metathesis chemistry III".

Guest Editors: K. Grela and A. Kajetanowicz

© 2018 Nocquet et al.; licensee Beilstein-Institut.

License and terms: see end of document.

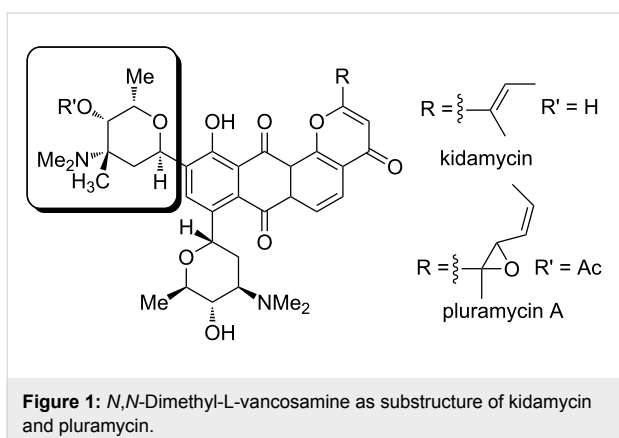
Abstract

In this paper, a new access to several chiral 3-aminoglycals as potential precursors for glycosylated natural products is reported from a common starting material, (−)-methyl-L-lactate. The stereodivergent strategy is based on the implementation of a ring-closing metathesis of vinyl ethers as key step of reaction sequences developed.

Introduction

Several classes of medicinally useful molecules with antibiotic and anticancer activity contain in their structures 3-amino-2-deoxy sugars [1]. For instance, *N,N*-dimethyl-L-vancosamine is an essential component of pluramycin antibiotics such as kidamycin and pluramycin A via a C-glycosidic linkage (Figure 1).

For constructing aryl C-glycoside bonds, glycal derivatives are versatile synthetic intermediates (Figure 2). Indeed, they can be converted into glycosyl donors but can also be considered as potential coupling partners or nucleophilic moieties via the formation of transient metalated species [2]. As example concerning their use in pluramycins' syntheses, an approach to the syn-



thesis of pluraflavin A was developed based on a Stille coupling to install the C-linked sugar residue [3]. Moreover, the addition of lithiated glycals to quinone derivatives followed by a rearrangement was also studied for the synthesis of kidamycin according to a “reverse polarity” strategy [4,5].

Considering that the glycal scaffolds are versatile building blocks with multiple applications in the field of natural product synthesis [6], the development of new asymmetric synthetic sequences with stereochemical diversity is still of high interest. Different approaches have been reported for the asymmetric synthesis of protected 3-aminoglycals from non-carbohydrate precursors. Most of them used a common methodology for the construction of the pyranosyl glycal ring which is based on a cycloisomerization reaction of chiral homopropargylic alcohols [7–10]. In some cases, the strategy used for the preparation of the corresponding alkynyl alcohols requires the handling of toxic tin reagents [8,9].

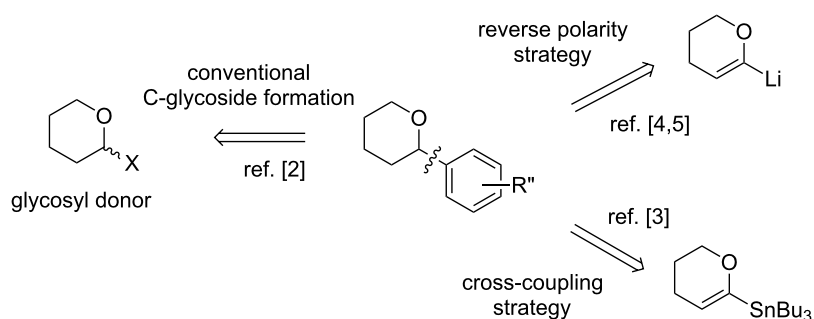
During these last years, ring-closing metathesis (RCM) of vinyl ethers have proved to be an efficient method for the preparation of chiral glycal scaffolds [11–18] as demonstrated in some total syntheses of marine polycyclic ethers [19–21]. However, to the best of our knowledge, this methodology was never

evaluated for the synthesis of this kind of nitrogen-containing substrates. Taking into account our interest about the development of new synthetic approaches to pluramycins [22,23], we speculated that the cyclic vinyl ether derivative **I**, with the prerequisite configuration of all stereogenic centers of the carbamate-protected glycal of L-vancosamine **1**, could be obtained from the alcohol derivative **II** using an O-vinyl-ation–ring-closing metathesis sequence (Figure 3). Afterwards, the introduction of nitrogen in the convenient position (C3) could be performed by a stereospecific nitrene insertion reaction catalyzed by rhodium(II) complexes [24,25].

Herein, we describe our outcomes related to the implementation of this strategy for the synthesis of L-vancosamine derivative **1**, as well as its diastereoisomer, the carbamate-protected 3-aminoglycal of L-saccharosamine **2**, employing the (*S*)-(*–*)-methyl lactate as common starting material. The efficiency and generality of this methodology was also demonstrated by a new synthesis of C-3 unbranched amino glycals, L-daunosamine **3** and L-ristosamine **4** derivatives, from the same source of chirality.

Results and Discussion

Synthesis of vancosamine and saccharosamine glycals. The chiral (–)-lactic methyl ester was identified as the privileged starting material considering that the Evans aldol reaction via boron enolates [26–28] with an appropriately O-protected aldehyde should afford the desired aldol adduct with a *syn* relative configuration between the two newly created chiral centers [29,30]. Moreover, the boron-mediated stereoselective aldol reaction is all the more interesting for our synthetic plan as stereochemical diversity can be generated depending on the absolute configuration of the chiral auxiliary used. The aldehyde **5** was first prepared according to a described procedure in two steps from methyl L-lactate (Scheme 1) [31]. The reaction with (*R*)- or (*S*)-oxazolidinones **6** led to the formation of 2,3-*syn* aldol products **7** in good yields with a very high level of diastereoselection (>20:1 for both).



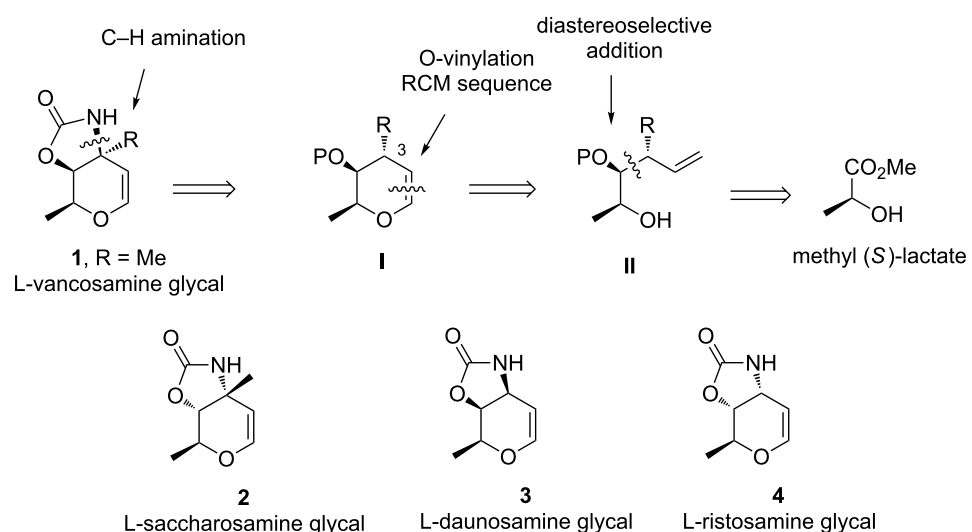
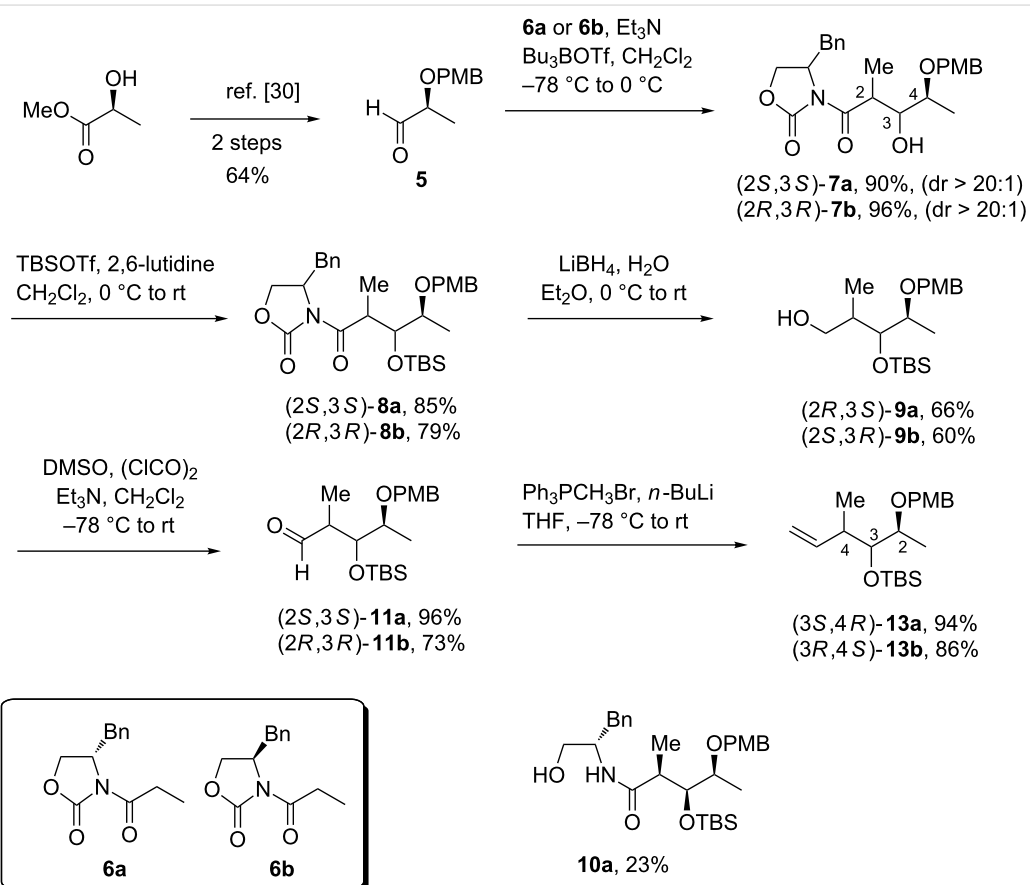


Figure 3: Strategy including a ring-closing metathesis of vinyl ethers as key step for the preparation of several carbamate-protected 3-aminoglycals.



Scheme 1: Evans aldol reaction for the preparation of diastereomeric compounds **13a** and **13b**.

After protection of the free hydroxy group, the reduction of the *N*-acyl oxazolidinones **8** into primary alcohols **9** was accomplished by LiBH₄ in presence of water or LiAlH₄ [32]. What-

ever the conditions used for this step, moderate yields were obtained for the desired products due to the formation of substantial amounts of ring-opened byproducts **10** resulting from the

hydride addition to the carbonyl group of the oxazolidinone ring [33,34]. The alcohols **9** were then subjected to a Swern oxidation followed by a Wittig reaction to generate the corresponding alkenes **13a,b** in 90% and 63% yield, respectively, over two steps. Alternatively, we envisioned that, from the same α -substituted chiral aldehyde **5**, compound **13b** could be obtained in a more straightforward manner employing a strategy based on a diastereoselective allylboration reaction (Scheme 2) [35]. Indeed, the reaction of achiral pinacol (*Z*)-crotylboronate with **5** under neat conditions at room temperature gave a good level of diastereoselectivity for the hitherto unreported 3,4-*syn*-2,3-*anti* product **12b** [36–39].

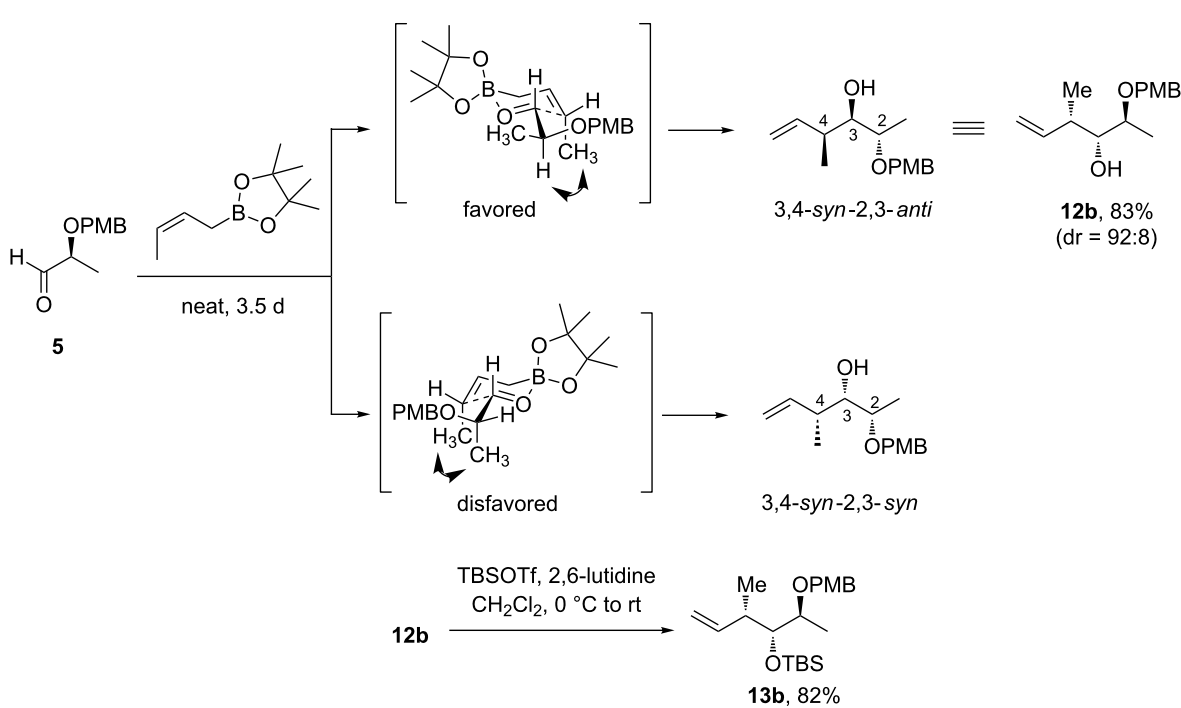
The *syn* relationship between C3 and C4 is controlled by the (*Z*)-geometry of the crotylboronate, while the 2,3-*anti* relationship can be rationalized by invoking Cornforth-like transition states [40–43]. Eventually, silylation of the homoallylic alcohol **12b** afforded the expected compound **13b** in 68% overall yield from **5** after purification, compared to 29% using a strategy based on an Evans' aldol reaction.

Mildly oxidizing conditions using 2,3-dichloro-5,6-dicyano-1,4-benzoquinone (DDQ) were used for the removal of the *p*-methoxybenzyl (PMB) group to provide alcohols **14** (Scheme 3). Several palladium(II) catalysts have been tested for the conversion of alcohols to vinyl ethers **15** [13,44–46]. We found that the best yields were obtained using $\text{Pd}(\text{TFA})_2$ and

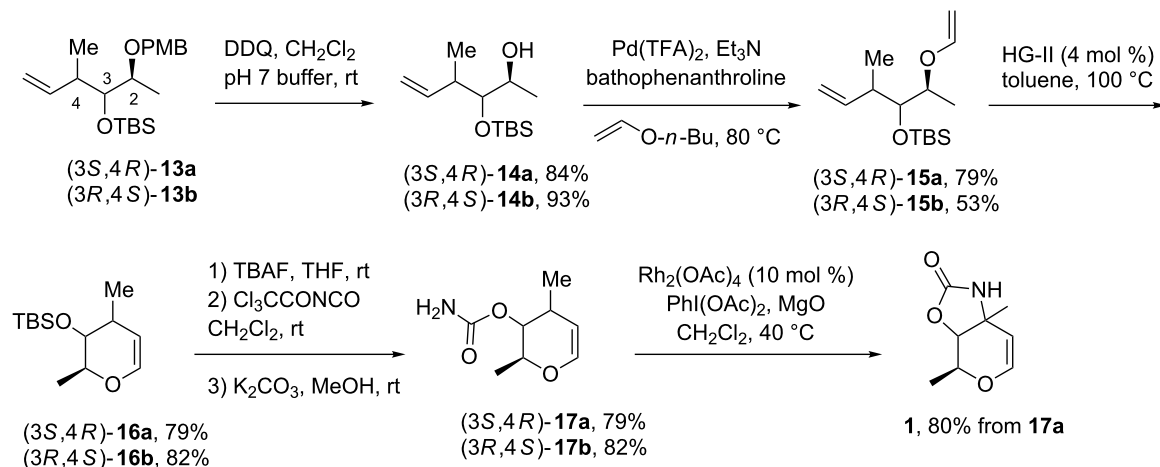
n-butyl vinyl ether as solvent in the presence of bathophenanthroline as ligand. In the case of $\text{Pd}(\text{OAc})_2$, the reaction was slower with moderate yields.

The ring-closing metathesis reaction was performed with Hoveyda–Grubbs second-generation (HG-II) catalyst to deliver the corresponding dihydropyran **16** in excellent yields given that this kind of reaction can be sensitive to the substitution pattern contained in the substrate [11]. After silyl deprotection, the key C–H amination precursors **17a,b** for the synthesis of the carbamate-protected glycal of L-vancosamine **1** and L-saccharosamine **2** were prepared in two steps by treatment of alcohols with the trichloroacetyl isocyanate reagent (TCA-NCO) followed by basic hydrolysis. The spectroscopic properties of carbamates **17** were identical to those reported in the literature [7,8]. Although the intramolecular C–H amination of compounds **17** under the Du Bois conditions [24] was already described in the literature [8,9], the reaction was nevertheless achieved with carbamate **17a** in order to check the reproducibility of the final step. As expected, L-vancosamine glycal **1** was obtained in similar yield than one reported [8,47].

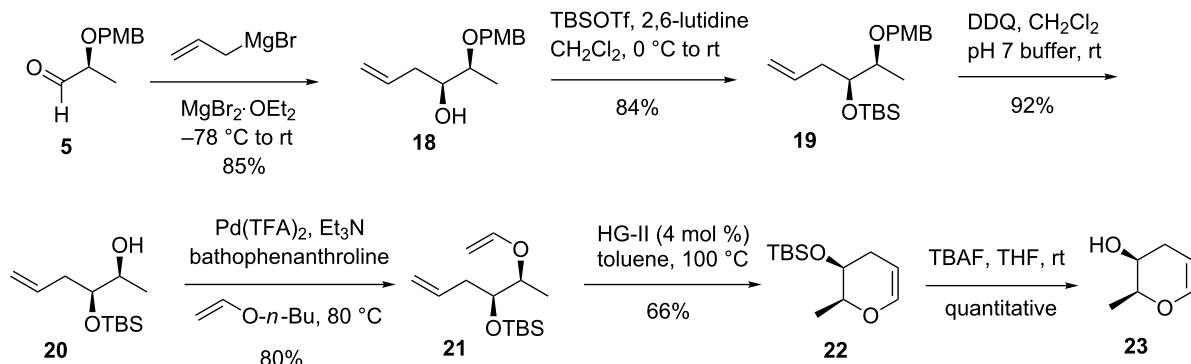
Synthesis of daunosamine and ristosamine glycals. As previously, the chiral pool material **5** was used for this unbranched glycal synthesis (Scheme 4). The first step was the chelation-controlled addition of allylmagnesium bromide to **5** to provide the *syn* diastereomer **18** in high stereoselectivity (93:7). After



Scheme 2: Alternative preparation of **13b** based on a diastereoselective allylboration.



Scheme 3: O-Vinylation-ring-closing metathesis sequence for access to 3-amino glycals.



Scheme 4: Synthesis of key intermediate 23 for the C-3 unbranched amino glycals preparation.

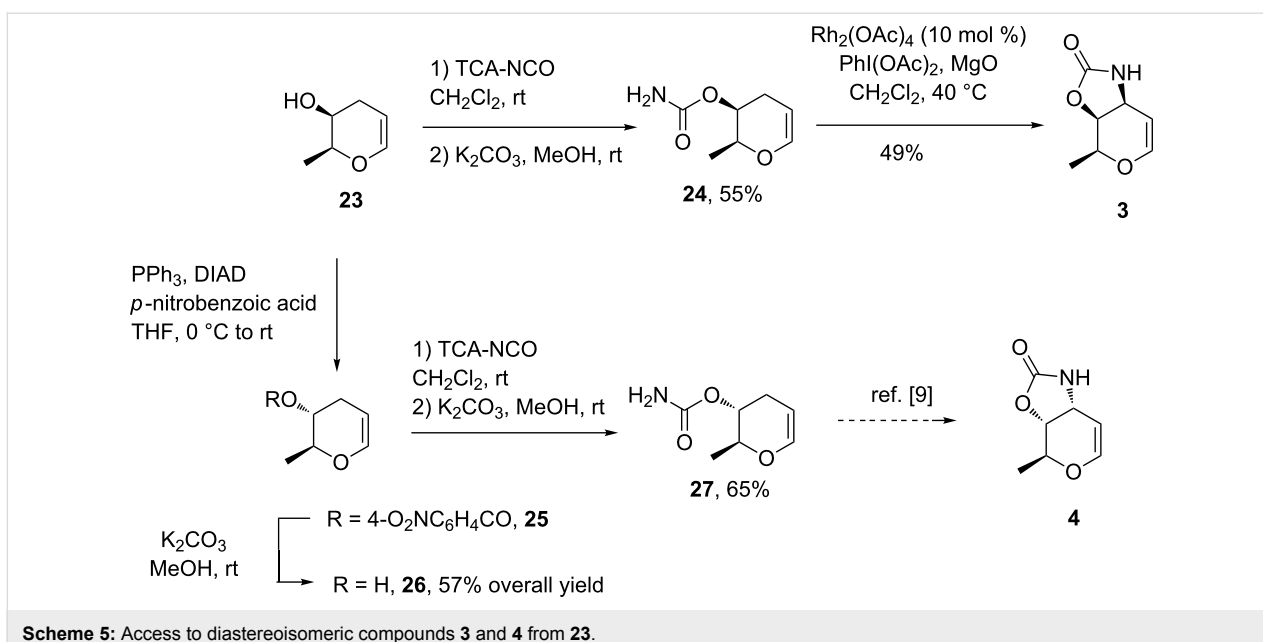
silylation of the free hydroxy group, the cleavage of the PMB ether with DDQ led to alcohol **20** in 77% yield for the two steps. Ring-closing metathesis of diene **21**, obtained by O-vinylation of **20**, gave the dihydropyran **22** in 53% overall yield for two steps. The silyl group of compound **22** was cleaved using tetrabutylammonium fluoride (TBAF) in THF to form alcohol **23** which was used directly in the next step [48].

At this stage, we envisioned that **23** could be also a key intermediate to access the ristosamine derivative by reversing the configuration of the stereogenic center bearing the hydroxy group (Scheme 5). With this in mind, the secondary alcohol **23** was engaged in a Mitsunobu reaction using *p*-nitrobenzoic acid as nucleophile to afford the expected compound **25**. Hydrolysis of the ester was achieved using potassium carbonate in methanol to afford the epimeric product **26**.

Both diastereomers **23** and **26** were converted to the corresponding known carbamates using a two step sequence. Reaction with TCA-NCO followed by a basic hydrolysis provided the desired compounds **24** and **27** in good yields and in full agreement with all reported spectroscopic data [9]. As an example, the expected protected glycal of L-daunosamine **3** [9,47] was obtained by regioselective rhodium nitrene insertion thus demonstrating the usefulness of this strategy for the synthesis of such compounds.

Conclusion

We developed an alternative route to 3-aminoglycals through ring-closing metathesis of vinyl ethers as key step in the synthesis and using a common noncarbohydrate starting material. The approach was first validated for the synthesis of protected L-vancosamine glycal and extended afterwards to prepare a dia-

**Scheme 5:** Access to diastereoisomeric compounds 3 and 4 from 23.

stereomeric compound as well as other unbranched C-3 amino-glycals. The use of these synthons in the synthesis of glycosylated antibiotics as kidamycin is underway in our laboratory.

Supporting Information

Supporting Information contains detailed experimental procedures with full characterization of all compounds and NMR spectra.

Supporting Information File 1

Experimental part and NMR spectra of all compounds.
[\[https://www.beilstein-journals.org/bjoc/content/supplementary/1860-5397-14-274-S1.pdf\]](https://www.beilstein-journals.org/bjoc/content/supplementary/1860-5397-14-274-S1.pdf)

Acknowledgements

This work was supported by the University of Rennes 1 and the Centre National de la Recherche Scientifique (CNRS). One of us, P.-A. N. thanks ANR for a postdoctoral fellowship (ANR-14-CE06-0008-01).

ORCID® IDs

Aurélie Macé - <https://orcid.org/0000-0003-4783-1621>
 Sylvain Collet - <https://orcid.org/0000-0002-7602-9585>
 Bertrand Carboni - <https://orcid.org/0000-0003-0529-715X>
 François Carreaux - <https://orcid.org/0000-0002-7406-8353>

References

1. Hauser, F. M.; Ellenberger, S. R. *Chem. Rev.* **1986**, *86*, 35–67. doi:10.1021/cr00071a003
2. Kitamura, K.; Ando, Y.; Matsumoto, T.; Suzuki, K. *Chem. Rev.* **2018**, *118*, 1495–1598. doi:10.1021/acs.chemrev.7b00380
3. Hartung, J.; Wright, B. J. D.; Danishefsky, S. J. *Chem. – Eur. J.* **2014**, *20*, 8731–8736. doi:10.1002/chem.201402254
4. Parker, K. A. *Pure Appl. Chem.* **1994**, *66*, 2135–2138. doi:10.1351/pac199466102135
5. Parker, K. A.; Koh, Y.-h. *J. Am. Chem. Soc.* **1994**, *116*, 11149–11150. doi:10.1021/ja00103a037
6. Danishefsky, S. J.; Bilodeau, M. T. *Angew. Chem., Int. Ed. Engl.* **1996**, *35*, 1380–1419. doi:10.1002/anie.199613801
7. Cutchins, W. W.; McDonald, F. E. *Org. Lett.* **2002**, *4*, 749–752. doi:10.1021/o1017195f
8. Parker, K. A.; Chang, W. *Org. Lett.* **2003**, *5*, 3891–3893. doi:10.1021/o1035479p
9. Parker, K. A.; Chang, W. *Org. Lett.* **2005**, *7*, 1785–1788. doi:10.1021/o10503561
10. Fei, Z.; McDonald, F. E. *Org. Lett.* **2007**, *9*, 3547–3550. doi:10.1021/o17014219
11. Sturino, C. F.; Wong, J. C. Y. *Tetrahedron Lett.* **1998**, *39*, 9623–9626. doi:10.1016/s0040-4039(98)02205-9
12. Gurjar, M. K.; Krishna, L. M.; Reddy, B. S.; Chorghade, M. S. *Synthesis* **2000**, 557–560. doi:10.1055/s-2000-6376
13. Peczuhi, M. W.; Snyder, N. L. *Tetrahedron Lett.* **2003**, *44*, 4057–4061. doi:10.1016/s0040-4039(03)00849-9
14. Postema, M. H. D.; Piper, J. L.; Liu, L.; Shen, J.; Faust, M.; Andreana, P. *J. Org. Chem.* **2003**, *68*, 4748–4754. doi:10.1021/jo030039x
15. Adam, J.-M.; de Fays, L.; Laguerre, M.; Ghosez, L. *Tetrahedron* **2004**, *60*, 7325–7344. doi:10.1016/j.tet.2004.05.058
16. Sharma, H.; Santra, S.; Debnath, J.; Antonio, T.; Reith, M.; Dutta, A. *Bioorg. Med. Chem.* **2014**, *22*, 311–324. doi:10.1016/j.bmc.2013.11.017
17. Sutton, A. E.; Seigal, B. A.; Finnegan, D. F.; Snapper, M. L. *J. Am. Chem. Soc.* **2002**, *124*, 13390–13391. doi:10.1021/ja028044q
18. Schmidt, B.; Biernat, A. *Chem. – Eur. J.* **2008**, *14*, 6135–6141. doi:10.1002/chem.200800567

19. Majumder, U.; Cox, J. M.; Johnson, H. W. B.; Rainier, J. D. *Chem. – Eur. J.* **2006**, *12*, 1736–1746. doi:10.1002/chem.200500993

20. Osei Akoto, C.; Rainier, J. D. *Angew. Chem., Int. Ed.* **2008**, *47*, 8055–8058. doi:10.1002/anie.200803791

21. Clark, J. S.; Romiti, F.; Sieng, B.; Paterson, L. C.; Stewart, A.; Chaudhury, S.; Thomas, L. H. *Org. Lett.* **2015**, *17*, 4694–4697. doi:10.1021/acs.orglett.5b02093

22. Mabit, T.; Siard, A.; Pantin, M.; Zon, D.; Foulgoc, L.; Sissouma, D.; Guingant, A.; Mathé-Allainmat, M.; Lebreton, J.; Carreaux, F.; Dujardin, G.; Collet, S. *J. Org. Chem.* **2017**, *82*, 5710–5719. doi:10.1021/acs.joc.7b00544

23. Mabit, T.; Siard, A.; Legros, F.; Guillarme, S.; Martel, A.; Lebreton, J.; Carreaux, F.; Dujardin, G.; Collet, S. *Chem. – Eur. J.* **2018**, *24*, 14069–14074. doi:10.1002/chem.201803674

24. Espino, C. G.; Du Bois, J. *Angew. Chem., Int. Ed.* **2001**, *40*, 598–600. doi:10.1002/1521-3773(20010202)40:3<598::aid-anie598>3.0.co;2-9

25. Du Bois, J. *Org. Process Res. Dev.* **2011**, *15*, 758–762. doi:10.1021/op200046v

26. Evans, D. A.; Vogel, E.; Nelson, J. V. *J. Am. Chem. Soc.* **1979**, *101*, 6120–6123. doi:10.1021/ja00514a045

27. Evans, D. A.; Nelson, J. V.; Vogel, E.; Taber, T. R. *J. Am. Chem. Soc.* **1981**, *103*, 3099–3111. doi:10.1021/ja00401a031

28. Mukaiyama, T.; Inoue, T. *Chem. Lett.* **1976**, 559–562. doi:10.1246/cl.1976.559

29. Cowden, C. J.; Paterson, I. *Org. React.* **1997**, 1–200. doi:10.1002/0471264180.or051.01

30. Zhang, Z.; Collum, D. B. *J. Org. Chem.* **2017**, *82*, 7595–7601. doi:10.1021/acs.joc.7b01365

See for a mechanistic study of the Evans aldol reaction.

31. Roush, W. R.; Bennett, C. E.; Roberts, S. E. *J. Org. Chem.* **2001**, *66*, 6389–6393. doi:10.1021/jo015756a

32. Heravi, M. M.; Zadsirjan, V.; Farajpour, B. *RSC Adv.* **2016**, *6*, 30498–30551. doi:10.1039/c6ra00653a

33. Penning, T. D.; Djuric, S. W.; Haack, R. A.; Kalish, V. J.; Miyashiro, J. M.; Rowell, B. W.; Yu, S. S. *Synth. Commun.* **1990**, *20*, 307–312. doi:10.1080/00397919008052299

34. Compound **10b** was not isolated.

35. Lachance, H.; Hall, D. G. Allylboration of carbonyl compounds. In *Organic reactions*; Denmark, S. E., Ed.; John Wiley & sons: Hoboken, New Jersey, 2008; Vol. 73. doi:10.1002/0471264180.or073.01

36. Hoffmann, R. W.; Weidmann, U. *Chem. Ber.* **1985**, *118*, 3966–3979. doi:10.1002/cber.19851181010

37. Brinkmann, H.; Hoffmann, R. W. *Chem. Ber.* **1990**, *123*, 2395–2401. doi:10.1002/cber.19901231223

38. Wuts, P. G. M.; Bigelow, S. S. *J. Org. Chem.* **1988**, *53*, 5023–5034. doi:10.1021/jo00256a023

39. Roush, W. R.; Adam, M. A.; Walts, A. E.; Harris, D. J. *J. Am. Chem. Soc.* **1986**, *108*, 3422–3434. doi:10.1021/ja00272a043

40. Cornforth, J. W.; Cornforth, R. H.; Mathew, K. K. *J. Chem. Soc.* **1959**, 112–127. doi:10.1039/jr9590000112

41. Roush, W. R. In *Houben-Weyl, Stereoselective Synthesis*; Helmchen, G.; Hoffmann, R. W.; Mulzer, J.; Schaumann, E., Eds.; Georg Thieme Verlag: Stuttgart, Germany, 1995; Vol. E21b, pp 1410–1486.

42. Cee, V. J.; Cramer, C. J.; Evans, D. A. *J. Am. Chem. Soc.* **2006**, *128*, 2920–2930. doi:10.1021/ja0555670

43. Díaz-Oltra, S.; Carda, M.; Murga, J.; Falomir, E.; Marco, J. A. *Chem. – Eur. J.* **2008**, *14*, 9240–9254. doi:10.1002/chem.200800956

44. Weintraub, P. M.; King, C.-H. R. *J. Org. Chem.* **1997**, *62*, 1560–1562. doi:10.1021/jo961182b

45. Handerson, S.; Schlaf, M. *Org. Lett.* **2002**, *4*, 407–409. doi:10.1021/o1017104e

46. Dechert-Schmitt, A.-M.; Cabral, S.; Kung, D. W. *Synlett* **2016**, *27*, 2611–2615. doi:10.1055/s-0036-1588615

47. A very clean carbamate product is required to obtain a good conversion into oxazolidinone.

48. A partial loss of product can occur during evaporation under reduced pressure due to its low boiling point.

License and Terms

This is an Open Access article under the terms of the Creative Commons Attribution License (<http://creativecommons.org/licenses/by/4.0>). Please note that the reuse, redistribution and reproduction in particular requires that the authors and source are credited.

The license is subject to the *Beilstein Journal of Organic Chemistry* terms and conditions: (<https://www.beilstein-journals.org/bjoc>)

The definitive version of this article is the electronic one which can be found at:

[doi:10.3762/bjoc.14.274](https://doi.org/10.3762/bjoc.14.274)



The activity of indenylidene derivatives in olefin metathesis catalysts

Maria Voccia¹, Steven P. Nolan^{*2,3}, Luigi Cavallo^{*4} and Albert Poater^{*1}

Full Research Paper

Open Access

Address:

¹Institut de Química Computacional i Catàlisi and Departament de Química, Universitat de Girona, c/ M^a Aurèlia Capmany 69, 17003 Girona, Catalonia, Spain, ²Department of Chemistry and Center for Sustainable Chemistry, Ghent University, Krijgslaan 281, S-3, B-9000 Ghent, Belgium, ³Department of Chemistry, College of Science King Saud University, P. O. Box 2455, Riyadh 11451, Saudi Arabia and ⁴King Abdullah University of Science & Technology, KAUST Catalysis Center (KCC), 23955-6900 Thuwal, Saudi Arabia

Email:

Steven P. Nolan^{*} - Steven.Nolan@UGent.be; Luigi Cavallo^{*} - luigi.cavallo@kaust.edu.sa; Albert Poater^{*} - albert.poater@udg.edu

* Corresponding author

Keywords:

activation; IMes; indenylidene; olefin metathesis; SIMes

Beilstein J. Org. Chem. **2018**, *14*, 2956–2963.

doi:10.3762/bjoc.14.275

Received: 06 September 2018

Accepted: 15 November 2018

Published: 30 November 2018

This article is part of the thematic issue "Progress in metathesis chemistry III".

Guest Editors: K. Grela and A. Kajetanowicz

© 2018 Voccia et al.; licensee Beilstein-Institut.

License and terms: see end of document.

Abstract

The first turnover event of an olefin metathesis reaction using a new family of homogenous Ru-based catalysts bearing modified indenylidene ligands has been investigated, using methoxyethylene as a substrate. The study is carried out by means of density functional theory (DFT). The indenylidene ligands are decorated with *ortho*-methyl and isopropyl groups at both *ortho* positions of their phenyl ring. DFT results highlight the more sterically demanding indenylidene have to undergo a more exothermic first phosphine dissociation step. Overall, the study emphasises advantages of increased steric hindrance in promoting the phosphine release, and the relative stability of the corresponding metallacycle over classical ylidene ligands. Mayer bond orders and steric maps provide structural reasons for these effects, whereas NICS aromaticity and conceptual DFT confirm that the electronic parameters do not play a significant role.

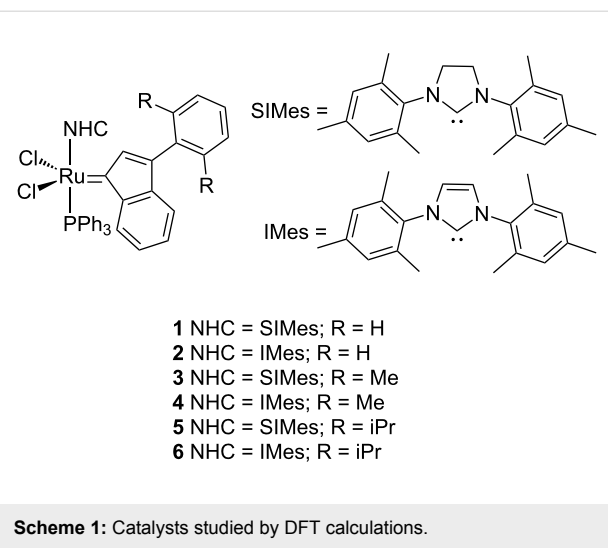
Introduction

Olefin metathesis has been an intensely studied reaction due to its wide use [1], in industrial applications, especially in petrochemistry [2], i.e., the Phillips Triolefin (PTP) process or the Shell Higher Olefin Process (SHOP) [3,4]. Additionally, the olefin metathesis reaction has provided a useful tool in poly-

merisation [5,6], as well as in the pharmaceutical industry in the formation of C=C bonds. Early catalyst examples were ill-defined entities and it is not until Grubbs [7] and Schrock [8] developed well-defined homogeneous catalysts that the area truly blossomed. Using a metal carbene complex as a catalyst,

making use of the Chauvin mechanism, olefin metathesis consists of the redistribution of two carbon–carbon double bonds [9]. The metal and its ligand environment in both ruthenium and molybdenum systems appear to confer the right environment that allows a productive alkene metathesis [10,11]. Little productive reactivity has been uncovered using other metals [12–14]. Apart from the metal, ruthenium-based olefin metathesis has seen several changes during the last decades, modifying the existing commercial catalysts, playing mainly with the electronic characteristics of the ligands (usually two chlorides and an ylidene ligand) [15–17], whereas basically the sterics of the substituents on the N-heterocyclic carbene (NHC) ligand have remained unchanged [18]. Overall, any modification of the available catalysts has been performed in order to increase the stability of the catalyst without losing any of its activity [19,20]. Although most of the olefin metathesis catalysts are based on ruthenium [21,22], because these are more stable to oxygen and moisture [23] than their molybdenum counterparts, they display sensitivity to decomposition while in solution [24,25]. Understanding and/or the elimination of potential pathways that leads to catalyst decomposition is extremely important [26–28], since any knowledge obtained in this area can guide the catalyst design efforts [29–31].

We are interested in evaluating, by density functional theory (DFT) calculations, the difference in the activation step between complexes **1–6** in Scheme 1, whose reactivity and properties have been reported already (for **1** and **2**) [24,32,33]. Predictive catalysis will be used here to generate and/or describe the activity in olefin metathesis of the new indenylidene derivatives. The phenyl substituent of the indenylidene is perpendicular to the indenyl moiety in the solid-state structure [34], as Nolan and co-workers first described in 1999 [35]. For complexes **3–6**, where the phenyl ring is *ortho*-substituted, there might be present steric repulsion with the NHCs, which might in turn facilitate the departure of the indenyl ligand [36]. Apart from reducing decomposition [37,38], this steric pressure should lead to faster rates for the initiation step of the metathesis reaction. This hypothesis will be examined computationally in order to assist catalyst design efforts.

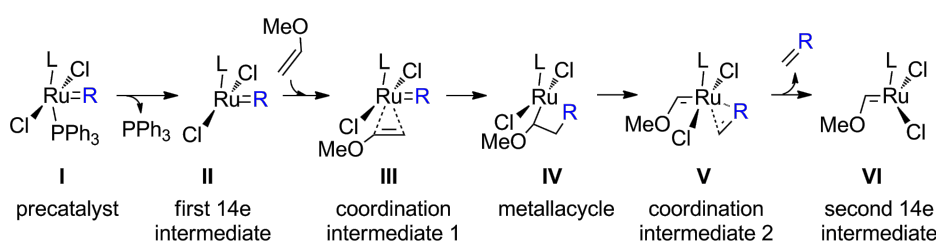


Scheme 1: Catalysts studied by DFT calculations.

Results and Discussion

We have studied the initiation cycle involving the transformation of the indenylidene precatalysts into the active methylidene for a series of olefin metathesis relevant complexes **1–6**, using methoxyethene as a substrate (Scheme 2). This substrate was selected in order to facilitate our analysis [39]. Computationally no significant differences exist by using ethene or methoxyethene [40,41]. The saturation of the backbone of the NHC has also been taken into account, thus considering either the SIMes (1,3-bis(2,4,6-trimethylphenyl)-4,5-dihydroimidazol-2-ylidene) and the IMes (1,3-bis(2,4,6-trimethylphenyl)imidazol-2-ylidene) NHC ligands. The group *trans* to the NHC ligand is triphenylphosphine for all catalysts.

Table 1 includes the energy profiles for the substituted indenylidene, bearing methyl or isopropyl groups at the *ortho* positions of the phenyl substituent, compared to the unsubstituted **1** and **2**. Comparing IMes vs SIMes, the activation is about 1 kcal/mol more favoured for the unsaturated system [42,43]. The absolute difference of 1 kcal/mol is maintained throughout the mechanism, however, we must point out that the opening of the metallacycle requires only 0.6 kcal/mol for the SIMes system versus 1.7 kcal/mol for the unsaturated system.



Scheme 2: Precatalyst initiation in olefin metathesis (L = NHC ligand).

Table 1: Precatalyst initiation reaction pathway for catalysts **1–6** (M06/TZVP~sdd//BP86/SVP~sdd; Gibbs free energies in kcal/mol).

	1	2	3	4	5	6
I	0.0	0.0	0.0	0.0	0.0	0.0
I–II	21.8	20.2	16.4	19.1 ^a	19.8	19.8
II	20.0	18.2	16.1	19.5	17.6	19.6
II–III	22.8	21.8	20.0	22.4	21.0	22.1
III	15.0	12.2	13.0	14.6	17.2	17.8
III–IV	22.1	21.1	19.0	20.1	17.8	19.3
IV	16.7	15.9	12.5	15.1	13.3	13.0
IV–V	17.3	17.6	13.7	15.8	15.6	16.2
V	7.0	3.7	2.0	3.5	2.9	2.9
V–VI	10.5	10.2	8.6	10.0	5.9	9.6
VI	8.1	7.0	3.8	5.4	4.3	5.0

^aThe transition state is somewhat lower in energy than the next 14e species **II** once included the solvent effects.

The methyl and isopropyl-substituted indenylidene moieties reveal a different performance between the SIMes and the IMes congeners. When the saturated NHC is considered, the substitution reduces dramatically the barriers of the first two transition states. Then the cycle **I**–**VI** is more exothermic with the substituted systems. On the other hand, the unsaturated system does not reduce the energy barriers with the substituted indenylidene moieties, because of the rigidity of its backbone. And the same

argument is valid for the entire catalytic system, which means that the substitution does not help to make the system significantly more exothermic than the saturated system, despite a slight stabilisation, especially for the second 14e species, **VI**.

Overall, among the catalysts with substituted indenylidene catalysts, the one bearing a SIMes NHC ligand and methyl groups in the indenylidene moiety is the most promising, in agreement with the experimental hypothesis that the release of the indenylidene ligand is more facile in such a case.

The concerted transition state that circumvents the formation of the 14e intermediate **II**, i.e., **I**–**III**, is higher in energy than **I**–**II** and **II**–**III** by 3.6 and 4.3 kcal/mol for systems **3** and **5**, compared to **1**, respectively. The unsaturated systems do not follow a concerted mechanism either, being 4.3 kcal/mol higher in energy for system **2**. Overall, for all substituted indenylidene this concerted transition state **I**–**III** is confirmed to be higher in energy.

The structural analysis included in Table 2 supports the fact that the substituted indenylidene display similar characteristics whatever the substituents are on both *ortho* positions of the corresponding phenyl ring in catalysts **1–6**. For instance, the Ru=C_{ylidene} bond changes by less than 0.008 Å, which is in perfect agreement with the insignificant changes in the Mayer Bond Order (MBO) results [44,45]. However, there is a clear

Table 2: Structural analysis for species **I**–**III** for catalysts **1–6** (in kcal/mol), including selected bond distances (d) in Å and Mayer Bond Orders (MBO).

	1	2	3	4	5	6
d(Ru=C _{ylidene})						
I	1.882	1.882	1.883	1.883	1.886	1.885
II	1.869	1.868	1.863	1.862	1.863	1.861
III	1.888	1.885	1.885	1.883	1.885	1.884
MBO(Ru=C _{ylidene})						
I	1.464	1.469	1.476	1.484	1.475	1.480
II	1.444	1.446	1.467	1.470	1.465	1.471
III	1.445	1.453	1.453	1.460	1.448	1.452
d(Ru–P)						
I	2.457	2.444	2.436	2.430	2.431	2.424
MBO(Ru–P)						
I	0.540	0.560	0.585	0.592	0.600	0.611
d(Ru–C _{NHC})						
I	2.071	2.089	2.087	2.103	2.093	2.111
II	1.947	1.956	1.941	1.955	1.941	1.953
III	2.020	1.885	2.019	1.883	2.014	2.029
MBO(Ru–C _{NHC})						
I	0.847	0.806	0.817	0.787	0.808	0.775
II	1.199	1.151	1.211	1.160	1.212	1.162
III	0.961	0.915	0.969	0.924	0.983	0.933

difference that shows that the saturated NHC backbone of the SIMes ligand facilitates the phosphine dissociation since the Ru–P bond distance is longer [24,38]. This is corroborated via the corresponding lower MBO values. More interestingly, the Ru–C_{NHC} bond is much shorter for SIMes, with a corresponding MBOs at least 0.030 larger, being more accentuated for the system with the unsubstituted indenylidene ligand, by 0.041. This effect is completely in agreement with the *trans* effect along the C_{NHC}–Ru–P axis [46]. On the other hand, the analysis of the substituted indenylidene systems **3–6** highlights that these are more difficult to activate since the MBO of the Ru–P is larger by 0.045, 0.042, 0.060 and 0.051, respectively. Overall, despite the unfavourable effect on the activation of the precatalytic species **I**, the substituted indenylidenes do not affect at all the 14e species **II** once generated through phosphine release.

To further understand how substituent sterics affect the indenylidene moieties of catalysts **3–6**, steric maps were calculated by means of the SambVca package [47], analyzing the %V_{Bur} [48]. Taking into account the precatalytic intermediate **I**, the %V_{Bur} for the NHC ligand ranges from 30.1% to 29.8% and 29.6% for SIMes-based catalysts **1**, **3** and **5**, respectively (see Figure 1). The same trend applies to the IMes-based catalysts **2**, **4** and **6**, with %V_{Bur} values of 30.0%, 29.7% and 29.6%, respectively. On the other hand, as expected since there is similarity in the part bonded to the metal [49], no significant difference in the steric hindrance towards the metal sphere was observed for the indenylidene and any of its derivatives, and the %V_{Bur} was found identical (see Supporting Information File 1 for steric maps of those ligands).

Table 3 includes the relevant information obtained from the frontier molecular orbitals. From conceptual DFT we reach

values for electrophilicity that describe a clear trend from species **II** that is prone to undergo nucleophilic attack by the entering olefin: the substituted indenylidene catalysts **3–6** exhibit lower electrophilicity, especially when bearing the saturated backbone NHC, systems **3** and **5**. Here the SIMes systems with lower electrophilicity are in perfect harmony with higher chemical hardness values [50], and the natural population analysis (NPA) on the C_{ylidene} confirms the more positive charge, which might favour the nucleophilic interaction with an olefin.

The NPA charges on ruthenium are not affected by the increase of steric hindrance on the phenyl rings of the indenylidene ligand, and only the IMes ligand shows a small decrease of the charge on the metal centre, on the precatalytic species **I**. Whereas **II** must be excluded from the discussion since there is a hydrogen bond (Ru···H) that affects the charge on the metal, especially strong when the indenylidene is substituted. The Ru···H distances for **1–6** are 3.110, 3.167, 3.004, 3.036 Å, 2.944, 2.929 Å, respectively (see Figure 2). This interaction is due to the rotation of 90° of the indenylidene ligand. But this Ru···H interaction deserves more attention since it is stronger for **3–6** and this in order to reduce the steric repulsion between the substituted phenyl ring of the indenylidene and the close mesityl group of the NHC ligand. One consequence for the more rigid unsaturated IMes systems **4** and **6** is that the next energy barrier for transition state **II–III** is larger, since the entering olefin requires a 90° rotation, and this is partially impeded when the phenyl group is substituted. However, the substituted indenylidene facilitates overcoming the energy barrier of the next transition state, the closure of the metallocycle in order to reduce the steric hindrance. Particularly, the latter transition state is 3.2 kcal/mol lower in energy for **5**, whereas only 0.7 kcal/mol more stable for **1**. And thermody-

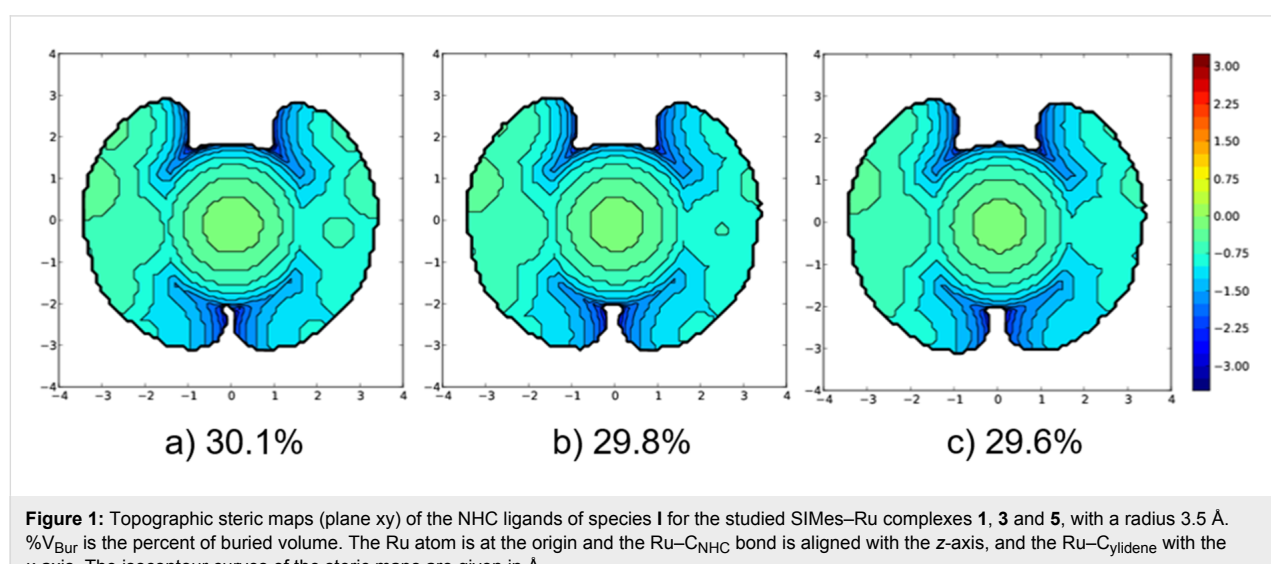


Figure 1: Topographic steric maps (plane xy) of the NHC ligands of species **I** for the studied SIMes–Ru complexes **1**, **3** and **5**, with a radius 3.5 Å. %V_{Bur} is the percent of buried volume. The Ru atom is at the origin and the Ru–C_{NHC} bond is aligned with the z-axis, and the Ru–C_{ylidene} with the x-axis. The isocontour curves of the steric maps are given in Å.

Table 3: Electronic analysis for species **I–III** for catalysts **1–6** (in kcal/mol) including energies of the frontier molecular orbitals (HOMO and LUMO); conceptual DFT parameters such as chemical hardness and electrophilicity; and natural population analysis (NPA) charges on ruthenium and ylidic carbon.

	1	2	3	4	5	6
HOMO						
I	-0.142	-0.143	-0.146	-0.145	-0.147	-0.147
II	-0.168	-0.162	-0.169	-0.162	-0.168	-0.161
III	-0.149	-0.150	-0.152	-0.152	-0.152	-0.152
LUMO						
I	-0.121	-0.121	-0.119	-0.119	-0.118	-0.119
II	-0.127	-0.127	-0.125	-0.125	-0.125	-0.125
III	-0.122	-0.123	-0.120	-0.121	-0.119	-0.120
chemical hardness						
I	0.011	0.011	0.014	0.013	0.014	0.014
II	0.021	0.018	0.022	0.019	0.022	0.018
III	0.014	0.013	0.016	0.015	0.016	0.016
electrophilicity						
I	0.788	0.784	0.642	0.663	0.611	0.629
II	0.526	0.593	0.491	0.545	0.499	0.557
III	0.676	0.694	0.588	0.602	0.560	0.575
q(Ru)						
I	-0.414	-0.434	-0.414	-0.430	-0.416	-0.431
II	-0.101	-0.100	-0.099	-0.110	-0.119	-0.121
III	-0.259	-0.265	-0.256	-0.263	-0.260	-0.258
q(C _{ylidene})						
I	0.126	0.126	0.127	0.129	0.125	0.127
II	0.098	0.094	0.101	0.104	0.110	0.109
III	0.130	0.134	0.136	0.139	0.139	0.139

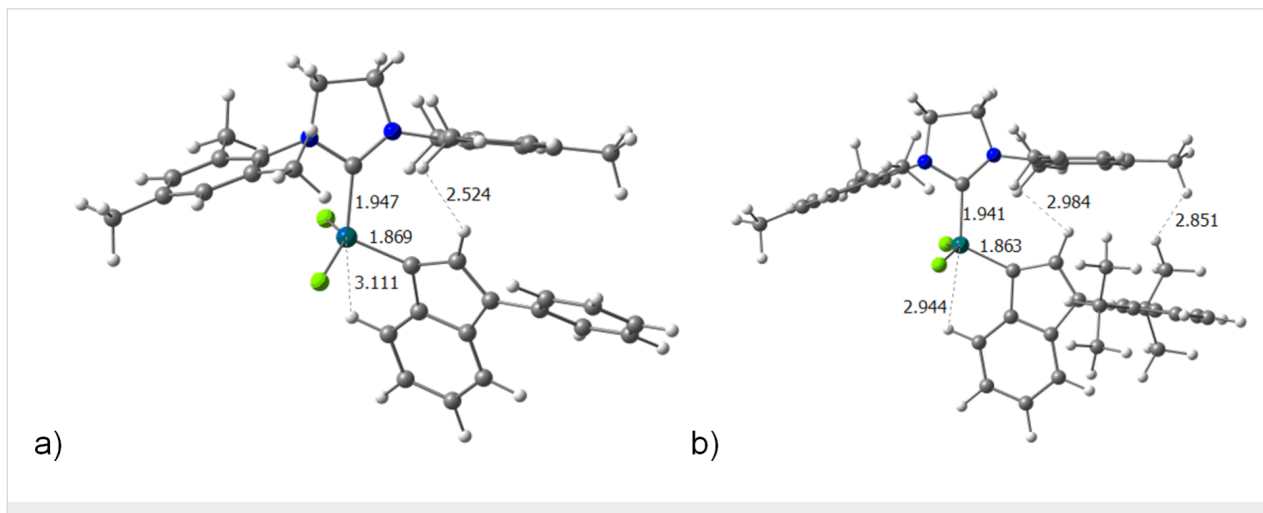


Figure 2: Intermediate **II** for catalysts a) **1** and b) **5** (important bond lengths are given in Å).

namically, the next metallacycle **IV** is also favoured with the indenylidene substitution, being 4.2 and 3.4 kcal/mol relatively more stable for systems **3** and **5**, respectively, with respect to **1**. This effect of reducing steric hindrance between the ylidene and the NHC ligands was examined previously, with the exchange

of benzylidene by indenylidene [51]; and with larger NHC ligands [52].

In order to evaluate the change of the aromaticity of the phenyl ring of the indenylidene derivatives **3–6**, we evaluated the

aromaticity of the six-membered aryl rings, as well as the ring current on the five-membered ring by means of magnetic-based aromaticity criterion NICS (GIAO, see all NICS values in Supporting Information File 1). The 5-membered rings turn out to be non-aromatic, whereas the changes of the aromaticity of the phenyl rings are minimal. Species **1**, **2** and **3** are 0.151 and 0.083 ppm more aromatic than **1**, nearly identical for the IMes systems **5** and **6**, 0.166 and 1.117 ppm and more aromatic than **4**. Once the phosphine has been dissociated, intermediate **II** becomes roughly 0.5 ppm more aromatic, but the trend for catalysts **1–6** is rather similar, being that **3–6** are approximately 0.1 ppm more aromatic than the non-substituted indenylidene systems **1** and **2**.

Conclusion

We have investigated the reaction pathway of a series of Ru-based olefin metathesis catalysts that leads to the methylidene catalytic active species, i.e., the activation of the precatalyst. The indenylidene ligand is substituted by congener ligands with *ortho*-methyl or isopropyl group on its phenyl ring. It was shown that to describe the reactivity, structural, and electronic parameters must be taken into account. The indenylidene ligands, especially the more sterically demanding, impose higher electrophilicity on the ruthenium centre, but structurally favour the relative stability of the metallacycle in order to reduce the steric hindrance between the mesityl groups of either the SIMes or IMes ligands with the *ortho* substituents on the phenyl group of the indenylidene.

The steric hindrance of the indenylidene derivatives does not affect the metal centre structurally since the steric maps confirm that the effect is far removed from the metal core where the reactivity with the entering olefin takes place. On the other hand, electronically the effect is rather small, with insignificant changes of the aromaticity in the phenyl ring. However, the 14e species that will accommodate the entering olefin in the next reaction step imposes a stronger Ru–H interaction thanks to the substituents on the indenylidene pushing downward the indenylidene ligand itself, to minimise the steric hindrance with the NHC ligand.

Computational Details

DFT static calculations were performed with the Gaussian 09 set of programs [53], using the BP86 functional of Becke and Perdew [54–56]. The electronic configuration of the molecular systems was described with the double- ζ basis set with polarisation of Ahlrichs for main group atoms (SVP keyword in Gaussian) [57], whereas for ruthenium the small-core quasi-relativistic Stuttgart/Dresden effective core potential, with an associated valence basis set (standard SDD keywords in Gaussian 09), was employed [58–60]. The geometry optimisa-

tions were performed without symmetry constraints. Analytical frequency calculations were performed to characterise the located stationary points, apart from calculating the unscaled zero-point energies (ZPEs) and the thermal corrections and entropy effects at 298 K, and all values at a pressure of 1354 atm using the approach of Martin and co-workers [61], excluding the potential overestimation of the entropy contribution [38,62,63]. Energies were obtained by single point calculations on the optimised geometries with the M06 functional [64] and the TZVP basis set [65], and solvent effects were estimated with the polarisable continuous solvation model PCM using dichloromethane as solvent [66,67]. The reported free energies in this work include energies obtained at the M06/TZVP~sdd level of theory corrected with zero-point energies, thermal corrections, and entropy effects evaluated at 298 K, achieved at the BP86/SVP~sdd level. This computational approach for olefin metathesis with Ru based catalysts turned out to display errors of less than 1 kcal/mol by Poater and co-workers [68].

The percent buried volume calculations were performed with the SambVca package developed by Cavallo et al. [42]. The radius of the sphere around the origin placed 2 Å below the metal centre was set to 3.5 Å, while for the atoms, we adopted the Bondi radii scaled by 1.17, and a mesh of 0.1 Å was used to scan the sphere for buried voxels. The steric maps were generated also with the SambVca package [69].

Aromaticity was evaluated by means of the nucleus independent chemical shift (NICS) [70,71], proposed by Schleyer et al., as a magnetic descriptor of aromaticity. NICS is defined as the negative value of the absolute shielding computed at a ring centre or at some other interesting point of the system. The more negative the NICS the higher the aromaticity of the ring is considered. NICS values were computed using the gauge-including atomic orbital method (GIAO), at the BP86/SVP level. The magnetic shielding tensor was calculated for ghost atoms located at the centre of the rings determined by the nonweighted mean of the heavy atom coordinates.

Supporting Information

Supporting Information File 1

All Cartesian coordinates, 3D view and energies of all species, steric maps and NICS aromaticity values.
[\[https://www.beilstein-journals.org/bjoc/content/supplementary/1860-5397-14-275-S1.pdf\]](https://www.beilstein-journals.org/bjoc/content/supplementary/1860-5397-14-275-S1.pdf)

Acknowledgements

A.P. thanks the Spanish MINECO for a project CTQ2014-59832-JIN, and EU for a FEDER fund (UNGI08-4E-003).

S.P.N. thanks King Saud University and King Abdullah University of Science and Technology (Award No. OSR-2015-CCF-1974-03) for support.

ORCID® IDs

Steven P. Nolan - <https://orcid.org/0000-0001-9024-2035>
 Luigi Cavallo - <https://orcid.org/0000-0002-1398-338X>
 Albert Poater - <https://orcid.org/0000-0002-8997-2599>

References

- Trnka, T. M.; Grubbs, R. H. *Acc. Chem. Res.* **2001**, *34*, 18–29. doi:10.1021/ar000114f
- Heckelsberg, L. F.; Banks, R. L.; Bailey, G. C. *Ind. Eng. Chem. Prod. Res. Dev.* **1968**, *7*, 29–31. doi:10.1021/i360025a007
- Reuben, B.; Wittcoff, H. *J. Chem. Educ.* **1988**, *65*, 605–607. doi:10.1021/ed065p605
- Lutz, E. F. *J. Chem. Educ.* **1986**, *63*, 202–203. doi:10.1021/ed063p202
- Buchmeiser, M. R. *Chem. Rev.* **2000**, *100*, 1565–1604. doi:10.1021/cr990248a
- Rosebrugh, L. E.; Ahmed, T. S.; Marx, V. M.; Hartung, J.; Liu, P.; López, J. G.; Houk, K. N.; Grubbs, R. H. *J. Am. Chem. Soc.* **2016**, *138*, 1394–1405. doi:10.1021/jacs.5b12277
- Scholl, M.; Ding, S.; Lee, C. W.; Grubbs, R. H. *Org. Lett.* **1999**, *1*, 953–956. doi:10.1021/o1990909q
- Schrock, R. R. *Tetrahedron* **1999**, *55*, 8141–8153. doi:10.1016/s0040-4020(99)00304-x
- Hérisson, J.-L.; Chauvin, Y. *Makromol. Chem.* **1971**, *141*, 161–176. doi:10.1002/macp.1971.021410112
- Perfetto, A.; Costabile, C.; Longo, P.; Grisi, F. *Organometallics* **2014**, *33*, 2747–2759. doi:10.1021/om5001452
- Poater, A.; Solans-Monfort, X.; Clot, E.; Copéret, C.; Eisenstein, O. *Dalton Trans.* **2006**, 3077–3087. doi:10.1039/b604481f
- Castarlenas, R.; Esteruelas, M. A.; Oñate, E. *Organometallics* **2005**, *24*, 4343–4346. doi:10.1021/om050569e
- Poater, A.; Chaitanya Vummaleti, S. V.; Pump, E.; Cavallo, L. *Dalton Trans.* **2014**, *43*, 11216–11220. doi:10.1039/c4dt00325j
- de Brito Sá, É.; Rodríguez-Santiago, L.; Sodupe, M.; Solans-Monfort, X. *Organometallics* **2016**, *35*, 3914–3923. doi:10.1021/acs.organomet.6b00641
- Aeilts, S. L.; Cefalo, D. R.; Bonitatebus, P. J., Jr.; Houser, J. H.; Hoveyda, A. H.; Schrock, R. R. *Angew. Chem.* **2001**, *113*, 1500–1504. doi:10.1002/1521-3757(20010417)113:8<1500::aid-ange1500>3.0.co;2-i
- Samojlowicz, C.; Bieniek, M.; Grela, K. *Chem. Rev.* **2009**, *109*, 3708–3742. doi:10.1021/cr800524f
- Schmid, T. E.; Bantrell, X.; Citadelle, C. A.; Slawin, A. M. Z.; Cazin, C. S. J. *Chem. Commun.* **2011**, *47*, 7060–7062. doi:10.1039/c1cc10825e
- Leitgeb, A.; Abbas, M.; Fischer, R. C.; Poater, A.; Cavallo, L.; Slugovc, C. *Catal. Sci. Technol.* **2012**, *2*, 1640–1643. doi:10.1039/c2cy20311a
- Clavier, H.; Caijo, F.; Borré, E.; Rix, D.; Boeda, F.; Nolan, S. P.; Mauduit, M. *Eur. J. Org. Chem.* **2009**, 4254–4265. doi:10.1002/ejoc.200900407
- Boeda, F.; Clavier, H.; Nolan, S. P. *Chem. Commun.* **2008**, 2726–2740. doi:10.1039/b718287b
- Lozano-Vila, A. M.; Monsaert, S.; Bajek, A.; Verpoort, F. *Chem. Rev.* **2010**, *110*, 4865–4909. doi:10.1021/cr900346r
- Diesendruck, C. E.; Tzur, E.; Lemcoff, N. G. *Eur. J. Inorg. Chem.* **2009**, 4185–4203. doi:10.1002/ejic.200900526
- Fürstner, A. *Angew. Chem., Int. Ed.* **2000**, *39*, 3012–3043. doi:10.1002/1521-3773(20000901)39:17<3012::aid-anie3012>3.0.co;2-g
- Vougioukalakis, G. C.; Grubbs, R. H. *Chem. Rev.* **2010**, *110*, 1746–1787. doi:10.1021/cr9002424
- Clavier, H.; Grela, K.; Kirschning, A.; Mauduit, M.; Nolan, S. P. *Angew. Chem., Int. Ed.* **2007**, *46*, 6786–6801. doi:10.1002/anie.200605099
- Rouen, M.; Queval, P.; Borré, E.; Falivene, L.; Poater, A.; Berthod, M.; Hugues, F.; Cavallo, L.; Baslé, O.; Olivier-Bourbigou, H.; Mauduit, M. *ACS Catal.* **2016**, *6*, 7970–7976. doi:10.1021/acscatal.6b01428
- Poater, A.; Bahri-Laleh, N.; Cavallo, L. *Chem. Commun.* **2011**, *47*, 6674–6676. doi:10.1039/c1cc11594d
- Manzini, S.; Nelson, D. J.; Lebl, T.; Poater, A.; Cavallo, L.; Slawin, A. M. Z.; Nolan, S. P. *Chem. Commun.* **2014**, *50*, 2205–2207. doi:10.1039/c3cc49481k
- Martínez, J. P.; Vummaleti, S. V. C.; Falivene, L.; Nolan, S. P.; Cavallo, L.; Solà, M.; Poater, A. *Chem. – Eur. J.* **2016**, *22*, 6617–6623. doi:10.1002/chem.201600383
- Poater, A.; Credendino, R.; Slugovc, C.; Cavallo, L. *Dalton Trans.* **2013**, *42*, 7271–7275. doi:10.1039/c3dt32884h
- Arnedo, L.; Chauvin, R.; Poater, A. *Catalysts* **2017**, *7*, 85. doi:10.3390/catal7030085
- Credendino, R.; Poater, A.; Ragone, F.; Cavallo, L. *Catal. Sci. Technol.* **2011**, *1*, 1287–1297. doi:10.1039/c1cy00052g
- Manzini, S.; Urbina Blanco, C. A.; Nelson, D. J.; Poater, A.; Lebl, T.; Meiries, S.; Slawin, A. M. Z.; Falivene, L.; Cavallo, L.; Nolan, S. P. *J. Organomet. Chem.* **2015**, *780*, 43–48. doi:10.1016/j.jorgchem.2014.12.040
- Jafarpour, L.; Schanz, H.-J.; Stevens, E. D.; Nolan, S. P. *Organometallics* **1999**, *18*, 5416–5419. doi:10.1021/om990587u
- Pump, E.; Slugovc, C.; Cavallo, L.; Poater, A. *Organometallics* **2015**, *34*, 3107–3111. doi:10.1021/om501246q
- Bantrell, X.; Poater, A.; Urbina-Blanco, C. A.; Bidal, Y. D.; Falivene, L.; Randall, R. A. M.; Cavallo, L.; Slawin, A. M. Z.; Cazin, C. S. J. *Organometallics* **2012**, *31*, 7415–7426. doi:10.1021/om300703p
- Manzini, S.; Urbina-Blanco, C. A.; Poater, A.; Slawin, A. M. Z.; Cavallo, L.; Nolan, S. P. *Angew. Chem., Int. Ed.* **2012**, *51*, 1042–1045. doi:10.1002/anie.201106915
- Manzini, S.; Poater, A.; Nelson, D. J.; Cavallo, L.; Slawin, A. M. Z.; Nolan, S. P. *Angew. Chem., Int. Ed.* **2014**, *53*, 8995–8999. doi:10.1002/anie.201403770
- Urbina-Blanco, C. A.; Poater, A.; Lebl, T.; Manzini, S.; Slawin, A. M. Z.; Cavallo, L.; Nolan, S. P. *J. Am. Chem. Soc.* **2013**, *135*, 7073–7079. doi:10.1021/ja402700p
- Poater, A.; Pump, E.; Vummaleti, S. V. C.; Cavallo, L. *Chem. Phys. Lett.* **2014**, *610–611*, 29–32. doi:10.1016/j.cplett.2014.06.063
- Luque-Urrutia, J. A.; Gimferrer, M.; Casals-Cruañas, É.; Poater, A. *Catalysts* **2017**, *7*, 389. doi:10.3390/catal7120389
- Poater, A.; Cavallo, L. *Beilstein J. Org. Chem.* **2015**, *11*, 1767–1780. doi:10.3762/bjoc.11.192
- Wappel, J.; Fischer, R. C.; Cavallo, L.; Slugovc, C.; Poater, A. *Beilstein J. Org. Chem.* **2016**, *12*, 154–165. doi:10.3762/bjoc.12.17
- Mayer, I. *Chem. Phys. Lett.* **1983**, *97*, 270–274. doi:10.1016/0009-2614(83)80005-0

45. Mayer, I. *Int. J. Quantum Chem.* **1984**, *26*, 151–154.
doi:10.1002/qua.560260111

46. Vummaleti, S. V. C.; Nelson, D. J.; Poater, A.; Gómez-Suárez, A.; Cordes, D. B.; Slawin, A. M. Z.; Nolan, S. P.; Cavallo, L. *Chem. Sci.* **2015**, *6*, 1895–1904. doi:10.1039/c4sc03264k

47. Falivene, L.; Credendino, R.; Poater, A.; Petta, A.; Serra, L.; Oliva, R.; Scarano, V.; Cavallo, L. *Organometallics* **2016**, *35*, 2286–2293.
doi:10.1021/acs.organomet.6b00371

48. Poater, A.; Cosenza, B.; Correa, A.; Giudice, S.; Ragone, F.; Scarano, V.; Cavallo, L. *Eur. J. Inorg. Chem.* **2009**, 1759–1766.
doi:10.1002/ejic.200801160

49. Lamberti, M.; Fortman, G. C.; Poater, A.; Broggi, J.; Slawin, A. M. Z.; Cavallo, L.; Nolan, S. P. *Organometallics* **2012**, *31*, 756–767.
doi:10.1021/om2012425

50. Poater, A.; Saliner, A. G.; Carbó-Dorca, R.; Poater, J.; Solà, M.; Cavallo, L.; Worth, A. P. *J. Comput. Chem.* **2009**, *30*, 275–284.
doi:10.1002/jcc.21041

51. Poater, A.; Ragone, F.; Correa, A.; Cavallo, L. *Dalton Trans.* **2011**, *40*, 11066–11069. doi:10.1039/c1dt10959f

52. Poater, A.; Falivene, L.; Urbina-Blanco, C. A.; Manzini, S.; Nolan, S. P.; Cavallo, L. *Dalton Trans.* **2013**, *42*, 7433–7439.
doi:10.1039/c3dt32980a

53. *Gaussian 09*, Revision E.01; Gaussian, Inc.: Wallingford, CT, 2009.

54. Becke, A. D. *Phys. Rev. A: At., Mol., Opt. Phys.* **1988**, *38*, 3098–3100.
doi:10.1103/physreva.38.3098

55. Perdew, J. P. *Phys. Rev. B: Condens. Matter Mater. Phys.* **1986**, *33*, 8822–8824. doi:10.1103/physrevb.33.8822

56. Perdew, J. P. *Phys. Rev. B* **1986**, *34*, 7406.
doi:10.1103/physrevb.34.7406

57. Schäfer, A.; Horn, H.; Ahlrichs, R. *J. Chem. Phys.* **1992**, *97*, 2571–2577. doi:10.1063/1.463096

58. Häussermann, U.; Dolg, M.; Stoll, H.; Preuss, H.; Schwerdtfeger, P.; Pitzer, R. M. *Mol. Phys.* **1993**, *78*, 1211–1224.
doi:10.1080/00268979300100801

59. Küchle, W.; Dolg, M.; Stoll, H.; Preuss, H. *J. Chem. Phys.* **1994**, *100*, 7535–7542. doi:10.1063/1.466847

60. Leininger, T.; Nicklass, A.; Stoll, H.; Dolg, M.; Schwerdtfeger, P. *J. Chem. Phys.* **1996**, *105*, 1052–1059. doi:10.1063/1.471950

61. Martin, R. L.; Hay, P. J.; Pratt, L. R. *J. Phys. Chem. A* **1998**, *102*, 3565–3573. doi:10.1021/jp980229p

62. Falivene, L.; Barone, V.; Talarico, G. *Mol. Catal.* **2018**, *452*, 138–144.
doi:10.1016/j.mcat.2018.04.012

63. Luque-Urrutia, J. A.; Poater, A. *Inorg. Chem.* **2017**, *56*, 14383–14387.
doi:10.1021/acs.inorgchem.7b02630

64. Zhao, Y.; Truhlar, D. G. *Theor. Chem. Acc.* **2008**, *120*, 215–241.
doi:10.1007/s00214-007-0310-x

65. Schäfer, A.; Huber, C.; Ahlrichs, R. *J. Chem. Phys.* **1994**, *100*, 5829–5835. doi:10.1063/1.467146

66. Barone, V.; Cossi, M. *J. Phys. Chem. A* **1998**, *102*, 1995–2001.
doi:10.1021/jp9716997

67. Tomasi, J.; Persico, M. *Chem. Rev.* **1994**, *94*, 2027–2094.
doi:10.1021/cr00031a013

68. Poater, A.; Pump, E.; Vummaleti, S. V. C.; Cavallo, L. *J. Chem. Theory Comput.* **2014**, *10*, 4442–4448.
doi:10.1021/ct5003863

69. Jacobsen, H.; Correa, A.; Poater, A.; Costabile, C.; Cavallo, L. *Coord. Chem. Rev.* **2009**, *293*, 687–703. doi:10.1016/j.ccr.2008.06.006

70. Schleyer, P. v. R.; Maerker, C.; Dransfeld, A.; Jiao, H.; van Eikema Hommes, N. J. R. *J. Am. Chem. Soc.* **1996**, *118*, 6317–6318. doi:10.1021/ja960582d

71. Chen, Z.; Wannere, C. S.; Corminboeuf, C.; Puchta, R.; Schleyer, P. v. R. *Chem. Rev.* **2005**, *105*, 3842–3888.
doi:10.1021/cr030088+

License and Terms

This is an Open Access article under the terms of the Creative Commons Attribution License (<http://creativecommons.org/licenses/by/4.0>). Please note that the reuse, redistribution and reproduction in particular requires that the authors and source are credited.

The license is subject to the *Beilstein Journal of Organic Chemistry* terms and conditions:
(<https://www.beilstein-journals.org/bjoc>)

The definitive version of this article is the electronic one which can be found at:
doi:10.3762/bjoc.14.275



Ring-closing-metathesis-based synthesis of annellated coumarins from 8-allylcoumarins

Christiane Schultze and Bernd Schmidt*

Full Research Paper

Open Access

Address:
Universität Potsdam, Institut fuer Chemie, Karl-Liebknecht-Straße
24–25, D-14476 Potsdam-Golm, Germany

Beilstein J. Org. Chem. **2018**, *14*, 2991–2998.
doi:10.3762/bjoc.14.278

Email:
Bernd Schmidt* - bernd.schmidt@uni-potsdam.de

Received: 13 September 2018
Accepted: 22 November 2018
Published: 05 December 2018

* Corresponding author

This article is part of the thematic issue "Progress in metathesis chemistry III".

Keywords:
coumarins; heterocycles; isomerization; olefin metathesis; ruthenium

Guest Editors: K. Grela and A. Kajetanowicz

© 2018 Schultze and Schmidt; licensee Beilstein-Institut.
License and terms: see end of document.

Abstract

8-Allylcoumarins are conveniently accessible through a microwave-promoted tandem Claisen rearrangement/Wittig olefination/cyclization sequence. They serve as a versatile platform for the annellation of five- to seven-membered rings using ring-closing olefin metathesis (RCM). Furano-, pyrano-, oxepino- and azepinocoumarins were synthesized from the same set of precursors using Ru-catalyzed double bond isomerizations and RCM in a defined order. One class of products, pyrano[2,3-*f*]chromene-2,8-diones, were inaccessible through direct RCM of an acrylate, but became available from the analogous allyl ether via an assisted tandem catalytic RCM/allylic oxidation sequence.

Introduction

Naturally occurring coumarins and synthetic derivatives have attracted considerable attention, because many of these compounds are pharmacologically active [1–4]. Their activity profiles are quite diverse and range from anticoagulant via anti-infective, anticancer to antineurodegenerative activities [2,3]. The majority of natural coumarins are secondary metabolites isolated from plants [5–7]. A commonly used taxonomy for these natural products (which has been extended to the non-natural analogues) is based on the coumarin structure (Figure 1) [4,8].

It distinguishes between simple coumarins with substituents only at the benzene part (e.g., osthole, a natural product with Ca^{2+} -channel antagonist activity) [9], coumarins with substituents at the pyrone part (e.g., warfarin, a synthetic clinically used anticoagulant) [10], and heteroannellated coumarins, in which a heterocycle is annellated to the benzene ring of the coumarin skeleton. In particular the latter group is often further divided into sections according to ring size (five-membered rings: furanocoumarins; six-membered rings: pyranocoumarins) and location of the annellated ring (linear vs angular). Angelicin (**3a**,

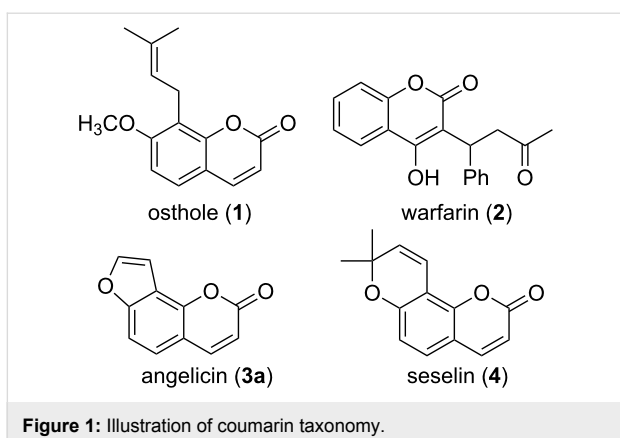


Figure 1: Illustration of coumarin taxonomy.

also named isopsoralen), for instance, is an angular furanocoumarin from *Psoralea corylifolia* [11,12] that is moderately cytotoxic [13] and exhibits anti-oxidative activity [14], but is significantly less phototoxic than the linear isomer psoralen, due to its inability to cross link DNA [15]. This consideration has, for example, led to the development of substituted angelicins rather than psoralens as potential anti-influenza drugs [16]. Seselin (4) is an example of an angular pyranocoumarin found in various plants, e.g., from the family of *Rutaceae* [17]. Among other bioactivities, the compound itself and some natural and non-natural derivatives induce apoptosis in melanoma HTB-140 cells [18].

Synthetic approaches to substituted coumarins in general and heteroannellated coumarins [19] in particular can start from other naturally occurring coumarins [20] or may involve the construction of the coumarin skeleton. For the latter group of syntheses several classical methods, such as the Perkin condensation, are available, which have been covered in earlier reviews [5,6,8]. Unfavorable reaction conditions, low yields and a sometimes limited scope make the development of alternatives to these established methods necessary. Examples from the past 15 years include transition metal-catalyzed transformations [21–23], solid-phase synthesis directed at combinatorial library design [24] and organocatalytic annellation reactions [25,26].

Sparked by our interest in the development and application of sequential one-pot transformations and motivated by the relevance of prenylated and other substituted coumarins in natural products and medicinal chemistry, we [27–29] and others [30] have investigated a microwave-promoted tandem reaction for the synthesis of 8-substituted coumarins over the past few years. Starting materials are allyl ethers of salicylic aldehydes or ketones **5** and the stable ylide ethyl (triphenylphosphoranylidene)acetate (**6**), which upon microwave irradiation undergo a tandem Claisen rearrangement/Wittig olefination/cyclization sequence. This sequence was pioneered by the groups of Harwood [31,32]

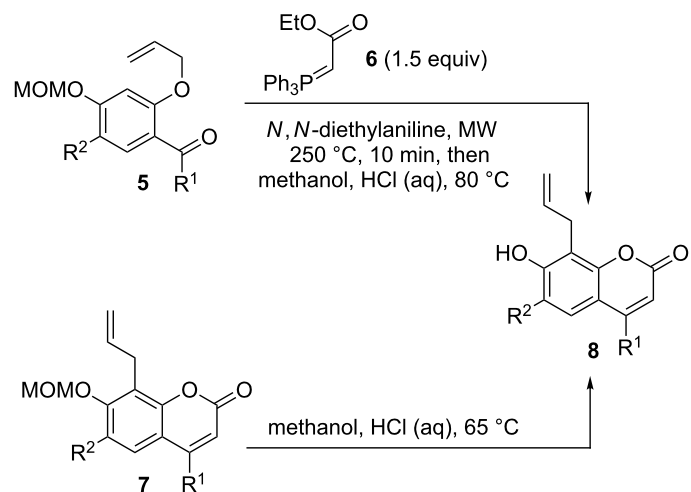
and Mali [33–36], and its Wittig olefination/cyclization part has been employed in the synthesis of various coumarins without alkyl substituents at position 8 [37–39]. In all previous reports conventional heating was used to induce the tandem sequence.

In this contribution we report how 8-allylcoumarins obtained through the microwave-promoted tandem sequence can be elaborated into heteroannellated coumarins that are either natural products or close ring-expanded analogues, using ring-closing olefin metathesis (RCM) reactions. Precedence for the use of RCM [40] in the synthesis and functionalization of coumarins is scarce, considering the vast number of applications olefin metathesis has found [41] and taking into account the high relevance of coumarins. Construction of the coumarin by RCM has been reported by few groups [42–45] and heteroannellations to the coumarin scaffold based on RCM are also limited in number and have mostly not been surveyed systematically [46–53].

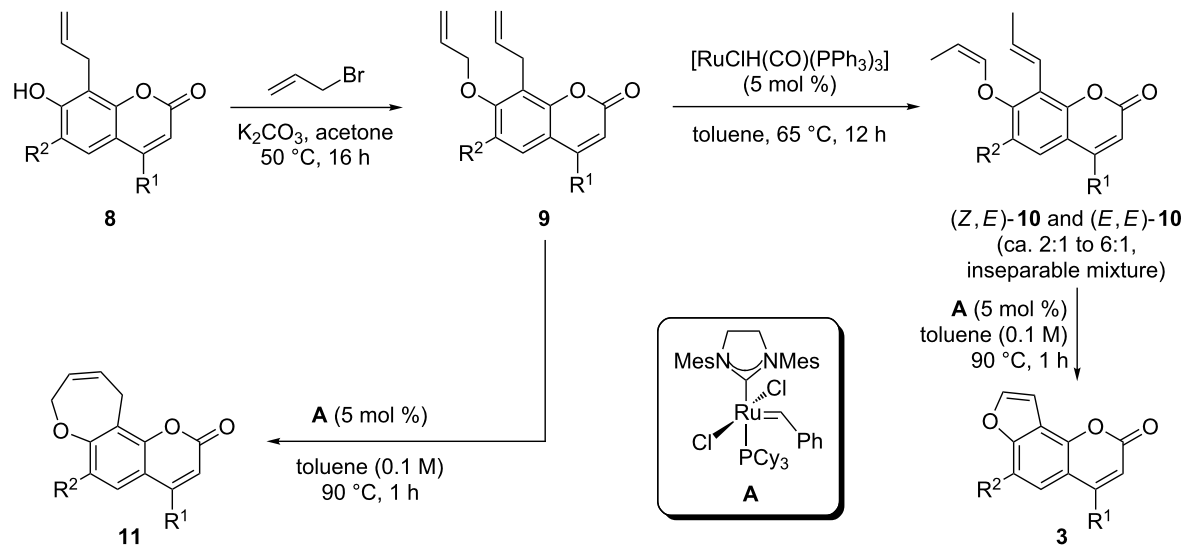
Results and Discussion

To study the heteroannellation reactions, a set of four 8-allyl-7-hydroxycoumarins **8** were synthesized starting from the MOM-protected precursors **5a–d** using the conditions of the microwave-promoted tandem sequence [29]. The intermediate MOM-protected coumarins were not isolated but immediately deprotected by treatment with aq HCl in methanol. Isolation of the MOM-protected coumarins **7** [29] and deprotection in a separate step resulted in virtually identical overall yields of coumarins **8** and did therefore not offer any advantage (Table 1).

For the synthesis of furanocoumarins **3** and their ring-expanded oxepino analogues **11** the 8-allylcoumarins **8** were first O-allylated. The resulting allyl ethers **9** underwent ring-closing metathesis to oxepines **11** smoothly in the presence of second-generation Grubbs' catalyst **A** [54] within one hour at 90 °C, except for the 4-phenyl-substituted derivative **9b**, which was recovered from the reaction mixture under these conditions. However, compound **9b** was successfully cyclized to **11b** using catalyst **A** in dichloromethane at ambient temperature, higher dilution and after prolonged reaction time. For the synthesis of furanocoumarins **3** the allyl ethers **9** were first subjected to a Ru hydride-catalyzed double bond isomerization [55,56] to furnish enol ethers **10** as inseparable mixtures of diastereoisomers. For these reasons a complete structural assignment turned out to be difficult, but the products with a 7-*Z*-propenylxyloxy- and an 8-*E*-propenyl substituent, as shown in Table 2, were in all cases predominant, followed by the *E,E*-configured products. The ratio of these two isomers was ca. 3:1 for compounds **10a,b,d** and ca. 10:1 for **10c** with an adjacent coordinating methoxy group. The other two diastereoisomers were present only in trace amounts.

Table 1: Synthesis of 8-allyl-7-hydroxycoumarins **8**.

entry	5	R ¹	R ²	8	yield (%) ^a	yield (%) ^b
1	5a	H	H	8a	59	82
2	5b	C ₆ H ₅	H	8b	70	91
3	5c	H	OCH ₃	8c	40	84
4	5d	CH ₃	H	8d	66	89

^aYield starting from **5** without isolation of **7**.^bYield starting from **7**.**Table 2:** Synthesis of oxepino- **11** and furanocoumarins **3** from a common precursor **9**.

entry	8	R ¹	R ²	9	yield (%)	10	yield (%)	11	yield (%)	3	yield (%)
1	8a	H	H	9a	97	10a	93	11a	92	3a	95
2	8b	C ₆ H ₅	H	9b	92	10b	94	11b	79 ^a	3b	89
3	8c	H	OCH ₃	9c	95	10c	quant.	11c	79	3c	98
4	8d	CH ₃	H	9d	91	10d	quant.	11d	77	3d	quant.

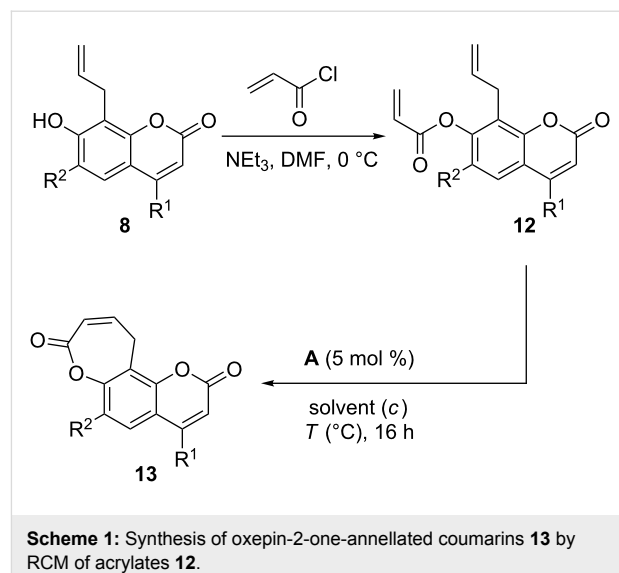
^a**A** (5 mol %), CH₂Cl₂ (0.05 M), 20 °C.

RCM of enol ethers [57,58] **10** under the same conditions used for the synthesis of the oxepino-annellated coumarins **11** gave furanocoumarins **3** in excellent yields (Table 2). Furanocoumarins **3a** (angelicin or isopsoralen, Table 2, entry 1) [11,12] and **3c** (sphondin, Table 2, entry 3) [59,60] are natural products. They have previously been synthesized from 7-hydroxy-8-iodocoumarins through Sonogashira coupling and cyclization [61] or via Dötz benzannellation [62] of furanyl carbene complexes and acetylenes [63]. Angelicin (**3a**) was also obtained via RCM of 8-(1-propenyl)-7-vinyloxycoumarin, but the synthesis of this precursor required four steps, starting from umbelliferone, and proceeded only with moderate regioselectivity for the second step [47].

Next, we investigated the synthesis of coumarins with annellated unsaturated lactones starting from the same 8-allylcoumarins **8** (Scheme 1). For the synthesis of oxepin-2-one-annellated coumarins **13** compounds **8** were first converted to the corresponding acrylates **12** with acryloyl chloride (Table 3). RCM of these acrylates turned out to be not straightforward but required some optimization (Table 4).

In particular, a reduced initial substrate concentration of 0.01 M and reaction temperatures of 110 °C (Table 4, entry 6) led to a smooth conversion to the desired oxepin-2-ones **13**, whereas ambient or slightly elevated temperatures in CH₂Cl₂ or toluene as a solvent (Table 4, entries 1, 2 and 5) resulted in incomplete conversions and low yields. Addition of the Lewis acid Ti(O*i*Pr)₄, which had previously been reported to prevent the formation of inactive catalyst–substrate chelates [64], inhibited the RCM reaction completely in this case (Table 4, entries 3 and 4). The beneficial effect of low initial substrate concentrations on RCM reactions with acrylates has previously been described [65] and was later systematically investigated by one of us [66].

A possible access to the pyran-2-one-annellated coumarin substitution pattern **15** was investigated starting from acrylate **12d**



Scheme 1: Synthesis of oxepin-2-one-annellated coumarins **13** by RCM of acrylates **12**.

Table 3: Synthesis of acrylates **12**.

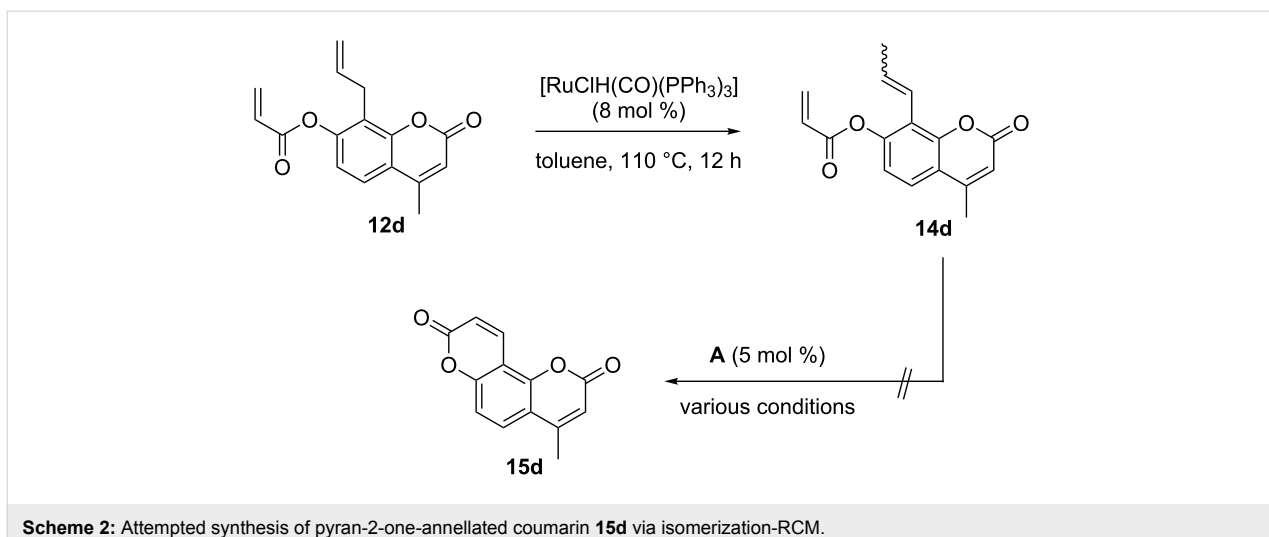
entry	8	R ¹	R ²	12	yield (%)
1	8a	H	H	12a	92
2	8b	C ₆ H ₅	H	12b	93
3	8c	H	OCH ₃	12c	89
4	8d	CH ₃	H	12d	86

(Scheme 2). The isomerization of the 8-allyl substituent to a prop-1-enyl substituent under the conditions used for the synthesis of precursors **10** (Table 2) stopped at 50% conversion. Higher catalyst loading and an increased reaction temperature, however, resulted in a quantitative conversion to **14d** as a mixture of *E*- and *Z*-isomers. Although the RCM of similarly substituted acrylates to coumarins was previously described in the literature, this reaction failed completely for the envisaged synthesis of **15d** from **14d** under various conditions. Initial substrate concentrations varying from 0.01 M to 0.10 M, the sol-

Table 4: Optimization of RCM conditions and synthesis of annellated coumarins **13**.

entry	12	R ¹	R ²	solvent	c (mol·L ⁻¹)	T (°C)	13	yield (%)
1	12a	H	H	CH ₂ Cl ₂	0.05	20	13a	16
2	12a	H	H	CH ₂ Cl ₂	0.01	40	13a	35
3 ^a	12a	H	H	CH ₂ Cl ₂	0.01	40	13a	— ^b
4 ^c	12a	H	H	CH ₂ Cl ₂	0.01	40	13a	— ^b
5	12a	H	H	toluene	0.01	20	13a	20
6	12a	H	H	toluene	0.01	110	13a	81
7	12b	C ₆ H ₅	H	toluene	0.01	110	13b	79
8	12c	H	OCH ₃	toluene	0.01	110	13c	91
9	12d	CH ₃	H	toluene	0.01	110	13d	86

^aAdditive Ti(O*i*Pr)₄ (1.0 equiv). ^bNo conversion. ^cAdditive Ti(O*i*Pr)₄ (2.0 equiv).



Scheme 2: Attempted synthesis of pyran-2-one-annellated coumarin **15d** via isomerization-RCM.

vents dichloromethane and toluene, and reaction temperatures between ambient temperature and 110 °C were tested, but to no avail.

As a method to circumvent notoriously difficult acrylate RCM steps we [45] and others [67] have developed an assisted tandem catalytic [68] RCM/allylic oxidation sequence. Such tandem sequences are characterized by the combination of two mechanistically distinct catalytic reactions in a defined order, which proceed with a single precatalyst that undergoes a transformation *in situ* upon addition of a suitable reagent, a “chemical trigger” [69]. In the case of the RCM/allylic oxidation sequence *tert*-butyl hydroperoxide is added after completion of the metathesis reaction, which most likely induces a conversion of the metathesis active Ru–carbene species to a Ru(IV)–oxo species. The latter are known to catalyze allylic and benzylic oxidation reactions through a radical mechanism [70].

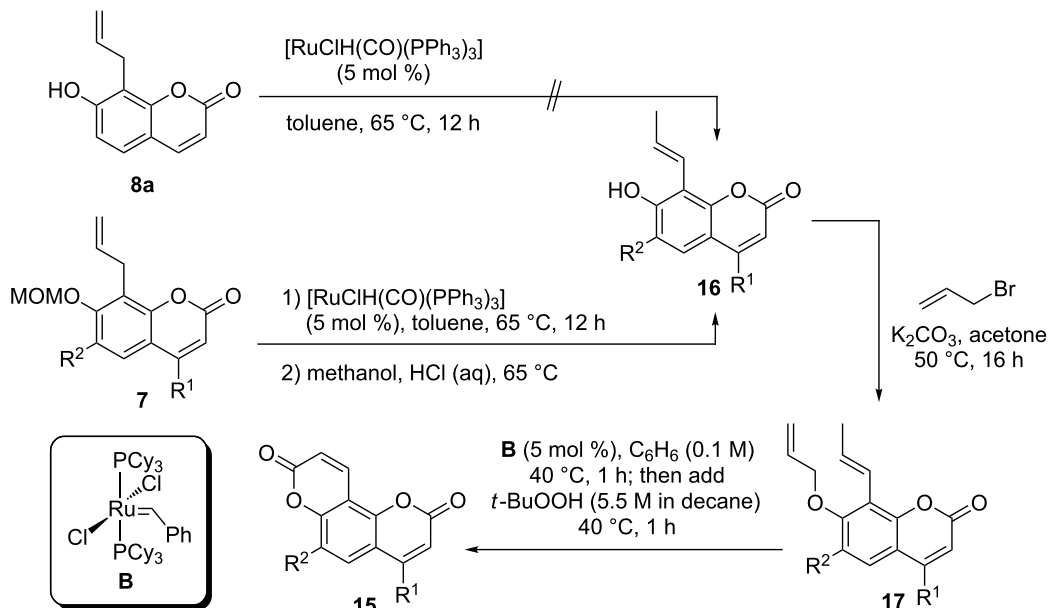
To implement this tandem sequence in the synthesis of pyran-2-one-annellated coumarins **15** an isomerization of the 8-allyl substituent to a prop-1-enyl substituent was first required. When 8-allyl-7-hydroxycoumarin (**8a**) was subjected to the isomerization conditions previously used for the synthesis of furanocoumarin precursors **10** (see Table 2) we observed no conversion. A plausible explanation is the formation of a stable six-membered Ru–O–chelate complex following hydroruthenation, which inhibits a subsequent β -hydride elimination and thus interrupts the catalytic cycle. For these reasons we started from the MOM-protected 8-allylcoumarins **7**, which underwent the Ru-hydride catalyzed double bond migration smoothly. The MOM group was cleaved off without isolation of the intermediate products and the required 7-hydroxy-8-(prop-1-enyl)coumarins **16** were isolated in high overall yields and *E*-selectivities. Allylation of phenols **16** furnished the RCM pre-

ursors **17**, which underwent the tandem RCM/allylic oxidation sequence to compounds **15** in fair yields (Table 5). All pyran-2-one-annellated coumarins **15** synthesized in the course of this study were previously described in the literature: compound **15a** was used to investigate the regioselectivity of [2 + 2]-photocycloadditions [71], compound **15d** was included in a comparative investigation into the fluorescence properties of 4-methylcoumarins [72], compounds **15b** and **15c** were tested for bacteriostatic activity [73] and insect-antifeedant activity [74], respectively. A common denominator of these reports is that a thorough investigation into the spectral and biological properties of these compounds is hampered by unsatisfactory yields and selectivities if classical coumarin syntheses are used. Compound **15a**, for instance, was obtained in only 14% yield from umbelliferone and malic acid in a Pechmann synthesis [71].

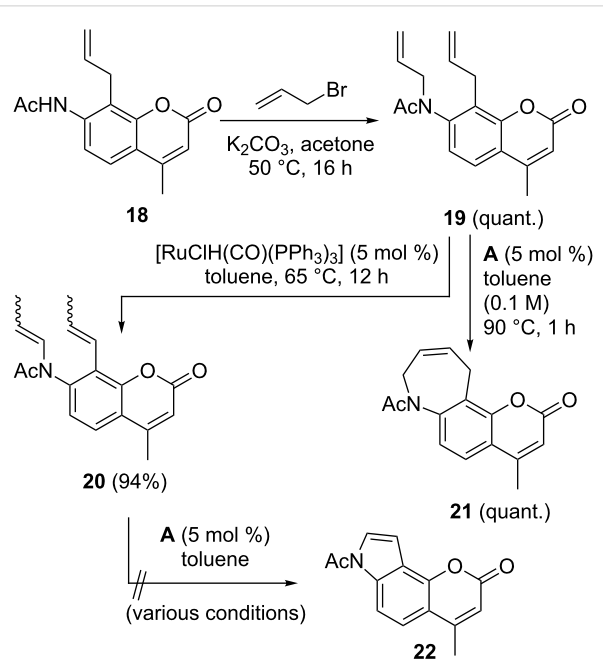
We concluded our study by investigating the possibility to transfer the syntheses of oxa-annellated coumarins described above to the aza-annellated derivatives. Starting point was the 7-acetamido-substituted coumarin **18** [29], which was first N-allylated to the allylamide **19**. Dual double bond migration was accomplished with the Ru–hydride complex used previously and furnished the enamide **20** in high yield and predominantly as the *E,E*-isomer. In light of previous work by Arisawa et al. [75], who reported a synthesis of indoles by RCM of sterically less encumbered enamides, we investigated the RCM of **20**. Unfortunately, no conversion to the indole **22** could be observed under various conditions. Ring-closing metathesis of **19** was, in contrast, successful and furnished the azepinocoumarin **21** in quantitative yield (Scheme 3).

Conclusion

In summary, we demonstrated that annellated coumarins become accessible from appropriately substituted benzene

Table 5: Synthesis of pyran-2-one-annellated coumarins **15** via tandem RCM/allylic oxidation.

entry	7	R ¹	R ²	16	yield (%)	17	yield (%)	15	yield (%)
1	7a	H	H	16a	95	17a	93	15a	56
2	7b	C ₆ H ₅	H	16b	81	17b	89	15b	41
3	7c	H	OCH ₃	16c	quant.	17c	90	15c	45
4	7d	CH ₃	H	16d	92	17d	quant.	15d	47

**Scheme 3:** Synthesis of aza-annellated coumarin **21** and attempted synthesis of indole **22**.

derivatives in few steps, using a microwave-promoted tandem Wittig olefination/Claisen rearrangement/cyclization sequence for the construction of the 8-allylcoumarin scaffold and combinations of double bond isomerization and ring-closing olefin metathesis for the annellation of a second heterocycle. Pyran-2-one-annellated coumarins, which are scarcely available in synthetically useful yields through classical methods, became accessible through a tandem RCM/allylic oxidation sequence.

Supporting Information

Supporting Information File 1

Full experimental procedures, characterization data and copies of ¹H and ¹³C NMR spectra of all compounds.
[\[https://www.beilstein-journals.org/bjoc/content/supplementary/1860-5397-14-278-S1.pdf\]](https://www.beilstein-journals.org/bjoc/content/supplementary/1860-5397-14-278-S1.pdf)

Acknowledgements

We thank Evonik Oxeno for generous donations of solvents and Umicore (Hanau, Germany) for generous donations of catalysts.

ORCID® iDs

Bernd Schmidt - <https://orcid.org/0000-0002-0224-6069>

References

- Kulkarni, M. V.; Kulkarni, G. M.; Lin, C.-H.; Sun, C.-M. *Curr. Med. Chem.* **2006**, *13*, 2795–2818. doi:10.2174/092986706778521968
- Riveiro, M. E.; De Kimpe, N.; Moglioni, A.; Vazquez, R.; Monczor, F.; Shayo, C.; Davio, C. *Curr. Med. Chem.* **2010**, *17*, 1325–1338. doi:10.2174/092986710790936284
- Peng, X.-M.; Damu, G. L. V.; Zhou, C.-H. *Curr. Pharm. Des.* **2013**, *19*, 3884–3930. doi:10.2174/1381612811319210013
- Venugopala, K. N.; Rashmi, V.; Odhav, B. *BioMed Res. Int.* **2013**, No. 963248. doi:10.1155/2013/963248
- Murray, R. D. H. *Nat. Prod. Rep.* **1995**, *12*, 477–505. doi:10.1039/np9951200477
- Murray, R. D. H. *Prog. Chem. Org. Nat. Prod.* **2002**, *83*, 1–673.
- Sarker, S. D.; Nahar, L. Progress in the Chemistry of Naturally Occurring Coumarins. In *Progress in the Chemistry of Organic Natural Products*; Kinghorn, A. D.; Falk, H.; Gibbons, S.; Kobayashi, J., Eds.; Springer International Publishing: Cham, 2017; Vol. 106, pp 241–304. doi:10.1007/978-3-319-59542-9_3
- Keating, G. J.; O'Kennedy, R. The Chemistry and Occurrence of Coumarins. In *Coumarins - Biology, Applications and Mode of Action*; O'Kennedy, R.; Thornes, R. D., Eds.; Wiley: Chichester, 1997; pp 23–66.
- Fusi, F.; Sgaragli, G.; Ha, L. M.; Cuong, N. M.; Saponara, S. *Eur. J. Pharmacol.* **2012**, *680*, 22–27. doi:10.1016/j.ejphar.2012.01.038
- Kleemann, A.; Engel, J.; Kutscher, B.; Reichert, D. *Pharmaceutical substances*, 5th ed.; Georg Thieme Verlag: Stuttgart; New York, 2009. doi:10.1055/b-003-108611
- Innocenti, G.; Cappelletti, E. M.; Caporale, G. *Int. J. Pharmacogn. (Lisse, Neth.)* **1991**, *29*, 311–316. doi:10.3109/13880209109082905
- Won, T. H.; Song, I.-H.; Kim, K.-H.; Yang, W.-Y.; Lee, S. K.; Oh, D.-C.; Oh, W.-K.; Oh, K.-B.; Shin, J. *J. Nat. Prod.* **2015**, *78*, 666–673. doi:10.1021/np500834d
- Mar, W.; Je, K.-H.; Seo, E.-K. *Arch. Pharmacal Res.* **2001**, *24*, 211–213. doi:10.1007/bf02978259
- Seo, E.; Lee, E.-K.; Lee, C. S.; Chun, K.-H.; Lee, M.-Y.; Jun, H.-S. *Oxid. Med. Cell. Longevity* **2014**, No. 897296. doi:10.1155/2014/897296
- Bethea, D.; Fullmer, B.; Syed, S.; Seltzer, G.; Tiano, J.; Rischko, C.; Gillespie, L.; Brown, D.; Gasparro, F. P. *J. Dermatol. Sci.* **1999**, *19*, 78–88. doi:10.1016/s0923-1811(98)00064-4
- Yeh, J.-Y.; Coumar, M. S.; Horng, J.-T.; Shiao, H.-Y.; Kuo, F.-M.; Lee, H.-L.; Chen, I.-C.; Chang, C.-W.; Tang, W.-F.; Tseng, S.-N.; Chen, C.-J.; Shih, S.-R.; Hsu, J. T.-A.; Liao, C.-C.; Chao, Y.-S.; Hsieh, H.-P. *J. Med. Chem.* **2010**, *53*, 1519–1533. doi:10.1021/jm901570x
- Gunatilaka, A. A. L.; Kingston, D. G. I.; Wijeratne, E. M. K.; Bandara, B. M. R.; Hofmann, G. A.; Johnson, R. K. *J. Nat. Prod.* **1994**, *57*, 518–520. doi:10.1021/np50106a013
- Ostrowska, K.; Olejarcz, W.; Wrzosek, M.; Głuszko, A.; Nowicka, G.; Szczepański, M.; Materek, I. B.; Koziol, A. E.; Struga, M. *Biomed. Pharmacother.* **2017**, *95*, 1412–1424. doi:10.1016/j.biopha.2017.09.050
- Medina, F. G.; Marrero, J. G.; Macías-Alonso, M.; González, M. C.; Córdova-Guerrero, I.; Teissier García, A. G.; Osegueda-Robles, S. *Nat. Prod. Rep.* **2015**, *32*, 1472–1507. doi:10.1039/c4np00162a
- Maes, D.; Syngel, K. V.; Debenedetti, S.; De Kimpe, N. *Tetrahedron* **2006**, *62*, 4426–4429. doi:10.1016/j.tet.2006.02.055
- Priyanka; Sharma, R. K.; Katiyar, D. *Synthesis* **2016**, *48*, 2303–2322. doi:10.1055/s-0035-1560450
- Kang, D.; Ahn, K.; Hong, S. *Asian J. Org. Chem.* **2018**, *7*, 1136–1150. doi:10.1002/ajoc.201800128
- Kitamura, T.; Otsubo, K. *J. Org. Chem.* **2012**, *77*, 2978–2982. doi:10.1021/jo300021a
- Nicolau, K. C.; Pfefferkorn, J. A.; Roecker, A. J.; Cao, G.-Q.; Barluenga, S.; Mitchell, H. J. *J. Am. Chem. Soc.* **2000**, *122*, 9939–9953. doi:10.1021/ja002033k
- Modrocká, V.; Veverková, E.; Baran, R.; Šebesta, R. *ChemistrySelect* **2018**, *3*, 1466–1471. doi:10.1002/slct.201800147
- Cheng, Y.; Zhang, P.; Jia, Y.; Fang, Z.; Li, P. *Org. Biomol. Chem.* **2017**, *15*, 7505–7508. doi:10.1039/c7ob01730h
- Schmidt, B.; Riemer, M. *Synthesis* **2016**, *48*, 141–149. doi:10.1055/s-0035-1560501
- Schmidt, B.; Schultze, C. *Eur. J. Org. Chem.* **2018**, *223*–227. doi:10.1002/ejoc.201701684
- Schultze, C.; Schmidt, B. *J. Org. Chem.* **2018**, *83*, 5210–5224. doi:10.1021/acs.joc.8b00667
- Konrádová, D.; Kozubíková, H.; Doležal, K.; Pospíšil, J. *Eur. J. Org. Chem.* **2017**, *5204*–5213. doi:10.1002/ejoc.201701021
- Cairns, N.; Harwood, L. M.; Astles, D. P. *J. Chem. Soc., Chem. Commun.* **1986**, 1264–1266. doi:10.1039/c39860001264
- Cairns, N.; Harwood, L. M.; Astles, D. P. *J. Chem. Soc., Perkin Trans. 1* **1994**, 3101–3107. doi:10.1039/p19940003101
- Mali, R. S.; Manekar, A. R.; Tilve, S. G. *Indian J. Chem., Sect. B: Org. Chem. Incl. Med. Chem.* **1987**, *26*, 1007.
- Mali, R. S.; Joshi, P. P.; Sandhu, P. K.; Manekar-Tilve, A. *J. Chem. Soc., Perkin Trans. 1* **2002**, 371–376. doi:10.1039/b109597h
- Patre, R. E.; Shet, J. B.; Parameswaran, P. S.; Tilve, S. G. *Tetrahedron Lett.* **2009**, *50*, 6488–6490. doi:10.1016/j.tetlet.2009.09.017
- Patre, R. E.; Parameswaran, P. S.; Tilve, S. G. *ARKIVOC* **2011**, No. ix, 68–76. doi:10.3998/ark.5550190.0012.905
- Ishii, H.; Ishikawa, T.; Wada, H.; Miyazaki, H.; Kaneko, Y.; Harayama, T. *Chem. Pharm. Bull.* **1992**, *40*, 2614–2619. doi:10.1248/cpb.40.2614
- Maes, D.; Riveiro, M. E.; Shayo, C.; Davio, C.; Debenedetti, S.; De Kimpe, N. *Tetrahedron* **2008**, *64*, 4438–4443. doi:10.1016/j.tet.2008.02.059
- Demyttenaere, J.; Vervisch, S.; Debenedetti, S.; Coussio, J.; Maes, D.; De Kimpe, N. *ChemInform* **2004**, *35*, 1844–1848. doi:10.1002/chin.200452188
- Schmidt, B.; Hauke, S.; Krehl, S.; Kunz, O. Ring-Closing Metathesis. In *Comprehensive Organic Synthesis II*, 2nd ed.; Molander, G. A.; Knochel, P., Eds.; Elsevier: Amsterdam, 2014; pp 1400–1482. doi:10.1016/b978-0-08-097742-3.00530-9
- Grela, K., Ed. *Olefin Metathesis - Theory and Practice*; John Wiley & Sons: Hoboken, 2014. doi:10.1002/9781118711613
- Chatterjee, A. K.; Toste, F. D.; Goldberg, S. D.; Grubbs, R. H. *Pure Appl. Chem.* **2003**, *75*, 421–425. doi:10.1351/pac200375040421
- Nguyen Van, T.; Debenedetti, S.; De Kimpe, N. *Tetrahedron Lett.* **2003**, *44*, 4199–4201. doi:10.1016/s0040-4039(03)00902-x

44. Polito, L.; Cravini, M.; Poletti, L.; Lay, L. *Synth. Commun.* **2006**, *36*, 2203–2209. doi:10.1080/00397910600638937

45. Schmidt, B.; Krehl, S. *Chem. Commun.* **2011**, *47*, 5879–5881. doi:10.1039/c1cc11347j

46. Chattopadhyay, S. K.; Maity, S.; Panja, S. *Tetrahedron Lett.* **2002**, *43*, 7781–7783. doi:10.1016/s0040-4039(02)01806-3

47. Tsai, T.-W.; Wang, E.-C. *J. Chin. Chem. Soc.* **2004**, *51*, 1019–1023. doi:10.1002/jccs.200400152

48. Majumdar, K. C.; Muhuri, S.; Rahaman, H.; Islam, R.; Roy, B. *Chem. Lett.* **2006**, *35*, 1430–1431. doi:10.1246/cl.2006.1430

49. Majumdar, K. C.; Samanta, S.; Chattopadhyay, B.; Nandi, R. K. *Synthesis* **2010**, 863–869. doi:10.1055/s-0029-1218620

50. Litinas, K. E.; Mangos, A.; Nikkou, T. E.; Hadjipavlou-Litina, D. J. *J. Enzyme Inhib. Med. Chem.* **2011**, *26*, 805–812. doi:10.3109/14756366.2011.555944

51. Chattopadhyay, S. K.; Mondal, P.; Ghosh, D. *Synthesis* **2014**, *46*, 3331–3340. doi:10.1055/s-0034-1379141

52. Yerrabelli, J. R.; Chakravarthula, V.; Yerrabelli, H.; Chitneni, P. R.; Batchu, V. R.; Nanubolu, J. B.; Krishnan, R. K. *Tetrahedron Lett.* **2015**, *56*, 2180–2182. doi:10.1016/j.tetlet.2015.02.106

53. Goud, E. Y.; Rao, B. K.; Thirupahi, G.; Hemasri, Y.; Rao, C. P.; Kumar, P. V.; Rao, Y. J. *ChemistrySelect* **2017**, *2*, 1170–1174. doi:10.1002/slct.201601614

54. Scholl, M.; Ding, S.; Lee, C. W.; Grubbs, R. H. *Org. Lett.* **1999**, *1*, 953–956. doi:10.1021/o1990909q

55. Krompiec, S.; Kužník, N.; Penczek, R.; Rzepa, J.; Mrowiec-Białoń, J. *J. Mol. Catal. A: Chem.* **2004**, *219*, 29–40. doi:10.1016/j.molcata.2004.04.039

56. Kužník, N.; Krompiec, S. *Coord. Chem. Rev.* **2007**, *251*, 222–233. doi:10.1016/j.ccr.2006.07.006

57. van Otterlo, W. A. L.; Morgans, G. L.; Madeley, L. G.; Kuzvidza, S.; Moleele, S. S.; Thornton, N.; de Koning, C. B. *Tetrahedron* **2005**, *61*, 7746–7755. doi:10.1016/j.tet.2005.05.090

58. Schmidt, B.; Wolf, F. *J. Org. Chem.* **2017**, *82*, 4386–4395. doi:10.1021/acs.joc.7b00447

59. Coassini Lokar, L. R.; Delben, S. *Phytochemistry* **1988**, *27*, 1073–1077. doi:10.1016/0031-9422(88)80276-0

60. O'Neill, T.; Johnson, J. A.; Webster, D.; Gray, C. A. *J. Ethnopharmacol.* **2013**, *147*, 232–237. doi:10.1016/j.jep.2013.03.009

61. Sardari, S.; Mori, Y.; Horita, K.; Micetich, R. G.; Nishibe, S.; Daneshthalab, M. *Bioorg. Med. Chem.* **1999**, *7*, 1933–1940. doi:10.1016/s0968-0896(99)00138-8

62. Dötz, K. H. *Angew. Chem., Int. Ed. Engl.* **1984**, *23*, 587–608. doi:10.1002/anie.198405871

63. Wulff, W. D.; McCallum, J. S.; Kunng, F. A. *J. Am. Chem. Soc.* **1988**, *110*, 7419–7434. doi:10.1021/ja00230a023

64. Fürstner, A.; Langemann, K. *J. Am. Chem. Soc.* **1997**, *119*, 9130–9136. doi:10.1021/ja9719945

65. Ghosh, A. K.; Cappiello, J.; Shin, D. *Tetrahedron Lett.* **1998**, *39*, 4651–4654. doi:10.1016/s0040-4039(98)00887-9

66. Schmidt, B.; Geißler, D. *ChemCatChem* **2010**, *2*, 423–429. doi:10.1002/cctc.200900282

67. Kato, H.; Ishigame, T.; Oshima, N.; Hoshiya, N.; Shimawaki, K.; Arisawa, M.; Shuto, S. *Adv. Synth. Catal.* **2011**, *353*, 2676–2680. doi:10.1002/adsc.201100303

68. Fogg, D. E.; dos Santos, E. N. *Coord. Chem. Rev.* **2004**, *248*, 2365–2379. doi:10.1016/j.ccr.2004.05.012

69. Schmidt, B.; Krehl, S. Domino and Other Olefin Metathesis Reaction Sequences. In *Olefin Metathesis - Theory and Practice*; Grela, K., Ed.; Wiley: Hoboken, 2014; pp 187–232. doi:10.1002/9781118711613.ch5

70. Murahashi, S.-I.; Komiya, N.; Oda, Y.; Kuwabara, T.; Naota, T. *J. Org. Chem.* **2000**, *65*, 9186–9193. doi:10.1021/jo001348f

71. Bethke, J.; Margaretha, P.; Wynne, A. M.; Caldwell, R. A. *J. Chem. Res.* **1998**, 142–143. doi:10.1039/a707819f

72. Maruyama, J.; Ito, K. *Chem. Pharm. Bull.* **1984**, *32*, 1178–1182. doi:10.1248/cpb.32.1178

73. Raju, M. S.; Subba Rao, N. V. *Proc. - Indian Acad. Sci., Sect. A* **1974**, *79*, 223–229. doi:10.1007/bf03051323

74. Nagaiah, K.; Krupadanam, G. L. D.; Srimannarayana, G. *Indian J. Chem., Sect. B: Org. Chem. Incl. Med. Chem.* **2002**, *41*, 858–862.

75. Arisawa, M.; Terada, Y.; Takahashi, K.; Nakagawa, M.; Nishida, A. *J. Org. Chem.* **2006**, *71*, 4255–4261. doi:10.1021/jo060308u

License and Terms

This is an Open Access article under the terms of the Creative Commons Attribution License (<http://creativecommons.org/licenses/by/4.0>). Please note that the reuse, redistribution and reproduction in particular requires that the authors and source are credited.

The license is subject to the *Beilstein Journal of Organic Chemistry* terms and conditions: (<https://www.beilstein-journals.org/bjoc>)

The definitive version of this article is the electronic one which can be found at:

[doi:10.3762/bjoc.14.278](https://doi.org/10.3762/bjoc.14.278)



A tutorial review of stereoretentive olefin metathesis based on ruthenium dithiolate catalysts

Daniel S. Müller, Olivier Baslé* and Marc Mauduit*

Review

Open Access

Address:

Univ. Rennes, Ecole Nationale Supérieure de Chimie de Rennes,
CNRS, ISCR – UMR 6226, F-35000 Rennes, France

Beilstein J. Org. Chem. **2018**, *14*, 2999–3010.

doi:10.3762/bjoc.14.279

Email:

Olivier Baslé* - olivier.basle@ensc-rennes.fr; Marc Mauduit* -
marc.mauduit@ensc-rennes.fr

Received: 04 September 2018

Accepted: 19 November 2018

Published: 07 December 2018

* Corresponding author

This article is part of the thematic issue "Progress in metathesis chemistry III".

Keywords:

catalysis; olefin metathesis; ruthenium; stereoretentive

Guest Editors: K. Grela and A. Kajetanowicz

© 2018 Müller et al.; licensee Beilstein-Institut.

License and terms: see end of document.

Abstract

Stereoretentive olefin metathesis based on ruthenium dithiolate complexes has become a very active field of research within the past years. This unique catalyst class is able to kinetically produce both *Z*- and *E*-alkenes in high stereochemical purity (typically >95:5) starting from stereochemically pure *Z*- or *E*-alkenes. The aim of this tutorial review is to organize the reported information concerning ruthenium dithiolate catalysts in a logic manner, thus providing an "operators handbook" for chemists who wish to apply this methodology in synthesis.

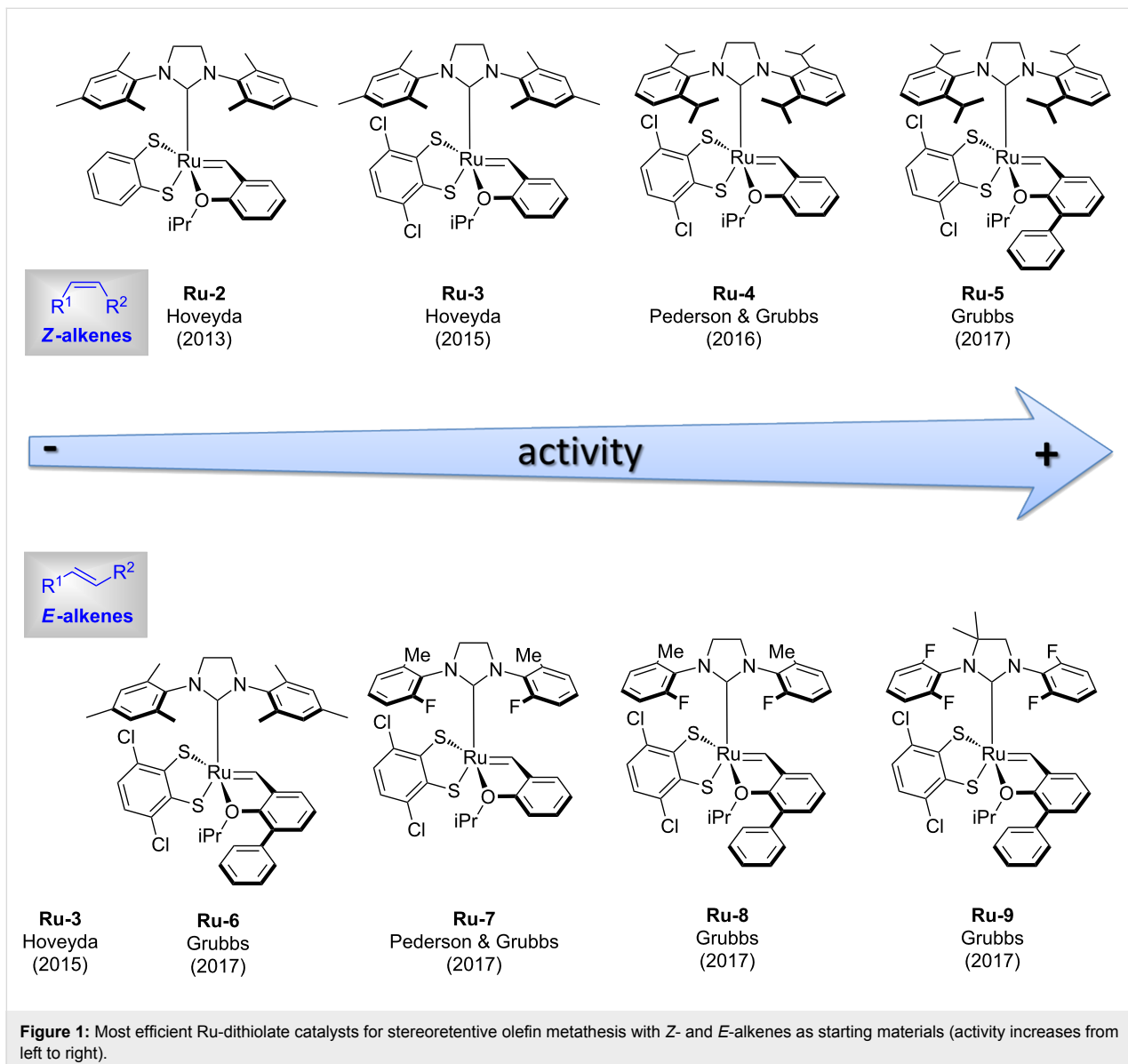
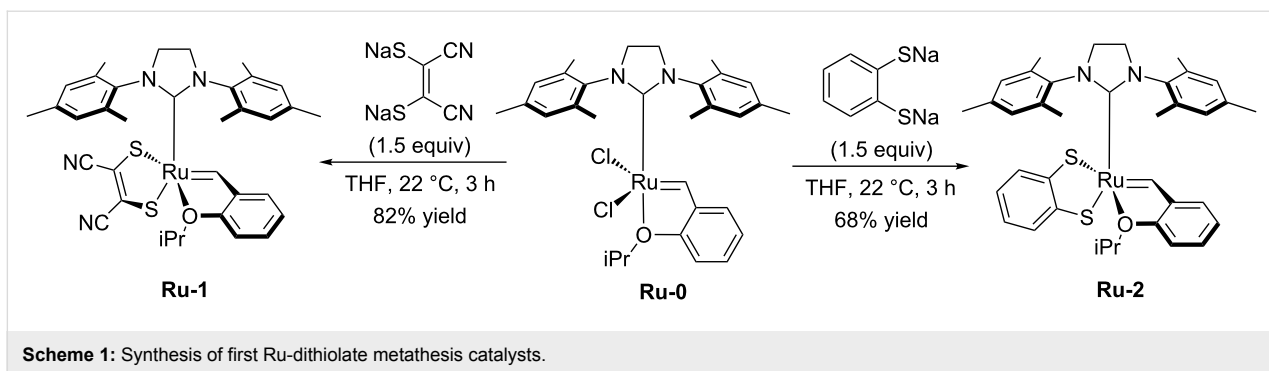
Review

1 Catalyst discovery and structure

optimization from 2013–2018

In stereoretentive metathesis the stereochemistry of the starting material is retained throughout the reaction: *Z*-alkenes starting materials lead to *Z*-alkene products and *E*-alkene starting materials lead to *E*-alkene products [1]. The first ruthenium dithiolate catalysts **Ru-1** and **Ru-2** were reported by Hoveyda in 2013 [2]. **Ru-1** and **Ru-2** were synthesized in one step from the commercially available Hoveyda–Grubbs catalyst **Ru-0** and the corresponding disodium dithiolate salts (Scheme 1).

Initially, Hoveyda described the complexes **Ru-1** and **Ru-2** as *Z*-selective catalysts [2]. However, subsequent studies by Pederson and the Grubbs group showed that Ru dithiolate catalysts are not stereoselective but stereoretentive catalysts [3]. Given the significant difference in geometry of *Z*- and *E*-alkenes it is obvious that each type of alkene requires a different catalyst (Figure 1). In both the *Z*- and *E*-stereoretentive processes, **Ru-3** introduced by Hoveyda in 2015 [4] showed



moderate to good catalytic activity and can therefore be considered as a relatively general catalyst (Figure 1). In 2016 Pederson and Grubbs reported SIPr-based catalyst **Ru-4** with

increased catalytic activity for *Z*-alkenes (Figure 1) [3]. Further improvement was made by the synthesis of **Ru-5** bearing the Blechert ligand (2-isopropoxy-3-phenylbenzylidene) which is

well known to lead to faster initiating Hoveyda-type ruthenium metathesis catalysts [5,6]. The same researchers also found the Blechert modification to significantly improve stereoretentive reactions with *E*-alkenes (**Ru-6**) [6]. Furthermore, Pederson and Grubbs also demonstrated that diminishing the size of the *ortho* substituents of the *N*-aryl groups of the NHC-ligand increased the efficiency for stereoretentive metathesis with *E*-alkenes (**Ru-7** [3], **Ru-8** [6], and **Ru-9** [6]). It should be noticed that the catalyst ranking shown in Figure 1 only applies to 1,2-disubstituted alkenes. Trisubstituted alkenes react very sluggishly and usually work only with catalysts that are efficient for *E*-alkenes (vide infra). Finally, it should be noted, that the precursors of catalysts **Ru-5** to **Ru-9** are not commercially available which limits their practicality [7].

Other attempts to improve the efficiency of dithiolate catalysts by steric and electronic variation of the Ru-dithiolate complexes were reported by several research groups (Figure 2). Hoveyda and co-workers studied a series of catecholate, mercaptophenolate and catecholthiolate catalysts (e.g., **Ru-10**) [8–10]. Variation of sterically demanding catecholthiolate ligands was reported by Grubbs in 2017 (e.g., **Ru-11**) [11]. In 2018 our group reported a series of electronically and sterically activated dithiolate ruthenium catalysts (e.g., **Ru-12**) [12]. However, none of these studies identified more efficient or practical catalysts compared to the ones shown in Figure 1.

2 Mechanistic models

The activity of the various catalysts vis-à-vis *Z*- or *E*-alkenes is best understood by a mechanistic model originally proposed by Pederson and Grubbs (Figure 3) [3]. A comprehensive computational study by Liu and Houk further validated this model, however, invoking distortion of the NHC ligand towards the dithiolate ligand as origin of the open pocket [13].

The proposed model assumes a side-bound mechanism, which results in a metallacycle perpendicular to the NHC ligand. To avoid steric repulsions, the substituents at the α -positions of the

metallacycle point away from the *N*-aryl groups of the NHC-ligands. In contrast, the substituents at the β -position can point up or down. For the reaction with *Z*-alkenes (Figure 3a), the substituent at the β -position has to point down thus creating a new *Z*-alkene with the residing substituent shown in red. It is obvious, that blocking the open space above the β -position of the metallacycle with a very bulky SiPr-NHC ligand (e.g., **Ru-4** and **Ru-5**) has a positive effect on reactions with *Z*-alkenes. Reactions with *E*-alkenes follow the same logic (Figure 3b), however, placing the substituent on the β -position above the plane of the metallacycle pointing towards the NHC ligand. Therefore, it is critical to keep the "pocket" above the β -position open to accommodate the substituent of the incoming alkene. This explains why the smaller 2-fluoro-6-methylphenyl substituent on the NHC ligand (**Ru-7**) leads to higher activity for reactions with *E*-alkenes compared to its *N*-mesityl-substituted congener **Ru-3**. The same applies for trisubstituted alkenes where one substituent is forced into the open "pocket" in the β -position. Therefore, trisubstituted alkenes work best with the same catalysts used for *E*-alkenes (e.g., **Ru-7**, **Ru-8** and **Ru-9**).

3 Kinetic studies

Grubbs studied the kinetic behavior of several Ru-dithiolate catalysts [6,14,15]. In a typical study the disappearance of the benzylidene proton of the ruthenium complex with time is recorded. The disappearance is attributed to the formation of the active catalyst without considering competitive degradation of the catalyst. Figure 4 shows the percentage of consumed precursor complexes **Ru-3** and **Ru-6** for the reaction with (*E*)-2-hexenyl acetate within 24 hours [6]. The Blechert modification (**Ru-6**) initiates much faster with (*E*)-2-hexenyl acetate compared to the parent catalyst **Ru-3**.

4 Selected applications

The synthetic usefulness of ruthenium dithiolate catalysts was demonstrated in numerous synthetic applications such as ring-opening metathesis polymerization (ROMP), ring-opening/cross

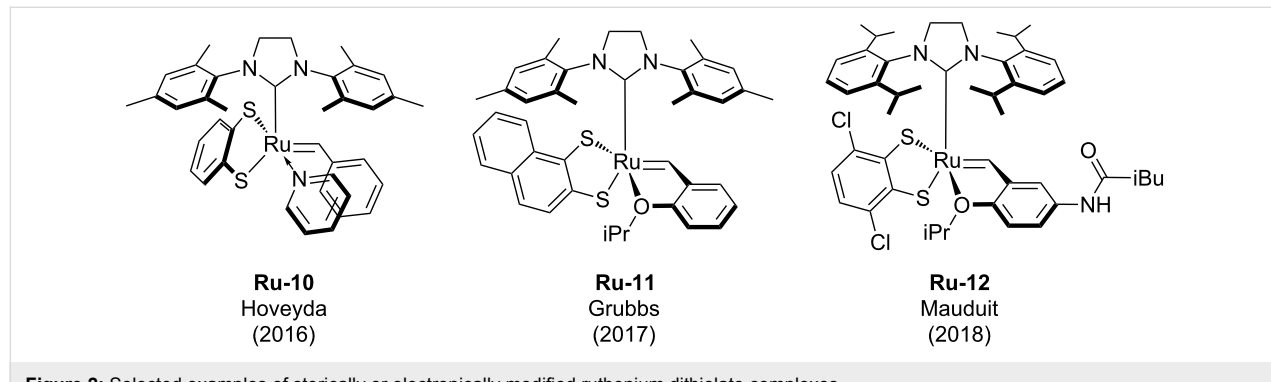


Figure 2: Selected examples of sterically or electronically modified ruthenium dithiolate complexes.

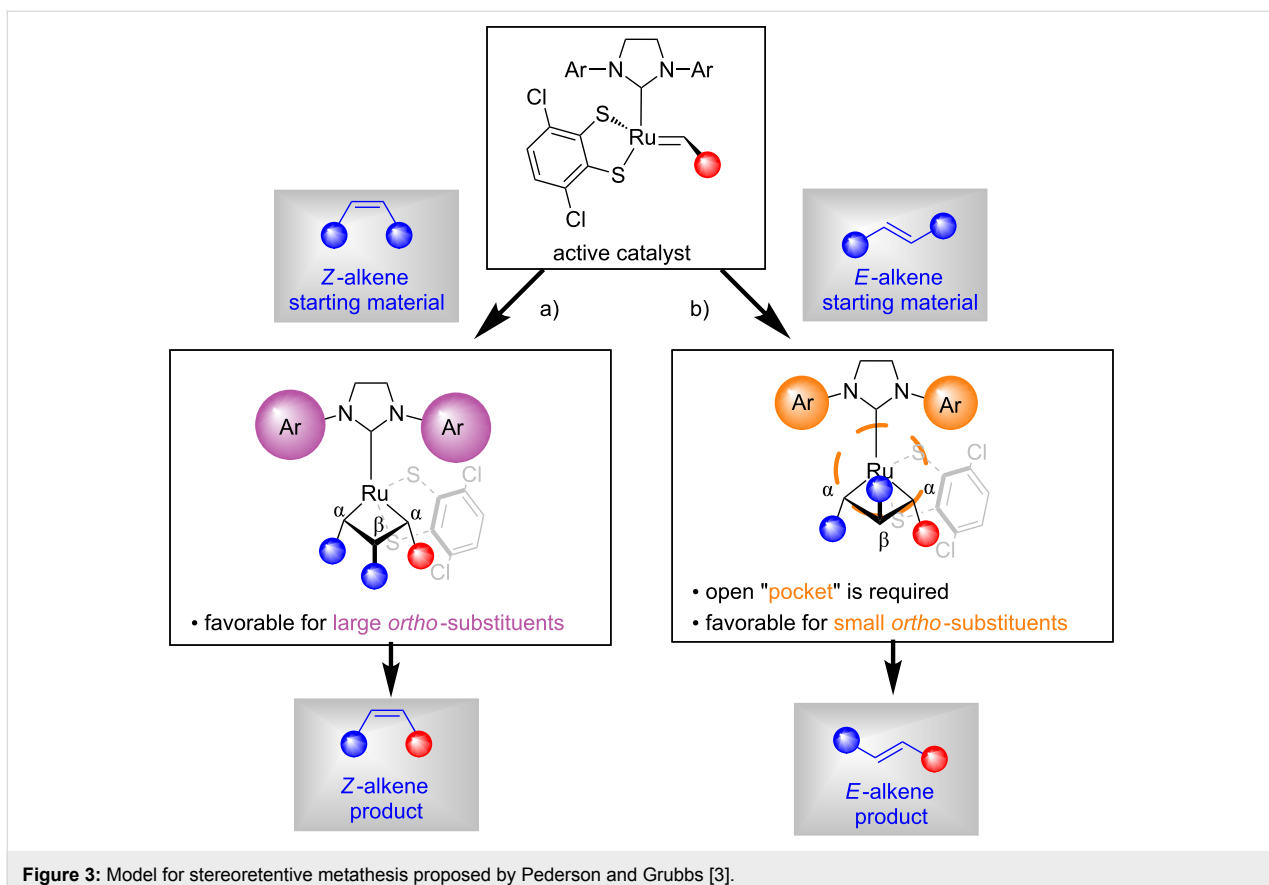


Figure 3: Model for stereoretentive metathesis proposed by Pederson and Grubbs [3].

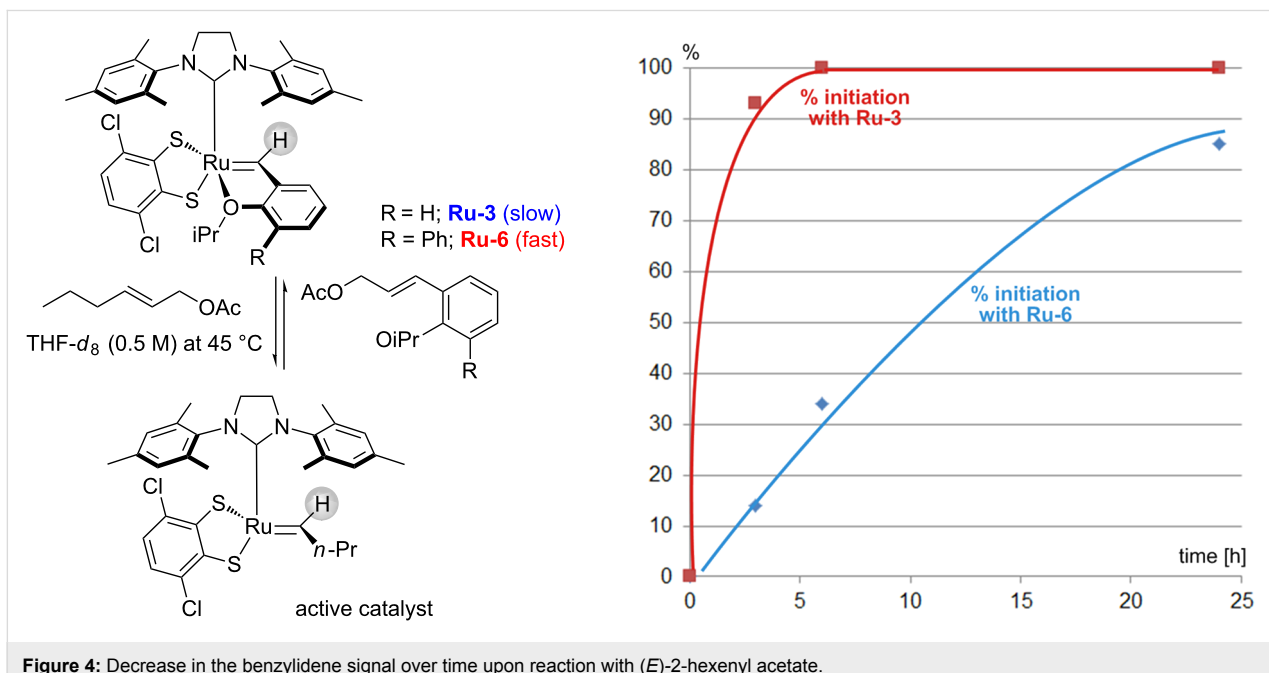
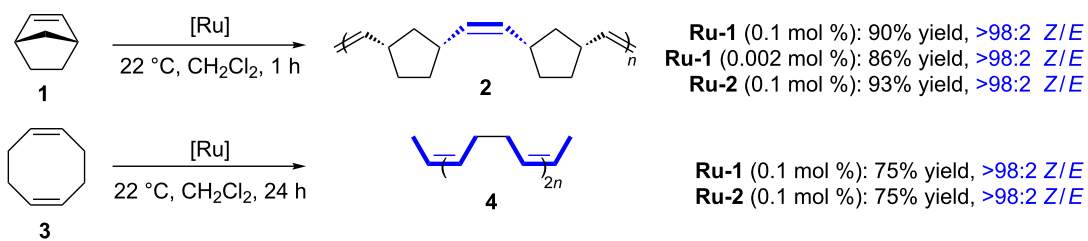


Figure 4: Decrease in the benzylidene signal over time upon reaction with (E) -2-hexenyl acetate.

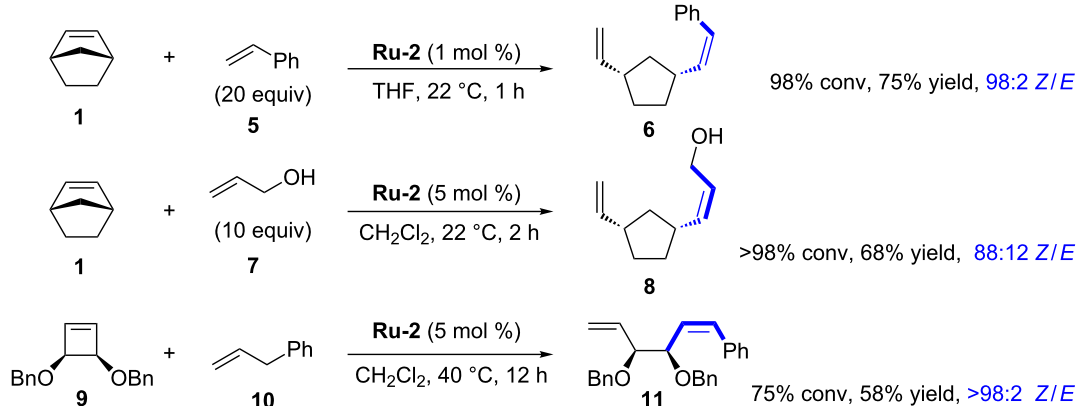
metathesis (ROCM), cross metathesis (CM), self-metathesis and ring-closing metathesis (RCM) reactions. Scheme 2 and Scheme 3 display selected examples for each of these reactions

[1]. ROMP is one of the most facile metathesis reactions, thus allowing for very low catalyst loadings (Scheme 2a). Both catalysts **Ru-1** and **Ru-2** achieved excellent selectivities and good

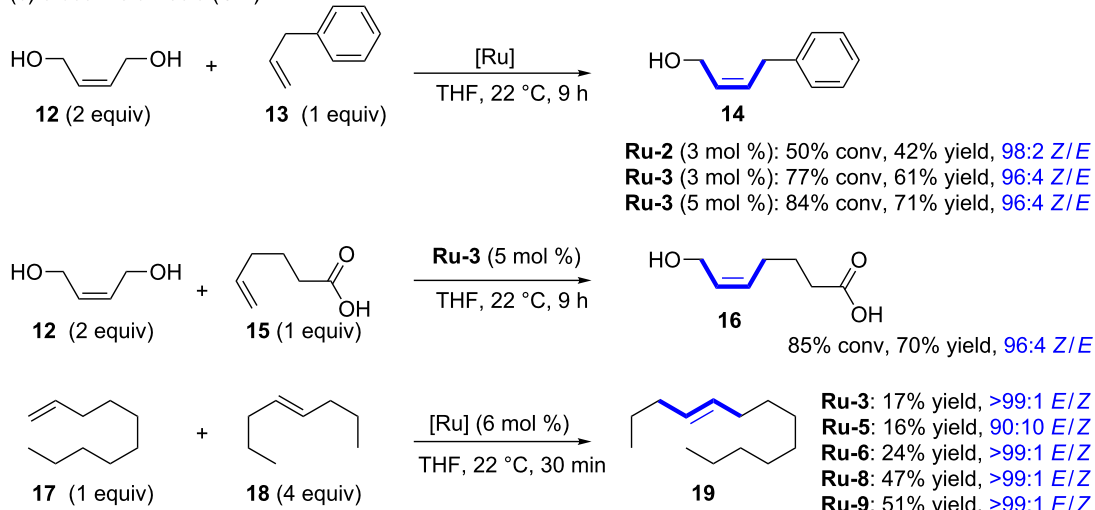
(a) ring-opening metathesis polymerization (ROMP)



(b) ring-opening/cross metathesis (ROCM)

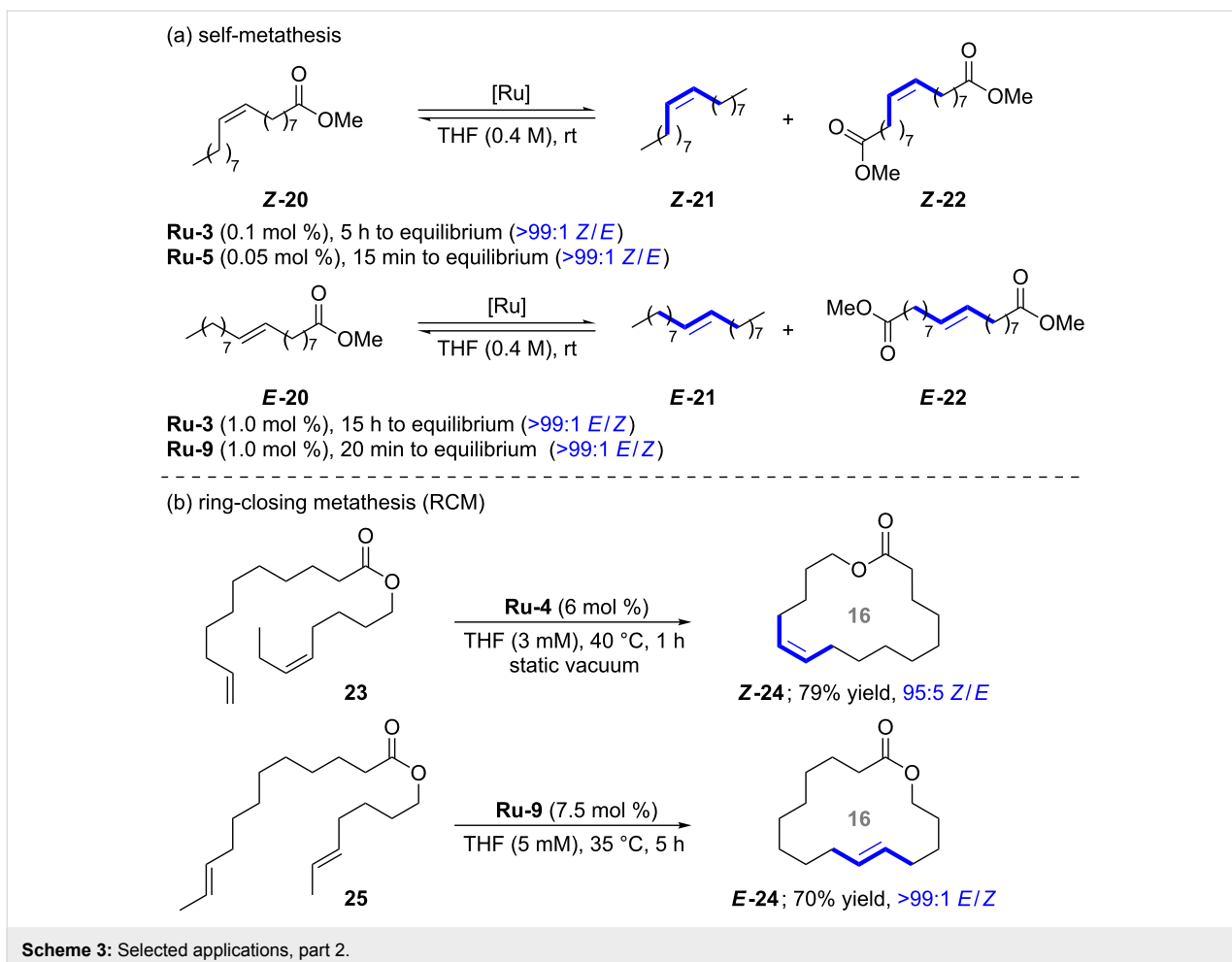


(c) cross metathesis (CM)

**Scheme 2:** Selected applications, part 1.

yields for the ROMP of norbornene (**1**) with catalyst loadings as low as 20 ppm (Scheme 2a) [2]. The ROMP of cyclooctadiene **3** was equally efficient with catalysts **Ru-1** and **Ru-2** [2]. It should be noted that the ROMP of norbornadiene was also investigated by Hoveyda [16]. A highly syndiotactic polymer was obtained by fine tuning of the steric and electronic characteristics of the catalyst (not depicted in this review) [16]. ROCM reactions of norbornene (**1**) with styrene (**5**) could be carried out

with only one mole percent of catalyst loading (Scheme 2b) [2]. Allylic alcohol (**7**) reacted cleanly with norbornene (**1**), albeit with lower stereoretention (**8**; 88:12 *Z/E*) [17]. Cyclobutenes (e.g., **9**) and cyclopropenes also delivered the corresponding products with good yields and excellent selectivity (Scheme 2b) [17]. It should also be noted that very recently Grubbs and Choi employed **Ru-3** for highly β -selective cyclopolymerization (not depicted in this review) [18]. Cross metathesis with *cis*-buten-

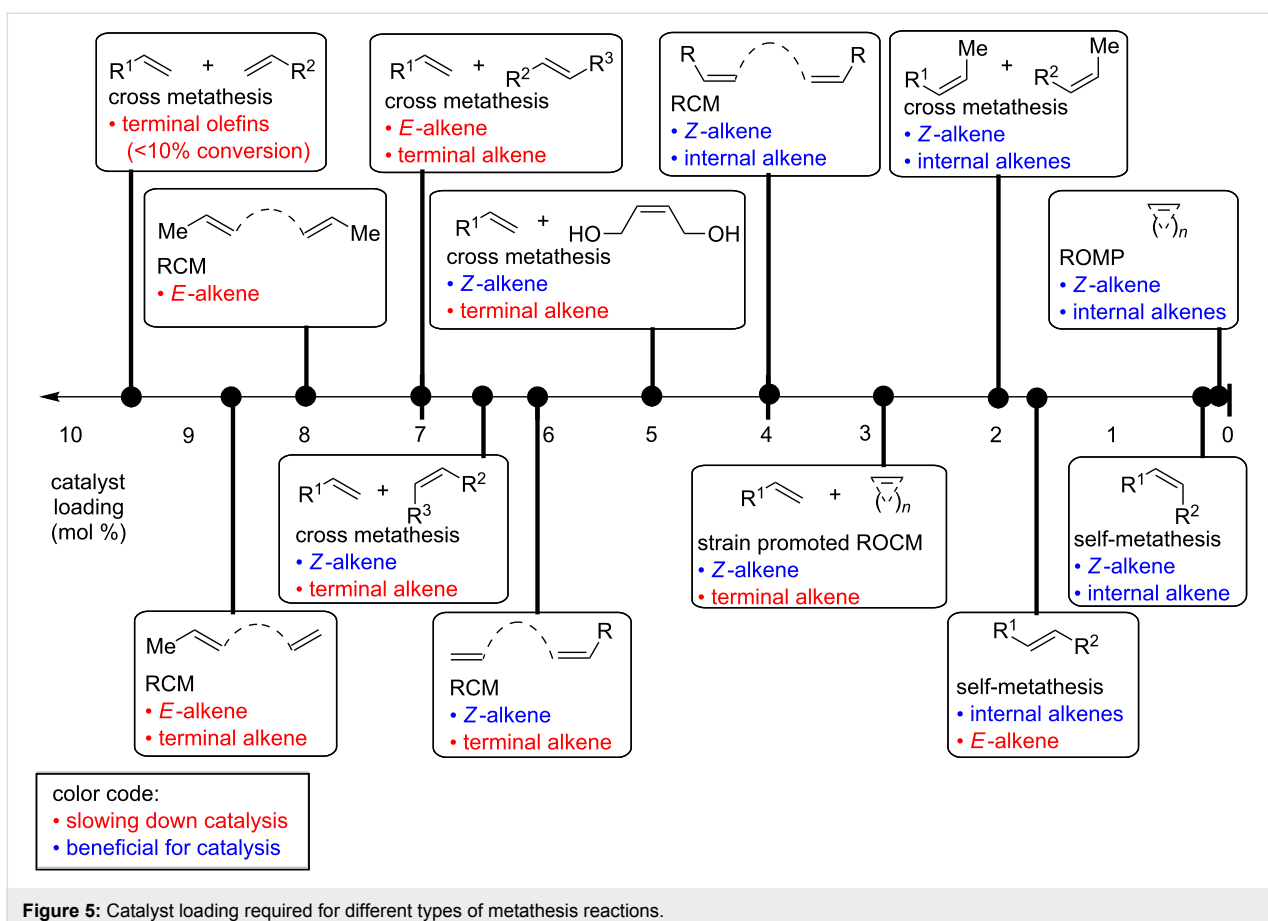


diol **12** was extensively explored by Hoveyda (Scheme 2c) [4]. The synthesis of *Z*-configured allylic alcohols is particularly attractive from the synthetic point of view. Allylic alcohols are highly versatile entities in organic chemistry and serve as starting materials in a multitude of reactions such as allylic substitutions [19]. Another advantage of this particular cross metathesis is that stereochemically pure *cis*-butenediol is commercially available and very inexpensive ($\approx 40 \text{ €/500 mL}$) [20]. Catalyst loadings of 3 to 5 mol % are typically required to obtain useful yields of the corresponding allylic alcohols. The cross metathesis with carboxylic acid **15** is particularly noteworthy as cyclometallated *Z*-selective ruthenium catalysts are inefficient in the presence of acidic functional groups [4]. More recently, Grubbs reported the cross metathesis of 1-decene (**17**) and (*E*)-4-octene (**18**) [6]. The results obtained follow the ranking displayed in Figure 1 concerning the catalyst efficiency for reactions with *E*-alkenes. In accordance with the proposed model by Pederson and Grubbs (Figure 3), sterically demanding catalyst **Ru-5** afforded a 90:10 *E/Z* mixture indicating severe steric interaction between the SiPr-NHC ligand and the β -substituent of the *E*-alkene. The most productive catalysts for the

cross metathesis with **E-18** are those with small aryl substituents on the NHC moieties (**Ru-8** and **Ru-9**).

The self-metathesis of (*Z*)- and (*E*)-methyl 9-octadecenoate (**20**) was studied by Grubbs in 2017 (Scheme 3a) [6]. The efficiency of the catalysts follows the common trend displayed in Figure 1. Catalyst **Ru-5** achieved an equilibrium with perfect selectivity at only 500 ppm of catalyst loading within 15 minutes in contrast to parent catalyst **Ru-3** that required 5 hours at higher catalyst loading. *E*-Alkenes react more sluggishly, even optimized catalyst **Ru-9** required 1 mole percent of catalyst loading to achieve equilibrium within 20 minutes. Grubbs also studied the stereoretentive RCM reaction for the synthesis of *Z*- and *E*-configured macrocycles (e.g., **24**) [14,15]. As predicted from the working model, bulky catalyst **Ru-4** performed very well for the RCM reaction with *Z*-alkene **23**, whereas the smaller catalyst **Ru-9** performed best for *E*-alkene **25**.

According to the literature Figure 5 summarizes the approximate catalyst loadings required for each type of reaction reported with dithiolate catalysts. The first determining factor



concerning the catalyst loadings is the configuration of the alkene: Z-alkenes react faster than E-alkenes and therefore require a lower catalyst loading (Figure 5). This can be easily understood by the mechanistic model proposed by Pederson and Grubbs (Figure 3). Z-Alkenes can easily approach to the catalyst via the widely open space underneath the metallacycle. In contrast, E-alkenes need to approach the catalyst in a way that the substituent above the metallacycle fits into the small open pocket; this is a less likely and slower process.

A second and even more important factor is the presence of terminal alkenes. Terminal alkenes are known to lead to catalyst degradation and therefore substrates containing terminal alkenes require high catalyst loading (see next section for details).

5 Catalyst stability

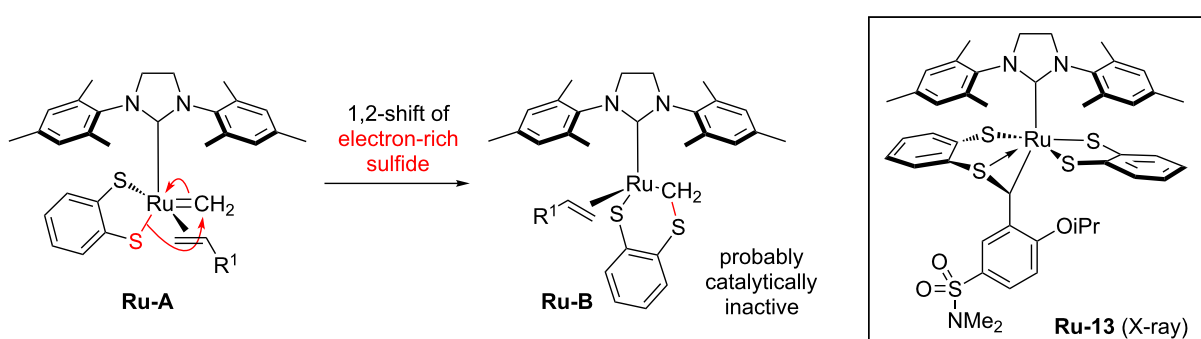
Hoveyda proposed that the catalyst degradation in the presence of terminal olefins is due to the generation of unstable methylidene-ruthenium species (Scheme 4) [4]. Terminal olefins inevitably produce ethylene which leads to the formation of methylidene-ruthenium species **Ru-A** (Scheme 4). Once complex **Ru-A** is formed, it is prone to be attacked by the electron-

rich sulfide ligand positioned opposite to the NHC ligand (*trans*-influence). This 1,2-sulfide shift generates a new ruthenium complex **Ru-B** which is probably catalytically inactive.

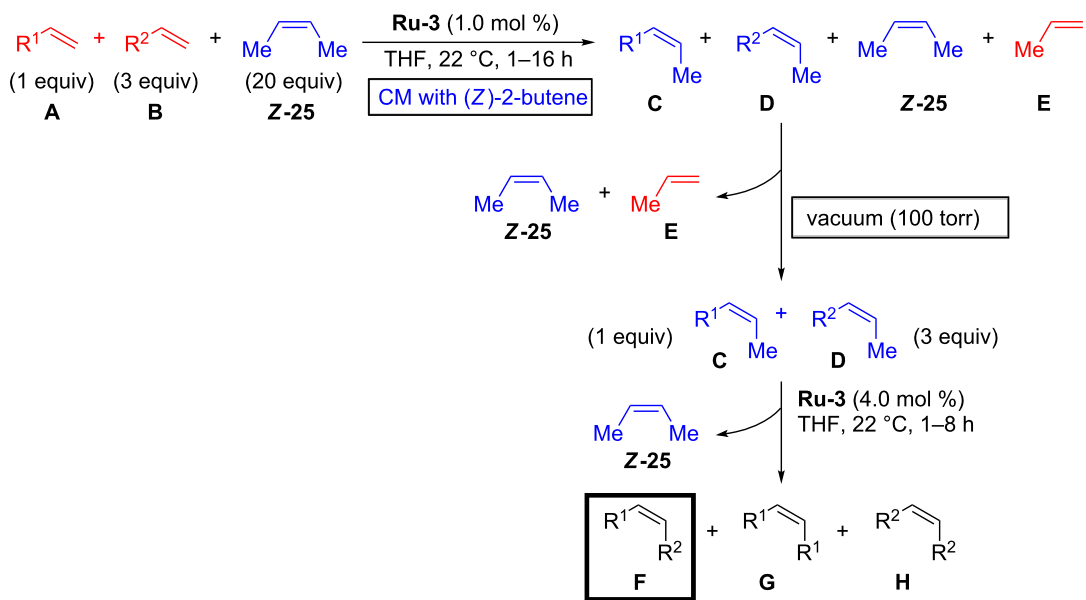
This assumption is supported by the isolation of ruthenium complex **Ru-13** which was formed by nucleophilic attack of a sulfide ligand onto the electron-poor benzylidene ligand [4]. Hoveyda reasoned that replacing the thiocatecholate ligand (**Ru-2**) by an electron-deficient dichloro catecholthiolate (**Ru-3**) should render the sulfide ligand less nucleophilic and therefore less prone for nucleophilic attack. This hypothesis gained credence by increased isolated yield for the cross metathesis of allylbenzene with *cis*-butenediol: **Ru-2** (42% yield) versus **Ru-3** (61% yield (Scheme 2c) [4].

6 The *in situ* methylene capping strategy

Experimental observations clearly indicate that terminal alkenes are detrimental for stereoretentive metathesis reactions with ruthenium dithiolate catalysts. In 2017 Hoveyda proposed the *in situ* methylene capping strategy as a solution to this problem [21]. The trick is to transform *in situ* the terminal olefins **A** and **B** into methylene capped olefins **C** and **D** by applying a large excess of (Z)-2-butene (**Z-25**, Scheme 5). (Z)-2-butene (**Z-25**)



Scheme 4: Proposed catalyst decomposition pathway occurring via attack of the electron-rich sulfide into methyldiene ruthenium complex.



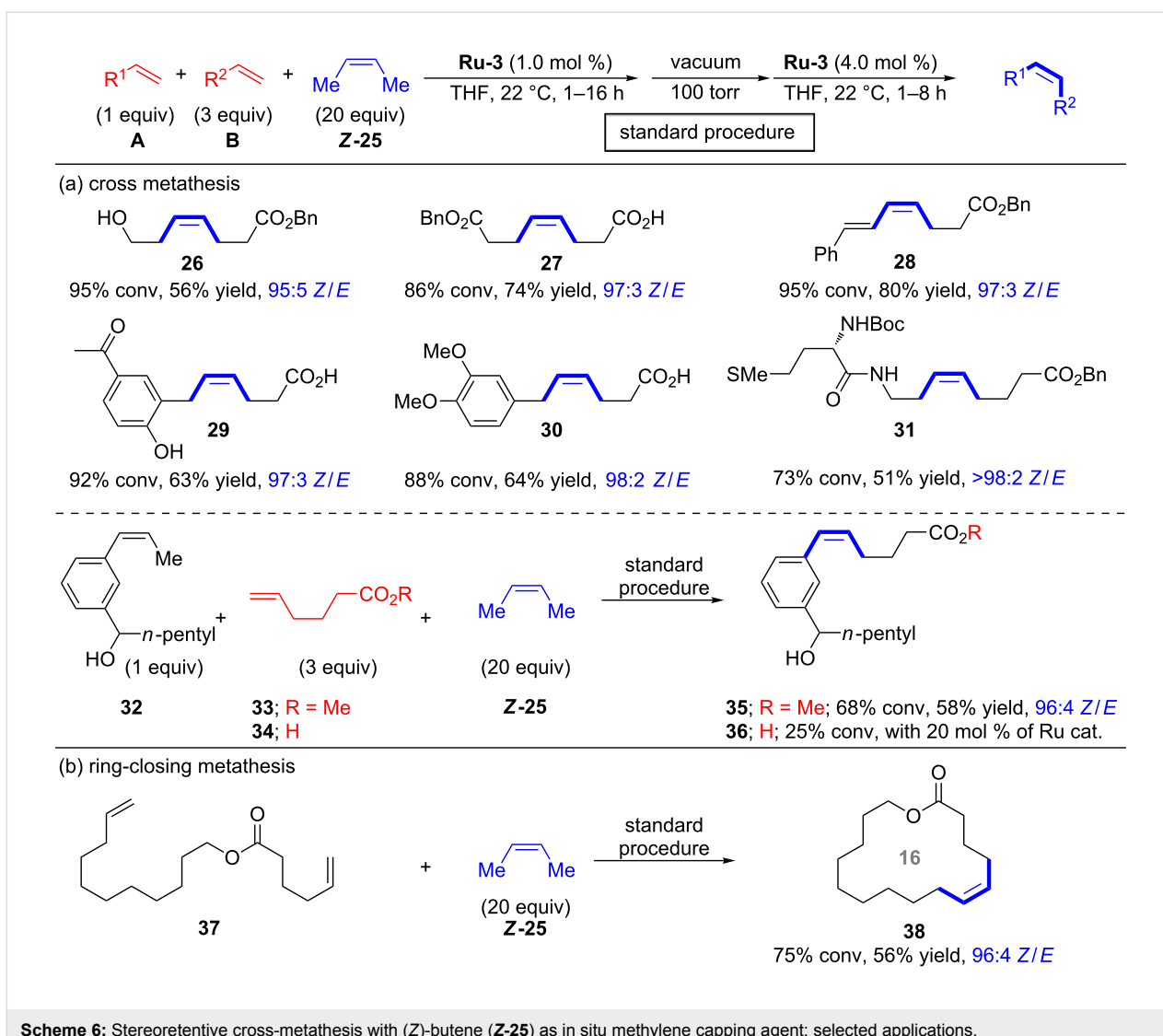
Scheme 5: In situ methylene capping strategy for stereoretention metathesis.

and propene **E** are then removed in vacuo (100 Torr) and a new portion of catalyst is added for the cross metathesis of **C** and **D** to give desired product **F** with excellent stereoisomeric purity along with side products **G** and **H** which require chromatographic removal. A major drawback of this strategy is that (Z)-2-butene (**Z-25**) is not commercially available in many countries (e.g., in Europe).

Selected applications of the in situ methylene capping strategy

Hoveyda and co-workers first applied the methylene capping strategy to cross-metathesis reactions (Scheme 6a) [21]. Almost 20 examples were isolated in modest to good yields and with excellent stereoisomeric purity. To assure high conversion in cross-metathesis reactions a 1:3 ratio of **A/B** was applied. Prac-

tical limitations are that **A** and **B** have to be of significantly different polarity for easy column chromatographic separation and that sterically hindered olefins are not tolerated. For some alkenes, e.g., styrenes, the homodimerization is too fast leading to stilbene formation. Replacing styrenes by (Z)- β -methylstyrenes (e.g., **32**) allowed for successful reactions with methyl ester **33** (Scheme 6a). Hoveyda noted that carboxylic acids (e.g., **34**) are not suitable cross-metathesis partners for (Z)- β -methylstyrenes. Hoveyda reasoned that with the sluggishly reacting styrene **32** the protonation and loss of the catecholthiolate ligand by Brønsted acid **34** is a faster process leading to catalyst degradation. It should be noted that stereoretention CM and RCM with (*E*)-2-butene (**E-25**) as capping reagent were also reported, however, these reactions required a significantly higher catalyst loading (10.0–12.5 mol %) [21]. Macrocyclic



Scheme 6: Stereoretentive cross-metathesis with (Z)-butene (**Z-25**) as in situ methylene capping agent; selected applications.

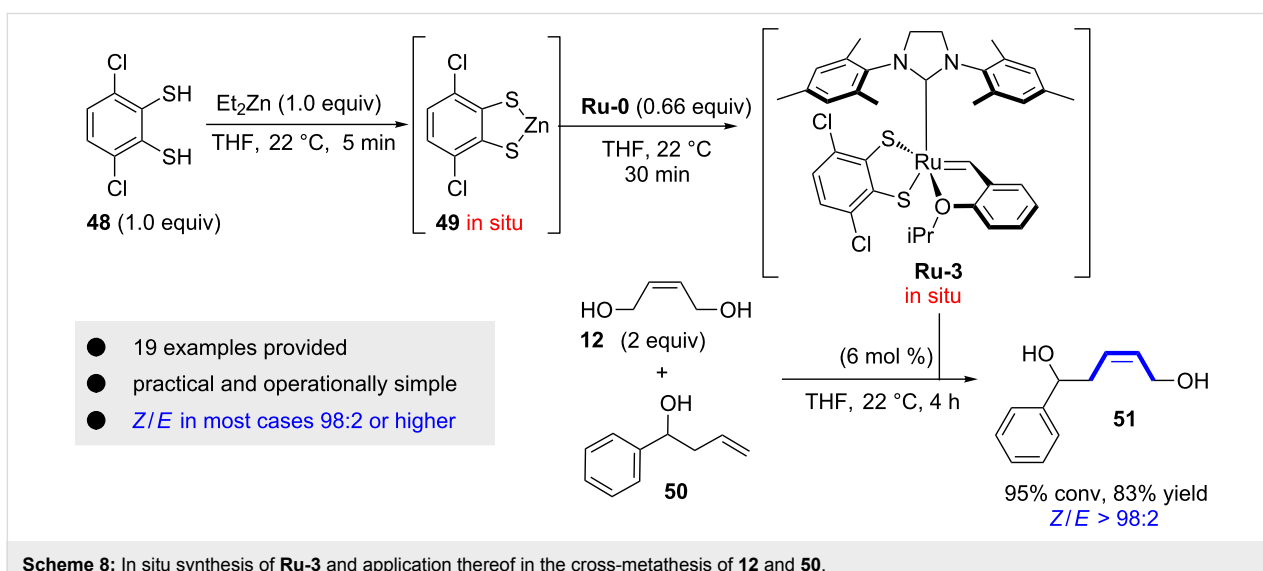
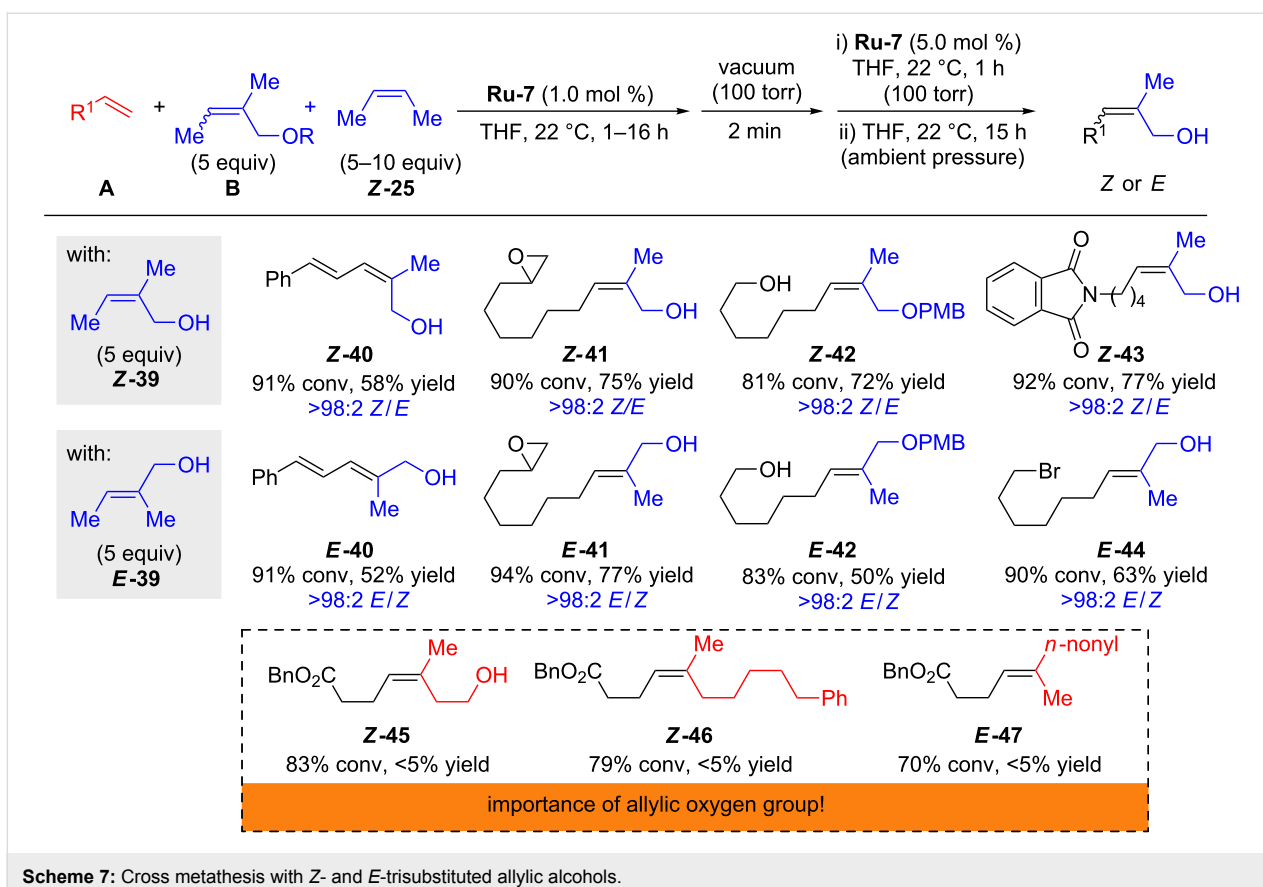
ring-closing metathesis (RCM) with (Z)-butene (**Z-25**) was also studied affording 14–21-membered macrocycles (e.g., **38**) in good yield and high stereoretention (Scheme 6b).

More recently Hoveyda disclosed his findings concerning the synthesis of *Z*- or *E*-trisubstituted allylic alcohols with ruthenium dithiolate catalysts (Scheme 7) [22]. In agreement with the proposed model (Figure 3), **Ru-7** was significantly more efficient compared to **Ru-3**. The reason for the higher reactivity of *E*-stereoretentive catalysts with trisubstituted substrates was previously discussed in the section "Mechanistic models". Cross metathesis utilizing the in situ methylene capping strategy with 1,1-disubstituted allylic alcohols **Z-39** or **E-39** afforded the products **40–42** in good yield and with excellent retention of stereochemistry independent of the configuration of the allylic alcohol. Allylic oxygen atoms often have an activating effect in metathesis [23]. This was confirmed by Hoveyda for stereore-

tentive metathesis by exposing homoallylic alcohol (product **Z-45**) and alkyl containing metathesis partners (products **Z-46** and **E-47**) to standard reaction conditions [22]. All the reactions were inefficient emphasizing the importance of an allylic alcohol, ether or acetate group.

7 The in situ catalyst synthesis strategy

Very recently, our group developed an in situ synthesis of dithiolate catalysts with the aim to avoid tedious isolation of Ru-dithiolate catalysts and to render this class of catalyst available to every practicing chemist [25]. A very practical and operationally simple protocol for the in situ generation of Ru-dithiolate catalysts was reported. First, the commercially available dithiol **48** is deprotonated with Et₂Zn to provide Zn-dithiolate **49** (Scheme 8). Then Hoveyda–Grubbs catalyst **Ru-0** is added to generate after another 30 minutes a solution of the desired catalyst **Ru-3**. Finally, the ruthenium stock solution of **Ru-3** is



added to the alkene starting material (e.g., for the cross metathesis of **12** and **50**) to give the product in high yields and excellent stereochemical purity. We applied the in situ generated catalyst to several reactions including cross metathesis, self-metathesis and RCM reactions. The selectivities are in general very high ($Z/E = 98:2$ or higher).

8 Applications in the synthesis of biologically active compounds

Several biologically active compounds, fragrance molecules and natural products were synthesized utilizing stereoretentive metathesis based on Ru-dithiolate catalysts, for example (+)-neopeltolide (**53**, Figure 6) [24]. For each of the examples

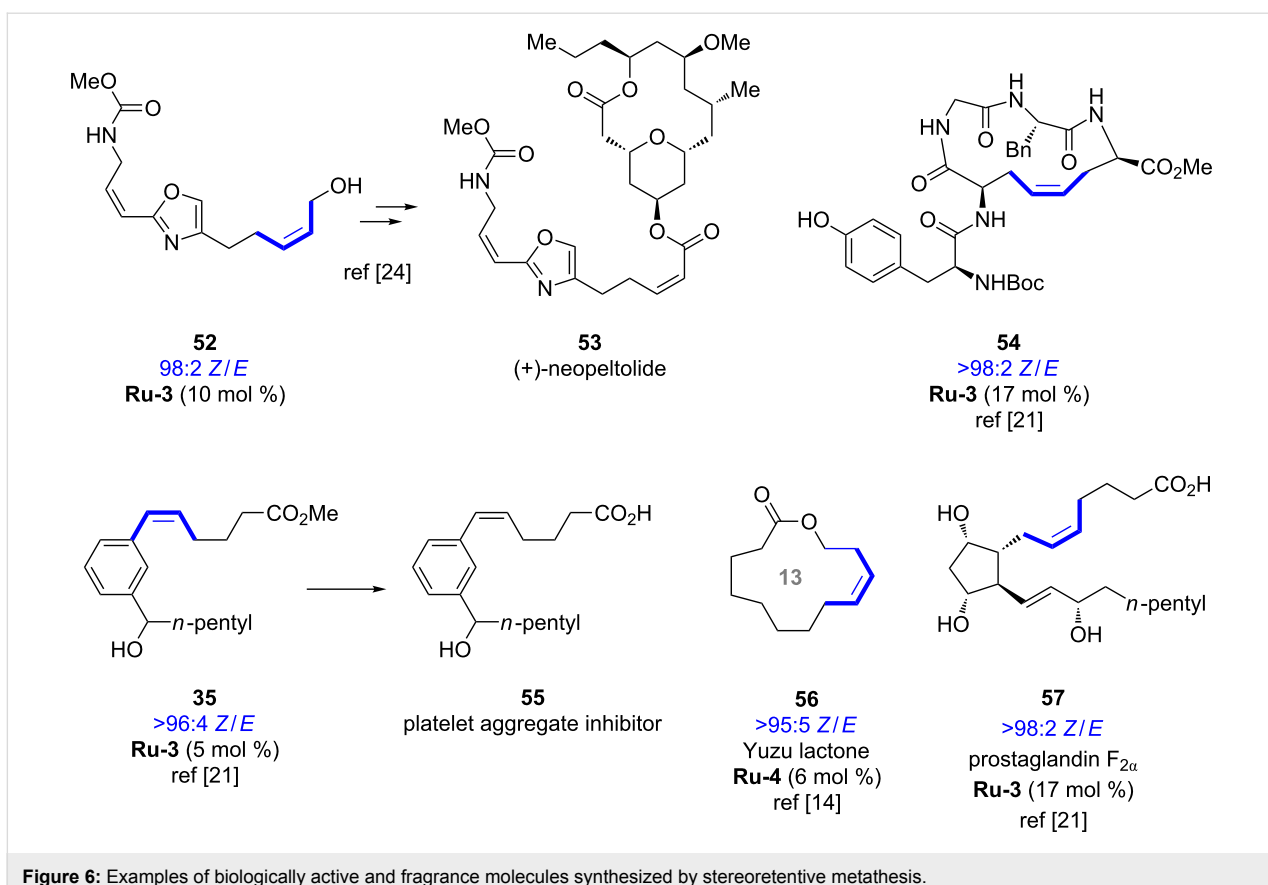


Figure 6: Examples of biologically active and fragrance molecules synthesized by stereoretention metathesis.

the catalyst loading of the Ru-dithiolate catalyst which was required to forge the corresponding *Z*-olefin is indicated. Given the high stereoisomeric purity of the obtained products we can expect many other examples to be reported in the near future.

Conclusion

Within only a few years the field of stereoretention metathesis using ruthenium dithiolate catalysts has attained a remarkable level of maturity. The fast development in this field is due to the complementary contributions of the Hoveyda and Grubbs groups who developed a set of general and highly stereoretention Ru-dithiolate catalysts. A major limitation at the moment is that the *Z*-stereoretention method is much more efficient and practical compared to stereoretention methods for *E*-alkenes. Certainly making the precursors of **Ru-6**, **Ru-7**, **Ru-8** and **Ru-9** commercially available would significantly help to further promote *E*-stereoretention metathesis. Nevertheless, it can be stated that the field has come a long way compared to where it was 5 years ago and certainly further important improvements will be reported in the near future.

Acknowledgements

This work was supported by the FASO (grant to DSM; Z-SELECT) and the Région Bretagne (SAD 2016 N° 9639 –

RZSELECT; grant to DSM). OB and MM acknowledge the Ecole Nationale Supérieure de Chimie de Rennes (ENSCR) and the Centre National de la Recherche Scientifique (CNRS) for financial support.

ORCID® IDs

Daniel S. Müller - <https://orcid.org/0000-0001-8184-1474>
 Olivier Baslé - <https://orcid.org/0000-0002-4551-473X>
 Marc Mauduit - <https://orcid.org/0000-0002-7080-9708>

References

- Montgomery, T. P.; Ahmed, T. S.; Grubbs, R. H. *Angew. Chem., Int. Ed.* **2017**, *56*, 11024–11036. doi:10.1002/anie.201704686
- Khan, R. K. M.; Torker, S.; Hoveyda, A. H. *J. Am. Chem. Soc.* **2013**, *135*, 10258–10261. doi:10.1021/ja404208a
- Johns, A. M.; Ahmed, T. S.; Jackson, B. W.; Grubbs, R. H.; Pederson, R. L. *Org. Lett.* **2016**, *18*, 772–775. doi:10.1021/acs.orglett.6b00031
- Koh, M. J.; Khan, R. K. M.; Torker, S.; Yu, M.; Mikus, M. S.; Hoveyda, A. H. *Nature* **2015**, *517*, 181–186. doi:10.1038/nature14061
- Wakamatsu, H.; Blechert, S. *Angew. Chem., Int. Ed.* **2002**, *41*, 2403–2405. doi:10.1002/1521-3773(20020703)41:13<2403::aid-anie2403>3.0.co;2-f

6. Ahmed, T. S.; Grubbs, R. H. *J. Am. Chem. Soc.* **2017**, *139*, 1532–1537. doi:10.1021/jacs.6b11330
7. Only Ru-catalyst precursors for **Ru-2**, **Ru-3** and **Ru-4** are commercially available. Hoveyda-Grubbs catalyst (CAS: 301224-40-8) and Grubbs catalyst C711TM (CAS: 635679-24-2).
8. Torker, S.; Khan, R. K. M.; Hoveyda, A. H. *J. Am. Chem. Soc.* **2014**, *136*, 3439–3455. doi:10.1021/ja410606b
9. Khan, R. K. M.; Torker, S.; Hoveyda, A. H. *J. Am. Chem. Soc.* **2014**, *136*, 14337–14340. doi:10.1021/ja505961z
10. Mikus, M. S.; Torker, S.; Xu, C.; Li, B.; Hoveyda, A. H. *Organometallics* **2016**, *35*, 3878–3892. doi:10.1021/acs.organomet.6b00773
11. Montgomery, T. P.; Grandner, J. M.; Houk, K. N.; Grubbs, R. H. *Organometallics* **2017**, *36*, 3940–3953. doi:10.1021/acs.organomet.7b00555
12. Dumas, A.; Müller, D. S.; Curbet, I.; Toupet, L.; Rouen, M.; Baslé, O.; Mauduit, M. *Organometallics* **2018**, *37*, 829–834. doi:10.1021/acs.organomet.7b00836
13. Grandner, J. M.; Shao, H.; Grubbs, R. H.; Liu, P.; Houk, K. N. *J. Org. Chem.* **2017**, *82*, 10595–10600. doi:10.1021/acs.joc.7b02129
14. Ahmed, T. S.; Grubbs, R. H. *Angew. Chem., Int. Ed.* **2017**, *56*, 11213–11216. doi:10.1002/anie.201704670
15. Ahmed, T. S.; Montgomery, T. P.; Grubbs, R. H. *Chem. Sci.* **2018**, *9*, 3580–3583. doi:10.1039/c8sc00435h
16. Mikus, M. S.; Torker, S.; Hoveyda, A. H. *Angew. Chem., Int. Ed.* **2016**, *55*, 4997–5002. doi:10.1002/anie.201601004
17. Koh, M. J.; Khan, R. K. M.; Torker, S.; Hoveyda, A. H. *Angew. Chem., Int. Ed.* **2014**, *53*, 1968–1972. doi:10.1002/anie.201309430
18. Jung, K.; Kim, K.; Sung, J.-C.; Ahmed, T. S.; Hong, S. H.; Grubbs, R. H.; Choi, T.-L. *Macromolecules* **2018**, *51*, 4564–4571. doi:10.1021/acs.macromol.8b00969
19. Butt, N. A.; Zhang, W. *Chem. Soc. Rev.* **2015**, *44*, 7929–7967. doi:10.1039/c5cs00144g
20. Acros OrganicsTM (2018) 40.90 € / 500 mL.
21. Xu, C.; Shen, X.; Hoveyda, A. H. *J. Am. Chem. Soc.* **2017**, *139*, 10919–10928. doi:10.1021/jacs.7b06552
22. Xu, C.; Liu, Z.; Torker, S.; Shen, X.; Xu, D.; Hoveyda, A. H. *J. Am. Chem. Soc.* **2017**, *139*, 15640–15643. doi:10.1021/jacs.7b10010
23. Lin, Y. A.; Davis, B. G. *Beilstein J. Org. Chem.* **2010**, *6*, 1219–1228. doi:10.3762/bjoc.6.140
24. Yu, M.; Schrock, R. R.; Hoveyda, A. H. *Angew. Chem., Int. Ed.* **2015**, *54*, 215–220. doi:10.1002/anie.201409120
25. Müller, D. S.; Curbet, I.; Raoul, Y.; Le Nôtre, J.; Baslé, O.; Mauduit, M. *Org. Lett.* **2018**, *20*, 6822–6826. doi:10.1021/acs.orglett.8b02943

License and Terms

This is an Open Access article under the terms of the Creative Commons Attribution License (<http://creativecommons.org/licenses/by/4.0>). Please note that the reuse, redistribution and reproduction in particular requires that the authors and source are credited.

The license is subject to the *Beilstein Journal of Organic Chemistry* terms and conditions: (<https://www.beilstein-journals.org/bjoc>)

The definitive version of this article is the electronic one which can be found at:
doi:10.3762/bjoc.14.279



Cross metathesis-mediated synthesis of hydroxamic acid derivatives

Shital Kumar Chattopadhyay*, Subhankar Ghosh and Suman Sil

Full Research Paper

Open Access

Address:
Department of Chemistry, University of Kalyani, Kalyani - 741235,
West Bengal, India, Fax: +91+33+25828282

Beilstein J. Org. Chem. **2018**, *14*, 3070–3075.
doi:10.3762/bjoc.14.285

Email:
Shital Kumar Chattopadhyay* - skchatto@yahoo.com

Received: 01 August 2018
Accepted: 29 November 2018
Published: 17 December 2018

* Corresponding author

This article is part of the thematic issue "Progress in metathesis chemistry III".

Keywords:
α-amino acid; catalysis; cross metathesis; hydroxamates

Guest Editors: K. Grela and A. Kajetanowicz

© 2018 Chattopadhyay et al.; licensee Beilstein-Institut.
License and terms: see end of document.

Abstract

An alternative synthesis of α,β -unsaturated hydroxamates via cross metathesis between a class-I olefin and *N*-benzyloxyacrylamide is reported. The reaction proceeds better in the presence of Grubbs' second generation catalyst within short time and in good yields (57–85%) with a range of substrates. Subsequent hydrogenation of each of the CM products delivers the title compounds in moderate to very good yield (70–89%). An important demonstration of the protocol is the preparation of the unusual amino acid component of the bioactive cyclic peptide Chap-31.

Introduction

Cross-metathesis reactions (CM) have rapidly grown [1-3] to be a reliable method for the preparation of functionalized alkenes and derivatives thereof. Intricacies regarding the electronic nature of olefins, their substitution patterns and steric demands are more or less settled through the works of many workers in many reports [4-7]. Yet, a number of new reports describing the CM-mediated synthesis of functionalized alkenes of various kinds continue to appear. For example, cross metathesis with acrylates [8-10], α,β -unsaturated acid chlorides [11], acrylamides [12-14], vinyl sulfones [15], vinylphosphine oxides [16], vinyl phosphonates [17], enones [18], and nitrile functionalities [19,20] have been shown to yield shorter routes to com-

pounds of interest as well as for green chemical applications [21,22].

Hydroxamates belong to a class of valuable biologically relevant compounds of proven record of utility. For example, the hydroxamate SAHA (**1**, Figure 1) [23] and the didehydrohydroxamate TSA (**2**) [24], display useful anticancer properties through inhibition of histone deacetylase enzymes (HDAC) and are used as FDA-approved drugs. Similarly, the cyclic peptide Chap-31 (**3**) [25] with a terminal hydroxamic acid residue has shown promising anticancer activity. Access to such derivatives usually involves the preparation of the corresponding acid

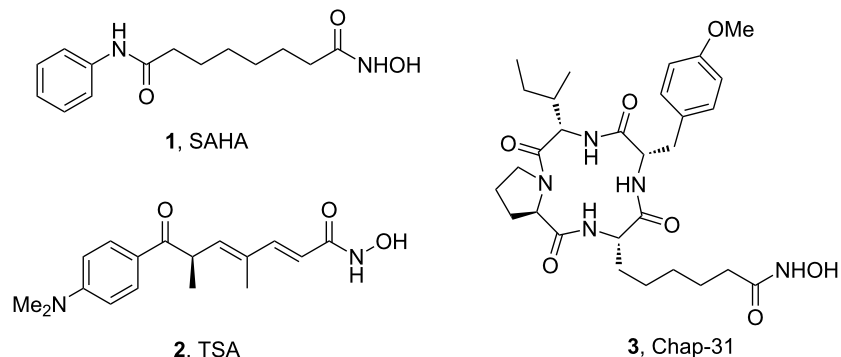


Figure 1: Some bioactive molecules containing hydroxamate functionality.

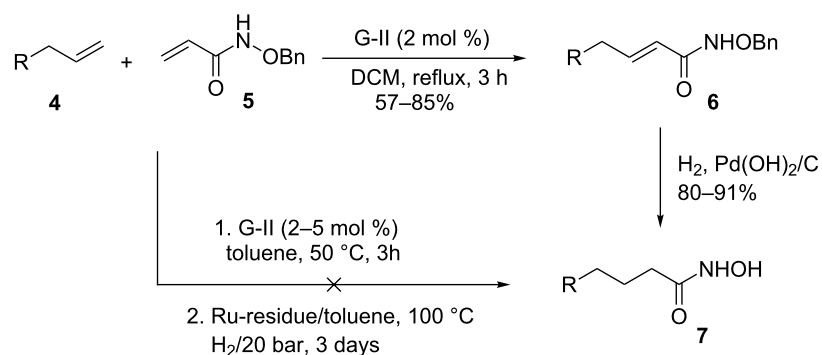
and subsequent amide bond formation with hydroxylamines. Although this two-step protocol is widely used, a direct access to α,β -unsaturated and saturated hydroxamates from cross metathesis of alkenes may prove to be of advantage. In continuation of our earlier studies [26,27] on HDAC inhibitors, we herein report a direct access to α,β -unsaturated hydroxamates through cross-metathesis reaction.

Results and Discussion

It is known that a CM reaction between a class-I olefin and a class-II olefin proceeds better in the presence of 2nd generation catalysts. Accordingly, CM between 1-decene (**4**, R = C₇H₁₅) and *N*-benzyloxyacrylamide **5** (Scheme 1) was attempted with Grubbs' second generation catalyst [(1,3-bis(2,4,6-trimethylphenyl)-2-imidazolidinylidene)dichloro(phenylmethylene) (tricyclohexylphosphine)ruthenium, G-II]. After some experimentation, it was found that the reaction proceeds quickly in refluxing dichloromethane to provide the CM product **6** (R = C₇H₁₅) in 81% yield. The yield of **6** was improved to 84% when Hoveyda–Grubbs 2nd generation catalyst [1,3-bis-(2,4,6-trimethylphenyl)-2-imidazolidinylidene]dichloro(*o*-isopropoxy-

phenylmethylene)ruthenium] (HG-II) was used under identical conditions. Hydrogenation of the later in the presence of Pd(OH)₂/C proceeded uneventfully resulting in the saturation of the double bond as well as concomitant deprotection of the *O*-benzyl group. The one-pot CM-hydrogenation sequence using the same ruthenium catalyst has recently found applications [28–30]. However, similar attempts in our case, i.e., direct conversion of **4** + **5** → **7** proved to be problematic and conversion to the desired product was not observed under the attempted conditions. An intractable mixture of compounds was the result.

Having established the conditions for stepwise CM and hydrogenation reactions, we extended the study to other substrates (Table 1). For example, the yields of the two steps for dodecene forming **6b** and **7b** were more or less similar with those for decene when either of the 2nd-generation catalysts was used. However, analogous reaction with bromobutene **4c** as CM partner proceeded with some compromise in yield with G-II. Moreover, HG-II in this case proved to be less successful. Similarly, the allylbenzene derivatives **4d–f** reacted with more or



Scheme 1: Cross metathesis between a class-I alkene and *N*-benzyloxyacryl amide.

Table 1: Hydroxamates prepared.

Entry	Alkene 4	CM product 6 (% yield)	reduction product 7 (% yield)
1		 6a (81)	 7a (85)
2		 6b (85)	 7b (83)
3		 6c (72)	 7c (70)
4		 6d (77)	 7d (89)
5		 6e (72)	 7e (85)
6		 6f (78)	 7f (80)
7		 6g (57)	 7g (83)
8		 6h (79)	 7h (81)
9		 6i (73)	 7i (78)
10		 6j (70)	 7j (75)
11		 6k (78)	 7k (86)
12		 6l (78)	 7l (84)

less similar ease with G-II to produce the corresponding CM products **6d–f**, respectively. Considerable isomerization (1:1 by ¹H NMR) of the CM-product **6d** to the corresponding styrene derivative was noticed when HG-II was used in place of G-II. **6e** behaved similarly. Reaction with the styrene derivative **4g** resulted in low conversion to the CM product **6g** (57%). Styrene derivatives, belonging to class-I olefins according to Grubbs' generalizations [31], are indeed known to be a sluggish partner in CM reactions, with homodimerization to stilbene being a recurring problem.

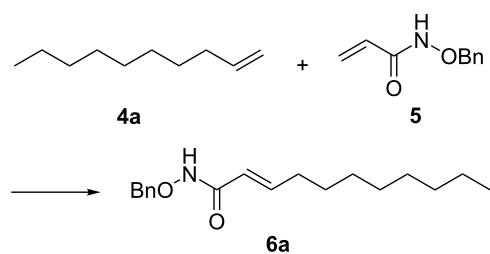
Alkenes **4h–j** containing a benzyl ester functionality at two, three and four carbons apart, respectively, participated in the reaction nearly equally well to give the corresponding CM products **6h–j**. Hydrogenation of each of these compounds separately led to the corresponding saturated hydroxamic acid derivatives **7h–j** with concommittant cleavage of the terminal benzyl ester functionality. In an extension to the synthesis of the unusual amino acid component of the important anticancer cyclic peptide compound Chap-31, we attempted the cross-metathesis reaction of *N*-benzyloxyacryl amide **5** with the homoallylglycine derivative **4k** (Table 1, entry 11) and the bis-homoallyl glycine derivative **4l** (Table 1, entry 12) [32], separately. Fortunately, both the reactions proceeded well and the desired amino acid derivatives **7k** and **7l** were obtained in good yields after hydrogenation.

Conclusion

In conclusion, we have developed a direct access to functionalized hydroxamic acid derivatives using a cross-metathesis reaction between *N*-benzyloxyacrylamide and a range of terminal alkenes. The products include hydroxamic acid derivatives with a long alkyl chain, aromatic and heteroaromatic cores, halogen residue, carboxylic acid moiety at the terminal relevant position for drug discovery. Moreover, an alternate preparation of the amino acid component of the important cyclic peptide Chap-31 may encourage the preparation of cyclic peptide based HDAC inhibitors. The developed methodology may hence complement the existing literature on the preparation of such class of compounds and may find applications.

Experimental

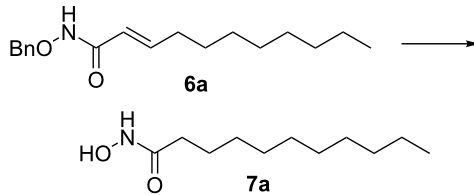
General procedure for cross metathesis



Grubbs' second generation catalyst G-II (10 mg, 2 mol %), was added to a stirred solution of the olefin **4a** (158 mg, 1.13 mmol), and olefin **5** (100 mg, 0.56 mmol), in anhydrous and degassed CH_2Cl_2 (3 mL) at rt and the reaction mixture was heated to reflux for 6 h under argon atmosphere. The reaction mixture was allowed to cool to room temperature and then concentrated in vacuo. The residue was purified by column chromatography on silica gel (hexane/ethyl acetate 60:40) to provide the CM product (*E*)-*N*-benzyloxyundec-2-enamide (**6a**, 133 mg, 81%) as a colourless viscous liquid.

IR (neat): 3183, 3064, 2926, 2855, 1669, 1683 cm^{-1} ; ¹H NMR (400 MHz, $\text{DMSO}-d_6$) δ 11.15 (s, 1H, NH), 7.38–7.29 (m, 5H, ArH), 6.74–6.67 (m, 1H, C3-H), 5.72 (d, J = 15.2 Hz, 1H, C2-H), 4.80 (s, 2H, OCH_2 -), 2.08 (q, J = 6.8 Hz, 2H, C4-H), 1.33 (brs, 3H, CH_2), 1.12 (s, 12H, CH_2), 0.81 (t, J = 6.8 Hz, 3H, C11-H3); ¹³C NMR (100 MHz, $\text{DMSO}-d_6$) δ 163.4 (CO), 144.3 (C3), 136.4 (ArC), 129.2 (ArCH), 128.7 (ArCH), 121.1 (C2), 77.4 (OCH_2), 31.8 (C4), 31.7 (C5), 29.3 (CH_2), 29.1 (CH_2), 29.0 (CH_2), 28.2 (CH_2), 22.6 (CH_2), 14.3 (C11); HRMS (TOF MS ES^+) m/z : [M + Na]⁺ calcd for $\text{C}_{18}\text{H}_{27}\text{NNaO}_2$, 312.1939; found, 312.1956.

General procedure for hydrogenation



CM product **6a** (50 mg, 0.17 mmol) was taken in a MeOH (3 mL) containing 1 drop of TFA [33]. Then $\text{Pd}(\text{OH})_2$ (10 mg) was added and the solution was degassed several times. Hydrogen gas was let in and the resulting heterogeneous mixture was vigorously stirred at atmospheric pressure for 2 h. It was filtered through Celite, the filter cake was washed with methanol (5 mL) and the combined filtrate was concentrated in vacuo. The residue was purified by column chromatography on silica gel ($\text{CHCl}_3/\text{MeOH}$ 97:3) to provide the product *N*-hydroxyundecanamide **7a** (85%) as a colorless solid.

Mp 85 °C; IR (neat): 3259, 3058, 2956, 1663, 1624 cm^{-1} ; ¹H NMR (400 MHz, $\text{DMSO}-d_6$) δ 10.52 (s, 1H, NH), 8.93 (brs, 1H, OH), 1.92 (t, J = 7.2 Hz, 2H, C2-H), 1.44 (m, 2H, C3-H), 1.19 (s, 14H, 7 \times CH_2), 0.81 (t, J = 6.8 Hz, 3H, C11-H); ¹³C NMR (100 MHz, $\text{DMSO}-d_6$) δ 170.4 (CO), 32.6 (C2), 31.6 (C3), 29.3 (CH_2), 29.3 (CH_2), 29.1 (CH_2), 28.9 (CH_2), 25.5 (CH_2), 22.5 (CH_2), 14.3 (C11); HRMS (TOF MS ES^+) m/z : [M + Na]⁺ calcd for $\text{C}_{11}\text{H}_{23}\text{NNaO}_2$, 224.1626; found, 224.1638.

Supporting Information

Supporting Information File 1

Analytical data of all new compounds as well as copies of their ^1H and ^{13}C NMR spectra.

[<https://www.beilstein-journals.org/bjoc/content/supplementary/1860-5397-14-285-S1.pdf>]

Acknowledgements

We are thankful to DST New Delhi, for funds (EMR/2017/001336), and University of Kalyani for assistance.

References

- O'Leary, D. J.; O'Neil, G. W. Cross-Metathesis. In *Handbook of Metathesis*; Grubbs, R. H.; Wenzel, A. G.; O'Leary, D. J.; Khosravi, E., Eds.; Wiley-VCH Verlag GmbH & Co. KGaA: Weinheim, Germany, 2015; Vol. 2, pp 171–294. doi:10.1002/9783527674107.ch16
- Zukowska, K.; Grela, K. In *Comprehensive Organic Synthesis*, 2nd ed.; Knochel, P.; Molander, G. A., Eds.; Elsevier: Amsterdam, Netherlands, 2014; Vol. 5, pp 1257–1301. doi:10.1016/b978-0-08-097742-3.00527-9
- Connon, S. J.; Blechert, S. *Angew. Chem., Int. Ed.* **2003**, *42*, 1900–1923. doi:10.1002/anie.200200556
- Zukowska, K.; Grela, K. Cross Metathesis. In *Olefin Metathesis-Theory and Practice*; Grela, K., Ed.; John Wiley and Sons: Hoboken, NJ, USA, 2014; pp 37–83. doi:10.1002/9781118711613.ch2
- Chatterjee, A. K. Olefin Cross-Metathesis. In *Handbook of Metathesis: Catalyst Development*, 1st ed.; Grubbs, R. H., Ed.; Wiley-VCH Verlag GmbH: Weinheim, Germany, 2003; Vol. 10, pp 246–295. doi:10.1002/9783527619481.ch20
- Montgomery, T. P.; Johns, A. M.; Grubbs, R. H. *Catalysts* **2017**, *7*, 87. doi:10.3390/catal7030087
- Ogba, O. M.; Warner, N. C.; O'Leary, D. J.; Grubbs, R. H. *Chem. Soc. Rev.* **2018**, *47*, 4510–4544. doi:10.1039/c8cs00027a
- Yu, E. C.; Johnson, B. M.; Townsend, E. M.; Schrock, R. R.; Hoveyda, A. H. *Angew. Chem., Int. Ed.* **2016**, *55*, 13210–13214. doi:10.1002/anie.201608087
See for a recent reference.
- Biermann, U.; Meier, M. A. R.; Butte, W.; Metzger, J. O. *Eur. J. Lipid Sci. Technol.* **2011**, *113*, 39–45. doi:10.1002/ejlt.201000109
- Bailey, G. A.; Fogg, D. E. *J. Am. Chem. Soc.* **2015**, *137*, 7318–7321. doi:10.1021/jacs.5b04524
- Fernié, L.; Bouzbouz, S.; Cossy, J. *Org. Lett.* **2009**, *11*, 5446–5448. doi:10.1021/ol9021386
- Choi, T.-L.; Chatterjee, A. K.; Grubbs, R. H. *Angew. Chem., Int. Ed.* **2001**, *40*, 1277–1279. doi:10.1002/1521-3773(20010401)40:7<1277::aid-anie1277>3.0.co;2-e
- Guan, J.; Hachey, M.; Puri, L.; Howieson, V.; Saliba, K. J.; Auclair, K. *Beilstein J. Org. Chem.* **2016**, *12*, 963–968. doi:10.3762/bjoc.12.95
See for a recent report of CM with *N*-alkylated acrylamides.
- Boufroura, H.; Mauduit, M.; Drège, E.; Joseph, D. *J. Org. Chem.* **2013**, *78*, 2346–2354. doi:10.1021/jo302435a
See for CM with Weinreb's amide.
- Michrowska, A.; Bieniek, M.; Kim, M.; Klajn, R.; Grela, K. *Tetrahedron* **2003**, *59*, 4525–4531. doi:10.1016/s0040-4020(03)00682-3
- Demchuk, O. M.; Pietrusiewicz, K. M.; Michrowska, A.; Grela, K. *Org. Lett.* **2003**, *5*, 3217–3220. doi:10.1021/o1035011m
- Malla, R. K.; Ridenour, J. N.; Spilling, C. D. *Beilstein J. Org. Chem.* **2014**, *10*, 1933–1941. doi:10.3762/bjoc.10.201
- Abbas, M.; Leitgeb, A.; Slugovc, C. *Synlett* **2013**, *24*, 1193–1196. doi:10.1055/s-0033-1338425
- Bidange, J.; Fischmeister, C.; Bruneau, C.; Dubois, J.-L.; Couturier, J.-L. *Monatsh. Chem.* **2015**, *146*, 1107–1113. doi:10.1007/s00706-015-1480-1
See for a detailed study of CM with acrylonitrile.
- Bruneau, C.; Fischmeister, C.; Miao, X.; Malacea, R.; Dixneuf, P. H. *Eur. J. Lipid Sci. Technol.* **2010**, *112*, 3–9. doi:10.1002/ejlt.200900105
- Bilel, H.; Hamdi, N.; Zagrouba, F.; Fischmeister, C.; Bruneau, C. *RSC Adv.* **2012**, *2*, 9584. doi:10.1039/c2ra21638h
- Miao, X.; Malacea, R.; Fischmeister, C.; Bruneau, C.; Dixneuf, P. H. *Green Chem.* **2011**, *13*, 2911. doi:10.1039/c1gc15569e
- Mann, B. S.; Johnson, J. R.; Cohen, M. H.; Justice, R.; Pazdur, R. *Oncologist* **2007**, *12*, 1247–1252. doi:10.1634/theoncologist.12-10-1247
- Yoshida, M.; Kijima, M.; Akita, M.; Beppu, T. *J. Biol. Chem.* **1990**, *265*, 17174.
- Komatsu, Y.; Tomizaki, K.-Y.; Tsukamoto, M.; Kato, T.; Nishino, N.; Sato, S.; Yamori, T.; Tsuruo, T.; Furumai, R.; Yoshida, M.; Horinouchi, S.; Hayashi, H. *Cancer Res.* **2001**, *61*, 4459.
- Mukherjee, J.; Sil, S.; Chattopadhyay, S. K. *Beilstein J. Org. Chem.* **2015**, *11*, 2487–2492. doi:10.3762/bjoc.11.270
- Mukherjee, J. P.; Sil, S.; Chattopadhyay, S. K. *Tetrahedron Lett.* **2016**, *57*, 739–742. doi:10.1016/j.tetlet.2016.01.005
- Schmidt, B.; Pohler, M. *Org. Biomol. Chem.* **2003**, *1*, 2512. doi:10.1039/b303441k
- Miao, X.; Fischmeister, C.; Bruneau, C.; Dixneuf, P. H.; Dubois, J.-L.; Couturier, J.-L. *ChemSusChem* **2012**, *5*, 1410–1414. doi:10.1002/cssc.201200086
- Skowerski, K.; Bialecki, J.; Czarnocki, S. J.; Żukowska, K.; Grela, K. *Beilstein J. Org. Chem.* **2016**, *12*, 5–15. doi:10.3762/bjoc.12.2
- Chatterjee, A. K.; Choi, T.-L.; Sanders, D. P.; Grubbs, R. H. *J. Am. Chem. Soc.* **2003**, *125*, 11360–11370. doi:10.1021/ja0214882
- Chattopadhyay, S. K.; Sil, S.; Mukherjee, J. P. *Beilstein J. Org. Chem.* **2017**, *13*, 2153–2156. doi:10.3762/bjoc.13.214
- Pahari, A. K.; Mukherjee, J. P.; Chattopadhyay, S. K. *Tetrahedron* **2014**, *70*, 7185–7191. doi:10.1016/j.tet.2014.07.045

License and Terms

This is an Open Access article under the terms of the Creative Commons Attribution License (<http://creativecommons.org/licenses/by/4.0>). Please note that the reuse, redistribution and reproduction in particular requires that the authors and source are credited.

The license is subject to the *Beilstein Journal of Organic Chemistry* terms and conditions: (<https://www.beilstein-journals.org/bjoc>)

The definitive version of this article is the electronic one which can be found at:
[doi:10.3762/bjoc.14.285](https://doi.org/10.3762/bjoc.14.285)



Ruthenium-based olefin metathesis catalysts with monodentate unsymmetrical NHC ligands

Veronica Paradiso, Chiara Costabile and Fabia Grisi*

Review

Open Access

Address:

Dipartimento di Chimica e Biologia "Adolfo Zambelli", Università di Salerno, Via Giovanni Paolo II 132, I-84084 Fisciano, Salerno, Italy

Email:

Fabia Grisi* - fgrisi@unisa.it

* Corresponding author

Keywords:

ligand design; olefin metathesis; ruthenium catalysts; selectivity; unsymmetrical N-heterocyclic carbenes

Beilstein J. Org. Chem. **2018**, *14*, 3122–3149.

doi:10.3762/bjoc.14.292

Received: 01 September 2018

Accepted: 22 November 2018

Published: 28 December 2018

This article is part of the thematic issue "Progress in metathesis chemistry III".

Guest Editors: K. Grela and A. Kajetanowicz

© 2018 Paradiso et al.; licensee Beilstein-Institut.

License and terms: see end of document.

Abstract

An overview on the catalytic properties of ruthenium complexes for olefin metathesis bearing monodentate unsymmetrical N-heterocyclic diaminocarbene ligands is provided. The non-symmetric nature of these NHC architectures strongly influences activity and selectivity of the resulting catalysts. The main achievements that have been accomplished in significant areas of olefin metathesis up to the current state of research are discussed.

Introduction

The transition metal-catalyzed olefin metathesis reaction is an indispensable synthetic tool for the construction of new carbon–carbon double bonds in various applications in both organic and polymer chemistry [1,2]. The great popularity of this methodology is mainly related to the development of well-defined ruthenium alkylidene catalysts with high air and moisture stability and functional group tolerance. Among them, ruthenium olefin metathesis complexes bearing N-heterocyclic carbene (NHC) ligands, known as second generation catalysts (Figure 1), have shown improved catalytic efficiency over other metathesis catalysts [3,4].

Moreover, their catalytic properties can be finely modulated through variation of the steric and electronic properties of the NHC ligand. Significant advances in ruthenium metathesis catalyst design have been achieved by the introduction of unsymmetrically substituted NHC (uNHC) ligands, namely presenting different substituents at the nitrogen atoms. They offer the possibility of strongly influencing the reactivity and selectivity of the resulting catalysts by creating different steric and/or electronic environments around the metal center. Indeed, ruthenium complexes coordinated with this kind of ligands can be easily tailored for challenging or specific metathesis applications in

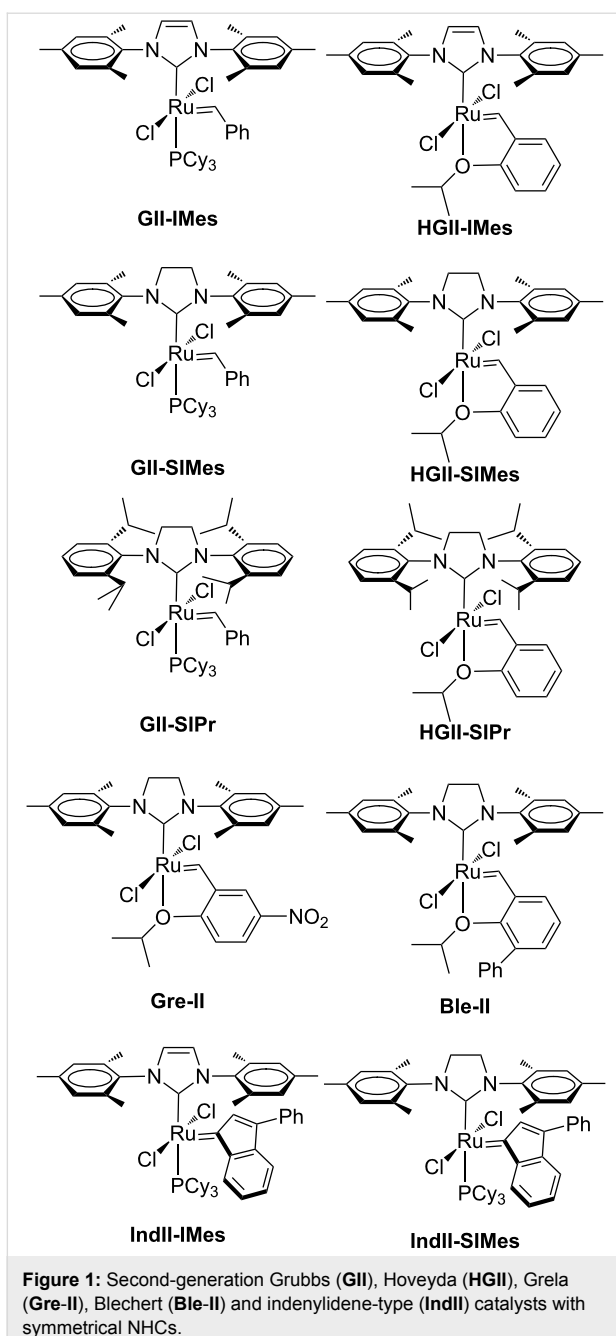


Figure 1: Second-generation Grubbs (GII), Hoveyda (HGII), Grela (Gre-II), Blechert (Ble-II) and indenylidene-type (IndII) catalysts with symmetrical NHCs.

which their symmetrical counterparts fail or show poor efficiency [5,6]. Moreover, the use of catalysts incorporating bidentate unsymmetrical NHCs has allowed for significant enhancements in the field of both asymmetric and Z-selective olefin metathesis reactions [7–9].

The aim of the present review is to provide a description of the catalytic behavior of ruthenium complexes bearing monodentate five-membered uNHCs. A special focus is given to the more recent advancements in the development of such unsymmetrical architectures for targeted metathesis applications.

Ruthenium complexes with NHCs presenting alternative heteroatoms, such as thiazol-2-ylidene ligands [10], or those containing one nitrogen substituent, such as the series of cyclic (alkyl) (amino) carbenes (CAACs) introduced by Bertrand et al. [11], are not included in this survey.

Review

Ruthenium catalysts coordinated with *N*-aryl, *N'*-aryl NHCs

The first ruthenium complexes with monodentate NHC ligands bearing unsymmetrical *N*-aryl, *N'*-aryl groups were reported by Blechert [12], who synthesized Grubbs and Hoveyda-type complexes with *N*-phenyl, *N'*-mesityl NHC substituents (**1a,b** in Figure 2). Both complexes were air stable, but in CH_2Cl_2 solution complex **1b** converted completely within a few hours into complex **2** due to the formation of an intramolecular carbene–arene bond between the benzylidene carbon atom and the *ortho* position of the *N*-phenyl ligand (Figure 3). According to the authors, the mechanism of the reaction that occurs only in the presence of oxygen, involves a pericyclic reaction followed by an irreversible oxidation step, and, finally, a rearomatization.

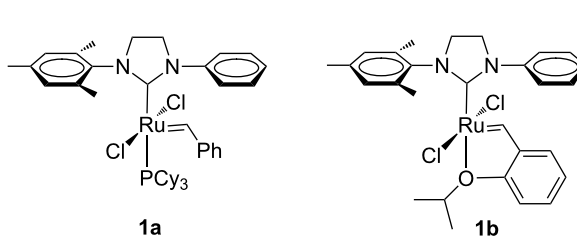


Figure 2: Grubbs (**1a**) and Hoveyda-type (**1b**) complexes with *N*-phenyl, *N'*-mesityl NHCs.

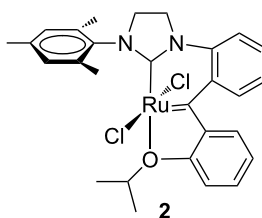


Figure 3: C–H insertion product **2**.

To avoid the C–H activation of aryl-substituted NHC ligands the corresponding *ortho* positions have to be substituted by different groups. Indeed, almost contemporaneously, Grubbs et al. reported on the synthesis of a family of corresponding *ortho*-substituted *N*-fluorophenyl, *N'*-aryl NHC Ru complexes (Figure 4) [13,14].

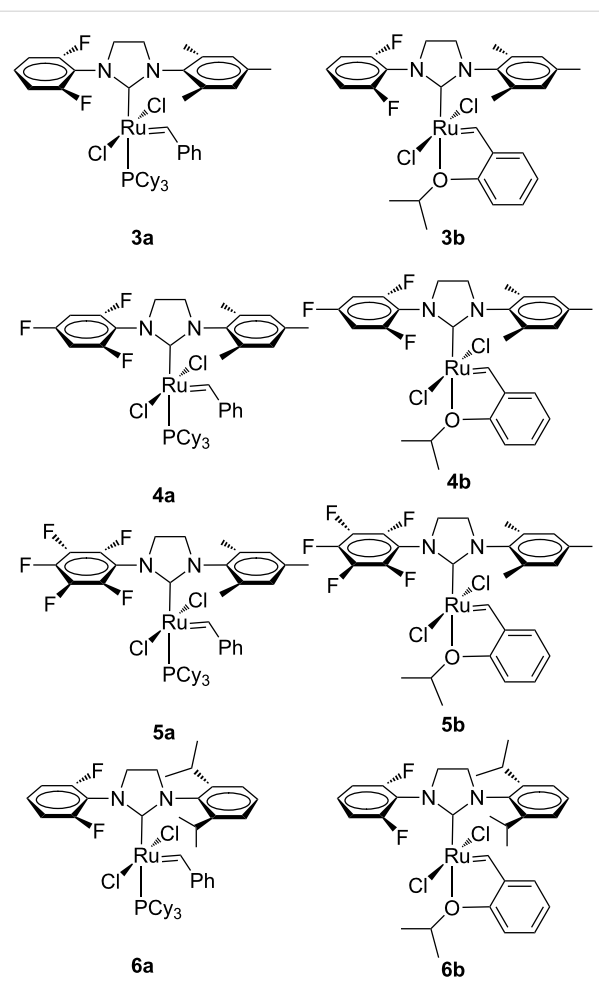
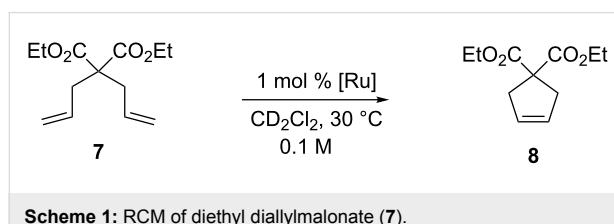


Figure 4: Grubbs (3a–6a) and Hoveyda-type (3b–6b) complexes with *N*-fluorophenyl, *N'*-aryl NHCs.

The behavior of this catalyst family was tested in the RCM of diethyl diallylmalonate (7, Scheme 1) and compared with that of **GII-SIMes** and **HGII-SIMes**.

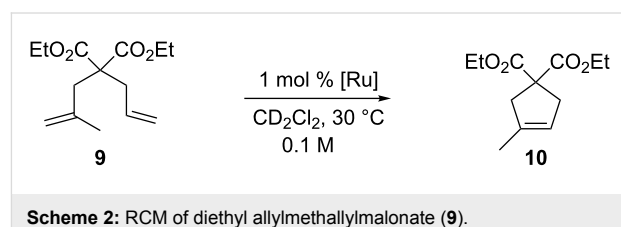


Scheme 1: RCM of diethyl diallylmalonate (7).

Interestingly, catalysts **3a** and **4a** clearly outperformed **GII-SIMes**, with catalyst **4a** emerging as the most efficient of all (>97% conversion in 9 min). Complex **5a** showed a higher initiation rate with respect to **GII-SIMes**, but eventually was found to be less efficient due to a decrease in its catalytic activity related to concomitant decomposition. As for Hoveyda-type catalysts **3b**, **4b** and **5b**, they all disclosed lower activity than

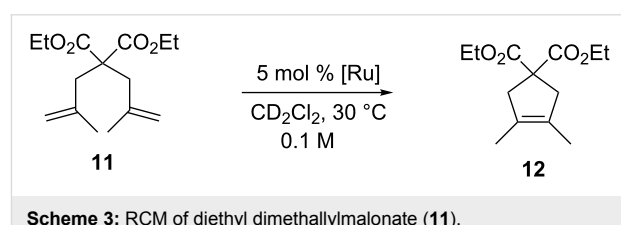
the parent complex **HGII-SIMes**, with catalyst **5b** being the least efficient of all in this series (>97% conversion in 100 min). Finally, **6a** as well as the phosphine-free **6b** showed to be very poor olefin metathesis catalysts.

Enhanced catalytic performances, with respect to **GII-SIMes**, were previously reported also for symmetrical NHC bearing *o*-fluorinated aryl groups. Possibly the presence of a Ru–F interaction is responsible for the positive impact on the reaction rates [15]. Similar results were observed in the RCM of the more hindered diethyl allylmethallylmalonate (**9**, Scheme 2), where **3a** and **4a** behaved as the most efficient catalysts.



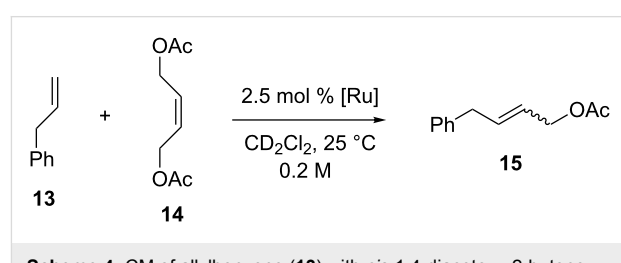
Scheme 2: RCM of diethyl allylmethallylmalonate (9).

Even in the challenging formation of tetrasubstituted olefin **12** via RCM (Scheme 3), catalysts **3a** and **4a** gave the best performances leading to 30% and 21% conversion, respectively, in four days.



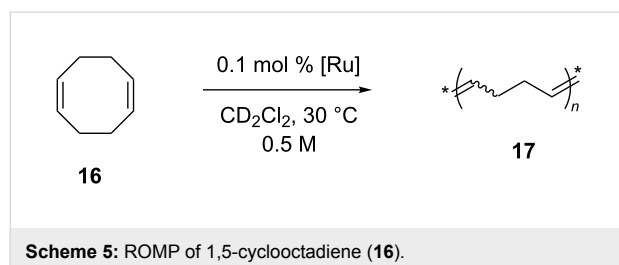
Scheme 3: RCM of diethyl dimethallylmalonate (11).

In the CM of allylbenzene (**13**) with *cis*-1,4-diacetoxy-2-butene (**14**, Scheme 4), the fluorinated complexes **3a–5a** and **3b–5b** exhibited activities comparable to **GII-SIMes** and **HGII-SIMes**, showing higher *Z*-selectivity at conversions above 60%. For example, catalyst **GII-SIMes** affords an *E/Z* ratio of ~10 at 79% conversion, whereas catalysts **3–5** gave an *E/Z* ratio of about 5.5 at the same conversion.



Scheme 4: CM of allylbenzene (13) with *cis*-1,4-diacetoxy-2-butene (14).

As for the ROMP of **16** (Scheme 5), **GII-SIMes** and **4a** displayed the highest activity with similar reactivity.



In the attempt to rationalize the catalytic performances of this family of *N*-fluorophenyl complexes the related $[\text{Rh}(\text{CO})_2\text{Cl}(\text{NHC})]$ complexes were synthesized. Unfortunately the shifts of the CO stretching frequencies showed that no correlation between the catalytic performances of Ru-cata-

lysts and electronic properties of the corresponding NHC ligand is found.

More recently, Osypov and co-workers introduced a new family of Grubbs (**18a–21a**) and Hoveyda-type (**18b–21b**) catalysts bearing unsymmetrical NHC ligands with one of the *N*-aryl substituents presenting a hexafluoroisopropylalkoxy $[(\text{CF}_3)_2(\text{OR})-\text{C}]$ group (Figure 5) [16,17].

Catalysts **18a** and **19a** showed efficiencies comparable to **GII-SIMes** and **HGII-SIMes** in the RCM of substrate **7** (Scheme 1), giving full conversion within 30 minutes, whereas the corresponding Hoveyda-type complexes **18b** and **19b** presented a more pronounced initiation period, giving good conversions in much longer reaction time (2–4 h) [16]. A similar trend was observed in the RCM of **9** (Scheme 2), but reaction rates were lower in all cases. As for **20a** and **21a**, the initiation rates in the

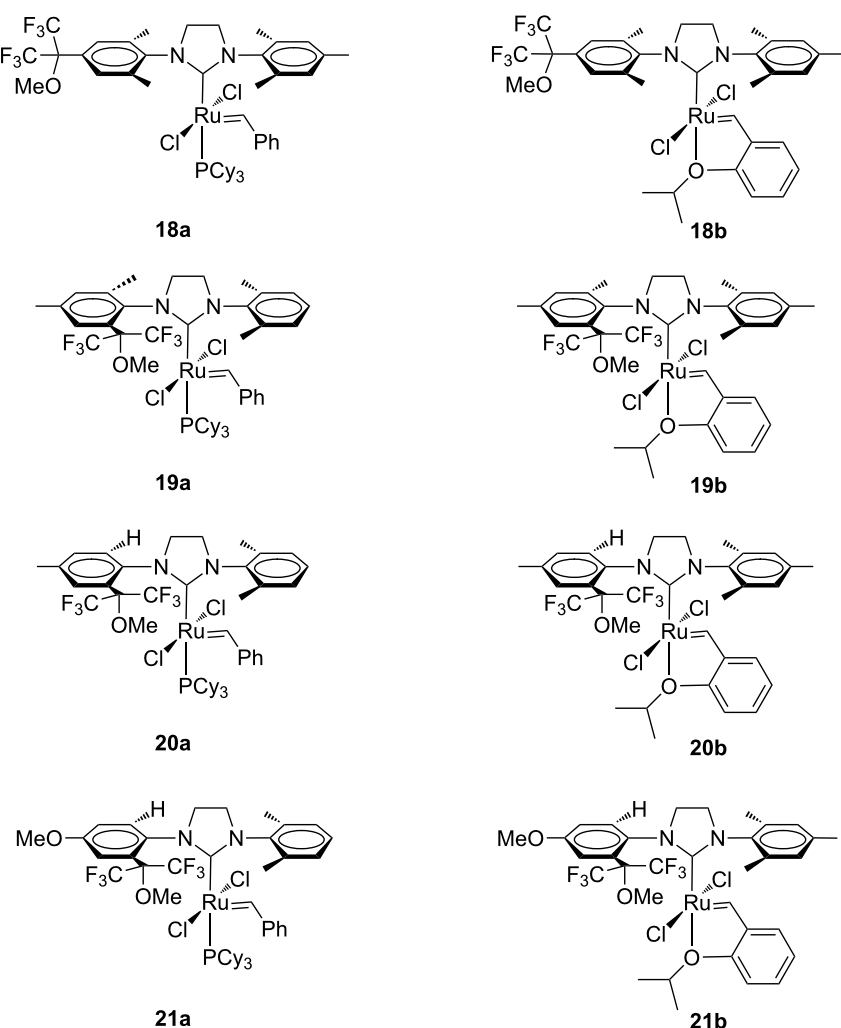


Figure 5: Grubbs (**18a–21a**) and Hoveyda-type (**18b–21b**) catalysts bearing uNHCs with a hexafluoroisopropylalkoxy $[(\text{CF}_3)_2(\text{OR})-\text{C}]$ group in one of the *N*-aryl substituents.

RCM of **7** were observed to be faster than **GII-SIMes**, **HGII-SIMes** and **19a**, while the initiation rates of **20b** and **21b** were lower than **GII-SIMes** and **HGII-SIMes**, but superior to **19b**, resulting in 90% conversion within 3 hours [17]. No relevant differences in the catalyst reactivity were observed for the CM of **13** and **14** (Scheme 4).

As a novel application of *N*-aryl, *N'*-aryl unsymmetrical ruthenium complexes in enantioselective catalysis, Grela and Schmidt very recently reported on the first example of a helically chiral Hoveyda-type metathesis complex. This catalyst, bearing a mesityl and a helicene as the aryl groups, was preliminary examined in some model asymmetric metathesis transformations and showed promising levels of enantioselectivity. Further studies on the development of this new concept for enantioinduction are still ongoing [18].

Ruthenium catalysts coordinated with *N*-alkyl, *N'*-aryl NHCs

N-Alkyl-substituents possessing no functionalities or heteroatoms

Unsymmetrical *N*-alkyl, *N'*-aryl NHC frameworks were initially developed in order to improve the catalytic activity of ruthenium-based complexes through enhanced electron-donating ability and different steric bulk of the NHC ligand. Mol et al. introduced complex **22** (Figure 6) in which one of the mesityl groups from **GII-SIMes** was replaced by the sterically more encumbered adamantyl group [19].

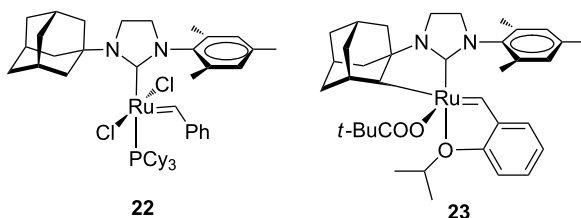


Figure 6: A Grubbs-type complex with an *N*-adamantyl, *N'*-mesityl NHC **22** and the Hoveyda-type complex with a chelating *N*-adamantyl, *N'*-mesityl NHC **23**.

However, no beneficial effect on the catalytic activity was observed. Indeed complex **22** revealed a very poor olefin metathesis catalyst, likely as a consequence of the excessive steric hindrance of the adamantyl moiety at the ruthenium center. It is worth to underline that the first *Z*-selective ruthenium catalyst (**23**, Figure 6), developed by Grubbs and co-workers, is based on a chelating NHC ligand that is derived from an intramolecular carboxylate-driven C–H bond insertion of the adamantyl N-substituent of the same NHC ligand in complex **22** [20]. Unsymmetrical complexes bearing smaller *N*-alkyl groups (Figure 7) were reported by Blechert and co-workers [21].

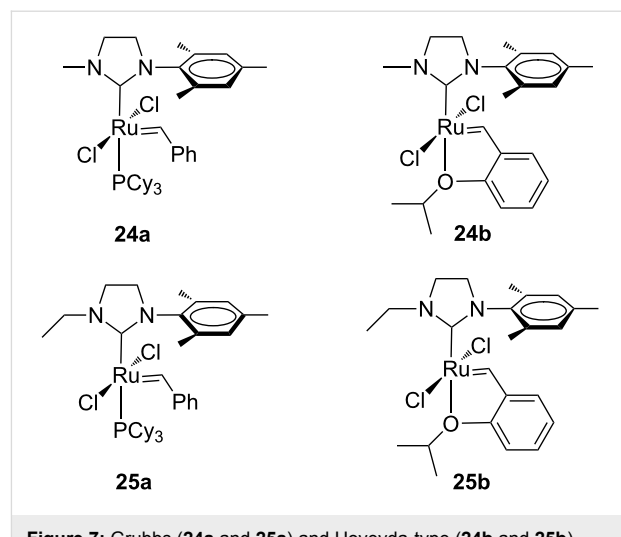


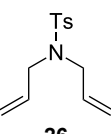
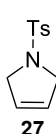
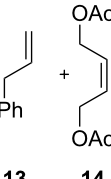
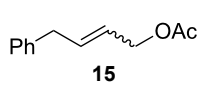
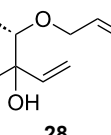
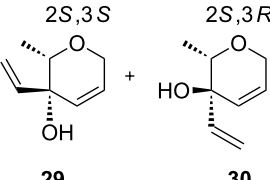
Figure 7: Grubbs (**24a** and **25a**) and Hoveyda-type (**24b** and **25b**) complexes with *N*-alkyl, *N'*-mesityl NHCs.

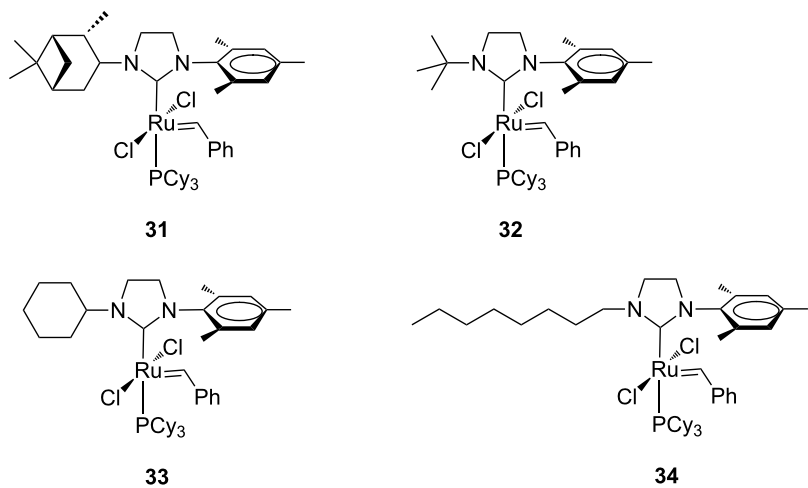
In addition to the concept that the presence of more electron-donating alkyl groups on the NHC could lead to enhanced σ -donor properties, and, consequently, to higher catalytic activity, the authors postulated that the unsymmetrical nature of the NHC ligands could improve *E/Z* selectivity in CM reactions and diastereoselectivity in RCM reactions altering the environment of key metathesis intermediates. Complexes **24** and **25** were found to exist in solution as a single rotational isomer having the benzylidene moiety located under the mesityl group, and for complexes **24b** and **25b** this orientation was observed also in the solid state. Some metathesis reactions performed in this study with **24b** and **25b** in comparison to **GII-SIMes** and **HGII-SIMes** are summarized in Table 1. In the model RCM reaction of *N,N*-diallyl-*p*-toluenesulfonamide (**26**, Table 1, entry 1), catalysts **24a** and **24b** showed activities similar to that of **GII-SIMes**. They also exhibited different *E/Z* selectivities in CM transformations (e.g., Table 1, entry 2), and gave improved selectivities in a diastereoselective RCM reaction (Table 1, entry 3).

Ledoux, Verpoort et al. described a series of phosphine-containing unsymmetrical catalysts **31–34** characterized by alkyl N-substituents with variable steric bulk (Figure 8) [22].

The catalytic performances of these complexes and of complex **24a** were evaluated for the RCM of diethyl diallylmalonate (**7**) and the ROMP of *cis*-1,5-cyclooctadiene (**16**). In the RCM reaction (Scheme 1), performed at 20 °C in CD₂Cl₂ at a catalyst concentration of 4.52 mM and a substrate/catalyst ratio of 200 (0.5 mol % of catalyst), a strong dependence of the catalytic activities on the steric bulkiness of the *N*-alkyl substituents was observed. Indeed, an increase in the size of the alkyl group resulted in a lower catalyst activity. Indeed, complex **24a** bear-

Table 1: Examples of metathesis reactions performed with catalysts **24a** and **24b**.^a

entry	substrate	product	complex	loading (mol %)	conversion (%)
1			GII-SIMes 24a HGII-SIMes 24b	0.02 0.02 0.02 0.02	50 56 66 56
2			GII-SIMes 24a HGII-SIMes 24b	3 3 3 3	79 (E/Z = 6:1) 72 (E/Z = 3:1) 84 (E/Z = 6:1) 76 (E/Z = 1:1)
3			GII-SIMes 24a HGII-SIMes 24b	3 3 3 3	95 (29/30 = 1.6:1) 92 (29/30 = 1.7:1) 95 (29/30 = 1.5:1) 95 (29/30 = 2.0:1)

^aReactions performed in refluxing dichloromethane [21].**Figure 8:** Grubbs-type complexes **31–34** with *N*-alkyl, *N'*-mesityl NHCs.

ing the small methyl moiety on the nitrogen, revealed as the best performing catalyst, even surpassing the parent complex **GII-SIMes**. In the ROMP reaction (Scheme 5), carried out in different solvents and monomer/catalyst ratios, the activities of complexes **31**, **33** and **34** were superior to that of the symmetrical counterpart **GII-SIMes** at low COD/catalyst loading in CDCl_3 . In general, the complexes were less dependent on the solvent used with respect to **GII-SIMes**. Catalyst **32**, having a bulky *N*-*tert*-butyl substituent on the NHC, displayed a consid-

erably lower activity than the other tested catalysts. The replacement of the mesityl group by a 2,6-diisopropylphenyl group as in complexes **24a** and **33** led preferentially to bis(NHC)-coordinated complexes, which showed metathesis activity only at elevated temperatures [23]. However, the mono(NHC) complex **35** (Figure 9) was isolated and tested in the RCM of **7** and the ROMP of *cis*-1,5-cyclooctadiene (**16**), where it displayed a fair olefin metathesis activity compared to the benchmark catalyst **GII-SIMes** [23].

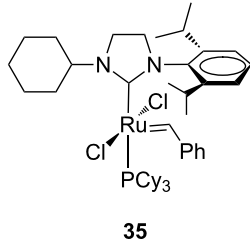


Figure 9: Grubbs-type complex **35** with an *N*-cyclohexyl, *N'*-2,6-diisopropylphenyl NHC.

Studies on this class of unsymmetrical NHC ligands were also extended to the Hoveyda-type complexes **36–40** (Figure 10) [24]. The effect of the modified NHC ligand was investigated in model metathesis reactions (RCM of **7**, ROMP of **16** and CM of **13** with acrylonitrile) in comparison to complex **24b** and the parent complexes **GII-SIMes** and **GII-SIPr**.

No real improvement in the catalytic activity was observed in any of the tested metathesis reactions, while different *E/Z* selectivities were observed in the CM of allylbenzene (**13**) with acrylonitrile. These results underline that steric differences in *N*-alkyl NHC ligands are more important than differences in their donor capacities in determining the activity and selectivity of the corresponding catalysts.

Quite recently, on the basis of a previous work, Verpoort et al. reported on the synthesis and characterization of second generation ruthenium indenylidene catalysts bearing *N*-alkyl, *N'*-mesityl-substituted NHCs **41–43** in which the alkyl group was methyl (**41**), octyl (**42**) or cyclohexyl (**43**, Figure 11) [25].

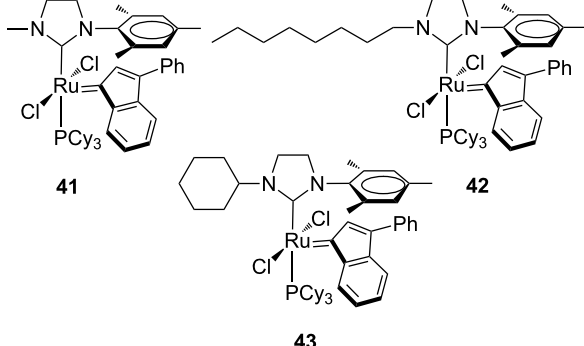


Figure 11: Indenylidene-type complexes **41–43** with *N*-alkyl, *N*-mesityl NHCs.

For all of the complexes, two rotamers were observed in solution, and the most abundant species was identified as the isomer with the indenylidene moiety located under the mesityl group. Solid-state structures of the complexes showed, consistently, the same relative orientation between the indenylidene and mesityl unit. Complexes **41–43** were tested in various representative metathesis reactions of standard substrates and compared to the benchmark catalysts **IndII-SIMes**. Interestingly, all complexes showed a faster catalytic initiation than **IndII-SIMes**. This faster initiation may be due to the stronger σ -donating properties of the unsymmetrical *N*-alkyl-substituted NHC ligands. Catalyst **41** bearing the smallest-sized *N*-alkyl group on the NHC emerged as the most performing catalyst in both initiation and propagation stages, even with respect to **IndII-SIMes**. Indeed, besides its faster initiation, complex **41** offers a less encumbered NHC for the approach of substrates to the metal center during the metathesis process. The performance of complex **41** also was compared with that of the benzylidene ana-

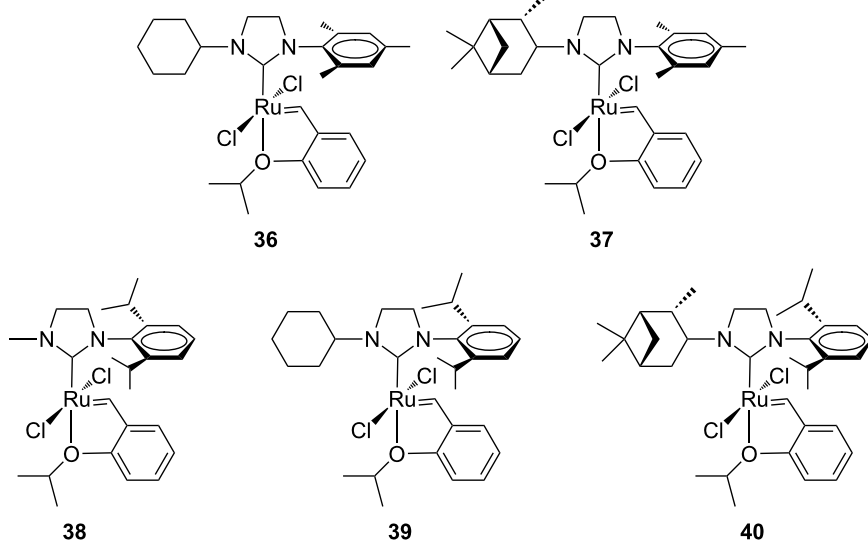


Figure 10: Hoveyda-type complexes with an *N*-alkyl, *N'*-mesityl (**36, 37**) and an *N*-alkyl, *N'*-2,6-diisopropylphenyl (**38–40**) NHC ligand.

logue **GII-SIMes** in the RCM of **7** (Scheme 1) using various catalyst loadings (0.125–0.5 mol %). Although the benzylidene complex **GII-SIMes** exhibited a faster initiation than the indenylidene complex **41** with all the used catalyst loadings, the latter outperformed **GII-SIMes** in the overall catalyst efficiency, especially at the lowest catalyst loading of 0.125 mol %.

In 2008, Blechert and Buchmeiser et al. introduced a ruthenium complex featuring an unsymmetrical, chiral NHC ligand **44** and its pyridine derivative **45** (Figure 12) [26].

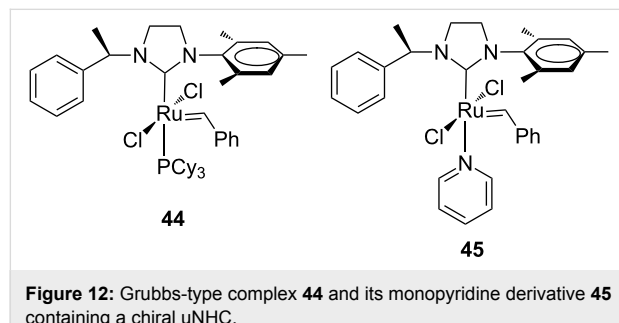


Figure 12: Grubbs-type complex **44** and its monopyridine derivative **45** containing a chiral uNHC.

Both complexes revealed as efficient systems to promote the alternating copolymerization of norbornene (NBE, **46**) with cyclooctene (COE, **47**) and cyclopentene (CPE, **48**), respectively (Scheme 6).

An NBE/COE ratio of 1:50 was found necessary to realize a copolymer containing 97% of alternating diads ([poly(NBE-*alt*-COE)_n]), while an NBE/CPE ratio of only 1:7 resulted in the formation of a copolymer with roughly 90% of alternating diads ([poly(NBE-*alt*-CPE)_n]), representing the highest value found until then. The selectivity in the copolymerization was mainly ascribed to the steric interaction between the 2-phenylethyl substituent at the nitrogen and the growing polymer chain. This study was then extended to a series of unsymmetrical pyridine-containing Ru benzylidenes (Figure 13) with *N*-alkyl (**49**, **50**),

N-phenyl (**51**) and *N*-benzyl (**52**) substituents in comparison to their parent phosphine-containing catalysts **24a**, **25a**, **1a** and **53** [27].

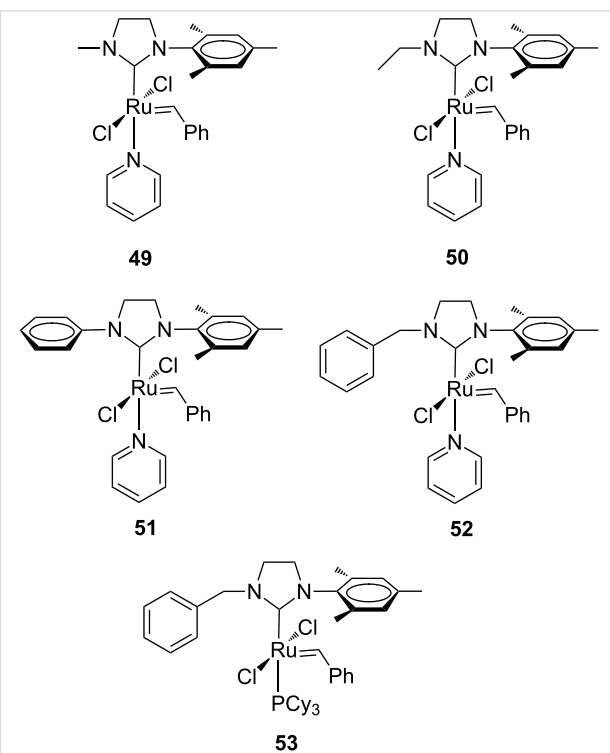
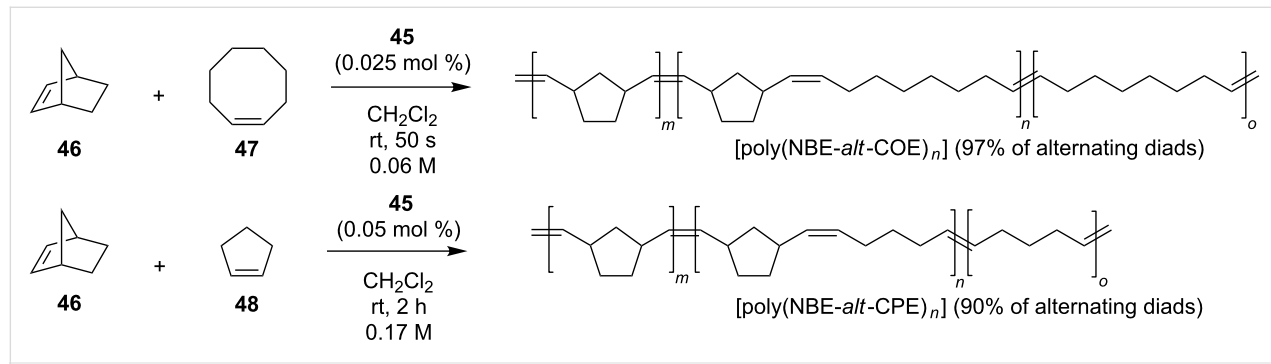


Figure 13: Pyridine-containing complexes **49–52** and Grubbs-type complex **53**.

Complexes **49** and **52** were obtained as monopyridine adducts, while complexes **50** and **51** were obtained as a mixture of mono- and bis(pyridine) adducts. In terms of initiation efficiency, the pyridine-derivatives turned out to be more efficient than the corresponding phosphine-containing complexes. In the copolymerization of NBE (**46**) and COE (**47**), complexes **49–52** afforded the corresponding copolymers with 95–97% of alternating diads and high *cis* content. In the copolymerization of NBE (**46**) and CPE (**48**), copolymers with 79–91% of alter-



Scheme 6: Alternating copolymerization of **46** with **47** and **48**.

nating diads were obtained. More recently, Plenio and co-workers described a new class of Hoveyda–Grubbs-type catalysts with an *N*-alkyl, *N'*-pentiphenyl NHC ligand (**54–57**, Figure 14). The complex **58** having an *N*-mesityl, *N'*-pentiphenyl NHC was also reported [28].

These complexes disclosed an excellent degree of alternation in the copolymerization of NBE and COE (0.05 mol % of catalyst, [NBE] = 0.14 M). Especially catalyst **56** having a cyclohexyl N-substituent provided the copolymer with the highest amount of alternating diads (98%) at an NBE/COE ratio of 1:10. However, the molecular mass of the copolymers was far lower than the theoretical value, suggesting that competitive chain-termination reactions occur. The pronounced steric bulk on the pentiphenyl side of the NHC ligand compared to the other less hindered side determines two differently accessible active sites around the metal and different rates of monomer incorporation, thus dominating the selectivity in the formation of alternating copolymers. The nature of the alkyl group also plays a role in the formation of alternating diads. Indeed, the proportion of alternating copolymer increases moving from the small methyl group (**54**) to the large cyclohexyl group (**56**).

Unsymmetrical catalysts based on NHC units possessing one alkyl substituent (propyl (**59**) or benzyl (**60**)) and one mesityl substituent (Figure 15) at the nitrogen atoms were investigated by Copéret and Thieuleux et al. in the tandem ring-

opening–ring-closing alkene metathesis (RO–RCM) of *cis*-cyclooctene (**47**) and their performance were compared to those of the classical **GII-SIMes** and **GII-IMes** [29].

The dissymmetry of the NHC ligand in **59** and **60** allowed for the selective formation of cyclic dimeric and trimeric products in place of polymers from cyclooctene, while the symmetrical analogues **GII-SIMes** and **GII-IMes** led mainly to polymers (Figure 15).

Following a study on degenerate metathesis reactions that had highlighted a strong catalytic preference of unsymmetrical *N*-alkyl, *N'*-aryl complexes to propagate as a methylidene species [30], Grubbs and co-workers developed a variety of unsymmetrical metathesis Hoveyda-type complexes (**61–69**, Figure 16) for applications in the ethenolysis of methyl oleate (**70**, Scheme 7) [31].

The ethenolysis reaction, in fact, requires catalyst stability as a propagating methylidene species to achieve high product selectivity and turnover numbers (TONs). The catalysts **61–69**, tested together to the phosphine-containing catalyst **32**, were found to be highly selective toward the formation of the desired ethenolysis products **71** and **72** (Scheme 7), and provided good yields and TONs at 50 °C and low catalyst loading (100 ppm, Table 2). Furthermore, many of the screened catalysts showed good stability toward propagation as a methylidene species. The

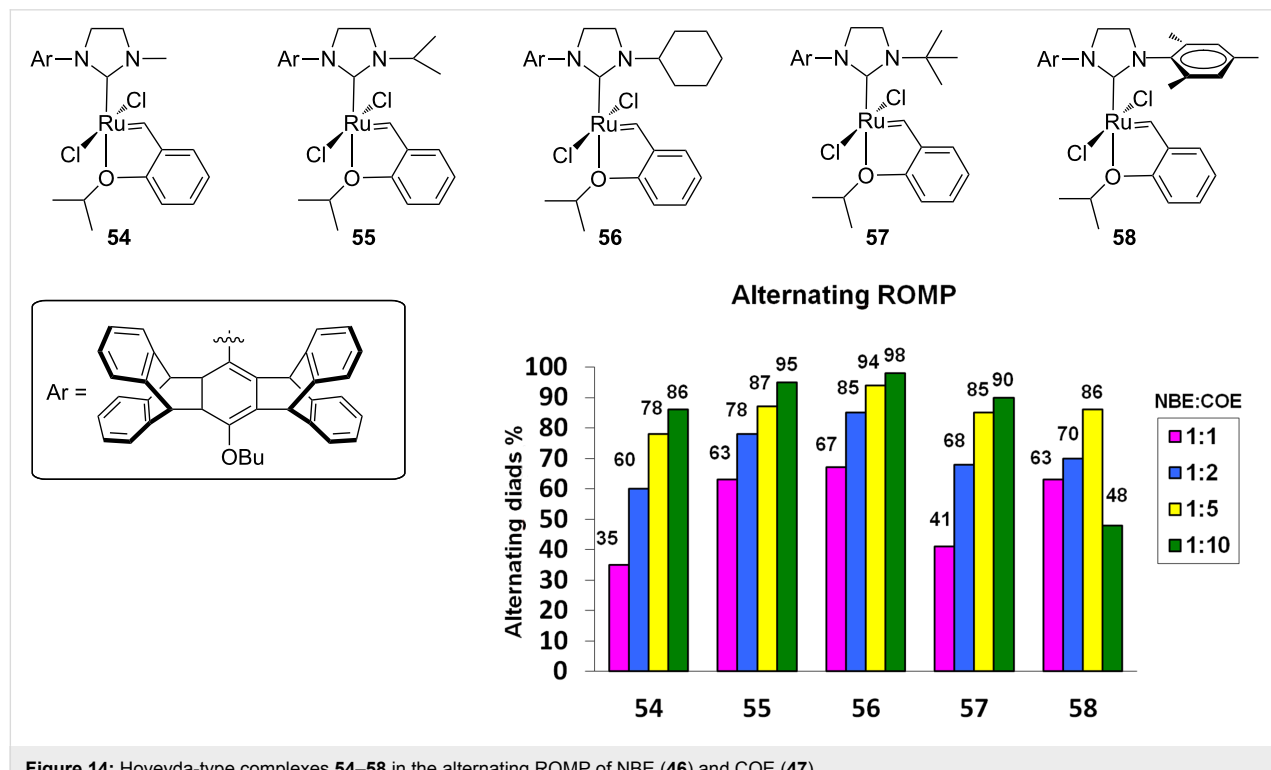
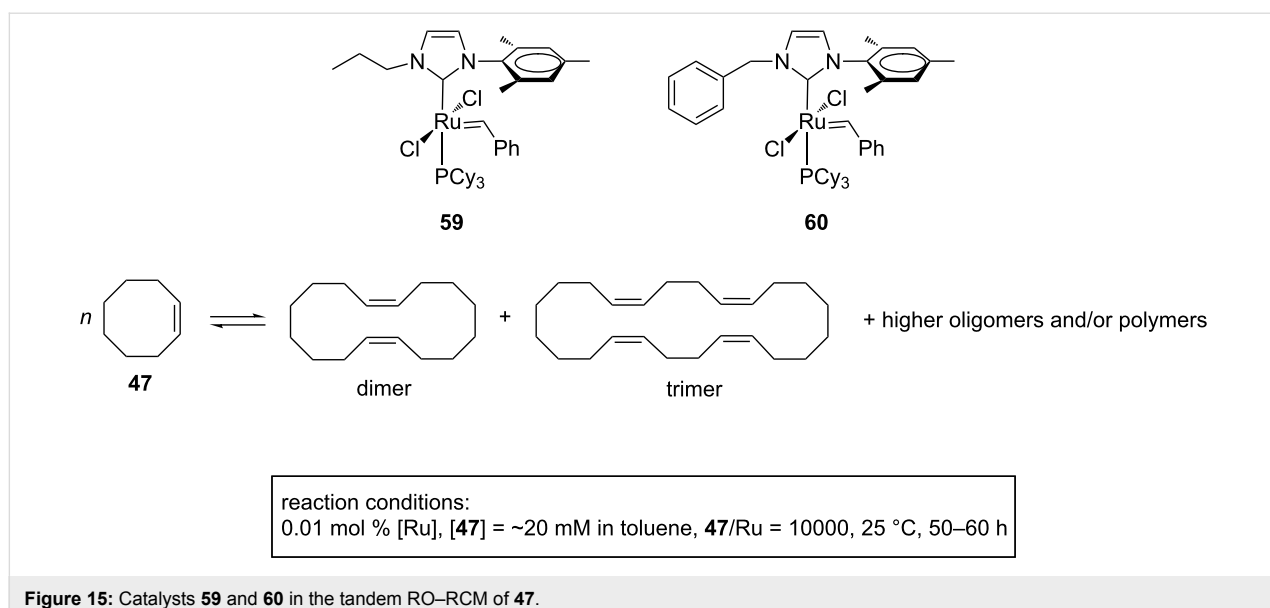
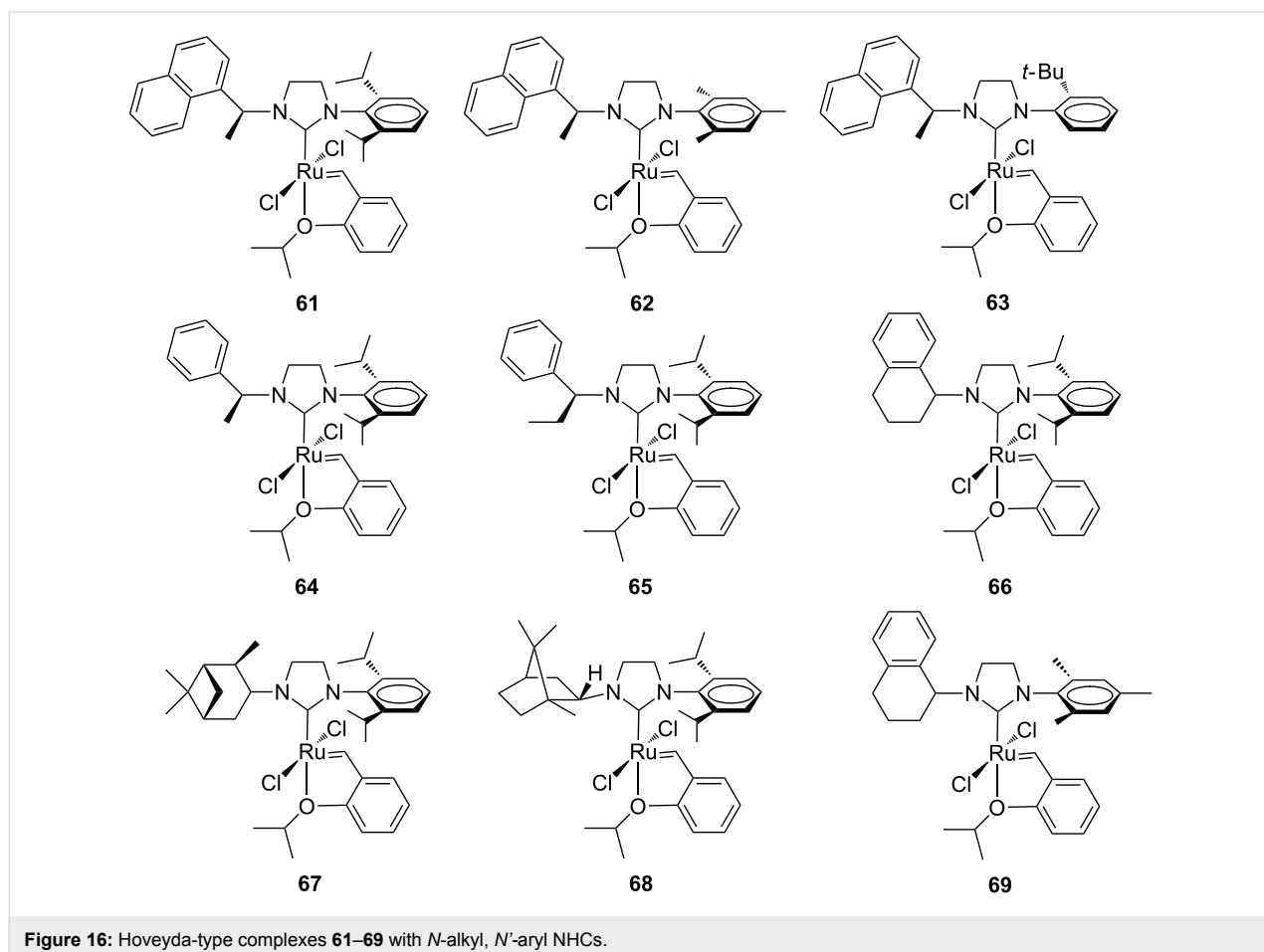
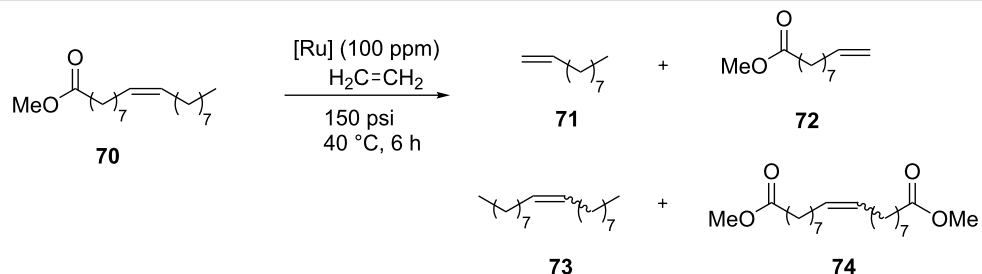


Figure 14: Hoveyda-type complexes **54–58** in the alternating ROMP of NBE (46) and COE (47).

Figure 15: Catalysts **59** and **60** in the tandem RO-RCM of **47**.Figure 16: Hoveyda-type complexes **61**–**69** with *N*-alkyl, *N'*-aryl NHCs.

observed selectivity seems to be controlled by the NHC sterics, as increasing steric bulkiness of the NHC ligand leads to greater selectivity and improves stability.

Catalyst **68** gave the highest selectivity (95%) toward terminal olefins observed until then for NHC–Ru complexes (Table 2, entry 7), but with 46% yield at 500 ppm of catalyst loading. The



Scheme 7: Ethenolysis of methyl oleate (70).

Table 2: Ethenolysis of methyl oleate (70) with catalysts 61–69.

entry	complex	conversion (%)	selectivity (%)	yield (%)	TON
1	61	54	86	46	4620
2	62	11	77	9	845
3	64	52	86	45	4450
4	65	42	86	36	3600
5	66	59	87	51	5070
6	67	52	89	46	4604
7	68	15	95	15	1460
8	69	17	69	11	1120

chiral catalysts **61**, **64**, **65**, **67** and **68** (Figure 16) were also investigated in the model asymmetric ring-opening cross metathesis (AROCM) of *cis*-5-norbornene-*endo*-2,3-dicarboxylic anhydride (**75**) with styrene (Scheme 8, Table 3) [32].

In this reaction complex **68** showed the highest selectivity for the formation of the desired product **76** (82% ee, Table 3, entry 5), comparable to the best ruthenium catalysts investigated in this AROCM reaction. All complexes gave side products **77** and/or **78** resulting from metathesis reactions of propagating ruthenium methylidene species.

In the same year, Grubbs and co-workers reported on the synthesis of highly thermally stable complexes containing a sterically encumbered *N*-*tert*-butyl substituent (**79**–**82**, Figure 17) which enables their application for latent olefin metathesis [33].

The complexes **79** and **81** having chloride ligands exhibited excellent latent behavior toward self-CM of 1-hexene, giving no conversion at room temperature and dimerization at 85 °C. Exchanging the chloride ligands for iodide ligands led to catalysts **80** and **82** with superior latent behavior that allowed

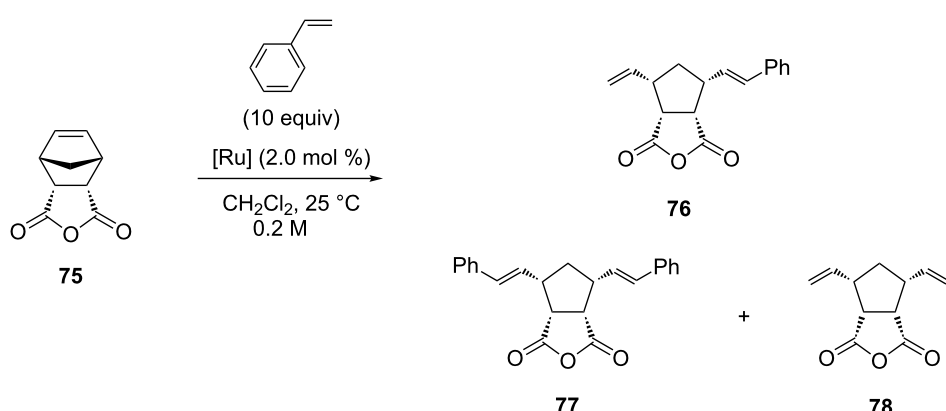
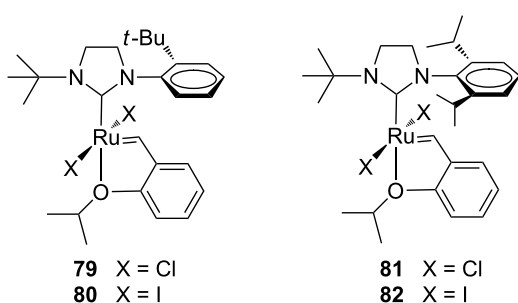
Scheme 8: AROCM of *cis*-5-norbornene-*endo*-2,3-dicarboxylic anhydride (75) with styrene.

Table 3: AROCM of *cis*-5-norbornene-*endo*-2,3-dicarboxylic anhydride (**75**) with catalysts **61**, **64**, **65**, **67** and **68**.

entry	complex	time (h)	conversion (%)	yield (%)	ee 76 (%)
1	61	5.5	60	60	69
2	64	0.5	99	69	14
3	65	0.5	99	73	9
4	67	5.5	98	65	33
5	68	10.5	98	54	82

**Figure 17:** Hoveyda-type catalysts **79–82** with *N*-*tert*-butyl, *N'*-aryl NHCs.

for the latent ROMP of norbornene derivatives (e.g., **83**, Scheme 9).

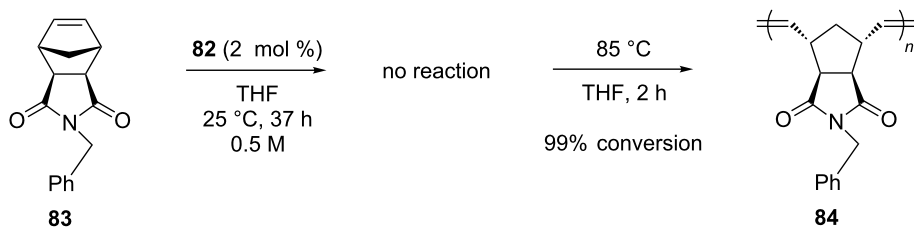
In order to improve the selectivities in olefin metathesis, a small library of indenylidene and Hoveyda-type complexes bearing unsaturated unsymmetrical NHCs combining a flexible cycloalkyl moiety and a mesityl unit as N-substituents (**85–89**, Figure 18) was synthesized by Mauduit and co-workers [34]. These systems were tested in the RCM of sterically demanding diethyl allylmethallylmalonate (**9**) under standard conditions (Scheme 2) and compared to their unsymmetrical saturated NHC–Ru complexes **90–92** (Figure 18) as well as a set of commercially available catalysts having symmetrical IMes or SIMes NHC ligands.

The unsaturated indenylidene catalysts **85** and **86** were found to be more active than their saturated homologues, giving full

conversions within 6 h and 24 h, respectively, thus showing better performances than **IndII-IMes** and Hoveyda-type catalysts **87–89**, **92**. As for the latter ones, the introduction of unsaturated NHCs with an *N*-cycloalkyl moiety did not provide any beneficial effect, since they were less efficient also than their symmetrical IMes and SIMes counterparts. The catalytic potential of the most active complex **85** with a cyclopentyl fragment on the NHC was explored in several RCM and CM reactions. Interestingly, in the RCM of *N,N*-dimethylallyl-*N*-tosylamide (**93**) only 2 mol % of **85** were required to produce 54% of the tetra-substituted tosylamide **94** within 3 h (Scheme 10).

Moreover, catalyst **85** was quite efficient under neat conditions for the self metathesis of allylbenzene (**13**), showing no trace of isomerized byproducts (Scheme 11).

More recently, Olivier-Bourbigou and Mauduit demonstrated the ability of unsymmetrical *N*-cycloalkyl Ru–indenylidene catalysts for the selective self metathesis of linear α -olefins to longer internal linear olefins in the absence of additives to prevent isomerization [35]. Catalyst **91** with a saturated NHC ligand containing a *N*-substituted cyclododecyl side chain was first evaluated at 50 ppm loading in the self metathesis of 1-octene (**96**), at 50 °C under neat conditions, in comparison to symmetrical benchmark second-generation ruthenium catalysts **IndII-SIMes**, **IndII-IMes**, **GII-SIMes** and **HGII-SIMes** (Table 4). Complex **91** was found to give 70% conversion of 1-octene (**96**) to the desired 7-tetradecene (**97**) with high selectivity (98% after 1 h, Table 4, entry 1). Moreover, the selectivity did not change over time (Table 4, entry 2). A lower

**Scheme 9:** Latent ROMP of **83** with catalyst **82**.

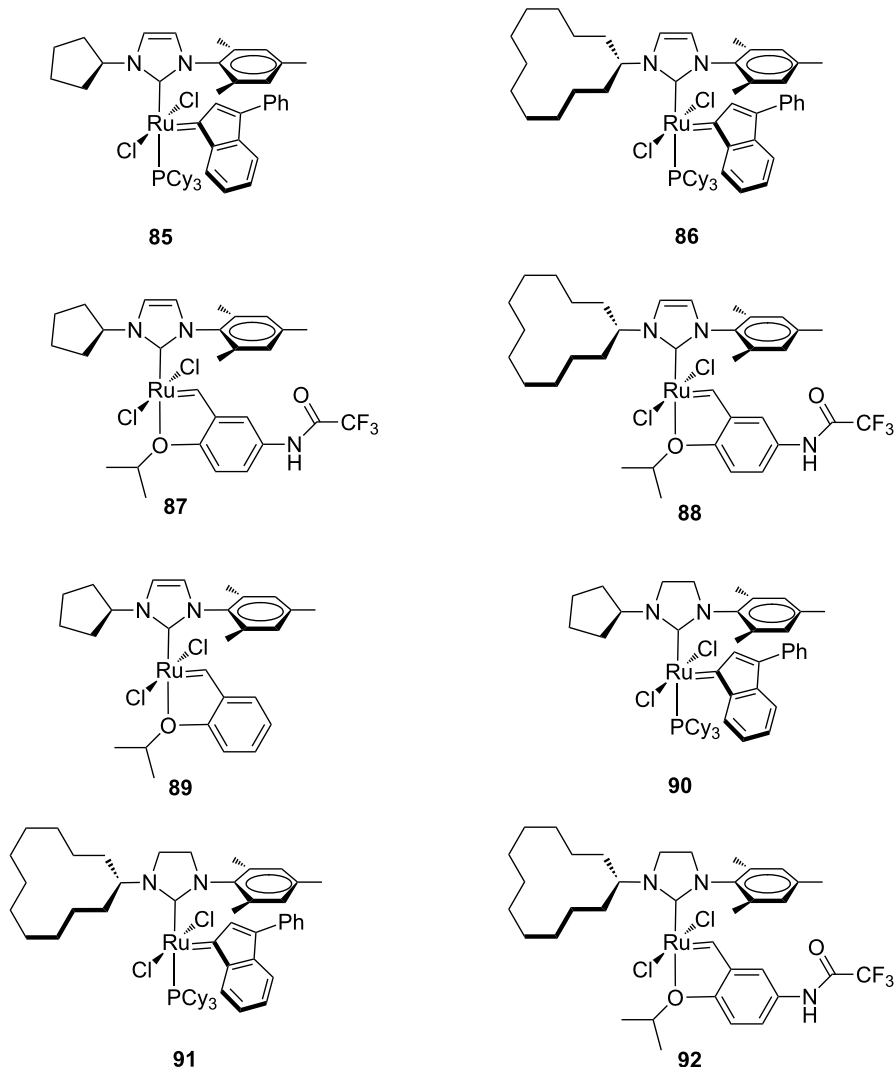
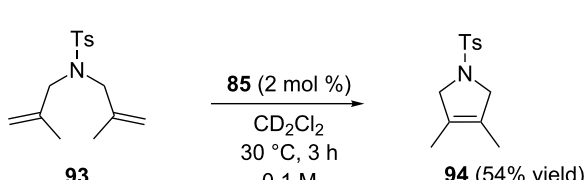
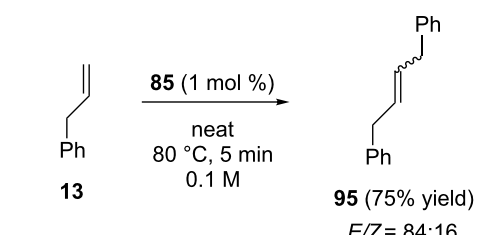


Figure 18: Indenylidene and Hoveyda-type complexes **85–92** with *N*-cycloalkyl, *N'*-mesityl NHCs.



Scheme 10: RCM of *N,N*-dimethyl-*N*-tosylamide (**93**) with catalyst **85**.

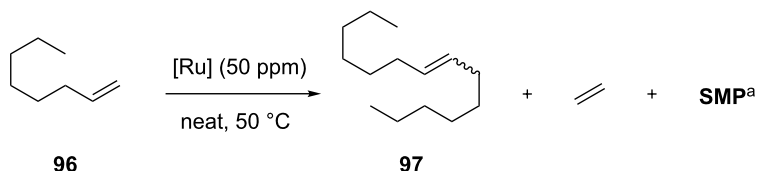


Scheme 11: Self metathesis of **13** with catalyst **85**.

selectivity was observed with **IndII-SIMes** (Table 4, entries 3 and 4) and **GII-SIMes** (Table 4, entry 5), while **IndII-IMes** was inactive (Table 4, entry 6) and **HGIIMes** gave only low conversion (Table 4, entry 7).

To render this process really attractive for industrial application, the authors also evaluated the lower-cost catalysts **85** and **86** in the self metathesis of **96** (Table 4, entries 8 and 9, respectively). Indeed, the one-step multicomponent synthesis of unsaturated

Table 4: Self metathesis of 1-octene (**96**).



entry	complex	time (h)	conversion (%)	selectivity (%)
1	91	1	70	98
2	91	4	70	98
3	IndII-SIMes	1	45	94
4	IndII-SIMes	2	76	80
5	GII-SIMes	2	80	85
6	IndII-IMes	4	<1	–
7	HGII-SIMes	4	30	98
8	85	2	59	99
9	86	4	55	98

^aSMP: secondary metathesis products (mixture of C₃–C₁₃ olefins) [35].

unsymmetrical NHCs could provide a cost-effective alternative to the multistep synthesis of their saturated counterparts [36]. The catalyst **85** was identified as the catalyst of choice for the selective metathesis of linear α -olefins and was successfully applied to selectively re-equilibrate the naphtha fraction (C₅–C₈) of a Fischer–Tropsch feed derived from biomass to higher value added olefins (C₉–C₁₄) that can serve as plasticizer and detergent precursors. An excellent olefin distribution with no isomerization was observed without the use of any additive even after 24 h of reaction performed at 50 °C under neat conditions.

N-Alkyl substituents possessing functionalities or heteroatoms

In 2001, the Fürstner group reported on phosphine-containing ruthenium complexes having unsymmetrical NHCs characterized by an alkenyl chain replacing one of the *N*-mesityl groups of the NHC ligand (**98–100**, Figure 19) [37]. The complexes **98–100** were able to metathesize their own ancillary ligands, thus leading to species in which the NHC ligand is bound to the Ru=CHR moiety to form a metallacycle (**101** and **102**, Figure 19). The basic idea was that these catalysts might be able to regenerate themselves upon consumption of the monomer in the reaction media. Variants of these complexes with a silyl ether or a perfluoroalkyl chain on one of the nitrogens of the NHC were also presented (**103** and **104**, Figure 19).

The catalytic behavior of complexes **98–100** and **101, 102** was tested in the RCM of *N,N*-dimethyl-*N*-tosylamide (**93**) to form the corresponding tetrasubstituted cycloolefin **94**.

(Scheme 10; reaction performed in toluene at 80 °C with 5 mol % of catalyst). All the complexes were able to achieve the cyclization, although the catalytic activity of the homologous series **98–100** was found to be strongly dependent on the tether length between the alkene group and the metal center. This effect is likely related to their different ability in forming the corresponding chelate complexes *in situ* (Figure 19).

Importantly, later on Grubbs and co-workers utilized this kind of catalysts, featuring a chelating N-to-Ru arm, for the preparation of cyclic polymers from cyclic monomers via a ring-expansion metathesis polymerization (REMP) process [38,39]. With the aim of developing catalysts suitable for covalent immobilization on various supports, Fürstner et al. reported on the preparation of some unsymmetrical complexes containing pendant protected (**105–108**) and unprotected (**109–111**) hydroxyalkyl chains on their NHCs (Figure 20) [40].

Complex **109** was easily immobilized on functionalized silica gel and the resulting complex **112** (Figure 20) was tested in prototype RCM reactions. In comparison to its homogeneously soluble analogues **109** and **110**, complex **112** required longer reaction times to give the same yields, but was reusable up to three times.

Interestingly, during investigations carried out to anchor this type of ruthenium complexes by physisorption rather than chemisorption, an unexpected molecular rearrangement of their ligand sphere, determining a *cis* orientation of the neutral ligands, was observed (113 and 114, Figure 20). The same

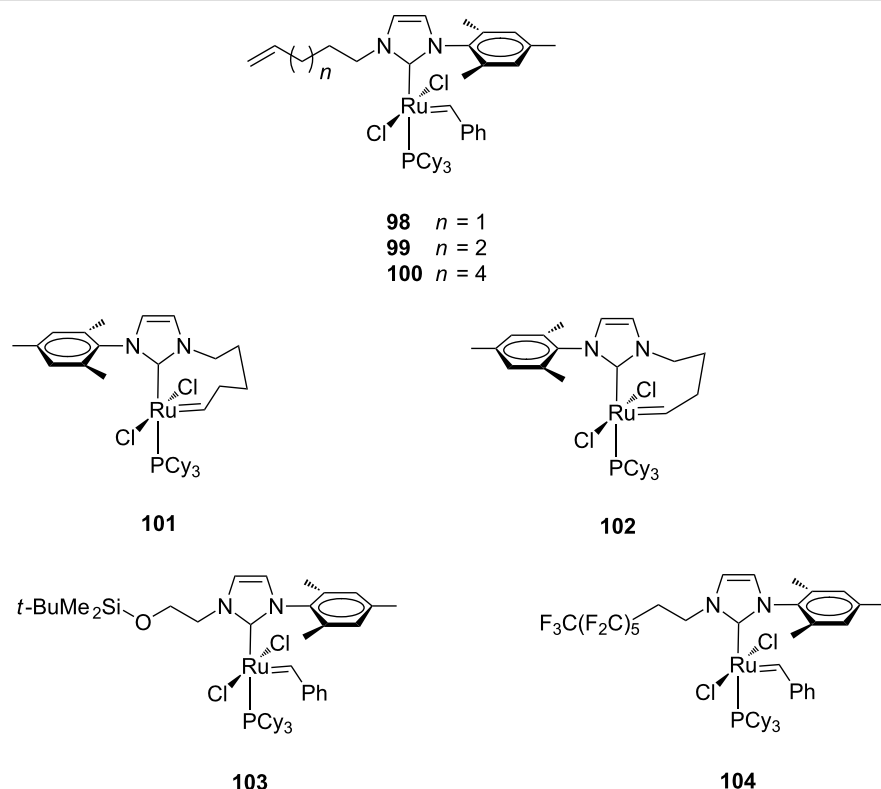


Figure 19: Grubbs-type complexes **98–104** with *N*-alkyl, *N'*-mesityl NHCs.

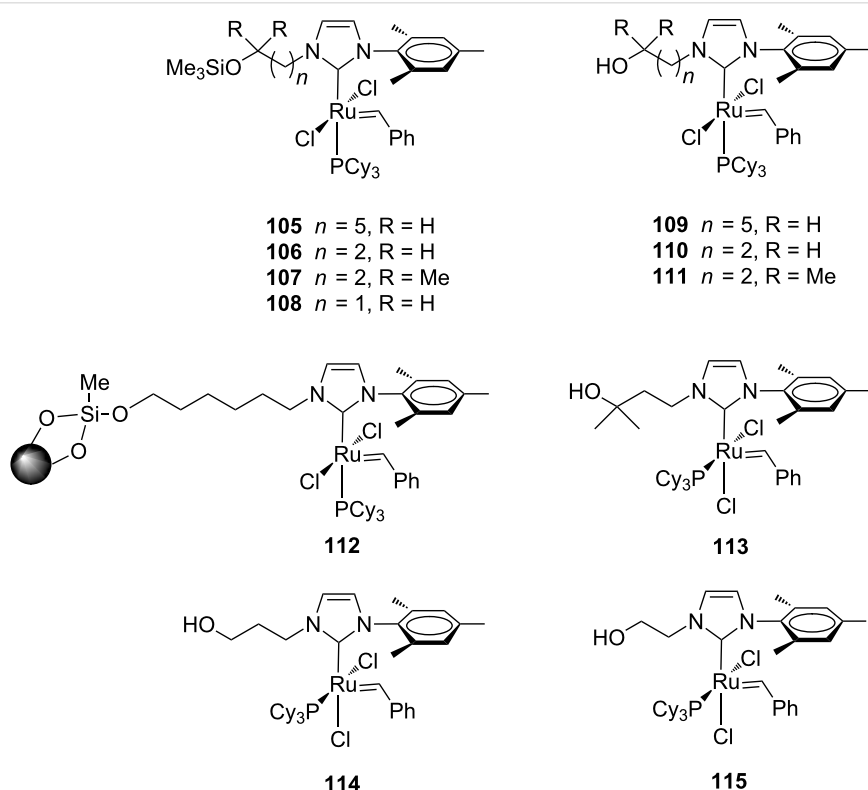


Figure 20: Grubbs-type complexes **105–115** with *N*-alkyl, *N'*-mesityl ligands.

unusual *cis* configuration was displayed by complex **115** (Figure 20) upon release from its precursor **108** by deprotection under acidic conditions.

The *cis* isomers **113–115** exhibited catalytic activity only at high temperatures, where they likely reassume the *trans* form which is characteristic for the Grubbs-type ruthenium carbene complexes.

In order to develop a new structural class of highly performing NHC-based metathesis catalysts with *N*-alkyl groups, ruthenium benzylidene complexes containing carbohydrate-based NHCs derived from glucose (**116**) and galactose (**117**, Figure 21) were reported in 2009 [41].

These complexes were characterized in solution by NMR techniques which revealed, at room temperature, the presence of rotameric species resulting from rotation about the Ru–C(benzylidene) bond. The catalytic behavior of **116** and **117** was examined in standard RCM, CM, ROMP olefin metathesis reactions. Interestingly, **116** and **117** differing only at

one stereocenter showed different kinetic behavior in the RCM of diethyl diallylmalonate (**7**, Scheme 1; reaction temperature 40 °C), where **117** displayed a higher activity than catalyst **116**. Furthermore, they showed surprising selectivity (*E/Z* ratio around 3) in the CM of allylbenzene (**13**) and *cis*-1,4-diacetoxy-2-butene (Scheme 4; reaction temperature 40 °C) compared to the benchmark catalysts **GII-IMes** and **GII-SIMes**, indicating that the steric bulk of the carbohydrate plays a role in influencing the geometry of the resulting olefinic product. Given the chiral nature of the carbohydrate attached to the NHC, complexes **116** and **117** were tested in the AROCM of a variety of norbornene derivatives with styrene. While isolated yields were generally excellent, enantiomeric excesses were poor.

The effect of a dangling amine tether incorporated into the NHC ligand on the catalytic efficiency of ruthenium benzylidene complexes was examined by Fryzuk et al. (**118**, Figure 22) [42].

NMR studies showed that complex **118** exists as a mixture of two rotational isomers in a 7:1 ratio. The major isomer was characterized by X-ray crystallography, while the minor isomer

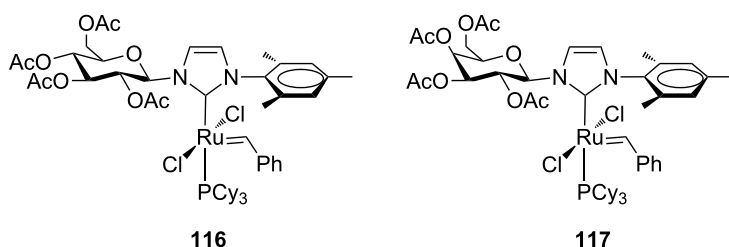


Figure 21: Complexes **116** and **117** bearing a carbohydrate-based NHC.

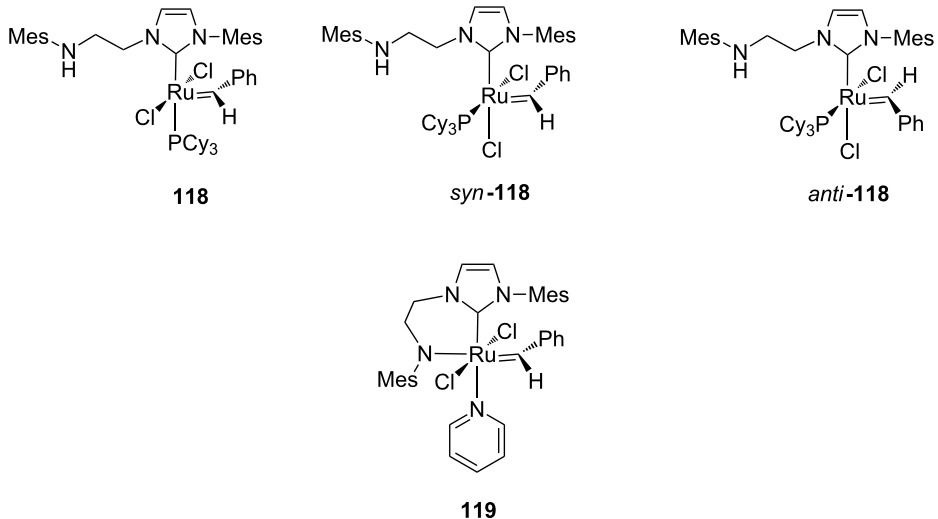


Figure 22: Complexes **118** and **119** bearing a hemilabile amino-tethered NHC.

was characterized only in solution and was identified as consistent with two possible structures (*syn*- and *anti*-**118**). In *syn*-**118** the two chloro ligands are *cis* disposed and the PCy_3 unit is *cis* to both the NHC and the benzylidene, whereas in *anti*-**118** the PCy_3 unit and the benzylidene are *trans* with respect to the $\text{Ru}=\text{CHPh}$ double bond. Moreover, no coordination of the tethered amine to the ruthenium center was detected in the species **118** by NMR spectroscopy. Evidence for coordination of the amino arm in solution and in the solid state was observed in its derived monopyridine adduct **119** (Figure 22). Complex **118** was found less active than **GII-SIMes** and **GII-IMes** in model RCM of **7** and ROMP of **16** (see Scheme 1 and Scheme 5, respectively). In the RCM of **7**, catalyst **118** gave 25% conversion in 30 min, while **GII-SIMes** and **GII-IMes** reached 96% and 74% conversion, respectively, within the same time. As for the ROMP of **16**, only 40% conversion was observed after 4 h with **118**, while full conversion was registered for **GII-SIMes** and **GII-IMes** in 6 and 80 min, respectively. The catalyst effi-

ciency is further reduced in the pyridine derivative **119**, suggesting that the pendant amine is deleterious for catalyst performance.

Ruthenium catalysts coordinated with *N*-benzyl, *N'*-aryl NHCs

The effect of replacing one of the mesityl groups of the NHC ligand with a flexible benzyl group on the catalytic properties of the resulting ruthenium complexes was studied by Grela and co-workers, who synthesized indenylidene complexes **120–126** [43,44] (Figure 23). Substituents in the benzyl group were introduced to modify the steric and electronic properties of the ligand and/or to allow additional coordination to the metal center.

The catalytic behavior of **120–126** was investigated in standard metathesis reactions using commercial grade solvents in air and compared to that of commercially available **IndII-SIMes**. Cata-

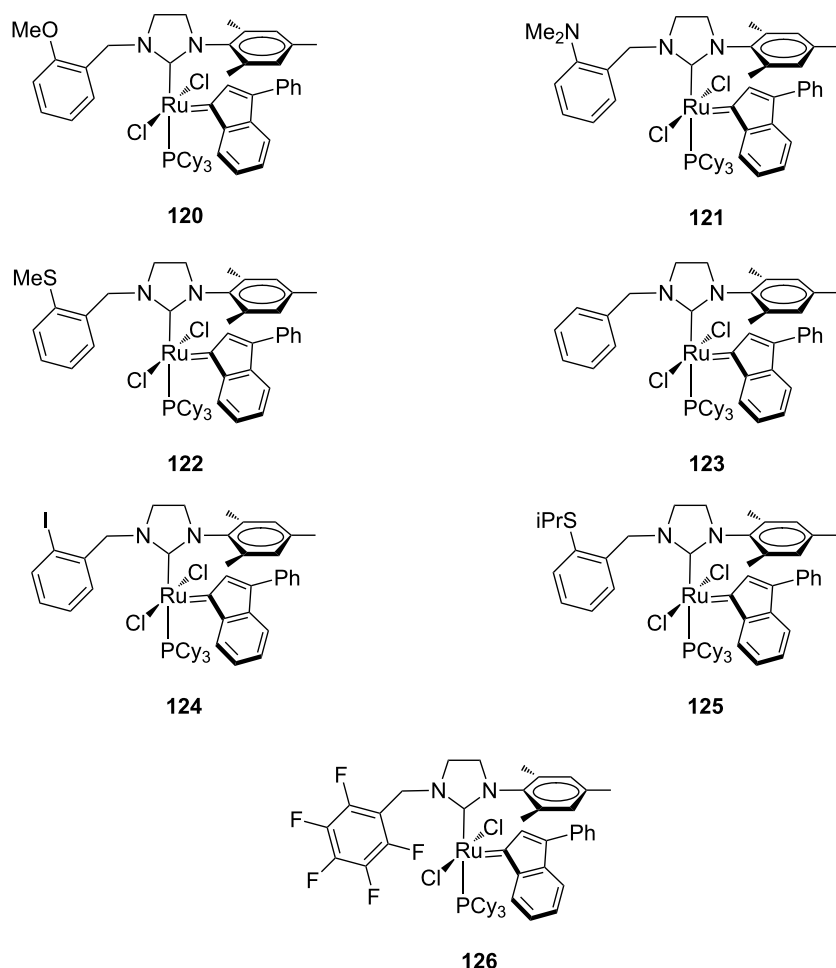


Figure 23: Indenylidene-type complexes **120–126** with *N*-benzyl, *N'*-mesityl NHCs.

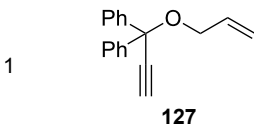
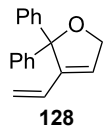
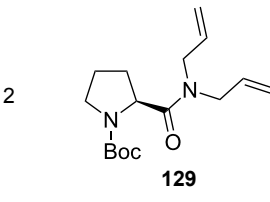
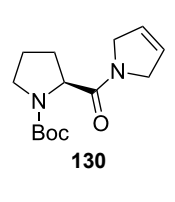
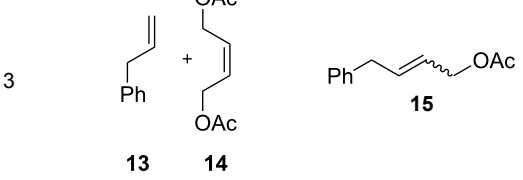
lysts **120**, **121**, **123**, **124** and **126** showed a better performance than **IndII-SIMes** in the RCM of **7** (Scheme 1), whereas the sulfur-containing catalysts **122** and **125** displayed lower activity. In more detail, **120**, **121**, **123** and **124** exhibited similar behavior, in spite of the different nature of aryl substituents, while **126** was found to be less efficient. Solvent tests on **IndII-SIMes**, **123** and **126** demonstrated that dichloromethane is a better solvent with respect to toluene, even if in toluene the initiation of catalyst **126** is faster. The low activity of **122**, **125** and **126** was rationalized by supposing the presence of an interaction between the metal and the heteroatoms of the benzyl substituents [15,43,44]. Complexes **120**, **121**, **123**, and **124** significantly outperformed commercial **IndII-SIMes** in the RCM of diethyl allylmethallylmalonate (**9**) as well. On the contrary, they appeared not suitable in the synthesis of tetrasubstituted olefins. Indeed, they were tested at 60 °C in the RCM of *N,N*-dimethylallyl-*N*-tosylamide (**93**, Scheme 10; reaction performed in toluene at 80 °C with 5 mol % of the catalyst), giving conversions between 30–40%, as observed also for the commercial catalyst **IndII-SIMes**.

The catalysts **120** and **121** were also tested in the ring-closing ene–yne metathesis reaction (RCEYMR) of standard substrate **127**. Both catalysts revealed slightly more active than **IndII-SIMes**, with **121** being the most efficient (Table 5, entry 1). Catalyst **120** showed the highest activity in the RCM of the amide-based substrate **129** (Table 5, entry 2) and in the CM of **13** with **14**, but with a slightly lower *Z*-selectivity (Table 5, entry 3).

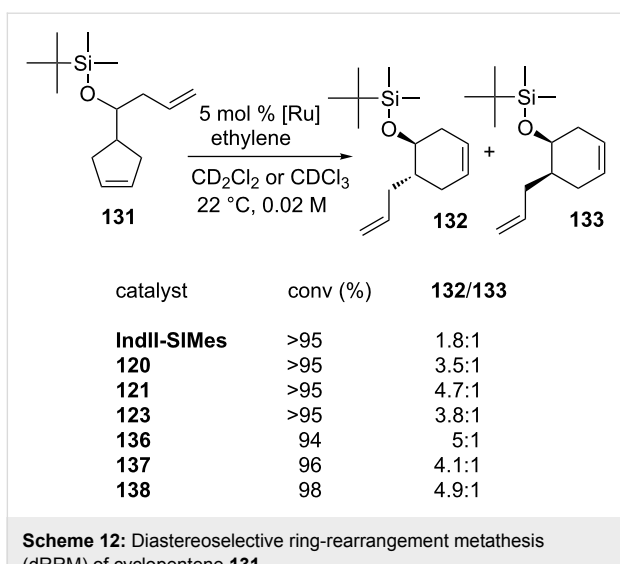
Finally, in the presence of catalysts **120**, **121** and **123**, diastereoselectivities higher than those achieved in the presence of **GII-SIMes**, **HGII-SIMes** and **IndII-SIMes** were observed in the diastereoselective ring-rearrangement metathesis (dRRM) of cyclopentene **131** (Scheme 12).

The presence of a nitro group at the *ortho* or *para* positions of the benzyl substituent (**134** and **135** in Figure 24), reported by Malinowska and co-workers [45], led to higher activities in the RCM of **7** and **9** (Schemes 1 and 2), with respect to the commercial **IndII-SIMes**, but significantly lower if compared to

Table 5: Metathesis reactions of standard substrates.

entry	substrate	product	catalyst (mol %)	T (°C)	t (h)	isolated yield (%)
1			IndII-SIMes (2) 120 (2) 121 (2) 134 (2) 135 (2) 136 (2) 137 (2) 138 (2) 139 (2) 140 (2) 141 (2) 142 (2)	30 30 30 40 40 50 50 50 50 50 50 50	8 6 5 8 8 2 2 2 1.5 1.5 1.5 1.5	96 ^a 94 ^a 96 ^a 99 ^b 99 ^b 92 ^c 91 ^c 92 ^c 89 ^c 91 ^c 89 ^c 91 ^c
2			IndII-SIMes (1) 120 (1) 121 (1) 136 (1) 137 (1) 138 (1) 139 (1) 140 (1) 141 (1) 142 (1)	50 50 50 50 50 50 50 50 50 50	2.5 1 2 1.25 2 1 3 3 3 3	94 ^a 96 ^a 91 ^a 87 ^c 89 ^c 92 ^c 85 ^c 94 ^c 88 ^c 90 ^c
3			IndII-SIMes (2.5) 120 (2.5) 121 (2.5) 134 (2.5) 135 (2.5) 136 (2.5) 137 (2.5) 138 (2.5) 139 (2.5) 140 (2.5) 141 (2.5) 142 (2.5)	30 30 30 30 30 50 50 50 50 50 50 50	20 20 20 20 20 2 2 2 2 1.5 1.5 1.5	74 (<i>E/Z</i> = 8:1) ^a 80 (<i>E/Z</i> = 9:1) ^a 74 (<i>E/Z</i> = 11:1) ^a 45 (<i>E/Z</i> = 4:1) ^b 86 (<i>E/Z</i> = 5:1) ^b 89 (<i>E/Z</i> = 7.1:1) ^c 76 (<i>E/Z</i> = 7.9:1) ^c 93 (<i>E/Z</i> = 6:1) ^c 74 (<i>E/Z</i> = 3.6:1) ^c 80 (<i>E/Z</i> = 7:1) ^c 81 (<i>E/Z</i> = 8:1) ^c 78 (<i>E/Z</i> = 6.5:1) ^c

^aRef [43]; ^bRef [45]; ^cRef [46].



Scheme 12: Diastereoselective ring-rearrangement metathesis (dRRM) of cyclopentene **131**.

catalysts **120**, **121**, **123** and **124**. A scarce activity toward the formation of tetrasubstituted olefin **12** (Scheme 3) was also observed. Complexes **134** and **135** were tested in RCEYM of **127** (Table 5, entry 1) showing a good efficiency and in the CM of **13** and **14** (Table 5, entry 3), where interesting Z-selectivities can be achieved.

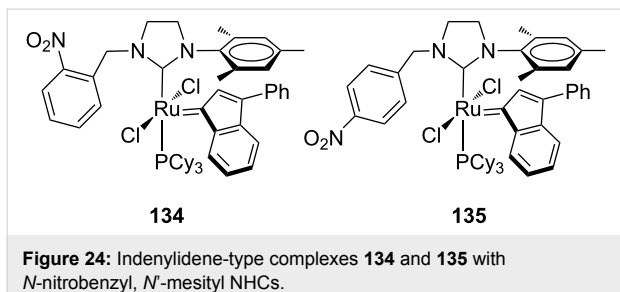


Figure 24: Indenylidene-type complexes **134** and **135** with *N*-nitrobenzyl, *N'*-mesityl NHCs.

Recently, Grela and co-workers modified the previously reported *N*-benzyl, *N'*-aryl NHC–Ru complexes **120**, **121** and **123**, by synthesizing the analogous Hoveyda-type derivatives **136–138** (Figure 25). Additionally, the behavior of catalysts **136–138** was compared with that of complexes bearing an *N*-Dipp (Dipp = 2,6-diisopropylphenyl) substituent in place of the *N*-mesityl group (**139–142** in Figure 26) [46].

As expected, the *N'*-Dipp complexes displayed a higher stability with respect to the *N'*-mesityl complexes. Nevertheless, complexes **136–138** were more active than **139–142** in the RCM of **7**, conducted at 50 °C and none of those catalysts outperformed **HGII-SIMes** and **HGII-SIPr**. Analogous results were observed in the RCM of more crowded substrates. The similar behavior of **141** and **142** indicated that steric effects are more relevant than electronic effects.

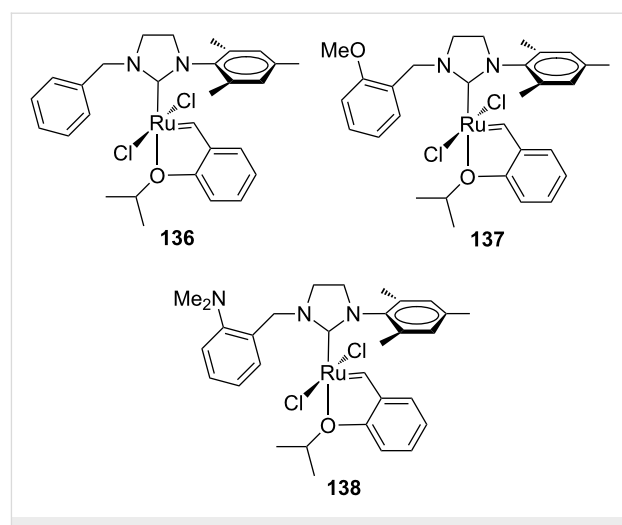


Figure 25: Hoveyda-type complexes **136–138** with *N*-benzyl, *N'*-mesityl NHCs.

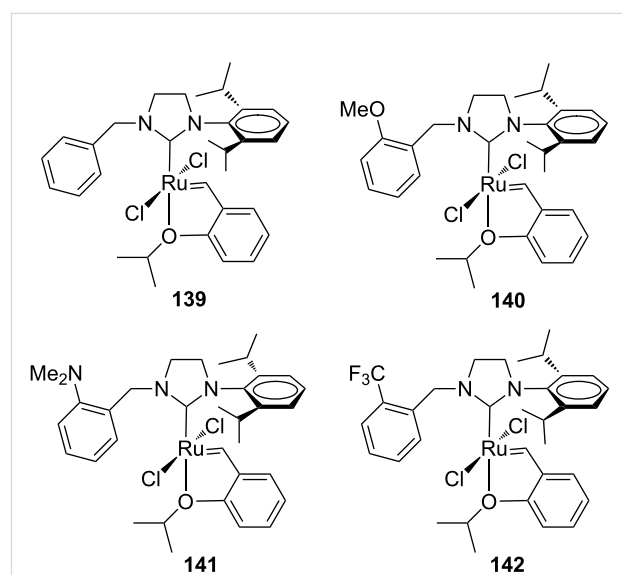


Figure 26: Hoveyda-type complexes **139–142** with *N*-benzyl, *N'*-Dipp NHCs.

Catalysts **136–142** were tested in the RCEYM of **127**, in the RCM of **129** and in the CM of **13** and **14** (Table 5, entry 3). According to the experimental results, mesityl-bearing catalysts generally gave better yields than Dipp-containing analogues. In the presence of **136–138**, a high selectivity in the dRRM of cyclopentene **131** was also observed (Scheme 12). Self metathesis of 1-octene (**96**) was conducted in the presence of **136**, **137**, **139** and **140**, in order to selectively obtain tetradec-7-ene (**97**). The presence of the *N*-benzyl substituent was crucial to achieve high yield (up to 80%) of the desired product, whereas commercial **HGII-SIMes** and **HGII-SIPr**, despite the higher reaction rate, gave mainly a mixture of byproducts.

Ruthenium catalysts coordinated with *N*-heteroaryl methyl, *N'*-aryl NHCs

To further modify the electronic and steric properties of the NHC ligand and consequently, to improve efficiency of the resulting ruthenium catalysts, the Grela group focused on the development of new ruthenium indenylidene and Hoveyda-type complexes bearing unsymmetrical NHCs containing a heteroaromatic moiety (**143–147**, Figure 27) [47].

The catalytic performances of **143–147** were examined in model RCM and CM metathesis reactions under air in commercial grade toluene and compared to benchmark complexes **IndII-SIMes** and **HGII-SIMes**. Under these conditions all the catalysts tested showed very high activity in RCM transformations, with the newly developed systems requiring shorter reaction times to give quantitative conversion. In the RCEYM of **127**, complexes **143**, **146** and **147** were performing less effectively than all the other ones, however, no clear relationship between heterocyclic substituents and activity can be found. In the CM of allylbenzene (**13**) and *cis*-1,4-diacetoxyl-2-butene (**14**), all of the new catalysts gave higher amounts of the *Z* isomer than **IndII-SIMes** and **HGII-SIMes**. Indeed, **143–147** showed *E/Z* ratios in the range of 3.2–4.0, while **IndII-SIMes** and **HGII-SIMes** provided *E/Z* ratios of 9.4 and 9.3, respectively. The complexes **143–147** displayed also better diastereoselectivities in the dRRM reaction of **131** (Scheme 12) than the commercial catalysts **GII-SIMes**, **HGII-SIMes** and **IndII-SIMes**.

The synthesis of indenylidene and Hoveyda-type complexes bearing *N*-phenylpyrrole and *N*-phenylindole moieties on their NHCs was also attempted [48]. Most of them revealed difficult to prepare and unstable apart from the Hoveyda-type complexes **148** and **149** (Figure 28).

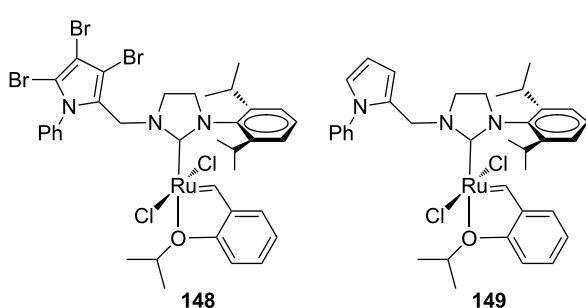


Figure 28: Hoveyda-type complexes **148** and **149** with *N*-phenylpyrrole, *N'*-mesityl NHCs.

These two systems were tested in standard RCM and CM reactions and complex **148** with a perbrominated *N*-phenylpyrrole moiety revealed as more stable and active than its parent catalyst **149**. Both complexes were found completely inactive in RCM at room temperature, becoming active only at higher temperature (80 °C). Computational studies suggested that the rarely occurring phenyl–ruthenium intramolecular interactions are responsible for lower stability and slower reaction initiation.

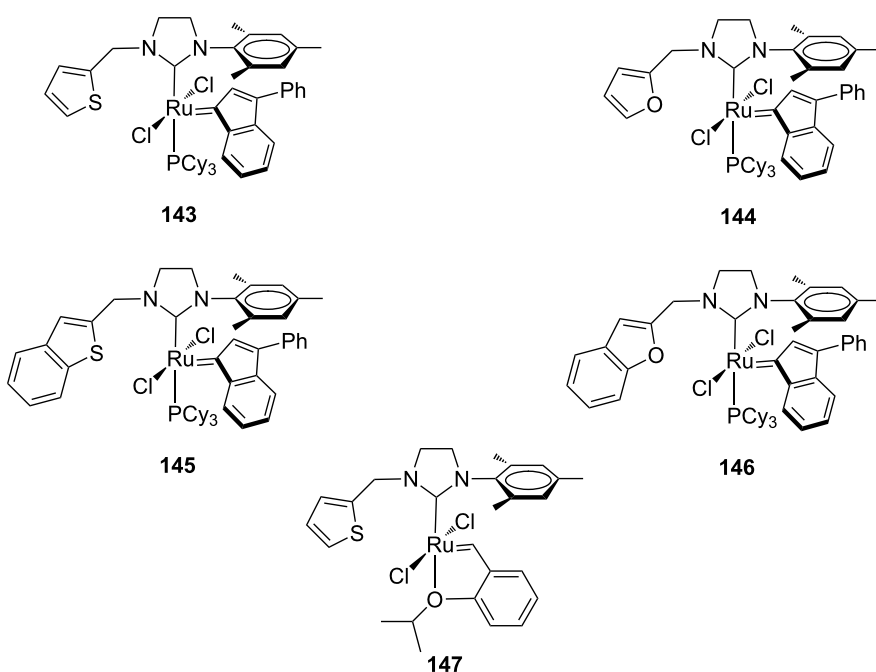


Figure 27: Indenylidene (**143–146**) and Hoveyda-type (**147**) complexes with *N*-heteroaryl methyl, *N'*-mesityl NHCs.

Ruthenium catalysts coordinated with *N*-trifluoromethyl benzimidazolidene NHCs

With the goal to develop chemoselective catalysts, ruthenium complexes containing unsymmetrical *N*-trifluoromethyl NHCs were introduced by Togni et al. (**150–152**, Figure 29) [49].

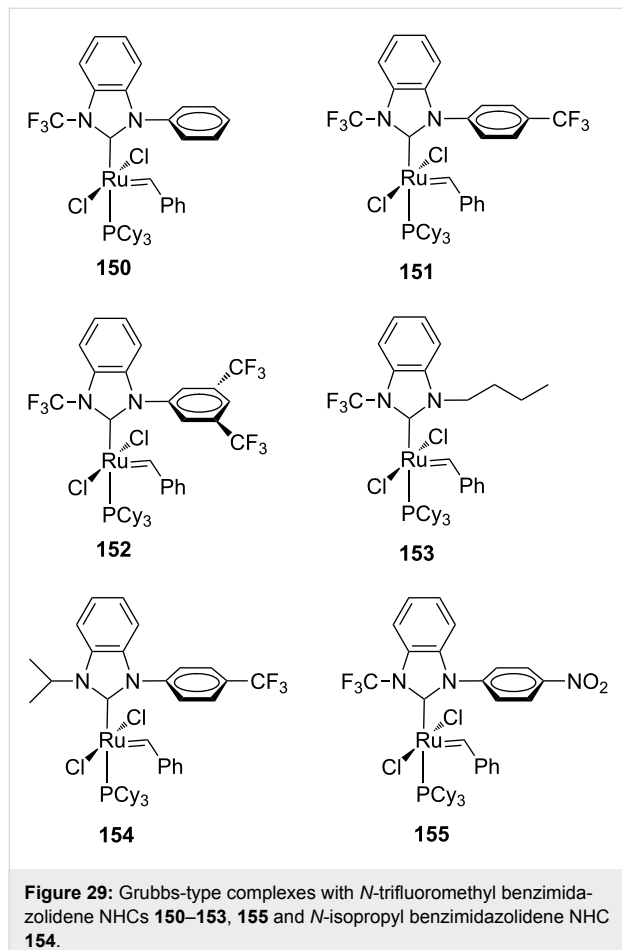


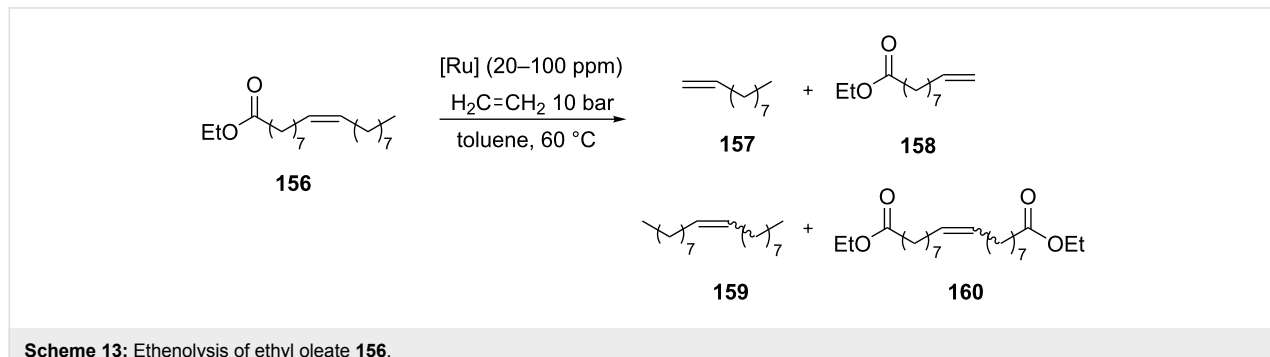
Figure 29: Grubbs-type complexes with *N*-trifluoromethyl benzimidazolidene NHCs **150–153**, **155** and *N*-isopropyl benzimidazolidene NHC **154**.

The presence of one *N*-trifluoromethyl substituent was supposed to impart positive effects on the catalytic performance, influencing both electronic and steric properties of the NHC ligand. Indeed, as already underlined, in symmetrical

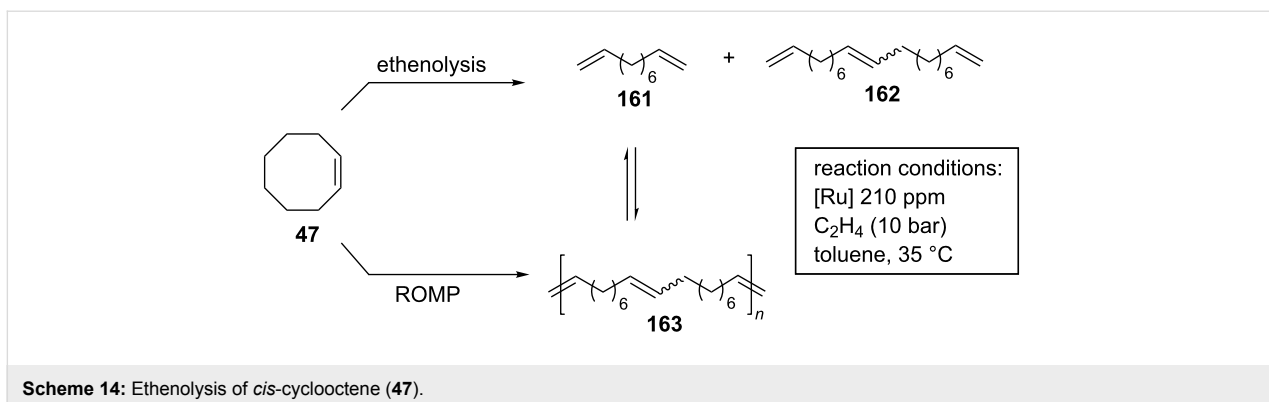
NHC ruthenium complexes with fluorinated *N*-aryl groups previously reported by Grubbs, a Ru–F interaction was considered as responsible for the observed enhanced metathesis activity [15]. X-ray crystallographic analysis of complexes **150**, **151** and **152** showed a Ru–F interaction in the solid state. All the catalysts were tested in benchmark RCM and CM reactions, where they displayed no improved performances compared to the commercial **GII-SIMes** catalyst. On the other hand, they showed a remarkable chemoselectivity (up to 97%) in the alternating copolymerization of norbornene (**46**) and cyclooctene (**47**). Moreover, in the ethenolysis of ethyl oleate (**156**, Scheme 13), they exhibited good selectivities (80–90%) for the formation of desired terminal olefins **157** and **158**.

Catalyst **154** containing an *N*-isopropyl group (Figure 29), which is considered to be sterically equivalent to the *N*-trifluoromethyl group, disclosed a substantially lower selectivity in both alternating copolymerization and ethenolysis reaction, underlining that the electronic effect determined by the strongly electron-withdrawing CF₃ group and/or a Ru–F interaction are the key factors for achieving a high selectivity in these transformations and, more general, could be used for modulating catalyst properties.

In another contribution by Coperet, Sigman and Togni, *N*-CF₃ complexes **150–155** (Figure 29) were tested for the ethenolysis of cyclic olefins to selectively form α,ω -dienes, along with other 23 Ru benzylidene complexes featuring NHC ligands that differ in steric and electronic properties [50]. It is worth to underline that this transformation mediated by ruthenium initiators is less well investigated, presumably as a consequence of the high activity of ruthenium catalysts toward the competitive ROMP that is leading to low yields of terminal dienes. Among all the investigated systems, *N*-CF₃ complex **153** emerged as the best performing catalyst in the ethenolysis of *cis*-cyclooctene (**47**), giving 96% conversion of cyclooctene and 53% selectivity for the ethenolysis product **161** (Scheme 14). Furthermore, catalyst **153** showed no detectable formation of poly(COE) (**163**) via ROMP in the absence of ethylene. On the



Scheme 13: Ethenolysis of ethyl oleate **156**.



Scheme 14: Ethenolysis of *cis*-cyclooctene (**47**).

contrary, the benchmark catalyst **GII-SIMes** displayed only 12% selectivity for the desired product, giving predominantly poly(COE).

Due to its superior activity, complex **153** was also investigated in the ethenolysis of more challenging substrates such as norbornene derivatives, which typically are among the most popular ROMP monomers because of their high ring strain. The efficient synthesis of valuable functionalized α,ω -dienes was thus accomplished in useful yields (>70%).

In order to explain the selectivity observed in the ethenolysis of cyclic olefins, steric and electronic descriptors of the NHC ligands obtained computationally were evaluated. The main role in controlling selectivity was ascribed to the π -acceptor ability of the NHC ligand that becomes more important with dissymmetric NHCs bearing an *N*-CF₃ group and drives the relative rate of degenerate metathesis and selectivity in ethenolysis of cyclic olefins.

Ruthenium catalysts coordinated with backbone substituted *N*-alkyl, *N'*-aryl NHCs

Substitution at the backbone positions of the NHC framework has represented a remarkable advancement in the design of ruthenium olefin metathesis catalysts, due to the significant effects exerted on complexes' stability, reactivity and selectivity [51].

The first example of *C*₁-symmetric ruthenium catalyst bearing a backbone-substituted *N*-alkyl, *N'*-aryl NHC ligand was reported by Collins et al. in 2007 (**164**, Figure 30) [52]. This complex represented an evolution of the chiral *C*₂-symmetric system previously proposed by Grubbs (**165**, Figure 30) [53], in which the replacement of the phenyl groups on the backbone with the more encumbered and electron-donating 1,2-di-*tert*-butyl units was made with the hope to enhance reactivity and enantioselectivity in Grubbs-type olefin metathesis catalysts. Moreover, in order to reduce the whole ligand's bulkiness which could have

hampered attempts to prepare the catalyst, one of the *N*-aryl substituents was replaced with the smaller methyl group.

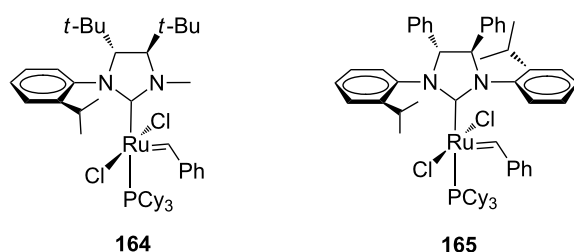


Figure 30: Grubbs-type *C*₁-symmetric (**164**) and *C*₂-symmetric (**165**) catalysts with a backbone-substituted NHC.

Complex **164** was obtained in poor yield (30%) and characterized through NOE and X-ray analysis, revealing the exclusive formation of the rotational isomer in which the *N*-methyl lies over the carbene unit (the *syn* isomer, Figure 31).

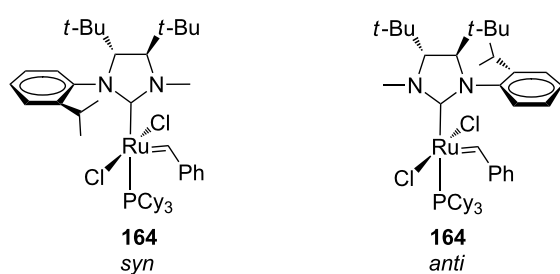


Figure 31: Possible *syn* and *anti* rotational isomers of catalyst **164**.

The catalytic performances of **164** were tested in the asymmetric ring-closing metathesis (ARCM) of prochiral trienes **166**, **168** and **170** (Scheme 15, Table 6) [52,54] achieving enantiomeric excesses (ee) that were generally lower with respect to those obtained with the *C*₂-symmetrical analogue **165** [55] (Table 6).

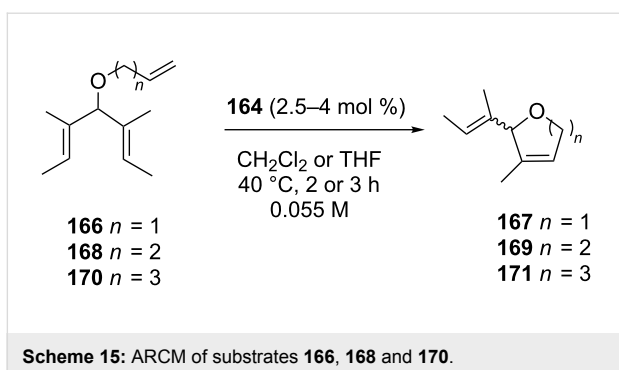


Table 6: ARCM of prochiral trienes **166**, **168**, and **170** promoted by catalysts **164** and **165**.

entry	catalyst	substrate	additive	ee (%)	conv (%)
1 ^a	164	166	none	82	>98
2 ^b			NaBr	68	>98
3 ^b			NaI	48	>98
4 ^a	164	168	none	28	>98
5 ^b			NaBr	34	>98
6 ^b			NaI	42	41
7 ^a	164	170	none	60	>98
8 ^b			NaBr	64	93
9 ^b			NaI	—	—
10 ^a	165^c	166	none	35	>98
11 ^b			NaI	90	>98
12 ^b	165^c	168	NaI	90	>98
13 ^b	165^c	170	NaI	85	5

^aCatalyst 2.5 mol %, solvent CH₂Cl₂; ^bcatalyst 4 mol %, solvent THF [54]; ^c[55].

The size of the ring formed was found to have a crucial influence on the enantioselectivity of the reaction with the enantiomeric excesses decreasing when passing from five to six and seven-membered rings (Table 6, entries 1, 4 and 7). The use of halide additives such as NaBr and NaI was also found to be dependent on the size of the ring formed, affecting both conversions and enantiomeric excesses with controversial results (Table 6). It should be underlined that the ambiguous halide influence constitutes a relevant difference between **164** and **165**. In fact, for the latter, the employment of halide additives had always a beneficial effect on the enantioselectivity [55].

The product ring size dependence observed in the desymmetrization of **166**, **168** and **170** with **164** was explained considering that an NHC rotation is possible during the catalytic cycle and that **166**, **168** and **170** should have different relative rates of cyclization. If the cyclization is slow, for instance in the case of seven-membered ring alkenes, an NHC rotation could occur during the catalytic cycle, thus determining a decrease of the enantiomeric excesses.

Rotation of the NHC ancillary ligand was detected in the case of **172**, the Hoveyda-type analogue of **164** (Figure 32), for which a room temperature interconversion between *syn* and *anti* rotamers, observed at a ratio of 7.8:1, was revealed by NOE experiments. Surprisingly, despite such rotation the reactivity profiles and the enantioselectivities observed for **164** and **172** in the desymmetrization of **166** and **170** were comparable. This suggested that the reaction occurs faster when the *N*-methyl group is *syn* to the ruthenium–carbene than when the *N*-aryl group is located *syn* to the ruthenium–carbene moiety.

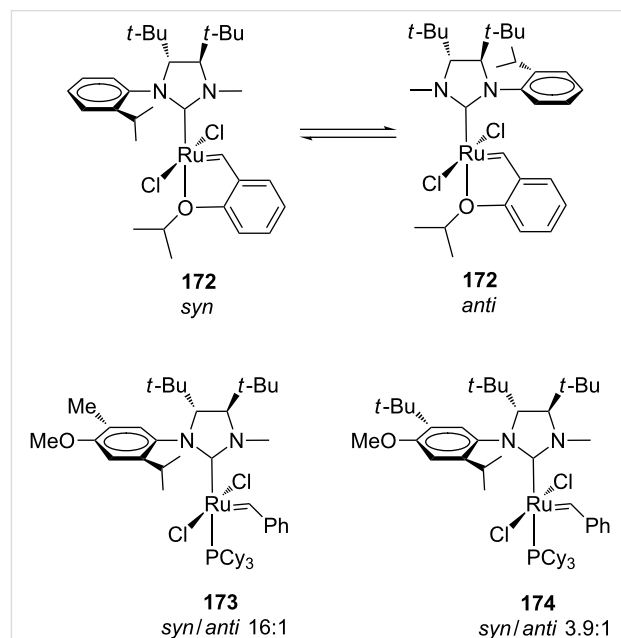
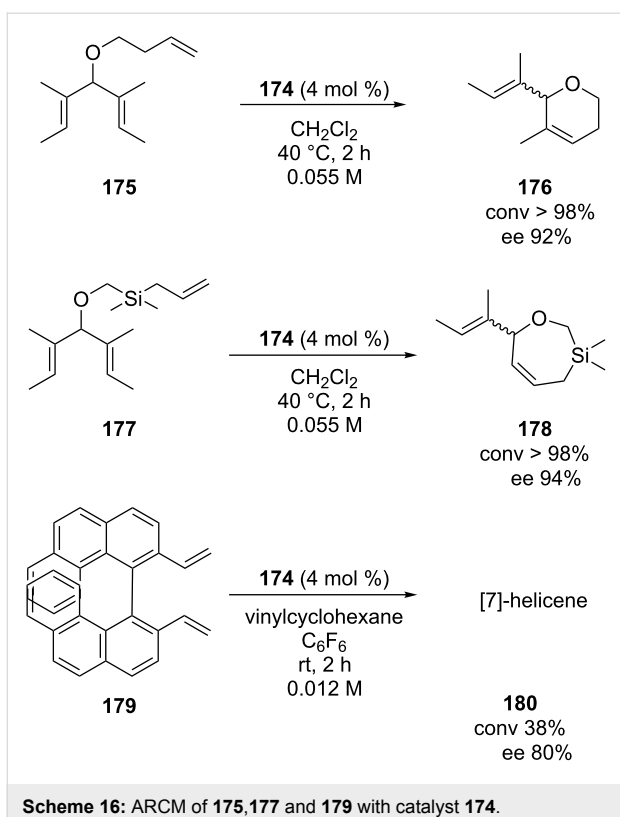


Figure 32: Hoveyda (**172**) and Grubbs-type (**173**, **174**) backbone-substituted C₁-symmetric NHC complexes.

In order to try suppressing the NHC rotation during the catalytic cycle, catalysts **173** and **174**, possessing additional substituents on the *N*-aryl group, were synthesized in moderate yields (42–44%, Figure 32). Both complexes were isolated as a mixture of rotamers, with a prevalence of the *syn* isomer and no interconversion between the *syn/anti* rotational isomers was detected at room temperature [54]. The catalytic behaviors of **173** and **174** were tested in a series of model ARCM reactions and similar or improved performances with respect to **164** and **172** were noticed, suggesting that the significant reactivity could result from the major *syn* isomer.

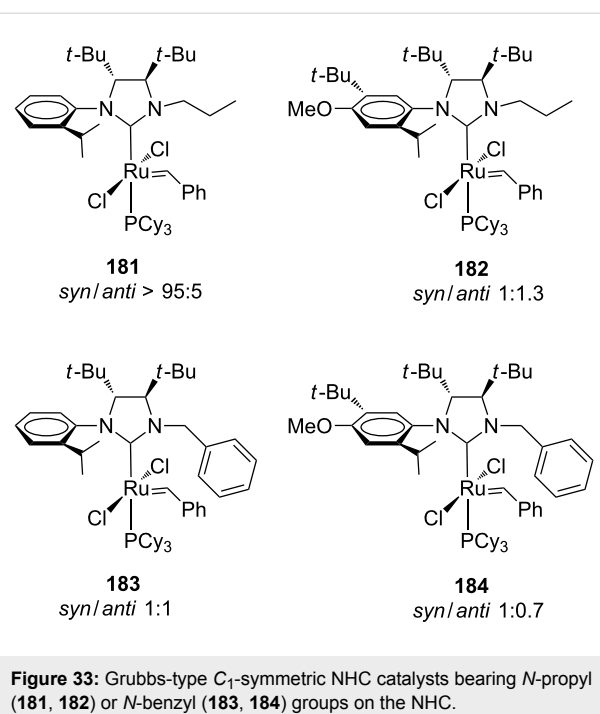
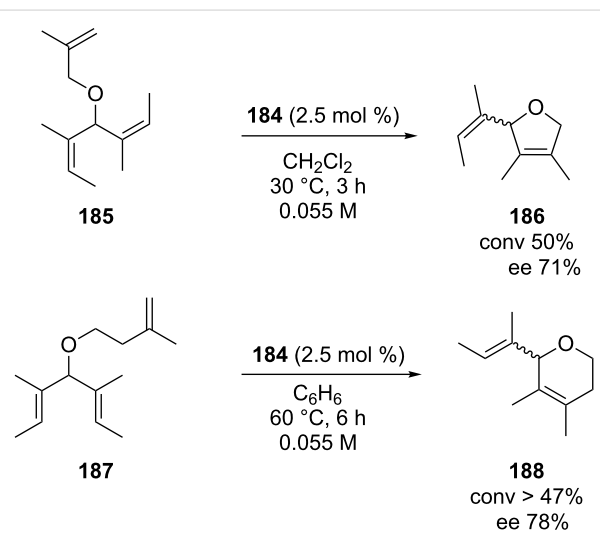
It is noteworthy that complex **174** was found to be very competent also in cyclizations to form six and seven-membered ring olefins (**175** and **177**, Scheme 16), conversely to the other C₁-symmetric systems previously reported. On the other hand, coherently with **164** and **172**, the best results were achieved without the use of any halide additive.

Scheme 16: ARCM of **175**, **177** and **179** with catalyst **174**.

The unsymmetrical NHC catalysts **164**, **173** and **174** were also examined in the asymmetric synthesis of [7]helicene (**180**). Among them, complex **174** exhibited the highest degree of selectivity, leading to the desired product with an enantiomeric excess of 80% [56]. An extension of this study, which examined the effect of the nature of the *N*-alkyl group on the complexes' efficiencies, was published a few years later by the same group [57]. In this paper, new *C*₁-symmetric NHC ruthenium catalysts **181**–**184** bearing the more encumbered *N*-propyl or *N*-benzyl substituents were presented. All catalysts were obtained as a mixture of *syn/anti* rotational isomers (Figure 33).

The catalytic efficiency of these complexes was generally lower with respect to their *N*-methyl analogues, both in terms of reactivity and enantioselectivity. However, despite this disadvantage, they showed an improved thermal and solution stability which allowed their application also in the ARCM forming tetrasubstituted alkenes, a reaction never examined so far with this family of complexes [58]. In particular, using a sample of catalyst **184** enriched in the *anti* rotational isomer (*syn/anti* 1:8), the hindered cycloolefins **186** and **188** were obtained with enantiomeric excesses of 71 and 78%, respectively (Scheme 17).

More recently, Grisi and co-workers investigated new Grubbs-type *C*₁-symmetric catalysts bearing methyl or cyclohexyl as the *N*-alkyl group and two phenyl units in *syn* or *anti* relative

Figure 33: Grubbs-type *C*₁-symmetric NHC catalysts bearing *N*-propyl (**181**, **182**) or *N*-benzyl (**183**, **184**) groups on the NHC.Scheme 17: ARCM of **185** and **187** promoted by **184** to form the encumbered alkenes **186** and **188**.

configuration on the backbone positions (**189**–**192**, Figure 34) [59,60]. These complexes were tested in several model RCM, ROMP and CM transformations and the size of the *N*-alkyl group and the backbone configuration seemed to determine the different catalytic behaviors. The most significant reactivity differences between catalysts having *syn* or *anti* phenyl groups on the backbone were observed in the presence of an *N*-cyclohexyl substituent. In particular, the *N*-cyclohexyl *anti* catalysts **192a** and **192b** showed high efficiencies in almost all tested metathesis transformations, especially in the most challenging

RCM reactions of hindered diolefins in which they rival the commercial second generation Grubbs and Hoveyda–Grubbs catalysts. On the other hand, in the CM of **13** and **14** (Scheme 4), *syn* catalysts **191a** and **191b** gave the most interesting results, leading to the desired cross product **15** in a lower *E/Z* ratio with respect to the *anti* congeners **192a** and **192b** (*E/Z* = 3.6 and 8.5 with **191a** and **192a**, respectively; *E/Z* = 2.6 and 7.6 with **191b** and **192b**, respectively).

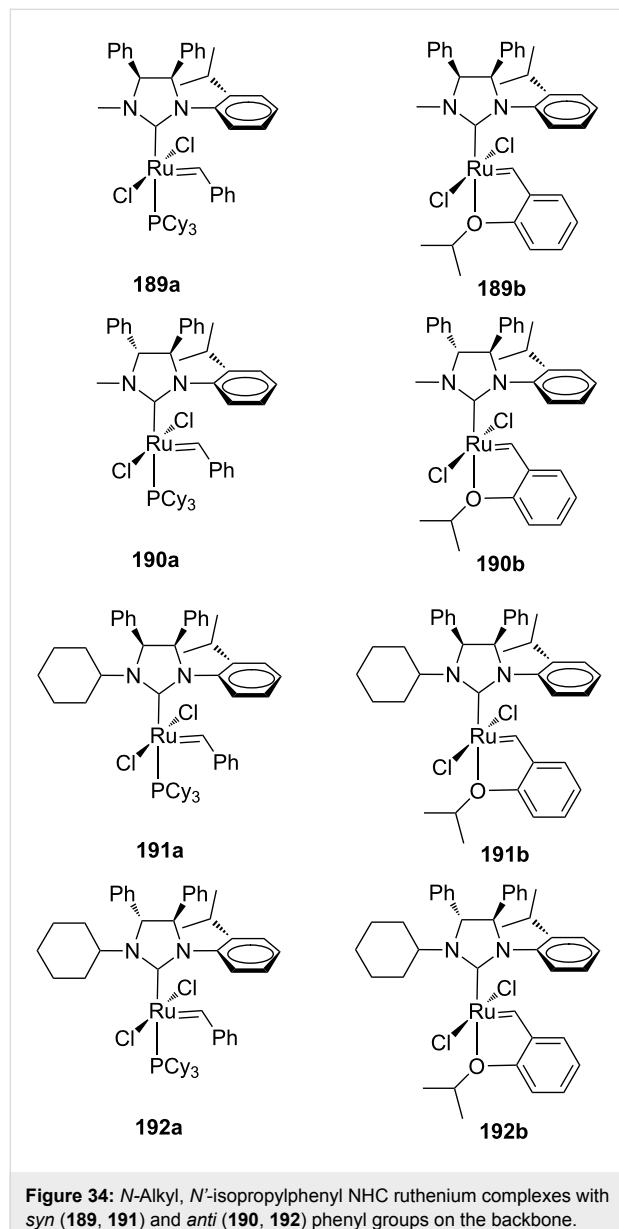


Figure 34: *N*-Alkyl, *N'*-isopropylphenyl NHC ruthenium complexes with *syn* (**189**, **191**) and *anti* (**190**, **192**) phenyl groups on the backbone.

The effect of the NHC backbone configuration on the catalytic properties has been justified considering a more electron-donating nature of the *anti* ligand with respect to the *syn* ligand, as suggested by experimental and theoretical studies on the steric and electronic properties of *N*-cyclohexyl, *N'*-isopropylphenyl

NHC ligands of **191** and **192** evaluated using the corresponding rhodium complexes [60].

A development of this study, which considered the utilization of other *N*-alkyl (neopentyl and neophyl) and *N*-aryl (mesityl) substituents, was published later [61]. Among these novel Hoveyda-type catalysts **193**–**198** (Figure 35), **198** was of particular interest due to its excellent thermal stability in solution and to the high efficiency in the enetholysis of ethyl oleate (**156**, Scheme 13). In this reaction, performed under neat conditions at 50 °C and at a catalyst loading of 100 ppm, **198** gave up to 90% selectivity towards enetholysis products **157** and **158** with a TON of 4400. At a lower catalyst loading (20 ppm), the same catalyst showed 83% selectivity with a TON of 7500, thus giving the best result reported up to now for enetholysis reactions performed with *N*-alkyl, *N'*-aryl NHC ruthenium catalysts.

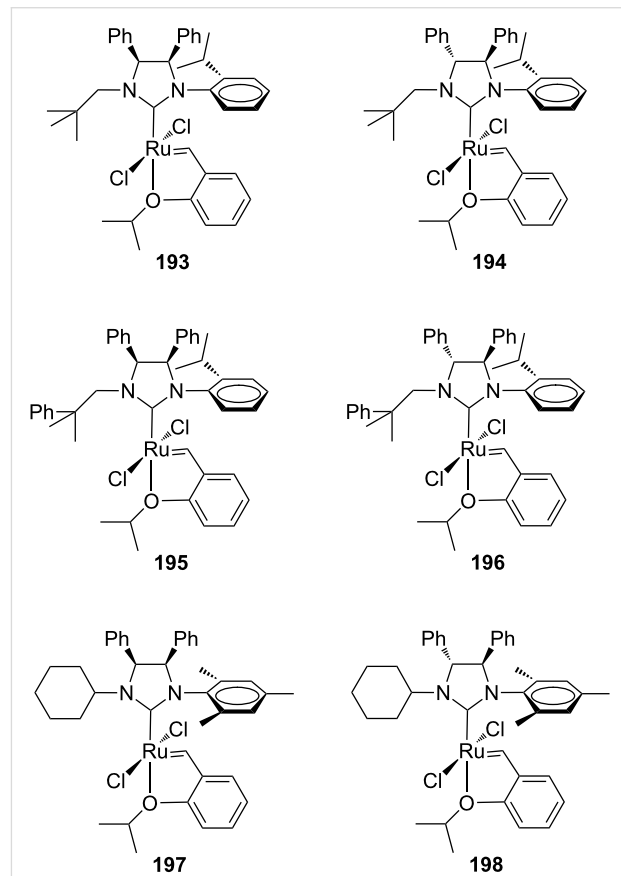
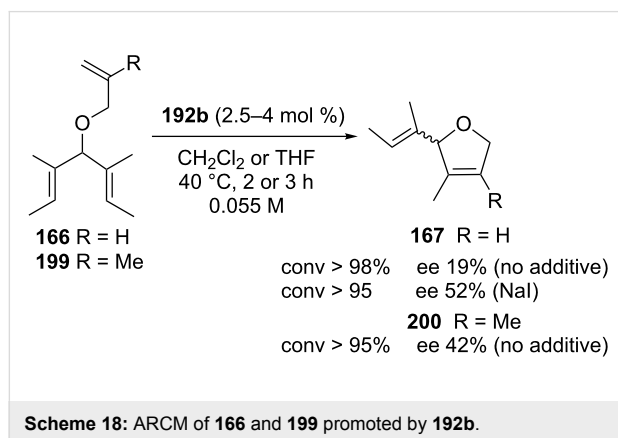


Figure 35: Hoveyda-type complexes **193**–**198** bearing *N*-alkyl, *N'*-aryl backbone-substituted NHC ligands.

All the aforementioned catalysts with an *anti* NHC backbone configuration (**190**, **192**, **194**, **196** and **198**) were tested in model ARCM and AROCM reactions displaying moderate enantioselectivities [60,61]. In the ARCM of **166**, differently from the other *C*₁-symmetric catalysts reported by Collins [52,54],

enantiomeric excesses were found to increase with the use of the halide additive. Interestingly, a pronounced efficiency towards the ring closing of the hindered alkene **199** was also observed (Scheme 18).



Scheme 18: ARCM of **166** and **199** promoted by **192b**.

In another contribution, the same group extended the feasibility in asymmetric metathesis transformations also to *C*₁-symmetric NHC catalysts bearing *syn*-related phenyl substituents on the backbone, that were obtained for the first time in an enantiopure form (**201a** and **201b**, Figure 36) [62]. These complexes were tested in model ARCM of trienes **166** and **199** showing moderate enantioselectivities (14–44% ee).

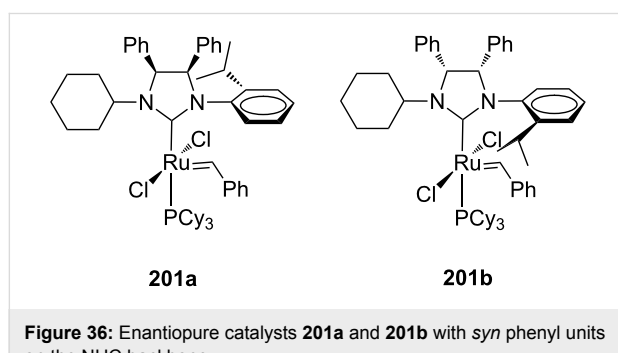


Figure 36: Enantiopure catalysts **201a** and **201b** with *syn* phenyl units on the NHC backbone.

Ruthenium catalysts coordinated with backbone monosubstituted *N*-aryl, *N'*-aryl NHCs

In 2010, Blechert and co-workers synthesized a new type of chiral NHC ruthenium catalysts containing a monosubstituted backbone and two different *N*-aryl groups (**202**–**204**, Figure 37) [63]. The idea behind this new category of compounds lied in the possibility of an efficient transfer of chirality from the backbone group to the metal center through a significant twisting of the monosubstituted arene unit. Additionally, the presence of the flat mesityl segment as the other *N*-aryl substituent could avoid steric hindrance reducing the reactivity.

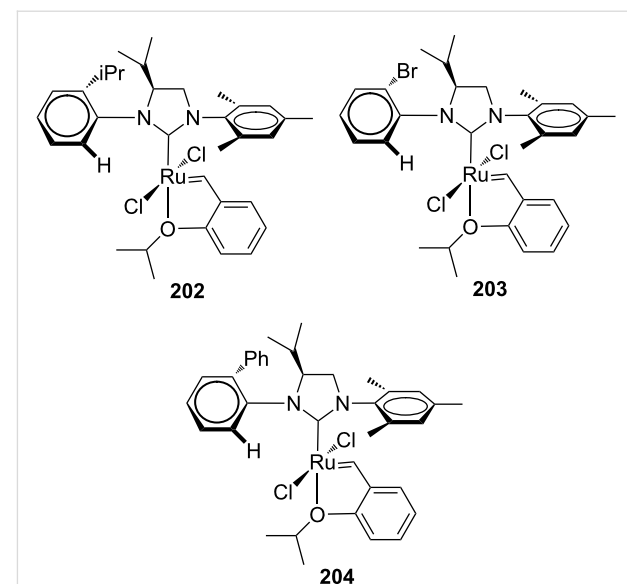


Figure 37: Backbone-monosubstituted catalysts **202**–**204**.

The catalysts **202**–**204** were tested in model ARCM and AROCM reactions. In the latter transformation, they were found to be highly efficient showing both excellent enantioselectivity and *E*-selectivity. In the AROCM of **75** with styrene (Scheme 8, reaction performed at –10 °C using 5 equiv styrene and 1 mol % of the catalyst), complex **204** gave the desired product **76** in >98% conversion, 93% ee and *E/Z* ratio > 30:1.

Pursuing on this concept, the same group subsequently published novel chiral backbone-monosubstituted NHC complexes in which a bridge connecting the *N*-aryl group and the backbone unit makes aryl rotation no longer possible, thus creating a rigid environment in the surroundings of the alkene coordination sphere (**205a,b**, Figure 38) [64].

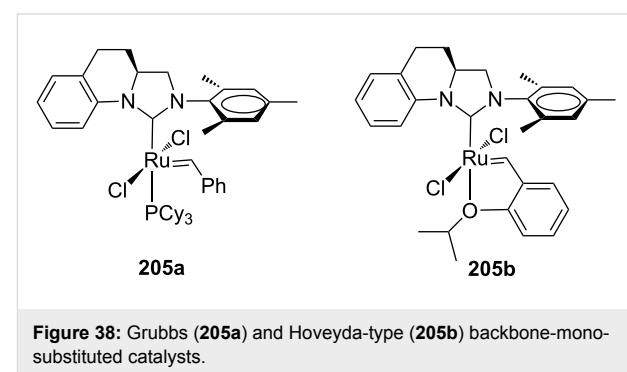
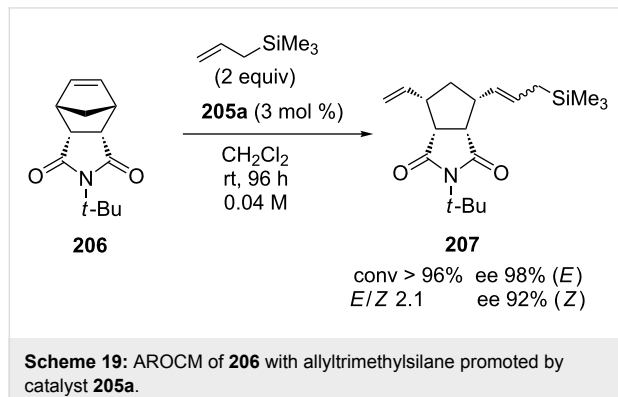


Figure 38: Grubbs (**205a**) and Hoveyda-type (**205b**) backbone-monosubstituted catalysts.

The performances of these catalysts in AROCM transformations were comparable with those of the congeners **202**–**204** albeit they showed a lower *E*-selectivity. These systems were successfully employed for the first time in the AROCM of **206**

with allyltrimethylsilane. Indeed, using catalyst **205a**, both *E* and *Z* geometric isomers of the desired cross product **207** were obtained in a high degree of enantioselectivity (Scheme 19).



Conclusion

In the last decades, a wide array of olefin metathesis ruthenium catalysts coordinated with monodentate unsymmetrical N-heterocyclic diaminocarbene ligands have been developed. The introduction of this class of second generation catalysts, especially those containing alkyl, aryl substituted NHCs, has offered new opportunities for various metathesis applications, giving access, for instance, to highly selective alternating ring-opening metathesis polymerization, ethenolysis reactions or self metathesis of α -olefins. Both steric and electronic properties of the unsymmetrical NHCs appear to influence stability, activity and selectivity of the resulting ruthenium complexes. Therefore, the possibility to further modify the NHC ligand architectures creating new steric and electronic environments around the ruthenium center represents one of the most appealing topic on which research efforts should be focused. The development of tailor-made unsymmetrical NHC ruthenium systems is desirable to improve the efficiency in targeted metathesis reactions of not only academic but also industrial interest.

Acknowledgements

Financial support from the Ministero dell'Università e della Ricerca Scientifica e Tecnologica is gratefully acknowledged.

ORCID® IDs

Chiara Costabile - <https://orcid.org/0000-0001-8538-7125>

Fabio Grisi - <https://orcid.org/0000-0003-3904-9541>

References

- Grubbs, R. H.; Wenzel, A. G.; O'Leary, D. J.; Khosravi, E. *Handbook of Metathesis*, 2nd ed.; Wiley-VCH: Weinheim, Germany, 2015. doi:10.1002/9783527674107
- Grela, K., Ed. *Olefin Metathesis Theory and Practice*; Wiley & Sons: Hoboken, NJ, 2014.
- Vougioukalakis, G. C.; Grubbs, R. H. *Chem. Rev.* **2010**, *110*, 1746–1787. doi:10.1021/cr9002424
- Samojlowicz, C.; Bieniek, M.; Grela, K. *Chem. Rev.* **2009**, *109*, 3708–3742. doi:10.1021/cr800524f
- Tornatzky, J.; Kannenberg, A.; Blechert, S. *Dalton Trans.* **2012**, *41*, 8215–8225. doi:10.1039/c2dt30256j
- Hamad, F. B.; Sun, T.; Xiao, S.; Verpoort, F. *Coord. Chem. Rev.* **2013**, *257*, 2274–2292. doi:10.1016/j.ccr.2013.04.015
- Herbert, M. B.; Grubbs, R. H. *Angew. Chem., Int. Ed.* **2015**, *54*, 5018–5024. doi:10.1002/anie.201411588
- Montgomery, T. P.; Johns, A. M.; Grubbs, R. H. *Catalysts* **2017**, *7*, 87. doi:10.3390/catal7030087
- Ogba, O. M.; Warner, N. C.; O'Leary, D. J.; Grubbs, R. H. *Chem. Soc. Rev.* **2018**, *47*, 4510–4544. doi:10.1039/c8cs00027a
- Vougioukalakis, G. C.; Grubbs, R. H. *J. Am. Chem. Soc.* **2008**, *130*, 2234–2245. doi:10.1021/ja075849v
- Lavallo, V.; Canac, Y.; Präsang, C.; Donnadieu, B.; Bertrand, G. *Angew. Chem., Int. Ed.* **2005**, *44*, 5705–5709. doi:10.1002/anie.200501841
- Vehlow, K.; Gessler, S.; Blechert, S. *Angew. Chem., Int. Ed.* **2007**, *46*, 8082–8085. doi:10.1002/anie.200702560
- Vougioukalakis, G. C.; Grubbs, R. H. *Organometallics* **2007**, *26*, 2469–2472. doi:10.1021/om0610593
- Vougioukalakis, G. C.; Grubbs, R. H. *Chem. – Eur. J.* **2008**, *14*, 7545–7556. doi:10.1002/chem.200800470
- Ritter, T.; Day, M. W.; Grubbs, R. H. *J. Am. Chem. Soc.* **2006**, *128*, 11768–11769. doi:10.1021/ja064091x
- Masoud, S. M.; Maiyan, A. K.; Dorcet, V.; Roisnel, T.; Dixneuf, P. H.; Bruneau, C.; Osipov, S. N. *Organometallics* **2015**, *34*, 2305–2313. doi:10.1021/om501077w
- Masoud, S. M.; Topchiy, M. A.; Peregudov, A. S.; Roisnel, T.; Dixneuf, P. H.; Bruneau, C.; Osipov, S. N. *J. Fluorine Chem.* **2017**, *200*, 66–76. doi:10.1016/j.jfluchem.2017.06.004
- Karras, M.; Dąbrowski, M.; Pohl, R.; Rybáček, J.; Vacek, J.; Bednárová, L.; Grela, K.; Starý, I.; Stará, I. G.; Schmidt, B. *Chem. – Eur. J.* **2018**, *24*, 10994–10998. doi:10.1002/chem.201802786
- Dinger, M. B.; Nieczypor, P.; Mol, J. C. *Organometallics* **2003**, *22*, 5291–5296. doi:10.1021/om034062k
- Endo, K.; Grubbs, R. H. *J. Am. Chem. Soc.* **2011**, *133*, 8525–8527. doi:10.1021/ja202818v
- Vehlow, K.; Maechling, S.; Blechert, S. *Organometallics* **2006**, *25*, 25–28. doi:10.1021/om0508233
- Ledoux, N.; Allaert, B.; Pattyn, S.; Vander Mierde, H.; Vercaemst, C.; Verpoort, F. *Chem. – Eur. J.* **2006**, *12*, 4654–4661. doi:10.1002/chem.200600064
- Ledoux, N.; Allaert, B.; Linden, A.; Van Der Voort, P.; Verpoort, F. *Organometallics* **2007**, *26*, 1052–1056. doi:10.1021/om060937u
- Ledoux, N.; Linden, A.; Allaert, B.; Vander Mierde, H.; Verpoort, F. *Adv. Synth. Catal.* **2007**, *349*, 1692–1700. doi:10.1002/adsc.200700042
- Yu, B.; Hamad, F. B.; Sels, B.; Van Hecke, K.; Verpoort, F. *Dalton Trans.* **2015**, *44*, 11835–11842. doi:10.1039/c5dt00967g
- Vehlow, K.; Wang, D.; Buchmeiser, M. R.; Blechert, S. *Angew. Chem., Int. Ed.* **2008**, *47*, 2615–2618. doi:10.1002/anie.200704822
- Lichtenheldt, M.; Wang, D.; Vehlow, K.; Reinhardt, I.; Kühnel, C.; Decker, U.; Blechert, S.; Buchmeiser, M. R. *Chem. – Eur. J.* **2009**, *15*, 9451–9457. doi:10.1002/chem.200900384
- Vasiuta, R.; Stockert, A.; Plenio, H. *Chem. Commun.* **2018**, *54*, 1706–1709. doi:10.1039/c7cc08476e

29. Kavitate, S.; Samantaray, M. K.; Dehn, R.; Deuerlein, S.; Limbach, M.; Schachner, J. A.; Jeanneau, E.; Copéret, C.; Thieuleux, C. *Dalton Trans.* **2011**, *40*, 12443–12446. doi:10.1039/c1dt11643f

30. Stewart, I. C.; Keitz, B. K.; Kuhn, K. M.; Thomas, R. M.; Grubbs, R. H. *J. Am. Chem. Soc.* **2010**, *132*, 8534–8535. doi:10.1021/ja1029045

31. Thomas, R. M.; Keitz, B. K.; Champagne, T. M.; Grubbs, R. H. *J. Am. Chem. Soc.* **2011**, *133*, 7490–7496. doi:10.1021/ja200246e

32. Thomas, R. M.; Grubbs, R. H. *Chem. N. Z.* **2011**, *75*, 65–71.

33. Thomas, R. M.; Fedorov, A.; Keitz, B. K.; Grubbs, R. H. *Organometallics* **2011**, *30*, 6713–6717. doi:10.1021/om200911e

34. Rouen, M.; Borré, E.; Falivene, L.; Toupet, L.; Berthod, M.; Cavallo, L.; Olivier-Bourbigou, H.; Mauduit, M. *Dalton Trans.* **2014**, *43*, 7044–7049. doi:10.1039/c4dt00142g

35. Rouen, M.; Queval, P.; Borré, E.; Falivene, L.; Poater, A.; Berthod, M.; Hugues, F.; Cavallo, L.; Baslé, O.; Olivier-Bourbigou, H.; Mauduit, M. *ACS Catal.* **2016**, *6*, 7970–7976. doi:10.1021/acscatal.6b01428

36. Queval, P.; Jahier, C.; Rouen, M.; Artur, I.; Legeay, J.-C.; Falivene, L.; Toupet, L.; Crévisy, C.; Cavallo, L.; Baslé, O.; Mauduit, M. *Angew. Chem., Int. Ed.* **2013**, *52*, 14103–14107. doi:10.1002/anie.201308873

37. Fürstner, A.; Ackermann, L.; Gabor, B.; Goddard, R.; Lehmann, C. W.; Mynott, R.; Stelzer, F.; Thiel, O. R. *Chem. – Eur. J.* **2001**, *7*, 3236–3253. doi:10.1002/1521-3765(20010803)7:15<3236::aid-chem3236>3.0.co;2-s

38. Bielawski, C. W.; Benitez, D.; Grubbs, R. H. *Science* **2002**, *297*, 2041–2044. doi:10.1126/science.1075401

39. Bielawski, C. W.; Benitez, D.; Grubbs, R. H. *J. Am. Chem. Soc.* **2003**, *125*, 8424–8425. doi:10.1021/ja034524l

40. Pröhls, S.; Lehmann, C. W.; Fürstner, A. *Organometallics* **2004**, *23*, 280–287. doi:10.1021/om0342006

41. Keitz, B. K.; Grubbs, R. H. *Organometallics* **2010**, *29*, 403–408. doi:10.1021/om900864r

42. Jong, H.; Patrick, B. O.; Fryzuk, M. D. *Organometallics* **2011**, *30*, 2333–2341. doi:10.1021/om2000844

43. Abrialimov, O.; Kędziora, M.; Torborg, C.; Malińska, M.; Woźniak, K.; Grela, K. *Organometallics* **2012**, *31*, 7316–7319. doi:10.1021/om300783g

44. Abrialimov, O.; Kędziora, M.; Malińska, M.; Woźniak, K.; Grela, K. *Organometallics* **2014**, *33*, 2160–2171. doi:10.1021/om4009197

45. Malinowska, M.; Kozłowska, M.; Hryniwicka, A.; Witkowski, S.; Morzycki, J. W. *Monatsh. Chem.* **2016**, *147*, 1091–1100. doi:10.1007/s00706-016-1697-7

46. Małecki, P.; Gajda, K.; Abrialimov, O.; Malińska, M.; Gajda, R.; Woźniak, K.; Kajetanowicz, A.; Grela, K. *Organometallics* **2017**, *36*, 2153–2166. doi:10.1021/acs.organomet.7b00211

47. Smoleń, M.; Kośnik, W.; Loska, R.; Gajda, R.; Malińska, M.; Woźniak, K.; Grela, K. *RSC Adv.* **2016**, *6*, 77013–77019. doi:10.1039/c6ra18210k

48. Grudzień, K.; Trzaskowski, B.; Smoleń, M.; Gajda, R.; Woźniak, K.; Grela, K. *Dalton Trans.* **2017**, *46*, 11790–11799. doi:10.1039/c7dt02180a

49. Engl, P. S.; Fedorov, A.; Copéret, C.; Togni, A. *Organometallics* **2016**, *35*, 887–893. doi:10.1021/acs.organomet.6b00028

50. Engl, P. S.; Santiago, C. B.; Gordon, C. P.; Liao, W.-C.; Fedorov, A.; Copéret, C.; Sigman, M. S.; Togni, A. *J. Am. Chem. Soc.* **2017**, *139*, 13117–13125. doi:10.1021/jacs.7b06947

51. Paradiso, V.; Costabile, C.; Grisi, F. *Molecules* **2016**, *21*, 117–136. doi:10.3390/molecules21010117

52. Fournier, P.-A.; Collins, S. K. *Organometallics* **2007**, *26*, 2945–2949. doi:10.1021/om700312c

53. Seiders, T. J.; Ward, D. W.; Grubbs, R. H. *Org. Lett.* **2001**, *3*, 3225–3228. doi:10.1021/o10165692

54. Fournier, P.-A.; Savoie, J.; Stenne, B.; Bédard, M.; Grandbois, A.; Collins, S. K. *Chem. – Eur. J.* **2008**, *14*, 8690–8695. doi:10.1002/chem.200800642

55. Funk, T. W.; Berlin, J. M.; Grubbs, R. H. *J. Am. Chem. Soc.* **2006**, *128*, 1840–1846. doi:10.1021/ja055994d

56. Grandbois, A.; Collins, S. K. *Chem. – Eur. J.* **2008**, *14*, 9323–9329. doi:10.1002/chem.200801033

57. Savoie, J.; Stenne, B.; Collins, S. K. *Adv. Synth. Catal.* **2009**, *351*, 1826–1832. doi:10.1002/adsc.200900269

58. Stenne, B.; Timperio, J.; Savoie, J.; Dudding, T.; Collins, S. K. *Org. Lett.* **2010**, *12*, 2032–2035. doi:10.1021/o1100511d

59. Paradiso, V.; Bertolasi, V.; Grisi, F. *Organometallics* **2014**, *33*, 5932–5935. doi:10.1021/om500731k

60. Paradiso, V.; Bertolasi, V.; Costabile, C.; Grisi, F. *Dalton Trans.* **2016**, *45*, 561–571. doi:10.1039/c5dt03758a

61. Paradiso, V.; Bertolasi, V.; Costabile, C.; Caruso, T.; Dąbrowski, M.; Grela, K.; Grisi, F. *Organometallics* **2017**, *36*, 3692–3708. doi:10.1021/acs.organomet.7b00488

62. Paradiso, V.; Menta, S.; Pierini, M.; Della Sala, G.; Ciogli, A.; Grisi, F. *Catalysts* **2016**, *6*, 177. doi:10.3390/catal6110177

63. Tiede, S.; Berger, A.; Schlesiger, D.; Rost, D.; Lühl, A.; Blechert, S. *Angew. Chem., Int. Ed.* **2010**, *49*, 3972–3975. doi:10.1002/anie.201000940

64. Kannenberg, A.; Rost, D.; Eibauer, S.; Tiede, S.; Blechert, S. *Angew. Chem., Int. Ed.* **2011**, *50*, 3299–3302. doi:10.1002/anie.201007673

License and Terms

This is an Open Access article under the terms of the Creative Commons Attribution License (<http://creativecommons.org/licenses/by/4.0>). Please note that the reuse, redistribution and reproduction in particular requires that the authors and source are credited.

The license is subject to the *Beilstein Journal of Organic Chemistry* terms and conditions: (<https://www.beilstein-journals.org/bjoc>)

The definitive version of this article is the electronic one which can be found at:

[doi:10.3762/bjoc.14.292](https://doi.org/10.3762/bjoc.14.292)



Selective ring-opening metathesis polymerization (ROMP) of cyclobutenes. Unsymmetrical ladderphane containing polycyclobutene and polynorbornene strands

Yuan-Zhen Ke^{1,2}, Shou-Ling Huang¹, Guoqiao Lai³ and Tien-Yau Luh^{*1}

Full Research Paper

Open Access

Address:

¹Department of Chemistry, National Taiwan University, Taipei 106, Taiwan, ²Shanghai Institute of Organic Chemistry, Chinese Academy of Sciences, 345 Lingling Lu, Shanghai 200032, China and ³Key Laboratory of Organosilicon Chemistry and Material Technology of Ministry of Education, Hangzhou Normal University, Hangzhou, Zhejiang 311121, China

Email:

Tien-Yau Luh^{*} - tyluh@ntu.edu.tw

* Corresponding author

Keywords:

cyclobutene; hydrolysis; linker; metathesis; norbornene; ROMP; selectivity; unsymmetrical ladderphane

Beilstein J. Org. Chem. **2019**, *15*, 44–51.

doi:10.3762/bjoc.15.4

Received: 20 August 2018

Accepted: 04 December 2018

Published: 03 January 2019

This article is part of the thematic issue "Progress in metathesis chemistry III". In memory of the late Professor Teruaki Mukaiyama.

Guest Editors: K. Grela and A. Kajetanowicz

© 2019 Ke et al.; licensee Beilstein-Institut.

License and terms: see end of document.

Abstract

At 0 °C in THF in the presence of Grubbs first generation catalyst, cyclobutene derivatives undergo ROMP readily, whereas norbornene derivatives remain intact. When the substrate contains both cyclobutene and norbornene moieties, the conditions using THF as the solvent at 0 °C offer a useful protocol for the selective ROMP of cyclobutene to give norbornene-appended polycyclobutene. Unsymmetrical ladderphane having polycyclobutene and polynorbornene as two strands is obtained by further ROMP of the norbornene appended polycyclobutene in the presence of Grubbs first generation catalyst in DCM at ambient temperature. Methanolysis of this unsymmetrical ladderphane gives polycyclobutene methyl ester and insoluble polynorbornene-amide-alcohol. The latter is converted into the corresponding soluble acetate. Both polymers are well characterized by spectroscopic means. No norbornene moiety is found to be incorporated into polycyclobutene strand at all. The double bonds in the polycyclobutene strand are mainly in *cis* configuration (ca 70%), whereas the *E/Z* ratio for polynorbornene strand is 8:1.

Introduction

Ring-opening metathesis polymerizations (ROMP) of strained cycloalkenes offer a powerful arsenal for the synthesis of polymers having a variety of fascinating properties [1-3]. To illustrate this, polynorbornenes and polycyclobutenes are readily ob-

tained from the corresponding monomeric norbornene and cyclobutene derivatives under various conditions. Symmetrical DNA-like double stranded ladderphanes are conveniently synthesized from bisnorbornene [4-15] or from biscyclobutene [16]

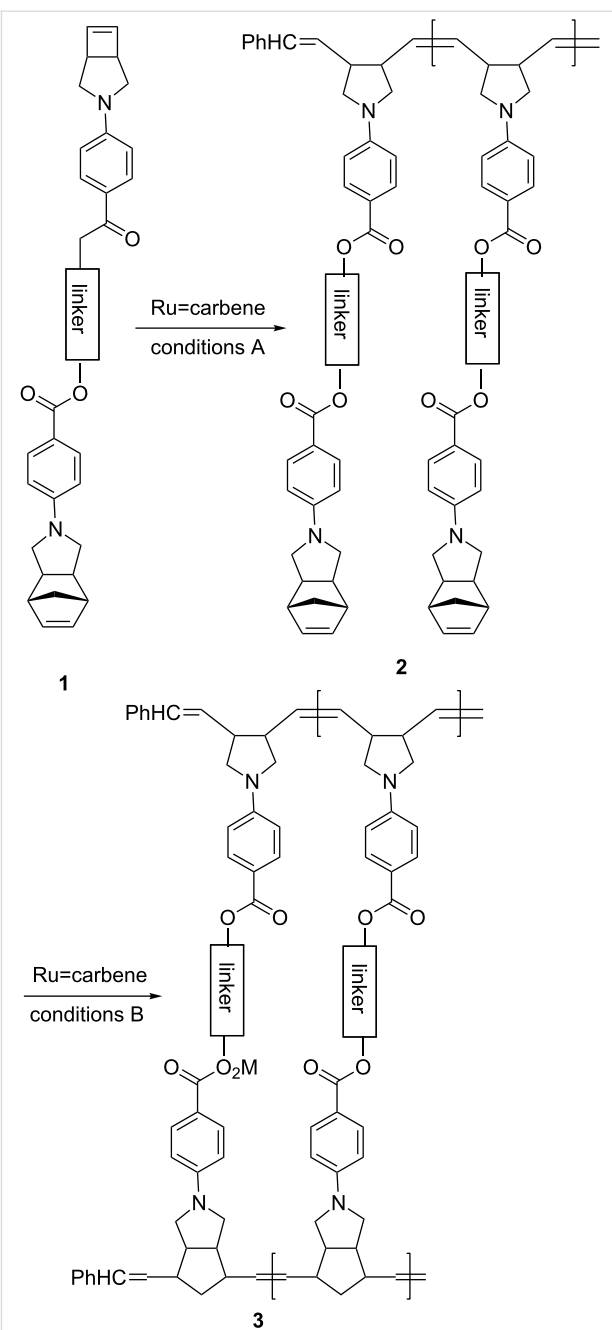
linked with a range of different rigid linkers. When a flexible linker is used, bisnorbornene derivatives undergo cascade metathetical cyclopolymerization giving the corresponding polynorbornenes with hammock-like pendants [17,18]. Unsymmetrical polynorbornene-based ladderphane is obtained by a replication protocol from a single stranded polynorbornene [19,20]. Alternatively, sequential polymerization of a monomer containing a norbornene moiety and other polymerizable group furnishes an unsymmetrical ladderphane having two structurally different polymeric backbones [21,22]. It is known that norbornenes having different substituents would have different reaction rates in ROMP [23]. These discrepancies in reactivity have been used for sequence control in polymer synthesis [24]. Since the first living ROMP methods for cyclobutenes were reported in 1992 [25], cyclobutene-containing block copolymers are well documented [26–34]. Alternating cyclobutene–cyclohexene copolymers have been synthesized by ROMP of the corresponding monomers [31–33]. However, to the best of our knowledge, selective ROMPs between cyclobutene and norbornene have not been reported.

The strain energies for norbornene and cyclobutene are 25 and 31 kcal/mol, respectively [35]. It is therefore envisaged that cyclobutene would react faster than norbornene under certain ROMP conditions. As such, when monomer **1** containing a cyclobutene moiety and a norbornene moiety connected by a bridge are subjected to ROMP, it would be feasible that the cyclobutene moiety would react preferentially giving the corresponding norbornene-appended polycyclobutene **2**. After all cyclobutene moieties have been consumed and quenched, further ROMP of **2** under different conditions would afford unsymmetrical double-stranded ladderphane **3** having both polycyclobutene and polynorbornene as two polymeric frameworks (Scheme 1). We have tested this viewpoint and now wish to report sequential ROMP of monomers containing both cyclobutene and norbornene moieties tethered by a linker.

Results and Discussion

A comparison of the reactivity of cyclobutene versus norbornene derivatives **4** and **5** in ROMP catalyzed by Grubbs I catalyst (**6**)

In the beginning of this study, we have examined the first order reaction kinetics of ROMPs of **4** and of **5** in the presence of 10 mol per cent of Grubbs first generation catalyst (**6**) [36] in DCM at 10 °C [37]. The rate constants for the reactions of **4** and **5** were 1.3×10^{-3} and $5.1 \times 10^{-4} \text{ s}^{-1}$, respectively. On the other hand, when the reaction was carried out in THF-*d*₈ at 273 K, the second order rate constant for **4** was $2.1 \times 10^{-3} \text{ M}^{-1} \text{ s}^{-1}$, whereas norbornene derivative **5** was inert



Scheme 1: Strategy for sequential ROMP of **1** to yield **3**.

under these conditions. The details are described in the Experimental section and Supporting Information File 1 (Figures S1, S2 and S8–S10).

It has been suggested that the metathesis reaction may involve a fourteen-electron ruthenium species as the active catalyst [38–40]. This active species might be stabilized when the reaction is carried out in polar solvent having weak coordination ability such as THF [41–43]. As mentioned above, the difference in reactivity between the ROMP of **4** and **5** in THF at 0 °C

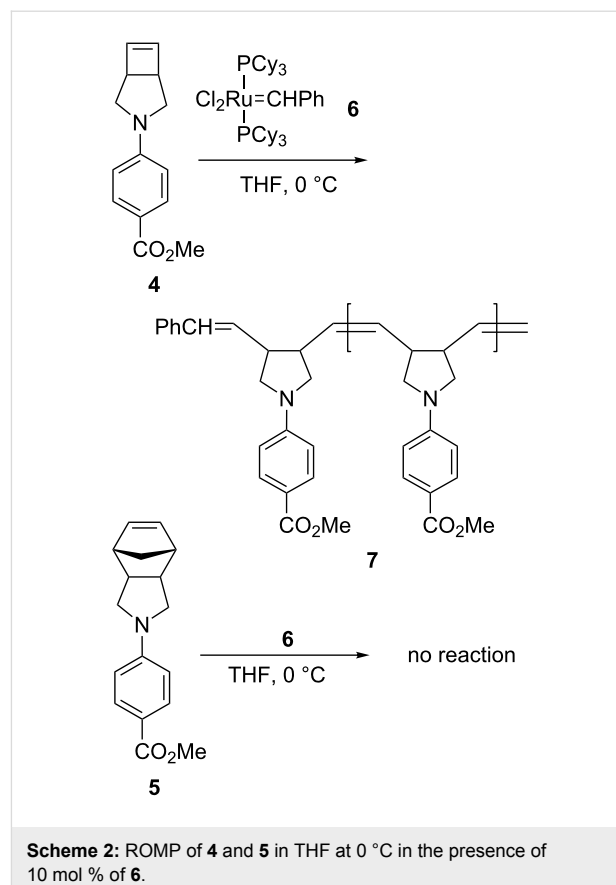
would offer useful conditions to selectively react with **4** in the presence of **5**. Thus, a mixture of an equal molar of **4** and **5** was treated with 10 mol % of **6** in THF-*d*₈ at 0 °C. Only **4** was consumed to give the corresponding polymer **7**, whereas **5** remained intact (Scheme 2). This promising observation prompted us to pursue the synthesis of unsymmetrical double-stranded ladderphane **8** by sequential ROMPs of **9** (Scheme 3).

Synthesis of monomer **9**

4-Aminobutanol (**11**) was used to link norbornene and cyclobutene moieties via amide and ester groups. The use of such a linker is because the ester group could be selectively hydrolyzed in the presence of amides. This selectivity will be helpful for the structural elucidation of polymer **8**. Thus, **10b** was allowed to react with **11** to afford amide-alcohol **12** in 79% yield. Esterification of **12** with **13b** furnished 70% yield of monomer **9** (Scheme 4).

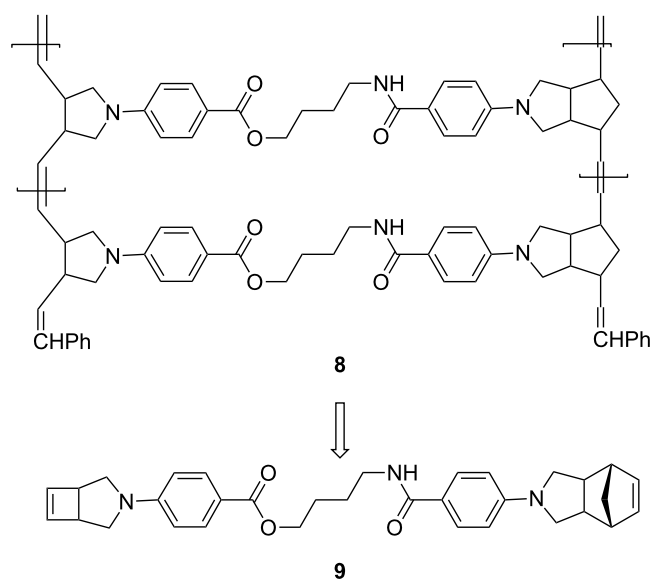
Synthesis of unsymmetrical ladderphane **8** by sequential ROMPs catalyzed by **6**

Polymerization of monomer **9** in the presence of 10 mol % of **6** was performed in THF at 0 °C for 4 h, followed by quenching with ethyl vinyl ether to give polymer **14** in 86% yield (Scheme 5). It is worth noting that no incorporation of the norbornene moiety into the polymeric backbone under these conditions was observed. The ¹H NMR spectrum of **14** shows the olefinic proton signals at δ 5.49 and 6.12 ppm in 1:1 ratio. These signals were assigned to the absorptions of olefinic protons on the polymeric backbone and the olefinic proton of unreacted norbornene pendants, respectively. In the ¹³C NMR spectrum, the peak at δ 139 ppm owing to the olefinic carbon of

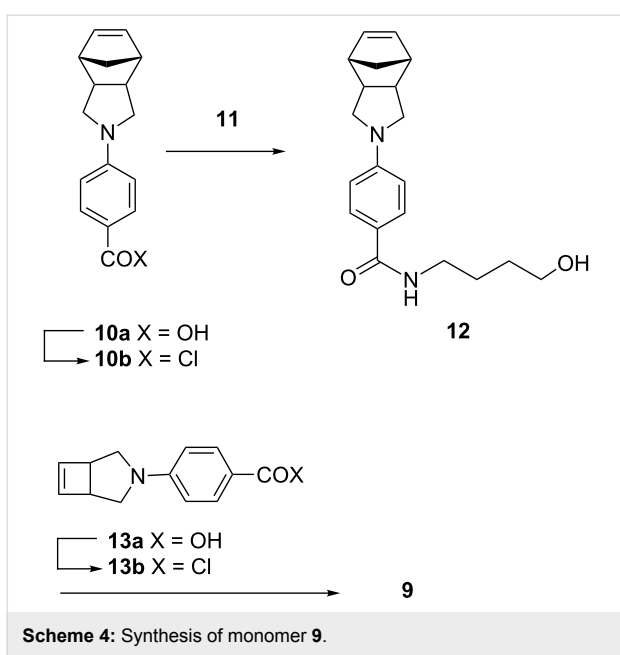


Scheme 2: ROMP of **4** and **5** in THF at 0 °C in the presence of 10 mol % of **6**.

cyclobutene shifts to δ 130 ppm due to ring opening, whereas the olefin carbon of the unreacted norbornene moiety at δ 136 ppm remained unchanged after first polymerization. These observations are consistent with the results of our prelim-



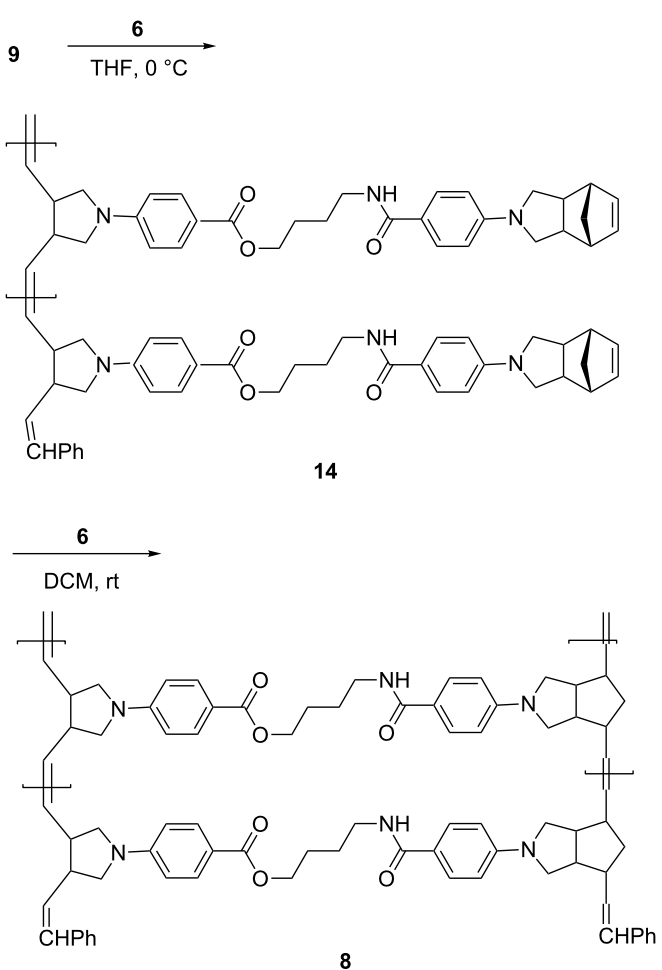
Scheme 3: Retrosynthesis of **8** from **9**.

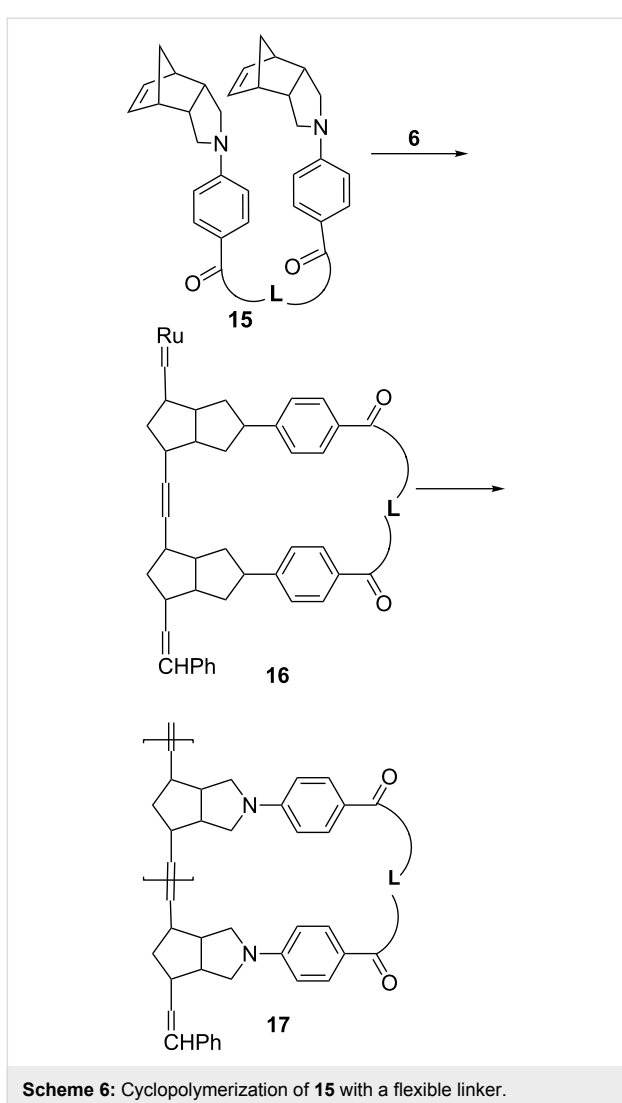


Scheme 4: Synthesis of monomer 9.

inary studies that only the cyclobutene moiety, but not norbornene in **9**, proceeds **6**-catalyzed ROMP under these conditions. The degree of polymerization of **14** was estimated to be 10 based on the ^1H NMR integration of relevant peaks.

We have previously found that two norbornene derivatives connected by a flexible linker **15** may undergo cascade ring-opening–ring-closing metathesis polymerization to give single-stranded hammock-like appended polynorbornenes **17** (Scheme 6) [17,18]. The linker in **8** is flexible, and, therefore, the possibility for similar intramolecular metathesis cyclopolymerization might take place to form intermediate **16** for further transformations. However, no such reaction was observed in this study. Presumably, the **6**-catalyzed metathesis reactivity of cyclobutenes would be much higher than that of norbornene derivatives. Accordingly, intermolecular metathesis reaction between two cyclobutene moieties would be favored over intramolecular ring-closing metathesis between a ruthenium carbene and the norbornene moiety.

Scheme 5: Synthesis of **14** and **8** by selective olefin metathesis.

Scheme 6: Cyclopolymerization of **15** with a flexible linker.

Polymer **14** was treated with 10 mol % **6** in DCM at rt to give **8** in 95% yield. The ^1H NMR spectrum of **8** shows that the relative intensity of the signals around δ 5.4 ppm was doubled, all signals due to olefinic protons in **9** and **14** being diminished.

Methanolysis of unsymmetrical ladderphane **8**

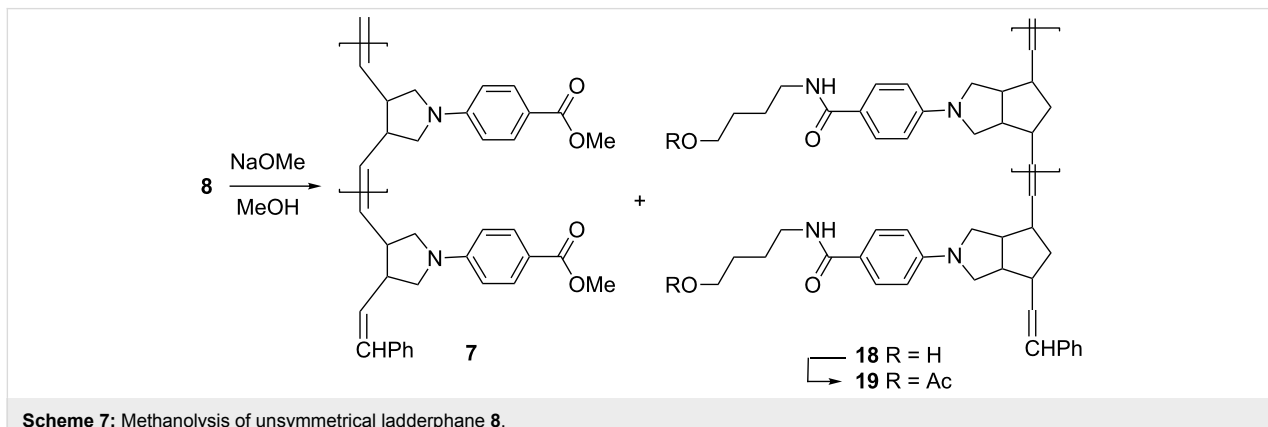
In order to confirm the uniformity of the polymerization leading to the formation of unsymmetrical ladderphane **8**, methanolysis of **8** with NaOMe in methanol at rt gave **7** and **18**. Chloroform was then added and **18** was collected as a grayish precipitate in 56% yield. After filtration, the filtrate was worked up to afford **7** in 64% yield with a degree of polymerization of 10 ($M_n = 2500$, PDI = 1.11), in good agreement with those of **14** and **8**. The ^{13}C NMR spectrum of **7** shows two peaks at δ 40.6 and 45.4 ppm, attributed to the allylic carbons attached to a *cis* and a *trans* double bond [13], respectively, and the relative ratio of these two peaks is roughly 7:3. This result suggests that about 70% of the double bonds in **7** might adopt *cis* configuration. Moreover, no norbornene moiety was detected by NMR on the polymeric backbones in **7** (Scheme 7).

Since **18** was insoluble in most organic solvents, acetylation of **18** with excess acetic anhydride and pyridine at 70 °C for 10 h gave the corresponding acetate **19**, which had good solubility in DCM or chloroform. GPC analysis showed that the degree of polymerization of **19** (DP = 10, PDI = 1.24) was again comparable with that of the corresponding ladderphane **8**, polycyclobutene **7** and **14**.

The ^1H NMR spectrum of **19** shows peaks at δ 5.6 and 5.3 ppm attributed to *trans* and *cis* olefinic protons, respectively, in a ratio of 8 to 1. It is well documented that **6**-catalyzed ROMP of *N*-arylpyrrolidene appended norbornene gives polynorbornene with all double bonds in *trans* configuration [44–46]. The existence of both *Z*- and *E*-double bonds in the parent polycyclobutene backbone in **14** may influence the stereoselectivity of the polynorbornene strand in **7** during the course of ROMP.

Conclusion

In summary, we have demonstrated useful ROMP conditions to selectively transform cyclobutene derivatives into the corre-

Scheme 7: Methanolysis of unsymmetrical ladderphane **8**.

sponding polycyclobutenes in THF at 0 °C, whereas the corresponding norbornene skeleton appears to be unreactive under these conditions. This protocol has been used for the selective synthesis of unsymmetrical ladderphane having polycyclobutene in one strand and polynorbornene in the other. Further applications of this selectivity to other systems are in progress in our laboratory.

Experimental

General

Unless otherwise specified, all commercially available starting materials were used without further purification. All air and moisture-sensitive reactions were carried out under an atmosphere of dry nitrogen in a glove box. All ¹H and ¹³C NMR spectra were recorded on a Varian 400 Unity Plus NMR spectrometer using CDCl₃ as solvent at ambient temperature. Chemical shifts were expressed in parts per million using residual solvent protons as internal standards (¹H: chloroform: 7.26 ppm). Gel permeation chromatography (GPC) was performed on a Waters GPC instrument equipped with Waters 1515 HPLC pump using Waters 2487 absorbance detector. Polymer (approximately 0.5 mg) in THF (0.1 mL) was filtered through a 0.5-micron filter and 20 μL of the sample was injected into Shodex KF-G, Styragel HR2, Styragel HR3 and Styragel HR4 column (7.8 × 300 mm) with oven temperature at 40 °C using standard polystyrene samples (1.84 × 10⁵ to 996 Da) for calibration. THF was used as eluent (flow rate 1.0 mL/min).

Synthesis of 12. Under N₂ atmosphere, to **10a** (560 mg, 2.2 mmol) in DCM (20 mL) was added oxalyl chloride (0.4 mL, 4.3 mmol) at 0 °C. The mixture was gradually warmed to rt and then stirred for 1 h. The solvent was removed in vacuo to give the crude acyl chloride **10b**, to which was added DCM (15 mL), DMAP (60 mg, 0.5 mmol) and Et₃N (2.0 mL, 15 mmol). 4-Amino-1-butanol (**11**, 178 mg, 2.0 mmol) was then added slowly at 0 °C. After stirring for 8 h at rt, the mixture was poured into H₂O (50 mL) and DCM (50 mL). The organic layer was separated, washed with brine (100 mL) and dried (MgSO₄). The solvent was removed in vacuo and the residue was chromatographed on silica gel (DCM/MeOH 20:1) to afford **12** (515 mg, 79%). mp 207–209 °C; IR (KBr): v 3455, 3306, 3056, 2940, 2867, 1606, 1554, 1514, 1473, 1379, 1309, 1199, 1130, 1047, 969, 826, 768, 733, 683 cm⁻¹; ¹H NMR (400 MHz) δ 1.52 (d, *J* = 8.4 Hz, 1H), 1.61–1.70 (m, 6H), 2.92–2.99 (m, 4H), 2.98–2.99 (m, 2H), 3.09 (m, 2H), 3.25–3.30 (m, 2H), 3.47–3.48 (m, 2H), 3.71 (t, *J* = 5.6 Hz, 2H), 6.15–6.16 (m, 3H), 6.39 (d, *J* = 9.0 Hz, 2H), 7.61 (d, *J* = 9.0 Hz, 2H); ¹³C NMR (100 MHz): δ 26.8, 30.1, 39.8, 45.6, 46.8, 50.6, 52.2, 62.3, 110.7, 120.1, 127.9, 135.3, 148.9, 167.1; HRMS (FAB, *m/z*): calcd for C₂₀H₂₆N₂O₂, 326.1994; found, 326.1997.

Synthesis of 9. Under N₂ atmosphere, to **13a** (321 mg, 1.4 mmol) in DCM (20 mL) was added oxalyl chloride (0.4 mL, 4.3 mmol) at 0 °C. The mixture was gradually warmed to rt and then stirred for 1 h. The solvent was removed in vacuo to give the crude acyl chloride **13b**, to which was added DCM (15 mL), DMAP (60 mg, 0.5 mmol) and Et₃N (2.0 mL, 15 mmol). Compound **12** (522 mg, 1.6 mmol) was then added slowly at 0 °C. After stirring for 8 h at rt, the mixture was poured into H₂O (50 mL) and DCM (50 mL). The organic layer was separated, washed with saturated brine (100 mL) and dried (MgSO₄). The solvent was removed in vacuo and the residue was chromatographed on silica gel (DCM/MeOH 20:1) to afford **9** (512 mg, 70%). mp 238–240 °C; IR (KBr): v 3333, 3051, 2949, 2843, 1699, 1606, 1547, 1511, 1473, 1376, 1274, 1216, 1180, 1106, 1050, 963, 828, 769, 740 cm⁻¹; ¹H NMR (400 MHz) δ 1.51 (d, *J* = 8.2 Hz, 1H), 1.61 (d, *J* = 8.2 Hz, 1H), 1.72–1.85 (m, 4H), 2.92–2.98 (m, 6H), 3.07–3.09 (m, 2H), 3.25–3.29 (m, 2H), 3.49–3.56 (m, 4H), 3.65 (d, *J* = 10.0 Hz, 2H), 4.30 (t, *J* = 6.4 Hz, 2H), 6.03 (m, 1H), 6.13–6.15 (m, 4H), 6.38 (d, *J* = 8.6 Hz, 2H), 6.62 (d, *J* = 8.4 Hz, 2H), 7.61 (d, *J* = 8.6 Hz, 2H), 7.87 (d, *J* = 8.4 Hz, 2H); ¹³C NMR (100 MHz) δ 26.4, 26.6, 39.4, 45.3, 46.4, 46.5, 48.8, 50.4, 52.0, 63.7, 110.8, 111.8, 117.5, 120.4, 128.0, 130.9, 135.5, 139.1, 149.1, 152.9, 166.6, 167.1; HRMS (FAB, *m/z*): calcd for C₃₃H₃₇N₃O₃, 523.2835; found, 523.2839.

Synthesis of 14. Under N₂ atmosphere, to a solution of **9** (84.0 mg, 0.16 mmol) in THF (10 mL) was added **6** (12.8 mg, 0.016 mmol) in THF (1 mL) at 0 °C. After stirring at 0 °C for 4 h, ethyl vinyl ether (1.0 mL) was then added and stirring was continued at 0 °C for 2 h. The mixture was concentrated and the residual solution was added to methanol. The precipitate was collected and redissolved in DCM. Reprecipitation by adding the DCM solution to methanol afforded **14** as a grayish powder (74.8 mg, 89%). IR (KBr): v 3350, 3054, 2954, 2847, 1695, 1605, 1512, 1476, 1381, 1275, 1179, 1107, 967, 827, 768, 733, 698 cm⁻¹; ¹H NMR (400 MHz) δ 1.51–1.72 (m, 6H), 2.92–3.48 (m, 16H), 4.26 (br, 2H), 5.49 (m, 2H), 6.12 (br, 2H), 6.36 (m, 5H), 7.63 (br, 2H), 7.86 (br, 2H); degree of polymerization (DP) analysis: δ 7.86/δ 5.07 = 10, indicating a DP of 10; ¹³C NMR (100 MHz) δ 26.6, 39.6, 40.9, 45.5, 46.6, 50.5, 52.1, 52.9, 64.0, 110.5, 110.9, 117.0, 120.5, 128.2, 129.8, 131.3, 135.6, 149.2, 150.2, 166.8, 167.4.

Synthesis of 8. Under N₂ atmosphere, to a solution of **14** (62.8 mg, 0.12 mmol) in DCM (40 mL) was added **6** (9.6 mg, 0.012 mmol) in DCM (5 mL). After stirring at rt for 4 h, ethyl vinyl ether (0.5 mL) was then added and stirring was continued for 30 min. The mixture was concentrated and the residual solution was added to methanol. The precipitate was collected and redissolved in DCM. Reprecipitation by adding the DCM solu-

tion to methanol afforded **8** as a grayish powder (59.7 mg, 95%). IR (KBr): ν 3373, 3054, 2929, 2849, 1694, 1605, 1512, 1478, 1381, 1274, 1179, 1106, 966, 827, 767, 733, 697 cm^{-1} ; ^1H NMR (400 MHz) δ 1.47 (br, 1H), 1.82 (m, 5H), 2.88–3.49 (m, 16H), 4.27 (br, 2H), 5.47 (m, 4H), 6.49 (m, 5H), 7.67–7.89 (m, 4H); DP analysis: δ 4.27/ δ 5.05 = 11, indicating a DP of 11. ^{13}C NMR (100 MHz) δ 26.6, 40.0, 46.1, 49.7, 53.2, 63.7, 110.6, 111.8, 116.9, 121.8, 126.0, 128.5, 131.3, 136.5, 138.7, 150.1, 166.7, 167.5.

Synthesis of 7 and 18. To a solution of **8** (52 mg, 0.1 mmol [calculated based on the molecular weight of the monomeric unit]) in DCM (20 mL) was added 30% NaOMe in methanol (6 mL). The mixture was stirred at 50 °C for 20 h and cooled to rt. The insoluble solid residue was collected and dried to give crude **18** as a grayish solid (18 mg, 56%). After filtration, the filtrate was washed with water and dried (MgSO_4). The mixture was concentrated and the residual solution was added to methanol. The precipitate was collected and redissolved in DCM. Reprecipitation by adding the DCM solution to methanol afforded **7** as a grayish powder (21 mg, 64%). IR (KBr): ν 3066, 2951, 2862, 1702, 1605, 1524, 1478, 1434, 1383, 1281, 1180, 1108, 970, 828, 769, 698, 507 cm^{-1} ; ^1H NMR (400 MHz) δ 3.02–3.49 (m, 6H), 3.86 (br, 3H), 5.49 (m, 2H), 6.43 (br, 2H), 7.87 (br, 2H), DP analysis by integration of peaks at δ 6.43/ δ 5.06 = 10, indicating a DP of 10. ^{13}C NMR (100 MHz) δ 40.8, 45.8, 51.6, 52.7, 110.5, 117.1, 128.4, 129.7, 131.3, 150.2, 167.2. GPC: M_n = 2500, M_w = 2800, PDI = 1.11.

Synthesis of 19. A mixture of crude **18** (16 mg, 0.05 mmol), obtained from the above experiment, in Ac_2O (0.5 mL) and pyridine (5 mL) was stirred at 70 °C for 10 h. The solvent was concentrated and the residue was dissolved in CHCl_3 (15 mL) and washed first with diluted HCl (pH 3) and then with water. The organic solvent was concentrated and the residual solution was added to methanol. The precipitate was collected and redissolved in CHCl_3 . Reprecipitation by adding the CHCl_3 solution to methanol afforded **19** as a grayish powder (12 mg, 63%). ^1H NMR (400 MHz) δ 1.73 (br, 6H) 2.05 (s, 3H), 2.73–3.62 (m, 10H), 4.07 (br, 2H), 5.50 (m, 2H), 6.48 (br, 2H), 7.73 (br, 2H), DP δ 5.50/ δ 5.05 = 10, indicating a DP of 10. ^{13}C NMR (100 MHz) δ 21.1, 28.0, 39.7, 45.0, 46.5, 50.8, 64.3, 112.2, 121.9, 128.5, 131.8, 132.0, 150.5, 168.1, 171.6.

General procedure for kinetic measurements

Monomer **4** or **5** (0.03 mmol) was dissolved in DCM- d_2 or THF- d_8 (0.5 mL) and was syringed into an NMR tube inside a glove-box under nitrogen atmosphere. The NMR tube was then covered with a standard tube cap and placed in the NMR spectrometer. The tube was left to equilibrate at the desired temperature and all parameters were adjusted. A solution of **6** (24 mg in

1.0 mL of the same solvent) was prepared under nitrogen atmosphere prior to the reaction. Catalyst **6** (10 mol %) was syringed into the NMR tube which was immediately put in the NMR probe again. The reaction was monitored by the decrease of the peak intensity for H-2 using the peaks for H-1 and H-1' as the internal reference (Supporting Information File 1, Figures S8–S10). The spectra were recorded every ten to twenty minutes interval depending on the reaction (Figures S8–S10). The rate constants were thus obtained (Figures S1 and S2).

Supporting Information

Supporting Information File 1

^1H and ^{13}C NMR spectra of both monomers and polymers, as well as GPC and kinetic investigation results.
[<https://www.beilstein-journals.org/bjoc/content/supplementary/1860-5397-15-4-S1.pdf>]

Acknowledgement

We thank the Ministry of Science and Technology in Taiwan for support of this work. YK thanks Shanghai Institute of Organic Chemistry for a fellowship.

References

1. Buchmeiser, M. R. *Chapter 19. In Synthesis of Polymers*; Schlüter, A. D.; Hawker, C. J.; Sakamoto, J., Eds.; Wiley-VCH, 2012.
2. Buchmeiser, M. R. *Chem. Rev.* **2000**, *100*, 1565–1604. doi:10.1021/cr990248a
3. Grubbs, R. H.; Khosravi, E., Eds. *Handbook of Metathesis. Polymer Synthesis*, 2nd ed.; Wiley-VCH, 2015; Vol. 3.
4. Luh, T.-Y. *Acc. Chem. Res.* **2013**, *46*, 378–389. doi:10.1021/ar300170b
5. Luh, T.-Y.; Ding, L. *Tetrahedron* **2017**, *73*, 6487–6513. doi:10.1016/j.tet.2017.09.029
6. Yang, H.-C.; Lin, S.-Y.; Yang, H.-C.; Lin, C.-L.; Tsai, L.; Huang, S.-L.; Chen, I. W.-P.; Chen, C.-h.; Jin, B.-Y.; Luh, T.-Y. *Angew. Chem., Int. Ed.* **2006**, *45*, 726–730. doi:10.1002/anie.200503406
7. Yang, H.-C.; Lee, S.-L.; Chen, C.-h.; Lin, N.-T.; Yang, H.-C.; Jin, B.-Y.; Luh, T.-Y. *Chem. Commun.* **2008**, 6158–6160. doi:10.1039/b814672a
8. Chou, C.-M.; Lee, S.-L.; Chen, C.-H.; Biju, A. T.; Wang, H.-W.; Wu, Y.-L.; Zhang, G.-F.; Yang, K.-W.; Lim, T.-S.; Huang, M.-J.; Tsai, P.-Y.; Lin, K.-C.; Huang, S.-L.; Chen, C.-h.; Luh, T.-Y. *J. Am. Chem. Soc.* **2009**, *131*, 12579–12585. doi:10.1021/ja9035362
9. Yang, K.-W.; Xu, J.; Chen, C.-H.; Huang, H.-H.; Yu, T. J.-Y.; Lim, T.-S.; Chen, C.-h.; Luh, T.-Y. *Macromolecules* **2010**, *43*, 5188–5194. doi:10.1021/ma100550q
10. Chen, C.-W.; Chang, H.-Y.; Lee, S.-L.; Hsu, I.-J.; Lee, J.-J.; Chen, C.-h.; Luh, T.-Y. *Macromolecules* **2010**, *43*, 8741–8746. doi:10.1021/ma101956n
11. Wang, H.-W.; Chen, C.-H.; Lim, T.-S.; Huang, S.-L.; Luh, T.-Y. *Chem. – Asian J.* **2011**, *6*, 524–533. doi:10.1002/asia.201000492

12. Huang, H.-H.; Chao, C.-G.; Lee, S.-L.; Wu, H.-J.; Chen, C.-h.; Luh, T.-Y. *Org. Biomol. Chem.* **2012**, *10*, 5948–5953. doi:10.1039/c2ob25114k

13. Yeh, N.-H.; Chen, C.-W.; Lee, S.-L.; Wu, H.-J.; Chen, C.-h.; Luh, T.-Y. *Macromolecules* **2012**, *45*, 2662–2667. doi:10.1021/ma300027k

14. Xu, J.; Zhang, Z.; Liu, Y.-H.; Guo, Q.; Wang, G.-W.; Lai, G.; Luh, T.-Y. *J. Polym. Sci., Part A: Polym. Chem.* **2017**, *55*, 2999–3010. doi:10.1002/pola.28572

15. Zhu, L.; Flook, M. M.; Lee, S.-L.; Chan, L.-W.; Huang, S.-L.; Chiu, C.-W.; Chen, C.-H.; Schrock, R. R.; Luh, T.-Y. *Macromolecules* **2012**, *45*, 8166–8171. doi:10.1021/ma301686f

16. Chen, C.-H.; Satyanarayana, K.; Liu, Y.-H.; Huang, S.-L.; Lim, T.-S.; Luh, T.-Y. *Chem. – Eur. J.* **2015**, *21*, 800–807. doi:10.1002/chem.201403806

17. Zhu, L.; Lin, N.-T.; Xie, Z.-Y.; Lee, S.-L.; Huang, S.-L.; Yang, J.-H.; Lee, Y.-D.; Chen, C.-h.; Chen, C.-H.; Luh, T.-Y. *Macromolecules* **2013**, *46*, 656–663. doi:10.1021/ma302293q

18. Lin, N.-T.; Xie, C.-Y.; Huang, S.-L.; Chen, C.-H.; Luh, T.-Y. *Chem. – Asian J.* **2013**, *8*, 1436–1440. doi:10.1002/asia.201300222

19. Lin, N.-T.; Lin, S.-Y.; Lee, S.-L.; Chen, C.-h.; Hsu, C.-H.; Hwang, L. P.; Xie, Z.-Y.; Chen, C.-H.; Huang, S.-L.; Luh, T.-Y. *Angew. Chem., Int. Ed.* **2007**, *46*, 4481–4485. doi:10.1002/anie.200700472

20. Lai, G.; Luh, T.-Y. *Bull. Chem. Soc. Jpn.* **2018**, *91*, 262–273. doi:10.1246/bcsj.20170354

21. Ke, Y.-Z.; Lee, S.-L.; Chen, C.-h.; Luh, T.-Y. *Chem. – Asian J.* **2011**, *6*, 1748–1751. doi:10.1002/asia.201000877

22. Ke, Y.-Z.; Ji, R.-J.; Wei, T.-C.; Lee, S.-L.; Huang, S.-L.; Huang, M.-J.; Chen, C.-h.; Luh, T.-Y. *Macromolecules* **2013**, *46*, 6712–6722. doi:10.1021/ma4012363

23. Moatsou, D.; Hansell, C. F.; O'Reilly, R. K. *Chem. Sci.* **2014**, *5*, 2246–2250. doi:10.1039/c4sc00752b

24. Lutz, J.-F., Ed. *Sequence-Controlled Polymers*; Wiley-VCH Verlag GmbH: Weinheim, Germany, 2018. doi:10.1002/9783527806096

25. Wu, Z.; Wheeler, D. R.; Grubbs, R. H. *J. Am. Chem. Soc.* **1992**, *114*, 146–151. doi:10.1021/ja00027a021

26. Wu, Z.; Grubbs, R. H. *Macromolecules* **1994**, *27*, 6700–6703. doi:10.1021/ma00101a002

27. Perrott, M. G.; Novak, B. M. *Macromolecules* **1995**, *28*, 3492–3494. doi:10.1021/ma00113a062

28. Perrott, M. G.; Novak, B. M. *Macromolecules* **1996**, *29*, 1817–1823. doi:10.1021/ma951516j

29. Maughon, B. R.; Grubbs, R. H. *Macromolecules* **1997**, *30*, 3459–3469. doi:10.1021/ma961780s

30. Charvet, R.; Novak, B. M. *Macromolecules* **2001**, *34*, 7680–7685. doi:10.1021/ma0109875

31. Lee, J. C.; Parker, K. A.; Sampson, N. S. *J. Am. Chem. Soc.* **2006**, *128*, 4578–4579. doi:10.1021/ja058801v

32. Song, A.; Parker, K. A.; Sampson, N. S. *J. Am. Chem. Soc.* **2009**, *131*, 3444–3445. doi:10.1021/ja809661k

33. Parker, K. A.; Sampson, N. S. *Acc. Chem. Res.* **2016**, *49*, 408–417. doi:10.1021/acs.accounts.5b00490

34. Lin, N.-T.; Ke, Y.-Z.; Satyanarayana, K.; Huang, S.-L.; Lan, Y.-K.; Yang, H.-C.; Luh, T.-Y. *Macromolecules* **2013**, *46*, 7173–7179. doi:10.1021/ma401007b

35. Greenberg, A.; Liebman, J. F. *Strained organic molecules*; Academic Press: New York, 1978.

36. Schwab, P.; Grubbs, R. H.; Ziller, J. W. *J. Am. Chem. Soc.* **1996**, *118*, 100–110. doi:10.1021/ja952676d

37. Rule, J. D.; Moore, J. S. *Macromolecules* **2002**, *35*, 7878–7882. doi:10.1021/ma0209489

38. Wenzel, A. G.; Grubbs, R. H. *J. Am. Chem. Soc.* **2006**, *128*, 16048–16049. doi:10.1021/ja0666598

39. Beligny, S.; Blechert, S. In *N-Heterocyclic Carbenes in Synthesis*; Nolan, S. P., Ed.; Wiley-VCH: Weinheim, 2006.

40. van der Eide, E. F.; Piers, W. E. *Nat. Chem.* **2010**, *2*, 571–576. doi:10.1038/nchem.653

41. Cazalis, C.; Héroguez, V.; Fontanille, M. *Macromol. Chem. Phys.* **2000**, *201*, 869–876. doi:10.1002/(sici)1521-3935(20000501)201:8<869::aid-macp869>3.3.c0;2-q

42. Al Samak, B.; Amir-Ebrahimi, V.; Corry, D. G.; Hamilton, J. G.; Rigby, S.; Rooney, J. J.; Thompson, J. M. *J. Mol. Catal. A: Chem.* **2000**, *160*, 13–21. doi:10.1016/s1381-1169(00)00228-4

43. Matos, J. M. E.; Lima-Neto, B. S. *J. Mol. Catal. A: Chem.* **2005**, *240*, 233–238. doi:10.1016/j.molcata.2005.07.003

44. Sattigeri, J. A.; Shiau, C.-W.; Hsu, C. C.; Yeh, F.-F.; Liou, S.; Jin, B.-Y.; Luh, T.-Y. *J. Am. Chem. Soc.* **1999**, *121*, 1607–1608. doi:10.1021/ja983433z

45. Lin, W.-Y.; Murugesh, M. G.; Sudhakar, S.; Yang, H.-C.; Tai, H.-C.; Chang, C.-S.; Liu, Y.-H.; Wang, Y.; Chen, I.-W. P.; Chen, C.-h.; Luh, T.-Y. *Chem. – Eur. J.* **2006**, *12*, 324–330. doi:10.1002/chem.200500770

46. Lin, W.-Y.; Wang, H.-W.; Liu, Z.-C.; Xu, J.; Chen, C.-W.; Yang, Y.-C.; Huang, S.-L.; Yang, H.-C.; Luh, T.-Y. *Chem. – Asian J.* **2007**, *2*, 764–774. doi:10.1002/asia.200700011

License and Terms

This is an Open Access article under the terms of the Creative Commons Attribution License (<http://creativecommons.org/licenses/by/4.0>). Please note that the reuse, redistribution and reproduction in particular requires that the authors and source are credited.

The license is subject to the *Beilstein Journal of Organic Chemistry* terms and conditions: (<https://www.beilstein-journals.org/bjoc>)

The definitive version of this article is the electronic one which can be found at: doi:10.3762/bjoc.15.4



Ammonium-tagged ruthenium-based catalysts for olefin metathesis in aqueous media under ultrasound and microwave irradiation

Łukasz Gułajski¹, Andrzej Tracz¹, Katarzyna Urbaniak¹, Stefan J. Czarnocki¹, Michał Bieniek¹ and Tomasz K. Olszewski^{*2}

Full Research Paper

Open Access

Address:

¹Aperion Synthesis SA, Duńska 9, 54-427 Wrocław, Poland and
²Wrocław University of Science and Technology, Faculty of Chemistry, Wybrzeże Wyspiańskiego 29, 50-370 Wrocław, Poland

Email:

Tomasz K. Olszewski* - tomasz.olszewski@pwr.edu.pl

* Corresponding author

Keywords:

catalysis; green chemistry; microwave; *N*-heterocyclic carbene; olefin metathesis; ruthenium; ultrasound

Beilstein J. Org. Chem. **2019**, *15*, 160–166.

doi:10.3762/bjoc.15.16

Received: 23 August 2018

Accepted: 22 December 2018

Published: 17 January 2019

This article is part of the thematic issue "Progress in metathesis chemistry III".

Associate Editor: M. Rueping

© 2019 Gułajski et al.; licensee Beilstein-Institut.

License and terms: see end of document.

Abstract

The influence of microwave and ultrasonic irradiation on the performance of ammonium-tagged Ru-based catalysts in olefin metathesis transformations in aqueous media was studied. Differences in the catalytic activity in correlation with the nature of the present counter ion and the size of the *N*-heterocyclic carbene (NHC) ligand were revealed. The presented methodology allows for preparation of a variety of polar and non-polar metathesis products under environmentally friendly conditions.

Introduction

Olefin metathesis is well established as a powerful transformation used for effective and elegant creation of new carbon–carbon double bonds [1,2]. The development of commercially available, stable and effective catalysts for that reaction [3–6] made possible for its wide application not only in academia but also in industry [7–12]. However, there is still a large interest in improving the catalytic activity of the existing Ru-based metathesis catalysts as there is no universal catalyst for all the metathesis transformations. This is especially true for olefin metathesis reactions carried out with the use of green solvents, for

which there is currently an increasing demand, especially in industrial practice, as a replacement for those with major regulatory issues such as chlorinated (dichloromethane, 1,2-dichloroethane) or aromatic solvents (toluene, benzene) [13–16]. In that aspect olefin metathesis in aqueous media appears to be an interesting alternative, especially in the case of preparation of biologically important molecules [17–20] as well as of highly polar compounds. Thus far, several strategies were applied to facilitate olefin metathesis in water including the development of specially designed water-soluble catalysts [21–28], addition

of organic solvents [29–31], or use of additives such as for example calixarenes or cyclodextrins [32,33], chloride salts [34], vitamin E-based amphiphiles [35], dodecyltrimethylammonium bromide (DTAB) [36], polymerised cyclooctadiene (COD) and cyclooctene (COE) [37], sodium dodecyl sulphate (SDS) [38] or DL- α -tocopherol methoxypolyethylene glycol succinate solution (TPGS-750-M) [39], to improve the solubility of reacting species and/or performance of the catalyst. Recent progress in the flourishing field of micellar catalysis and the use of surfactants that self-aggregate in water into micelles in which the hydrophobic core provides an environment for effecting homogeneous reactions between organic molecules has been reviewed by Scarso et al. [40] and very recently by Lipshutz and co-workers [41]. Worth mentioning are also reports of heterogenous and recyclable catalysis able to mediate metathesis in aqueous media [42–45]. Although the aforementioned examples show a significant progress in the olefin metathesis in aqueous media, some limitations such as complex structure of the tailored catalysts and thus difficulties associated with their synthesis, or the need to use additives or co-solvents to improve the solubility of reacting species, still remain. Therefore, further development of catalytic systems would provide a complementary extension to the scope of this interesting transformation.

Furthermore, in the continuous search for new sustainable protocols for chemical reactions to induce new reactives or

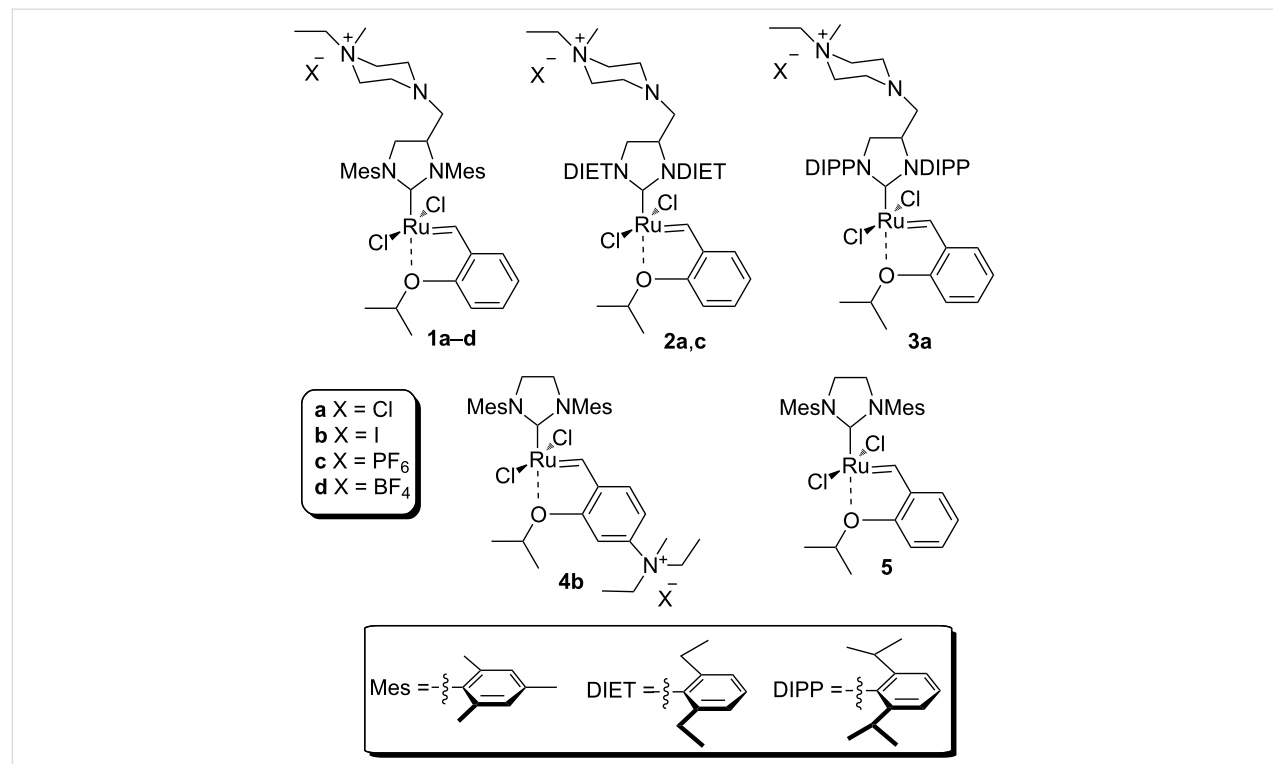
reduce the energetic cost of the processes, the replacement of mechanical mixing and/or heating of the reacting species with microwave (μW) [46–48] and ultrasonic irradiation (US) [49–55] appears as a promising approach. Both methods were shown in the past to be responsible for shortening the reaction time, increasing the reaction yield or even favour the formation of the desired product when compared to traditional protocols [56,57]. In the case of olefin metathesis, examples of application of those techniques are well documented for organic solvents [58–66], surprisingly, examples describing reactions in aqueous media are scarce and thus merit further investigation [67,68].

In line with our ongoing research on synthesis of catalysts for olefin metathesis and to expand the utility of ammonium-tagged ruthenium-based catalysts [69–76], herein we present the use of such catalysts for olefin metathesis in aqueous media promoted by microwave and ultrasound irradiation.

Results and Discussion

The structures of the catalysts **1–5** used in this work are depicted in Figure 1.

Catalyst **1b** was prepared by alkylation of the non-ionic tertiary amine-containing analogue with methyl iodide [71]. Complexes **1c,d** were prepared from their commercially available



corresponding chloride salt **1a** [72] by exchange of the Cl^- counter-ion to PF_6^- or BF_4^- [76]. The exchange was performed in water, and after addition of NH_4PF_6 or NH_4BF_4 the formed catalysts were collected by filtration. Catalyst **2c** was prepared from the new complex **2a** using a similar procedure (see Supporting Information File 1 for details). The complexes **3a** [75] and **5** are commercially available and catalyst **4b** was obtained according to a literature procedure from commercially available Grubbs 2nd generation catalyst through ligand exchange [68]. In general, the solubility of the catalysts containing Cl^- as counter ion in water is good (e.g., 50 mg mL^{-1} for **1a** or **3a**) whereas for those with I^- as counter-ion is much lower (e.g., 4.0 mg mL^{-1} for **1b**). In turn catalysts bearing PF_6^- or BF_4^- as counter ions are not soluble in water [71].

We have started our study with the comparison of the catalytic activity of complex **4b**, having the ionic tag attached to the benzylidene ligand, with that of catalyst **1a**, bearing an ionic tag placed on the *N*-heterocyclic carbene (NHC) fragment. As model reactions we have selected the ring-closing metathesis (RCM) of the water-soluble substrate **6**, the homometathesis of alcohol **8**, and more challenging, the cross metathesis (CM) between alcohol **8** and the electron-deficient cross partner methyl acrylate (**10**, Table 1).

All reactions were run at 36 °C in D_2O promoted either by microwave (μW) or ultrasound (US) irradiation, and for comparison purposes also with standard magnetic stirring. In the case of the RCM (Table 1, entries 1 and 2) both tested catalysts (1 mol %) under classical conditions exhibited similar activities with **4b** being slightly less active (52 vs 48%, respectively). The

reaction performed under ultrasound irradiation proved to be ca. 10% more productive with both catalysts compared to the classical conditions. On the other hand, microwave irradiation turned out to be less effective leading to a drop in the reaction yield for **1a** (48%) and a slightly increased yield in the case of **4b** (55%). In the homometathesis reaction of allyl alcohol **8** (Table 1, entries 3 and 4) both catalysts (5 mol %) produced the desired product again with quite similar yields under classical conditions. However, the use of microwave or ultrasound irradiation promoted the undesired isomerisation of the $\text{C}=\text{C}$ bond, thus lowering the yields of the desired product **9** (Table 1, entries 3 and 4). This result is in agreement with the known fact that in protic solvents ruthenium hydrides are formed leading to isomerisation byproducts [66]. Finally, we were pleased to see that the use of ultrasound or microwave irradiation were beneficial for the CM of alcohol **8** with methyl acrylate (**10**, Table 1, entries 5 and 6) resulting not only in increased conversion but also reducing the amount of the unwanted product of self-metathesis of **8**.

In general, the results obtained with catalysts **4b** and **1a** were comparable. However, we expected that **1a** should be much more effective because it remains tagged after the initiation step. This unexpected catalytic activity might be due to the fact that catalysts **4b** and **1a** have different counter ions and therefore we decided to examine if there is an influence of counter ions on the catalytic activity. To achieve this we used analogues of **1a** bearing different counter ions (**1b–d**) and also included catalysts having differently sized NHC ligands (**2a,c**). For testing the catalysts performances, we selected the RCM of the water-soluble substrate **12** (Table 2).

Table 1: Effect of microwave (μW) and ultrasound (US) irradiation on RCM, homometathesis and CM in water mediated by complexes **1a** and **4b**.

Entry	Substrate	Product	Ru complex	Classical conditions ^a	US ^a	μW^{a}
1 ^b			1a 4b	52 48	63 59	48 55
2 ^b			1a 4b	81 (78) 77 (88)	73 (60) 38 (66)	64 (68) 75 (84)
3 ^c			1a 4b	69 (74) 35 (45)	71 (79) 71 (80)	81 (88) 80 (86)
4 ^c			1a 4b	69 (74) 35 (45)	71 (79) 71 (80)	81 (88) 80 (86)
5 ^c			1a 4b	69 (74) 35 (45)	71 (79) 71 (80)	81 (88) 80 (86)
6 ^c			1a 4b	69 (74) 35 (45)	71 (79) 71 (80)	81 (88) 80 (86)
10 (4 equiv)						

^aConversion and selectivity (in parentheses, referring to the formation of an aldehyde, having a signal at 9.60 ppm, resulting from double bond migration) have been determined based on ^1H NMR. ^bReaction conditions: D_2O , catalyst (1 mol % Ru), c 0.1 M, 36 °C, 2 h. ^cReaction conditions: D_2O , catalyst (5 mol % Ru), c 0.1 M, 36 °C, 2 h.

Table 2: Effect of the counter ion and substituents size of the NHC ligand in catalysts **1b–d**, and **2a,c** on their efficiency in the RCM of substrate **12** in water under μ W and US irradiation.^a

Entry	Substrate	Product	Ru	Classical conditions ^b	US ^b	μ W ^b
1			1a	33	41	58
2			1b	13	53	77
3			1c	53	49	81
4			1d	35	46	72
5	12	13	2a	54	12	51
6			2c	33	32	61
7			5	3	1	1

^aReaction conditions: D₂O, Ru catalyst (0.25 mol %), c 0.2 M, 36 °C, 2 h. ^bConversions determined based on NMR.

Under the reaction conditions the classical catalyst **5** (0.25 mol %) was not soluble resulting in poor yields and justifying the use of modified catalysts. For the ammonium NHC-tagged catalysts (0.25 mol %), the use of microwave irradiation was more productive than ultrasound treatment. This effect was most pronounced in the case of catalysts with low solubility in water such as **1b** or the insoluble catalysts **1d** and **2c**. Additionally, under classical conditions, we observed a higher activity of catalyst **2a** with Cl[−] as counter ion and a larger NHC ligand when compared to **1a**. In turn, the use of US and μ W had an inverse effect on that reaction furnishing lower yields of the product in the case of **2a** when compared with **1a**. In case of catalysts bearing a large hexafluorophosphate counter ion (PF₆[−]; **1c** and **2c**) an increase of the NHC's size had a negative effect on the catalyst performance (Table 2, entries 3 and 6, respectively).

Examining further the influence of the steric hindrance of the NHC ligand we tested complexes **1a**, **2a** and **3a** (1 mol %) all with Cl[−] as counter ion in the RCM of polar substrate **6** (Table 3).

In order to maintain homogeneity of the reaction mixture addition of isopropanol (iPrOH) was necessary. Under the applied conditions the activity of the tested complexes decreased with

increasing size of the NHC ligand. This result suggests that a fast propagation ensured by a smaller carbene ligand rather than robustness ascribed to larger catalysts is a prerequisite for the efficient metathesis in homogeneous aqueous conditions. Except in the case of catalyst **3a**, exhibiting the lowest activity under classical conditions, we noted a positive effect of US increasing the reaction yield from 22 to 61%.

Finally, we have tested the influence of μ W and US irradiation on the RCM of lipophilic substrates **14**, **16** and **18** in water (Table 4).

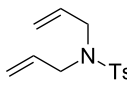
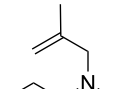
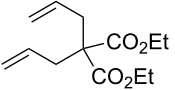
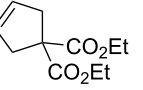
Regardless of the conditions and substrate used, the lowest yields were observed for the water-soluble complexes **1a** and **2a**. This is most probably due to the reduced stability of those catalysts in aqueous medium and additionally to their limited contact with the substrates, being in a different phase (organic layer), and in a process that resembles more to a “heterogeneous reaction”. In turn, reactions with the use of catalysts **1b**, **1c**, **1d** and **2c** with much lower solubility in water gave significantly better results. With only two exceptions the use of μ W or US irradiation provided poorer results when compared to the classical conditions. Only catalysts **1c** and **2c** bearing PF₆[−] as counter ion performed better with both, μ W and US irradiation. However, this effect was observed only for the simplest sub-

Table 3: Effect of the size of the NHC ligand in the catalysts **1a**, **2a**, and **3a** on their catalytic efficiency in the RCM of substrate **6** under μ W and US irradiation.^a

Entry	Substrate	Product	Ru	Classical conditions ^b	US ^b	μ W ^b
1			1a	61	48	51
2			2a	43	38	36
3	6	7	3a	22	61	39

^aReaction conditions: D₂O/iPrOH 2:1 (v/v), Ru catalyst (1 mol %), 36 °C, 2 h. ^bConversions determined based on NMR.

Table 4: Effect of microwave (μW) and ultrasound irradiation (US) irradiation on the RCM of lipophilic substrates in water.^a

Entry	Substrate ^b	Product ^b	Ru	Classical conditions ^c	US ^c	μW^{c}
1			1a	21	6	17
2			1b	95	95	97
3	14	15	1c	83	92	93
4			1d	93	80	89
5			2a	20	6	12
6			2c	73	91	97
7			5	49	63	96
8			1a	24	3	11
9			1b	82	29	46
10	16	17	1c	96	73	74
11			1d	90	25	55
12			2a	12	2	7
13			2c	96	95	83
14			5	88	78	77
15 ^d			1a	3	2	3
16 ^d			1b	78	15	56
17 ^d	18	19	1c	93	27	64
18 ^d			1d	78	11	57
19 ^d			2a	3	2	2
20 ^d			2c	93	37	67
21 ^d			5	80	69	50

^aReaction conditions: H_2O , Ru catalyst (0.5 mol %), *c* 0.2 M, 36 °C, 2 h. ^bTs: *p*-toluenesulfonyl. ^cConversions determined based on GC. ^dReaction conditions: H_2O , Ru catalyst (1.0 mol %), *c* 0.2 M, 36 °C, 2 h.

strate **14**. The results collected in Table 4 can be explained by the fact that the reactions actually occurred under heterogeneous conditions between water-insoluble components at the water–reagents phase boundary [26,77,78]. Such conditions can imply a positive impact on the rate of a reaction and are the result of a “hydrophobic effect” [78,79]. This phenomenon, mentioned by Sharpless and co-workers in their seminal paper [78] is not well understood yet [80]. Jung and Marcus postulated a trans-phase hydrogen bonding from water OH groups to H-bond acceptor sites of organic reactants contributing to a stabilisation of organic transition states enables the on-water catalysis [77]. Ben-Amotz et al. demonstrated that the effect of the water OH groups depends either on the surface area involved or on the electrostatic nature of the surface itself [81]. Additionally, the packing density of supramolecular clusters of water created by strong intermolecular hydrogen bonds may also play a key role. Indeed, various effects may be depending on the solubility of the reactants in water [82,83]. The hydrophobic and water molecules stay in minimal contact between each other because a sphere of water molecules is formed around the non-polar components resulting in higher (local) concentration and higher pressure in water [26,79]. The application of US and μW irradiation could, to some extent, disturb the “hydrophobic

effect” and thus may explain the less satisfactory results of the reactions using those techniques compared to those obtained under classical conditions.

Conclusion

We have examined the effect of microwave and ultrasonic irradiation on a range of different olefin metathesis transformations in water catalysed by ammonium-tagged Ru-based catalysts. It was noted that placing the water solubilising ionic tag on the NHC ligand gives catalysts with improved catalytic activity and more suitable for reactions in water than those having an ionic tag on the benzylidene part. In general, a more prominent positive effect of microwave irradiation on the reaction outcome compared to ultrasound was observed. This effect was shown in a CM reaction, where an improvement in the reaction yield and selectivity was noted, as well as in the RCM of water-soluble substrates. In reactions with lipophilic substrates the solubility of the tested catalysts had a crucial influence on the reaction outcome. In turn, the use of microwave and ultrasonic irradiation did not have a positive effect on the reaction productivity. In contrast, catalysts that are sparingly or even insoluble in water gave better results that were explained by the “hydrophobic effect”.

Supporting Information

Supporting Information File 1

Experimental procedures and characterisation data for all previously unreported compounds.

[<https://www.beilstein-journals.org/bjoc/content/supplementary/1860-5397-15-16-S1.pdf>]

Acknowledgements

L. G. and M. B. acknowledge the National Science Centre (NCN) for financial support within the “Preludium” project (decision number UMO-2012/05/N/ST5/02312).

ORCID® iDs

Tomasz K. Olszewski - <https://orcid.org/0000-0001-8243-9313>

References

1. Grela, K., Ed. *Olefin Metathesis: Theory and Practice*, 1st ed.; Wiley-VCH: Weinheim, Germany, 2014. doi:10.1002/9781118711613
2. Grubbs, R. H.; Wenzel, A. G.; O’Leary, D. J.; Khosravi, E., Eds. *Handbook of Metathesis*, 2nd ed.; Wiley-VCH: Weinheim, Germany, 2015. doi:10.1002/9783527674107
3. Herbert, M. B.; Grubbs, R. H. *Angew. Chem., Int. Ed.* **2015**, *54*, 5018–5024. doi:10.1002/anie.201411588
4. Fuster, S.; Simón-Fuentes, A.; Barrio, P.; Haufe, G. *Chem. Rev.* **2015**, *115*, 871–930. doi:10.1021/cr500182a
5. Hoveyda, A. H. *J. Org. Chem.* **2014**, *79*, 4763–4792. doi:10.1021/jo500467z
6. Olszewski, T. K.; Bieniek, M.; Skowerski, K.; Grela, K. *Synlett* **2013**, 903–919. doi:10.1055/s-0032-1318497
7. Higman, C. S.; Lummiss, J. A. M.; Fogg, D. E. *Angew. Chem., Int. Ed.* **2016**, *55*, 3552–3565. doi:10.1002/anie.201506846
8. Hughes, D.; Wheeler, P.; Ene, D. *Org. Process Res. Dev.* **2017**, *21*, 1938–1962. doi:10.1021/acs.oprd.7b00319
9. Olszewski, T. K.; Figlus, M.; Bieniek, M. *Chim. Oggi* **2014**, *32*, 22–29.
10. Behr, A.; Vorholt, A. J.; Ostrowski, K. A.; Seidensticker, T. *Green Chem.* **2014**, *16*, 982–1006. doi:10.1039/c3gc41960f
11. Chikkali, S.; Mecking, S. *Angew. Chem., Int. Ed.* **2012**, *51*, 5802–5808. doi:10.1002/anie.201107645
12. Leimgruber, S.; Trimmel, G. *Monatsh. Chem.* **2015**, *146*, 1081–1097. doi:10.1007/s00706-015-1501-0
13. Piola, L.; Nahra, F.; Nolan, S. P. *Beilstein J. Org. Chem.* **2015**, *11*, 2038–2056. doi:10.3762/bjoc.11.221
14. Guidone, S.; Songis, O.; Nahra, F.; Cazin, C. S. J. *ACS Catal.* **2015**, *5*, 2697–2701. doi:10.1021/acscatal.5b00197
15. Skowerski, K.; Bialecki, J.; Tracz, A.; Olszewski, T. K. *Green Chem.* **2014**, *16*, 1125–1130. doi:10.1039/c3gc41943f
And the references cited therein.
16. Skowerski, K.; Kasprzycki, P.; Bieniek, M.; Olszewski, T. K. *Tetrahedron* **2013**, *69*, 7408–7415. doi:10.1016/j.tet.2013.06.056
17. Lin, Y. A.; Chalker, J. M.; Davis, B. G. *ChemBioChem* **2009**, *10*, 959–969. doi:10.1002/cbic.200900002
18. Lin, Y. A.; Chalker, J. M.; Floyd, N.; Bernardes, G. J. L.; Davis, B. G. *J. Am. Chem. Soc.* **2008**, *130*, 9642–9643. doi:10.1021/ja8026168
19. Lin, Y. A.; Chalker, J. M.; Davis, B. G. *J. Am. Chem. Soc.* **2010**, *132*, 16805–16811. doi:10.1021/ja104994d
20. Lin, Y. A.; Boutureira, O.; Lercher, L.; Bhushan, B.; Paton, R. S.; Davis, B. G. *J. Am. Chem. Soc.* **2013**, *135*, 12156–12159. doi:10.1021/ja403191g
21. Wright, D. B.; Touve, M. A.; Thompson, M. P.; Gianneschi, N. C. *ACS Macro Lett.* **2018**, *7*, 401–405. doi:10.1021/acsmacrolett.8b00091
22. Wang, Z. J.; Jackson, W. R.; Robinson, A. J. *Green Chem.* **2015**, *17*, 3407–3414. doi:10.1039/c5gc00252d
23. Gleeson, E. C.; Wang, Z. J.; Jackson, W. R.; Robinson, A. J. *J. Org. Chem.* **2015**, *80*, 7205–7211. doi:10.1021/acs.joc.5b01091
24. Levin, E.; Ivry, E.; Diesendruck, C. E.; Lemcoff, N. G. *Chem. Rev.* **2015**, *115*, 4607–4692. doi:10.1021/cr400640e
25. Szczepaniak, G.; Kosiński, K.; Grela, K. *Green Chem.* **2014**, *16*, 4474–4492. doi:10.1039/c4gc00705k
26. Tomasek, J.; Schatz, J. *Green Chem.* **2013**, *15*, 2317–2338. doi:10.1039/c3gc41042k
27. Diaz Velazquez, H.; Verpoort, F. *Chem. Soc. Rev.* **2012**, *41*, 7032–7060. doi:10.1039/c2cs35102a
28. Burtscher, D.; Grela, K. *Angew. Chem., Int. Ed.* **2009**, *48*, 442–454. doi:10.1002/anie.200801451
29. Connan, S. J.; Blechert, S. *Bioorg. Med. Chem. Lett.* **2002**, *12*, 1873–1876. doi:10.1016/s0960-894x(02)00260-3
30. Connan, S. J.; Rivard, M.; Zaja, M.; Blechert, S. *Adv. Synth. Catal.* **2003**, *345*, 572–575. doi:10.1002/adsc.200202201
31. Binder, J. B.; Blank, J. J.; Raines, R. T. *Org. Lett.* **2007**, *9*, 4885–4888. doi:10.1021/ol7022505
32. Tomasek, J.; Seßler, M.; Gröger, H.; Schatz, J. *Molecules* **2015**, *20*, 19130–19141. doi:10.3390/molecules201019130
33. Brendgen, T.; Fahlbusch, T.; Frank, M.; Schühle, D. T.; Seßler, M.; Schatz, J. *Adv. Synth. Catal.* **2009**, *351*, 303–307. doi:10.1002/adsc.200800637
34. Matsuo, T.; Yoshida, T.; Fujii, A.; Kawahara, K.; Hirota, S. *Organometallics* **2013**, *32*, 5313–5319. doi:10.1021/om4005302
35. Lipshutz, B. H.; Aguinaldo, G. T.; Ghorai, S.; Voigtritter, K. *Org. Lett.* **2008**, *10*, 1325–1328. doi:10.1021/ol800028x
36. Lynn, D. M.; Kanaoka, S.; Grubbs, R. H. *J. Am. Chem. Soc.* **1996**, *118*, 784–790. doi:10.1021/ja950327d
37. Claverie, J. P.; Viala, S.; Maurel, V.; Novat, C. *Macromolecules* **2001**, *34*, 382–388. doi:10.1021/ma001570m
38. Davis, K. J.; Sinou, D. *J. Mol. Catal. A: Chem.* **2002**, *177*, 173–178. doi:10.1016/s1381-1169(01)00239-4
39. Lipshutz, B. H.; Bošković, Z.; Crowe, C. S.; Davis, V. K.; Whittemore, H. C.; Vosburg, D. A.; Wenzel, A. G. *J. Chem. Educ.* **2013**, *90*, 1514–1517. doi:10.1021/ed300893u
40. La Sorella, G.; Strukul, G.; Scarso, A. *Green Chem.* **2015**, *17*, 644–683. doi:10.1039/c4gc01368a
41. Lipshutz, B. H.; Ghorai, S.; Cortes-Clerget, M. *Chem. – Eur. J.* **2018**, *24*, 6672–6695. doi:10.1002/chem.201705499
42. Wang, W.; Cui, L.; Sun, P.; Shi, L.; Yue, C.; Li, F. *Chem. Rev.* **2018**, *118*, 9843–9929. doi:10.1021/acs.chemrev.8b00057
43. Dewaele, A.; Verpoort, F.; Sels, B. *ChemCatChem* **2016**, *8*, 3010–3030. doi:10.1002/cctc.201600591
44. Mwangi, M. T.; Runge, M. B.; Bowden, N. B. *J. Am. Chem. Soc.* **2006**, *128*, 14434–14435. doi:10.1021/ja0642212
45. Hensle, E. M.; Tobis, J.; Tiller, J. C.; Bannwarth, W. *J. Fluorine Chem.* **2008**, *129*, 968–973. doi:10.1016/j.fluchem.2008.05.024
46. Kappe, C. O.; Pieber, B.; Dallinger, D. *Angew. Chem., Int. Ed.* **2013**, *52*, 1088–1094. doi:10.1002/anie.201204103
47. Kappe, C. O. *Angew. Chem., Int. Ed.* **2004**, *43*, 6250–6284. doi:10.1002/anie.200400655

48. Kappe, C. O.; Dallinger, D. *Nat. Rev. Drug Discovery* **2006**, *5*, 51–63. doi:10.1038/nrd1926

49. Chatel, G. *Ultrason. Sonochem.* **2018**, *40*, 117–122. doi:10.1016/j.ultsonch.2017.03.029

50. Cravotto, G.; Cintas, P. *Chem. Soc. Rev.* **2006**, *35*, 180–196. doi:10.1039/b503848k

51. Cravotto, G.; Cintas, P. *Chem. Sci.* **2012**, *3*, 295–307. doi:10.1039/c1sc00740h

52. Lupacchini, M.; Mascitti, A.; Giachi, G.; Tonucci, L.; d'Alessandro, N.; Martinez, J.; Colacicco, E. *Tetrahedron* **2017**, *73*, 609–653. doi:10.1016/j.tet.2016.12.014

53. Banerjee, B. *Ultrason. Sonochem.* **2017**, *35*, 15–35. doi:10.1016/j.ultsonch.2016.10.010

54. Cravotto, G.; Borgetto, E.; Oliverio, M.; Procopio, A.; Penoni, A. *Catal. Commun.* **2015**, *63*, 2–9. doi:10.1016/j.catcom.2014.12.014

55. Cravotto, G.; Gaudino, E. C.; Cintas, P. *Chem. Soc. Rev.* **2013**, *42*, 7521–7534. doi:10.1039/c2cs35456j

56. Varma, R. S. *Green Chem.* **2014**, *16*, 2027–2041. doi:10.1039/c3gc42640h

57. Bruckmann, A.; Krebs, A.; Bolm, C. *Green Chem.* **2008**, *10*, 1131–1141. doi:10.1039/b812536h

58. Dallinger, D.; Irfan, M.; Sujanovic, A.; Kappe, C. O. *J. Org. Chem.* **2010**, *75*, 5278–5288. doi:10.1021/jo1011703

59. Garbacia, S.; Desai, B.; Lavastre, O.; Kappe, C. O. *J. Org. Chem.* **2003**, *68*, 9136–9139. doi:10.1021/jo035135c

60. Mayo, K. G.; Nearhoof, E. H.; Kiddle, J. *J. Org. Lett.* **2002**, *4*, 1567–1570. doi:10.1021/o1025789s

61. Nosse, B.; Schall, A.; Jeong, W. B.; Reiser, O. *Adv. Synth. Catal.* **2005**, *347*, 1869–1874. doi:10.1002/adsc.200505137

62. Debleds, O.; Campagne, J.-M. *J. Am. Chem. Soc.* **2008**, *130*, 1562–1563. doi:10.1021/ja0780986

63. Gebauer, J.; Arseniyadis, S.; Cossy, J. *Eur. J. Org. Chem.* **2008**, 2701–2704. doi:10.1002/ejoc.200800203

64. Goldup, S. M.; Pilkington, C. J.; White, A. J. P.; Burton, A.; Barrett, A. G. M. *J. Org. Chem.* **2006**, *71*, 6185–6191. doi:10.1021/jo060931e

65. Fürstner, A.; Stelzer, F.; Rumbo, A.; Krause, H. *Chem. – Eur. J.* **2002**, *8*, 1856–1863. doi:10.1002/1521-3765(20020415)8:8<1856::aid-chem1856>3.0.co;2-r

66. Sacco, M.; Charnay, C.; De Angelis, F.; Radoiu, M.; Lamaty, F.; Martinez, J.; Colacicco, E. *RSC Adv.* **2015**, *5*, 16878–16885. doi:10.1039/c4ra14938f
See for a recent example on simultaneous microwaves-ultrasound irradiation (SMUI) hybrid technology.

67. Castagnolo, D.; Botta, L.; Botta, M. *J. Org. Chem.* **2009**, *74*, 3172–3174. doi:10.1021/jo900205x

68. Gułajski, Ł.; Śledź, P.; Lupa, A.; Grela, K. *Green Chem.* **2008**, *10*, 271–274. doi:10.1039/b719493e

69. Knapkiewicz, P.; Skowerski, K.; Jaskólska, D. E.; Barbasiewicz, M.; Olszewski, T. K. *Org. Process Res. Dev.* **2012**, *16*, 1430–1435. doi:10.1021/op300116j

70. Olszewski, T. K.; Jaskólska, D. E. *Heteroat. Chem.* **2012**, *23*, 605–609. doi:10.1002/hc.21056

71. Tracz, A.; Gawin, A.; Bieniek, M.; Olszewski, T. K.; Skowerski, K. *New J. Chem.* **2018**, *42*, 8609–8614. doi:10.1039/c8nj00614h

72. Skowerski, K.; Szczepaniak, G.; Wierzbicka, C.; Gułajski, Ł.; Bieniek, M.; Grela, K. *Catal. Sci. Technol.* **2012**, *2*, 2424–2427. doi:10.1039/c2cy20320k

73. Skowerski, K.; Wierzbicka, C.; Szczepaniak, G.; Gułajski, Ł.; Bieniek, M.; Grela, K. *Green Chem.* **2012**, *14*, 3264–3268. doi:10.1039/c2gc36015b

74. Skowerski, K.; Bialecki, J.; Czarnocki, S. J.; Zukowska, K.; Grela, K. *Beilstein J. Org. Chem.* **2016**, *12*, 5–15. doi:10.3762/bjoc.12.2

75. Skowerski, K.; Pastva, J.; Czarnocki, S. J.; Janoscova, J. *Org. Process Res. Dev.* **2015**, *19*, 872–877. doi:10.1021/acs.oprd.5b00132

76. Pastva, J.; Skowerski, K.; Czarnocki, S. J.; Žilková, N.; Čejka, J.; Bastl, Z.; Balcar, H. *ACS Catal.* **2014**, *4*, 3227–3236. doi:10.1021/cs500796u

77. Jung, Y.; Marcus, R. A. *J. Am. Chem. Soc.* **2007**, *129*, 5492–5502. doi:10.1021/ja068120f

78. Narayan, S.; Muldoon, J.; Finn, M. G.; Fokin, V. V.; Kolb, H. C.; Sharpless, K. B. *Angew. Chem., Int. Ed.* **2005**, *44*, 3275–3279. doi:10.1002/anie.200462883

79. Pirrung, M. C. *Chem. – Eur. J.* **2006**, *12*, 1312–1317. doi:10.1002/chem.200500959

80. García-Álvarez, J.; Hevia, E.; Capriati, V. *Chem. – Eur. J.* **2018**, *24*, 14854–14863. doi:10.1002/chem.201802873

81. Davis, J. G.; Rankin, B. M.; Gierszal, K. P.; Ben-Amotz, D. *Nat. Chem.* **2013**, *5*, 796–802. doi:10.1038/nchem.1716

82. Chanda, A.; Fokin, V. V. *Chem. Rev.* **2009**, *109*, 725–748. doi:10.1021/cr800448q

83. Butler, R. N.; Coyne, A. G. *Chem. Rev.* **2010**, *110*, 6302–6337. doi:10.1021/cr100162c

License and Terms

This is an Open Access article under the terms of the Creative Commons Attribution License (<http://creativecommons.org/licenses/by/4.0>). Please note that the reuse, redistribution and reproduction in particular requires that the authors and source are credited.

The license is subject to the *Beilstein Journal of Organic Chemistry* terms and conditions: (<https://www.beilstein-journals.org/bjoc>)

The definitive version of this article is the electronic one which can be found at:

[doi:10.3762/bjoc.15.16](https://doi.org/10.3762/bjoc.15.16)



Catalysis of linear alkene metathesis by Grubbs-type ruthenium alkylidene complexes containing hemilabile α,α -diphenyl-(monosubstituted-pyridin-2-yl)methanolato ligands

Tegene T. Tole^{1,2}, Johan H. L. Jordaan¹ and Hermanus C. M. Vosloo^{*1}

Full Research Paper

Open Access

Address:

¹Research Focus Area for Chemical Resource Beneficiation, Catalysis and Synthesis Research Group, North-West University, Hoffmann Street, 2531 Potchefstroom, South Africa and ²Department of Chemistry, College of Natural and Computational Sciences, Hawassa University, Hawassa, Ethiopia

Beilstein J. Org. Chem. **2019**, *15*, 194–209.

doi:10.3762/bjoc.15.19

Received: 02 September 2018

Accepted: 21 December 2018

Published: 22 January 2019

Email:

Hermanus C. M. Vosloo^{*} - manie.vosloo@nwu.ac.za

This article is part of the thematic issue "Progress in metathesis chemistry III".

* Corresponding author

Guest Editors: K. Grela and A. Kajetanowicz

Keywords:

Grubbs-type precatalyst; hemilabile; 1-octene metathesis; pyridinyl-alcoholato ligand

© 2019 Tole et al.; licensee Beilstein-Institut.

License and terms: see end of document.

Abstract

Four new Grubbs-type precatalysts $[\text{RuCl}(\text{H}_2\text{IMes})(\text{O}^{\text{N}})(=\text{CHPh})]$, where $[\text{O}^{\text{N}} = \alpha,\alpha\text{-diphenyl-(3-methylpyridin-2-yl)methanolato, } \alpha,\alpha\text{-diphenyl-(4-methylpyridin-2-yl)methanolato, } \alpha,\alpha\text{-diphenyl-(5-methylpyridin-2-yl)methanolato and } \alpha,\alpha\text{-diphenyl-(3-methoxypyridin-2-yl)methanolato}]$ were synthesized and tested for their activity, stability and selectivity in the 1-octene metathesis reaction. Overall the precatalysts showed good activity and high stability for the metathesis of 1-octene at temperatures above 80 °C and up to 110 °C. Selectivities towards the primary metathesis products, i.e., 7-tetradecene and ethene, above 85% were obtained with all the precatalysts at 80 and 90 °C. High selectivities were also observed at 100 °C for the 4-Me- and 3-OMe-substituted precatalysts. With an increase in temperature an increase in isomerisation products and secondary metathesis products were observed with the latter reaching values >20% for the 3-OMe- and 3-Me-substituted precatalysts at 110 and 100 °C, respectively. All the precatalysts exhibits first-order kinetics at 80 °C with the 3-substituted precatalysts the slowest. The behaviour of the 3-substituted precatalysts can be attributed to electronic and steric effects associated with the adjacent bulky phenyl groups.

Introduction

The alkene metathesis reaction is now well established as a powerful synthetic tool in organic and polymer chemistry [1,2]. The development of metal alkylidene precatalysts based on ruthenium, starting with the so-called Grubbs 1 (**1**) and 2 (**2**) metal carbenes, played a major role to extend the versatility of

the reaction including the application of these in industrial processes (Figure 1). Of course, the role of the so-called Schrock metal carbenes based on tungsten and molybdenum should not be ignored in the success story of the alkene metathesis reaction but it is not the focus of this article.

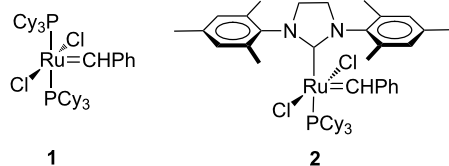
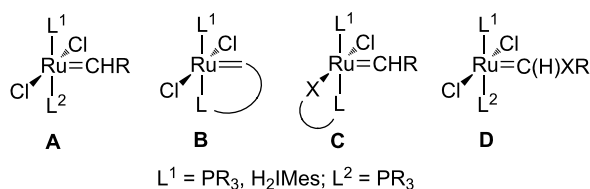


Figure 1: Structures of Grubbs 1 (**1**) and 2 (**2**) precatalysts.

The large number of ruthenium alkylidene precatalysts that has been developed is based on the design concepts illustrated in Scheme 1 [3]. The design concept **C** is of interest because of the potential hemilabile nature and latent metathesis activity of these complexes [4]. Of particular interest to us are the ruthenium alkylidene complexes containing the pyridinyl alcoholato bidentate ligands investigated by a number of research groups [5].



Scheme 1: Design concepts for ruthenium alkylidene precatalysts [3].

The pyridinyl alcohol found its way to the Grubbs-type complexes from research by Van Der Schaaf and co-workers on the Schrock-type analogues [6,7]. Grubbs 1-type complexes **3a–f** (Figure 2) were used to catalyse the ring-closing metathesis (RCM) of dialkenes, ring-opening metathesis polymerisation (ROMP), isomerisation of alkenes and cross-metathesis (CM) of alkenes [7]. The complexes were synthesized by reacting the lithium salts of the corresponding pyridinyl alcohols with $[\text{RuCl}_2(\text{=CHC}_6\text{H}_5)(\text{P}(\text{iPr})_3)]_2$. These complexes catalysed inter alia the cyclisation of hex-5-enyl undec-10-enoate to oxacyclohexadec-11-en-2-one (50% at 60 °C in toluene) and the ROMP of dicyclopentadiene. They were also able to immobilise these Grubbs 1-type precatalysts using dendritic pyridinyl alcohols [8]. These complexes catalysed the RCM reaction (at 80 °C) of

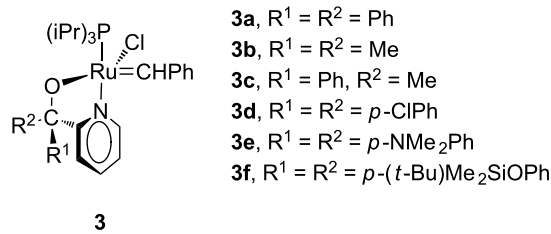


Figure 2: Structures of Grubbs 1-type (**3**) and 2-type (**4**) pyridinyl-alcoholato precatalysts.

diethyl diallylmalonate with 100% conversion after 30 min, results comparable to the unimolecular catalyst.

Denk et al. [9] synthesised *N*-heterocyclic (NHC) ruthenium alkylidene complexes containing pyridinyl-alcoholato ligands (**4**). These complexes were tested as precatalysts at different temperatures in the ROMP of norbornene and cyclooctene. Oligomers were obtained at room temperature in the presence of **4a** and **4d**, while **4b** and **4c** yielded polymers. At 60 °C, ROMP was observed with norbornene (98–100%) and cyclooctene (72–80%) in the presence of **4**.

We investigated a number of Grubbs 1- and Grubbs 2-type (**5**) metal carbenes with pyridinyl alcoholato ligands for the 1-octene metathesis reaction (Figure 3) [10–14]. The incorporation of pyridinyl-alcoholato ligands in the Grubbs-type precatalysts has shown an increase in the thermal stability, activity and lifetime of the precatalysts when compared to **1** and **2** [10]. The pyridinyl-alcoholato Grubbs 2-types exhibited higher activities and selectivities than the Grubbs 1-types and were investigated in more detail. It is clear from the results that the chelating ability of the pyridinyl alcoholato ligands combined with the NHC ligand is responsible for the activity and improved stability of the precatalyst at high temperatures. In general **5d** performed the best in the 1-octene metathesis reactions when compared to complexes **5a–c** and **5e–h**. The catalytic perfor-

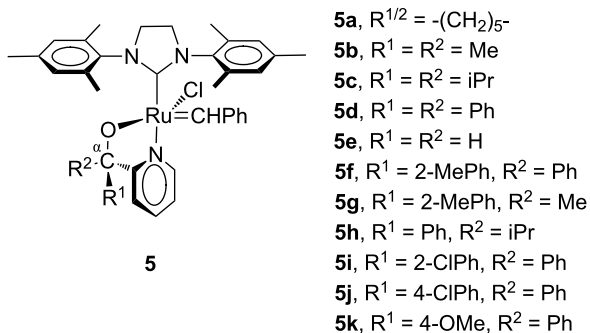
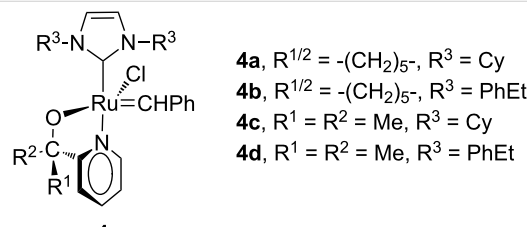


Figure 3: Structures of Grubbs 2-type (**5**) pyridinyl-alcoholato precatalysts.



mance could be further tuned by the incorporation of an electron-donating (e.g., OMe, **5k**) or electron-withdrawing (e.g. Cl, **5i** and **5j**) group at the 2- or 4-position of one of the α -phenyl groups of **5d** [14]. At 80–110 °C these complexes showed improved catalytic performance in the metathesis of oct-1-ene. At 110 °C complex **5k**, with 96% conversion and 95% selectivity towards the primary metathesis products tetradec-7-ene and ethene, outperformed the other complexes. In a computational study the improved catalytic performance was attributed to strengthening of the Ru–N bond due to steric repulsion between the substituted phenyl group and the NHC ligand [14]. An 8-quinolinolate Grubbs 2-type derivative, patented by Slugovc and Wappel [15] for use in ROPM reactions, was found to be inactive (<1% conversion) for 1-octene metathesis at 60 °C [12].

Schachner et al. [16] evaluated the catalytic activity of **5b**, **5d** and related complexes for the ROPM of cyclooctene, CM of hex-5-enyl acetate with dec-5-ene and the RCM of hex-5-en-1-yl undec-10-enoate. Superior (CM, RCM) to moderate (ROPM) activities were observed for most of these precatalysts. An interesting result was the very high affinity (“stickiness”) to untreated, unmodified and commercially available chromatography-grade silica. This was exploited further by Cabrera et al. [17,18] when **5b** and related complexes were investigated as heterogeneous precatalysts in biphasic RO-RCM and CM reactions. The substrate and catalyst were adsorbed on a thin layer silica plate and developed in EtOAc/hexane (1:7 v/v) for the CM of methyl 9-dodecene and in hexane for the RO-RCM of *cis*-cyclooctene.

The above-mentioned studies clearly illustrate the versatility and use of ruthenium alkylidene complexes with pyridinyl-alcoholato ligands. In principle these studies had one approach in common concerning the pyridinyl-alcoholato ligand, and that was to focus on substituents on the α -carbon of the ligand. To our knowledge, there are no reports on investigations of electronic and/or steric effect(s) of pyridinyl substituents on the chelation efficiency of pyridinyl alcoholato ligands, and subsequently its metathesis activity. Therefore, in this paper, we investigated the influence of a monosubstituent on the pyridinyl moiety on the 1-octene metathesis activity of a Grubbs 2-type precatalyst with an α,α -diphenyl methanolato ligand. For the synthesis of the pyridinyl methanol compounds, commercially available substituted bromopyridines were reacted with benzophenone followed by a reaction of the lithiated alcohol with **2**. Four new ruthenium alkylidene complexes, i.e., **6–9** (Figure 4), were successfully obtained and investigated as precatalyst in 1-octene metathesis in the temperature range 40–110 °C. The stability, selectivity and turnover frequency (TOF) of **2** increased upon substituting Me and OMe groups on the various

positions of the pyridine ring of the pyridinyl-alcoholato ligands at high temperatures (80–110 °C). The increase in stability is attributed to the electronic and steric influence of the Me and OMe groups on Ru–N chelation. The activity of the precatalysts also showed a significant improvement upon increasing the reaction temperature from 40 to 110 °C. The increase in the activity of the precatalysts is relatively low in the 40–60 °C range, but a high activity difference is observed upon increasing the temperature in 10 °C intervals between 70 and 110 °C.

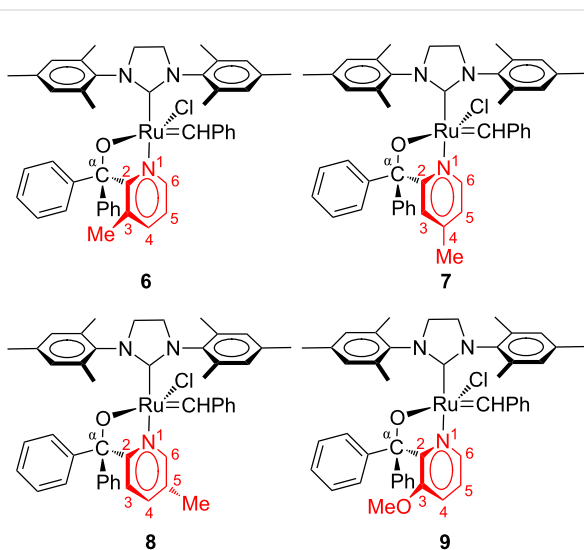


Figure 4: Structures of pyridinyl-substituted Grubbs 2-type pyridinyl-alcoholato precatalysts.

Results and Discussion

A mixture of products, summarised in Table 1, is obtained during the metathesis of 1-octene, i.e., primary metathesis products (PMPs), isomerisation products (IPs) and secondary me-

Table 1: Mixture of products formed during 1-octene metathesis in the presence of ruthenium alkylidene precatalysts.

Reaction	Substrate ^a	Products ^a	Abbrev.
primary metathesis			PMPs
self-metathesis	C=C ₇	C=C + C ₇ =C ₇	
isomerisation	C=C ₇	C ₂ =C ₆ + C ₃ =C ₅ + C ₄ =C ₄	IPs
secondary metathesis			SMPs
cross metathesis	C=C ₇ + C ₂ =C ₆	C ₂ =C ₇ + C ₂ =C ₆ + C=C ₂ + C ₆ =C ₇	
self-metathesis	C ₂ =C ₆	C ₂ =C ₂ + C ₆ =C ₆	

^aGeometrical isomers and hydrogens are not shown for simplicity.

tathesis products (SMPs). The PMPs, 7-tetradecene (*cis* and *trans*) and ethene, forms as a result of the self-metathesis (SM) of 1-octene. Simultaneously 1-octene is isomerised to 2-, 3- and 4-octene (IPs). The subsequent SM and CM reactions of the internal alkenes yield alkenes (*cis* and *trans*) in the C₃–C₁₃ range (SMPs).

All the reactions were followed by GC at regular sampling intervals until 540 min. Because the observed formation of IPs is mostly below 2% and never above 4% it is also not shown in the figures.

Effect of the reaction temperature

The results of the metathesis of 1-octene at temperatures 40–100 °C are presented in Figure 5 and Table 2 for precatalyst 7. The rate of self-metathesis of 1-octene showed an increase upon raising the reaction temperature from 40 to 100 °C. The metathesis reaction is insignificant at lower temperatures (40 to 60 °C). Upon raising the temperature beyond 70 °C, an increase in the reaction rate was observed, resulting in a significant increase in 1-octene conversion greater than 80% at 90 °C after 540 min. Increasing the temperature further to 100 °C showed a dramatic increase in the metathesis reaction rate and a

high PMPs formation are observed at 100 °C (>85% after ca. 200 min).

The formation of PMPs did not equilibrate within 540 min for the temperature range 50 to 80 °C; however, its formation equilibrated at ca. 400 min at 90 °C and ca. 200 min at 100 °C. This shows that 7 is stable at high temperatures, with moderate to very good PMPs (ca. 25–80%) formation. On the other hand, the formation of SMPs (ca. 0.2–2.0%) and IPs (ca. 0.2–0.5%) is negligible in the range 40–80 °C, while a more significant amount is formed at temperatures greater than 90 °C (ca. 10–14% SMPs and 1.7–2.1% IPs) after 540 min.

Table 2 summarises the overall catalytic performance of 7 at 420 min. In this period it can be seen that the PMPs and SMPs formation, TON, and TOF of the precatalyst show a direct relationship with temperature. The highest PMPs formation is observed for the temperature changes from 80 to 90 °C (29.3%) and the least for 40 to 50 °C (0.7%) at 420 min.

The selectivity towards PMPs showed a dramatic increase upon increasing the temperature from 40 to 80 °C (23–97%); however, it showed a decrease going from 80 (97%) to 90 °C (89%),

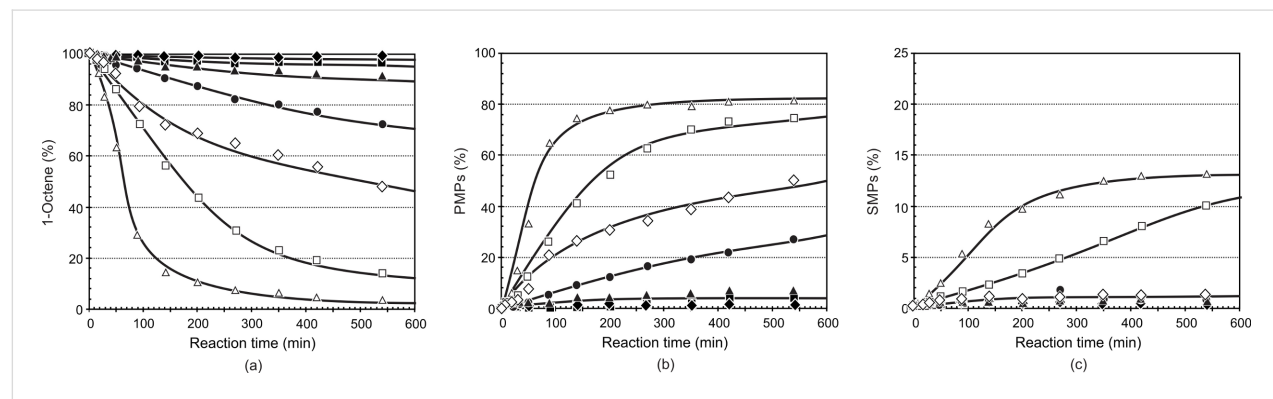


Figure 5: The influence of the reaction temperature on the (a) conversion of 1-octene, (b) formation of PMPs and (c) formation of SMPs using precatalyst 7 (Ru/1-octene = 1:9000). [◆ 40 °C, ■ 50 °C, ▲ 60 °C, ● 70 °C, ◇ 80 °C, □ 90 °C, △ 100 °C].

Table 2: Summary of the catalytic performance of precatalyst 7 at different temperatures (Ru/1-octene molar ratio 1:9 000, 420 min).

Entry	Temp. [°C]	Conv. ^a	PMPs ^a	SMPs ^a	IPs ^a	S ^b	TON ^c	TOF ^d
1	40	0.8	0.2	0.2	0.4	23	18	0.07×10^{-2}
2	50	2.1	0.9	0.4	0.8	44	81	0.32×10^{-2}
3	60	7.2	5.8	1.1	0.3	80	522	2.07×10^{-2}
4	70	22.3	21.2	0.9	0.2	95	1908	7.57×10^{-2}
5	80	44.4	43.1	1.1	0.2	97	3879	15.39×10^{-2}
6	90	81.4	72.4	8.0	1.0	89	6516	25.86×10^{-2}
7	100	95.2	83.1	11.0	1.1	87	7479	29.68×10^{-2}

^aConversion or yield in mol %; ^bS (selectivity) in percent toward PMPs; ^cTON (turnover number) = [%PMPs × (Oct/Ru)]/100; ^dTOF (turnover frequency) = TON/time in s.

and then to 100 °C (87%). An overall assessment of the results show that at 80 °C the catalyst showed a high selectivity for PMPs with a negligible amount of SMPs and IPs. Although the activity of the precatalyst increased a great deal at 90 and 100 °C, the selectivity for PMPs decreased as a result of the high amount of SMPs and IPs formation. The TOF increased significantly as a result of increasing the temperature. The highest TOF increase was observed upon increasing the temperature from 80 to 90 °C. Generally, precatalyst 7 showed very good activity, selectivity and stability at high temperatures.

The results of the metathesis of 1-octene at temperatures 40–100 °C are presented in Figure 6 and Table 3 for precatalyst 8. A similar overall trend for 8 is observed, i.e., very low reaction rates at temperatures below 60 °C with a rapid increase in reaction rates above 70 °C resulting in 1-octene conversions above ca. 70% after 540 min. Although the formation of PMPs equilibrated quickly at ca. 70% after ca. 150 min at 100 °C and at ca. 65% only after ca. 400 min for 90 °C it did not equilibrate at 80 °C even after 540 min.

The formation of SMPs is very low (below 4%) for 8 in the temperature range 40–80 °C after 540 min, while it is relatively high at 14 and 21% at 90 and 100 °C, respectively. In the same

period the formation of IPs remained below 3% even at the high temperatures. At 100 °C and 540 min, a larger amount of SMPs is formed for precatalyst 8 than that of 7.

Table 3 summarises the overall catalytic performance of precatalyst 8 at 420 min. The PMPs and SMPs formation, TON and TOF all show a direct relationship with temperature. Precatalysts 7 and 8 share similarities in having the same temperature range for the highest PMPs formation, i.e., 70 to 80 °C at 420 min. The biggest difference, however, is observed for 8 (37%). Relatively higher SMPs are formed for 8 (11%, 19%) than that of 7 (8%, 11%) at 90 and 100 °C, respectively. The relatively low PMPs formation of 8 compared to that of 7 is due to the relatively high SMPs and IPs formations with precatalyst 8. The IPs formation in 8 follows a similar pattern to that of 7, i.e., it showed an increase upon increasing the temperature from 40 to 50 °C, followed by a decrease from 50 to 60 °C and then an increase from 60 to 100 °C. The selectivity in 8 increased upon increasing the temperature from 40 to 70 °C, and then showed a decrease from 70 to 100 °C.

A maximum selectivity for 8 is observed at 70 °C (94%) (see Table 3, entry 4) and for that of 7 at 80 °C (97%) (see Table 2, entry 5). Generally, precatalyst 7 showed a better selectivity

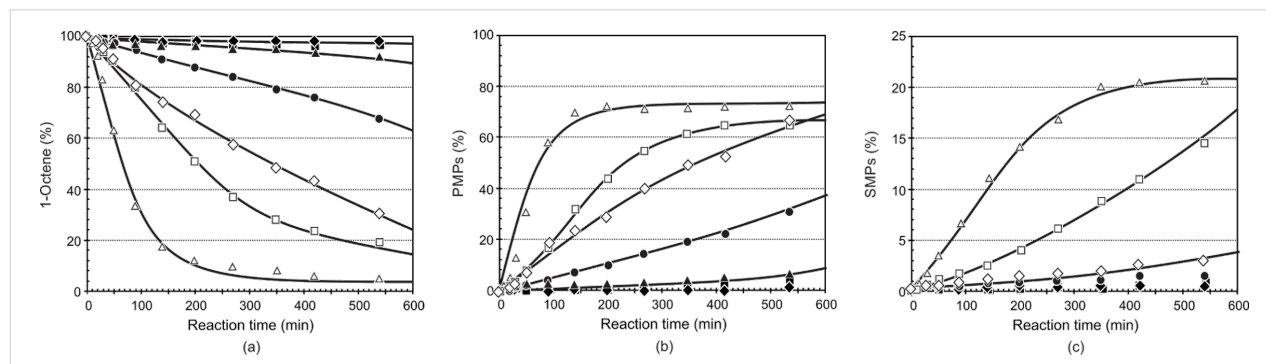


Figure 6: The influence of the reaction temperature on the (a) conversion of 1-octene, (b) formation of PMPs and (c) formation of SMPs using precatalyst 8 (Ru/1-octene = 1:9000). ◆ 40 °C, ■ 50 °C, ▲ 60 °C, ● 70 °C, ◇ 80 °C, □ 90 °C, △ 100 °C].

Table 3: Summary of catalytic performance of precatalyst 8 at different temperatures (Ru/1-octene molar ratio 1:9 000, 420 min).

Entry	Temp. [°C]	Conv. ^a	PMPs ^a	SMPs ^a	IPs ^a	S ^b	TON ^c	TOF ^d
1	40	1.5	0.8	0.3	0.4	56	72	0.28×10^{-2}
2	50	2.9	1.4	0.6	0.9	49	126	0.50×10^{-2}
3	60	5.3	4.5	0.7	0.1	85	405	1.61×10^{-2}
4	70	24.0	22.7	1.1	0.2	94	2043	8.11×10^{-2}
5	80	65.4	60.5	4.1	0.8	92	5445	21.61×10^{-2}
6	90	77.3	65.0	11.0	1.3	84	5850	23.21×10^{-2}
7	100	93.8	73.0	19.0	1.8	78	6570	26.07×10^{-2}

^aConversion or yield in mol %; ^bS (selectivity) in percent toward PMPs; ^cTON (turnover number) = [%PMPs × (Oct/Ru)]/100; ^dTOF (turnover frequency) = TON/time in s.

compared to that of **8** at 420 min. Although the TOF of **8** is in direct relation with temperature, it follows the following order upon comparing with **7**; **8** > **7** at 40 and 50 °C (see Table 2 and Table 3, entries 1–7), at 60 °C **7** > **8** (see Table 2 and Table 3, entry 3), at 70 and 80 °C **8** > **7** (see Table 2 and Table 3, entries 4 and 5) and **7** > **8** at 90 and 100 °C (see Table 2 and Table 3, entries 6 and 7).

Summarising the comparisons of precatalysts **7** and **8**, it is noted that precatalyst **7** showed better activity, selectivity and stability in the 60–100 °C temperature range, except for 80 °C, at 420 min. It also showed higher TOF at 60, 90 and 100 °C at 420 min. According to a DFT study by Getty et al. [19] the more positively charged the Ru, the slower the initiation rate of the catalyst. The calculated Mulliken atomic charge of Ru in **7** (0.934) is less positive than in **8** (0.976).

The results of the metathesis of 1-octene at temperatures of 60 to 110 °C are presented in Figure 7 and Figure 8 for precatalysts **6** and **9**, respectively. Because of their low activity and high stability, the metathesis reactions were done between 60 and 110 °C. Metathesis of 1-octene by the 3-Me-substituted

precatalyst **6** showed an increase in the activity of the precatalyst upon increasing the temperature from 60 to 110 °C. A large increase in the rate of the metathesis reaction is observed upon increasing the temperature from 80 to 90 °C. Although the activity of the precatalyst has shown an increase upon increasing the temperature from 60 to 110 °C, a very high (ca. 45%) increase in the PMPs formation is observed upon increasing the temperature from 80 to 90 °C at 540 min. The PMPs formation did not equilibrate at 90 °C and this shows the stability of precatalyst **6** at high temperatures. The PMPs formation, however, equilibrated from ca. 270 min at 100 °C and ca. 140 min at 110 °C. At 80 °C, the activity of precatalyst **6** (ca. 25%) is very low compared to precatalysts **7** (ca. 50%) and **8** (ca. 70%) during the course of PMPs formation, at 540 min. Generally, in the first 100 to 300 minutes, the rate of formation of PMPs increases dramatically and slows down afterwards in the temperature range of 90 to 110 °C. A similar trend is observed during the course of SMPs formation. Significant amounts (16–36%) of SMPs are formed by **6** for temperatures 90 to 110 °C, while negligible amounts (1.3–3.6%) of SMPs are formed from 60 to 80 °C. Large amounts of SMPs (ca. 36%) and IPs (5%) were formed by **6** at 540 min at 100 °C. A comparison of precata-

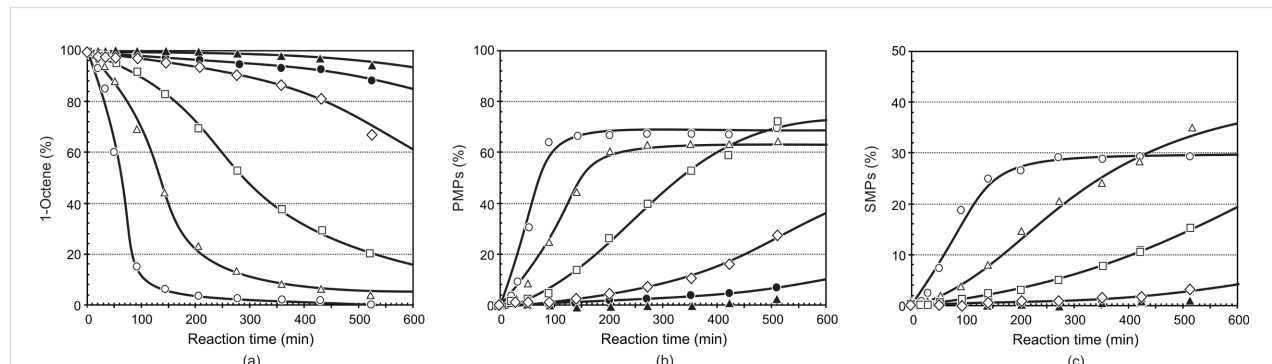


Figure 7: The influence of the reaction temperature on the (a) conversion of 1-octene, (b) formation of PMPs and (c) formation of SMPs using precatalyst **6** (Ru/1-octene = 1:9000). [▲ 60 °C, ● 70 °C, ◊ 80 °C, □ 90 °C, △ 100 °C, ○ 110 °C].

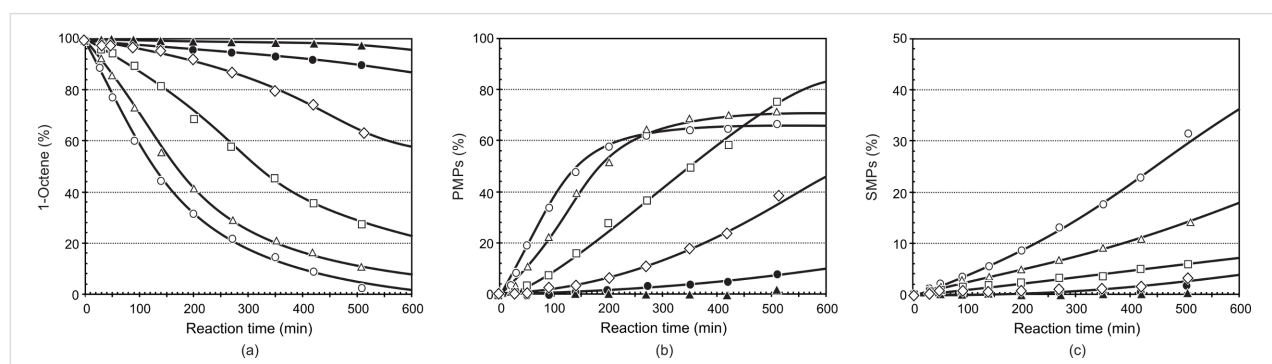


Figure 8: The influence of the reaction temperature on the (a) conversion of 1-octene, (b) formation of PMPs and (c) formation of SMPs using precatalyst **9** (Ru/1-octene = 1:9000). [▲ 60 °C, ● 70 °C, ◊ 80 °C, □ 90 °C, △ 100 °C, ○ 110 °C].

lysts **6**, **7** and **8** with regard to SMPs and IPs formation at 100 °C and 540 min shows a decreasing order of **6** > **8** > **7**. Generally, a relatively large amount of IPs is formed by precatalyst **6**. Although the rate of PMPs formation is slow at 80 °C, high selectivity and stability are attained at this temperature for precatalyst **6**, similar to precatalysts **7** and **8**. The highest difference in the PMPs formation (ca. 45%) is observed between 80 and 90 °C. Although the SMPs formation has shown a direct relationship with temperature, the formation of high SMPs (16–36%) from 90 to 110 °C limited the PMPs formation to only a maximum of ca. 68% at 540 min. The contribution of the IPs formation in limiting the formation of PMPs is not negligible as a result of the relatively high (ca. 3.5%) IPs formation. The SMPs formation increased approximately six-fold upon increasing the temperature from 80 to 90 °C, which was then followed by approximately a two-fold increase upon increasing the temperature from 90 to 100 °C.

Table 4 presents the overall catalytic performance of precatalyst **6** at 420 min. At 420 min, 1-octene conversion is 98.0% (110 °C), 93.0% (100 °C), 70.5% (90 °C), 19.4% (80 °C), 6.8% (70 °C) and 2.5% (60 °C). This shows the dramatic increase of the catalytic activity upon increasing the temperature. An investigation of the PMPs formation reveals a huge 66% increase for the PMPs formation upon increasing the reaction temperature from 60 to 110 °C. The IPs formation, on the other hand, increased two-fold upon increasing the temperature from 60 to 70 °C, 80 to 90 °C and 90 to 100 °C.

The selectivity toward PMPs (67.2%) and the SMPs (28.8%) are relatively high at 110 °C. The TOF is also directly related to the reaction temperature. The TOF of precatalyst **6** are generally lower than for precatalysts **7** and **8**. This, therefore, shows the relatively high stability of precatalyst **6** compared to those of **7** and **8**. As a result of having a more positive Ru charge, precatalyst **6** showed a low initiation rate. This is also in agreement with the DFT study of Getty et al. [19], i.e., precatalyst **6** (0.988) has more positive Mulliken's atomic charge on Ru than

both **7** (0.934) and **8** (0.976). Its high activity at 110 °C with 69% selectivity is, however, remarkable for linear alkene metathesis catalysed by ruthenium alkylidene precatalysts.

The 3-OMe-substituted precatalyst **9** showed a negligible activity for the metathesis of 1-octene at 60 °C (Figure 8), similar to the 3-Me-substituted precatalyst **6**. The overall activity of the precatalyst, however, showed a significant increase upon increasing the temperature from 60 to 110 °C. In a similar way to that of **6**, the largest increase in the activity of the precatalyst is observed upon increasing the temperature from 80 to 90 °C (ca. 38%) at 420 min. The activity of the catalyst showed a small difference between 100 and 110 °C, on the overall metathesis reaction.

During the course of PMPs formation, high catalytic activity for **9** is observed within 200 min at temperatures above 90 °C (ca. 60%), while the activity of the precatalyst showed a dramatic increase from 70 to 90 °C after ca. 500 min, similar to that of **6** (see Figure 7b). For both **6** and **9** the highest PMPs (>60%) is observed from 90 to 110 °C after 420 min. The rate of formation of SMPs is very high for **9** at 110 °C within 420 min. This is the reason for the decrease in the formation of PMPs from 71% at 100 °C to 64.2% at 110 °C.

Table 5 presents the overall catalytic performance of precatalyst **9** at 420 min. Firstly, PMPs formation increased from 0.5 to 71% when increasing the temperature from 60 to 100 °C; however, from 100 to 110 °C the PMPs yield decreased from 71 to 64.2%. The reason for this is the formation of a very large amount of SMPs (23.2%) and IPs (2.6%), which is, more than twice the amount at 100 °C. Similarly, the selectivity and TOF showed a decrease when going from 100 to 110 °C.

The selectivity showed a dramatic (50%) increase upon increasing the temperature from 60 (43%) to 80 °C (93%) and then begins to decrease to 91% (at 90 °C), 85% (at 100 °C) and finally to 71% (at 110 °C). Although the catalyst showed signif-

Table 4: Summary of catalytic performance of precatalyst **6** at different temperatures (Ru/1-octene molar ratio 1:9000, 420 min).

Entry	Temp. [°C]	Conv. ^a	PMPs ^a	SMPs ^a	IPs ^a	S ^b	TON ^c	TOF ^d
1	60	2.5	1.0	0.9	0.6	41	93	0.36×10^{-2}
2	70	6.8	4.5	1.0	1.3	66	406	1.61×10^{-2}
3	80	19.4	16.4	2.3	0.7	85	1479	5.86×10^{-2}
4	90	70.5	59.0	10.3	1.2	83	5310	21.07×10^{-2}
5	100	93.0	61.3	28.5	3.9	66	5514	21.88×10^{-2}
6	110	98.0	67.2	28.8	2.1	69	6051	24.01×10^{-2}

^aConversion or yield in mol %; ^bS (selectivity) in percent toward PMPs; ^cTON (turnover number) = [%PMPs × (Oct/Ru)]/100; ^dTOF (turnover frequency) = TON/time in s.

Table 5: Summary of catalytic performance of precatalyst **9** at different temperatures (Ru/1-octene molar ratio 1:9000, 420 min).

Entry	Temp. [°C]	Conv. ^a	PMPs ^a	SMPs ^a	IPs ^a	S ^b	TON ^c	TOF ^d
1	60	1.1	0.5	0.3	0.3	43	45	0.18×10^{-2}
2	70	7.3	5.3	1.1	0.9	73	477	1.89×10^{-2}
3	80	25.7	24.0	1.4	0.3	93	2160	8.57×10^{-2}
4	90	64.0	58.3	5.1	0.6	91	5247	20.82×10^{-2}
5	100	83.3	71.0	11.1	1.2	85	6390	25.36×10^{-2}
6	110	90.0	64.2	23.2	2.6	71	5778	22.93×10^{-2}

^aConversion or yield in mol %; ^bS (selectivity) in percent toward PMPs; ^cTON (turnover number) = [%PMPs × (Oct/Ru)]/100; ^dTOF (turnover frequency) = TON/time in s.

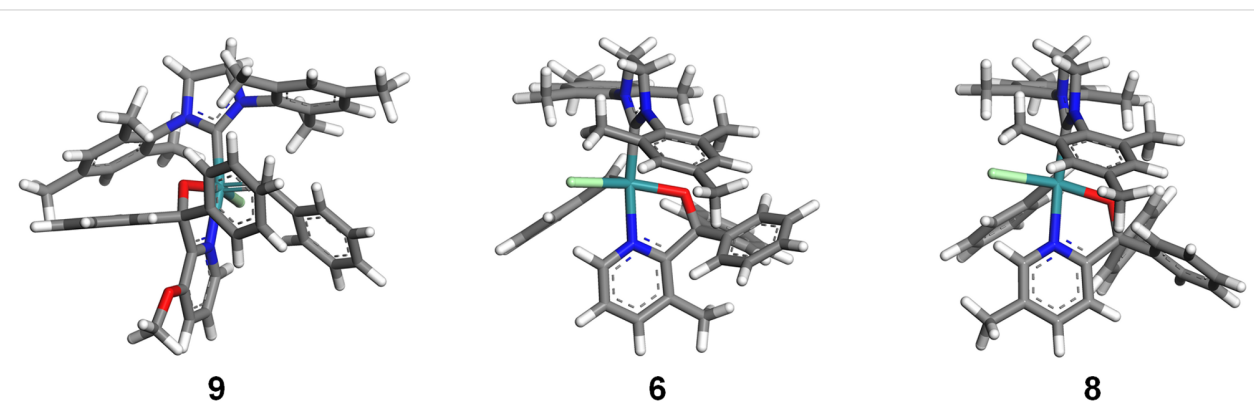
icant stability and very good (71%) selectivity at 110 °C, it is advisable not to go beyond 100 °C, as the formation of SMPs and IPs doubled that will affect the overall PMPs yield. It is also worthwhile to note the decrease in the turnover frequency at 110 °C.

Similar to the Me-substituted precatalysts **6** (85%) (see Table 4, entry 3), **7** (97%) (see Table 2, entry 5) and **8** (92%) (see Table 3, entry 5), precatalyst **9** showed high selectivity (93%) towards PMPs and good stability at 80 °C after 420 min. It is also observed from the results that precatalyst **9** showed relatively high selectivity (91%) for PMPs and good activity, higher than its methyl counterparts **6** (83%) (see Table 4, entry 4), **7** (84%) (see Table 2, entry 6) and **8** (89%) (see Table 3, entry 6), at 90 °C after 420 min.

A general comparison of the overall performance of the precatalysts, in terms of PMPs, SMPs, IPs, selectivity, TON and TOF, exhibits the decreasing order of **7** > **9** > **8** > **6** at 60, 90 and 100 °C. The order, however, changes at 80 °C to **8** > **7** > **9** > **6** and at 70 °C to **7** ≈ **8** > **9** > **6**. In all cases, the small amounts of SMPs and IPs are positive for the application of these systems at higher temperatures. Overall precatalyst **7** performed the best

at all temperatures (except at 80 °C). In an attempt to understand the significance of these results, DFT calculations were performed on the precatalysts.

Precatalyst **6** showed the lowest activity of all precatalysts in the specified temperature ranges. It is also worthwhile to note that increasing the reaction temperature showed a significant increase in the activity of **6**. Precatalyst **9**, on the other hand, showed better performance at high temperatures (≥ 70 °C) compared to **6**. This may be explained by the longer Ru–N bond (2.181 Å) in the geometry-optimised structure (Figure 9) of precatalyst **9** compared to that of the Ru–N bond (2.166 Å) of **6**. A longer bond suggests a weaker Ru–N chelation thus a more active hemilabile complex. The difference in the Ru–N bond length may be attributed to the electron-withdrawing inductive effect of the OMe group making the Ru–N chelation weaker. Furthermore, a type of orbital interaction between the oxygen of the 3-OMe group and the two α -phenyl rings, i.e., an oxygen lone pair-aromatic π interaction illustrated in Figure 10, may add to the inductive effect. The longer Ru–O bond (2.031 Å), shorter C α –O bond (1.420 Å) and C α –C₂ bond (1.541 Å) observed in precatalyst **9** when compared to the corresponding bonds in **6**, i.e., 2.028, 1.425 and 1.544 Å, respectively, supports

**Figure 9:** Geometry-optimised structures of precatalyst **9**, **6** and **8**.

such a premise. It may also be a plausible explanation for the envelope geometry of the five-membered ruthenacycle. In addition, the relatively low ruthenium metal positive charge on **9** would cause it to have a high initiation rate constant [19].

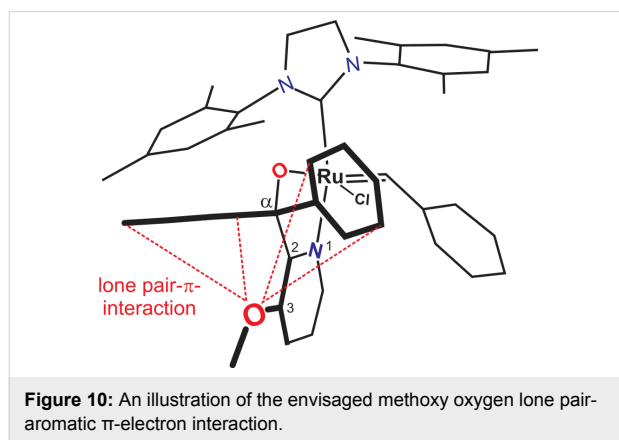


Figure 10: An illustration of the envisaged methoxy oxygen lone pair–aromatic π -electron interaction.

On the other hand, the 3-Me group in **6** will strengthen the Ru–N chelation via inductive electron-donation and steric repulsion between the methyl group and the two phenyl rings. As a result of the steric interaction **6** has a planar five-membered ruthenacycle geometry (Figure 9). In the absence of substituents on the pyridinyl moiety it is expected that the resulting precatalyst will be more active at lower temperatures. This is indeed the case when **5d** is used as catalyst.

As we have discussed earlier, the 4-Me-substituted precatalyst **7** has shown better catalytic performance in all temperatures under investigation except at 80 °C. The reason for this is that the Me group is, relatively speaking, further removed from the pyridine nitrogen so that the inductive electron-donation by the methyl group cannot significantly influence the electron density on the pyridine nitrogen. There is also no steric effect that would interfere with the Ru–N bond strength. The strengthening effect on the Ru–N chelation would, therefore, possibly be low compared to the other precatalysts.

If this is a plausible explanation for the relatively better performance of the 4-Me-substituted precatalyst **7**, one might ask what about the difference between the 3-Me-, **6**, and 5-Me-substituted, **8**, precatalysts that are at the same distance from the pyridine nitrogen? In the optimised structure of **6**, the Me group is in a crowded environment due to its proximity to the two α -phenyl groups, which upon opening the Ru–N chelation, would even become more sterically crowded. This results in a planar geometry of the five-membered ruthenacycle while **8** exhibits an envelope geometry. The Ru–N (2.179 Å) bond length in **8** is longer and the C α –O (1.417 Å) and C α –C₂ (1.532 Å) bonds are shorter than the corresponding bonds in **6**.

In order to overcome the combined effect of the resistance that resulted from the steric crowdedness and the inductive electron-donation by the 3-Me group and open the strong Ru–N chelation, it needs relatively high energy. In **8** the methyl group is in exactly the opposite orientation to the two α -phenyl groups. Therefore, the steric crowdedness that is observed in **6** that will lead to steric resistance to open the Ru–N chelation does not exist. Thus **8** is more susceptible to hemilability than **6** and exhibits higher activity. Therefore, for 4-Me- and 5-Me-substituted precatalysts, only the inductive electron-donation effect of the methyl group is the reason for the increased stability. In the 3-Me- and 3-OMe-substituted precatalysts, however, the steric effect and orbital interactions work towards the stability of the precatalyst in addition to inductive effects.

Stability of precatalysts

In previous studies [11,12,14] we investigated the stability of pyridinyl-alcoholate Grubbs-type precatalysts as seen in the improved catalytic lifetimes of these complexes. Plots of $\ln([\text{starting material}])$ versus time, proposed by Grubbs and co-workers [20], were used as a measure of the stability of the precatalyst, i.e., a linear plot indicates a reaction with pseudo-first order rate kinetics, while a curved plot points towards catalyst decomposition. We used the conversion of 1-octene at a Ru/1-octene molar ratio of 1:9000 and a reaction temperature of 80 °C to compare the stability of **5d** with that of **5i**, **5j** and **5k** [14]. In Figure 11 the literature data (% 1-octene conversion and $\ln(\%)$ 1-octene) of **5d** is compared with that of precatalysts **6–9** at a Ru/1-octene molar ratio of 1:9000 and a reaction temperature of 80 °C over 540 min.

The overall activity order of the catalysts follows the order **5d** > **8** > **9** > **6** up to ca. 540 min. The order **8** > **5d** ≈ **7** > **9** > **6** is observed for both the overall metathesis and the PMPs formation. All the precatalysts exhibits first-order kinetics over the first ca 540 min when the $\ln(\%)$ 1-octene plots (Figure 11b) are considered. The substituted precatalysts show better stability than **5d**, thus longer lifetimes, with **6** and **9** the slowest and **8** close to but slower than **5d**.

It is interesting to note that the stability of **5j** and **5k** correlates very well with that of **7**, while **5i** is more stable than **7** but less than **9** (comparison of current results with results in [14]). This clearly indicates that a substituent on one of the α -phenyl groups or the pyridinyl moiety has a stabilising effect on the corresponding precatalyst with a substituent on the 3-position (**6** and **9**) of the pyridinyl rendering the precatalyst the most stable. The latter two is also active at higher temperatures.

Table 6 presents the overall catalytic performance of precatalysts **5d**, and **6–9** at a Ru/1-octene molar ratio of 1:9000, 80 °C

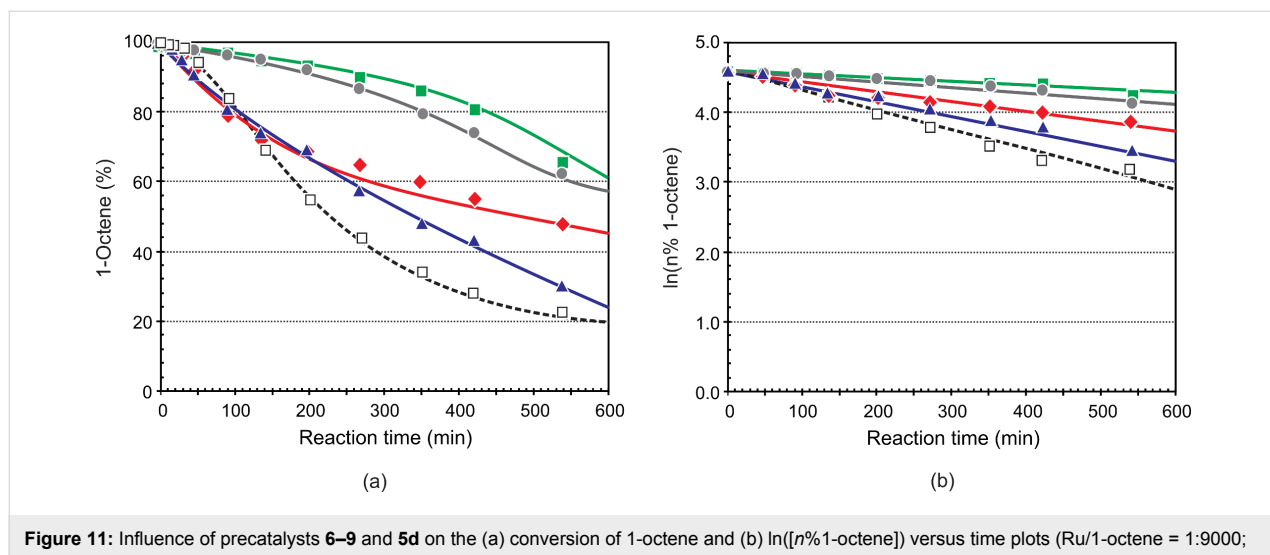


Figure 11: Influence of precatalysts **6**–**9** and **5d** on the (a) conversion of 1-octene and (b) $\ln([n\% \text{1-octene}])$ versus time plots (Ru/1-octene = 1:9000; 80 °C). [■ **6**, ◆ **7**, ▲ **8**, ● **9**, □ **5d**]

Table 6: Summary of catalytic performances of different precatalyst (Ru/1-octene molar ratio 1:9000, 80 °C, 420 min).

Entry	Precat.	Conv. ^a	PMPs ^a	SMPs ^a	IPs ^a	S ^b	TON ^c	TOF ^d
1	5d^e	71.2	68.0	3.0	0.3	96	6120	24.29×10^{-2}
2	8	65.4	60.5	4.1	0.8	92	5445	21.61×10^{-2}
3	7	44.4	43.1	1.1	0.2	97	3879	15.39×10^{-2}
4	9	25.7	24.0	1.4	0.3	93	2160	8.57×10^{-2}
5	6	19.4	16.4	2.3	0.7	85	1476	5.86×10^{-2}

^aConversion or yield in mol %; ^bS (selectivity) in percent toward PMPs; ^cTON (turnover number) = [%PMPs × (Oct/Ru)]/100; ^dTOF (turnover frequency) = TON/time in s; ^eSee reference [14].

and 420 min. According to these results precatalyst **5d** shows the highest PMPs, TON and TOF. Although it has relatively high SMPs compared to most of the precatalysts, its overall performance prevails over the other precatalysts. The second best performance was observed for **8**, as it resulted in relatively high PMPs, TON and TOF compared to the rest of the precatalysts, although its SMPs ranks as first. The rest of the precatalysts can be ranked in a decreasing order of activity of **7 > 9 > 6**. It is clear from the data in Table 6 that the unsubstituted precatalyst **5d** is more active compared to the substituted precatalysts at 420 min. This will only be due to the substituent effect on the activity of the precatalyst.

Effect of catalyst concentration

Earlier studies indicated that 80 °C is the optimum temperature for **5d** [10,11]. It was therefore decided to investigate the effect of the concentration of the precatalyst on the metathesis of 1-octene at 80 °C. Precatalyst **8** was chosen for this investigation at Ru/1-octene molar ratios of 1:6000, 1:9000, 1:10000 and 1:15000.

Table 7 presents the overall catalytic performance of precatalyst **8** at different Ru/1-octene molar ratios, 80 °C and 420 min. With a decrease in precatalyst concentration a direct relationship was observed with the conversion of 1-octene and PMPs,

Table 7: Summary of the catalytic performance of precatalyst **8** present in different concentrations (80 °C, 420 min).

Entry	C ₈ :Ru	Conv. ^a	PMPs ^a	SMPs ^a	IPs ^a	S ^b	TON ^c	TOF ^d
1	6000	76.9	70.7	5.9	0.4	92	4240	16.83×10^{-2}
2	9000	65.4	60.5	4.1	0.8	92	5445	21.61×10^{-2}
3	10000	60.2	55.4	4.5	0.4	92	5539	21.98×10^{-2}
4	15000	52.8	48.4	3.8	0.7	92	7254	28.78×10^{-2}

^aConversion or yield in mol %; ^bS (selectivity) in percent toward PMPs; ^cTON (turnover number) = [%PMPs × (Oct/Ru)]/100; ^dTOF (turnover frequency) = TON/time in s.

they all decreased, while the TON and TOF increased. The SMPs and IPs did not follow a specific trend while the selectivity remained the same, i.e., 92%, at all the concentrations.

¹H NMR investigation of precatalyst 7 and 5d

Proton nuclear magnetic resonance spectrometry (¹H NMR) is a powerful tool to study ruthenium alkylidene complexes and was used to study 1-octene metathesis in the presence of **1** and **2** [10,21,22]. The conversion of the benzylidene, $[\text{Ru}]=\text{CHPh}$, to the heptylidene, $[\text{Ru}]=\text{CHC}_6\text{H}_{13}$, and methylidene, $[\text{Ru}]=\text{CH}_2$, (where $[\text{Ru}] = \text{RuL}_2\text{Cl}_2$) could be clearly distinguished using the carbene- H_α signals; they appeared as a singlet, triplet and singlet in the δ 18.5–20.2 ppm region, respectively. We also investigated **5a** and observed five carbene- H_α signals attributing three to the alkylidene species when the pyridinyl-alcoholato ligand was in the “closed” (coordinated) position; δ_{CHPh} 18.05 ppm, δ_{CHHx} 16.71 ppm and δ_{CHH} 16.08 ppm [10]. The other two was attributed to the benzylidene (δ_{CHPh} 19.48 ppm) and methylidene (δ_{CHH} 19.76 ppm) species in the “open” (uncoordinated) position with the uncoordinated heptylidene signal not appearing probably due to the fast reaction of this species. Four signals at δ 9.48 ppm (for the coordinated ligand), 9.05 ppm, 9.22 ppm, and 9.71 ppm attributed to the H_α signals

of the pyridine ring were also observed. The latter three signals overlapped too much to be useful.

We performed a ¹H NMR investigation of the metathesis of 1-octene by precatalyst **7** in the temperature region 60–90 °C in order to gain some insight into the reaction mechanism. The carbene- H_α ¹H NMR signals at 90 °C over a period of 345 min are presented in Figure 12. Three signals attributed to the benzylidene (δ 17.33 ppm, singlet), heptylidene (δ 16.85 ppm, triplet) and methylidene (δ 15.68 ppm) were observed. A small signal at δ 16.66 ppm appeared at 270 min and was not assigned (inter alia multiplicity not discernable). A different development of carbene signals over time is observed than what was reported before for **5a** [10], i.e., the methylidene signal starts to appear at 12 min while the heptylidene signal only starts to appear at 165 min. The benzylidene signal rapidly declines after 194 min and is not observed at 345 min. No clear indication of an “open” or “closed” complex was observed, so it assumed that the signals represent the “closed” species. It can be concluded that the alkylidene species of the pyridinyl-alcoholato Grubbs 2-type precatalysts are quite stable at high temperatures explaining the activity of these precatalyst at high temperatures and the slow rate of disappearance/formation of these signals confirms the longer lifetimes observed in the catalytic reactions.

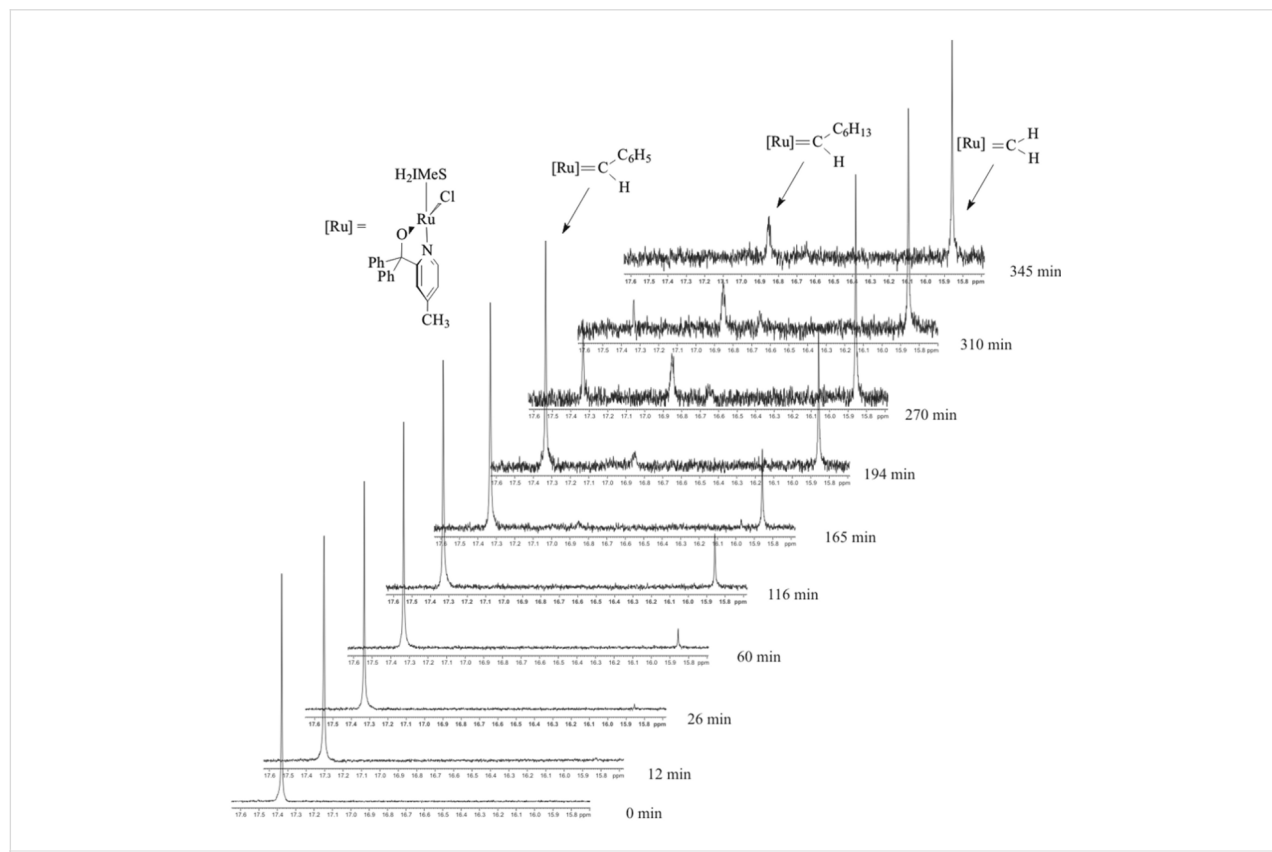


Figure 12: ¹H NMR spectra of the carbene- H_α region at different time intervals of the 1-octene/7 reaction mixture in toluene- d_8 at 90 °C.

The H_α pyridine ring ^1H NMR signals at 90 °C at 345 min are presented in Figure 13. Five H_α signals of the pyridine ring that are not observed at the beginning of the reaction were observed at δ 9.57 ppm (doublet), δ 9.22 ppm (doublet), δ 9.08 ppm (unknown multiplicity), δ 8.91 ppm (doublet) and δ 8.85 ppm (doublet). The signal at δ 9.70 ppm (singlet) was the only signal observed at the beginning of the reaction. These signals are probably due to the “open” and “closed” pyridinyl-alcoholato ligands of alkylidene species and a possible assignment is shown in Figure 13. Further research is required to gain a comprehensive understanding of the operation of the active species of the pyridinyl-alcoholato ruthenium alkylidene precatalysts.

Effect of solvent on 1-octene metathesis using precatalyst 7

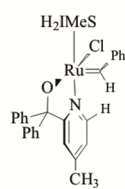
Because toluene- d_8 was used in the ^1H NMR study it was decided to investigate if toluene as solvent has any effect on the 1-octene metathesis reaction using precatalyst 7. Results of this investigation are presented in Table 8.

An increase in SMPs formation is the only difference that was observed when toluene was used as solvent with an 8.9% in-

crease at 420 min. This affected the other performance indicators, i.e., PMPs, S, TON and TOF; lower values than the neat reactions were obtained. The results suggest that no significant solvent effect appears to exist. However, the increase in SMPs (associated with an increase in IPs) indicates decomposition of the precatalyst to active isomerisation species, probably metal hydride species. In our NMR study no indication of the existence of metal hydride species was found.

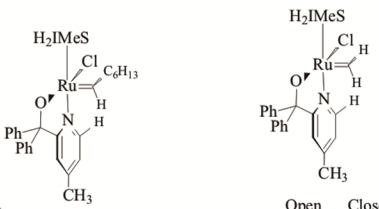
Conclusion

The aim of our research is to control the Ru–N bond strength of the bidentate hemilabile pyridinyl-alcoholato ligands in precatalyst **5d** in an attempt to synthesise a precatalyst with high performance for linear alkene metathesis at high temperatures. To reach this aim, we synthesised ruthenium alkylidene precatalysts by substituting one of the hydrogens of the pyridine ring of the bidentate pyridinyl-alcoholato ligand by Me and OMe groups. We synthesised the 3-, 4-, and 5-methyl and 3-methoxy-substituted **5d** precatalysts. The catalytic activity, selectivity and stability results of the Me- and OMe-substituted **5d** precatalysts, in 1-octene metathesis, showed promising results at high temperatures. The high stability, very good activity, selectivity, TON and TOF of the four precatalysts, at high temperatures,



Open

Close



Open

Close

Figure 13: ^1H NMR spectra of the H_α region of the pyridine ring of the 1-octene/7 reaction mixture in toluene- d_8 at 90 °C at 345 min.

Table 8: Summary of the catalytic performance of precatalyst 7 present in the presence of toluene as solvent (Ru/1-octene = 1:9000, 90 °C, 420 min).

Entry	Solvent	Conv. ^a	PMPs ^a	SMPs ^a	IPs ^a	S ^b	TON ^c	TOF ^d
1	neat	81.4	72.4	8.0	1.0	89	6516	25.86×10^{-2}
2	toluene ^e	79.8	61.8	16.9	1.2	77	5564	22.08×10^{-2}

^aConversion or yield in mol %; ^bS (selectivity) in percent toward PMPs; ^cTON (turnover number) = [%PMPs × (Oct/Ru)]/100; ^dTOF (turnover frequency) = TON/time in s; ^e $V_{\text{toluene}} = 4 \text{ mL}$.

proved that the hemilability of the bidentate hemilabile pyridinyl alcoholato ligand can be influenced by monosubstitution on the pyridinyl moiety. A Ru/1-octene precatalyst concentration of 1:9000 and 80 °C were found to be the best reaction conditions for the precatalysts. Although **8** performed better than the rest of the precatalysts at 80 °C, **7** showed the best performance in the other temperatures under investigation. ¹H NMR spectrometry was used to investigate precatalyst **7** and the active alkylidene species, i.e., benzylidene, heptylidene and methylidene, were observed. NMR evidence of the hemilabile nature of these precatalysts was found in the H_α region of the pyridine ring of the pyridinyl alcoholato ligand.

Experimental

Instruments and reagents

¹H NMR (600 MHz) spectra were obtained using a Bruker Ultrashield Plus 600 Avance III spectrometer.

GC/FID: The progress of the metathesis reactions was followed on an Agilent 6890 gas chromatograph equipped with an Agilent 7683 auto sampler, HP-5 5% phenyl methyl siloxane capillary column and a flame ionisation detector (FID). The following general GC settings were used: Column: HP-5, 30.0 m × 320 μm × 0.25 μm, nominal; detector: FID at 250 °C; H₂ flow rate: 40 mL/min at 20 °C; air flow rate: 450 mL/min at 20 °C; inlet temperature: 200 °C, 60.6 kPa; N₂ carrier gas flow rate: 45 mL/min at 20 °C; injection volume: 2 μL (auto injection); syringe size 10.0 μL; split ratio: 50.4:1; split flow 94.3 mL/min; oven programming: 60 °C for 5 min; 60 to 110 °C at 25 °C/min; 110 °C hold for 10 min; 110 to 290 °C at 25 °C/min; 290 to 300 °C at 25 °C for 5 min.

GC/MSD analyses was performed on an Agilent 6890 gas chromatograph equipped with an Agilent 7683B autosampler, HP-5 capillary column and an Agilent 5973 mass selective detector (MSD). The oven programme was used with either a two-minute solvent delay or no solvent delay. Helium was used as carrier gas with a 1.5 mL/min flow rate at 20 °C. The following general GC settings were used: Column: HP-5, 30.0 m × 320 μm × 0.25 μm; Split ratio: 0.1:1; Split flow: 0.1 mL/min; Inlet: 250 °C, 16.6 kPa; Injection volume: 0.2 μL; Detector: 50–550 Dalton mass range; scan speed of 2.94 seconds per decade; oven programming: 60 °C (hold time 2 min); 60 to 110 °C at 25 °C/min; 110 °C (hold time 10 min); 110 to 290 °C at 25 °C/min (hold time 16 min).

Reagents: 2-Bromo-3-methylpyridine (95%), 2-bromo-4-methylpyridine (97%), 2-bromo-5-methylpyridine (98%), 2-bromo-3-methoxypyridine (97%), *n*-BuLi (2.5 M in hexane), benzophenone (99%), 2-*N,N*-dimethylaminoethanol (≥ 99.5%), Grubbs 2 (**2**) (97%), 1-octene (99% GC), nonane (reagent plus

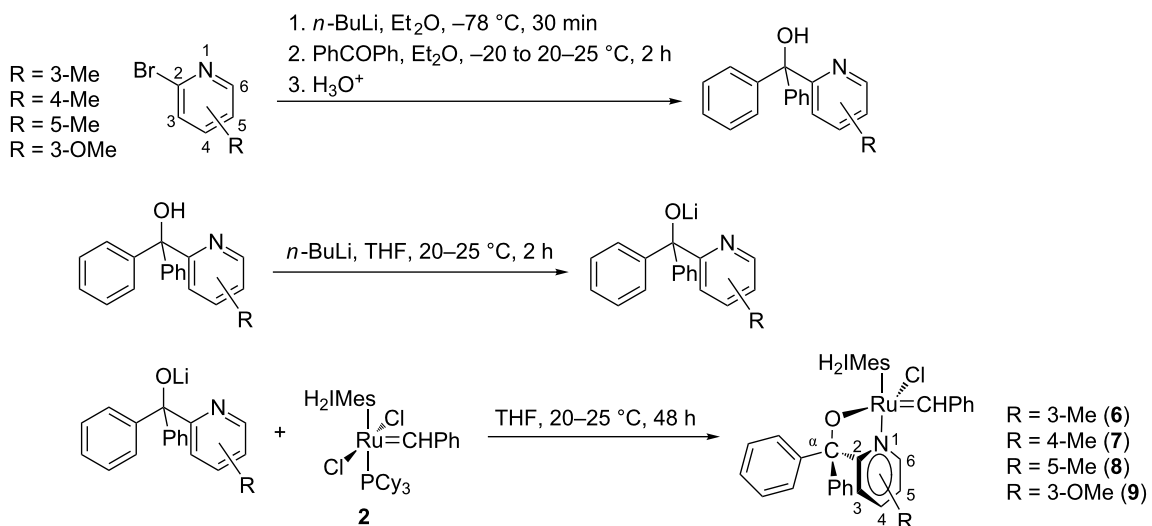
99%) and toluene (99%) were purchased from Sigma-Aldrich. Toluene-*d*₈ (99.5%) was purchased from MERCK and *tert*-butyl hydrogen peroxide (80%) from Riedel-de Haen. Diethyl ether and THF were dried over Na in the presence of benzophenone. Pentane was distilled over CaH₂ in an inert atmosphere before using as solvent. 2-*N,N*-Dimethylaminoethanol and *n*-hexane were dried over molecular sieves (4 Å) and kept under nitrogen before use. Gas-tight Hamilton syringes were used to add reagents and dried solvents to the reactor. Acrodisc Premium 25 mm syringe filter with GxF/0.45 μm GHP membrane (PALL) was used to filter the lithium salt from the precatalyst.

Experimental procedures

Precatalyst synthesis: The well-established methods of Herrmann et al. [23] and Van Der Schaaf et al. [7] were used to synthesize precatalysts **6–9**. This is illustrated in Scheme 2.

Benzylidene chloro(1,3-bis(2,4,6-trimethylphenyl)-2-imidazolidinylidene)[1-(3'-methyl-2'-pyridinyl)-1,1-diphenylmethanolato]ruthenium (6): Yield 0.422 g, 89%, green powder, decomp.: 190 °C, ¹H NMR (600 MHz, CDCl₃) δ 16.89 (s, 1H, H of Ru=CHPh), 9.70 (t, *J* = 3.8 Hz, 1H, H-6 of C₅H₃N), 7.24 (m, 1H, *para* H of Ru=CHPh), 7.24 (m, 2H, *meta* H of Ru=CHPh), 7.15 (m, 2H, *ortho* H of Ph), 7.05/7.28 (m, 4H, *meta* H of mesityl), 7.00 (m, 1H, H-4 of C₅H₃N), 6.90 (s, 2H, *para* H of Ph), 6.97 (d, *J* = 3.7 Hz, 2H, *ortho* H of Ru=CHPh), 6.49 (s, 1H, H-5 of C₅H₃N), 6.75 (s, 2H, *meta* H of Ph), 4.01–3.87 (m, 4H, H of NHC), 2.56/2.18/2.11 (3 × s, 3 × 6H, H of 6-CH₃ on mesityl), 1.18 (s, 3H, H of CH₃ on C₅H₃N); MALDI-MS (*m/z*): [M]⁺ 807.2646 (C₄₇H₄₈ClN₃ORu); IR (in cm^{−1}): *v*(OH, moisture) = 3386, *v*(=C-H) = 3054, 3018, 776, *v*(CH₃) = 2921, 2852, 1396, *v*(C=N) = 1604, *v*(C=C) = 1584–1443, *v*(C-N) = 1254, *v*(C-O) = 1157; ¹³C NMR (150 MHz) δ 290.4, 214.5, 169.9, 151.2, 148.4, 144.6, 144.4, 139.2, 137.8, 132.4, 128.8, 128.7, 126.8, 126.7, 121.3, 93.7, 51.2, 21.0, 19.1, 18.8.

Benzylidene chloro(1,3-bis(2,4,6-trimethylphenyl)-2-imidazolidinylidene)[1-(4'-methyl-2'-pyridinyl)-1,1-diphenylmethanolato]ruthenium (7): Yield 0.456 g, 96%, green powder, decomp.: 190 °C, ¹H NMR (600 MHz, CDCl₃) δ 17.09 (s, 1H, H of Ru=CHPh), 9.42 (d, *J* = 5.9 Hz, 1H, H-6 of C₅H₃N), 7.27 (m, 1H, H-3 of C₅H₃N), 7.27 (m, 2H, *para* H of Ru=CHPh), 7.24 (s, 2H, *meta* H of Ru=CHPh), 7.24/7.04 (m, 4H, *meta* H of mesityl), 7.10 (m, 4H, *ortho* H of Ph), 6.96 (t, *J* = 7.6 Hz, 2H, *para* H of Ph), 6.92 (s, 2H, *ortho* H of Ru=CHPh), 6.76 (s, 1H, H-5 of C₅H₃N), 6.63 (s, 4H, *meta* H of Ph), 4.04–3.90 (m, 4H, H of NHC), 2.60/2.25/2.19 (3 × s, 3 × 6H, H of 6-CH₃ on mesityl), 1.99 (s, 3H, H of CH₃ on C₅H₃N); IR (in cm^{−1}): *v*(OH, moisture) = 3393, *v*(=C-H) =



Scheme 2: Synthesis of pyridinyl-alcohol ligands and Grubbs 2-type pyridinyl-alcoholato complexes.

3052, 3018, 755, $\nu(\text{CH}_3) = 2919$, 2850, 1290, $\nu(\text{C}=\text{N}) = 1611$, $\nu(\text{C}=\text{C}) = 1448$ –1443, $\nu(\text{C}-\text{N}) = 1258$, $\nu(\text{C}-\text{O}) = 1248$; ^{13}C NMR (150 MHz, CDCl_3) δ 291.7, 214.7, 170.6, 151.5, 149.8, 146.2, 143.8, 139.2, 137.8, 136.7, 129.0, 128.5, 126.8, 126.6, 122.3, 93.0, 51.3, 21.0, 19.1, 18.8.

Benzylidene chloro(1,3-bis(2,4,6-trimethylphenyl)-2-imidazolidinylidene)-[1-(5'-methyl-2'-pyridinyl)-1,1-diphenylmethanolato]ruthenium (8): Yield 0.304 g, 64%, dark-green crystalline powder, decomp.: 125 °C, ^1H NMR (600 MHz, CDCl_3) δ 17.07 (s, 1H, H of Ru=CHPh), 9.37 (s, 1H, H-6 of $\text{C}_5\text{H}_3\text{N}$), 7.26 (m, 1H, *para* H of Ru-CHPh), 7.24 (s, 4H, *meta* H of mesityl), 7.14 (m, 1H, H-3 of $\text{C}_5\text{H}_3\text{N}$), 7.10–7.02 (m, 4H, *ortho* H of Ph), 6.97 (t, $J = 7.5$ Hz, 2H, *meta* H of Ru=CHPh), 6.92 (s, 2H, *ortho* H of Ru=CHPh), 6.92 (s, 1H, H-4 of $\text{C}_5\text{H}_3\text{N}$), 6.75 (t, $J = 7.6$ Hz, 2H, *para* H of 2Ph), 6.68/6.58 (2d, $J = 7.3$ Hz, 4H, *meta* H of 2Ph), 4.00–3.95 (m, 4H, H of NHC), 2.60/2.26/2.19 (3 × s, 3 × 6H, 6-CH₃ of mesityl), 2.17 (s, 3H, H of CH₃ on $\text{C}_5\text{H}_3\text{N}$); MALDI-MS (m/z): [M]⁺ 807.2660 ($\text{C}_{47}\text{H}_{48}\text{ClN}_3\text{ORu}$); IR (in cm^{-1}): $\nu(\text{OH, moisture}) = 3391$, $\nu(\text{C}=\text{H}) = 3055$, 3020, 755, $\nu(\text{CH}_3) = 2920$, 2849, 1377, $\nu(\text{C}=\text{N}) = 1605$, $\nu(\text{C}=\text{C}) = 1481$ –1410, $\nu(\text{C}-\text{N}) = 1261$, $\nu(\text{C}-\text{O}) = 1163$; ^{13}C NMR (150 MHz, CDCl_3) δ 291.2, 214.5, 168.2, 151.6, 149.9, 146.3, 143.9, 139.2, 137.3, 134.9, 129.0, 128.5, 126.8, 126.5, 121.7, 92.9, 51.3, 20.9, 19.1, 18.8.

Benzylidene chloro(1,3-bis(2,4,6-trimethylphenyl)-2-imidazolidinylidene)-[1-(3'-methoxy-2'-pyridinyl)-1,1-diphenylmethanolato]ruthenium (9): Yield 0.465 g, 96%, green powder, decomp.: 197 °C, ^1H NMR (600 MHz, CDCl_3) δ 16.97 (s, 1H, H of Ru=CH), 9.38 (d, $J = 5.5$ Hz, 1H, H-6 of

$\text{C}_5\text{H}_3\text{N}$), 7.30 (m, 1H, *para* H of Ru=CHPh), 7.29 (m, 2H, *meta* H of Ru=CHPh), 7.25 (m, 4H, *ortho* H of 2Ph), 7.16 (m, 1H, H-4 of $\text{C}_5\text{H}_3\text{N}$), 6.91/6.54 (s, 4H, *meta* H of mesityl), 7.04 (m, 1H, H-4 of $\text{C}_5\text{H}_3\text{N}$), 6.99 (m, 2H, *para* H of 2Ph), 6.99 (m, 1H, H-5 of $\text{C}_5\text{H}_3\text{N}$), 6.73 (m, 4H, *meta* H of 2Ph), 6.73 (m, 2H, *para* H of 2Ph), 6.43 (d, $J = 7.7$ Hz, *ortho* H of Ru=CHPh), 4.01–3.89 (m, 4H, H of NHC), 2.57/2.19/2.16 (3 × s, 3 × 6H, 6-CH₃ of mesityl), 2.90 (s, 3H, H of OCH₃); MALDI-MS (m/z): [M]⁺ 823.2417 ($\text{C}_{47}\text{H}_{48}\text{ClN}_3\text{O}_2\text{Ru}$); IR (in cm^{-1}): $\nu(\text{OH, moisture}) = 3388$, $\nu(\text{C}=\text{H}) = 3054$, 3015, 755, $\nu(\text{CH}_3) = 2920$, 2848, 1316, $\nu(\text{C}=\text{N}) = 1601$, $\nu(\text{C}=\text{C}) = 1586$ –1457, $\nu(\text{C}-\text{N}) = 1258$, $\nu(\text{C}-\text{O}) = 1230$; ^{13}C NMR (150 MHz, CDCl_3) δ 290.5, 214.5, 162.9, 151.5, 151.4, 149.1, 142.3, 139.2, 137.3, 137.2, 129.0, 128.6, 126.8, 122.1, 93.6, 55.4, 51.3, 20.9, 19.1, 18.8.

Metathesis reactions: The metathesis reactions were carried out in 5 mL small-scale glass reactors. The reactor containing a small magnetic bar was flushed with nitrogen and an appropriate amount of precatalyst added by weighing. Once again, the contents of the reactor were carefully flushed with nitrogen and the reactor was sealed. The sealed reactor was placed in an aluminium block on a magnetic stirrer. The temperature was set to the desired temperature and allowed to stabilise prior to the reactor being placed in the block. The temperature was regulated throughout the reaction using a temperature controller fitted with a thermocouple. After one minute of heating nonane (0.25 mL) was added via gastight syringe (1 mL) as an internal standard, followed by the addition of 1-octene (5 mL) via gastight syringe (5 mL). Samples (0.1 mL) were withdrawn at time intervals for ca. 520 min with a gastight syringe (1 mL), transferred to a GC vial (1 mL), quenched with toluene

(0.3 mL) and *tert*-butyl hydrogen peroxide (2 drops), and then injected into a GC/FID by auto sampler. The metathesis reaction was terminated after 1440 minutes and analysed by GC/FID. Some samples were also analysed by GC/MSD. Each experiment was repeated at least three times.

¹H NMR investigation of metathesis reaction: An NMR tube was placed in a Schlenk tube, evacuated with a vacuum pump and then flushed with a stream of argon. The same procedure was repeated and then 12 mg (0.015 mmol) of precatalyst 7 was added to the NMR tube. Once again, the contents of the NMR tube were flushed with argon and toluene-*d*₃ (0.65 mL) added. The catalyst was dissolved by shaking the contents and 1-octene (0.1 mL, 0.64 mmol) added immediately before putting the tube in the spectrometer for temperature ranges 30–50 °C. ¹H NMR spectra were recorded at 5–6 minute intervals for 5–8.5 h. For temperature ranges 60–90 °C, ¹H NMR of the precatalyst was done alone before adding the 1-octene. The precatalyst (11.5 mg, 0.014 mmol) and anthracene (5.2 mg, 0.03 mmol) were mixed in the metathesis reaction where anthracene was used as an internal standard.

Computational details

Geometry optimisation: Geometry optimisation of the precatalysts was done using the DFT module DMol³ of Materials Studio 6.1. The generalized gradient approximation (GGA) with a double numerical basis set and a p-function (DNP) was used. The exchange correlation functional PW91 was investigated. All electrons were treated explicitly and the net charge of all the structures was set to zero. Energies were calculated with frequencies using coarse-grained parallelisation in order to avoid optimised structures with negative frequencies.

Atomic charge calculation: Total electron density was calculated with fine grid resolution, 0.15 Å grid interval and 3.0 Å border. Mulliken atomic charges of Ru were calculated from population analysis and total electron density.

Ru-atom bond length measurement: All bond lengths were measured from the optimised complexes with α,α -diphenyl-(monosubstituted-pyridin-2-yl)alcoholato ligands.

Hardware: 1. Personal computer (HP); (Windows 7 Enterprise © 2009 Microsoft Service Pack 1, Intel® Core™ i5-2450M CPU @ 2.50 GHz, 2.50 GHz; 64-bit operating system).

2. HPC: 336 CPU Cluster with 1 × Master Node: (HP BL460C G6 - 2 Quad Core 2.93 GHz, 16 GB RAM, 2 146 GB HDD), 40 × Compute Nodes: (HP BL460C G6 - 2 Quad Core 2.93 GHz, 16 GB RAM, 2 146 GB HDD, ProLiant BL2 x 220 G5, HP BL460C G1), 1 × 3 TB HP EVA 4400 SAN and 1x HP

BL460C G6 Storage Server, Operating system on compute nodes: Scientific Linux SL release 5.3, Cluster operating system: Rocks 5.2 - Scientific Linux SL release 5.3.

Acknowledgements

The financial support of the North-West University (NWU) and the South African Department of Science and Technology (DST)-National Research Foundation (NRF) Centre of Excellence in Catalysis (c*change) towards this research is hereby gratefully acknowledged. Opinions expressed and conclusions arrived at, are those of the authors and are not necessarily to be attributed to the NWU or c*change.

ORCID® IDs

Tegene T. Tole - <https://orcid.org/0000-0002-5858-9239>
Johan H. L. Jordaan - <https://orcid.org/0000-0002-8134-6753>
Hermanus C. M. Vosloo - <https://orcid.org/0000-0002-5879-323X>

References

1. Grubbs, R. H.; Wenzel, A. G.; O'Leary, D. J.; Khosravi, E., Eds. *Handbook of Metathesis*, 2nd ed.; Wiley-VCH Verlag GmbH: Weinheim, Germany, 2015. doi:10.1002/9783527674107
2. Grela, K., Ed. *Olefin Metathesis: Theory and Practice*; Wiley-VCH: Weinheim, Germany, 2014. doi:10.1002/9781118711613
3. Slugovc, C.; Burtscher, D.; Stelzer, F.; Mereiter, K. *Organometallics* **2005**, 24, 2255–2258. doi:10.1021/om050141f
4. Monsaert, S.; Vila, A. L.; Drozdak, R.; Van Der Voort, P.; Verpoort, F. *Chem. Soc. Rev.* **2009**, 38, 3360–3372. doi:10.1039/b902345n
5. Tole, T.; Jordaan, J.; Vosloo, H. *Molecules* **2018**, 23, 896. doi:10.3390/molecules23040896
6. van der Schaaf, P. A.; Abbenhuis, R. A. T. M.; Grove, D. M.; Smeets, W. J. J.; Spek, A. L.; van Koten, G. *J. Chem. Soc., Chem. Commun.* **1993**, 504–506. doi:10.1039/c39930000504
7. Van Der Schaaf, P. A.; Mühlbach, A.; Hafner, A.; Kolly, R. Heterocyclig ligand containing ruthenium and osmium catalysts. U.S. Patent 6,417,363 B1, July 9, 2002.
8. Wijkens, P.; Jastrzebski, J. T. B. H.; van der Schaaf, P. A.; Kolly, R.; Hafner, A.; van Koten, G. *Org. Lett.* **2000**, 2, 1621–1624. doi:10.1021/o10059100
9. Denk, K.; Fridgen, J.; Herrmann, W. A. *Adv. Synth. Catal.* **2002**, 344, 666–670. doi:10.1002/1615-4169(200208)344:6/7<666::aid-adsc666>3.0.co;2-0
10. Jordaan, M.; Vosloo, H. C. M. *Adv. Synth. Catal.* **2007**, 349, 184–192. doi:10.1002/adsc.200600474
11. van der Gryp, P.; Barnard, A.; Cronje, J.-P.; de Vlieger, D.; Marx, S.; Vosloo, H. C. M. *J. Membr. Sci.* **2010**, 353, 70–77. doi:10.1016/j.memsci.2010.02.032
12. du Toit, J. I.; Jordaan, M.; Huijsmans, C. A. A.; Jordaan, J. H. L.; van Sittert, C. G. C. E.; Vosloo, H. C. M. *Molecules* **2014**, 19, 5522–5537. doi:10.3390/molecules19055522
13. du Toit, J. I.; van der Gryp, P.; Loock, M. M.; Tole, T. T.; Marx, S.; Jordaan, J. H. L.; Vosloo, H. C. M. *Catal. Today* **2016**, 275, 191–200. doi:10.1016/j.cattod.2015.12.004
14. Tole, T. T.; du Toit, J. I.; van Sittert, C. G. C. E.; Jordaan, J. H. L.; Vosloo, H. C. M. *Catalysts* **2017**, 7, 22. doi:10.3390/catal7010022

15. Slugovc, C.; Wappel, J. Olefin Metathesis. WIPO/PCT Patent WO2013/029079 A1, March 7, 2013.
16. Schachner, J. A.; Cabrera, J.; Padilla, R.; Fischer, C.; van der Schaaf, P. A.; Pretot, R.; Rominger, F.; Limbach, M. *ACS Catal.* **2011**, *1*, 872–876. doi:10.1021/cs2002109
17. Cabrera, J.; Padilla, R.; Bru, M.; Lindner, R.; Kageyama, T.; Wilckens, K.; Balof, S. L.; Schanz, H.-J.; Dehn, R.; Teles, J. H.; Deuerlein, S.; Müller, K.; Rominger, F.; Limbach, M. *Chem. – Eur. J.* **2012**, *18*, 14717–14724. doi:10.1002/chem.201202248
18. Cabrera, J.; Padilla, R.; Dehn, R.; Deuerlein, S.; Gulajski, Ł.; Chomiszcza, E.; Teles, J. H.; Limbach, M.; Grela, K. *Adv. Synth. Catal.* **2012**, *354*, 1043–1051. doi:10.1002/adsc.201100863
19. Getty, K.; Delgado-Jaime, M. U.; Kennepohl, P. *J. Am. Chem. Soc.* **2007**, *129*, 15774–15776. doi:10.1021/ja0747674
20. Ritter, T.; Hejl, A.; Wenzel, A. G.; Funk, T. W.; Grubbs, R. H. *Organometallics* **2006**, *25*, 5740–5745. doi:10.1021/om060520o
21. Ulman, M.; Grubbs, R. H. *Organometallics* **1998**, *17*, 2484–2489. doi:10.1021/om9710172
22. Jordaan, M.; van Helden, P.; van Sittert, C. G. C. E.; Vosloo, H. C. M. *J. Mol. Catal. A: Chem.* **2006**, *254*, 145–154. doi:10.1016/j.molcata.2006.03.022
23. Herrmann, W. A.; Lobmaier, G. M.; Priermeier, T.; Mattner, M. R.; Scharbert, B. *J. Mol. Catal. A: Chem.* **1997**, *117*, 455–469. doi:10.1016/s1381-1169(96)00381-0

License and Terms

This is an Open Access article under the terms of the Creative Commons Attribution License (<http://creativecommons.org/licenses/by/4.0>). Please note that the reuse, redistribution and reproduction in particular requires that the authors and source are credited.

The license is subject to the *Beilstein Journal of Organic Chemistry* terms and conditions: (<https://www.beilstein-journals.org/bjoc>)

The definitive version of this article is the electronic one which can be found at:
[doi:10.3762/bjoc.15.19](https://doi.org/10.3762/bjoc.15.19)



Olefin metathesis in multiblock copolymer synthesis

Maria L. Gringolts, Yulia I. Denisova, Eugene Sh. Finkelshtein
and Yaroslav V. Kudryavtsev*

Review

Open Access

Address:
Topchiev Institute of Petrochemical Synthesis, Russian Academy of Sciences, Leninsky prosp. 29, 119991 Moscow, Russia

Beilstein J. Org. Chem. **2019**, *15*, 218–235.
doi:10.3762/bjoc.15.21

Email:
Yaroslav V. Kudryavtsev* - yar@ips.ac.ru

Received: 10 September 2018
Accepted: 21 December 2018
Published: 24 January 2019

* Corresponding author

This article is part of the thematic issue "Progress in metathesis chemistry III".

Keywords:
ADMET; macromolecular cross metathesis; multiblock copolymers; olefin metathesis; ROMP

Guest Editors: K. Grela and A. Kajetanowicz

© 2019 Gringolts et al.; licensee Beilstein-Institut.
License and terms: see end of document.

Abstract

Multiblock copolymers constitute a basis for an emerging class of nanomaterials that combine various functional properties with durability and enhanced mechanical characteristics. Our mini-review addresses synthetic approaches to the design of multiblock copolymers from unsaturated monomers and polymers using olefin metathesis reactions and other ways of chemical modification across double C=C bonds. The main techniques, actively developed during the last decade and discussed here, are the coupling of end-functionalized blocks, sequential ring-opening metathesis polymerization, and cross metathesis between unsaturated polymers, or macromolecular cross metathesis. The last topic attracts special interest due to its relative simplicity and broad opportunities to tailor the structure and hence the properties of the copolymer products. Whenever possible, we analyze the structure–property relations for multiblock copolymers and point to their possible practical applications.

Introduction

Nowadays, olefin metathesis has become a well-established field of organic and polymer chemistry. The discovery of metal–locarbene initiators that are capable of catalyzing metathesis polymerization in a living fashion turned it into a powerful tool of polymer design [1]. Hundreds of linear, comb-like, graft-, bottle-brush, ladder, and other homopolymers and copolymers were synthesized [2–7]. Block copolymers combining properties of two or more individual polymers in one material attract ongoing attention from both experimentalists and theoreticians

due to their intrinsic tendency to self-assemble into diverse microstructures [8–11]. Technological applications of block copolymers cover lithography [12], photovoltaics [13], membranes [14] and many other areas [15]. Most of the research is devoted to diblock and triblock copolymers, whereas multiblock copolymer studies are still much less common [3,4,16–18]. Aside from more complicated synthesis and characterization of multiblock copolymers, for decades it was thought that any sequence disorder along polymer chains hinders their

ordering [19] so that the only interesting are regular multiblock copolymers that can form structures with more than one periodicity [20]. Meanwhile, theoretical investigations [21–23] and computer simulations [24–27] gradually revealed the high potential of random multiblock copolymers with respect to self-assembly. In recent years, it was demonstrated that such polymers can be prepared with many of the available techniques, including polycondensation [28], chain-shuttling polymerization [29], copper-mediated radical polymerization [30–32], reversible addition–fragmentation chain transfer polymerization [33,34], and intermacromolecular reactions [35–37]. Though the properties of multiblock copolymers are far from being fully explored and understood, their applications already include adhesives, barrier materials, emulsifiers, impact modifiers, and materials for electronics, fuel cells, gene and drug delivery [8,9,15,38–40]. Compared with diblock and triblock copolymers, not to speak about polymer blends, multiblock copolymers often demonstrate superior mechanical properties, biocompatibility, biodegradability, compatibilizing ability, and tendency to form bicontinuous phases needed for ionic and molecular transport [8–10,41–45]. On the other side, they retain individual properties of their comonomers, which are usually aver-

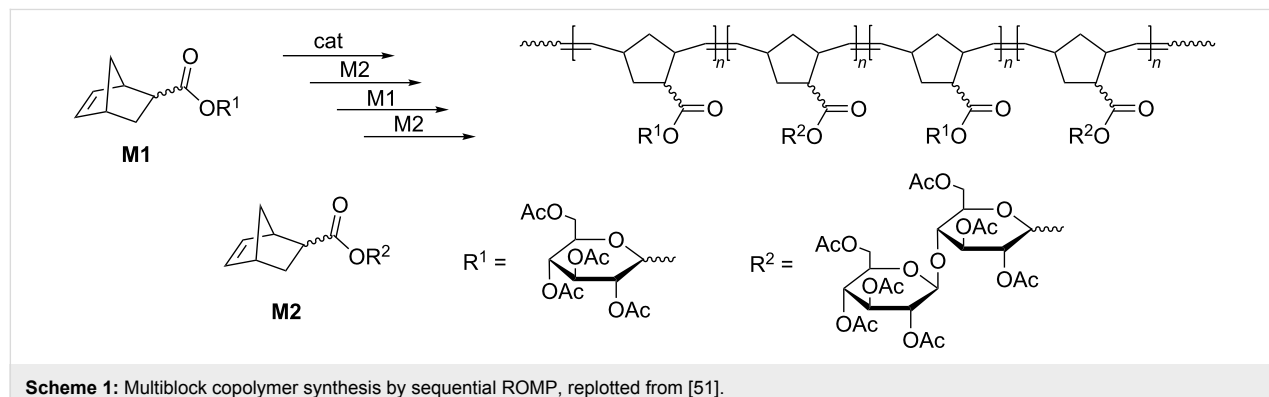
aged and therefore lost in fully random copolymers of similar composition [46,47].

In this mini-review we consider the approaches to multiblock copolymer syntheses via olefin metathesis reactions developed mainly over the past ten years. The following sections address the achievements and perspectives of three main techniques used for this purpose, namely, sequential ring-opening metathesis polymerization, coupling of end-functionalized blocks, and macromolecular cross metathesis.

Review

Synthesis by sequential ring-opening metathesis polymerization

Living ring-opening metathesis polymerization (ROMP) provides an opportunity to use a well-established route to multiblock copolymers based on the repetitive addition of different monomers to living polymer chains after full consumption of a previous monomer [48,49]. This technique was effectively applied for the synthesis of di-, tri- and tetrablock carbohydrate copolymers mediated by Schrock' and Grubbs' catalysts of the 1st (Gr1) and 2nd (Gr2) generations (Scheme 1, Figure 1)



Scheme 1: Multiblock copolymer synthesis by sequential ROMP, reprinted from [51].

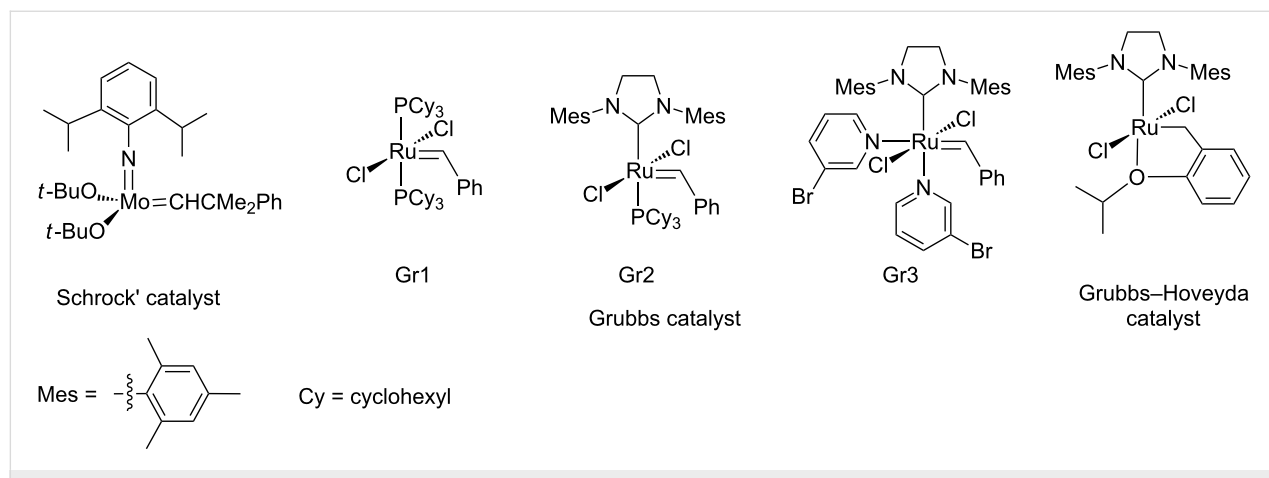


Figure 1: The most known commercially available catalysts for olefin metathesis.

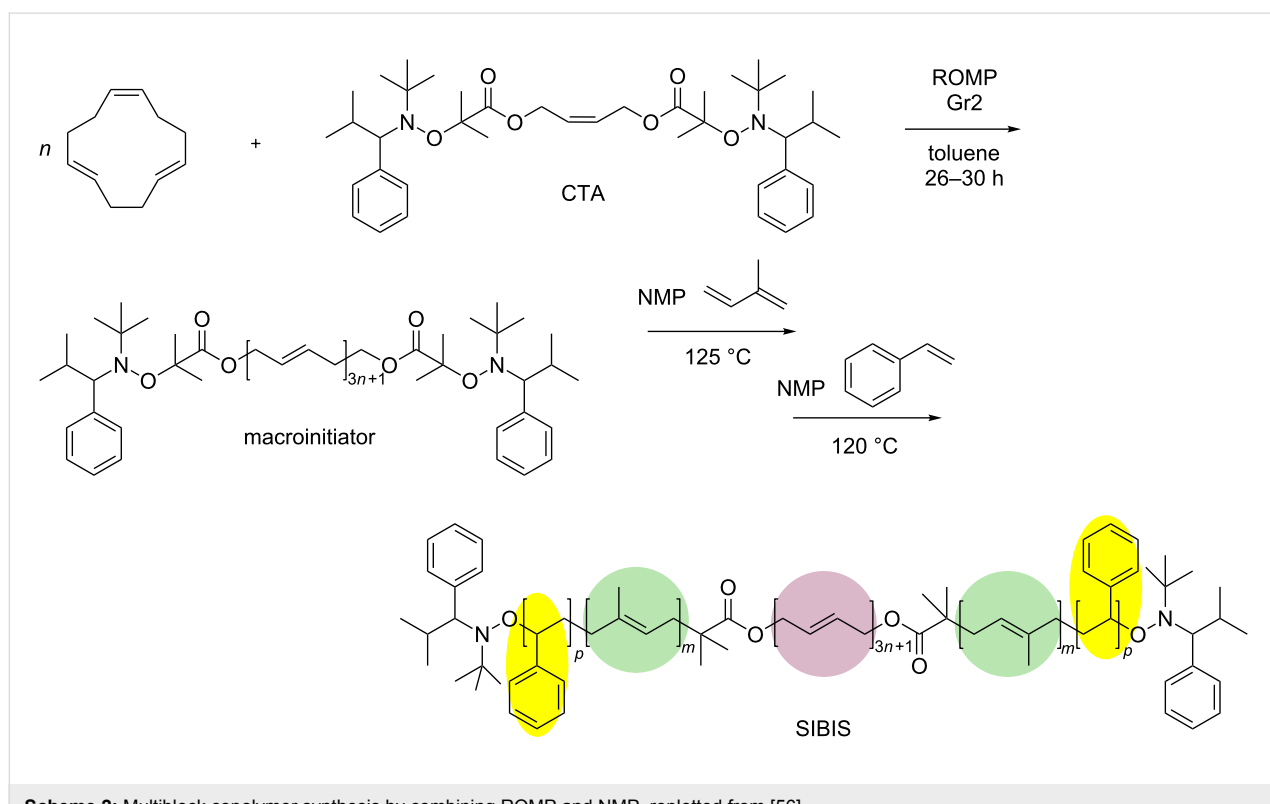
[50,51]. It yields copolymers of the desired average molecular mass and narrow molecular mass distribution ($D = M_w/M_n = 1.0\text{--}1.19$) and enables control over the block sequence and length in the copolymer chains (sequence-controlled multiblock copolymers). However, in practice this method is restricted to copolymers with a limited number of blocks, such as tetrablocks or pentablocks [52], because each time a new monomer is added some of the living chains cannot initiate polymerization being terminated with trace impurities. Besides, in the course of ROMP main-chain double bonds are prone to secondary metathesis in a chain-transfer process that leads to reshuffling of the monomer unit sequences. Since less sterically encumbered groups are more easily involved into the secondary metathesis, this effect can be minimized by first polymerizing a more bulky monomer and then conducting a fast polymerization of another monomer [53–55].

Synthesis from end-functionalized blocks

Another strategy to multiblock copolymer preparation is to assemble them by using pre-synthesized telechelic polymers with α,ω -bifunctional end groups, which can be coupled in different ways. The classical technique for preparing telechelics uses a symmetrical difunctional olefin compound as a chain-transfer agent (CTA). This was applied for the synthesis of styrene (S)–isoprene (I)–butadiene (B) multiblock copolymers by combining ROMP with nitroxide-mediated polymerization

(NMP) [56]. A perfectly regioregular α,ω -telechelic poly(1,4-butadiene) bearing alkoxyamine termini was obtained by ROMP of *trans,trans,cis*-1,5,9-cyclododecatriene in the presence of a symmetric acyclic olefin CTA (Scheme 2). This telechelic polybutadiene was used as the macroinitiator for the NMP of styrene and diene monomers to yield unimodal SBS, IBI, and SIBIS multiblock copolymers, which include glassy, rubbery, and semicrystalline polymer segments and demonstrate peculiar mechanical behavior [57,58].

References [59] and [60] report on the preparation of fluorescent polymer nanoparticles for bioimaging and in vivo targeting of tumors and the nanoparticles were formed by a ABCBA pentablock copolymer. In this polymer A stands for hydrophilic oligo(ethylene glycol) (OEG)-grafted polynorbornene possessing stealth-like and antifouling properties that are useful for in vivo applications. The B block is formed by polynorbornene functionalized with *N*-hydroxysuccinate esters (NHS) that can be used as a carrier for antitumor drugs, and the C block is a far-red emitting conjugated random copolymer of *p*-phenylene ethynylene (PPE) and perylene monoimide (PMI, Figure 2). For the synthesis, the random PPE–PMI copolymer was end-capped with norbornadiene (NB–(PPE–PMI)–NB) to allow further functionalization through olefin metathesis. The separately prepared by ROMP living diblock copolymers comprising norbornene with OEG (A block) and an NHS (B block)



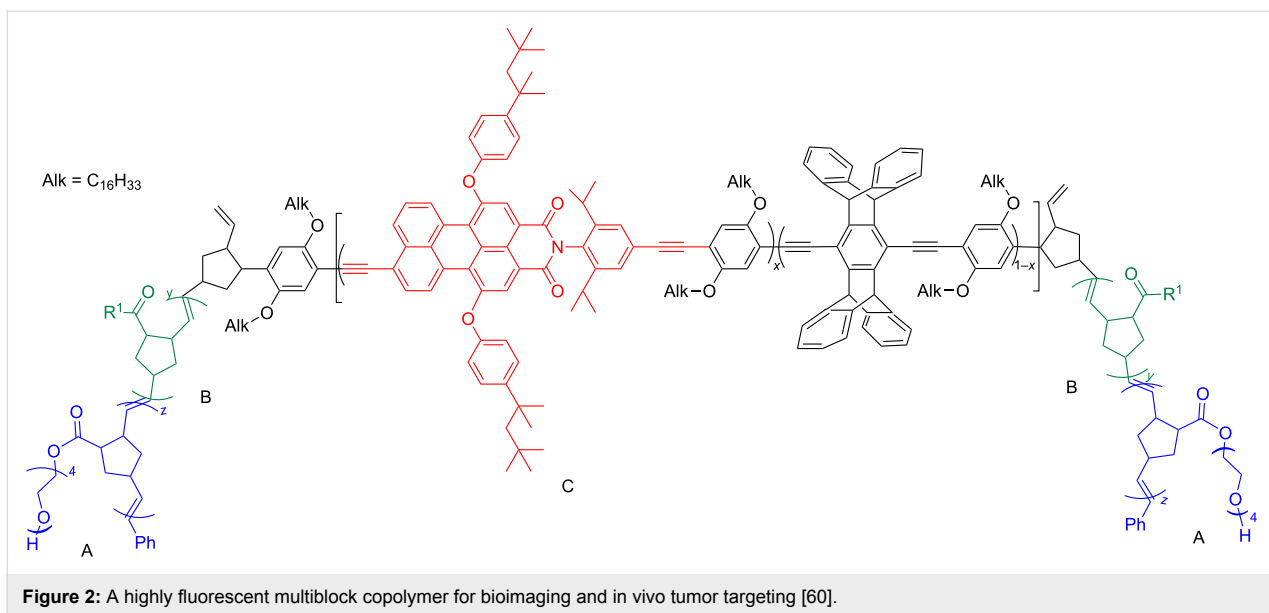


Figure 2: A highly fluorescent multiblock copolymer for bioimaging and in vivo tumor targeting [60].

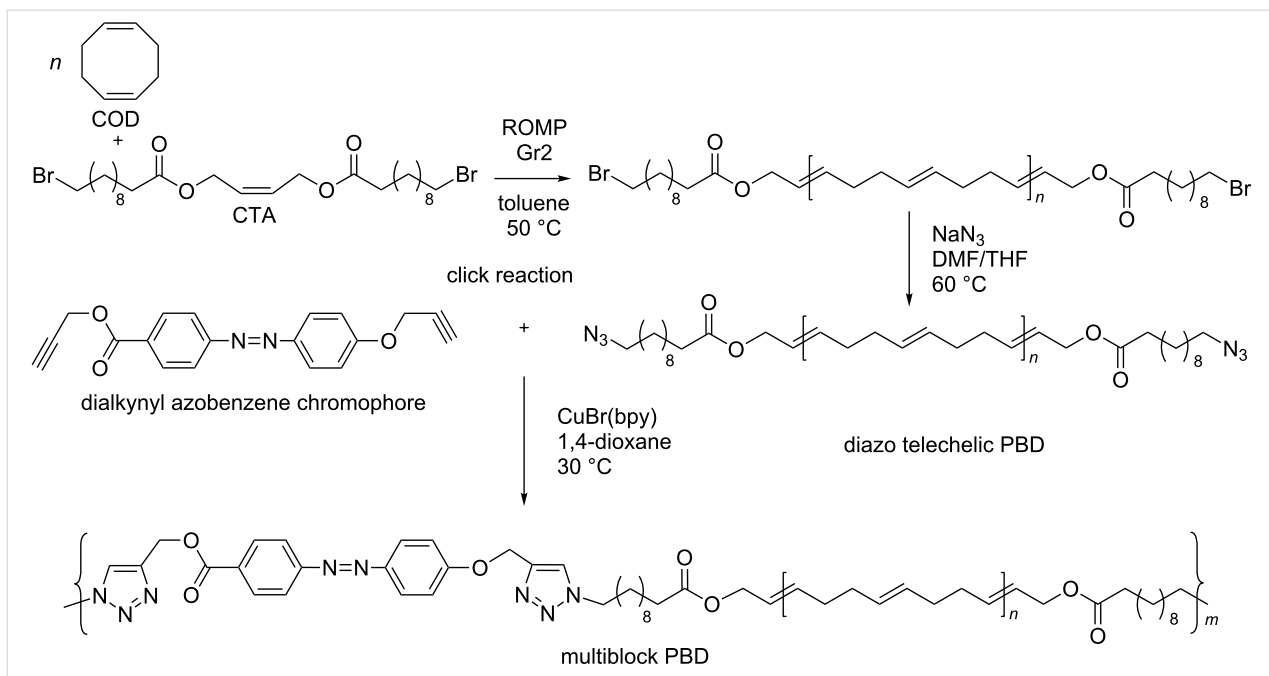
were synthesized in the presence of Gr1 and terminated by the reaction with NB–(PPE–PMI)–NB to obtain the ABCBA pentablock copolymers.

This copolymer forms nanoparticles with a central hydrophobic core capable of accommodating fluorescent dyes and conventional therapeutics and a hydrophilic biocompatible outer shell.

The efficient combination of the ROMP process and click chemistry led to the highly photoresponsive multiblock polybu-

tadiene [61]. Initially, ROMP of 1,5-cyclooctadiene (COD) in the presence of a difunctional CTA provided dibromo-telechelic polybutadiene (PBD), which was transformed into diazido-functionalized telechelic PBD (Scheme 3).

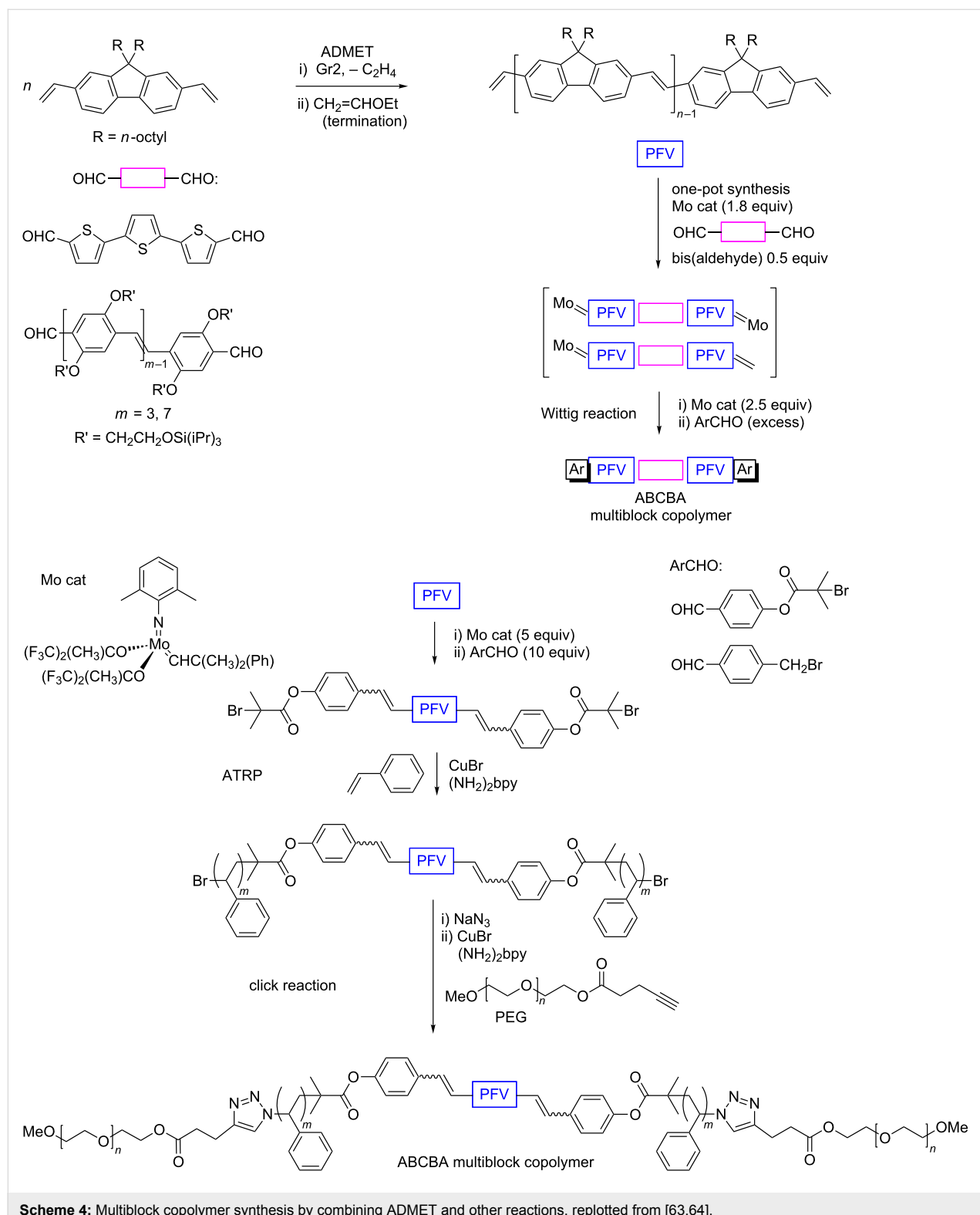
The multiblock PBD then was assembled by multiple click reactions of the diazido-telechelic PBD with a dialkynyl-containing azobenzene chromophore. The newly formed triazole moieties can tune and improve the photoresponsive properties of PBD.



Scheme 3: Multiblock copolymer synthesis by combining ROMP and click reactions replotted from [61].

α,ω -Functional telechelic polymers also can be synthesized by acyclic diene metathesis (ADMET) polymerization. This approach was implemented for the preparation of fluorene-containing multiblock copolymers [62,63]. Poly(9,9-di-*n*-octylfluore-

rene-2,7-vinylene, PFV) obtained by ADMET polymerization of 2,7-divinyl-9,9-di-*n*-octylfluorene in the presence of Gr2 under reduced pressure (Scheme 4), possessed exclusive *trans* regularity and contained vinyl groups at the both polymer chain



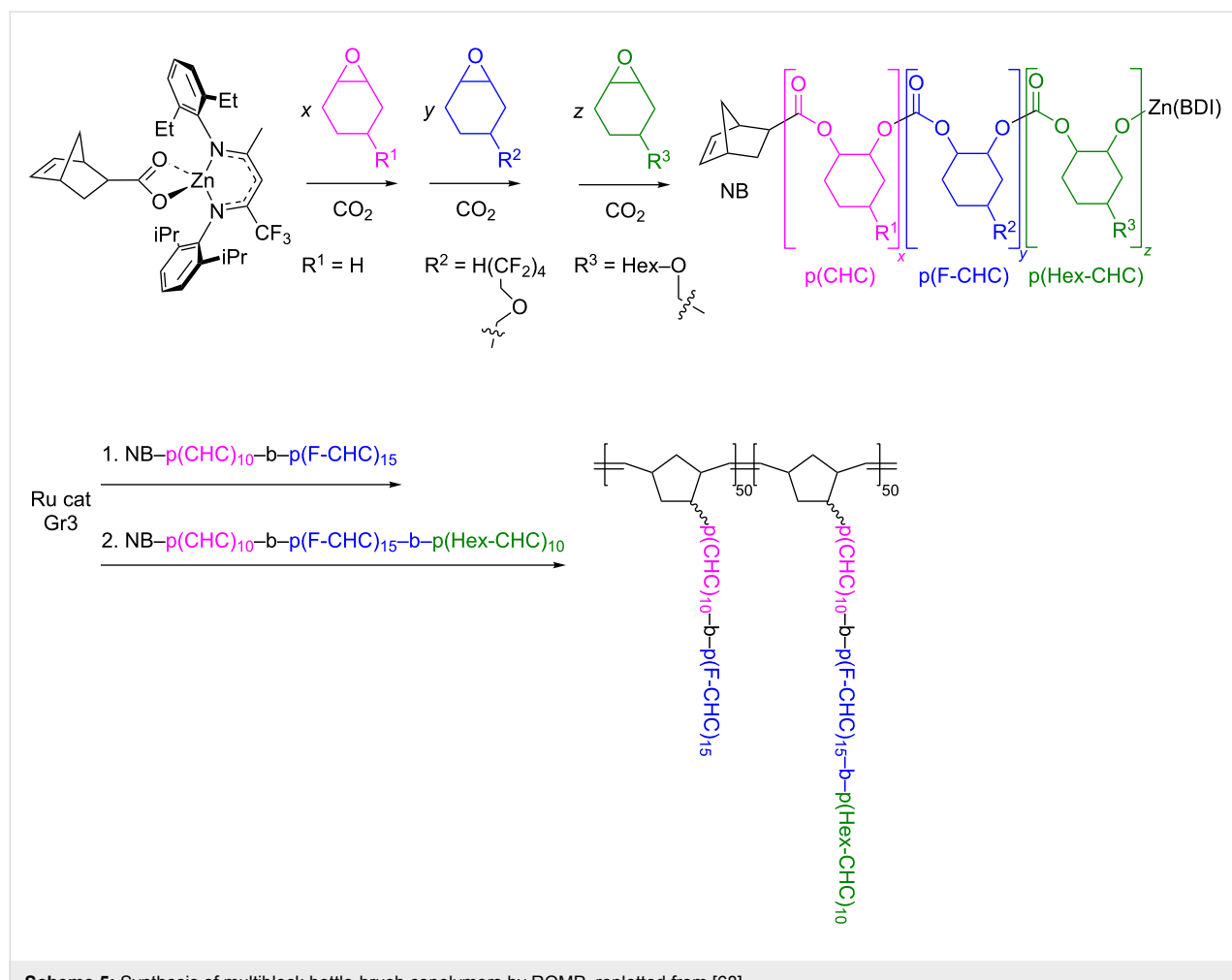
Scheme 4: Multiblock copolymer synthesis by combining ADMET and other reactions, replotted from [63,64].

ends. These groups were treated with a Mo catalyst to generate the corresponding Mo-alkylidene moieties followed by the Wittig-type cleavage with various aldehydes, gave an opportunity to utilize atom transfer radical polymerization (ATRP) and click reactions for the precise synthesis of amphiphilic ABCBA-type block copolymers (Scheme 4) [63]. A more facile “one-pot” procedure for the synthesis of an end-functionalized conjugated multiblock copolymer with PFV main chain was accomplished by combining olefin metathesis and subsequent Wittig coupling (Scheme 4) [64].

The ADMET technique was used not only for the synthesis of polymer telechelics but also for their assembling into multiblock copolymers. A simple one-pot way for the preparation of random multiblock copolymers was proposed in reference [65]. A mixture of semicrystalline and amorphous samples of partly hydrogenated PBD underwent ethenolysis in the presence of the Ru-carbene catalyst. This depolymerization procedure resulted in the formation of telechelics with both end vinylated. Then, the ethylene atmosphere was replaced with argon and an addi-

tional amount of catalyst added. Under these conditions, the ADMET polymerization led to the multiblock copolymers with randomly distributed semicrystalline and amorphous blocks, which exhibited noticeably improved mechanical properties compared with the blend of the initial polymers.

An approach utilizing macromonomers or macrocycles was used for the synthesis of multiblock copolymers with random or sequence-controlled structure [66]. The ROMP is also suitable for the synthesis of bottle-brush block copolymers, in which linear or branched side chains are densely grafted to a linear backbone, being easily functionalized for recognition, imaging, and drug delivery in aqueous media [4-6,67]. They have a low tendency to entangle and can rapidly self-assemble in selective solvents even at very low concentrations forming large-domain microstructures. The facile synthesis of norbornenyl-terminated di- and triblock poly(cyclohexene carbonate)s was carried out by the β -diiminate (BDI) zinc-catalyzed block copolymerization of functionalized epoxides and CO_2 with a norbornenyl-containing initiator (Scheme 5) [68]. The subsequent “grafting



through” by ROMP of norbornene resulted in the synthesis of multiblock copolymer brushes. Changes in the synthetic stage sequence led to variable layer compositions.

Various linear and star-shaped (triarm) ABA and ABCBA amphiphilic multiblock copolymers containing acetal-protected sugars (APS) were prepared by the coupling of an end-functionalized ROMP copolymer of norbornene (NB) and APS-substituted NB with poly(ethylene glycol) (PEG) [69]. Ring-opening metathesis copolymerization of the rather strained cyclooctene (COE) and a strainless 27-membered macrocyclic olefin (MCO) led to the multiblock copolymer consisting of octenylene blocks linked with ring-opened MCO segments (Scheme 6) [70]. The higher reactivity of COE in ROMP is the reason for the formation of long octenylene sequences.

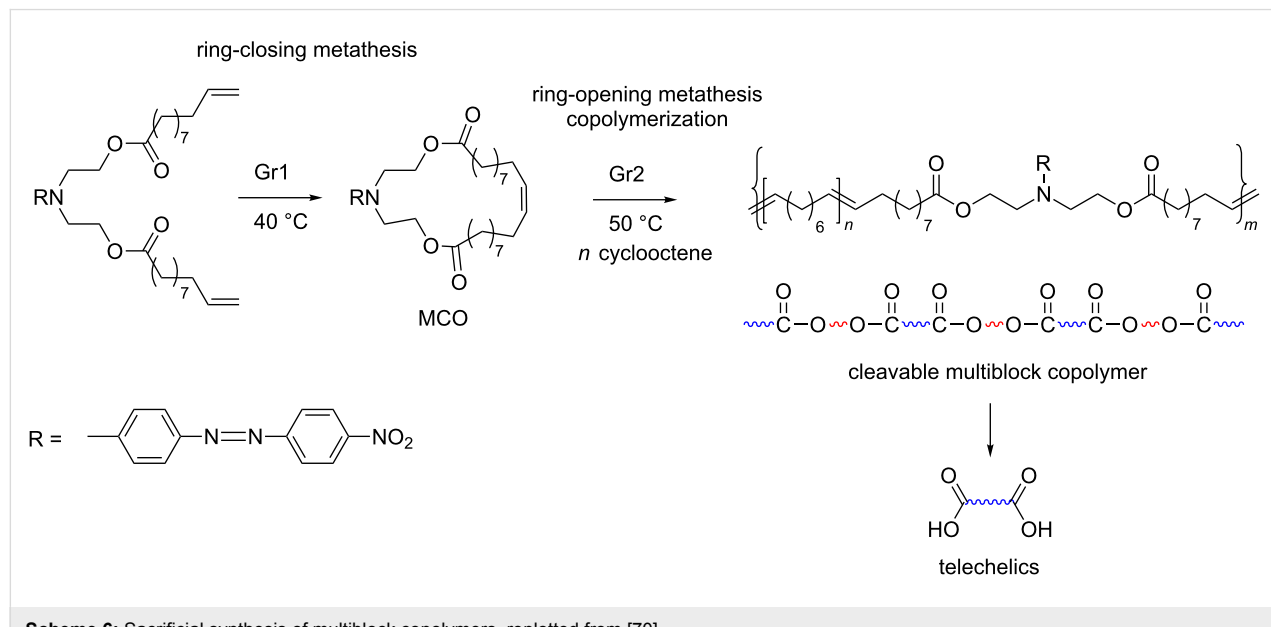
The MCO was obtained by ring-closing metathesis and contained easily cleavable ester linkages. It gave the possibility to cut the multiblock copolymer into pieces under alkaline conditions in order to obtain telechelic polyoctenylene with carboxyl end groups. The last reaction represents an example of the so-called sacrificial synthesis, another effective approach to telechelics [71].

Hiff and Kilbinger generated cleavable ABAB pentablock and ABABABA heptablock metathesis copolymers via the sequential ROMP of seven-membered cyclic acetals (2-methyl-1,3-dioxepine and 2-phenyl-1,3-dioxepine) and N-substituted NB dicarboximide derivatives [72]. The subsequent hydrolysis of the prepared copolymers resulted in well-defined telechelics in good yields per initiator molecule and thus significantly im-

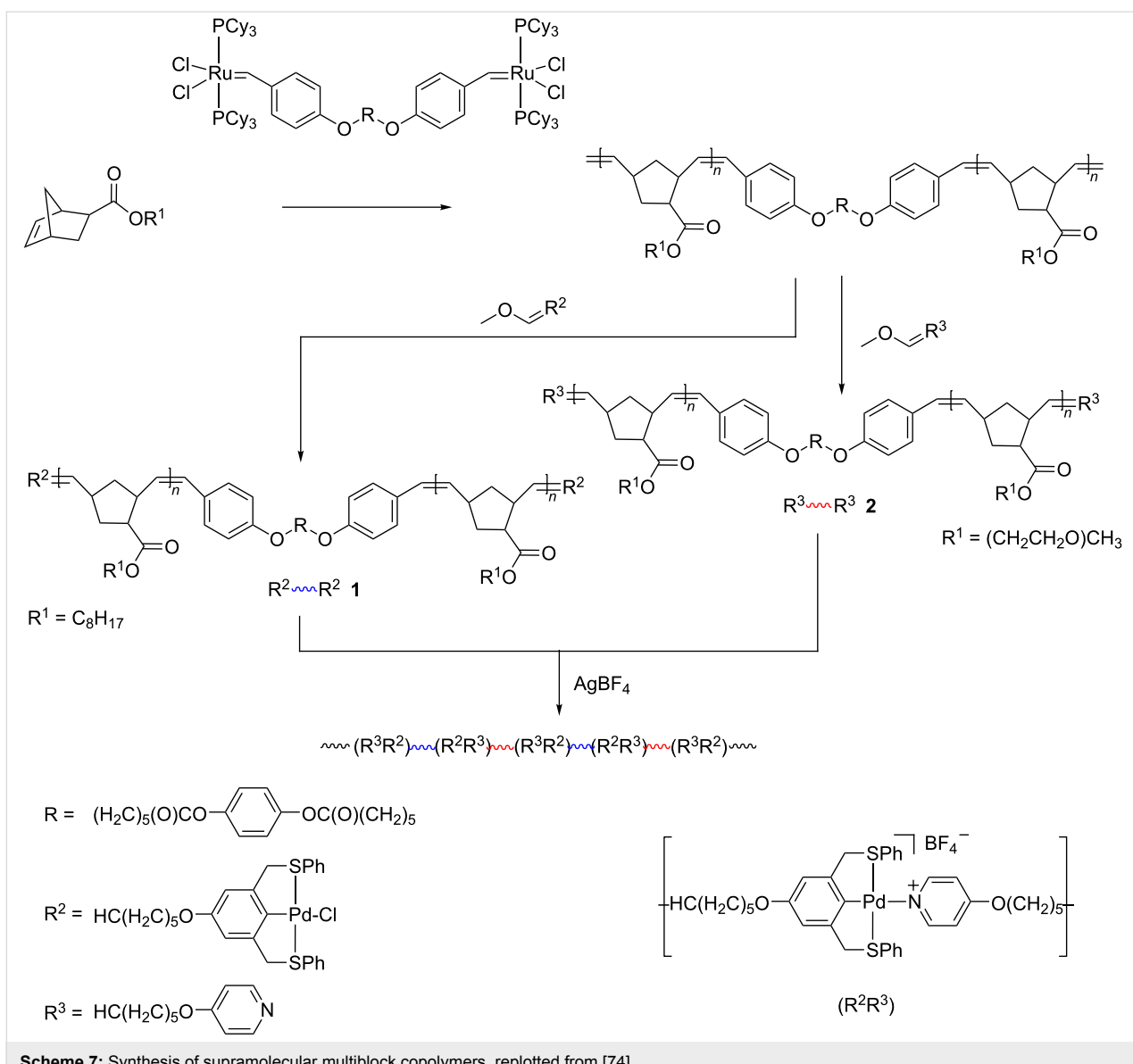
proved the initiator efficiency. The sacrificial approach also helps to describe the multiblock copolymer structure: owing to the acid-labile acetal group, polymer scission takes place at the point of the dioxepin insertion thus providing an indirect way to detect the monomer location [73].

Supramolecular multiblock copolymers with the possibility to introduce stimuli-responsive functionalities were obtained using a bimetallic ruthenium initiator [74]. The initiator allowed for the single-step fabrication of symmetrically end-functionalized telechelic polymers using ROMP and functional chain terminators (Scheme 7). In more detail, the synthesis included ROMP of NB octyl ester or NB by means of metal coordination using the obtained telechelic polymers methyl triglycol ester in the presence of the bimetallic ruthenium catalyst followed by the addition of an excess of either a Pd-containing chain terminator to obtain pincer-functionalized telechelic polymer **1** or a pyridine-containing end-terminator to yield pyridine-functionalized telechelic polymers **2**. On this basis, supramolecular copolymers with alternating blocks were constructed using AgBF_4 to remove Cl from the pincer complex and generate a cationic Pd ligand, which can coordinate with pyridyl ligands in a new pincer complex.

A range of Zr(IV) and Hf(IV)-based bisamido complexes can catalyze both ROMP and addition (AP or vinyl) (co)polymerization of NB [74,75]. The presence of a 2-pyridyl moiety, along with a boron-containing group, and activation by MAO makes it possible to synthesize a NB copolymer with ethylene, containing both NB-ROMP and NB-AP monomer units. This approach allows obtaining multiblock copolymers that are capable



Scheme 6: Sacrificial synthesis of multiblock copolymers, reprinted from [70].



Scheme 7: Synthesis of supramolecular multiblock copolymers, reprinted from [74].

of simple post-polymerization functionalization across double bonds (Figure 3). For instance, the introduction of polar groups imparts adhesive properties to the copolymers, which are essential for coatings.

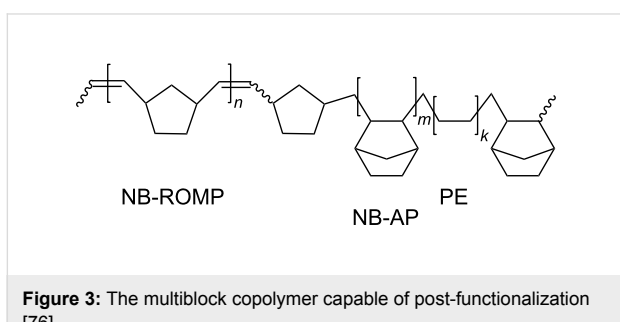


Figure 3: The multiblock copolymer capable of post-functionalization [76].

Synthesis by macromolecular cross metathesis

Cross metathesis between polymers containing main-chain C=C double bonds is a recent and actively developing approach to random multiblock copolymers. For years, the cross metathesis involving double bonds in the polymer backbone was considered as an undesired chain-transfer process that broadens molecular mass distribution, leads to the formation of cyclooligomers and reshuffling of monomer units in the course of the polymer synthesis [77]. The cross metathesis reactions on polymers were mostly studied with regard to the intramolecular polymer–catalyst interactions [77–79] or intermolecular degradation of polymers via the cometathesis with different olefins [77,80,81]. Only recently, the cross metathesis between macromolecules, or macromolecular cross metathesis (MCM), began

to be considered as a promising reaction for various applications [82–93]. It was shown that the random copolymers produced by the cross metathesis of chemically dissimilar polymers, such as polycarbonate and PCOE, demonstrate an ability to ordering via microphase separation (Figure 4A) [82]. The MCM was shown to be effective in the preparation of multiblock copolymers from parent polymers synthesized according to different polymerization mechanisms. New multiblock copolymers were obtained by the cross metathesis of ROMP-derived 1,4-polybutadiene or natural polyisoprene and olefin-containing polyester or polyurethane prepared via step-growth polymerization (Figure 4B and C) [83–85]. The multiblock copolymers from polybutadiene and olefin-containing polyurethane demonstrated improved mechanical properties [85]. Head-to-tail regioregular and *E*-stereoregular multiblock copolymers and heterottelechelic polymers were successfully synthesized by the cross metathesis between different ROMP-derived poly(3-substituted cyclooctenes), (Figure 4D) [86]. The MCM between immiscible commercial polybutadiene and polyisoprene led to the formation of single-phase block copolymers (Figure 4E) [87]. The cross metathesis between functionalized polyoctenamers (PCOE) and polynorbornenes (PNB) opened the way to new multiblock copolymers that are difficult to obtain by other methods (Figure 4F) [88–93]. With a large excess of COE, the ring-opening metathesis copolymerization of NB and COE results in the formation of a mixture of the homopolymers and copolymers enriched with NB units [94,95]. The substantial difference in the monomer strain energy (NB: 100 kJ mol^{−1}, $-\Delta G^\circ$ ROMP = 47 kJ mol^{−1}; COE: 16 kJ mol^{−1}, $-\Delta G^\circ$ ROMP = 13 kJ mol^{−1}) [77,96] is the reason for such behavior. Unlike copolymerization, the MCM starts from two homopolymers, PNB and PCOE, in which there is no difference in the strain energy, so that multiblock copolymers with various block lengths are easily formed [88,89,91,93]. Obtaining of multiblock polymers using cross metathesis is synthetically much simpler than using the earlier described sequential ROMP or pre-synthesized block-coupling techniques so that MCM can be advantageous when a strict sequence control over the copolymer structure is not needed. Nevertheless, random block copolymers obtained by interchain exchange reactions, like MCM, retain the ability to ordering [82].

MCM is an interchain cross reaction characterized by reshuffling of monomer units in the macromolecular backbones via break up and formation of new double bonds according to the olefin metathesis mechanism. In the beginning, an exchange of chain segments between the parent homopolymers results in the formation of diblock copolymers. Then random multiblock copolymers are formed (Scheme 8), their average block lengths are decreased until they gradually reach the values typical of a copolymer with the fully random unit sequence.

Therefore, the copolymer chain structure can be controlled by altering the reaction time, molar ratio of the starting polymers, catalyst type and concentration, as well as solvent type and initial polymer concentration [83–89,93]. It is important to keep a relatively high polymer concentration in the reaction mixture to prevent intramolecular metathesis that leads to cyclooligomers. It is worth noting that the Gr2, Gr3 and Grubbs–Hoveyda (Gr–H) catalysts (Figure 1) are much more active than Gr1 in MCM and concentrations of 0.036–0.049% are sufficient to carry out the process effectively [86,87]. In the PBD–polyisoprene (PI) cross metathesis, Gr1 can be replaced by Gr–H1 but longer reaction times are needed [87]. A control over the reaction kinetics can be sometimes complicated because the overall composition of a polymer mixture does not change in the course of MCM. Nevertheless, it can be successfully implemented using a complex of NMR, GPC, and DSC methods. As a rule, the parent polymers are characterized by different molecular masses, which allow using GPC to track how two peaks in the chromatogram merge into one with conversion. If the initial polymers display different glass transition temperatures, DSC can be also used to monitor the kinetics (Figure 5). At the beginning of the MCM reaction, two T_g values are observed which get closer and finally merge into one, when long sequences of chemically identical units stemming from the parent homopolymers are exhausted.

¹H NMR spectroscopy was implemented to track the evolution of the chain structure in the course of MCM between polybutadiene (PBD) or polyisoprene (PI) and olefin-containing polyesters or polyurethane, as well as changes in the chain stereospecificity during the reaction between 3-substituted PCOEs [83–86]. Cross metathesis in the PNB/PCOE (Figure 6) and PBD/PI pairs was monitored by ¹³C NMR [87–91,93]. The fraction of heterodyads in the copolymer gradually increased with conversion thus indicating the formation of random multiblocks. The average block length L was calculated from an integral ratio of homo (A–A, B–B) and heterodyad (A–B) signals in the NMR spectra:

$$L_A = [I(C^{A-A}) + I(C^{A-B})]/I(C^{A-B}); L_B = [I(C^{B-B}) + I(C^{B-A})]/I(C^{B-A}); \text{ where } I(C^{A-A}) \text{ and } I(C^{B-B}) \text{ are the peak intensities of the initial homodyads, A–A and B–B, and } I(C^{A-B}) \text{ and } I(C^{B-A}) \text{ are the peak intensities related to the alternating dyads.}$$

The average block lengths decreased with the conversion, reaction time, and catalyst concentration and asymptotically approached the value of 2, characteristic of a completely random (Bernoullian) equimolar copolymer. Thus, a proper choice of the MCM conditions enables one to obtain copolymers with a controllable average block length ranging from the initial homopolymer length to a few monomer units.

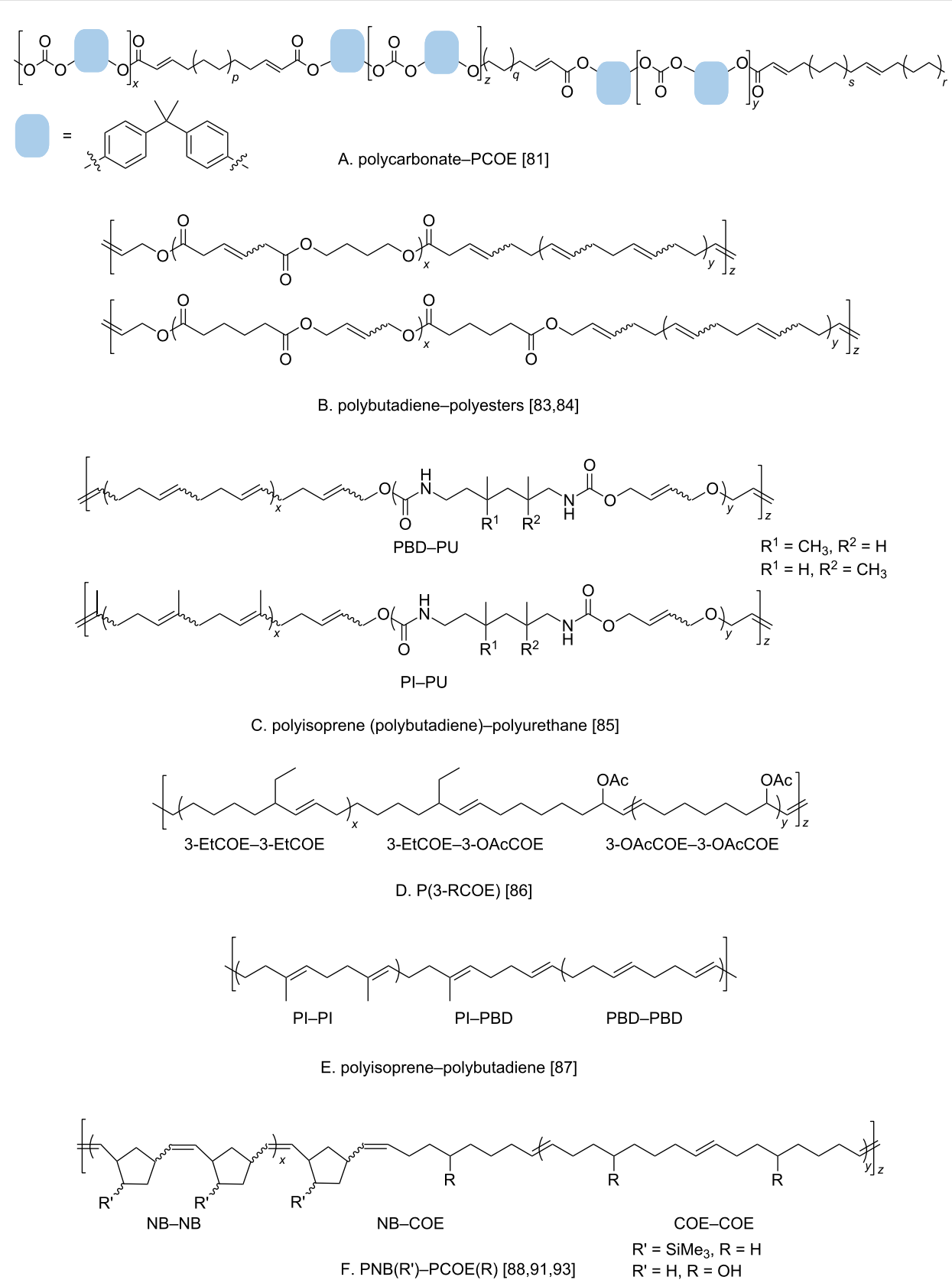
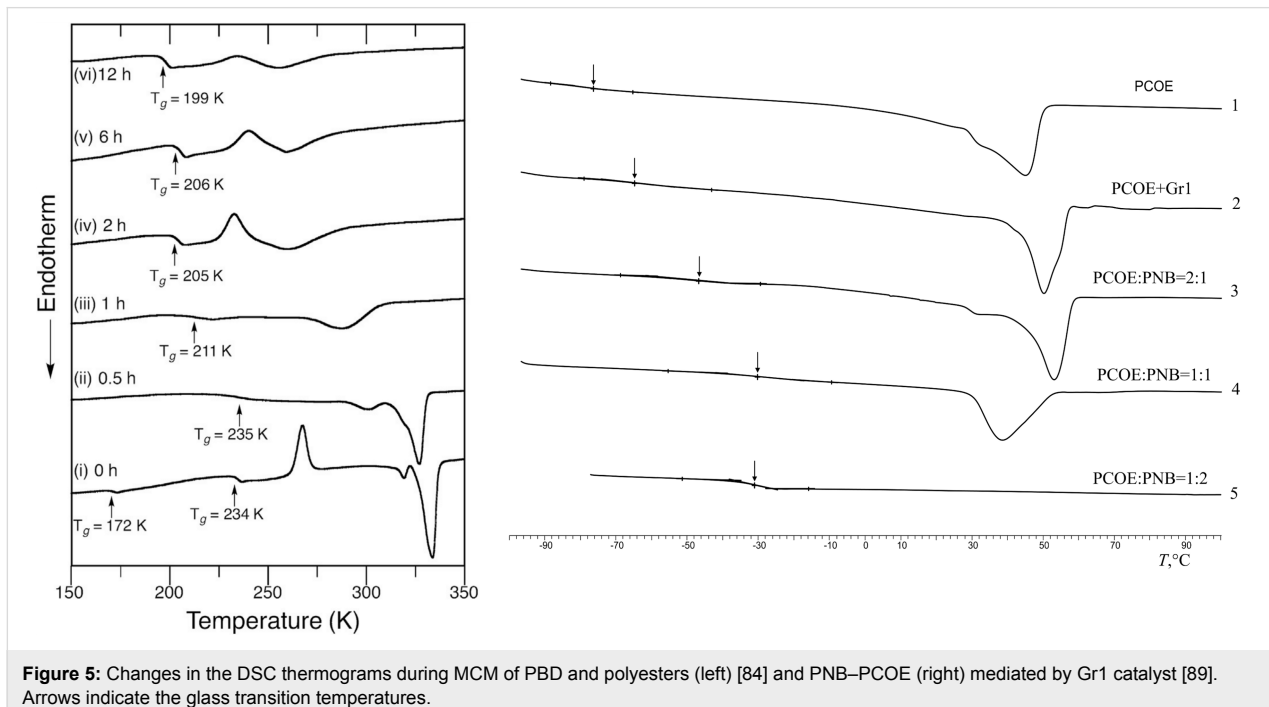
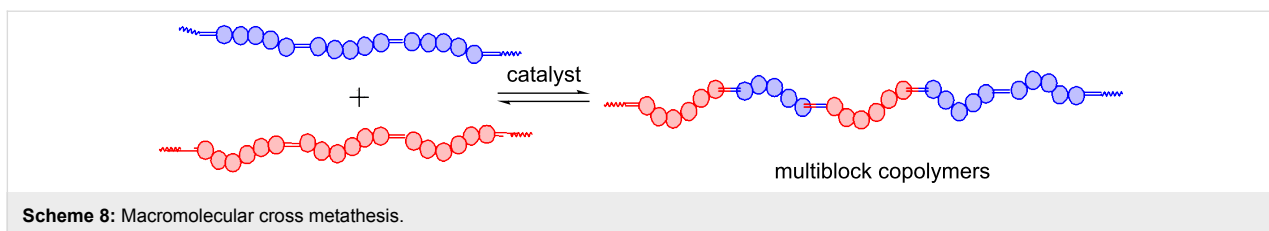


Figure 4: Multiblock copolymers synthesized by macromolecular cross metathesis.



Important data on the kinetics of MCM between PNB and PCOE mediated by Gr1 were obtained by combining in situ NMR studies of the Ru-carbene transformations and ex situ NMR monitoring of the dyad composition evolution [90]. It was found that Gr1 first interacts with PCOE so that all Ru-carbenes become bound to those macromolecules approximately within one hour (Scheme 9, reaction 1 and Figure 7). Recall that the addition of Gr1 to a mixture of NB and COE first causes rapid metathesis polymerization of NB and only after that COE monomers are involved. An early MCM stage is also characterized by a decrease in the average molar mass of the mixture, which indicates that polymer backbones break during their interaction with the catalyst.

It takes about a day for the interchain exchange between the homopolymers with carbene-functionalized end groups to yield a statistical NB–COE copolymer and during this process its molar mass remains almost unchanged. The slowest elementary reaction, which controls the overall kinetics, is the interaction between [Ru]=PCOE carbenes and C=C bonds in PNB chains (Scheme 9, reaction 2). Its low rate is consistent with the

bulky structure of NB units. During the cross metathesis, the concentration of [Ru]=PNB carbenes is very low but they are necessary for the cross reaction to proceed (Scheme 9, reaction 3).

An increase of the PNB concentration in the mixture results in a growth of the copolymer degree of blockiness [89]. This feature of the cross metathesis between PNB and PCOE is also opposite to what is expected for the metathesis copolymerization of NB and COE, where a high excess of COE is needed to allow for the formation of NB–COE copolymer [95].

Some results regarding the *cis/trans*-isomerization of double bonds in the MCM process were obtained [85,87,89]. In the systems PNB–PCOE (68% *cis*)–Gr1 and PBD–*cis*-olefin-containing polyurethane (*cis*-PU)–Gr2, *cis*-double bonds partly transform to a more thermodynamically stable *trans*-configuration, which is well-known for olefin metathesis [85,89]. The *cis/trans*-isomerization is observed for homodyads in MCM and even in the course of the homopolymer–catalyst interaction as a result of self-metathesis reactions that do not directly

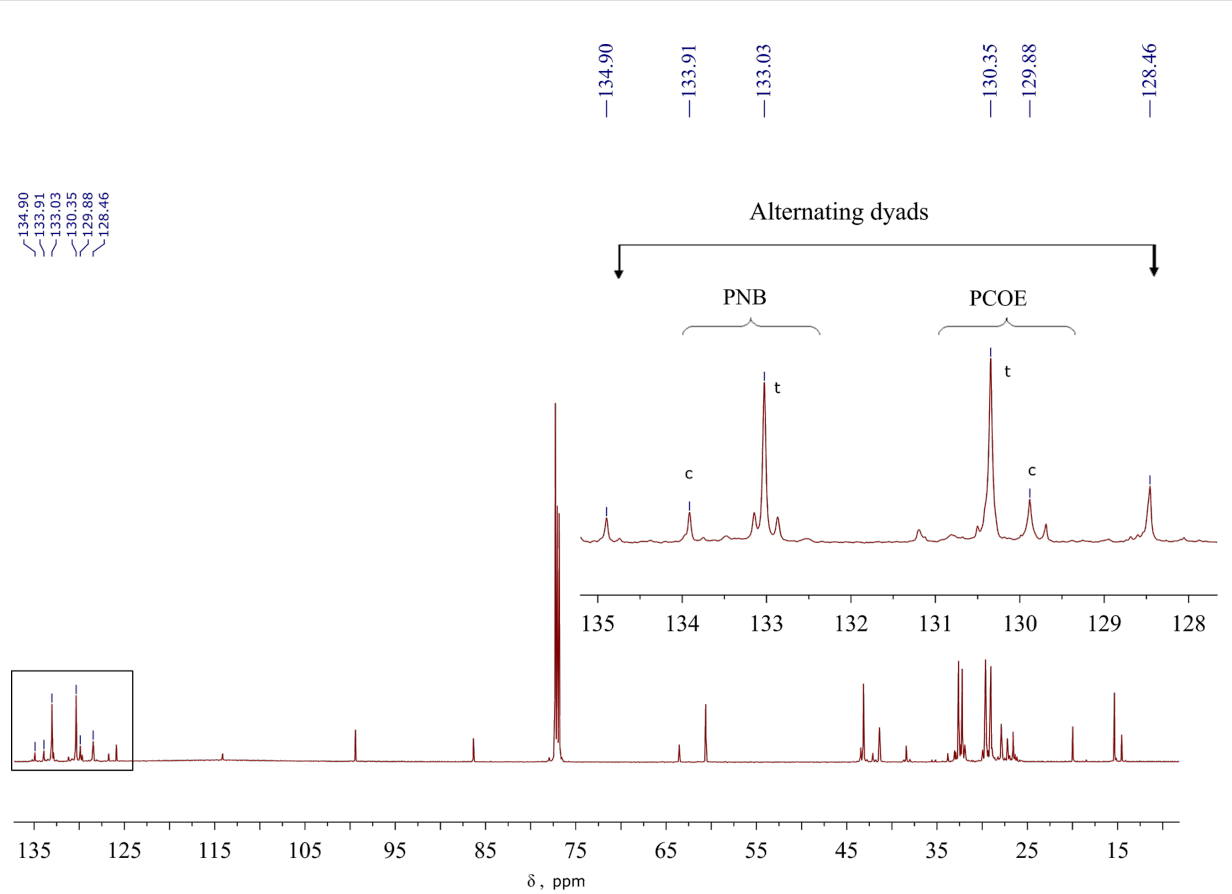
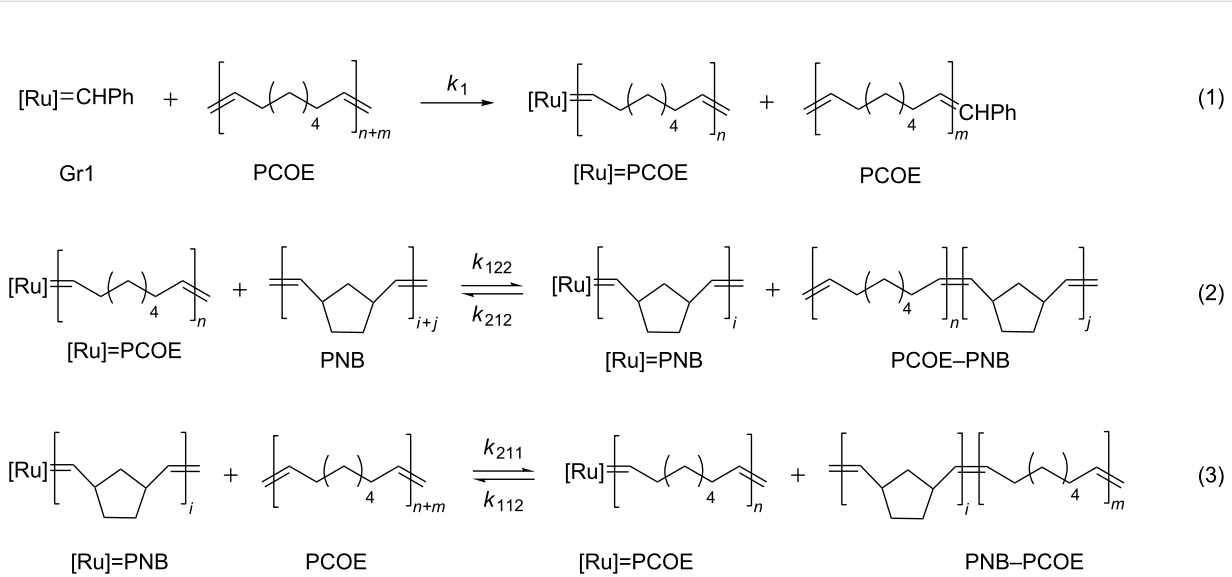


Figure 6: The ^{13}C NMR spectrum recorded after 8 h of the reaction between PCOE, PNB, and Gr1; the homo- and heterodyad signals are enlarged in the inset [90].



Scheme 9: Elementary reactions of MCM between PNB and PCOE, replotted from [90].

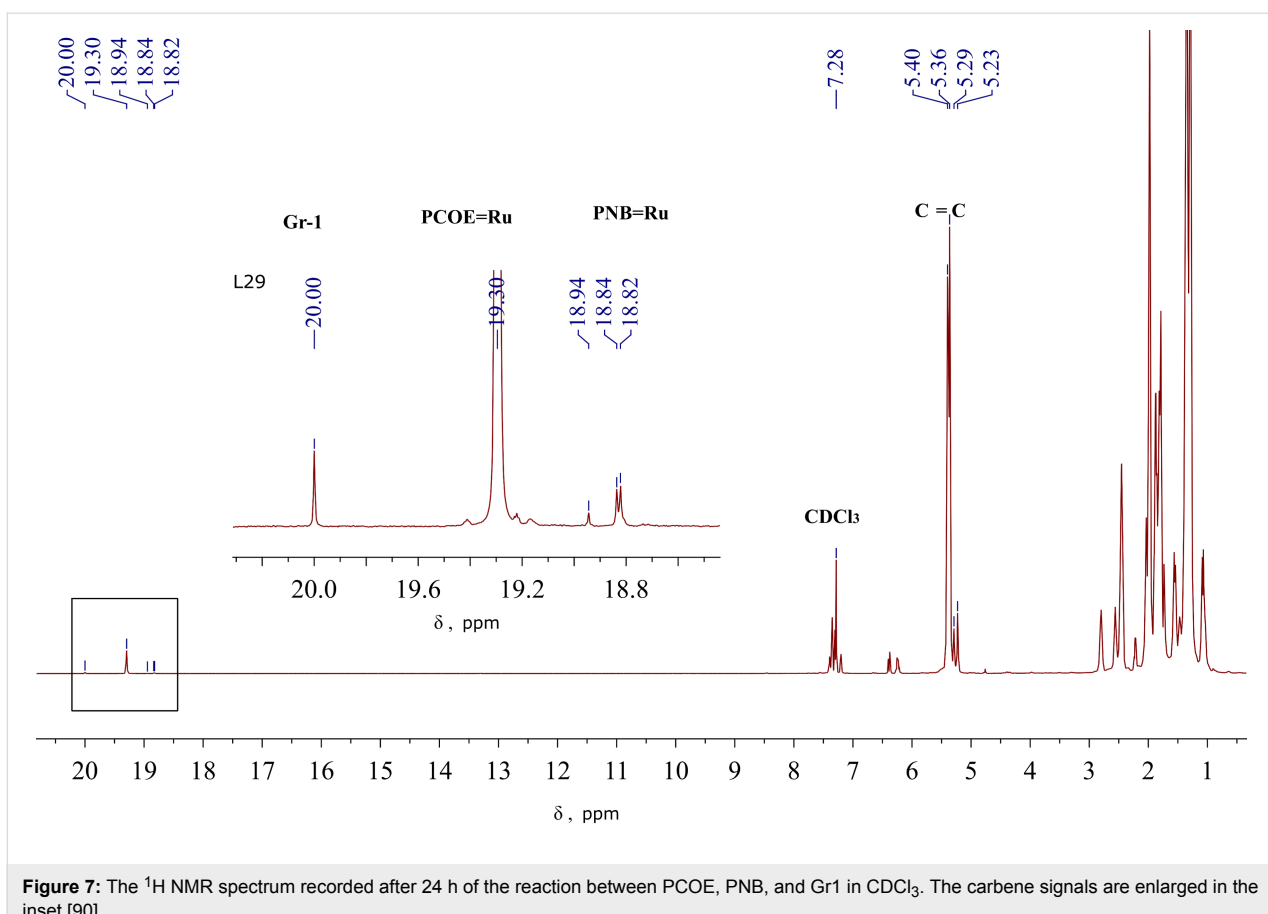


Figure 7: The ^1H NMR spectrum recorded after 24 h of the reaction between PCOE, PNB, and Gr1 in CDCl_3 . The carbene signals are enlarged in the inset [90].

influence the copolymer formation. For instance, the cross metathesis of commercial *cis*-PBD (97% *cis*, 2% *trans*, 1% vinyl) with *cis*-PI (94.5% *cis*, 5.5% *trans*) mediated by Gr1 led to a partial conversion of *cis*-double bonds in PBD units into the *trans*-configuration increasing its content from 2 to 9% [87]. On the opposite, the amount of *trans*-double bonds in PI decreased, which resulted in the increase of the *cis*-double bonds content from 94.5 to 99%. The authors explained this observation by the higher reactivity of isoprene *trans* units. However, the *cis*-PU was more active in the MCM reaction with PBD than *trans*-PU [85]. It seems that more research on this topic is needed. It is also worth mentioning that the MCM of 3-substituted PCOEs proceeds in a regioselective fashion, similar to the ROMP of 3-substituted COE monomers [86].

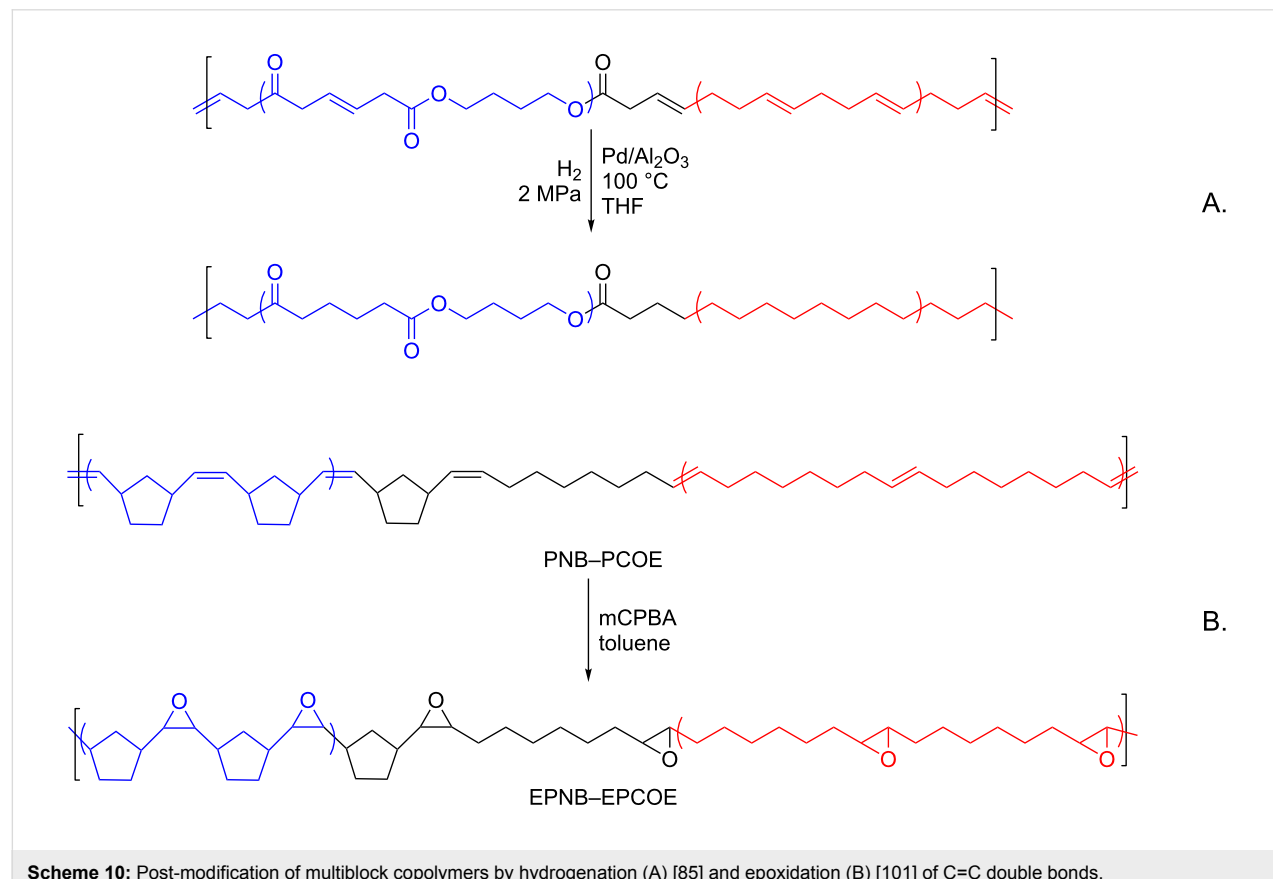
Choosing a suitable solvent is of vital importance for the effective implementation of MCM reactions. It should provide homogeneity of the reaction medium at a highest possible polymer concentration to minimize the impact of intrachain reactions [79]. At the same time increasing polymer concentration can lead to polymer/solvent and polymer/polymer phase separation. These issues can be controlled by light scattering

[90]. Another possible concern is related to the high viscosity of the initial polymer mixture, especially in the case of high molecular mass components, like PNB. Fortunately, upon the catalyst addition such mixtures rapidly become more fluid because of polymer-chain scission. The effect of solvent (THF and CH_2Cl_2) was studied for the MCM in the PBD–PU–Gr2 system [85] and it was found that the reaction in THF proceeded at a higher rate than in CH_2Cl_2 .

A decrease in the polymer molecular mass can be considered as a disadvantage of the MCM process. It takes place at the first stage of the reaction when Ru–polymer carbene active sites are formed as a result of the catalyst–polymer interaction. The decrease in M_n is observed during the first 1–2 hours and then it remains nearly unchanged [84]. The molecular mass of the resulting multiblock copolymer decreases with increasing the catalyst concentration [84,88]. Another reason for lowering the copolymer molecular mass is related to intramolecular metathesis that leads to low molecular mass cyclooligomers [77], which are lost during isolation of the reaction product. This negative effect can be partially counteracted by increasing the polymer concentration in the reaction mixture [84] in order to suppress intramolecular reactions.

The range of practical applications of multiblock copolymers can be significantly broadened through their functionalization. This goal can be achieved by introducing substituents into the parent homopolymers before MCM, just to mention 3-substituted PCOEs that are able to form stereoregular structures [86]. We introduced substituents into NB–COE copolymers by premodification of NB blocks or COE blocks (Figure 4F) [91,93]. A bulky Me_3Si -substituent that can enhance gas separation properties was introduced into NB copolymer blocks by the cross metathesis of poly(5-trimethylsilylnorbornene) with PCOE [89]. Kinetic studies demonstrated that a substituent in the NB monomer units considerably lowers the MCM rate. The introduction of hydroxy groups into COE units of a NB–COE copolymer met certain difficulties mainly related to the poor solubility of the parent poly(5-hydroxycyclooct-2-ene), PCOE(OH), homopolymer in common solvents [91,97]. The cross metathesis of PNB with PCOE(OH) in the presence of Gr2 was carried out only in a mixed solvent, CHCl_3 (10%)/MeOH. However, MCM was accompanied by partial hydrogenation of double bonds, especially for long reaction times. The ability of the Gr2 catalyst to form Ru–hydride complexes in the presence of alcohols is well-known and described in the literature [98,99]. Such complexes promoting C=C bond hydrogenation were detected in the PNB–PCOE(OH)–Gr2 system using

NMR [97]. It is curious that the resulting multiblock copolymers reveal some crystallinity, whereas the parent PNB and PCOE(OH) are fully amorphous. It can be explained if we recall that hydrogenated PNB is a semicrystalline polymer [100]. The $\text{Pd}/\text{Al}_2\text{O}_3$ catalyst was used to promote the hydrogenation of multiblock copolymers formed with the cross metathesis of PBD and olefin-containing polyester (Scheme 10A) [84]. It was shown that shortening the block length in both the olefinically unsaturated and hydrogenated copolymers resulted in a decrease, and, finally, in the extinction of T_m . At the same time multiblock copolymers with long blocks demonstrated two glass temperatures, which get closer to each other upon block shortening and then a single-phase copolymer with one T_g was formed [84,86–88]. Besides, the semitransparent, hard, and brittle copolymers obtained by MCM of PBD and polyesters became nearly transparent and flexible upon hydrogenation [84]. Another approach to the post-functionalization of NB–COE multiblock copolymers was implemented in reference [101] via double-bond epoxidation in the presence of *m*-chloroperbenzoic acid (Scheme 10B). It was found that this reaction proceeds more actively in the COE copolymer blocks than in the parent PCOE homopolymer. The epoxidation, as well hydrogenation, influenced the thermal and crystalline properties of the multiblock copolymers resulting in the increase of T_g



by 40–50 °C and T_m by 20–30 °C. It is quite natural that the degree of crystallinity and melting temperature are higher for the copolymers with longer COE blocks.

Copolymer crystallinity can be studied in detail by combining WAXD and DSC methods, including recently emerged technique of thermal fractionation by successive self-nucleation and annealing [84,92,102,103]. It was found that the width distribution of crystalline lamellae in NB–COE copolymers correlates with the average length of the *trans*-octenylene blocks. Compared with the pure PCOE or its equimolar blend with PNB, the NB–COE copolymers form considerably smaller crystallites (Figure 8) [92].

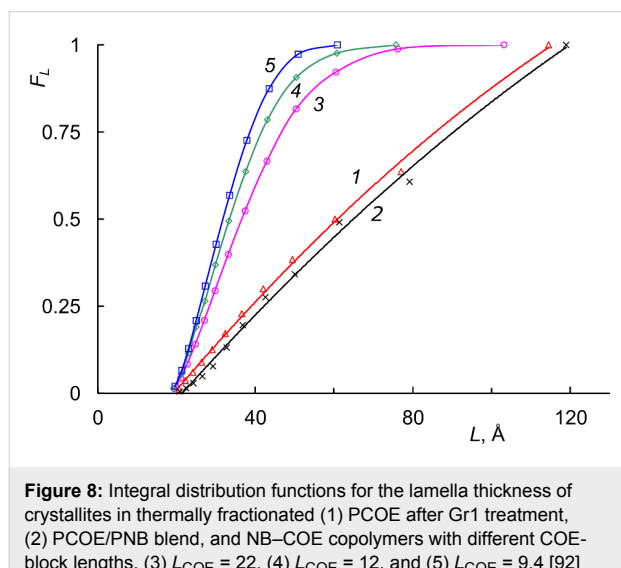


Figure 8: Integral distribution functions for the lamella thickness of crystallites in thermally fractionated (1) PCOE after Gr1 treatment, (2) PCOE/PNB blend, and NB–COE copolymers with different COE-block lengths, (3) $L_{COE} = 22$, (4) $L_{COE} = 12$, and (5) $L_{COE} = 9.4$ [92]

Conclusion

It is rather clear nowadays that the olefin-metathesis reaction is a versatile tool for the synthesis of multiblock copolymers with diverse chemical structures. Due to the rapid progress in the catalyst design for living polymerization, sequential ROMP has become a well-established method of obtaining copolymers with sequence-defined structures. However, in many aspects, this technique remains laborious and even cumbersome. Most publications report on the multiblock copolymers synthesis by the coupling of premade individual blocks. A key point here is related to advances in the development of synthetic approaches for fabricating symmetric and asymmetric telechelics and monochelics, macromonomers and macrocycles based on different olefin-metathesis techniques like CTA, ADMET, etc. A subsequent assembling of macroblocks into copolymers can be carried out by combining olefin metathesis with other reactions such as ATRP, RAFT, click-reaction, and so on, which permit to gain certain control over the final copolymer structures. The most recent approach to the multiblock copolymer synthesis

implements the macromolecular cross-metathesis reaction, which is still poorly studied. For this method, the simplicity of realization is counterweighted by inability of precise control over block sequences and considerable drop in the average molecular mass of reacting polymers as a result of their interaction with metathesis catalysts. Nevertheless, the average block lengths can be easily tailored and the resulting copolymers reveal the ability to self-assemble into ordered structures, enhanced mechanical properties, and nontrivial crystalline and thermal characteristics. Recent kinetic studies with the use of *in situ* and *ex situ* NMR have shed some light on the regularities of the macromolecular cross-metathesis reaction, which appeared to be somewhat opposite to the notions about metathesis copolymerization. Perspectives of the entire field under review are related to the elaboration of novel post-modification methods for obtaining new functionalities and enhancing various characteristics of multiblock copolymers. In our opinion, further development of the olefin metathesis methods for the multiblock copolymer synthesis will be directed by the search for new properties and possible applications.

Acknowledgements

The authors are thankful to the Russian Foundation for Basic Research (project 17-03-00596). Yu. I. Denisova was personally supported by the same foundation (project 16-33-60213).

ORCID® IDs

Maria L. Gringolts - <https://orcid.org/0000-0002-4607-2558>
 Yulia I. Denisova - <https://orcid.org/0000-0002-0778-0930>
 Eugene Sh. Finkelshtein - <https://orcid.org/0000-0002-9460-9081>
 Yaroslav V. Kudryavtsev - <https://orcid.org/0000-0002-5462-6792>

References

1. Bielawski, C. W.; Grubbs, R. H. *Prog. Polym. Sci.* **2007**, *32*, 1–29. doi:10.1016/j.progpolymsci.2006.08.006
2. Grubbs, R. H., Ed. *Handbook of Metathesis. Vol. 3: Applications in Polymer Synthesis*; Wiley-VCH Verlag GmbH & Co: Weinheim, Germany, 2003. doi:10.1002/9783527619481
3. Grubbs, R. H.; Khosravi, E., Eds. *Handbook of Metathesis. Vol. 3: Polymer Synthesis*, 2nd ed.; Wiley-VCH Verlag GmbH & Co: Weinheim, Germany, 2015.
4. Verduzco, R.; Li, X.; Pesek, S. L.; Stein, G. E. *Chem. Soc. Rev.* **2015**, *44*, 2405–2420. doi:10.1039/c4cs00329b
5. Liberman-Martin, A. L.; Chu, C. K.; Grubbs, R. H. *Macromol. Rapid Commun.* **2017**, *38*, 1700058. doi:10.1002/marc.201700058
6. Yu, Y.-G.; Chae, C.-G.; Kim, M.-J.; Seo, H.-B.; Grubbs, R. H.; Lee, J.-S. *Macromolecules* **2018**, *51*, 447–455. doi:10.1021/acs.macromol.7b02447
7. Descour, C.; Macko, T.; Schreur-Piet, I.; Pepels, M. P. F.; Duchateau, R. *RSC Adv.* **2015**, *5*, 9658–9666. doi:10.1039/c4ra11056k
8. Bates, C. M.; Bates, F. S. *Macromolecules* **2017**, *50*, 3–22. doi:10.1021/acs.macromol.6b02355

9. Bates, F. S.; Hillmyer, M. A.; Lodge, T. P.; Bates, C. M.; Delaney, K. T.; Fredrickson, G. H. *Science* **2012**, *336*, 434–440. doi:10.1126/science.1215368
10. Constantinou, A. P.; Georgiou, T. K. Thermoresponsive Multiblock Copolymers: Chemistry, Properties and Applications. In *Temperature-Responsive Polymers: Chemistry, Properties, and Applications*; Khutoryanskiy, V. V.; Georgiou, T. K., Eds.; Wiley, 2018; pp 35–67. doi:10.1002/9781119157830.ch2
11. Lutz, J.-F., Ed. *Sequence-Controlled Polymers*; Wiley-VCH Verlag GmbH & Co: Weinheim, Germany, 2017. doi:10.1002/9783527806096
12. Bates, C. M.; Maher, M. J.; Janes, D. W.; Ellison, C. J.; Willson, C. G. *Macromolecules* **2014**, *47*, 2–12. doi:10.1021/ma401762n
13. Topham, P. D.; Parnell, A. J.; Hiorns, R. C. *J. Polym. Sci., Part B: Polym. Phys.* **2011**, *49*, 1131–1156. doi:10.1002/polb.22302
14. Abetz, V. *Macromol. Rapid Commun.* **2015**, *36*, 10–22. doi:10.1002/marc.201400556
15. Kim, H.-C.; Park, S.-M.; Hinsberg, W. D. *Chem. Rev.* **2010**, *110*, 146–177. doi:10.1021/cr900159v
16. Hillmyer, M. *Curr. Opin. Solid State Mater. Sci.* **1999**, *4*, 559–564. doi:10.1016/s1359-0286(00)00006-1
17. Riegler, S.; Slugovc, C.; Trimmel, G.; Stelzer, F. *Macromol. Symp.* **2004**, *217*, 231–246. doi:10.1002/masy.2004451319
18. Schacher, F. H.; Rupar, P. A.; Manners, I. *Angew. Chem., Int. Ed.* **2012**, *51*, 7898–7921. doi:10.1002/anie.201200310
19. de Gennes, P. G. *Faraday Discuss. Chem. Soc.* **1979**, *68*, 96–103. doi:10.1039/dc9796800096
20. Fleury, G.; Bates, F. S. *Macromolecules* **2009**, *42*, 1691–1694. doi:10.1021/ma900060f
21. Angerman, H.; ten Brinke, G.; Erukhimovich, I. *Macromolecules* **1996**, *29*, 3255–3262. doi:10.1021/ma950961b
22. Subbotin, A.; Klymko, T.; ten Brinke, G. *Macromolecules* **2007**, *40*, 2915–2918. doi:10.1021/ma062889v
23. Govorun, E. N.; Chertovich, A. V. *J. Chem. Phys.* **2017**, *146*, 034903. doi:10.1063/1.4973933
24. Houdayer, J.; Müller, M. *Macromolecules* **2004**, *37*, 4283–4295. doi:10.1021/ma035814p
25. Chertovich, A. V.; Guseva, D. V.; Kudryavtsev, Y. V.; Litmanovich, A. D. *Polym. Sci., Ser. A* **2008**, *50*, 451–461. doi:10.1134/s0965545x08040147
26. Gavrilov, A. A.; Kudryavtsev, Y. V.; Khalatur, P. G.; Chertovich, A. V. *Chem. Phys. Lett.* **2011**, *503*, 277–282. doi:10.1016/j.cplett.2011.01.024
27. Govorun, E. N.; Gavrilov, A. A.; Chertovich, A. V. *J. Chem. Phys.* **2015**, *142*, No. 204903. doi:10.1063/1.4921685
28. Ueda, M. *Prog. Polym. Sci.* **1999**, *24*, 699–730. doi:10.1016/s0079-6700(99)00014-3
29. Chum, P. S.; Swogger, K. W. *Prog. Polym. Sci.* **2008**, *33*, 797–819. doi:10.1016/j.progpolymsci.2008.05.003
30. Lutz, J.-F. *Acc. Chem. Res.* **2013**, *46*, 2696–2705. doi:10.1021/ar400097a
31. Soeriyadi, A. H.; Boyer, C.; Nyström, F.; Zetterlund, P. B.; Whittaker, M. R. *J. Am. Chem. Soc.* **2011**, *133*, 11128–11131. doi:10.1021/ja205080u
32. Alsubaie, F.; Anastasaki, A.; Wilson, P.; Haddleton, D. M. *Polym. Chem.* **2015**, *6*, 406–417. doi:10.1039/c4py01066c
33. Engelis, N. G.; Anastasaki, A.; Nurumbetov, G.; Truong, N. P.; Nikolaou, V.; Shegiwal, A.; Whittaker, M. R.; Davis, T. P.; Haddleton, D. M. *Nat. Chem.* **2017**, *9*, 171–178. doi:10.1038/nchem.2634
34. Martin, L.; Gody, G.; Perrier, S. *Polym. Chem.* **2015**, *6*, 4875–4886. doi:10.1039/c5py00478k
35. Litmanovich, A. D.; Platé, N. A.; Kudryavtsev, Y. V. *Prog. Polym. Sci.* **2002**, *27*, 915–970. doi:10.1016/s0079-6700(02)00003-5
36. Maeda, T.; Otsuka, H.; Takahara, A. *Prog. Polym. Sci.* **2009**, *34*, 581–604. doi:10.1016/j.progpolymsci.2009.03.001
37. Ayres, N.; Weck, M. *Polym. Chem.* **2012**, *3*, 3031–3032. doi:10.1039/c2py90036j
38. Ghassemi, H.; McGrath, J. E.; Zawodzinski, T. A., Jr. *Polymer* **2006**, *47*, 4132–4139. doi:10.1016/j.polymer.2006.02.038
39. You, Y.-Z.; Zhou, Q.-H.; Manickam, D. S.; Wan, L.; Mao, G.-Z.; Oupický, D. *Macromolecules* **2007**, *40*, 8617–8624. doi:10.1021/ma071176p
40. Zhang, H.; Shen, P. K. *Chem. Rev.* **2012**, *112*, 2780–2832. doi:10.1021/cr200035s
41. Zhang, J.; Bates, F. S. *J. Am. Chem. Soc.* **2012**, *134*, 7636–7639. doi:10.1021/ja301770v
42. Lee, I.; Bates, F. S. *Macromolecules* **2013**, *46*, 4529–4539. doi:10.1021/ma400479b
43. Liu, G.; Guan, Y.; Wen, T.; Wang, X.; Zhang, X.; Wang, D.; Li, X.; Loos, J.; Chen, H.; Walton, K.; Marchand, G. *Polymer* **2011**, *52*, 5221–5230. doi:10.1016/j.polymer.2011.09.009
44. Lee, I.; Panthani, T. R.; Bates, F. S. *Macromolecules* **2013**, *46*, 7387–7398. doi:10.1021/ma401508b
45. Park, C. H.; Lee, C. H.; Guiver, M. D.; Lee, Y. M. *Prog. Polym. Sci.* **2011**, *36*, 1443–1498. doi:10.1016/j.progpolymsci.2011.06.001
46. Ilyin, S. O.; Malkin, A. Y.; Kulichikhin, V. G.; Denisova, Y. I.; Krentsel, L. B.; Shandryuk, G. A.; Litmanovich, A. D.; Litmanovich, E. A.; Bondarenko, G. N.; Kudryavtsev, Y. V. *Macromolecules* **2014**, *47*, 4790–4804. doi:10.1021/ma5003326
47. Li, S.; Register, R. A.; Weinhold, J. D.; Landes, B. G. *Macromolecules* **2012**, *45*, 5773–5781. doi:10.1021/ma300910m
48. Choi, T.-L.; Grubbs, R. H. *Angew. Chem.* **2003**, *115*, 1785–1788. doi:10.1002/ange.200250632
49. Trnka, T. M.; Grubbs, R. H. *Acc. Chem. Res.* **2001**, *34*, 18–29. doi:10.1021/ar000114f
50. Nomura, K.; Schrock, R. R. *Macromolecules* **1996**, *29*, 540–545. doi:10.1021/ma9512519
51. Miyamoto, Y.; Fujiki, M.; Nomura, K. *J. Polym. Sci., Part A: Polym. Chem.* **2004**, *42*, 4248–4265. doi:10.1002/pola.20286
52. Rahman, M. A.; Lokupitiya, H. N.; Ganewatta, M. S.; Yuan, L.; Stefk, M.; Tang, C. *Macromolecules* **2017**, *50*, 2069–2077. doi:10.1021/acs.macromol.7b00001
53. Alonso-Villanueva, J.; Rodríguez, M.; Vilas, J. L.; Laza, J. M.; León, L. M. *J. Macromol. Sci., Part A: Pure Appl. Chem.* **2010**, *47*, 1130–1134. doi:10.1080/10601325.2010.511539
54. Liaw, D.-J.; Wu, P.-L. *J. Mol. Catal. A: Chem.* **2000**, *160*, 35–43. doi:10.1016/s1381-1169(00)00230-2
55. Pitet, L. M.; Zhang, J.; Hillmyer, M. A. *Dalton Trans.* **2013**, *42*, 9079–9088. doi:10.1039/c2dt32695g
56. Banik, S. M.; Monnot, B. L.; Weber, R. L.; Mahanthappa, M. K. *Macromolecules* **2011**, *44*, 7141–7148. doi:10.1021/ma201278x
57. Mahanthappa, M. K.; Lim, L. S.; Hillmyer, M. A.; Bates, F. S. *Macromolecules* **2007**, *40*, 1585–1593. doi:10.1021/ma0617421
58. Bishop, J. P.; Register, R. A. *Macromolecules* **2010**, *43*, 4954–4960. doi:10.1021/ma100314z
59. Miki, K.; Kimura, A.; Oride, K.; Kuramochi, Y.; Matsuoka, H.; Harada, H.; Hiraoka, M.; Ohe, K. *Angew. Chem., Int. Ed.* **2011**, *50*, 6567–6570. doi:10.1002/anie.201101005

60. Ahmed, E.; Morton, S. W.; Hammond, P. T.; Swager, T. M. *Adv. Mater.* **2013**, *25*, 4504–4510. doi:10.1002/adma.201301656

61. Ding, L.; Zhang, L.; Yang, D.; Huang, W.; Xie, M.; Zhang, Y. *Polymer* **2010**, *51*, 1285–1292. doi:10.1016/j.polymer.2010.02.001

62. Copenhafer, J. E.; Meyer, T. Y. *Polym. Prepr.* **2005**, *46*, 1022–1023.

63. Abdellatif, M. M.; Nomura, K. *ACS Macro Lett.* **2012**, *1*, 423–427. doi:10.1021/mz300061a

64. Nomura, K.; Haque, T.; Onuma, T.; Hajjaj, F.; Asano, M. S.; Inagaki, A. *Macromolecules* **2013**, *46*, 9563–9574. doi:10.1021/ma4022554

65. Hu, N.; Mai, C.-K.; Fredrickson, G. H.; Bazan, G. C. *Chem. Commun.* **2016**, *52*, 2237–2240. doi:10.1039/c5cc09200k

66. Gutekunst, W. R.; Hawker, C. J. *J. Am. Chem. Soc.* **2015**, *137*, 8038–8041. doi:10.1021/jacs.5b04940

67. Xia, Y.; Olsen, B. D.; Kornfield, J. A.; Grubbs, R. H. *J. Am. Chem. Soc.* **2009**, *131*, 18525–18532. doi:10.1021/ja908379q

68. Kim, J. G.; Coates, G. W. *Macromolecules* **2012**, *45*, 7878–7883. doi:10.1021/ma301137q

69. Murphy, J. J.; Kawasaki, T.; Fujiki, M.; Nomura, K. *Macromolecules* **2005**, *38*, 1075–1083. doi:10.1021/ma047887u

70. Xie, M.; Wang, W.; Ding, L.; Liu, J.; Yang, D.; Wei, L.; Zhang, Y. *J. Polym. Sci., Part A: Polym. Chem.* **2010**, *48*, 380–388. doi:10.1002/pola.23795

71. Hilf, S.; Kilbinger, A. F. M. *Macromolecules* **2009**, *42*, 4127–4133. doi:10.1021/ma900036c

72. Hilf, S.; Kilbinger, A. F. M. *Macromolecules* **2009**, *42*, 1099–1106. doi:10.1021/ma802440k

73. Moatsou, D.; Nagarkar, A.; Kilbinger, A. F. M.; O'Reilly, R. K. *J. Polym. Sci., Part A: Polym. Chem.* **2016**, *54*, 1236–1242. doi:10.1002/pola.27964

74. Yang, S. K.; Ambade, A. V.; Weck, M. *Chem. – Eur. J.* **2009**, *15*, 6605–6611. doi:10.1002/chem.200900573

75. Meng, X.; Tang, G.-R.; Jin, G.-X. *Chem. Commun.* **2008**, 3178–3180. doi:10.1039/b803382j

76. Zou, Y.; Wang, D.; Wurst, K.; Kühnel, C.; Reinhardt, I.; Decker, U.; Gurram, V.; Camadanli, S.; Buchmeiser, M. R. *Chem. – Eur. J.* **2011**, *17*, 13832–13846. doi:10.1002/chem.201101829

77. Ivin, K. J.; Mol, J. C. *Olefin Metathesis and Metathesis Polymerization*; Academic Press: London, 1997. doi:10.1016/b978-0-12-377045-5.x5000-9

78. Bertrand, A.; Hillmyer, M. A. *J. Am. Chem. Soc.* **2013**, *135*, 10918–10921. doi:10.1021/ja4050532

79. Monfette, S.; Fogg, D. E. *Chem. Rev.* **2009**, *109*, 3783–3816. doi:10.1021/cr800541y

80. Gutiérrez, S.; Tlenkopatchev, M. A. *Rev. Latinoam. Metal. Mater.* **2009**, *S1*, 1463–1467.

81. Michel, X.; Fouquay, S.; Michaud, G.; Simon, F.; Brusson, J.-M.; Carpentier, J.-F.; Guillaume, S. M. *Eur. Polym. J.* **2017**, *96*, 403–413. doi:10.1016/j.eurpolymj.2017.09.027

82. Wagner, N. L.; Timmers, F. J.; Arriola, D. J.; Jueptner, G.; Landes, B. G. *Macromol. Rapid Commun.* **2008**, *29*, 1438–1443. doi:10.1002/marc.200800344

83. Otsuka, H.; Muta, T.; Sakada, M.; Maeda, T.; Takahara, A. *Chem. Commun.* **2009**, 1073–1075. doi:10.1039/b818014h

84. Maeda, T.; Kamimura, S.; Ohishi, T.; Takahara, A.; Otsuka, H. *Polymer* **2014**, *55*, 6245–6251. doi:10.1016/j.polymer.2014.10.001

85. Ohishi, T.; Suyama, K.; Kamimura, S.; Sakada, M.; Imato, K.; Kawahara, S.; Takahara, A.; Otsuka, H. *Polymer* **2015**, *78*, 145–153. doi:10.1016/j.polymer.2015.09.076

86. Radlauer, M. R.; Matta, M. E.; Hillmyer, M. A. *Polym. Chem.* **2016**, *7*, 6269–6278. doi:10.1039/c6py01231k

87. Daniele, S.; Mariconda, A.; Guerra, G.; Longo, P.; Giannini, L. *Polymer* **2017**, *130*, 143–149. doi:10.1016/j.polymer.2017.10.008

88. Gringolts, M. L.; Denisova, Y. I.; Shandryuk, G. A.; Krentsel, L. B.; Litmanovich, A. D.; Finkelshtein, E. S.; Kudryavtsev, Y. V. *RSC Adv.* **2015**, *5*, 316–319. doi:10.1039/c4ra12001a

89. Denisova, Y. I.; Gringolts, M. L.; Krentsel', L. B.; Shandryuk, G. A.; Litmanovich, A. D.; Finkelshtein, E. S.; Kudryavtsev, Y. V. *Polym. Sci., Ser. B* **2016**, *58*, 292–297. doi:10.1134/s1560090416030040

90. Denisova, Y. I.; Gringolts, M. L.; Peregudov, A. S.; Krentsel, L. B.; Litmanovich, E. A.; Litmanovich, A. D.; Finkelshtein, E. S.; Kudryavtsev, Y. V. *Beilstein J. Org. Chem.* **2015**, *11*, 1796–1808. doi:10.3762/bjoc.11.195

91. Denisova, Y. I.; Gringolts, M. L.; Roenko, A. V.; Shandryuk, G. A.; Finkelshtein, E. S.; Kudryavtsev, Y. V. *Mendeleev Commun.* **2017**, *27*, 416–418. doi:10.1016/j.mencom.2017.07.034

92. Shandryuk, G. A.; Denisova, Y. I.; Gringolts, M. L.; Krentsel, L. B.; Litmanovich, A. D.; Finkelshtein, E. S.; Kudryavtsev, Y. V. *Eur. Polym. J.* **2017**, *86*, 143–153. doi:10.1016/j.eurpolymj.2016.11.025

93. Denisova, Y. I.; Gringolts, M. L.; Krentsel', L. B.; Shandryuk, G. A.; Peregudov, A. S.; Finkelshtein, E. S.; Kudryavtsev, Y. V. *Polym. Sci., Ser. B* **2017**, *59*, 412–420. doi:10.1134/s1560090417040030

94. Naga, N.; Kikuchi, G.; Toyota, A. *Polymer* **2006**, *47*, 6081–6090. doi:10.1016/j.polymer.2006.06.015

95. Bornand, M.; Chen, P. *Angew. Chem., Int. Ed.* **2005**, *44*, 7909–7911. doi:10.1002/anie.200502606

96. Schleyer, P. v. R.; Williams, J. E.; Blanchard, K. R. *J. Am. Chem. Soc.* **1970**, *92*, 2377–2386. doi:10.1021/ja00711a030

97. Denisova, Y. I.; Roenko, A. V.; Gringolts, M. L.; Krentsel, L. B.; Peregudov, A. S.; Shandryuk, G. A.; Finkelshtein, E. S.; Kudryavtsev, Y. V. *Polym. Sci., Ser. B* **2019**, *61*, in press. doi:10.1134/s1560090418060052

98. Digner, M. B.; Mol, J. C. *Eur. J. Inorg. Chem.* **2003**, 2827–2833. doi:10.1002/ejic.200200702

99. Edwards, M. G.; Jazzar, R. F. R.; Paine, B. M.; Shermer, D. J.; Whittlesey, M. K.; Williams, J. M. J.; Edney, D. D. *Chem. Commun.* **2004**, 90–91. doi:10.1039/b312162c

100. Lee, L.-B. W.; Register, R. A. *Macromolecules* **2005**, *38*, 1216–1222. doi:10.1021/ma048013a

101. Morontsev, A. A.; Denisova, Y. I.; Gringolts, M. L.; Filatova, M. P.; Shandryuk, G. A.; Finkelshtein, E. S.; Kudryavtsev, Y. V. *Polym. Sci., Ser. B* **2018**, *60*, 688–698. doi:10.1134/s1560090418050111

102. Müller, A. J.; Amal, M. L. *Prog. Polym. Sci.* **2005**, *30*, 559–603. doi:10.1016/j.progpolymsci.2005.03.001

103. Müller, A. J.; Michell, R. M.; Pérez, R. A.; Lorenzo, A. T. *Eur. Polym. J.* **2015**, *65*, 132–154. doi:10.1016/j.eurpolymj.2015.01.015

License and Terms

This is an Open Access article under the terms of the Creative Commons Attribution License (<http://creativecommons.org/licenses/by/4.0>). Please note that the reuse, redistribution and reproduction in particular requires that the authors and source are credited.

The license is subject to the *Beilstein Journal of Organic Chemistry* terms and conditions:
(<https://www.beilstein-journals.org/bjoc>)

The definitive version of this article is the electronic one which can be found at:
[doi:10.3762/bjoc.15.21](https://doi.org/10.3762/bjoc.15.21)



Application of olefin metathesis in the synthesis of functionalized polyhedral oligomeric silsesquioxanes (POSS) and POSS-containing polymeric materials

Patrycja Źak and Cezary Pietraszuk*

Review

Open Access

Address:

Adam Mickiewicz University in Poznań, Faculty of Chemistry,
Umultowska 89b, 61-614 Poznań, Poland

Beilstein J. Org. Chem. **2019**, *15*, 310–332.

doi:10.3762/bjoc.15.28

Email:

Cezary Pietraszuk* - pietrasz@amu.edu.pl

Received: 26 October 2018

Accepted: 07 January 2019

Published: 04 February 2019

* Corresponding author

This article is part of the thematic issue "Progress in metathesis chemistry III".

Keywords:

olefin metathesis; POSS; silsesquioxanes

Guest Editors: K. Grela and A. Kajetanowicz

© 2019 Źak and Pietraszuk; licensee Beilstein-Institut.

License and terms: see end of document.

Abstract

This mini-review summarizes the applications of olefin metathesis in synthesis and functionalization of polyhedral oligomeric silsesquioxanes (POSS) and POSS-containing polymeric materials. Three types of processes, i.e., cross metathesis (CM) of vinyl-substituted POSS with terminal olefins, acyclic diene metathesis (ADMET) copolymerization of divinyl-substituted POSS with α,ω -dienes and ring-opening metathesis polymerization (ROMP) of POSS-substituted norbornene (or other ROMP susceptible cycloolefins) are discussed. Emphasis was put on the synthetic and catalytic aspects rather than on the properties and applications of synthesized materials.

Introduction

Silsesquioxanes are nanostructures described by the empirical formula $RSiO_{3/2}$, where R represents hydrogen, alkyl, alkenyl, aryl, arylene or their functionalized derivatives. A number of silsesquioxane structures have been reported including random, ladder, cage and partial cage structures. Silsesquioxanes with specific cage structures are commonly referred as polyhedral oligomeric silsesquioxanes (POSS). From among POSS structures the most thoroughly studied is a cubic silsesquioxane unit, denoted also as T_8 . It contains an inorganic cubic core

composed of eight Si atoms at the vertices, connected through O atoms along the edges, chemically bonded with eight different or similar organic substituents so that it represents a truly hybrid architecture. The cubic silsesquioxane unit is characterized by a three-dimensional nanoscopic size structure with approximate Si–Si distance equal to 0.5 nm and an approximate R–R distance of 1.5 nm (Figure 1). The synthesis, structure and properties of POSS have been extensively reviewed [1–3].

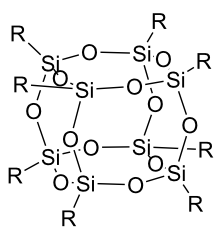


Figure 1: Cubic octasilsesquioxane.

Proper selection of organic substituents R allows the modification of solubility of POSS in reaction media, its compatibility with polymers, biological systems, or surfaces. The introduction of one or more reactive groups into the POSS structure permits their further chemical modification. Because of the ease of the synthesis as well as the commercial availability of polyhedral oligomeric silsesquioxanes containing vinyl groups (which is a common functional group used in organosilicon chemistry), POSS are often functionalized through the chemical processes of C=C bond transformation, e.g., hydrosilylation, Heck coupling, silylative coupling and olefin metathesis.

Olefin metathesis, i.e., catalytic exchange of double bonds between carbon atoms, is a powerful tool in organic synthesis. The use of metathesis in organic and polymer synthesis is comprehensively described in excellent monographs [4–6]. However, the literature does not offer a more detailed review on the application of metathesis in the synthesis of functionalized polyhedral oligomeric silsesquioxanes (POSS). The lack of a pertinent overview in this field has prompted us to summarize the reported applications of olefin metathesis in the synthesis and functionalization of oligomeric silsesquioxanes and POSS-containing polymeric materials. This review is focused on the synthetic and catalytic aspects rather than on the properties and applications of the resulting materials.

Vinylsilanes show a specific reactivity towards alkylidene ruthenium complexes because of a strong effect of the silyl group on the properties of the double bond. In general, the substituents at the silicon atom determine the regioselectivity of the vinylsilane cycloaddition to the Ru=C bond. The knowledge of this untypical reactivity is pivotal for the application of metathesis for the modification of vinylsilanes, vinyl-substituted siloxanes, spherasilicates and silsesquioxanes. The appropriate choice of substituents permits the control of the process to a certain degree. The reactivity of vinylsilanes with different substituents at silicon towards alkylidene ruthenium complexes is illustrated in Scheme 1 [7].

According to Scheme 1a, as a result of the reaction of trialkoxy-, tris(trimethylsiloxy)-, trichloro- or dichloromethyl-substi-

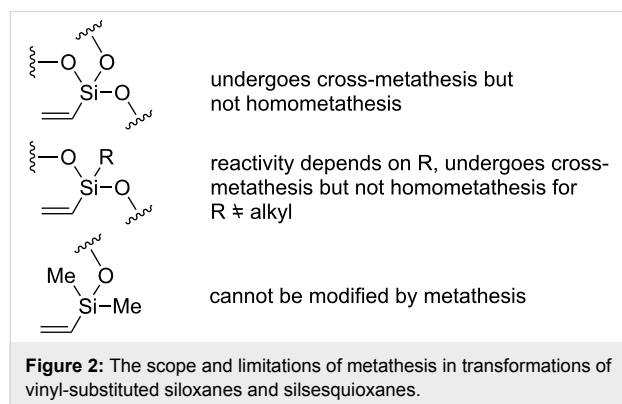
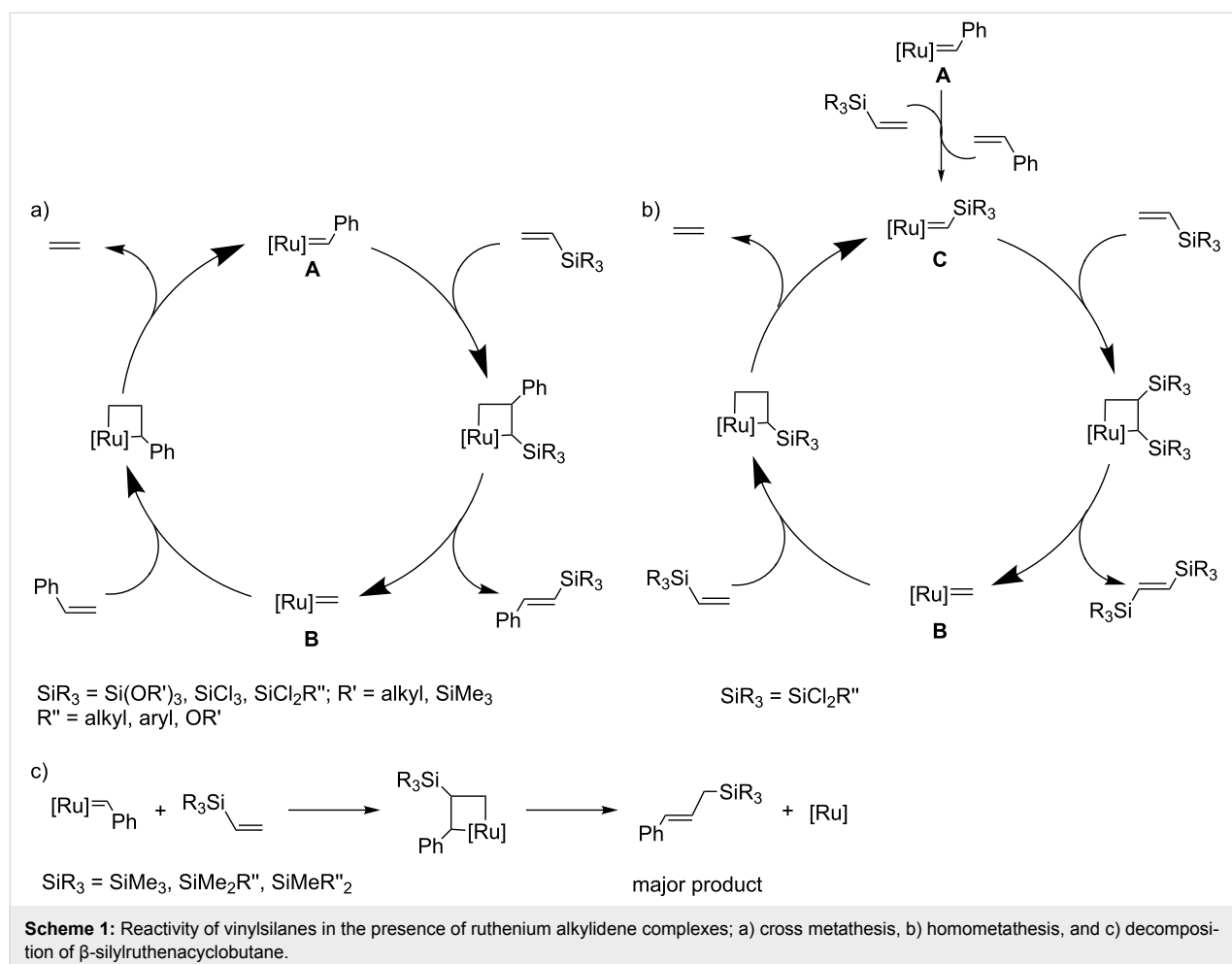
tuted vinylsilanes with Grubbs catalyst of first or second generation (**A**), the active methylene complex **B** and the corresponding (*E*)-1-phenyl-2-(silyl)ethene are formed. The methylene complex **B** in the presence of styrene undergoes metathetic conversion to benzylidene complex **A** and ethene. When dichloro-substituted vinylsilanes are used, the pathway shown in Scheme 1b is also possible. Metathesis of dichloro-substituted vinylsilanes with Grubbs catalyst **A** leads to styrene and (silyl)methylidene complex **C**. Formation of (silyl)methylidene complex **C** has not been confirmed by spectroscopic methods. The reaction of the postulated complex **C** with vinylsilane gives the corresponding (*E*)-1,2-bis(silyl)ethenes and the methylene complex **B**. The methylene complex **B** may react with vinylsilane to form ethene and regenerate complex **C**. In the presence of vinylsilanes containing alkyl substituents the Grubbs catalyst undergoes fast decomposition as a result of β -transfer of the silyl group in the appropriate β -(silyl)rutenacyclobutane complex to ruthenium followed by reductive elimination of the corresponding propene derivative (Scheme 1c). The transformation resulted in complexes that do not contain a carbene ligand and do not show catalytic activity in metathesis.

The most important consequences of the above-described reactivity in metathesis of vinyl-substituted siloxanes, spherasilicates and silsesquioxanes are presented in Figure 2. It should be indicated that one of the consequences of the described reactivity is the inactivity of vinylsilsesquioxane in homo-metathesis.

The limitations apply to silanes containing a double bond located directly at the silyl group and do not apply to allylsilanes and other alkenylsilanes, which behave like terminal olefins and readily undergo metathesis.

Application of metathesis in chemistry of unsaturated derivatives of POSS is limited to three types of processes, i.e., cross metathesis (CM) of vinyl-substituted POSS with terminal olefins, acyclic diene metathesis (ADMET) copolymerization of divinyl-substituted POSS with α,ω -dienes and ring-opening metathesis polymerization (ROMP) of POSS-substituted norbornene (or other ROMP susceptible cycloolefins, Scheme 2).

Nearly all metathetic transformations described in this review have been performed in the presence of commonly used ruthenium-based catalysts (Figure 3). In contrast, there are only a few examples of application of molybdenum-based complexes in modification of silsesquioxanes (Figure 3), which can be explained as related to the sensitivity of these complexes toward atmospheric oxygen, moisture and functional groups of reagents.



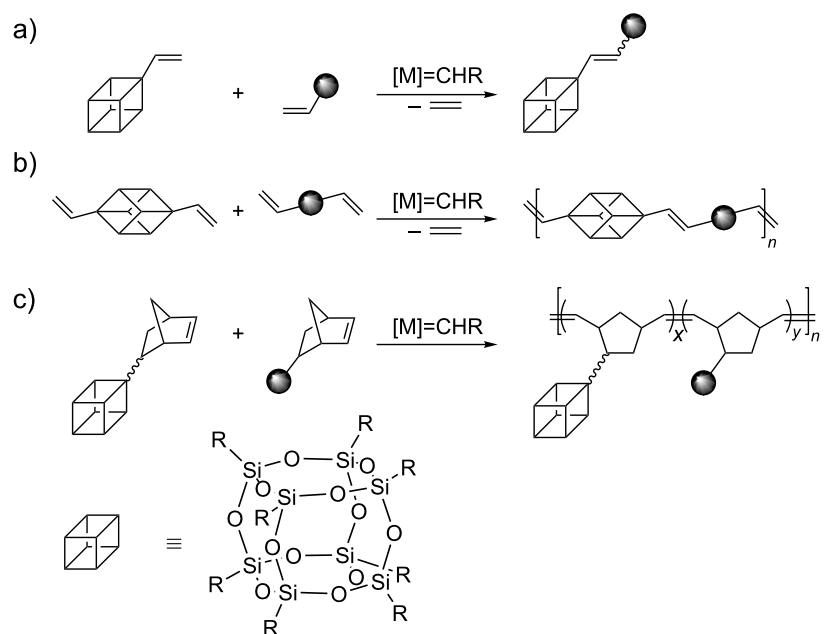
Review

Cross metathesis of vinyl-substituted silsesquioxanes

The first metathetic transformations of vinyl-substituted silsesquioxanes and spherocilicates (Figure 4) were reported by Feher in 1997 [8]. In the presence of molybdenum alkylidene complex **Mo-1** octavinylsilsesquioxane (OVS) underwent cross metathesis of terminal and internal olefins, functionalized

olefins (such as allyltrimethoxysilane, ethyl undec-10-enylate, oct-7-enyltrimethoxysilane, 5-bromopentene, pent-4-en-1-ol) and styrene.

Moreover, the catalytic activity of the first generation Grubbs' catalyst (**Ru-1**) was demonstrated in CM of OVS with pent-4-en-1-ol and 5-bromopentene. It has been found that terminal alkenes undergo cross metathesis much more readily and are clearly better than internal alkenes from the cost perspective. However, internal alkenes are less volatile and cannot produce any ethene, which makes them interesting starting materials. A slight vacuum had to be applied to reactions with terminal alkenes in order to remove ethene, because ethene would strongly slow down the desired cross metathesis and inactivate Schrock-type metathesis catalysts. CM of OVS with styrenes proceeded stereoselectively. A mixture of *cis*- and *trans*-isomers was obtained in the transformations of other olefins tested. Spherocilicate was shown to undergo CM with pent-1-ene and styrene in the presence of **Mo-1**. No data on the activity of **Ru-1** in metathesis transformation of spherocilicates was provided.



Scheme 2: Application of olefin metathesis in the synthesis and modification of POSS-based materials: a) functionalization of vinyl-substituted POSS via cross metathesis; b) synthesis of POSS-containing polymers via acyclic diene metathesis; c) synthesis of POSS-containing copolymers via ROMP.

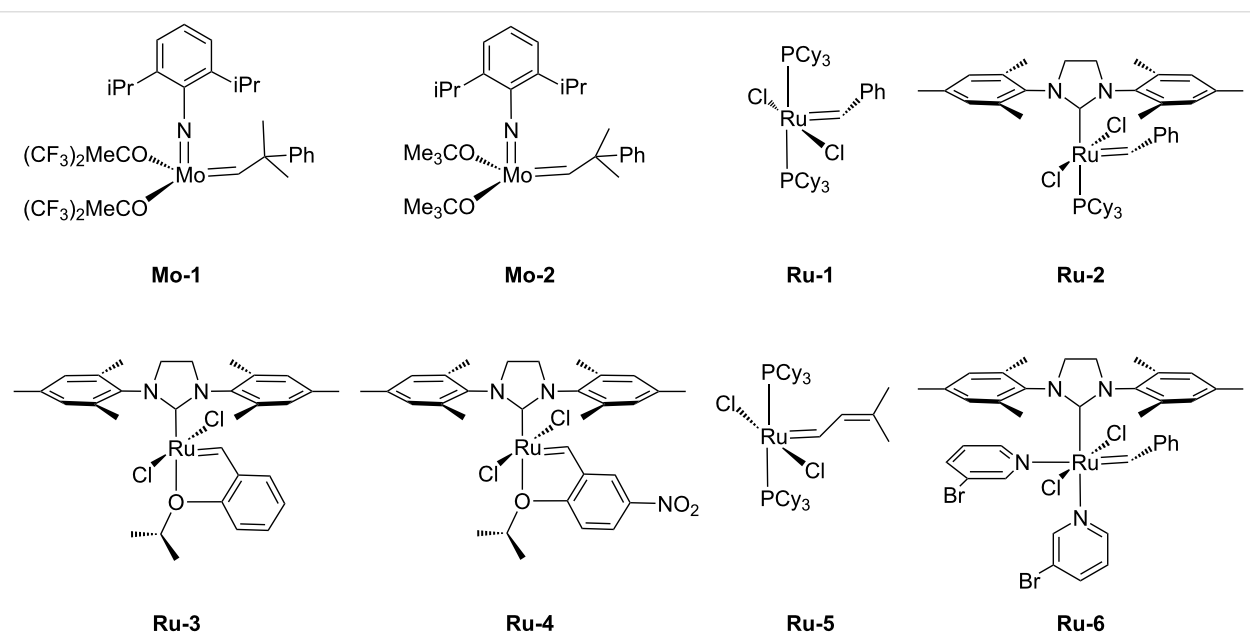


Figure 3: Olefin metathesis catalysts used in transformations of silsesquioxanes.

In 2004 Marciniec reported the first efficient cross metathesis of octavinylsilsesquioxane (OVS) occurring in the presence of first generation Grubbs' catalyst (**Ru-1**, Scheme 3) [9].

Octavinylsilsesquioxane (OVS) has been effectively transformed via cross metathesis with styrene, 1-hexene and allyltrimethylsilane. The reactions were carried out in the presence of

first-generation Grubbs catalyst at room temperature using a 12- or 24-fold molar excess of olefin relative to silsesquioxane. The reaction with styrene led to the formation of the expected product with an exclusive *E*-stereochemistry around the newly formed C=C double bond, while aliphatic α -alkenes (1-hexene, allyltrimethylsilane) gave a mixture of stereoisomers (*E/Z* = 94:6). Additionally, when 1-hexene was used as reacting

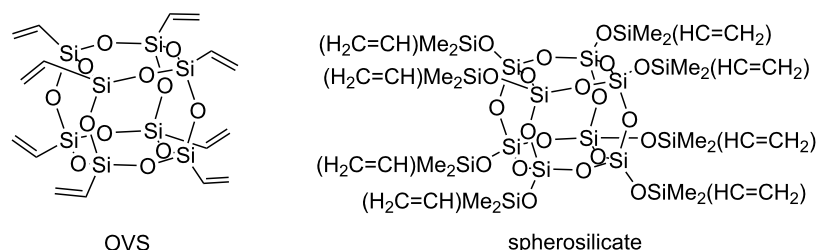
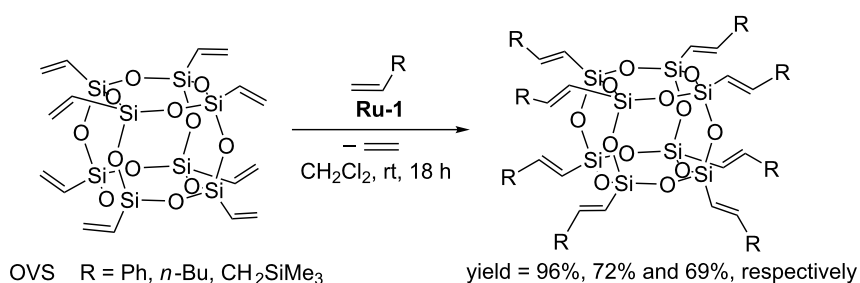


Figure 4: Octavinyl-substituted cubic silsesquioxane (OVS) and spherosilicate.

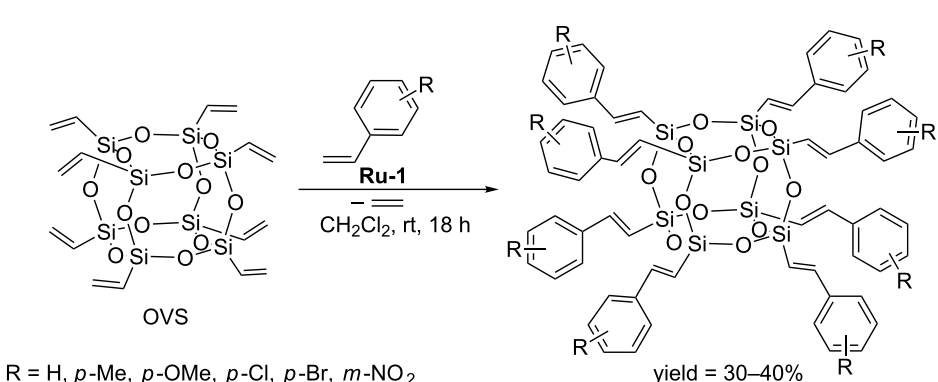


Scheme 3: Cross metathesis of OVS with terminal olefins (stereoselectivity as discussed in the text).

partner, the product of the cross metathesis was accompanied by considerable amounts of those of olefin homometathesis. Under optimized conditions, CM of OVS with styrene proceeds quantitatively despite the low loading of the catalyst (0.5 mol % relative to the vinylsilyl group, Scheme 3) [9]. Effective cross metathesis was observed when OVS was treated with vinyl sulfide in the presence of second generation Grubbs' catalyst (**Ru-2**). The product was obtained in 91% isolated yield, however, the process required a temperature elevation to 60 °C and the use of a catalyst amount of 4 mol % [9].

Laine has described the cross metathesis of OVS with a series of substituted styrenes (Scheme 4) [10].

Cross metathesis was carried out using a 1.5-fold excess of commercially available functionalized styrenes and 0.5 mol % of **Ru-1**. The reaction mixtures were stirred for 72 h to ensure complete conversion of the silsesquioxane. The quantitative conversion of the substrate can be achieved by blowing a gentle stream of nitrogen above the reaction mixture to remove the ethylene formed. The resulting 4-bromostyryl derivatives were subsequently modified via Heck coupling with a set of 4-substituted styrenes to give the next generation of functionalized derivatives. The authors also demonstrated the possibility of further functionalization of an amino-substituted derivative via the reaction with 3,5-dibromo or dinitrobenzoyl chloride. The proposed synthetic method based on the gradual development of



Scheme 4: Cross metathesis of OVS with substituted styrenes.

the organic part can be used for the synthesis of new star polymers, dendrimers or hyperbranched molecules. Further examples of the use of cross metathesis of OVS with styrenes in order to form functionalizable dendrimer cores have been reported by Cole-Hamilton [11]. Procedures allowing the syntheses of POSS derivatives with synthetically useful functional groups in multigram quantities have been proposed (Scheme 5).

A similar procedure permits the synthesis of a series of vinyl-biphenyl chromophore-decorated cubic oligosilsesquioxanes [12,13]. In the process conditions applied (methylene chloride at 55 °C, **Ru-1**) cross metathesis has been accompanied by competitive olefin homometathesis. The authors have developed a method for the isolation and purification of the expected materials and obtained the desired derivatives (Figure 5) with isolated yields exceeding 60%.

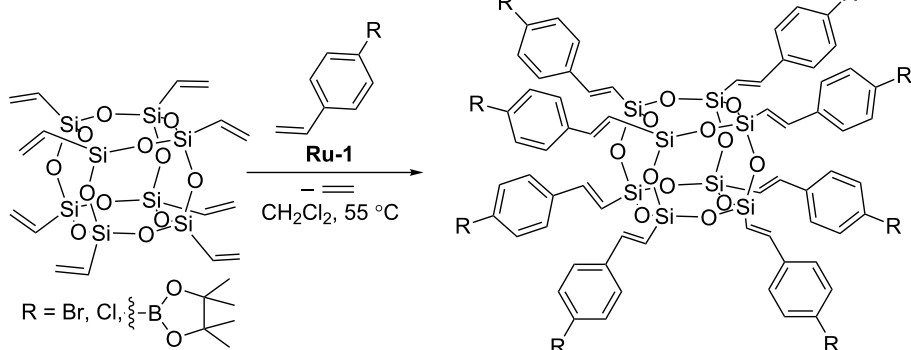
Chromophore-functionalized silsesquioxane-core dendrimers were obtained to investigate their photophysical properties [12,14]. In the synthesized compounds chromophore properties were only slightly influenced by the core. The possibility of fine-tuning of the photophysical properties of the POSS-based dendritic molecule not only by changing the chromophore but also by providing tailored steric interactions between bridges and/or chromophores was proved [14]. Interestingly, the 4'-vinylbiphenyl-3,5-dicarbaldehyde group modified macromolecule (Figure 5d) displayed the ability to become luminescent when exposed to reducing agents such as NaBH₄, LiAlH₄ or BH₃ [13].

Procedures for high yield and selective modification of octavinylsilsesquioxane (OVS) via CM with a variety of substituted styrenes, including the ones bearing highly π -conjugated substituents such as phenyl, 1-naphthyl, 9-anthracenyl and 2-thienyl have been reported by Marciniec [15]. For all styrene derivatives tested, the procedures described permitted highly

regioselective metathesis leading to exclusive formation of the *E*-isomer. Cross-metathesis experiments were performed under mild reaction conditions (CH₂Cl₂, 40 °C, 24 h), in the presence of the first generation Grubbs catalyst (**Ru-1**). Under such conditions, a fully selective course of the reaction was observed.

Núñez has described the synthesis of fluorescent POSS derivatives with carboranylstyrene fragments attached to each corner. The procedure involves CM of OVS with carboranylstyrene compounds with different substituents (Ph, Me, or H, Scheme 6) [16].

The reactions catalyzed by **Ru-1**, occurred with quantitative conversion and excellent regio- and stereoselectivity leading to exclusive formation of *E*-isomers. However, CM was accompanied by a minor amount of homometathesis. Fortunately, the product of homocoupling could be easily separated from the desired CM products. The presence of the carborane clusters was shown to enhance the thermal stability of the materials. Absorption and emission data of carborane–POSS hybrids indicate a large red-shift with respect to the precursors. Dautel and Moreau have synthesized octakis[2-(*p*-carboxyphenyl)ethyl] (Scheme 7) and octakis[2-(4-carboxy-1,1'-biphenyl)ethyl]-silsesquioxane via cross-metathesis methodology [17]. In the presence of palladium and dihydrogen the synthesized derivatives undergo, under mild conditions, hydrogenolysis of the benzyl ester group to the carboxylic acid and hydrogenation of the C=C double bonds at the silicon atoms (Scheme 7). The ability of the obtained derivatives, in particular the carboxylic acids, to generate nanostructured materials through self-organization processes was tested. The X-ray crystal structures of the octaester showed an interpenetrated compact packing of the molecular building blocks without any specific supramolecular interaction. The structure of the octaacid was found to contain hydrogen-bonded ribbons, thanks to the two-dimensional char-



Scheme 5: Modification of OVS via CM with styrenes.

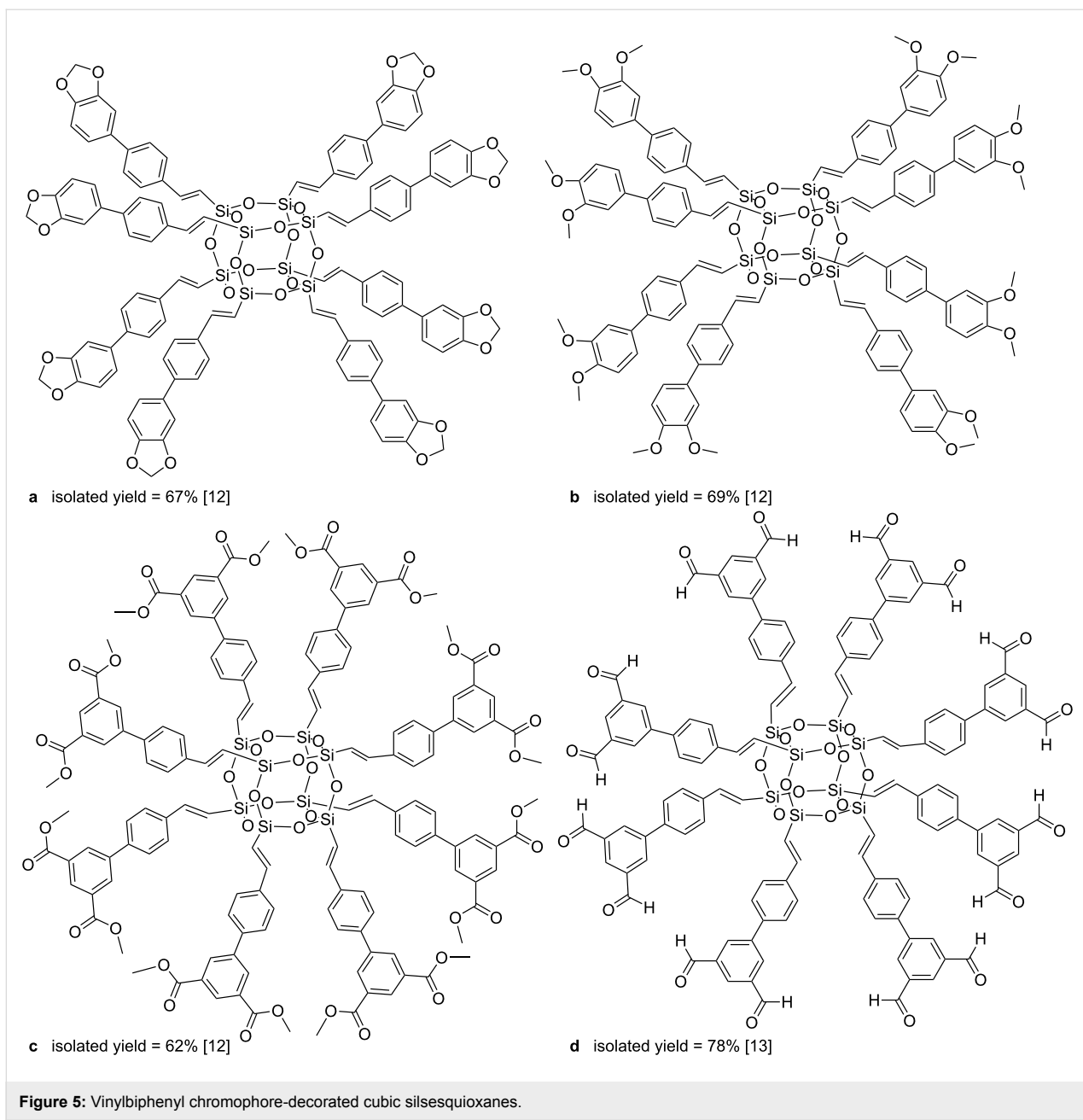


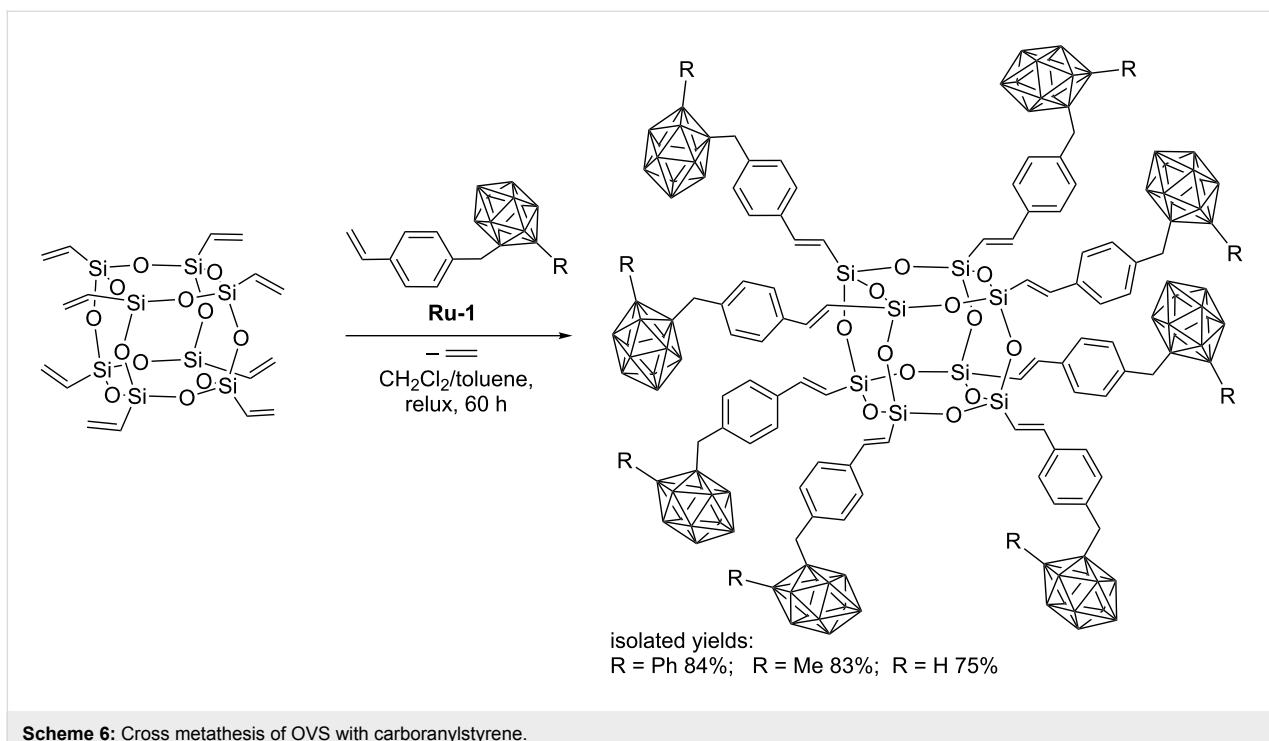
Figure 5: Vinylbiphenyl chromophore-decorated cubic silsesquioxanes.

acter of the acid and the directionality of the hydrogen bond pattern of the acid dimer.

Cross metathesis of monovinyl-substituted POSS with olefins has been reported for the first time by Marciniec [18]. It was demonstrated that monovinylhepta isobutyl-substituted octasilsesquioxane (monovinyl-POSS) underwent highly efficient CM with styrenes as well as vinyl and allyl organic derivatives in the presence of **Ru-1** (Scheme 8).

The reactions were performed in refluxing methylene chloride in the presence of usually 1 mol % of first generation Grubbs

catalyst (**Ru-1**) and led to the formation of the expected products with isolated yields ranging from 85% to 97%. In all cases the exclusive formation of *E*-isomers was detected and the formation of competitive olefin homometathesis was not observed. The reactions were carried out using a small excess of olefin (1.5–3 equiv) to ensure complete conversion of the reactants. In the reaction of monovinyl-POSS with allylbenzene, CM was accompanied by double bond migration, which results in reduction of the isolated yield of the CM product (85%) and the formation of minor amounts (15%) of 1-propenylbenzene. No similar isomerization was observed in the reaction of POSS with allyltrimethylsilane. Further research enabled Marciniec to



Scheme 6: Cross metathesis of OVS with carboranylstyrene.

extend the scope of the reaction by reporting efficient CM of monovinyl-POSS with a series of substituted styrenes. The reported procedures permit efficient and selective functionalization of mono- and octavinylsilsesquioxanes with π -conjugated substituents via cross metathesis (Scheme 9) [15].

In 2016 Marciniec reported the synthesis of a series of new cubic POSS in which one vertex silicon atom was replaced by a germanium atom bearing a vinyl group [19]. Monovinylgermasilsesquioxanes were successfully converted into the corresponding styryl derivatives via CM with styrenes (Scheme 10). Under optimized reaction conditions complete conversion of reacting partners and selective formation of CM products with exclusive *E*-arrangement around the C=C double bonds was observed.

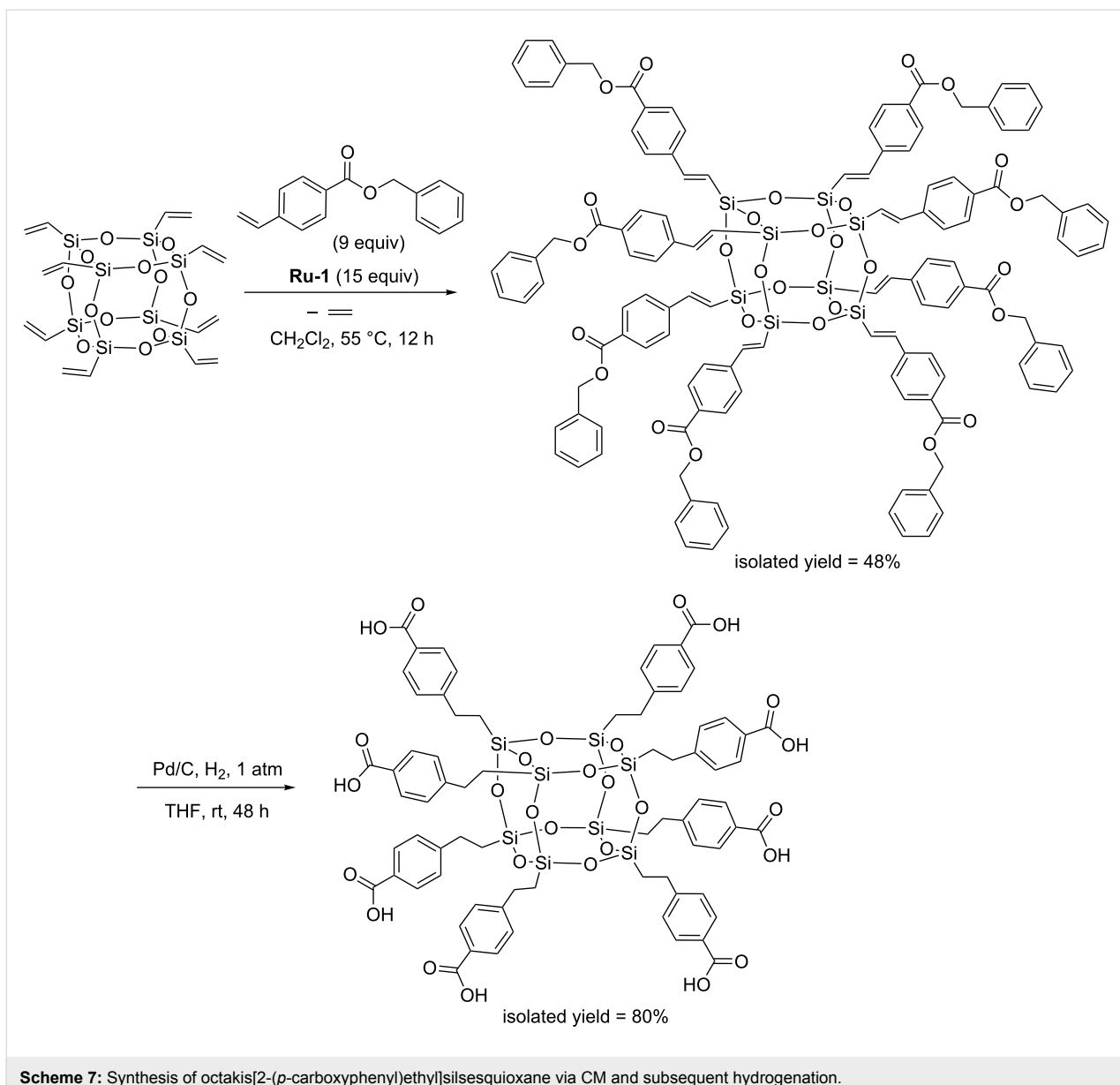
The most suitable catalyst for CM was found to be **Ru-1**, in whose presence no undesirable competitive reaction of olefin homometathesis occurred. Full conversion of monovinylgermasilsesquioxane required the use of 1 mol % of the catalyst. The reactions described are the first examples of metathesis activity of vinylgermanium compounds.

More than a decade ago Yoshida developed a new class of silsesquioxyl compounds containing rigid Si–O–Si bonds, called double-decker silsesquioxanes [20,21]. This class of compounds has recently been reviewed [22]. Marciniec found that divinyl-substituted double-decker silsesquioxanes (DDSQ-

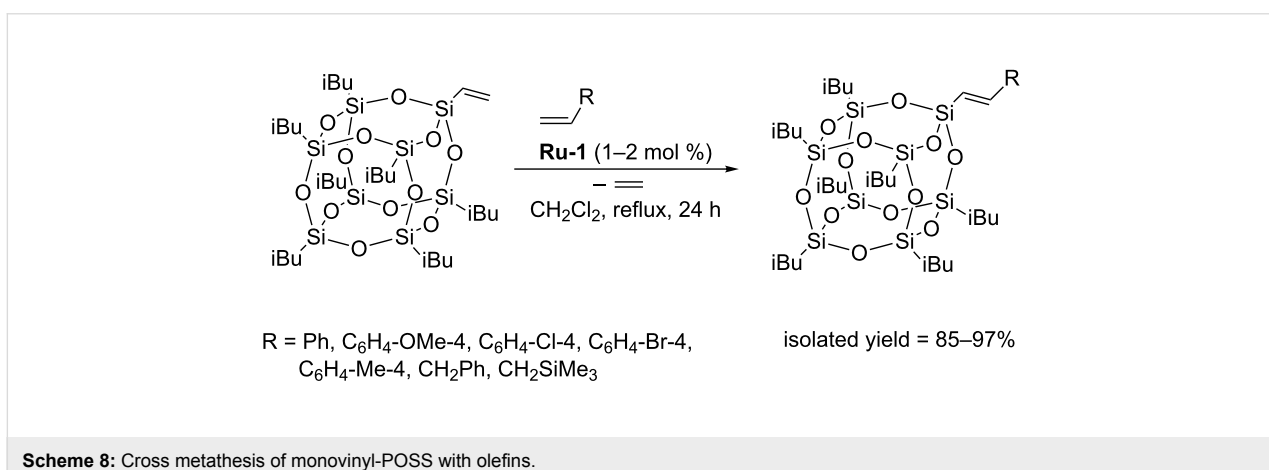
2SiVi) can be functionalized via cross metathesis and provided a series of examples of effective CM of DDSQ-2SiVi with styrenes and selected allyl derivatives (Scheme 11) [23].

Under optimized reaction conditions (Scheme 11), CM led to the exclusive formation of *E*-isomers and was not accompanied by competitive homometathesis. This selectivity was obtained thanks to the use of the **Ru-1** catalyst, moderately active in homometathesis of the olefins studied. Effective transformation was observed for substituted styrenes. Expected products were isolated with yields in the range of 88–95%. When allyl derivatives (allyltrimethylsilane, allylbenzene and allyl alcohol) were tested as olefinic partners, incomplete conversions of reactants (55–60%) were observed, despite the increased catalyst loading (2 mol %). Effective metathesis transformation was observed also in the presence of **Ru-2** but then considerable amounts of olefin homometathesis product were formed. The presence of a methyl group at the vinylsilyl moiety was responsible for the lack of activity, which was consistent with earlier studies (Scheme 1). The scope of the reaction was further extended to the palette of olefins containing conjugated systems of π -bonds (Scheme 12) [24].

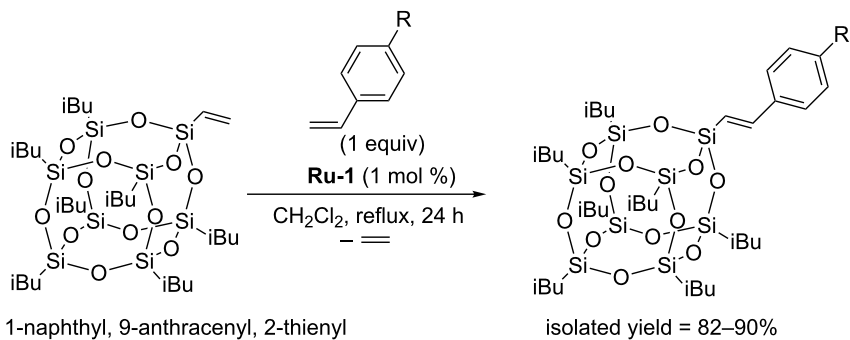
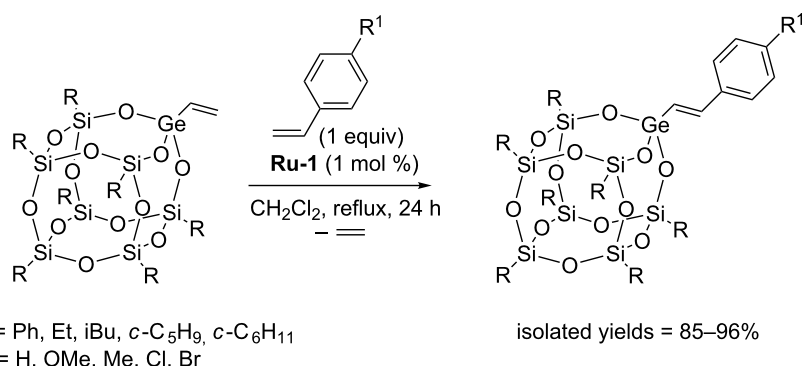
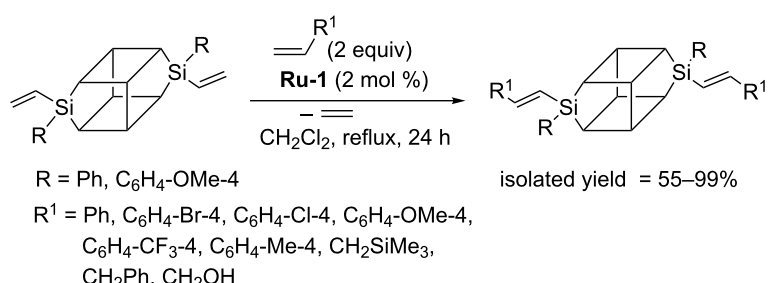
Irrespective of the type of olefin used, under optimized conditions all reactions proceeded with high yields and stereoselectivity, leading to exclusive formation of the *E,E*-isomer. Marciniec reported the synthesis of divinylgermasilsesquioxane (DDSQ-2GeVi) and proved effective functionalization of such



Scheme 7: Synthesis of octakis[2-(*p*-carboxyphenyl)ethyl]silsesquioxane via CM and subsequent hydrogenation.



Scheme 8: Cross metathesis of monovinyl-POSS with olefins.

**Scheme 9:** Cross metathesis of monovinyl-POSS with highly π -conjugated substituted styrenes.**Scheme 10:** Cross metathesis of monovinylgermasilsesquioxane with styrenes.**Scheme 11:** Cross metathesis of DDSQ-2SiVi with olefins.

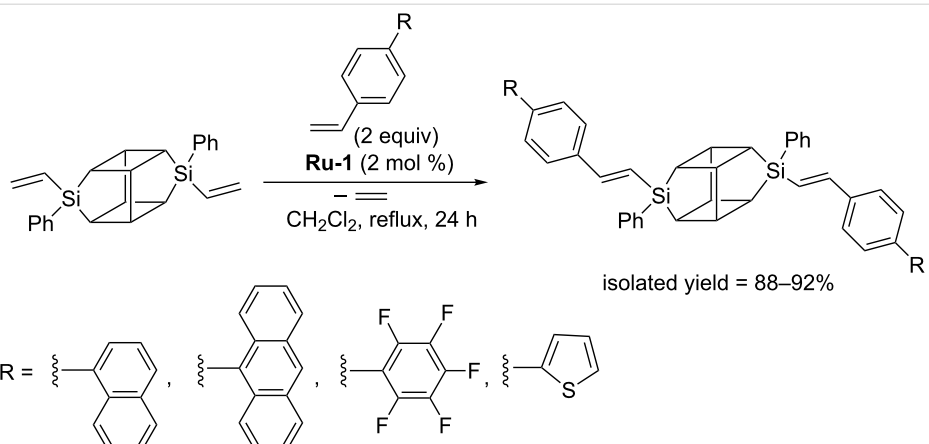
compounds by cross metathesis with a series of 4-substituted styrenes and allylbenzene, in the presence of **Ru-1** (Scheme 13) [19].

Under optimized conditions reactions led to fully chemo- and stereoselective formation of disubstituted germasilsesquioxanes. The ability of alkylsiloxyvinylgermane to be converted in metathesis is worth noting as the analogous vinylsilane does not undergo metathesis.

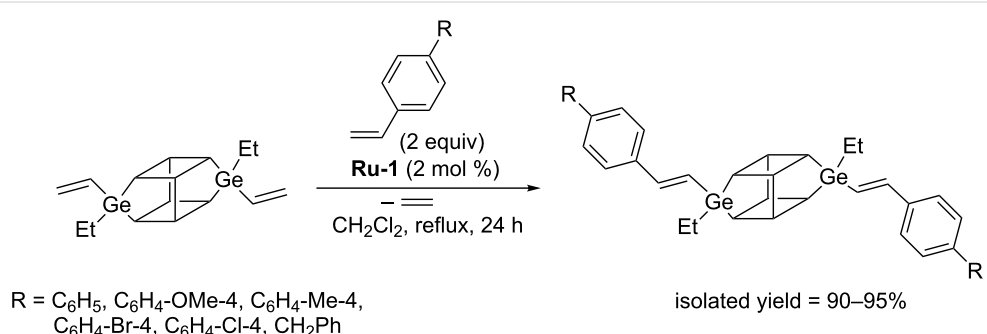
In 2010 Laine reported a procedure enabling the synthesis of polyhedral vinylphenyl-substituted deca- and dodeca-

silsesquioxanes (denoted **T₁₀** and **T₁₂**, respectively) [25]. Divinyl octa- or decaphenylsubstituted **T₁₀** and **T₁₂** derivatives (mixture of isomers) were demonstrated to effectively undergo cross metathesis with 4-bromostyrene in the presence of **Ru-1** (Scheme 14).

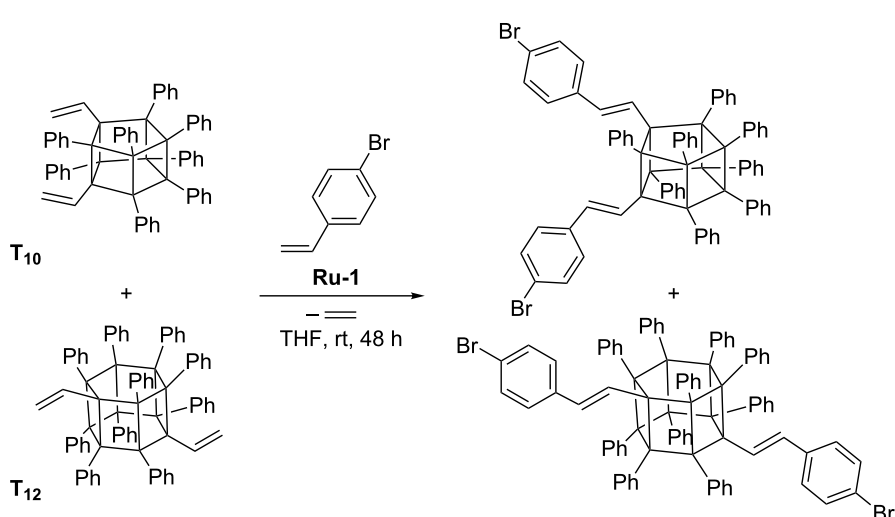
Attempts of homometathesis of vinylsilsesquioxanes have failed, which is understandable in view of the above presented scheme of reactivities of vinylsilanes (Scheme 1). The possibility to modify vinyl and styryl derivatives of silsesquioxanes via Heck reaction has been proved. The Heck coupling of 4-bromostyrene and vinyl-POSS derivatives leads to the formation of



Scheme 12: Cross metathesis of DDSQ-2SiVi with substituted styrenes.

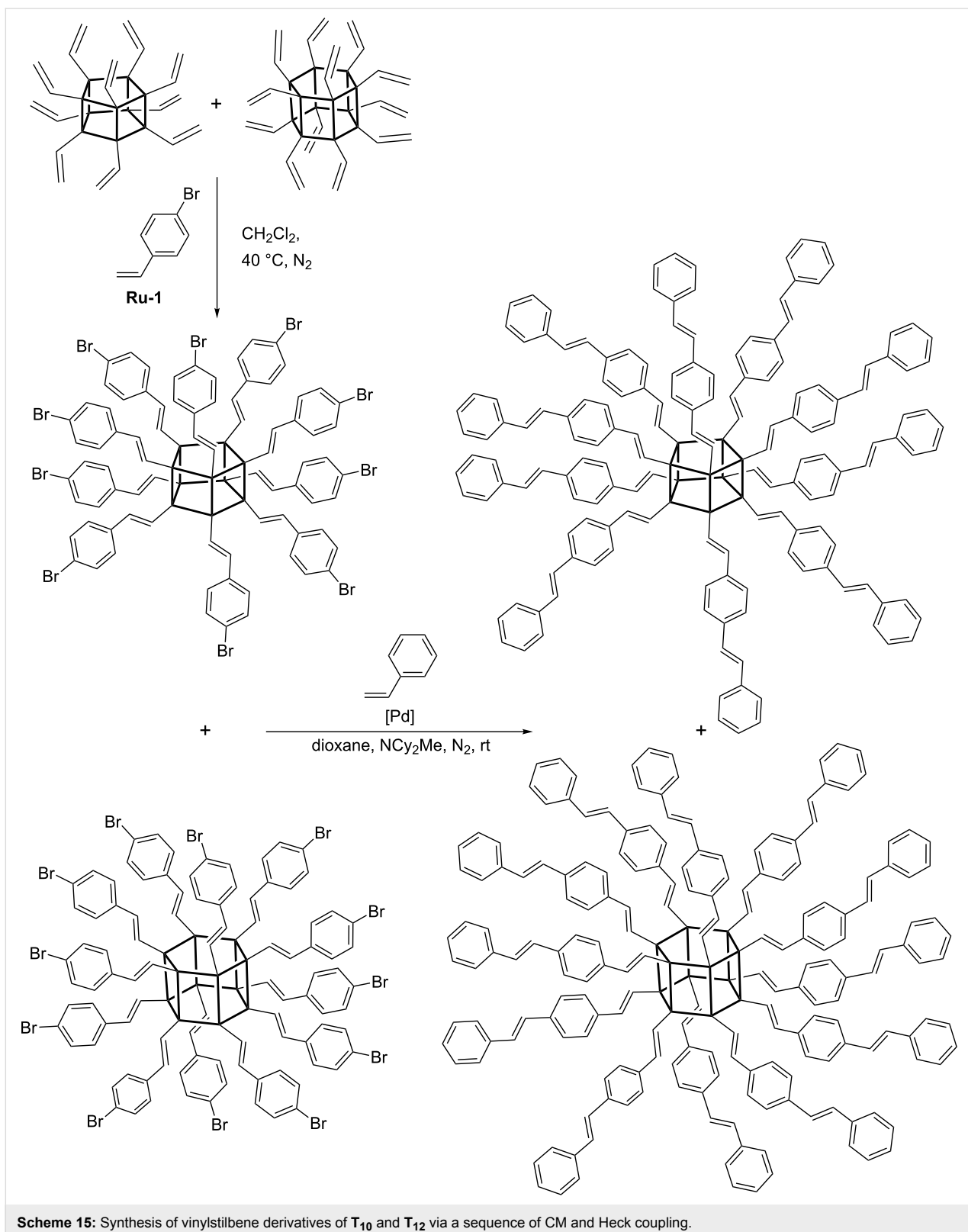


Scheme 13: Cross metathesis of (DDSQ-2GeVi) with olefins.

Scheme 14: CM of divinyl-substituted **T**₁₀ and **T**₁₂ with 4-bromostyrene (selected isomers are shown).

oligomeric products containing a silsesquioxane core in the polymer backbone. The deca- and dodecavinyldervatives of **T**₁₀ and **T**₁₂, respectively, undergo cross metathesis with

4-bromostyrene in the presence of **Ru-1** to form 4-bromostyryl derivatives, which in turn can be modified by Heck coupling with styrene to produce stilbenevinyl derivatives (Scheme 15)



Scheme 15: Synthesis of vinylstilbene derivatives of **T₁₀** and **T₁₂** via a sequence of CM and Heck coupling.

[26]. Laine has proposed a procedure for the separation of **T₁₀** and **T₁₂** derivatives, which enabled detailed photophysical studies of pure **T₁₀** and **T₁₂** core-based materials [26].

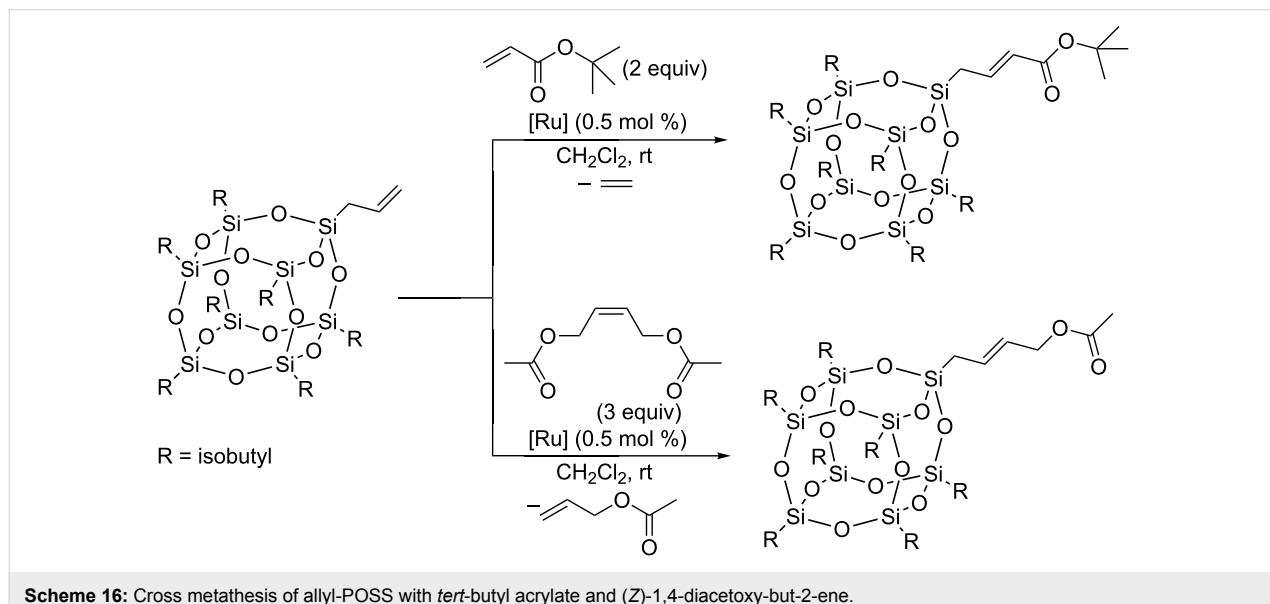
Detailed photophysical studies of chromophore-functionalized **T₁₀** and **T₁₂** silsesquioxanes have shown that the cage size and/or the symmetry can strongly affect photophysical properties

[26]. In the subsequent paper the authors describe the use of OVS or mixtures of **T₁₀** and **T₁₂** units in the synthesis of hydroxyphenyl-terminated silsesquioxanes. Such derivatives were obtained via cross metathesis with 4-acetoxystyrene or via a sequence of cross metathesis with 4-bromostyrene and Heck coupling with 4-acetoxystyrene. The resulting acetoxy compounds were then hydrolyzed to produce hydroxy-functionalized derivatives. These compounds, after purification, were reacted with adipic acid chloride to form POSS-moiety containing highly crosslinked polyesters with some porosity [27].

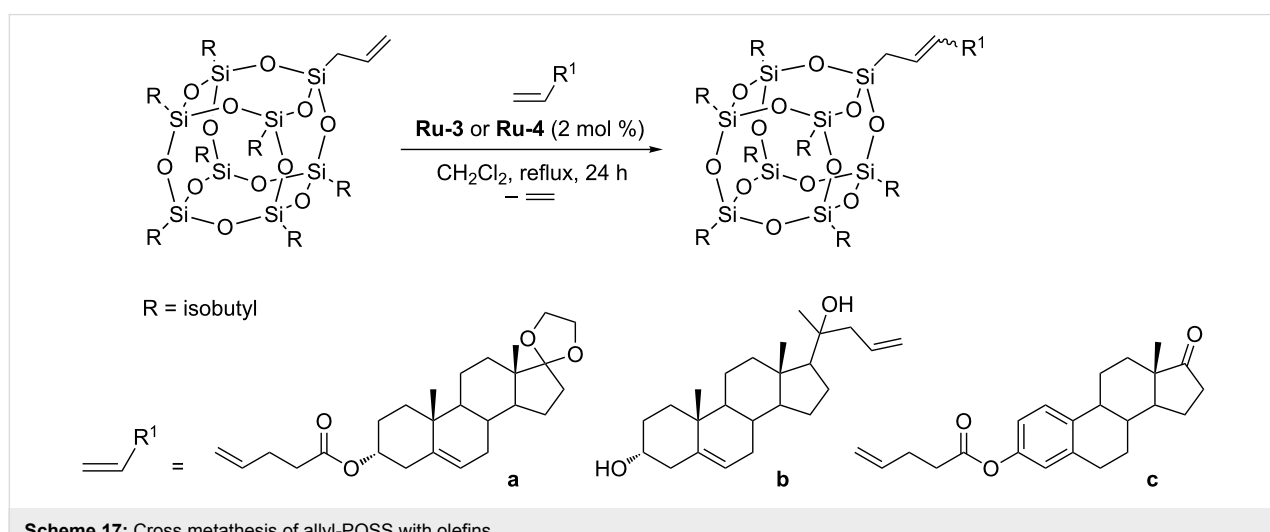
Czaban-Józwiak and Grela have studied the metathetic transformation of allyl-substituted cubic silsesquioxane [28]. In search for the optimum catalyst a variety of ruthenium complexes were

tested in the CM of allylsilsesquioxane with *tert*-butyl acrylate and (Z)-1,4-diacetoxybut-2-ene as model olefins (Scheme 16).

For the majority of the ruthenium catalysts tested, despite the mild reaction conditions, high yields were observed. No reaction or lower yields of the test reaction products were observed for first generation catalysts and indenylidene complexes. For further research, active in preliminary tests and commercially available second generation Grubbs–Hoveyda catalyst **Ru-3** and its nitro derivative **Ru-4** were selected. The same authors were able to successfully functionalize allylsilsesquioxane with more challenging, three different steroid derivatives. The reactions were performed in toluene at 100 °C in the presence of 2 mol % of **Ru-3** or **Ru-4** (Scheme 17, substrate **a**) or in CH₂Cl₂ at 45 °C in the presence of 2 mol % of **Ru-4** (Scheme 17, substrates **b** and **c**).



Scheme 16: Cross metathesis of allyl-POSS with *tert*-butyl acrylate and (Z)-1,4-diacetoxybut-2-ene.



Scheme 17: Cross metathesis of allyl-POSS with olefins.

and **c**). The products were obtained with yields of 62–72% as a mixture of *Z/E* isomers in the ratio of 20:80. Efficient homometathesis of allylsilsesquioxane occurring in toluene at 100 °C in the presence of 0.5 mol % of **Ru-4** was noted. The observed activity of allylsilsesquioxane in homometathesis is understandable because allylsilanes (unlike vinylsilanes) behave in metathesis like terminal olefins.

There are scarce reports on the application of ADMET in the synthesis of oligomers or polymers containing a POSS unit in the main chain. Marciniec disclosed ADMET copolymerization of DDSQ-2SiVi with dienes in the stereoselective synthesis of a new class of vinylene–arylene copolymers containing double-decker silsesquioxanes in the main chain (Scheme 18) [24].

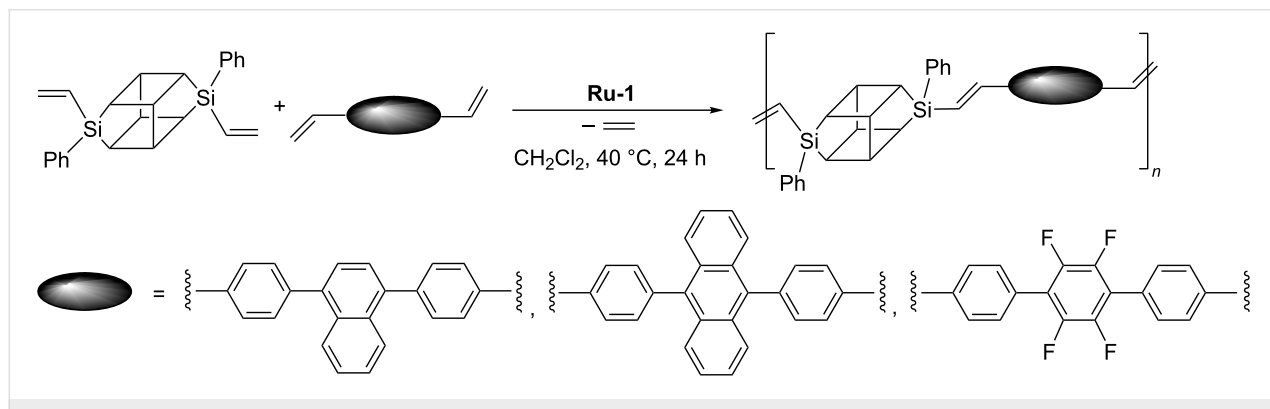
The products were polymers characterized by M_n in the range from 9100 to 18300 Da and M_w in the range from 13600 to 46100 Da. Thermogravimetric analyses indicate a high level of thermal resistance of the obtained systems, reaching the temperature values over 550 °C. Analogous ADMET copolymerization of divinylgermasilsesquioxanes with 4,4'-divinylbiphenyl or 4,4'-divinylterphenyl can be used in the synthesis of stereoregular *trans*-germasilsesquioxyl–vinylene–phenylene oligomers (Scheme 19) [19].

This method permitted obtaining a polymer with M_w in the range from 9057 to 11033 Da and polydispersity index (PDI) = 1.5.

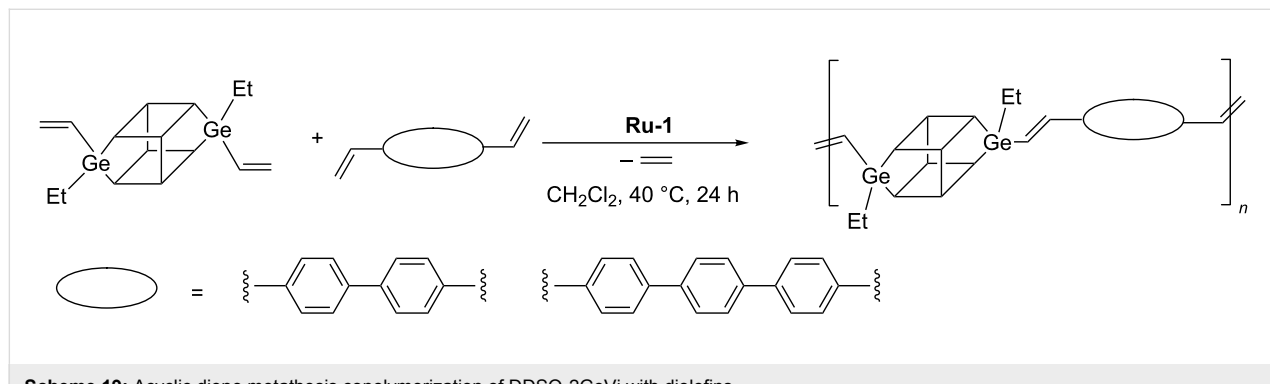
Ring-opening metathesis polymerization (ROMP) of POSS-functionalized monomers

The chemistry of inorganic–organic hybrid materials has emerged as a fascinating new field of modern nanotechnology. The inclusion of POSS cages into the polymeric material can significantly improve such properties of the polymer as thermal and oxidative resistance, surface properties, improvement of mechanical properties as well as reduced flammability, heat release and viscosity during processing [29]. Synthesis, properties and applications of POSS-containing materials are the subject of numerous reviews [30–37]. From among the methods for preparation of organic–inorganic hybrid materials, polymerization or copolymerization is particularly convenient to incorporate POSS units into polyolefins.

Ring-opening metathesis polymerization (ROMP) is the type of olefin metathesis chain-growth polymerization that uses metathesis catalysts to generate polymers from cyclic olefins [38–41]. To obtain polymers functionalized with POSS in the side chain, a susceptible to the ROMP monomer connected via a suitable



Scheme 18: Acyclic diene metathesis copolymerization of DDSQ-2SiVi with diolefins.



Scheme 19: Acyclic diene metathesis copolymerization of DDSQ-2GeVi with diolefins.

linker to the silsesquioxane cage should be used. Due to the ease of polymerization and functionalization, norbornene derivatives are the most often used monomers.

The aim of this section is to indicate the applications of ROMP in the synthesis of hybrid materials containing the POSS moiety covalently bonded to organic polymeric chains rather than the discussion of the properties of the obtained materials.

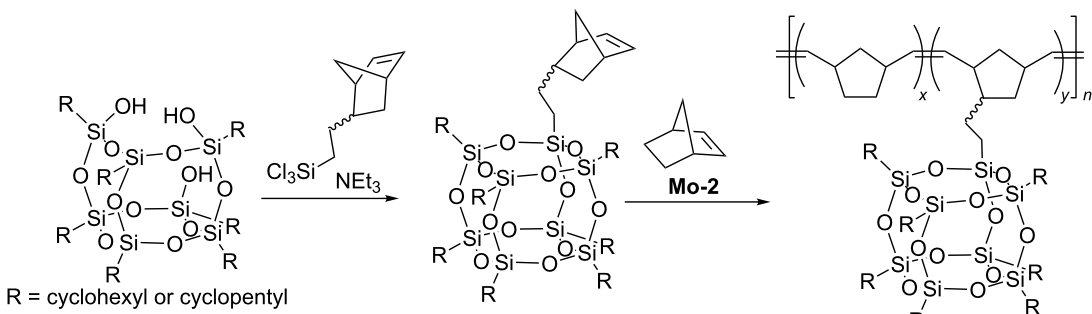
The synthesis of polymers by ROMP is carried out almost exclusively in the presence of ruthenium-based catalysts **Ru-1–Ru-6** because of their tolerance to moisture, atmospheric oxygen and most functional groups as well as commercial availability. The choice of solvents is determined by the solubility of monomers, with methylene chloride, chloroform, and toluene being the most commonly used. Polymerization is terminated by addition of ethyl vinyl ether to the reaction mixture. Ruthenium residues from the obtained copolymer are removed on a short alumina plug.

In 1999 Lichtenhan reported ring-opening metathesis copolymerization of POSS-functionalized norbornene with norbornene in the presence of the Mo-based catalyst **Mo-2** (Figure 3,

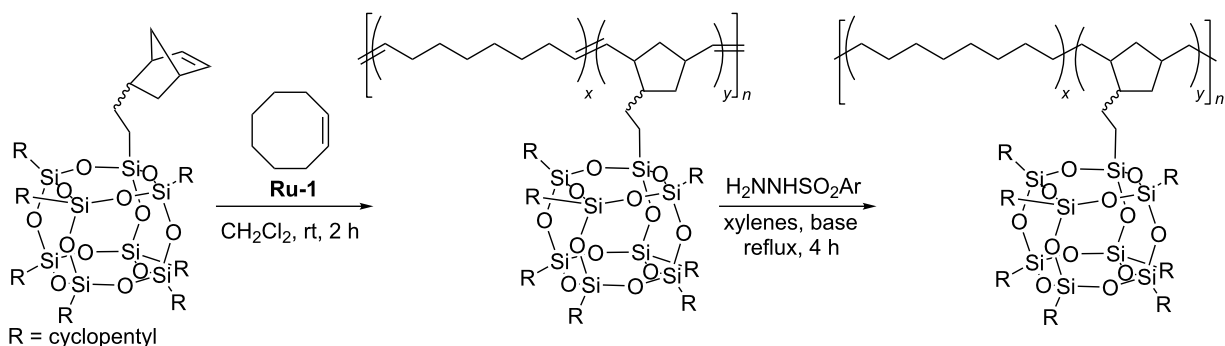
Scheme 20) [42]. The polymerization was carried out in CHCl_3 under nitrogen atmosphere. The reactions were terminated by the addition of benzaldehyde. A series of random copolymers with different weight percentage of POSS containing comonomer were synthesized.

Ruthenium alkylidene catalyst **Ru-1** was successfully used by Caughlin who reported ring-opening metathesis polymerization of heptacyclopentylnorbornenylethyloctasilsesquioxane and its copolymerization with cyclooctene [43]. The obtained copolymer was subsequently hydrogenated to afford polyethylene–POSS random copolymer (Scheme 21). Thermogravimetric analysis of the polyethylene–POSS copolymers under air showed a significant improvement of the thermal stability relative to that of polyethylene.

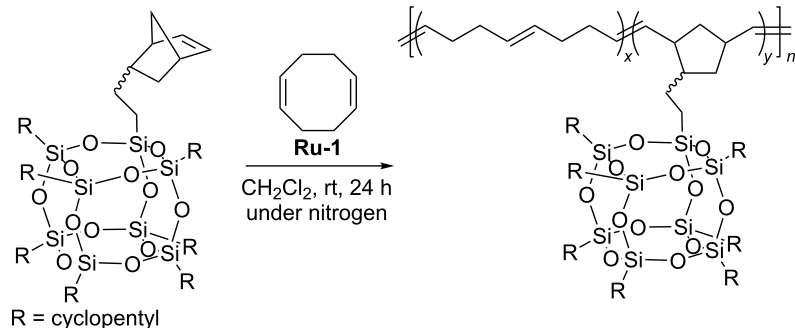
In subsequent studies Caughlin used ring-opening metathesis copolymerization of POSS-functionalized norbornene with 1,5-cyclooctadiene in the presence of **Ru-1** for the synthesis of a series of random copolymers in which POSS loading varied in the range from 0 to 53 wt % (Scheme 22) [44]. Polymers with a weight-average molecular mass in the range from 67000 to 88000 Da were obtained.



Scheme 20: Ring-opening metathesis copolymerization of norbornenylethyl-POSS with norbornene.



Scheme 21: Synthesis of a polyethylene–POSS copolymer via ring-opening metathesis copolymerization of norbornenylethyl-POSS with cyclooctene and subsequent hydrogenation.



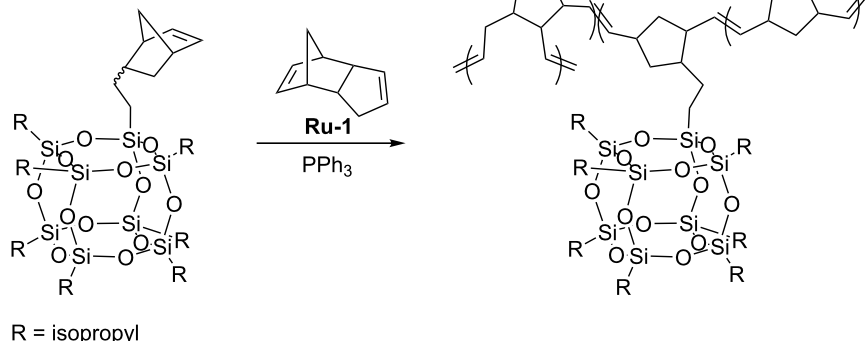
Scheme 22: ROMP of norbornenylethyl-POSS with 1,5-cyclooctadiene.

In the random copolymers obtained, the associative interactions between the particles were shown to result in the formation of ordered nanostructures. TEM micrographs indicate that the copolymers assemble into small, randomly oriented lamellae with lateral dimensions of approximately 50 nm and a thickness of ca 3–5 nm that corresponds to twice the diameter of a POSS nanoparticle. With increasing POSS concentration, the nanostructures extend to longer continuous lamellae having lateral lengths in the order of microns. Ruthenium alkylidene catalyst **Ru-5** was successfully used in copolymerization of cubic silsesquioxane bearing four β -styryl and four (3-phenyl-oxiran-2-yl) substituents with dicyclopentadiene (DCPD) [45]. Moreover, octanorbornenyl cubic silsesquioxane was found to undergo ring-opening metathesis copolymerization with DCPD. Due to limited solubility only 0.1 mol % of POSS was used in the copolymerization. Such a small content of the POSS-containing comonomer caused, however, an increase in T_g up to 15 °C in relation to that of polyDCPD. Similar examinations were reported by Coughlin who used first generation Grubbs catalyst (**Ru-1**) for copolymerization of POSS-functionalized norbornene with DCPD (Scheme 23) [46]. During polymerization, PPh_3 had to be added to reduce the activity of **Ru-1**.

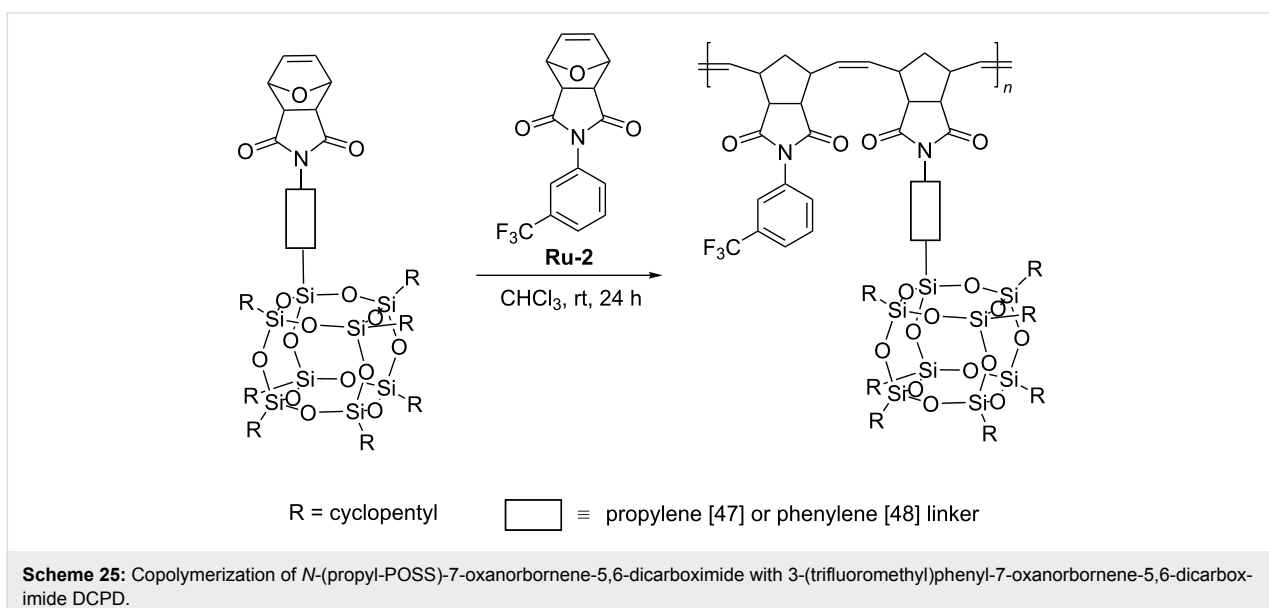
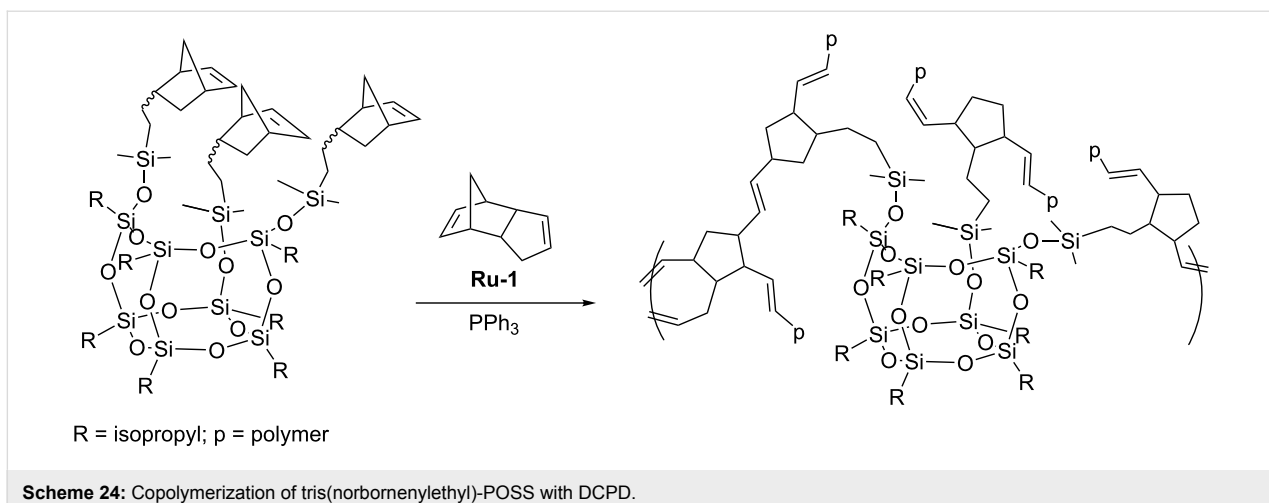
Dicyclopentadiene and norbornenylethyl-POSS or tris(norbornenylethyl)-POSS (Scheme 24) have been copolymerized over a range of POSS loadings. In the copolymers obtained using mononorbornenylethyl-POSS, the aggregates containing three to four POSS molecules were observed for high POSS loadings. When tris(norbornenylethyl)-POSS was used as comonomer, the POSS remained uniformly dispersed over all loadings. No improvements in thermal properties were observed in the copolymers obtained.

Another POSS-containing monomer – *N*-(propyl-POSS)-7-oxanorbornene-5,6-dicarboximide was tested in ring-opening metathesis copolymerization with 3-(trifluoromethyl)phenyl-7-oxanorbornene-5,6-dicarboximide in the presence of second generation Grubbs catalyst (**Ru-2**, Scheme 25) [47].

The use of specified proportions of the two comonomers allowed obtaining a series of copolymers with different POSS contents characterized by average molecular weights in the range of 42,000–200,000 Da and PDI values in the range of 1.3–1.9. The surface morphology and thermal properties of hybrids were found to be affected by the POSS macromer. TEM



Scheme 23: Copolymerization of POSS-functionalized norbornene with DCPD.



analysis of copolymer films revealed the presence of POSS agglomerates. An analogous macromer bearing POSS-bound via phenylene linker was used in the synthesis of a series of polymers and copolymers with 3-(trifluoromethyl)phenyl-7-oxanorbornene-5,6-dicarboximide (Scheme 25) [48]. It was found that the increase in the content of POSS units in the copolymer results in a decrease in thermal stability and T_g values. TEM and AFM microimages show spherical POSS aggregates uniformly dispersed within the copolymer. POSS-substituted polynorbornenes, in which POSS groups are linked to the polynorbornene backbone through the flexible spacer with different lengths, were subjected to homopolymerization by ROMP and copolymerization with norbornene substituted with a butyl ester group, to determine the effect of the spacer length on POSS crystallization ability and the composition dependence of physical properties of the copolymers [49]. A

series of homopolymers and random copolymers were synthesized in the presence of third generation Grubbs catalyst **Ru-6** in CH_2Cl_2 , at room temperature (Figure 6) [49].

It has been demonstrated that the length of the spacer affects the crystallizability of POSS groups so that the use of a reasonably long spacer to link the POSS groups to the main chain can make POSS groups crystallizable.

Kim and Kwon have shown that ring-opening metathesis copolymerization of norbornenylethyl-POSS with methyltetracyclododecene in the presence of first generation Grubbs catalyst (**Ru-1**) is a practical route to the synthesis of block copolymers containing POSS nanoparticles (Scheme 26) [50]. ROMP of norbornenylethyl-POSS produced the corresponding homopolymer in relatively controlled molecular weights

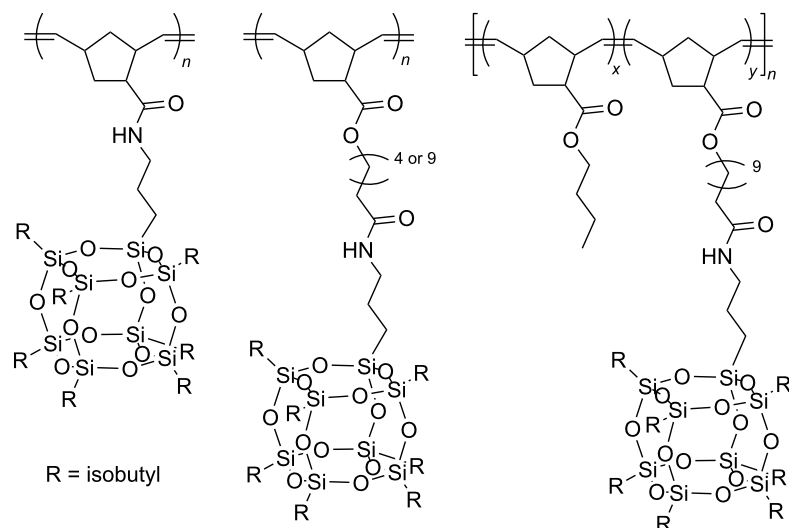
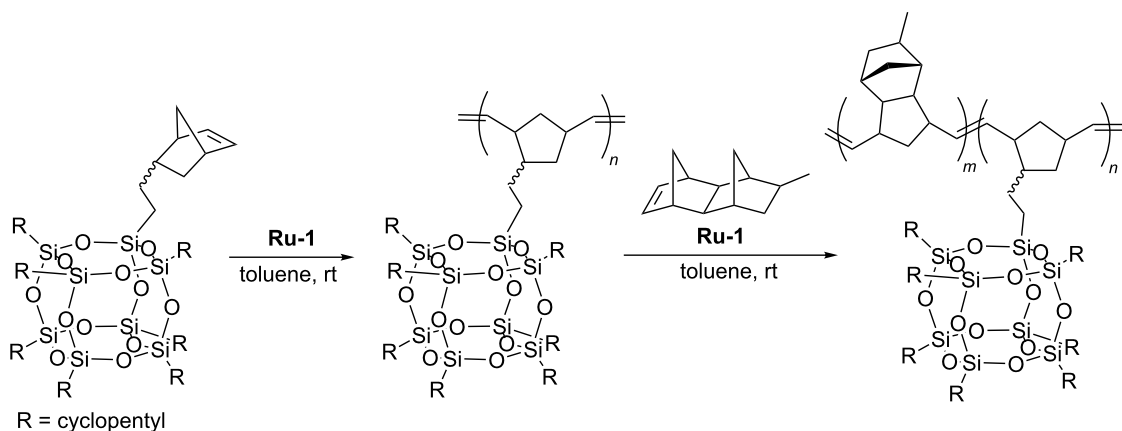


Figure 6: Homopolymers and copolymers having POSS groups attached to the main chain via flexible spacers of different lengths.



Scheme 26: Ring-opening metathesis copolymerization of POSS-NBE with methyltetracyclododecene.

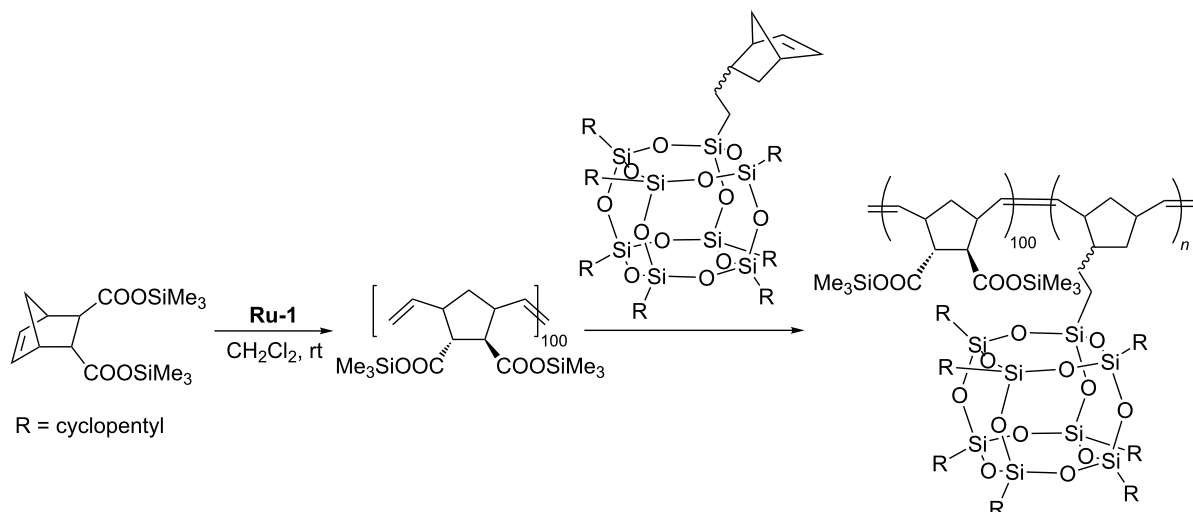
($M_n = 17,900$ – $26,300$ Da) and narrow molecular weight distributions (in the range $M_n/M_w = 1.19$ – 1.29). Copolymerization was employed by a sequential monomer addition. At first, the POSS-NBE was introduced into the reaction system containing the catalyst and after its complete conversion methyltetracyclododecene was added. The reaction was terminated with ethyl vinyl ether as soon as the second monomer was fully converted. A series of copolymers with different POSS-NBE content were obtained. The PDI values were in the range of 1.32–1.53 with average molecular weights of ca. 48000–63000 Da.

The synthesized POSS containing nanocomposites displayed significant improvements in their thermal stability relative to that of the polynorbornenes formed in the absence of POSS cages. Xu has reported an example of the synthesis of POSS-containing block copolymers via “living” ROMP [51]. Copoly-

merization of norbornenylethylotcasilsesquioxane with 2-*endo*-3-*exo*-5-norbornene-2,3-dicarboxylic acid trimethylsilyl ester was performed in the presence of **Ru-1**. The block copolymer was obtained via sequential monomer addition (Scheme 27). After hydrolysis of the ester function, the polymer was isolated by precipitation.

As a result two block copolymers were obtained. The one containing 5% of POSS units was characterized by $M_n = 26200$ Da and PDI = 1.16 and the other one bearing 10% of POSS-substituted monomeric units, has a number average molecular weight $M_n = 33200$ Da and a polydispersity index PDI = 1.23.

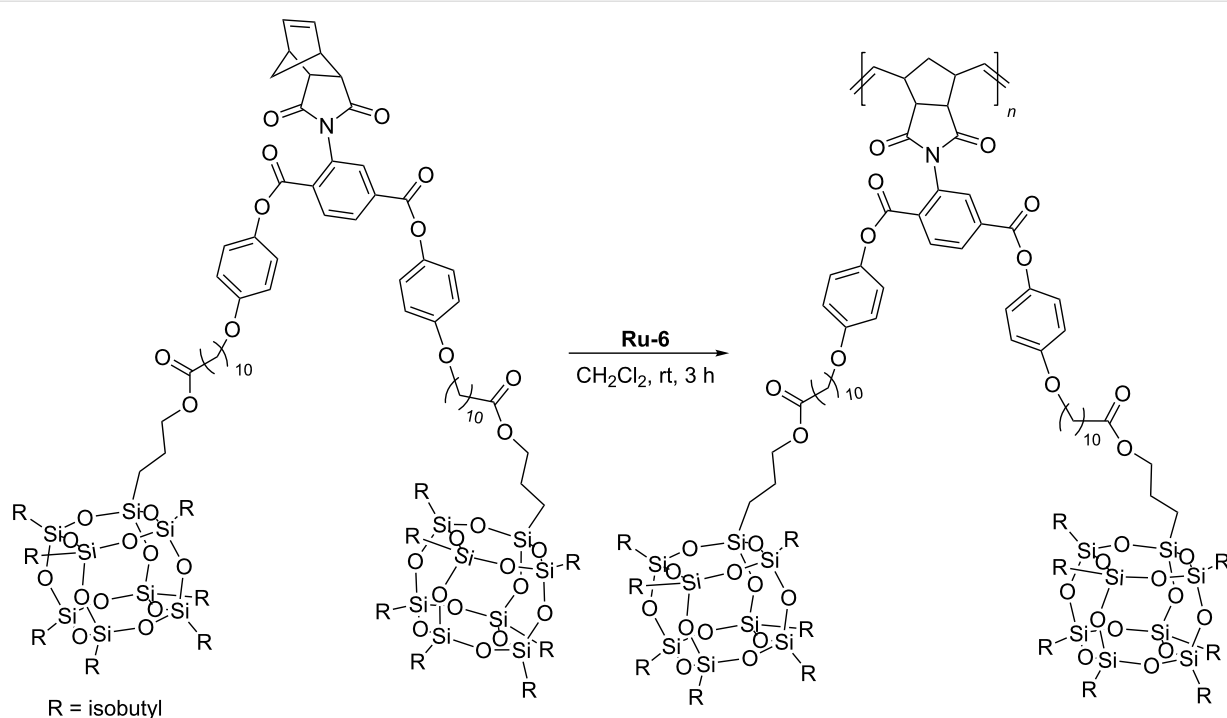
The possibility of employing ROMP as a key step in the synthesis of a polynorbornene-based mesogen-jacketed liquid crystalline polymer (MJLCP) containing polyhedral oligomeric



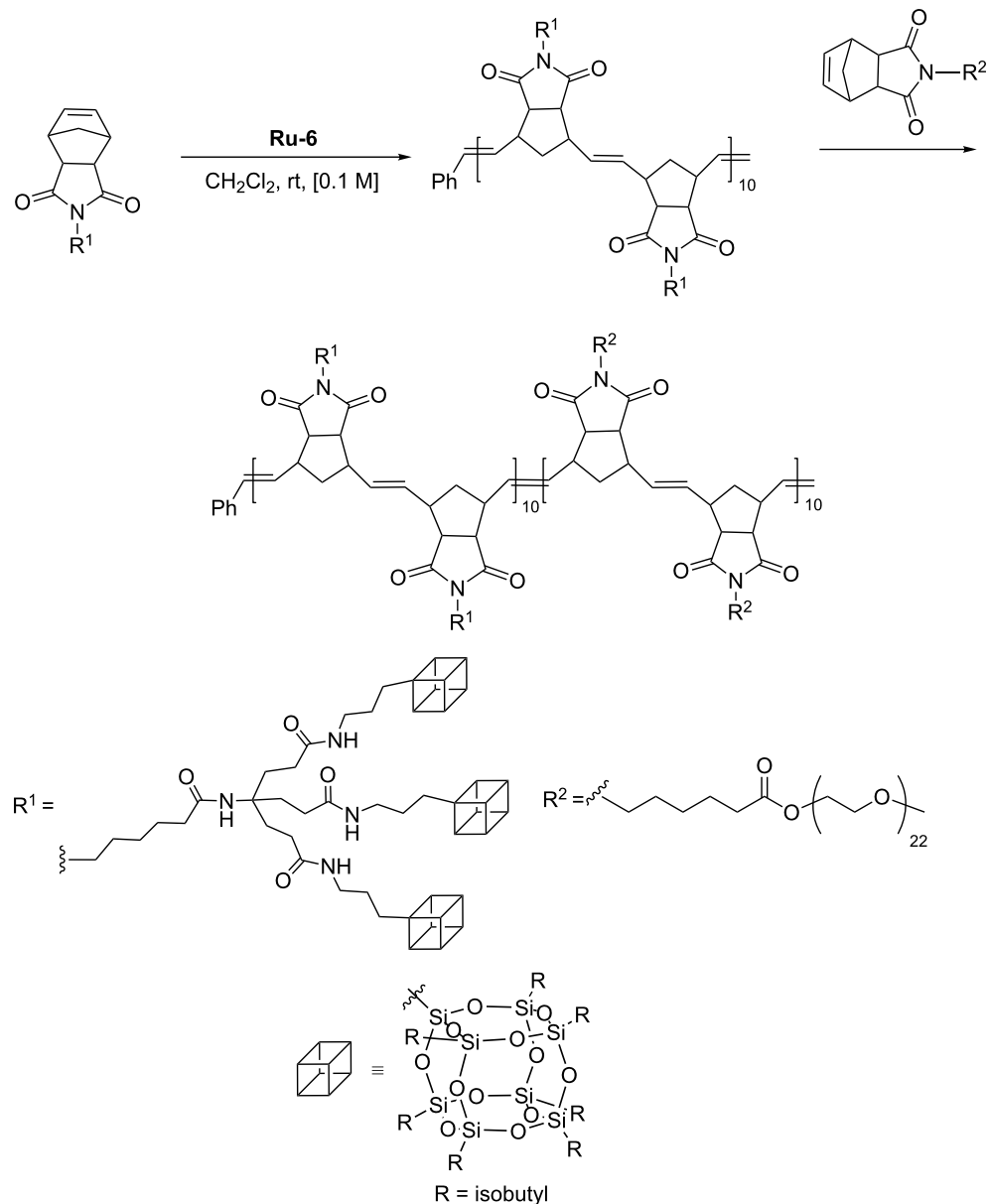
Scheme 27: Synthesis of block copolymer via ROMP by sequential monomer addition.

silsesquioxane (POSS) in the side chain was demonstrated by Shen and Fan (Scheme 28) [52]. The reaction was performed in the presence of third generation Grubbs catalyst **Ru-6** under inert atmosphere. The synthesized polymer showed various phase structures including POSS crystal and a hexagonal columnar phase, which, depending on temperature, can coexist with each other. The POSS crystal was shown to have a tremendous effect on the liquid crystalline behavior of the polymer.

Wang has reported living ROMP of a series of monomers bearing a polymerizable norbornene dicarboxyimide group attached via an appropriate linker to 1–4 POSS units [53]. Copolymerization of POSS-bearing monomers with norbornene containing pendant poly(ethylene oxide) group permitted the synthesis of a number of block copolymers, containing blocks of hydrophobic nature (POSS containing block) and those of hydrophilic nature (polyether containing block, Scheme 29). The block copolymer



Scheme 28: Synthesis of a liquid crystalline polymer with POSS core in the side chain.



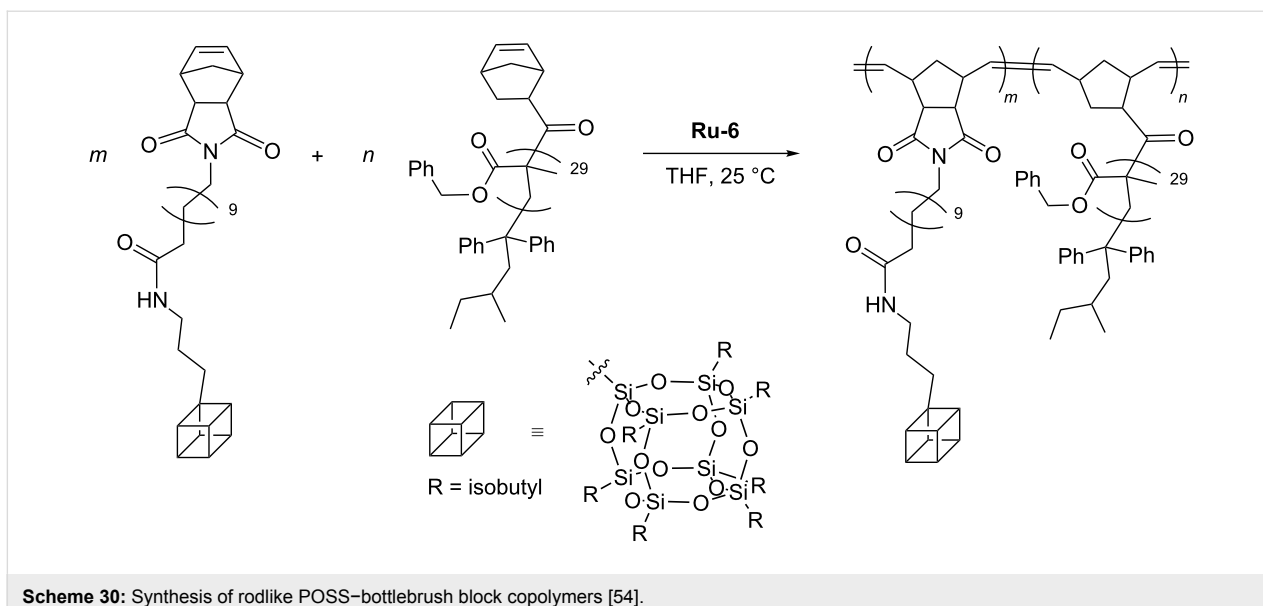
Scheme 29: Sequential synthesis of copolymers of polynorbornene containing POSS and PEO pendant groups.

was synthesized via sequential monomer addition starting from the POSS-containing macromer. The synthesis of the copolymers was carried out under mild reaction conditions in the presence of **Ru-6**. It was shown that the polymers obtained can self-assemble in THF solution into aggregates, when water was added.

Lee has performed a series of sequential ring-opening metathesis copolymerization of norbornene-*exo*-2,3-dicarboxyimido)dodecanoylethylamino)propylheptaisobutyl-POSS and *exo*-5-norbornene-2-carbonyl-end poly(benzyl methacrylate, Scheme 30) [54] and obtained rodlike POSS–bottlebrush block

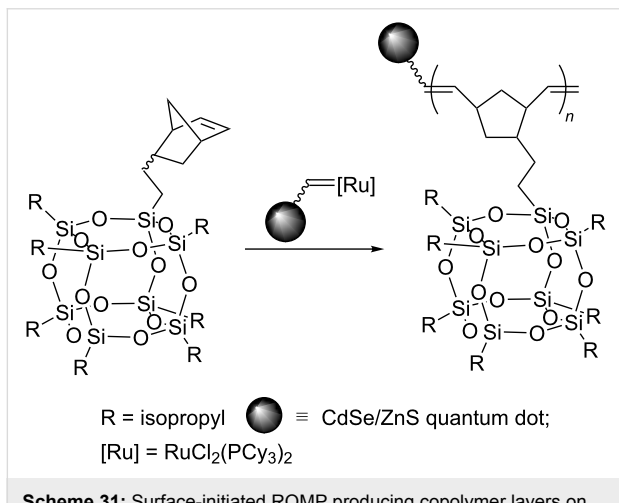
copolymers containing crystalline POSS pendants in one block and amorphous polymeric grafts in another block. Hierarchical self-assembly of rodlike copolymer was studied from the point of view of its utility in producing highly ordered 1D photonic crystals.

Surface-initiated ROMP was used to grow an organic corona phase on the surface of CdSe/ZnS quantum dots [39]. Functionalization of the surface with the octenylidemethylsilyl group allowed the attachment of a ruthenium alkylidene complex as a catalyst. Subsequent ROMP of norbornenylethylisobutyl cubic silsesquioxane or norbornenedicarbonyl chloride produced dif-



Scheme 30: Synthesis of rodlike POSS–bottlebrush block copolymers [54].

ferent molecular weights and narrow polydispersity homo- or copolymer layers directly onto the quantum dots (Scheme 31) [55].



Scheme 31: Surface-initiated ROMP producing copolymer layers on the surface of CdSe/ZnS quantum dots.

Conclusion

Olefin metathesis, a universal tool in organic and polymer synthesis, offers numerous advantages for the synthesis of POSS-based materials. Ruthenium-based olefin metathesis catalysts tolerate the presence of water, air and nearly all functional groups. Commercially available vinylsilsesquioxanes can be easily modified and/or functionalized by cross metathesis. According to the CM product-selectivity model [56], vinylsilsesquioxane is an olefin type III (it does not undergo homodimerization). The correct choice of olefin and catalyst permits selective CM. Another metathetic transformation – acyclic

diene metathesis copolymerization – permits introduction of a POSS group to the copolymer main chain. This methodology has not been thoroughly studied so far. In turn, ring-opening metathesis (co)polymerization is a convenient tool for introducing a number of functional groups, including POSS, in the side chain of polymers. This method is limited by the small number of monomers susceptible to ROMP. In view of the dynamic development of the studies on synthesis and properties of inorganic–organic hybrid materials, it is reasonable to expect that olefin metathesis thanks to its advantages and charm will find numerous further applications in the synthesis of POSS-based materials.

Acknowledgements

Financial support from the National Science Centre (Poland), (project No. UMO-2011/03/B/ST5/01047) is gratefully acknowledged.

ORCID® IDs

Patrycja Źak - <https://orcid.org/0000-0002-9138-2416>

Cezary Pietraszuk - <https://orcid.org/0000-0003-2413-0478>

References

1. Applications of Polyhedral Oligomeric Silsesquioxanes. In *Advances in Silicon Science*; Hartmann-Thompson, C., Ed.; Springer Netherlands: Dordrecht, Netherlands, 2011. doi:10.1007/978-90-481-3787-9
2. Cordes, D. B.; Lickiss, P. D.; Rataboul, F. *Chem. Rev.* **2010**, *110*, 2081–2173. doi:10.1021/cr900201r
3. Lickiss, P. D.; Rataboul, F. *Adv. Organomet. Chem.* **2008**, *57*, 1–116. doi:10.1016/s0065-3055(08)00001-4
4. Grubbs, R. H.; Wenzel, A. G.; O'Leary, D. J.; Khosravi, E., Eds. *Handbook of Metathesis*; Wiley-VCH Verlag GmbH: Weinheim, Germany, 2015. doi:10.1002/9783527674107

5. Grela, K., Ed. *Olefin Metathesis. Theory and Practice*; Wiley: Hoboken, 2014.
6. Grubbs, R. H., Ed. *Handbook of Metathesis*; Wiley-VCH: Weinheim, 2003.
7. Pietraszuk, C.; Fischer, H.; Rogalski, S.; Marciniec, B. *J. Organomet. Chem.* **2005**, *690*, 5912–5921. doi:10.1016/j.jorgancchem.2005.07.091
8. Feher, F. J.; Soulivong, D.; Eklund, A. G.; Wyndham, K. D. *Chem. Commun.* **1997**, 1185–1186. doi:10.1039/a701996c
9. Itami, Y.; Marciniec, B.; Kubicki, M. *Chem. – Eur. J.* **2004**, *10*, 1239–1248. doi:10.1002/chem.200305433
10. Sulaiman, S.; Bhaskar, A.; Zhang, J.; Guda, R.; Goodson, T., III; Laine, R. M. *Chem. Mater.* **2008**, *20*, 5563–5573. doi:10.1021/cm801017e
11. Cheng, G.; Vautravers, N. R.; Morris, R. E.; Cole-Hamilton, D. J. *Org. Biomol. Chem.* **2008**, *6*, 4662–4667. doi:10.1039/b812140k
12. Vautravers, N. R.; André, P.; Slawin, A. M. Z.; Cole-Hamilton, D. J. *Org. Biomol. Chem.* **2009**, *7*, 717–724. doi:10.1039/b814496f
13. Vautravers, N. R.; André, P.; Cole-Hamilton, D. J. *J. Mater. Chem.* **2009**, *19*, 4545–4550. doi:10.1039/b818060a
14. André, P.; Cheng, G.; Ruseckas, A.; van Mourik, T.; Früchtli, H.; Crayston, J. A.; Morris, R. E.; Cole-Hamilton, D.; Samuel, I. D. W. *J. Phys. Chem. B* **2008**, *112*, 16382–16392. doi:10.1021/jp806031q
15. Źak, P.; Marciniec, B.; Majchrzak, M.; Pietraszuk, C. *J. Organomet. Chem.* **2011**, *696*, 887–891. doi:10.1016/j.jorgancchem.2010.10.021
16. Ferrer-Ugalde, A.; Juárez-Pérez, E. J.; Teixidor, F.; Viñas, C.; Núñez, R. *Chem. – Eur. J.* **2013**, *19*, 17021–17030. doi:10.1002/chem.201302493
17. Voisin, D.; Flot, D.; Van der Lee, A.; Dautel, O. J.; Moreau, J. J. E. *CrystEngComm* **2017**, *19*, 492–502. doi:10.1039/c6ce02369j
18. Źak, P.; Pietraszuk, C.; Marciniec, B.; Spólnik, G.; Danikiewicz, W. *Adv. Synth. Catal.* **2009**, *351*, 2675–2682. doi:10.1002/adsc.200900400
19. Źak, P.; Frąckowiak, D.; Grzelak, M.; Bolt, M.; Kubicki, M.; Marciniec, B. *Adv. Synth. Catal.* **2016**, *358*, 3265–3276. doi:10.1002/adsc.201600489
20. Yoshida, K. *Polym. Prepr. Jpn.* **2003**, *52*, 316.
21. Ootake, N.; Yoshida, K. US Pat. Appl. 2006/0196091(A1), July 13, 2006.
22. Dudziec, B.; Marciniec, B. *Curr. Org. Chem.* **2017**, *21*, 2794–2813. doi:10.2174/1385272820666151228193728
23. Źak, P.; Dudziec, B.; Kubicki, M.; Marciniec, B. *Chem. – Eur. J.* **2014**, *20*, 9387–9393. doi:10.1002/chem.201402862
24. Źak, P.; Majchrzak, M.; Wilkowski, G.; Dudziec, B.; Dutkiewicz, M.; Marciniec, B. *RSC Adv.* **2016**, *6*, 10054–10063. doi:10.1039/c5ra20848c
25. Asuncion, M. Z.; Laine, R. M. *J. Am. Chem. Soc.* **2010**, *132*, 3723–3736. doi:10.1021/ja0987743
26. Furgal, J. C.; Hung, J. H.; Goodson, T., III; Laine, R. M. *J. Am. Chem. Soc.* **2013**, *135*, 12259–12269. doi:10.1021/ja4043092
27. Jung, J. H.; Chou, K.; Furgal, J. C.; Laine, R. M. *Appl. Organomet. Chem.* **2013**, *27*, 666–672. doi:10.1002/aoc.3054
28. Czaban-Józwiak, J.; Woźniak, Ł.; Ulikowski, A.; Kwiecińska, K.; Rajkiewicz, A.; Grela, K. *Molecules* **2018**, *23*, 1722. doi:10.3390/molecules23071722
29. Kuo, S.-W.; Chang, F.-C. *Prog. Polym. Sci.* **2011**, *36*, 1649–1696. doi:10.1016/j.progpolymsci.2011.05.002
30. Zhou, H.; Ye, Q.; Xu, J. *Mater. Chem. Front.* **2017**, *1*, 212–230. doi:10.1039/c6qm00062b
31. Kausar, A. *Polym.-Plast. Technol. Eng.* **2017**, *56*, 1401–1420. doi:10.1080/03602559.2016.1276592
32. Ye, Q.; Zhou, H.; Xu, J. *Chem. – Asian J.* **2016**, *11*, 1322–1337. doi:10.1002/asia.201501445
33. Croissant, J. G.; Cattoën, X.; Durand, J.-O.; Wong Chi Man, M.; Khashab, N. M. *Nanoscale* **2016**, *8*, 19945–19972. doi:10.1039/c6nr06862f
34. Zhang, W.; Müller, A. H. E. *Prog. Polym. Sci.* **2013**, *38*, 1121–1162. doi:10.1016/j.progpolymsci.2013.03.002
35. Ayandele, E.; Sarkar, B.; Alexandridis, P. *Nanomaterials* **2012**, *2*, 445–475. doi:10.3390/nano2040445
36. Pieliuchowski, K.; Njuguna, J.; Janowski, B.; Pieliuchowski, J. *Adv. Polym. Sci.* **2006**, *201*, 225–296. doi:10.1007/12_077
37. Li, G.; Wang, L.; Ni, H.; Pittman Jr., C. U. *J. Inorg. Organomet. Polym.* **2001**, *11*, 123–154. doi:10.1023/a:1015287910502
38. Nuyken, O.; Schneider, M.; Frenzel, U. Metathesis polymerization. In *Encyclopedia of Polymer Science and Technology*; Mark, H. F., Ed.; Wiley, 2014; Vol. 8, pp 149–206.
39. Knall, A.-C.; Slugovc, C. Olefin metathesis polymerization. In *Olefin Metathesis. Theory and Practice*; Grela, K., Ed.; Wiley: Hoboken, 2014; pp 269–284. doi:10.1002/9781118711613.ch7
40. Suthasupa, S.; Shiotsuki, M.; Sanda, F. *Polym. J.* **2010**, *42*, 905–915. doi:10.1038/pj.2010.94
41. Leitgeb, A.; Wappel, J.; Slugovc, C. *Polymer* **2010**, *51*, 2927–2946. doi:10.1016/j.polymer.2010.05.002
42. Mather, P. T.; Jeon, H. G.; Romo-Uribe, A.; Haddad, T. S.; Lichtenhan, J. D. *Macromolecules* **1999**, *32*, 1194–1203. doi:10.1021/ma981210n
43. Zheng, L.; Farris, R. J.; Coughlin, E. B. *J. Polym. Sci., Part A: Polym. Chem.* **2001**, *39*, 2920–2928. doi:10.1002/pola.1272
44. Zheng, L.; Hong, S.; Cardoen, G.; Burgaz, E.; Gido, S. P.; Coughlin, E. B. *Macromolecules* **2004**, *37*, 8606–8611. doi:10.1021/ma048557c
45. Pittman, C. U., Jr.; Li, G.-Z.; Ni, H. *Macromol. Symp.* **2003**, *196*, 301–325. doi:10.1002/masy.200390170
46. Constable, G. S.; Lesser, A. J.; Coughlin, E. B. *Macromolecules* **2004**, *37*, 1276–1282. doi:10.1021/ma034989w
47. Gnanasekaran, D.; Madhavan, K.; Tsibouklis, J.; Reddy, B. S. R. *Aust. J. Chem.* **2011**, *64*, 309–315. doi:10.1071/chi10367
48. Gnanasekaran, D.; Madhavan, K.; Tsibouklis, J.; Reddy, B. S. R. *Polym. Int.* **2013**, *62*, 190–195. doi:10.1002/pi.4278
49. Zheng, X.-H.; Zhao, J.-F.; Zhao, T.-P.; Yang, T.; Ren, X.-K.; Liu, C.-Y.; Yang, S.; Chen, E.-Q. *Macromolecules* **2018**, *51*, 4484–4493. doi:10.1021/acs.macromol.8b00302
50. Kwon, Y.; Kim, K.-H. *Macromol. Res.* **2006**, *14*, 424–429. doi:10.1007/bf03219105
51. Xu, W.; Chung, C.; Kwon, Y. *Polymer* **2007**, *48*, 6286–6293. doi:10.1016/j.polymer.2007.08.014
52. Hou, P.-P.; Gu, K.-H.; Zhu, Y.-F.; Zhang, Z.-Y.; Wang, Q.; Pan, H.-B.; Yang, S.; Shen, Z.; Fan, X.-H. *RSC Adv.* **2015**, *5*, 70163–70171. doi:10.1039/c5ra12152c
53. Meng, C.-S.; Yan, Y.-K.; Wang, W. *Polym. Chem.* **2017**, *8*, 6824–6833. doi:10.1039/c7py01344b
54. Chae, C.-G.; Yu, Y.-G.; Seo, H.-B.; Kim, M.-J.; Grubbs, R. H.; Lee, J.-S. *Macromolecules* **2018**, *51*, 3458–3466. doi:10.1021/acs.macromol.8b00298
55. Vatansever, F.; Hamblin, M. R. *J. Nanopart. Res.* **2016**, *18*, No. 302. doi:10.1007/s11051-016-3328-y

56. Chatterjee, A. K.; Choi, T.-L.; Sanders, D. P.; Grubbs, R. H.
J. Am. Chem. Soc. **2003**, *125*, 11360–11370. doi:10.1021/ja0214882

License and Terms

This is an Open Access article under the terms of the Creative Commons Attribution License (<http://creativecommons.org/licenses/by/4.0>). Please note that the reuse, redistribution and reproduction in particular requires that the authors and source are credited.

The license is subject to the *Beilstein Journal of Organic Chemistry* terms and conditions:
(<https://www.beilstein-journals.org/bjoc>)

The definitive version of this article is the electronic one which can be found at:
doi:10.3762/bjoc.15.28



Aqueous olefin metathesis: recent developments and applications

Valerio Sabatino and Thomas R. Ward*

Review

Open Access

Address:

Department of Chemistry, University of Basel, Building 1096, Mattenstraße 24a, Biopark Rosental, 4058, Basel, Switzerland

Email:

Thomas R. Ward* - thomas.ward@unibas.ch

* Corresponding author

Keywords:

aqueous catalysis; artificial metalloenzymes; chemical biology; green chemistry; olefin metathesis; ruthenium catalysts; stapled peptides

Beilstein J. Org. Chem. **2019**, *15*, 445–468.

doi:10.3762/bjoc.15.39

Received: 31 October 2018

Accepted: 24 January 2019

Published: 14 February 2019

This article is part of the thematic issue "Progress in metathesis chemistry III".

Guest Editors: K. Grela and A. Kajetanowicz

© 2019 Sabatino and Ward; licensee Beilstein-Institut.

License and terms: see end of document.

Abstract

Olefin metathesis is one of the most powerful C–C double-bond-forming reactions. Metathesis reactions have had a tremendous impact in organic synthesis, enabling a variety of applications in polymer chemistry, drug discovery and chemical biology. Although challenging, the possibility to perform aqueous metatheses has become an attractive alternative, not only because water is a more sustainable medium, but also to exploit biocompatible conditions. This review focuses on the progress made in aqueous olefin metatheses and their applications in chemical biology.

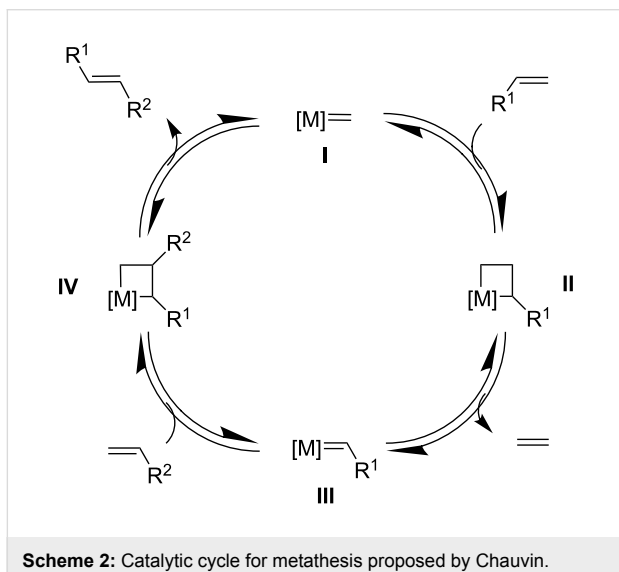
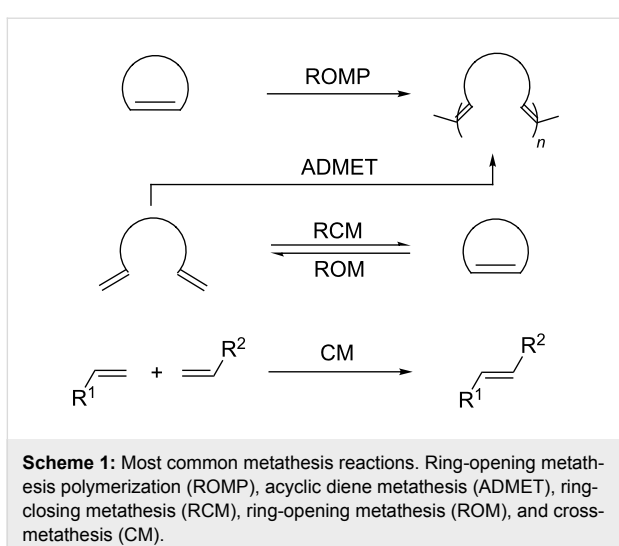
Introduction

Olefin metathesis represents a versatile synthetic tool for the construction of carbon–carbon bonds [1–9]. Since its first report in 1956, a Ti(II)-catalyzed polymerization of norbornene [10], metathesis rapidly attracted interest among organic chemists and has been used in different research fields spanning polymer chemistry [11,12] to drug discovery [13–15]. Scheme 1 displays the most common metathesis reactions.

The metathesis reaction mechanism, proposed by Chauvin in 1971, suggests that the reaction proceeds via the reversible formation of a metallacyclobutane intermediate (Scheme 2, intermediates **II** and **IV**) [16]. The catalytic cycle involves an initial

[2 + 2] cycloaddition between a metal carbene **I** and an olefin, followed by a retro [2 + 2] cycloaddition, leading to the release of a “scrambled” olefin (e.g., ethylene in Scheme 2) and the metal carbene species **III** as key intermediate. A [2 + 2] cycloaddition with a second olefin leads to the formation of intermediate **IV**, followed by a retro [2 + 2] cycloaddition that regenerates catalyst **I** and releases the metathesis product. This visionary mechanistic proposal was later confirmed by experimental studies [17–20].

Ruthenium-based catalysts are among the most tolerant and stable metathesis catalysts and are widely employed for metath-



eses in aqueous media [21,22]. There is a growing interest in performing metathesis reactions in water as a greener alternative to chlorinated or aromatic solvents [23,24]. Water is inexpensive, non-flammable, non-toxic and environmentally friendly, all characteristics that make it an ideal solvent. Furthermore, water is the media of biochemical reactions, and metathesis is a bioorthogonal reaction that can be exploited in a biological setting. Figure 1 illustrates some of the most representative catalysts developed for aqueous metathesis. Water-soluble catalysts are obtained by derivatization of classical catalysts **G-II** and **HG-II** (Figure 1a), resulting from the introduction of ionic tags and highly polar groups such as ammonium tags (Figure 1b) and PEGs (Figure 1c). This review focuses on the recent improvements of olefin metathesis in aqueous media and the resulting applications in bioinorganic chemistry and chemical biology.

Review

Challenges in aqueous metathesis

The first examples of aqueous metathesis were reported in the late 1980s [25,26]. ROMP reactions of 7-oxanorbornene derivatives **13** and **14** were carried out with the so-called “ill-defined” catalysts, namely $\text{RuCl}_3 \cdot \text{H}_2\text{O}$ and $\text{Ru}(\text{OTs})_2(\text{H}_2\text{O})_6$ [27,28] (Scheme 3). However, these catalysts had limited usefulness due to a slow initiation rate and detrimental effect of water on the reaction mixture.

Water can lead to the formation of catalytically inactive Ru hydride species. Fürstner et al. isolated these complexes as by-products during the synthesis of Grubbs second generation-type catalysts with saturated NHC ligands [29]. In this specific case, the formation of the metal hydride complex is believed to occur during the work-up with methanol. Dinger and Mol also carried out studies supporting this theory [30]. In their report, they elucidated the degradation pathway of the first generation Grubbs catalyst (**G-I**) in the presence of primary alcohols and water (Scheme 4). The detrimental effect of water is more likely to occur at high temperatures and in the presence of a base.

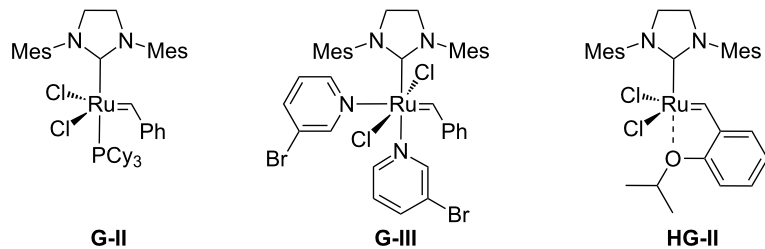
^1H NMR studies revealed that methanol is the source of hydride and this was later confirmed by Grubbs and co-workers [31]. The proposed mechanism for the degradation of **G-I** occurs via alcohol dehydrogenation followed by decarbonylation of the ruthenium hydride **16**.

In 2015, Cazin and co-workers showed that the detrimental effect of H_2O also occurs with the more innovative catalysts **Caz-I**, **Ind-II** and **HG-II** (Table 1) [32]. The authors performed the RCM of the challenging substrate **17** in toluene at 110 °C, reporting excellent yields in reactions carried out on a benchtop under air using non-degassed technical-grade solvents. However, upon addition of 100 μL of distilled degassed water to the reaction mixture, the conversions dropped to 36%, 15% and 8%, respectively, for **HG-II**, **Caz-I**, and **Ind-II** (Table 1). Thus, the presence of H_2O (ca. 6%) severely affects the phosphine-based catalysts **Caz-I** and **Ind-II**, while it has a less pronounced detrimental effect on the isopropoxy-benzylidene catalyst **HG-II**.

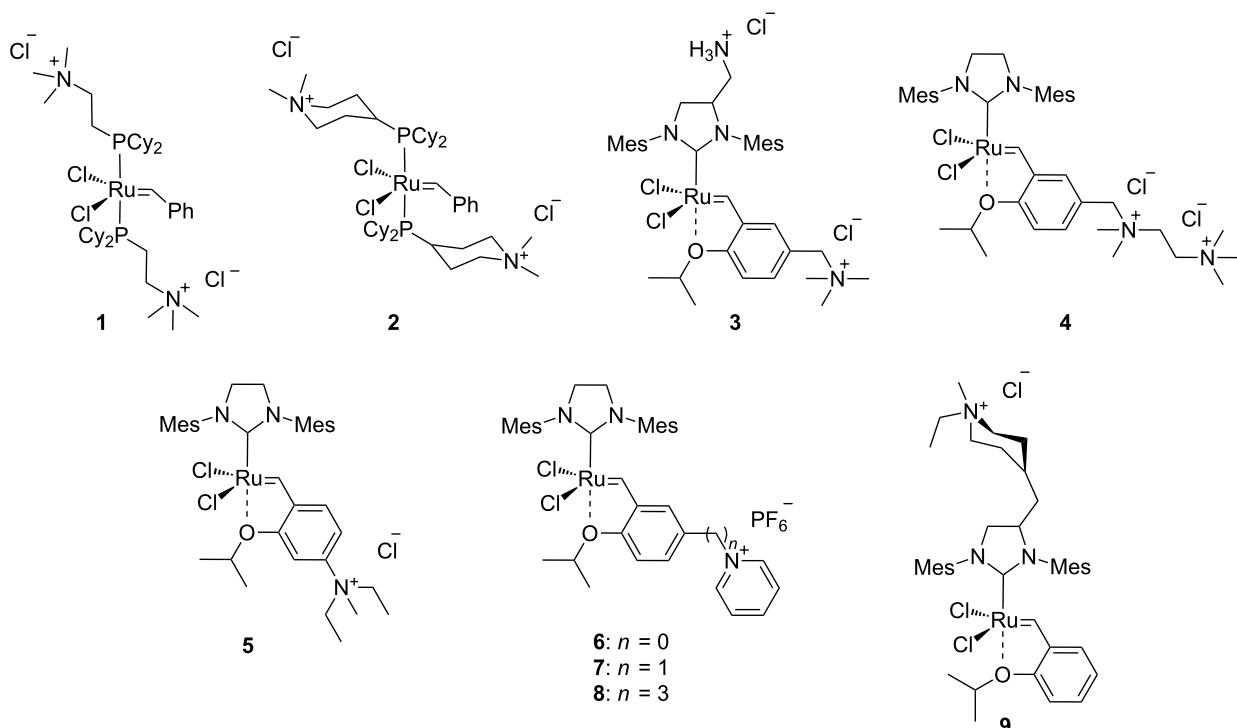
“On water” vs “in water” metathesis

Hydrophobic catalysts are able to perform metathesis in aqueous mixtures. Blechert and Raines reported examples of RCM, CM and ROMP in heterogeneous conditions with hydrophobic catalysts [21,33]. Blechert prepared alkoxy- and cyano-substituted catalysts **19** and **20** from **G-II** (Scheme 5) [34], while Raines and co-workers employed the conventional catalysts **G-II** and **HG-II** [35].

a) well-defined catalysts



b) ammonium-tagged catalysts



c) PEG-tethered catalysts

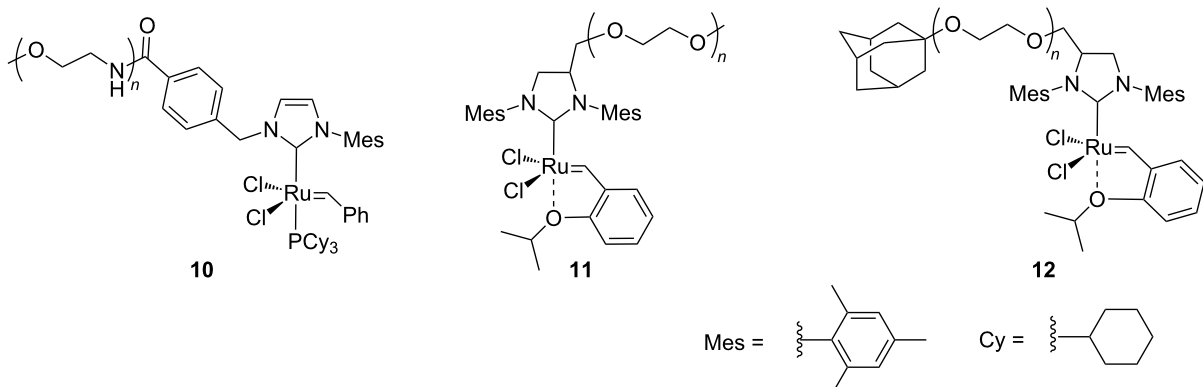


Figure 1: Some of the most representative catalysts for aqueous metathesis. a) Well-defined ruthenium catalysts. b) Catalysts bearing ammonium tags. c) PEG-tethered catalysts.

Blechert and Raines both performed RCM reactions with the benchmark substrate **21** in mixtures of water/organic solvent at room temperature in air (Table 2).

Table 2 summarizes the activities of the different ruthenium catalysts in protic media. The ratio water/co-solvent affects the RCM of substrate **21** catalyzed by **G-II** (77% conversion in

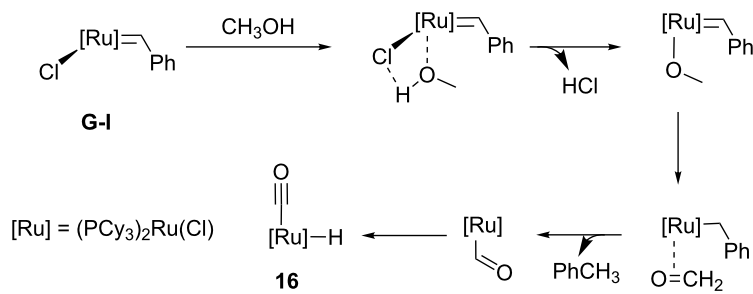
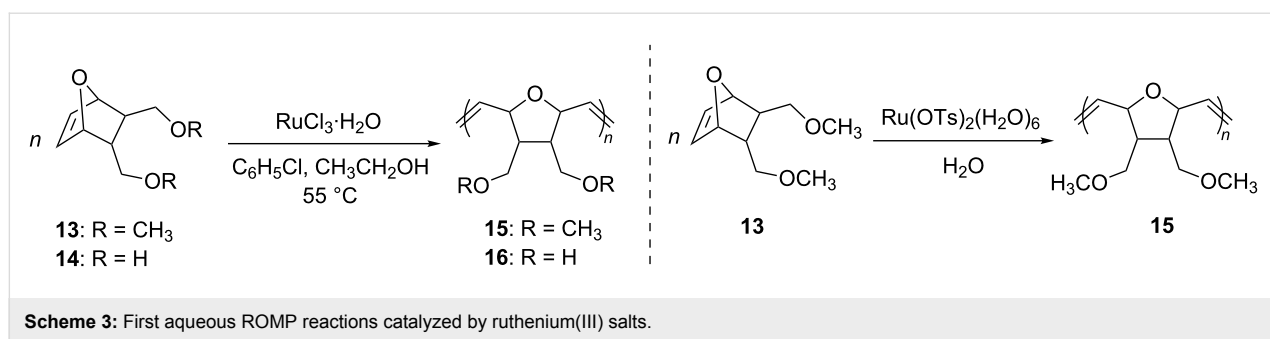
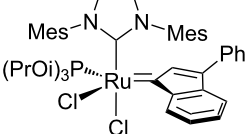
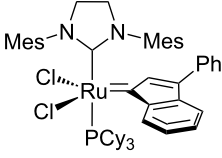
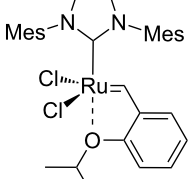
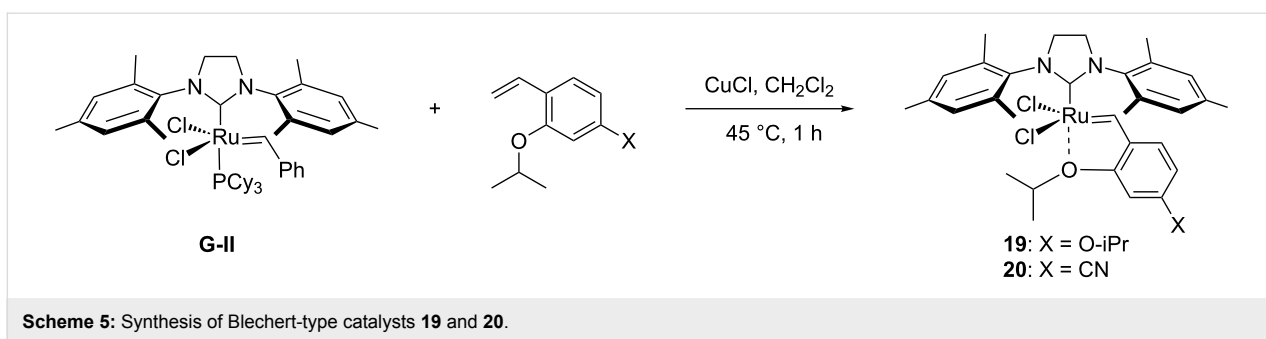


Table 1: RCM of challenging substrate 17 in air and in the presence of water.

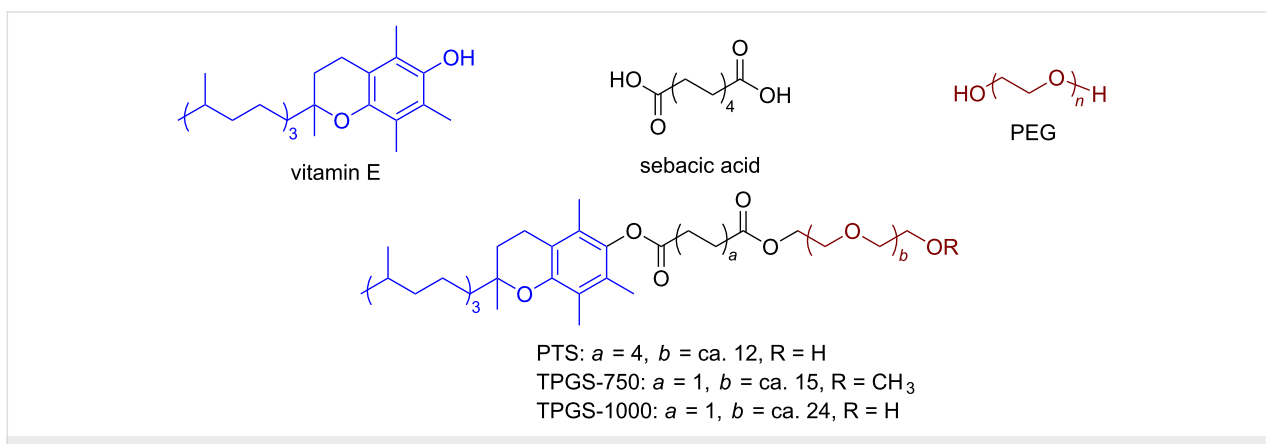
	Ru cat.	dry air (conv. %)	air (conv. %)	H ₂ O (conv. %)
Caz-I		90	60	15
Ind-II		70	22	8
HG-II		60	38	36

**Scheme 5:** Synthesis of Blechert-type catalysts **19** and **20**.**Table 2:** RCM of *N,N*-diallyltoluenesulfonamide (**21**) with ruthenium catalysts.

catalyst (mol %)	solvent	21	Ru (mol %)		conv. (%)	reference
			solvent, rt, in air	22		
G-II (5)	acetone/H ₂ O 2:1		24	rt	>95	[35]
G-II (5)	THF/H ₂ O 4:1		24	rt	3	[35]
G-II (3)	MeOH/H ₂ O 3:1		12	22	29	[34]
G-II (3)	MeOH/H ₂ O 1:3		12	22	77	[34]
G-II (3)	DMF/H ₂ O 1:3		12	22	82	[34]
9 (3)	MeOH/H ₂ O 3:1		12	22	87	[34]
9 (3)	MeOH/H ₂ O 1:3		12	22	94	[34]
9 (3)	DMF/H ₂ O 1:3		12	22	94	[34]
HG-II (3)	acetone/H ₂ O 2:1		2	rt	>95	[35]
HG-II (1)	DME/H ₂ O 2:1		24	rt	95	[35]

MeOH/H₂O 1:3 and 29% conversion in MeOH/H₂O 3:1). The drastic loss of activity can be traced back to the better activity of **G-II** under aqueous-emulsion conditions and the poor solubility of **G-II** in MeOH. These results suggest how important the role of the hydrophobic effect is on the catalytic activity of the reaction. In fact, catalyst and substrate are encapsulated into emulsion droplets formed in the reaction media above the aqueous layer, making the reaction proceed “on water” [21,22].

The introduction of amphiphilic molecules for aqueous micellar catalysis allows metathesis to proceed efficiently “in water” [36]. Lipshutz and co-workers generalized the application of a three-component non-ionic surfactant for numerous reactions in water, including olefin metathesis [37–39]. The surfactant, PTS, incorporates α -tocopherol, sebacic acid and PEG moieties as part of its structure, resulting in a non-ionic amphiphile (Figure 2).

**Figure 2:** Chemical structure and components of amphiphilic molecule PTS and derivatives.

In water, PTS forms nanomicelles which contribute to the solubilization of water-insoluble substrates and catalysts, thus contributing significantly to improve olefin metathesis yields. The positive effect of this strategy was demonstrated by Lipshutz and co-workers for RCM and for CM reactions [40,41]. Scheme 6 displays the RCM of selected substrates with **G-II** as catalyst in the presence of PTS as surfactant. The work of Lipshutz and co-workers is extensively reported elsewhere [21,33,42,43].

Catalyst encapsulation is a recent example of “in water” metathesis with a heterogenous catalytic system. Pauly et al. used alginate beads as a matrix to encapsulate the **G-II** catalyst for the RCM of substrate **31** and **33** (Scheme 7) [44]. Alginate amide beads perform best in neat water as they facilitate the diffusion of hydrophobic substrates through the beads. However, the reaction rates are very low compared to the non-encapsulated catalyst **G-II**. The main advantage of the catalyst encapsulation is the catalyst recycling, as the alginate beads can be reused up to 10 times, retaining about 80% of activity.

Catalysts bearing quaternary ammonium tags

Classical metathesis catalysts such as **G-II** and **HG-II** are among the most active, stable and versatile ruthenium complexes. Despite their high activity and remarkable stability, they are sparingly soluble in neat water, thus challenging their use as homogeneous catalysts in pure water. To overcome this challenge, a small amount of organic co-solvent (or surfactant) is frequently used.

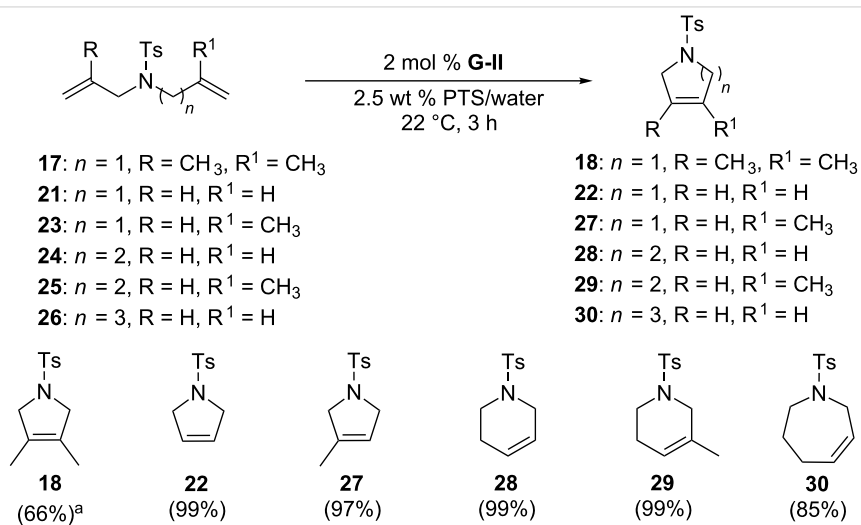
The removal of residual ruthenium traces is a crucial step for most industrial applications [45–50]. Indeed, the purifica-

tion of products from metathesis reaction mixtures often requires multiple tedious steps, primarily because metal complexes’ impurities in the final product may cause isomerization or decomposition of the products and may be toxic. The latter is a very critical issue for the pharmaceutical industry, as the amount of ruthenium in APIs (active pharmaceutical ingredients) may not exceed 100 µg/day for drugs administered per os (oral administration) and 1 µg/day by inhalation [51].

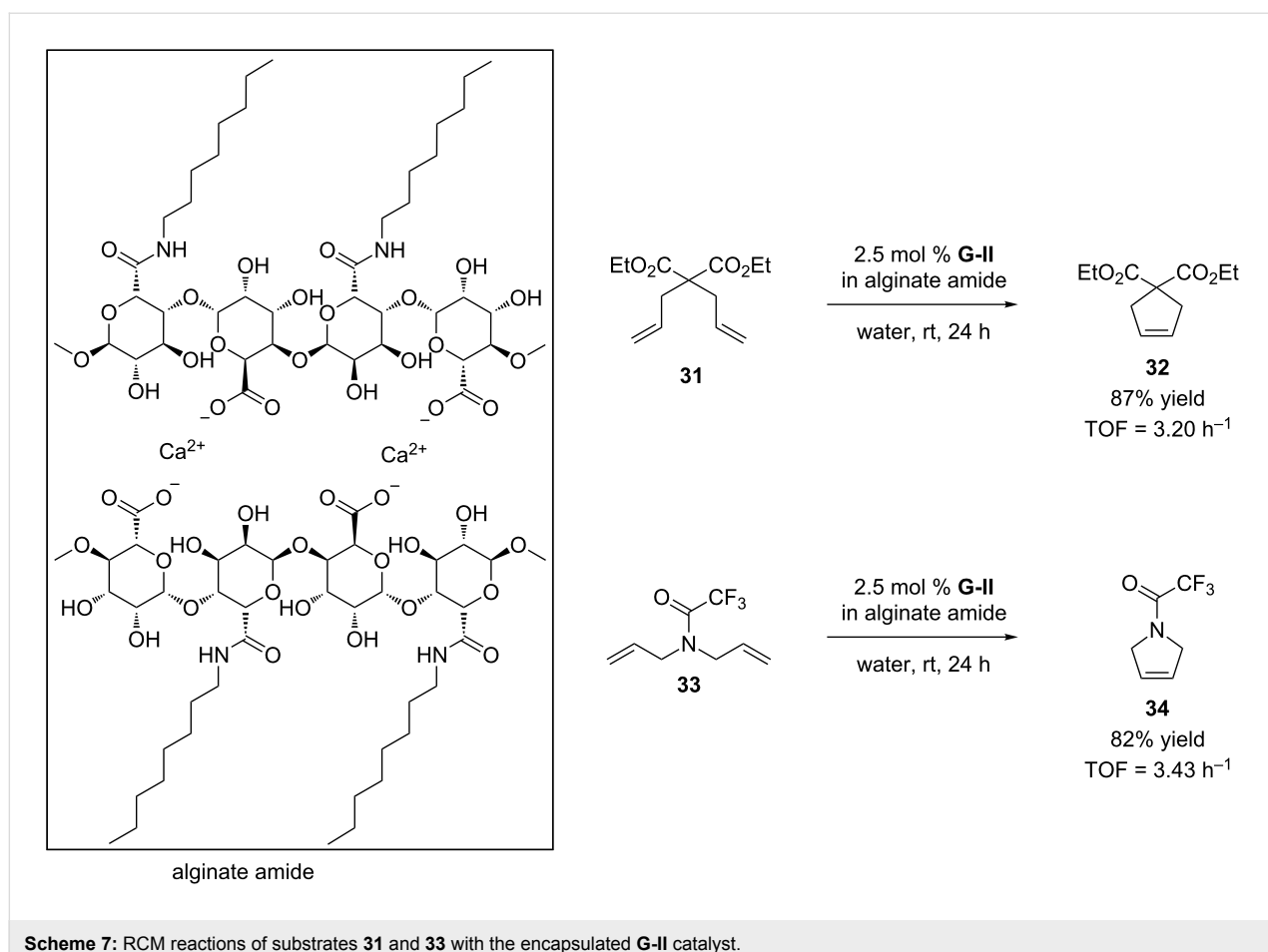
Some of the difficulties highlighted above can be overcome by the incorporation of quaternary ammonium tags, which simplify product purification as well as olefin metathesis in pure water [52,53].

Grubbs and co-workers were the first to introduce water-soluble catalysts which displayed metathesis activity in aqueous media [54]. In 1996, Grubbs et al. reported that complexes **1** and **2** catalyze the living opening polymerization of norbornene derivatives **35** and **36** in neat water. Interestingly, the presence of a Brønsted acid led to the protonation of one phosphine ligand rather than reacting with the ruthenium alkylidene moiety. Scavenging of the trialkylphosphine moiety resulted in a more active complex capable of initiating the ROMP of 2,3-difunctionalized norbornadienes and 7-oxo analogues (Scheme 8).

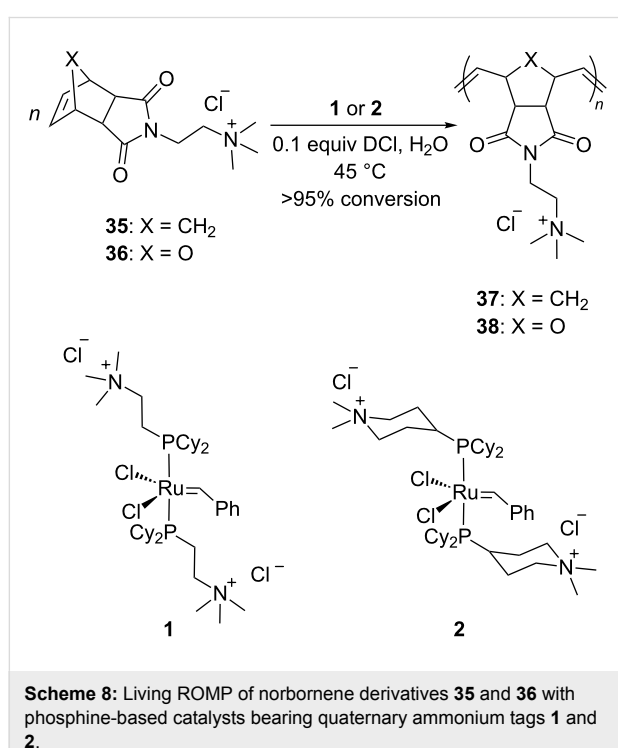
However, catalysts **1** and **2** are unstable in water and their use is limited to ROMP. Polyethylene glycol (PEG)-tagged catalysts (**10** and **11**, Figure 1c) showed significantly improved RCM activities in water, but they tend to form aggregates in water due to their high molecular weight (ca. 5,000 g·mol^{−1}) [55]. A few years later, Grubbs and co-workers reported the use of NHC complexes containing quaternary ammonium tags [56].



Scheme 6: RCM of selected substrates in the presence of the surfactant PTS. Conditions^a: The reaction was carried out at 60 °C for 24 hours.



Scheme 7: RCM reactions of substrates **31** and **33** with the encapsulated **G-II** catalyst.

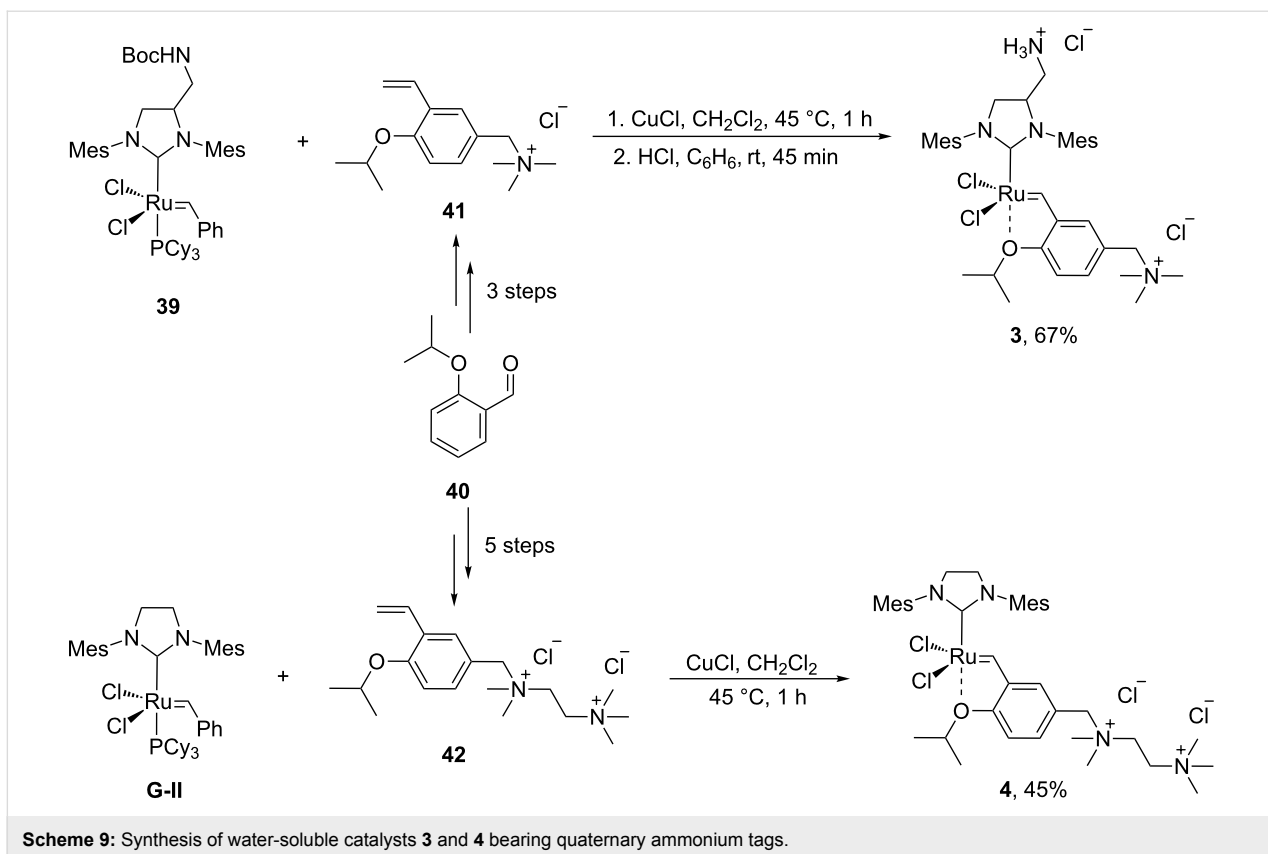


Scheme 8: Living ROMP of norbornene derivatives **35** and **36** with phosphine-based catalysts bearing quaternary ammonium tags **1** and **2**.

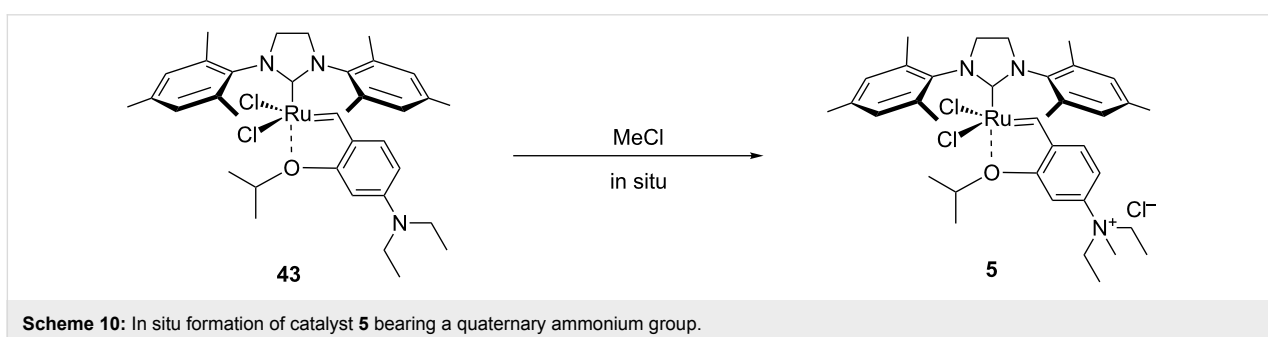
The catalysts **3** and **4** were obtained by the reactions of **G-II** and the asymmetric Boc-protected derivative **39** with 2-isopropyloxystyrene derivatives **41** and **42** (Scheme 9). Catalysts **3** and **4** showed modest activities in the ROMP of substrate **35**.

In 2006, Grela and co-workers reported the synthesis of the metathesis catalyst **5** also bearing a quaternary ammonium tag [57]. Following their previous studies highlighting the beneficial effect of an electron-withdrawing group (EWG) on the benzylidene moiety, such as NO_2 [58], they proposed an “electron-donating to electron-withdrawing activity switch”, consisting of an *in situ* formation of quaternary ammonium salts by treatment with Brønsted acids (Scheme 10). Several metathesis reactions were performed in methanol/water mixtures with EWG-substituted catalyst **5**.

The “*in situ*” strategy was successfully applied to the preparation of catalysts **47**, **48** and **49** by Skowerski et al. [59]. Treatment of the free bases **44**, **45** and **46** with methyl chloride (MeCl) yielded the corresponding ammonium quaternized groups (Table 3).



Scheme 9: Synthesis of water-soluble catalysts 3 and 4 bearing quaternary ammonium tags.



Scheme 10: In situ formation of catalyst 5 bearing a quaternary ammonium group.

In a recent publication, catalyst **9** was used for an aqueous living ring-opening metathesis polymerization-induced self-assembly (ROMPISA). The authors demonstrated the possibility of performing living ROMP in water selecting a quaternary ammonium-based phenyl norbornene carboximide as core-forming monomer [60]. This polymer is currently being investigated for possible biomedical applications.

Table 4 summarizes the activities of the different ammonium-tagged catalysts discussed above with several water-soluble substrates. Catalysts **3** and **4** showed modest to excellent activities in the RCM of *N,N*-diallylated substrate **50** (respectively 36% and >95% yield with **3** and **4**) and substrate **54** (>95% yield with both catalysts). There is no obvious explanation why

the RCM of **52** does not occur under identical conditions. Catalysts **9**, **47** and **48** display good activities for the ring-closing of substrates **54** and **56**, for the self-metathesis of allyl alcohol (**59**) and the *cis-trans* isomerization of *cis*-butenedienol (*Z*-**58**).

Metathesis catalysts bearing quaternary ammonium groups provide an attractive alternative to classical ruthenium catalysts. Although they do not represent a great improvement in terms of catalytic activity, they significantly improve the water solubility and facilitate the removal of ruthenium residues from reaction mixtures [52,59]. The majority of such ruthenium complexes can easily be removed, especially for the metathesis of water-insoluble substrates, as demonstrated by Grela and co-workers for the RCM of diallylmalonate **31** in DCM

Table 3: The “in situ” formation of quaternary ammonium-tagged catalysts.

precursor	R	R ¹	catalyst	R ²	R ³
44			47		
45		H	48		H
46	iPr		49	iPr	

Table 4: Aqueous metathesis of selected substrates with water-soluble catalysts bearing quaternary ammonium groups.

substrate	product	cat. (mol %)	T (°C)	t (h)	yield % (E:Z)
50	51	3 (5) 4 (5)	rt rt	4 24	36 >95
52	53	3 (5) 4 (5)	rt rt	24 24	<5 <5
54	55	3 (5) 4 (5) 9 (5) 47 (5) 48 (5)	rt rt rt rt rt	12 24 2.5 2.5 3.5	>95 >95 96 88 49
56	57	9 (5) 47 (5) 48 (5)	rt rt rt	5 5 5	46 41 62

Table 4: Aqueous metathesis of selected substrates with water-soluble catalysts bearing quaternary ammonium groups. (continued)

		3 (5) 4 (5) 9 (0.5) 47 (0.5) 48 (0.5)	30 30 rt rt rt	2 24 0.16 0.13 1.1	94 92 94 94 71
		3 (5) 4 (5) 9 (5) 47 (5) 48 (5)	45 45 rt rt rt	6 24 24 24 24	69 82 77 (16.7:1) 38 (12.5:1) 74 (16.7:1)

(Scheme 11). Upon reaction completion, the catalyst is extracted from the organic reaction mixture with D_2O and (re)-used for the isomerization of *cis*-butenediol **Z-58** in water.

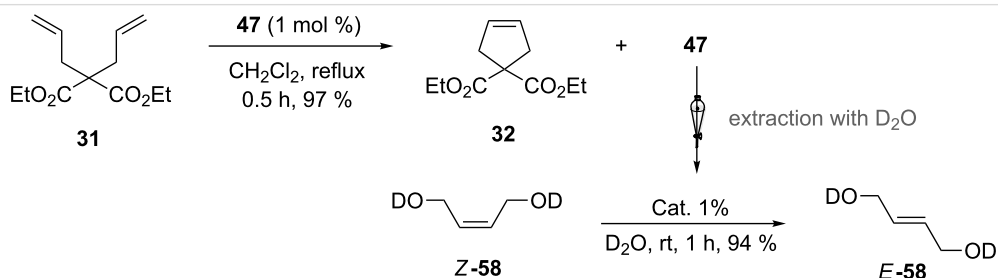
Recently the removal of a water-soluble catalyst from reaction mixtures was also achieved with catalyst **12** (Figure 1c) through host–guest interactions [61]. Chung and co-workers used a PEG-tethered adamantyl ligand for various metathesis reactions in water and DCM [62]. The authors showed that the catalyst can be easily removed by generating a host–guest complex between silica-grafted β -cyclodextrin and the adamantyl group of catalyst **12**. A simple filtration of the crude mixture through a cotton plug after RCM of substrate **54** yields the purified product with 53 ppm of residual ruthenium (Scheme 12).

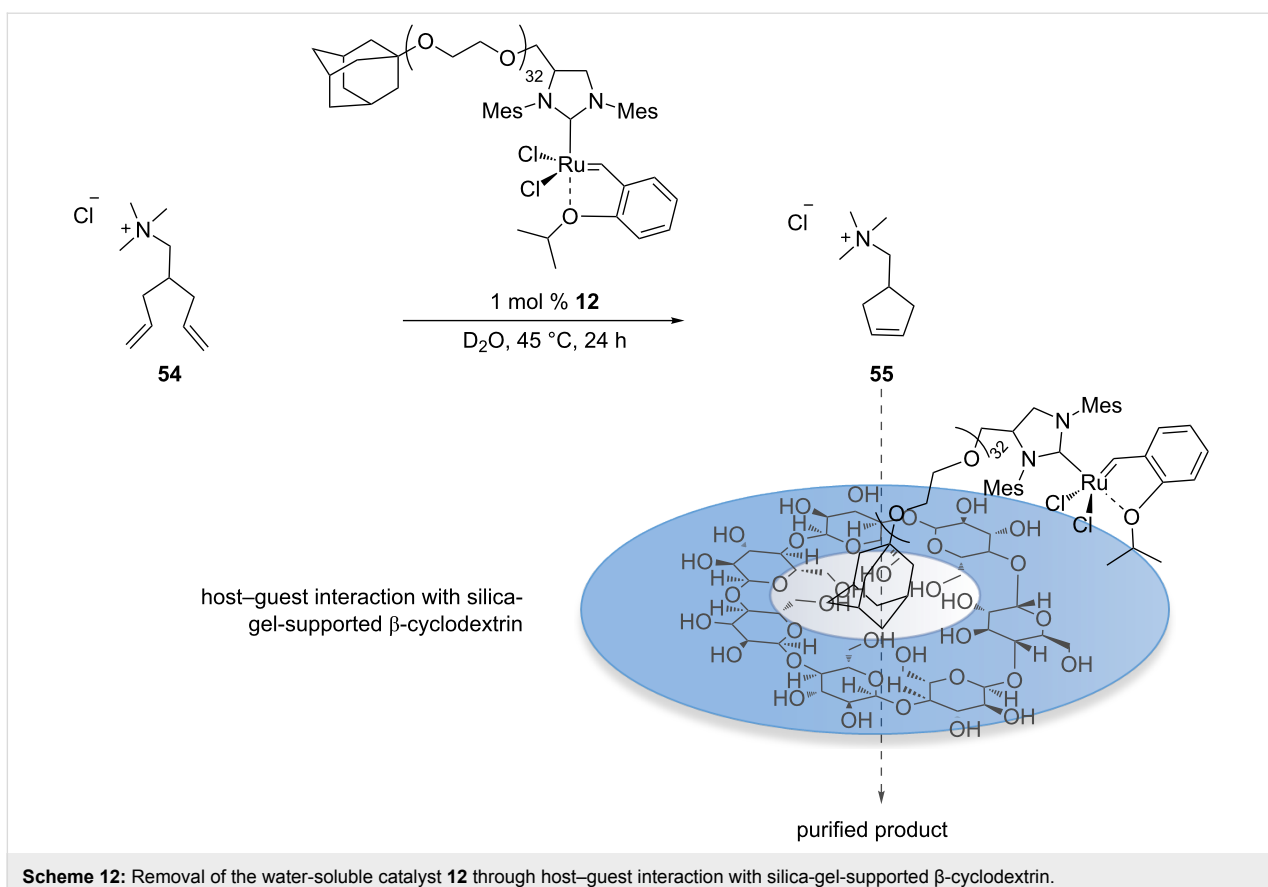
Metathesis with artificial metalloenzymes

Directed evolution allows an iterative improvement by successive rounds of mutation and screening the performances of genetically-encoded enzymes. Hypothesizing that this tool may be applicable to the optimization of artificial metalloenzymes (ArMs) for olefin metathesis, a new-to-nature bioorthogonal reaction might be introduced in a biological system. ArMs result from the incorporation of a catalytically active organometallic moiety within a protein scaffold. Such biohybrid catalysts enable a chemogenetic optimization of their catalytic performances. As olefin metathesis is bioorthogonal, it offers attractive features for the manipulation of biological systems. Comprehensive reviews on ArMs can be found elsewhere

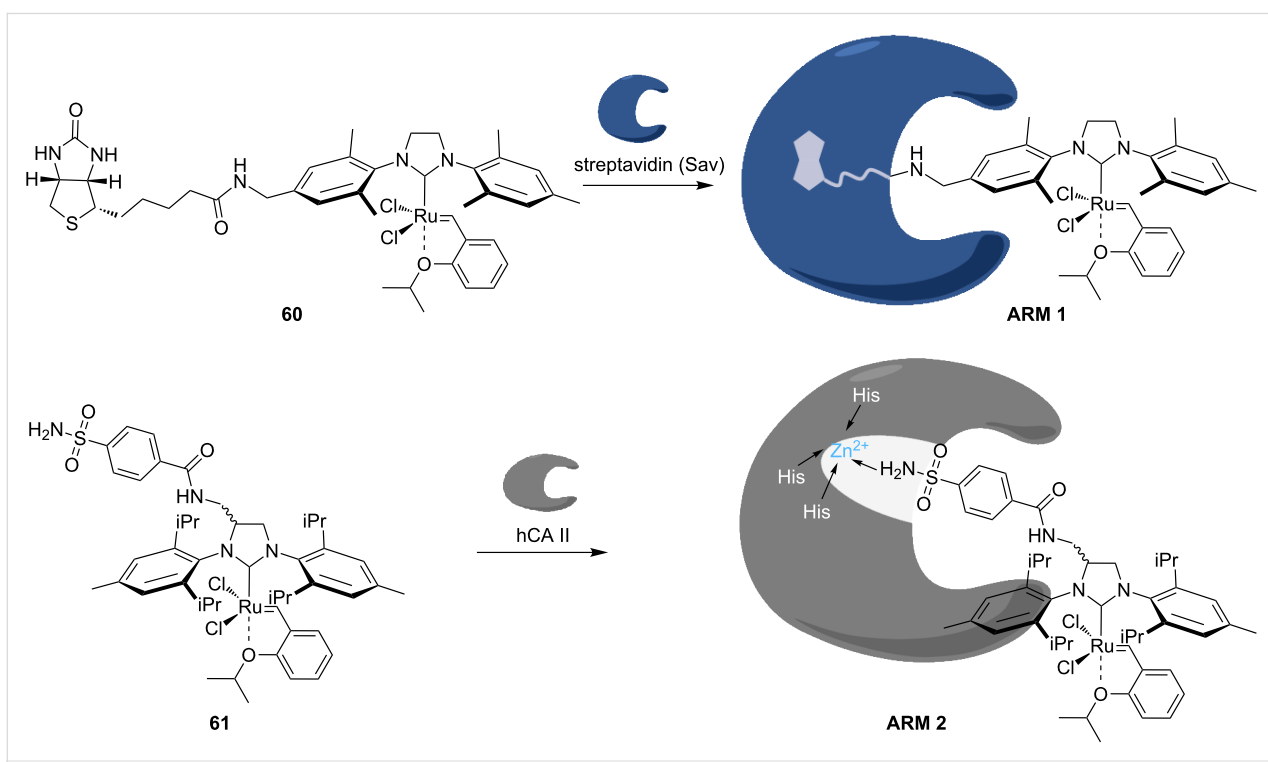
[63,64]. Several artificial metalloenzymes able to perform metathesis, coined artificial metathases, have been reported since 2011. The artificial metathases rely on different strategies to anchor the organometallic moiety to the protein scaffold and include supramolecular, dative, as well as covalent anchoring. Ward and co-workers reported the first artificial metathase based on the biotin–(strept)avidin technology in 2011 [65], thus expanding the set of reported reactions with this class of ArMs [66]. It is well known that the biotin–(strept)avidin couple possesses one of the highest non-covalent binding affinities ($K_d = 10^{-12}$ – 10^{-15} M). This exceptional affinity warrants the ArM remaining assembled throughout catalysis. Biotinylated HG-type catalysts anchored within (strept)avidin through supramolecular interactions were tested in the RCM of *N,N*-diallyltoluenesulfonamide (**21**) in aqueous media, achieving encouraging results at pH 4 and in the presence of MgCl_2 [65]. The chemical optimization of the organometallic moiety revealed catalyst **60**, which was combined with streptavidin (Sav) to afford **ArM 1** (Scheme 13). Ward and co-workers reported another artificial metathase based on the dative anchoring of a biotinylated HG-type catalyst to human carbonic anhydrase II (hCAII) in 2015 [67]. The active site of hCAII contains Zn^{2+} which is coordinated to three histidines. Catalyst **61** contains an arylsulfonamide moiety that coordinates the metal with high affinity ($K_d = 205$ nM), affording **ArM 2** (Scheme 13).

From the different organometallic moieties tested, the catalyst containing 2,6-diisopropylphenyl groups on the NHC ligand afforded the highest activity for the aqueous RCM of *N,N*-dial-

**Scheme 11:** Catalyst recycling of an ammonium-bearing catalyst.



Scheme 12: Removal of the water-soluble catalyst **12** through host–guest interaction with silica-gel-supported β -cyclodextrin.



Scheme 13: Selection of artificial metathases reported by Ward and co-workers (**ARM 1** based on biotin–(strept)avidin technology and **ARM 2** based on dative anchoring to hCAII).

lyltosylamine (**21**). Metathase **ArM 2** performed best in phosphate buffer at pH 5.0, yielding 85% of product **22** (Table 5). A substitution of lysine with histidine at position 198 (Table 5, entries 8 and 9) did not improve the catalytic efficiency of **ArM 2** at pH 7.0.

Jeschek et al. subsequently evolved **ArM 1** *in vivo* by directed evolution of an artificial metathase [68]. Tethering an OmpA leader sequence to the *N*-terminus of streptavidin (Sav) allowed the secretion and assembly of functional tetrameric Sav in the periplasm of *E. coli*. The passive diffusion of the biotinylated Hoveyda–Grubbs catalyst **60** through the outer membrane of *E. coli* containing Sav in its periplasm then affords the artificial metathase **ArM 1**. Upon addition of the umbelliferone precursor **62**, RCM reaction occurs in AcONa/AcOH buffer (pH 4.0) in the presence of 0.5 M MgCl₂. The formed umbelliferone (**63**) can be detected by fluorescence (Figure 3).

The fifth generation Sav-mutant resulting from directed evolution (Sav_mut^{5*}) displayed a cell-specific activity

Table 5: Selected RCM reaction with hCAII-based artificial metathase ArM 2.

entry ^a	hCAII ^b	MgCl _n (mol/L)	pH	TON	
				1 mol % 61	1.2 mol % hCAII
1	–	MgCl ₂ (0.1)	6.0	48 ± 0.8	
2	WT	MgCl ₂ (0.1)	6.0	45 ± 2.0	
3	–	–	7.0	23 ± 2.1	
4	–	MgCl ₂ (0.5)	5.0	85 ± 1.0	
5	WT	MgCl ₂ (0.5)	5.0	78 ± 2.5	
6	–	NaCl (0.154)	7.0	32 ± 2.0	
7	WT	NaCl (0.154)	7.0	21 ± 1.8	
8	L198H	NaCl (0.154)	7.0	28 ± 0.6	
9	L198H	–	7.0	22 ± 0.1	

^aReaction conditions: [21]: 1 mM, [61]: 10 µM, [hCA II]: 12 µM, V_{tot}: 200 µL (DMSO 10%), 37 °C. Reactions carried out in triplicate.

^bWT = wild-type.

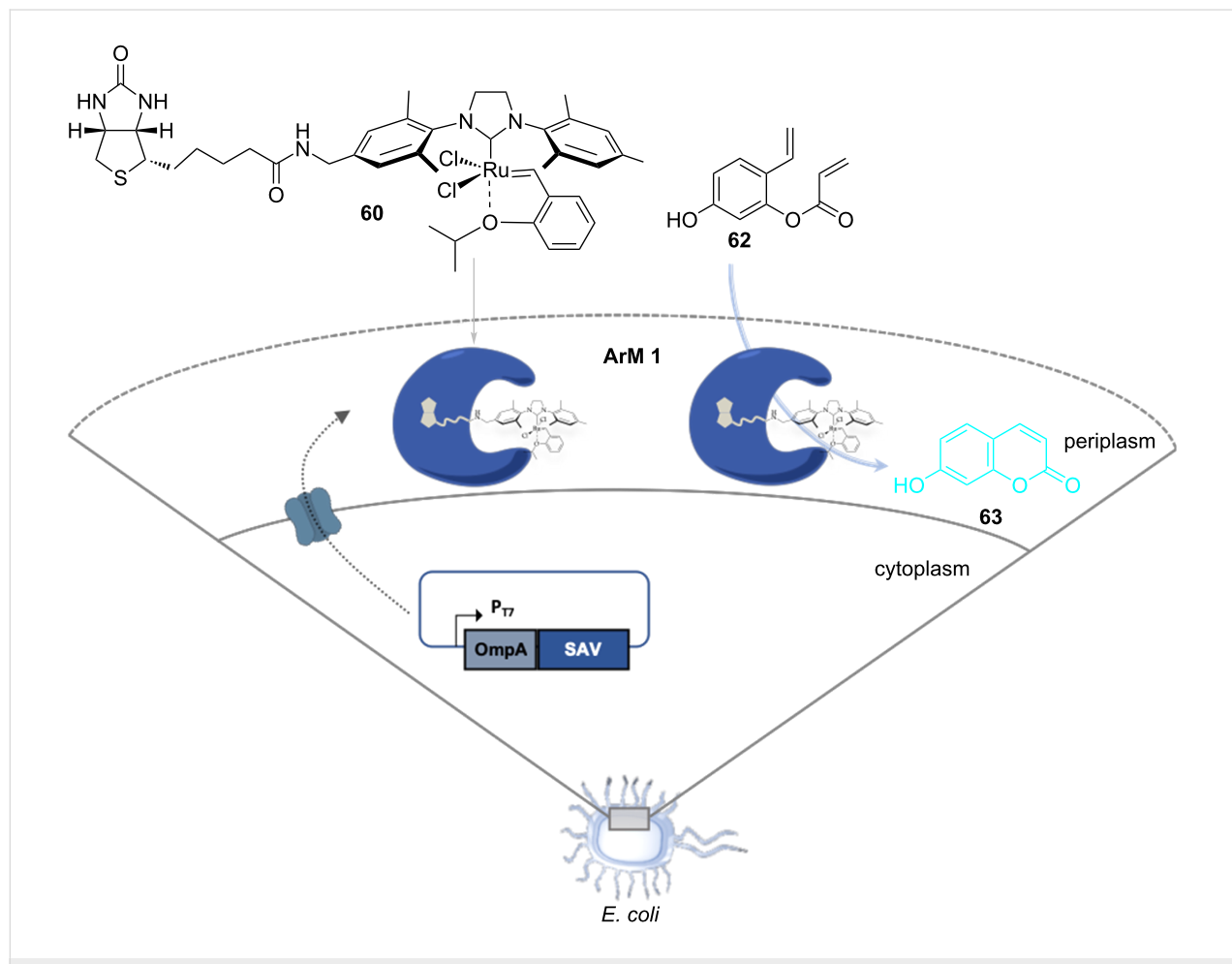


Figure 3: In vivo metathesis with an artificial metalloenzyme based on the biotin–streptavidin technology.

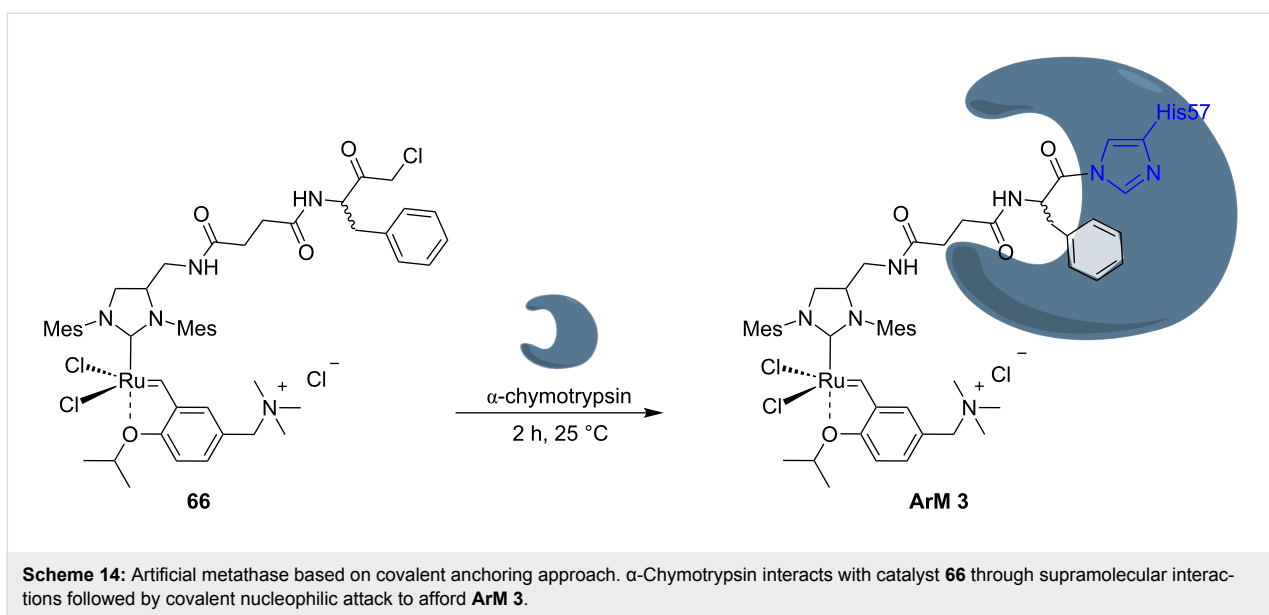
5.4 ± 1.2 times higher than the wild-type enzyme. Table 6 summarizes the different RCM reactions tested using purified **ArM 1** in aqueous buffer at 37 °C [68,69].

Matsuo et al. used α -chymotrypsin as protein scaffold to assemble an artificial metathase by covalent anchoring [70]. α -Chymotrypsin is a serine protease that recognizes hydro-

Table 6: Selected RCM results obtained with artificial metathase **ArM 1** using purified Sav samples.

entry ^a	substrate	catalyst (%)	protein ^b	TON
1		60	–	1.1
2		60	Sav	1.7
3		60	Sav_mut ^{5*}	4.4
4		60	–	180 ± 4 ^c
5		60	Sav	430 ± 3 ^c
6		60	Sav_mut ^{5*}	650 ± 35 ^c
7 ^d		60	–	30 ± 1
8 ^d		60	Sav	52 ± 2
9 ^d		60	Sav_mut ^{5*}	90 ± 3

^aReaction conditions: 100 mM acetate buffer, 0.5 M MgCl₂, pH 3.6, [catalyst] = 50 μ M, 16 h at 37 °C and 200 rpm. ^bSav_mut^{5*} = Sav V47A/N49K/T114Q/A119G/K121R. ^cTON determined by ¹H NMR. ^d[Substrate] = 20 mM; TON determined by UPLC-MS analysis.



phobic residues in one of its clefts. A modified HG-type catalyst (**66**) contains an L-phenyl chloromethyl ketone moiety that acts as inhibitor and is first recognized by supramolecular anchoring and then covalently attaches upon nucleophilic attack at the chloromethyl moiety by the imidazole of His57, to afford the artificial metathase **ArM 3** (Scheme 14).

Matsuo et al. tested the RCM of three different substrates with the protein-free catalyst **66** as well as **ArM 3** (Table 7). No RCM occurred with substrate **52** (<2 TON) with catalyst **66**, while the RCM of **67** reached 20 and 14 TON, respectively, with **ArM 3** and catalyst **66**. However, **ArM 3** decreased the RCM activity of **21** to 4 TON compared to 20 TON with catalyst **66**.

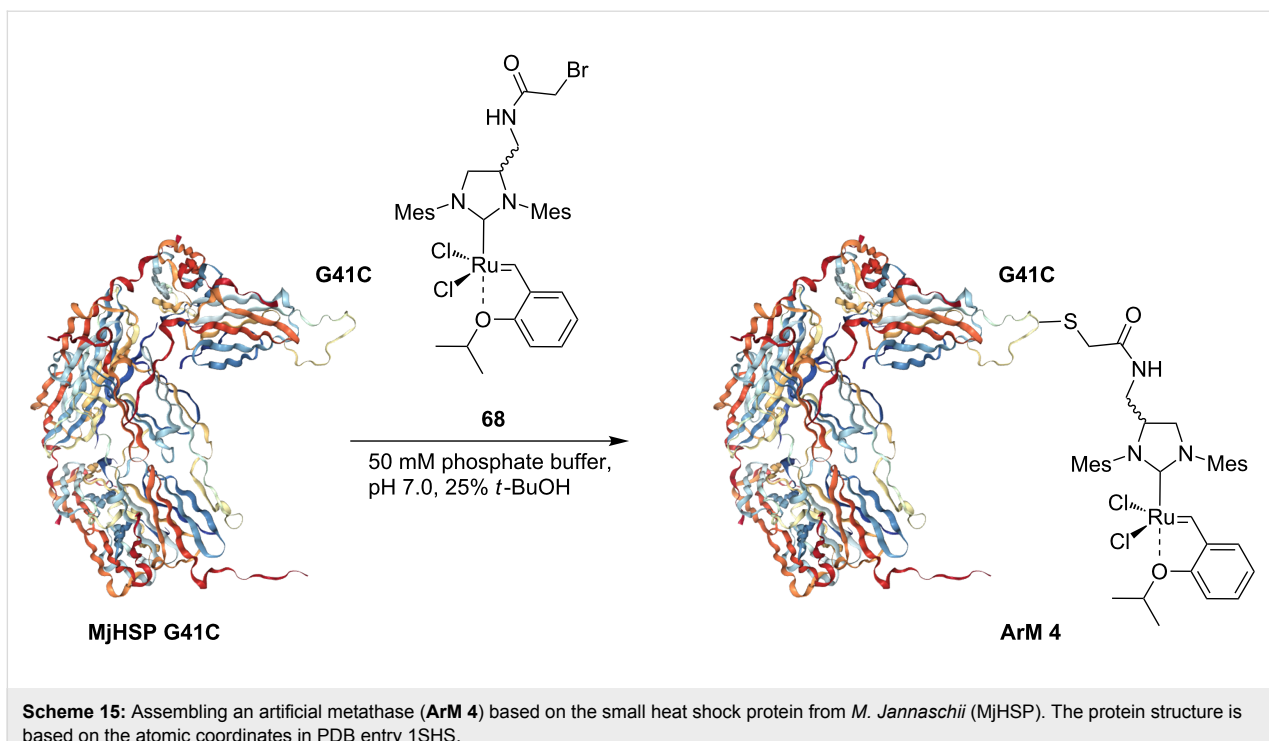
In 2011, Hilvert and co-workers reported an ArM based on the covalent anchoring of a metathesis catalyst to a small heat shock protein from *M. Jannaschii* (MjHSP) [71]. The authors reported a HG-II-type catalyst modified on its NHC backbone with an α -bromoacetyl unit (**68**) that is reacted with the unique cysteine of the modified MjHSP variant (G41C) to afford **ArM 4** (Scheme 15).

The hybrid catalyst **ArM 4** was then tested for the aqueous RCM of substrate **21**. In a $\text{H}_2\text{O}/t\text{-BuOH}$ mixture, the catalytic efficiency of **ArM 4** markedly increases upon lowering the pH (Table 8, entry 6), although under the same conditions, the free catalyst **68** performs better (Table 8, entry 3).

Cavity-size engineered ArMs are the first example of biohybrid catalysts able to catalyze all three main olefin metathesis reactions (RCM, ROMP and CM) [72]. Schwaneberg and Okuda

Table 7: RCM activities of catalyst **66** and **ArM 3** with substrates **67**, **52** and **21**.

entry	substrate	catalyst	TON
1			20
2			14
3			N.D.
4			<2
5			4
6			20



Scheme 15: Assembling an artificial metathase (**ArM 4**) based on the small heat shock protein from *M. Jannaschii* (MjHSP). The protein structure is based on the atomic coordinates in PDB entry 1SHS.

Table 8: RCM of *N,N*-diallyltoluenesulfonamide (**21**) with **ArM 4**.

		2–4 mol % catalyst		
entry	catalyst (mol %)	buffer	pH	TON
1	68 (2)	50 mM phosphate	7.0	2 ± 0.2
2	68 (2)	50 mM MES	3.9	16 ± 0.4
3	68 (2)	10 mM HCl	2.0	33 ± 0.5
4	ArM 4 (4)	50 mM phosphate	7.0	3 ± 0.1
5	ArM 4 (4)	50 mM MES	3.9	12 ± 1.5
6	ArM 4 (4)	10 mM HCl	2.0	25 ± 2.1

engineered the cavity size of the β -barrel protein nitrobindin (variant 4, NB4) to accommodate HG-type catalysts. The authors followed a similar approach developed earlier with a variant of the β -barrel protein FhuA [73,74]. To do so, the authors duplicated multiple β -barrel strands to enlarge the cavity of the protein. HG-type catalysts bearing a maleimide moiety with different spacer lengths (**69–71**) were covalently anchored to a cysteine of the expanded nitrobindin variant (**NB4exp**). The coupling reaction in aqueous buffer at pH 7.5 finally affords **ArM 5**, **ArM 6** and **ArM 7**, respectively (Scheme 16).

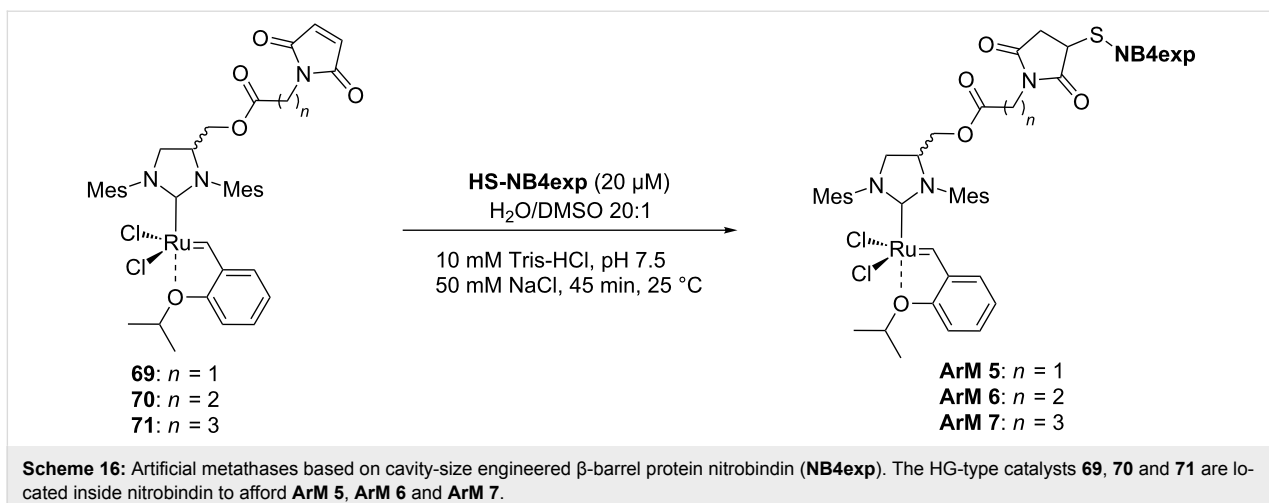
The obtained hybrid catalysts were tested for the RCM with substrates **21** and **64** (Table 9). Overall, **ArM 6** and **ArM 7** are

comparable and perform best in both reactions with 35% conversion of substrate **21** and quantitative conversion of substrate **64**. The water-soluble catalyst **9** was compared to the hybrid catalysts, displaying a higher TON in the RCM of **21** (Table 9, entry 4). Interestingly, the activity of catalyst **9** is inhibited in the presence of **NB4exp** (Table 9, entries 5 and 10).

In the ROMP of the norbornene derivative **13**, **ArM 6** and **ArM 7** performed best, outperforming catalyst **9**. A near ten-fold increase is observed for **ArM 6** (Table 10, entry 2).

In the cross metathesis of terminal olefins **73**, **74**, and **75**, with the commercial catalyst **9** conversions of 79%, 98% and 94%, respectively, were achieved. As in the RCM, the combination with **NB4exp** did not give any conversion (Table 11, entry 5). All three ArMs converted the three substrates with good yields of products **76**, **77** and **78**. **ArM 6** performed the best, affording quantitative conversion for all three substrates (Table 11, entries 2, 7 and 12).

Gebbink and co-workers anchored the HG-type catalyst **79** to cutinase, a serine hydrolase [75]. The phosphonate ester moiety acts as a suicide inhibitor forming an irreversible covalent bond to a serine residue present in the active site of the enzyme. Assembly of **ArM 8** occurs at pH 5 (Scheme 17). The activity of the artificial metalloenzyme was tested with the benchmark RCM substrate **21**, yielding 84% of product **22** in acetate buffer

**Table 9:** Selected RCM results of *N,N*-diallyltoluenesulfonamide (**21**) and diol **64**.

 21	$1 \text{ mol \% catalyst}$ $5 \text{ mM MES buffer, pH 6}$ $200 \text{ mM NaCl, } 40^\circ\text{C, 24 h}$ 750 mbar	 22: $X = N$; $R = \text{Tos}$ 72: $X = C$; $R = (\text{CH}_2\text{OH})_2$	 64	$1 \text{ mol \% catalyst}$ $5 \text{ mM MES buffer, pH 6}$ $200 \text{ mM NaCl, } 40^\circ\text{C, 24 h}$ 750 mbar
entry	catalyst	substrate	substrate	conversion (%) = TON
1	ArM 5	21		16
2	ArM 6	21		35
3	ArM 7	21		35
4	9	21		41
5	9 + NB4exp	21		0
6	ArM 5	64		45
7	ArM 6	64		100
8	ArM 7	64		100
9	9	64		100
10	9 + NB4exp	64		0

Table 10: ROMP of 7-oxonorbornene derivative **13** with β -barrel engineered artificial metalloenzymes.^a

 13	$0.008 \text{ mol \% catalyst}$ $5 \text{ mM MES buffer, pH 6.0}$ $200 \text{ mM NaCl, } 23^\circ\text{C, 12 h}$	 15			
			entry	catalyst	conversion ^b (%)
1	ArM 5	25		TON	PDI ^c
2	ArM 6	81		3000	1.29
3	ArM 7	75		10000	1.21
4	9	16		9300	1.29
				1700	N.D.

^a[13] = 0.2 M. ^bDetermined by ¹H NMR spectroscopy. ^cPDI = polydispersity index.

Table 11: Selected CM results with cavity-size engineered ArMs.

	1 mol % catalyst	
5 mM MES buffer, pH 6.0 200 mM NaCl, 40 °C, 24 h 750 mbar		
73: R = CH ₂ OH		76: R = CH ₂ OH
74: R = Ph		77: R = Ph
75: R = C ₆ H ₄ - <i>p</i> -OMe		78: R = C ₆ H ₄ - <i>p</i> -OMe
entry ^a	catalyst	substrate
conversion ^b (%)	TON	
1	ArM 5	73
>99 ^c	100	
2	ArM 6	73
>99 ^c	100	
3	ArM 7	73
69 ^c	69	
4	9	73
79 ^c	79	
5	9 + NB₄exp	73, 74, 75
0	0	
6	ArM 5	74
45 ^c	45	
7	ArM 6	74
>99 ^c	100	
8	ArM 7	74
>99 ^c	100	
9	9	74
98 ^d	98	
10	ArM 5	75
40 ^d	40	
11	ArM 6	75
>99 ^d	100	
12	ArM 7	75
>99 ^d	100	
13	9	75
94 ^d	94	

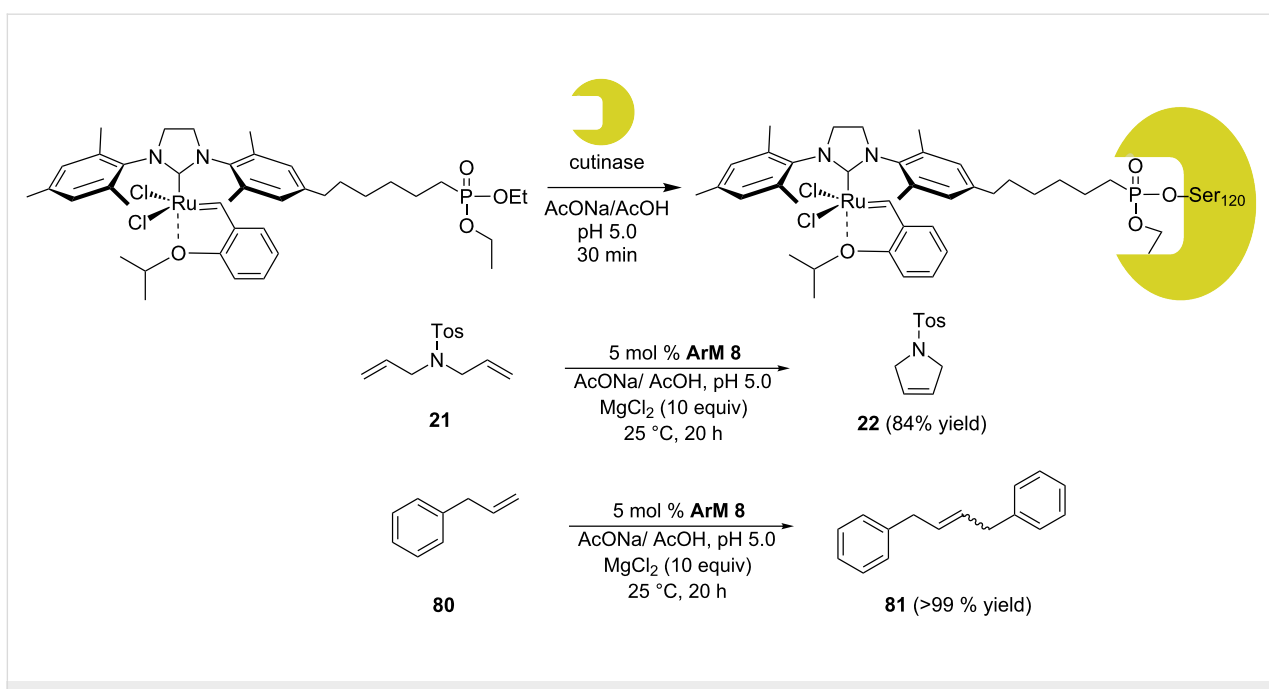
^a[Substrate] = 0.05 M. ^bConversions determined by ¹H NMR. ^cE/Z = 20:1. ^dE/Z = 99:1.

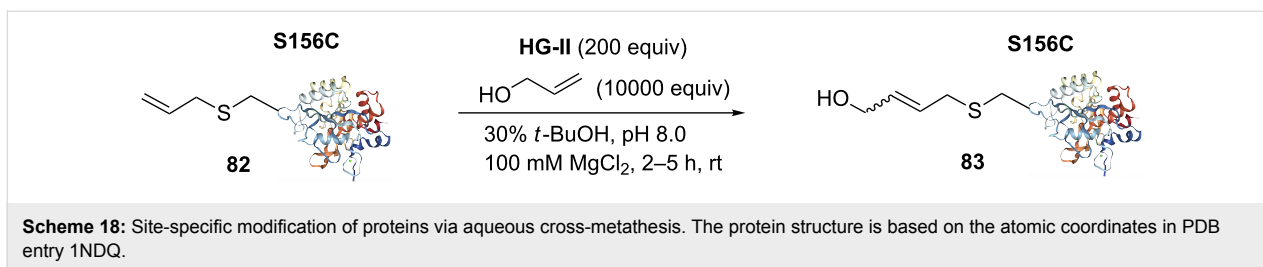
Olefin metathesis: applications in chemical biology

Synthetic compounds are increasingly being used as chemical tools to scrutinize and modulate biological systems [76]. Olefin metathesis is a prime example of bioorthogonal reactions and the ruthenium catalysts display good stability and chemoselectivity. The first applications of olefin metathesis in chemical biology were reported with “ill-defined” catalysts such as RuCl₃·H₂O to synthesize insect pheromones by olefin metathesis [77,78]. The development of well-defined ruthenium-based catalysts increased the number of olefin metathesis applications in chemical biology thanks to their tolerance against various functional groups such as amides, alcohols and carboxylic acids. However, one major hurdle for olefin metathesis in chemical biology remains the necessity to perform catalysis under mild conditions in buffered aqueous media.

The aqueous ROMP introduced by Grubbs and co-workers led to several biological applications [79,80]. Kiessling and co-workers were the first to use ROMP for the synthesis of biologically active polymers and for the synthesis of multivalent antigens to probe signaling pathways *in vivo* [81,82].

In 2008, Davis and co-workers performed site-selective protein modification through aqueous CM [83], thus expanding the catalytic repertoire of protein modification with transition-metal catalysts [84–87]. A variant of subtilisin from *Bacillus lenthus* containing a single cysteine (SBL-S156C) was modified by direct allylation to install an allyl-sulfide on the surface of the



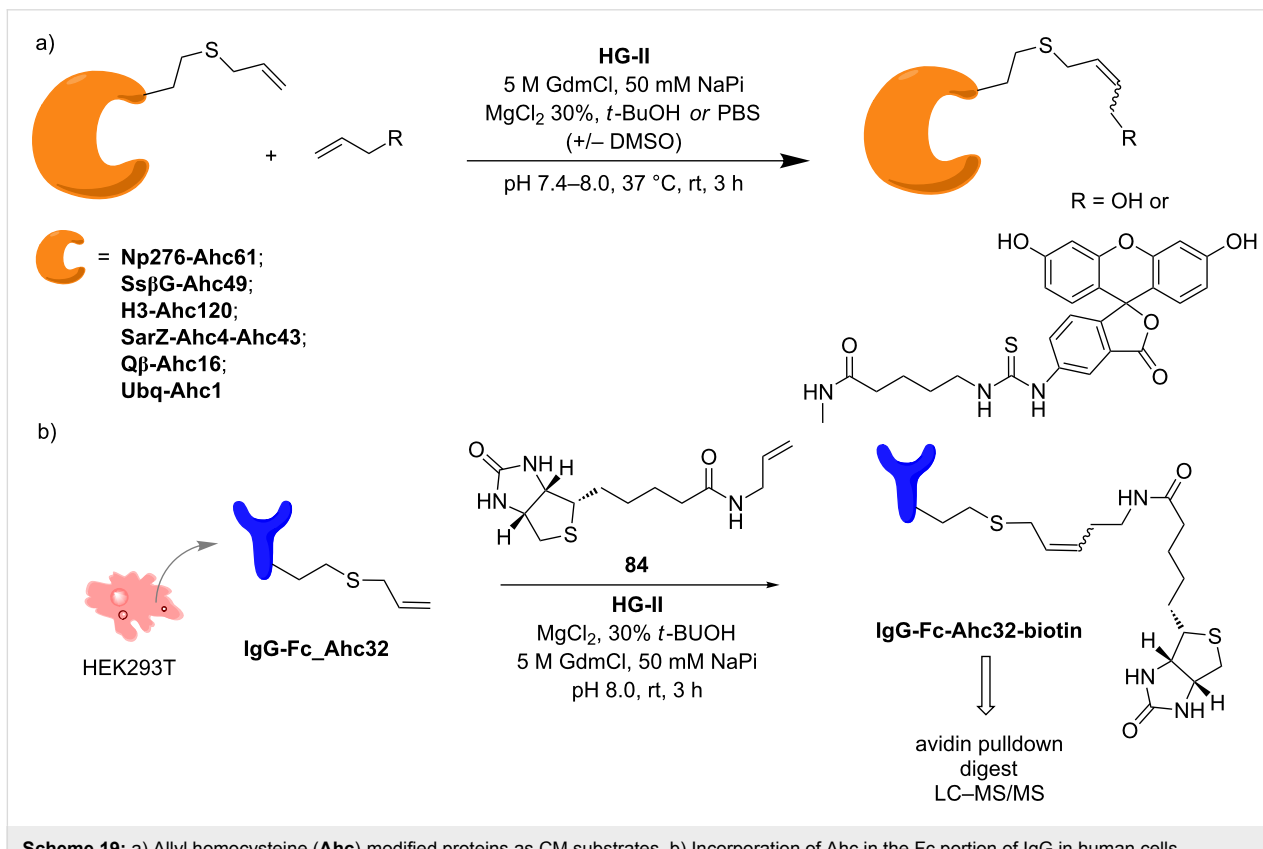


protein. Cross metathesis of the modified protein **82** with allyl alcohol gave the CM product with over 90% conversion (Scheme 18).

To achieve this challenging reaction, 200 equivalents (equiv) of **HG-II** catalyst were employed in a reaction mixture containing 0.01 mM **82**. Remarkably, no conversion was observed in the absence of $MgCl_2$, which prevents the non-productive binding of the amino acid side chains to ruthenium. The authors suggested that the positive effect of allyl sulfides may be due to the coordination of the sulfur atom to the ruthenium center, favoring the formation of the metallacyclobutane intermediate. The modest activities of butenyl and pentenyl sulfides were rationalized by the formation of five and six-membered ring chelates. The aqueous CM with allyl sulfides was also exploited

by Hunter et al. for the generation of a metathesis-based dynamic combinatorial library [88].

The work carried out by Davis and co-workers led to the metabolic incorporation of unnatural amino acids (uAAs) bearing a terminal alkene as CM substrates for protein modification [89]. The authors investigated the possibility to incorporate methionine (Met) analogues in a Met-auxotrophic strain of *E. coli* (B834DE3). Allyl-homocysteine (**Ahc**) resulted in the only uAA successfully incorporated into 6 different proteins, namely Histone H3 (**H3-Ahc120**), Np276 (**Np276-Ahc61**), Ss β G (**Ss β G-Ahc49**), SarZ (**SarZ-Ahc4-Ahc43**), Q β (**Q β -Ahc16**), and Ubq (**Ubq-Ahc1**). The modified proteins were tested for cross metathesis with allyl alcohol or with a fluorescein derivative (Scheme 19a).



Scheme 19: a) Allyl homocysteine (**Ahc**)-modified proteins as CM substrates. b) Incorporation of **Ahc** in the Fc portion of IgG in human cells (HEK 293T) and CM reaction with **84**.

To further advance the chemical tagging through cross metathesis, genetic incorporation of **Ahc** was performed in human cells (HEK 293T) for the modification of the Fc region of IgG (IgG-Fc-Ahc32, Scheme 19b). An olefin-bearing biotin **84** was selected as olefinic partner for the CM reaction with the modified antibody, yielding **IgG-Fc-Ahc32-biotin** (Scheme 19b). The conjugated protein can be selectively pulled-down with avidin beads and analyzed by tandem MS after tryptic digestion. This strategy suggests that CM reactions can be integrated in the toolbox of chemical proteomics.

Recently, following a similar strategy, Lu et al. reported on-DNA RCM and CM, an application potentially useful to generate DNA-encoded libraries for hit identification and target validation [90]. Substrates appended to oligonucleotides undergo Ru-promoted RCM and CM when the **G-III** catalyst is used under heterogeneous conditions (water/*tert*-butanol 3:2)

with a large excess of Mg^{2+} . Also in this case, the role of Mg^{2+} is to protect the oligonucleotide from Ru-induced decomposition by binding to the phosphate backbone. Table 12 summarizes the activities of 7 different DNA-tethered substrates for RCM. Good conversions were achieved in water mixtures (40% *t*-BuOH) at room temperature after 1 hour of reaction. However, these reactions are not catalytic as they require 150 equivalents of the **G-III** catalyst.

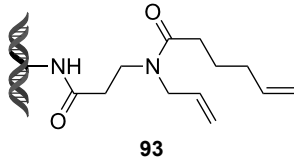
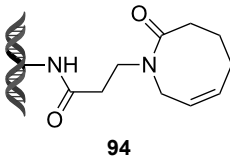
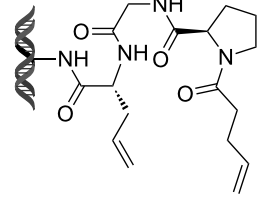
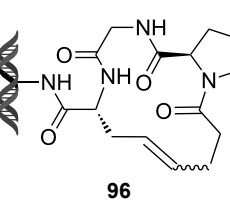
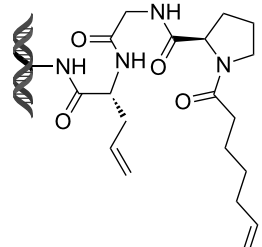
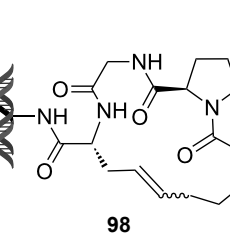
The same conditions were tested for the cross metathesis of the allyl-sulfide **99** with allyl alcohol, yielding 50% of product **100** in aqueous mixture (40% *t*-BuOH) in the presence of 4000 equiv of Mg^{2+} (Scheme 20).

In another recent study, Toussaint et al. described the synthesis of two metathesis-based fluorescent probes suitable for the detection of ethylene in live cells [91]. BODIPY fluorophores

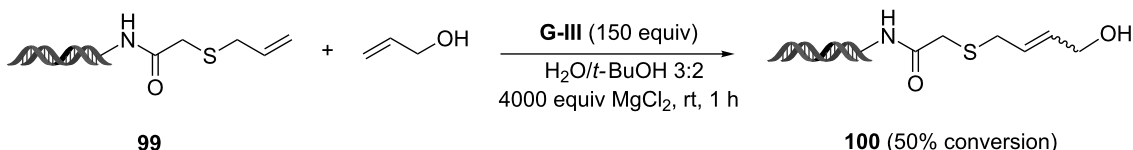
Table 12: Scope of RCM reactions using DNA-tethered substrates.^a

entry	substrate	product	conversion (%)
1			50
2			85
3			65
4			65

Table 12: Scope of RCM reactions using DNA-tethered substrates.^a (continued)

5			50
6			55
7			50

^a150 equiv **G-III** catalyst, [substrate] = 0.09 mM.

**Scheme 20:** On-DNA cross-metathesis reaction of allyl sulfide **99**.

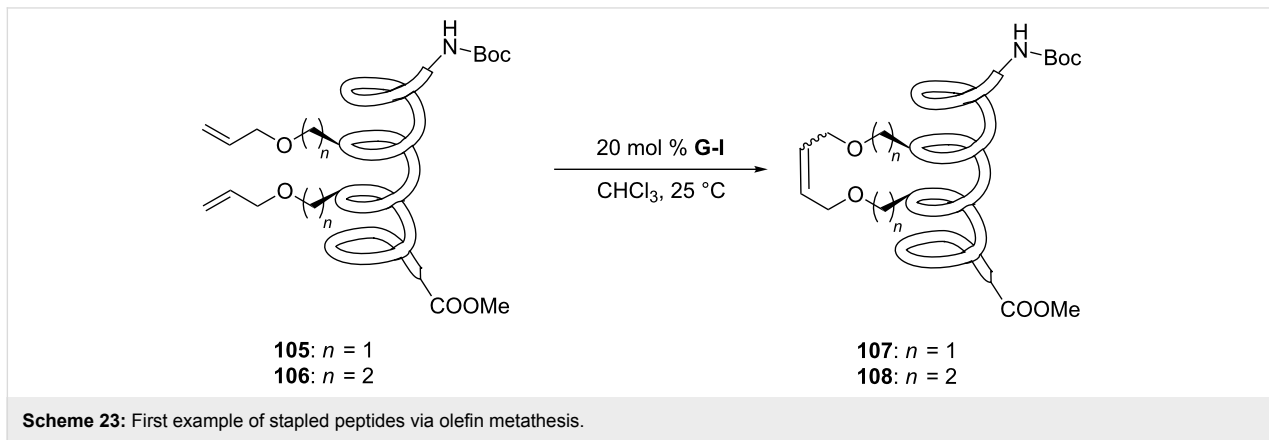
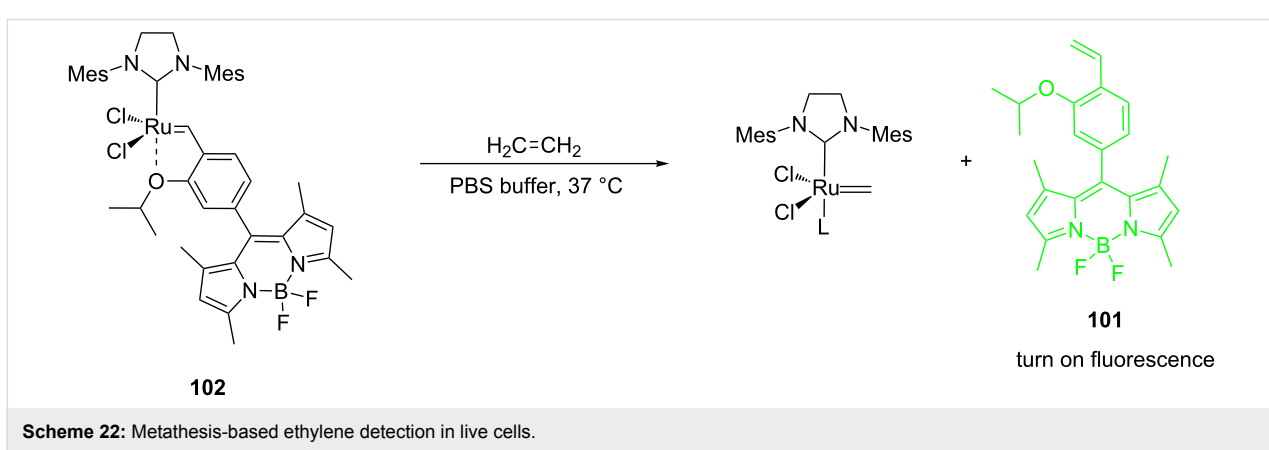
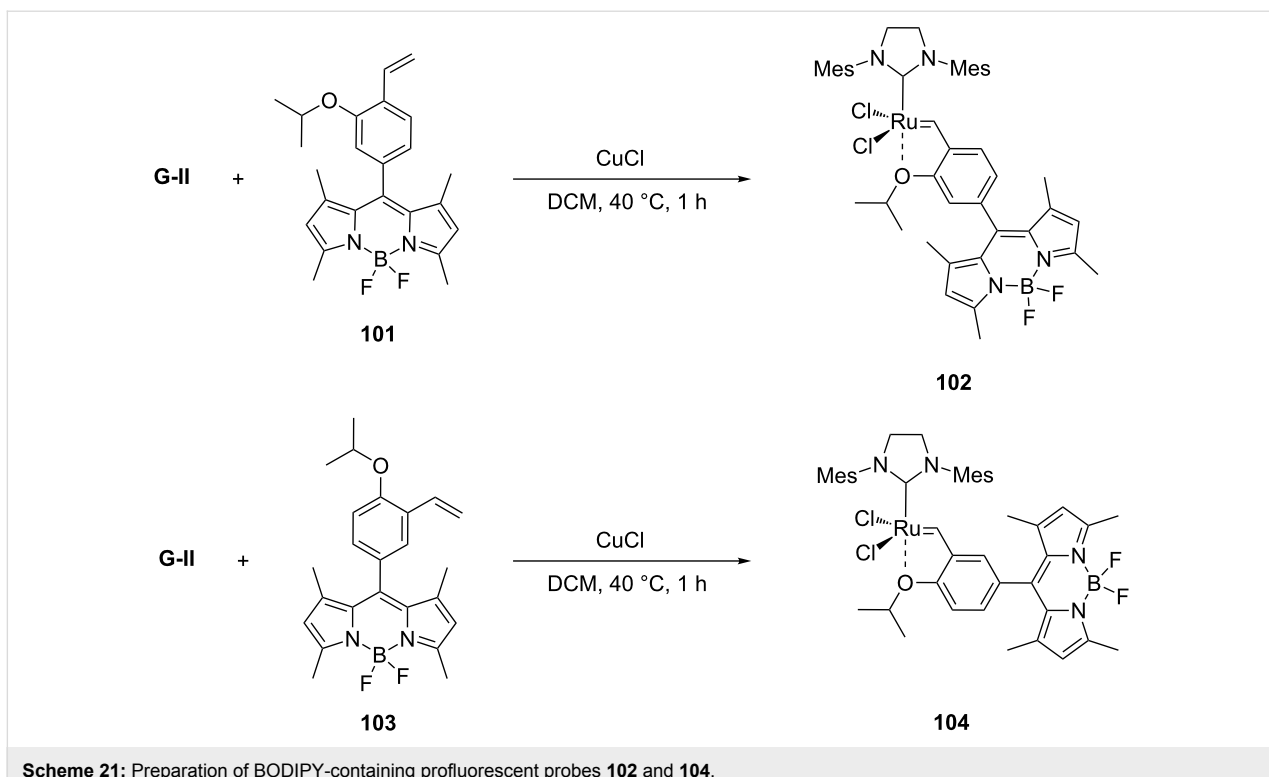
bearing the isopropoxybenzylidene moiety (**101** and **103**) reacted with the **G-II** catalyst to form the **HG-II** derivatives **102** and **104**, respectively (Scheme 21).

The resulting compounds are Ru-based profluorescent probes that become fluorescent in the presence of ethylene, thus leading to the release of **101** from the Ru-catalyst (Scheme 22).

Live cell experiments with *Chlamydomonas reinhardtii* suggest that 20 μM of probe **102** in PBS buffer are sufficient to turn fluorescence on in cells flushed with exogenous ethylene or ethylene gas derived from ripe fruit (e.g., banana or mango). Control experiments reveal however a steady increase in fluorescence in the absence of ethylene, suggesting that further optimization of the probes is required. As ethylene plays an important role as a plant hormone, metathesis-based probes might have interesting applications in plant biology.

Olefin metathesis is also used to cross-link peptide fragments. This technology is known as peptide stapling [92]. Blackwell et al. engineered the first stapled peptide in 1998 by introducing two non-natural amino acids bearing a terminal alkene in a peptide sequence (e.g., **105**, **106**) [93]. The cross-linking of the two amino acids by metathesis results in a more rigid and stabilized alpha helix (products **107** and **108**, Scheme 23).

Although the reaction cannot be classified as aqueous metathesis (the reaction is carried out in CHCl_3 and the peptide remains attached to the solid phase), this technology has been exploited to disrupt protein–protein interactions (PPIs) in cancer cells [94–96]. Aileron Therapeutics recently launched a stapled peptide platform aiming at developing molecules like ALRN-6924, a stapled peptide that interacts with p53 inhibitors MDMX and MDM4. The drug candidate is currently being evaluated in clinical trials for different types of cancer [97].



Conclusion

Over the past 20 years, the number of applications of olefin metathesis in water has dramatically increased. The field of metathesis is continuously growing and scientists seek new opportunities to exploit this powerful C–C double-bond-forming reaction in different fields of research. Several biological applications have emerged over the past 10 years as a result of the extensive efforts to establish biocompatible protocols. While aqueous metathesis offers the advantage of performing catalysis in a more sustainable medium, it still remains challenging to achieve due to the detrimental effect of water. Despite this limitation, olefin metathesis widely contributes to polymer chemistry, drug discovery and biocatalysis. Several technologies relying on aqueous metathesis have been developed (e.g., protein modification, on-DNA metathesis, directed evolution of artificial metalloenzymes, etc.) and are paving the way to future interesting applications.

Acknowledgements

The picture in the background of the graphical abstract was taken from <https://www.maxpixel.net/Summer-Water-Droplets-Lotus-Leaf-2192811> (CC0 Public Domain; Free for commercial use).

ORCID® IDs

Thomas R. Ward - <https://orcid.org/0000-0001-8602-5468>

References

1. Grubbs, R. H.; Wenzel, A. G.; O'Leary, D. J.; Khosravi, E., Eds. *Handbook of Metathesis*, 2nd ed.; Wiley-VCH Verlag GmbH: Weinheim, Germany, 2015; Vol. 1–3. doi:10.1002/9783527674107
2. *Alkene Metathesis in Organic Synthesis*; Fürstner, A., Ed.; *Topics in Organometallic Chemistry*, Vol. 1; Springer-Verlag: Berlin, Heidelberg, 1998. doi:10.1007/3-540-69708-x
3. Ogbu, O. M.; Warner, N. C.; O'Leary, D. J.; Grubbs, R. H. *Chem. Soc. Rev.* **2018**, *47*, 4510–4544. doi:10.1039/c8cs00027a
4. Herbert, M. B.; Grubbs, R. H. *Angew. Chem., Int. Ed.* **2015**, *54*, 5018–5024. doi:10.1002/anie.201411588
5. Fustero, S.; Simón-Fuentes, A.; Barrio, P.; Haufe, G. *Chem. Rev.* **2015**, *115*, 871–930. doi:10.1021/cr500182a
6. Olszewski, T. K.; Bieniek, M.; Skowerski, K.; Grela, K. *Synlett* **2013**, *24*, 903–919. doi:10.1055/s-0032-1318497
7. Olszewski, T. K.; Figlus, M.; Bieniek, M. *Chim. Oggi* **2014**, *32* (5), 22–29.
8. Hughes, D.; Wheeler, P.; Ene, D. *Org. Process Res. Dev.* **2017**, *21*, 1938–1962. doi:10.1021/acs.oprd.7b00319
9. Grela, K., Ed. *Olefin Metathesis: Theory and Practice*, 1st ed.; Wiley-VCH: Weinheim, Germany, 2014.
10. Anderson, A. W.; Merckling, M. G. *Chem. Abstr.* **1956**, *50*, 3008.
11. Bielawski, C. W.; Grubbs, R. H. *Prog. Polym. Sci.* **2007**, *32*, 1–29. doi:10.1016/j.progpolymsci.2006.08.006
12. Sinclair, F.; Alkattan, M.; Prunet, J.; Shaver, M. P. *Polym. Chem.* **2017**, *8*, 3385–3398. doi:10.1039/c7py00340d
13. McCauley, J. A.; McIntyre, C. J.; Rudd, M. T.; Nguyen, K. T.; Romano, J. J.; Butcher, J. W.; Gilbert, K. F.; Bush, K. J.; Holloway, M. K.; Swestock, J.; Wan, B.-L.; Carroll, S. S.; DiMuzio, J. M.; Graham, D. J.; Ludmerer, S. W.; Mao, S.-S.; Stahlhut, M. W.; Fandozzi, C. M.; Trainor, N.; Olsen, D. B.; Vacca, J. P.; Liverton, N. J. *J. Med. Chem.* **2010**, *53*, 2443–2463. doi:10.1021/jm9015526
14. Tsantrizos, Y. S.; Ferland, J.-M.; McClory, A.; Poirier, M.; Farina, V.; Yee, N. K.; Wang, X.-j.; Haddad, N.; Wei, X.; Xu, J.; Zhang, L. *J. Organomet. Chem.* **2006**, *691*, 5163–5171. doi:10.1016/j.jorgchem.2006.09.027
15. Higman, C. S.; Lummiss, J. A. M.; Fogg, D. E. *Angew. Chem., Int. Ed.* **2016**, *55*, 3552–3565. doi:10.1002/anie.201506846
16. Hérisson, J.-L.; Chauvin, Y. *Makromol. Chem.* **1971**, *141*, 161. doi:10.1002/macp.1971.021410112
17. Casey, C. P.; Burkhardt, T. J. *J. Am. Chem. Soc.* **1974**, *96*, 7808–7809. doi:10.1021/ja00832a032
18. Katz, T. J.; McGinnis, J. *J. Am. Chem. Soc.* **1975**, *97*, 1592–1594. doi:10.1021/ja00839a063
19. Grubbs, R. H.; Burk, P. L.; Carr, D. D. *J. Am. Chem. Soc.* **1975**, *97*, 3265–3267. doi:10.1021/ja00844a082
20. Grubbs, R. H.; Carr, D. D.; Hoppin, C.; Burk, P. L. *J. Am. Chem. Soc.* **1976**, *98*, 3478–3483. doi:10.1021/ja00428a015
21. Tomasek, J.; Schatz, J. *Green Chem.* **2013**, *15*, 2317–2338. doi:10.1039/c3gc41042k
22. Burtscher, D.; Grela, K. *Angew. Chem., Int. Ed.* **2009**, *48*, 442–454. doi:10.1002/anie.200801451
23. Piola, L.; Nahra, F.; Nolan, S. P. *Beilstein J. Org. Chem.* **2015**, *11*, 2038–2056. doi:10.3762/bjoc.11.221
24. Skowerski, K.; Bialecki, J.; Tracz, A.; Olszewski, T. K. *Green Chem.* **2014**, *16*, 1125–1130. doi:10.1039/c3gc41943f
25. Novak, B. M.; Grubbs, R. H. *J. Am. Chem. Soc.* **1988**, *110*, 7542–7543. doi:10.1021/ja00230a047
26. Novak, B. M.; Grubbs, R. H. *J. Am. Chem. Soc.* **1988**, *110*, 960–961. doi:10.1021/ja00211a043
27. Mühlbach, A.; Bernhard, P.; Bühler, N.; Karlen, T.; Ludi, A. *J. Mol. Catal.* **1994**, *90*, 143–156. doi:10.1016/0304-5102(94)00005-0
28. Feast, W. J.; Harrison, D. B. *Polym. Bull.* **1991**, *25*, 343–350. doi:10.1007/bf00316904
29. Fürstner, A.; Ackermann, L.; Gabor, B.; Goddard, R.; Lehmann, C. W.; Mynott, R.; Stelzer, F.; Thiel, O. R. *Chem. – Eur. J.* **2001**, *7*, 3236–3253. doi:10.1002/1521-3765(20010803)7:15<3236::aid-chem3236>3.0.co;2-s
30. Dinger, M. B.; Mol, J. C. *Organometallics* **2003**, *22*, 1089–1095. doi:10.1021/om0208218
31. Lynn, D. M.; Grubbs, R. H. *J. Am. Chem. Soc.* **2001**, *123*, 3187–3193. doi:10.1021/ja0020299
32. Guidone, S.; Songis, O.; Nahra, F.; Cazin, C. S. *J. ACS Catal.* **2015**, *5*, 2697–2701. doi:10.1021/acscatal.5b00197
33. Levin, E.; Ivry, E.; Diesendruck, C. E.; Lemcoff, N. G. *Chem. Rev.* **2015**, *115*, 4607–4692. doi:10.1021/cr400640e
34. Connon, S. J.; Rivard, M.; Zaja, M.; Blechert, S. *Adv. Synth. Catal.* **2003**, *345*, 572–575. doi:10.1002/adsc.200202201
35. Binder, J. B.; Blank, J. J.; Raines, R. T. *Org. Lett.* **2007**, *9*, 4885–4888. doi:10.1021/o17022505
36. Davis, K. J.; Sinou, D. *J. Mol. Catal. A: Chem.* **2002**, *177*, 173–178. doi:10.1016/s1381-1169(01)00239-4
37. Lipshutz, B. H.; Taft, B. R. *Org. Lett.* **2008**, *10*, 1329–1332. doi:10.1021/o1702755g

38. Lipshutz, B. H.; Ghorai, S.; Aguinaldo, G. T. *Adv. Synth. Catal.* **2008**, *350*, 953–956. doi:10.1002/adsc.200800114

39. Lipshutz, B. H.; Petersen, T. B.; Abela, A. R. *Org. Lett.* **2008**, *10*, 1333–1336. doi:10.1021/ol702714y

40. Lipshutz, B. H.; Aguinaldo, G. T.; Ghorai, S.; Voigtritter, K. *Org. Lett.* **2008**, *10*, 1325–1328. doi:10.1021/ol800028x

41. Lipshutz, B. H.; Ghorai, S.; Leong, W. W. Y.; Taft, B. R.; Krogstad, D. V. *J. Org. Chem.* **2011**, *76*, 5061–5073. doi:10.1021/jo200746y

42. Lipshutz, B. H.; Ghorai, S.; Cortes-Clerget, M. *Chem. – Eur. J.* **2018**, *24*, 6672–6695. doi:10.1002/chem.201705499

43. García-Álvarez, J.; Hevia, E.; Capriati, V. *Chem. – Eur. J.* **2018**, *24*, 14854–14863. doi:10.1002/chem.201802873

44. Pauly, J.; Gröger, H.; Patel, A. V. *Green Chem.* **2018**, *20*, 5179–5187. doi:10.1039/c8gc02164c

45. Cho, J. H.; Kim, B. M. *Org. Lett.* **2003**, *5*, 531–533. doi:10.1021/ol027423l

46. Michrowska, A.; Gułajski, Ł.; Grela, K. *Chem. Commun.* **2006**, 841–843. doi:10.1039/b517088e

47. Vougioukalakis, G. C. *Chem. – Eur. J.* **2012**, *18*, 8868–8880. doi:10.1002/chem.201200600

48. Wheeler, P.; Phillips, J. H.; Pederson, R. L. *Org. Process Res. Dev.* **2016**, *20*, 1182–1190. doi:10.1021/acs.oprd.6b00138

49. Skowerski, K.; Kasprzycki, P.; Bieniek, M.; Olszewski, T. K. *Tetrahedron* **2013**, *69*, 7408–7415. doi:10.1016/j.tet.2013.06.056

50. Tracz, A.; Gawin, A.; Bieniek, M.; Olszewski, T. K.; Skowerski, K. *New J. Chem.* **2018**, *42*, 8609–8614. doi:10.1039/c8nj00614h

51. U. S. Department of Health and Human Services, Food and Drug Administration. Q3D Elemental Impurities Guidance for Industry. ICH, 2015; <http://www.fda.gov/Drugs/GuidanceComplianceRegulatoryInformation/Guidances/default.htm>.

52. Jana, A.; Grela, K. *Chem. Commun.* **2018**, *54*, 122–139. doi:10.1039/c7cc06535c

53. Szczepaniak, G.; Kosiński, K.; Grela, K. *Green Chem.* **2014**, *16*, 4474–4492. doi:10.1039/c4gc00705k

54. Lynn, D. M.; Kanaoka, S.; Grubbs, R. H. *J. Am. Chem. Soc.* **1996**, *118*, 784–790. doi:10.1021/ja950327d

55. Hong, S. H.; Grubbs, R. H. *J. Am. Chem. Soc.* **2006**, *128*, 3508–3509. doi:10.1021/ja058451c

56. Jordan, J. P.; Grubbs, R. H. *Angew. Chem., Int. Ed.* **2007**, *46*, 5152–5155. doi:10.1002/anie.200701258

57. Michrowska, A.; Gułajski, Ł.; Kaczmarśka, Z.; Mennecke, K.; Kirschning, A.; Grela, K. *Green Chem.* **2006**, *8*, 685–688. doi:10.1039/b605138c

58. Michrowska, A.; Bujok, R.; Harutyunyan, S.; Sashuk, V.; Dolgonos, G.; Grela, K. *J. Am. Chem. Soc.* **2004**, *126*, 9318–9325. doi:10.1021/ja048794v

59. Skowerski, K.; Szczepaniak, G.; Wierzbicka, C.; Gułajski, Ł.; Bieniek, M.; Grela, K. *Catal. Sci. Technol.* **2012**, *2*, 2424–2427. doi:10.1039/c2cy20320k

60. Wright, D. B.; Touve, M. A.; Thompson, M. P.; Gianneschi, N. C. *ACS Macro Lett.* **2018**, *7*, 401–405. doi:10.1021/acsmacrollett.8b00091

61. Kim, C.; Ondrusk, B. A.; Chung, H. *Org. Lett.* **2018**, *20*, 736–739. doi:10.1021/acs.orglett.7b03871

62. Kim, C.; Chung, H. *J. Org. Chem.* **2018**, *83*, 9787–9794. doi:10.1021/acs.joc.8b01312

63. Schwizer, F.; Okamoto, Y.; Heinisch, T.; Gu, Y.; Pellizzoni, M. M.; Lebrun, V.; Reuter, R.; Köhler, V.; Lewis, J. C.; Ward, T. R. *Chem. Rev.* **2018**, *118*, 142–231. doi:10.1021/acs.chemrev.7b00014

64. Rosati, F.; Roelfes, G. *ChemCatChem* **2010**, *2*, 916–927. doi:10.1002/cctc.201000011

65. Lo, C.; Ringenberg, M. R.; Gnandt, D.; Wilson, Y.; Ward, T. R. *Chem. Commun.* **2011**, *47*, 12065–12067. doi:10.1039/c1cc15004a

66. Heinisch, T.; Ward, T. R. *Acc. Chem. Res.* **2016**, *49*, 1711–1721. doi:10.1021/acs.accounts.6b00235

67. Zhao, J.; Kajetanowicz, A.; Ward, T. R. *Org. Biomol. Chem.* **2015**, *13*, 5652–5655. doi:10.1039/c5ob00428d

68. Jeschek, M.; Reuter, R.; Heinisch, T.; Trindler, C.; Klehr, J.; Panke, S.; Ward, T. R. *Nature* **2016**, *537*, 661–665. doi:10.1038/nature19114

69. Kajetanowicz, A.; Chatterjee, A.; Reuter, R.; Ward, T. R. *Catal. Lett.* **2014**, *144*, 373–379. doi:10.1007/s10562-013-1179-z

70. Matsuo, T.; Imai, C.; Yoshida, T.; Saito, T.; Hayashi, T.; Hirota, S. *Chem. Commun.* **2012**, *48*, 1662–1664. doi:10.1039/c2cc16898g

71. Mayer, C.; Gillingham, D. G.; Ward, T. R.; Hilvert, D. *Chem. Commun.* **2011**, *47*, 12068–12070. doi:10.1039/c1cc15005g

72. Grimm, A. R.; Sauer, D. F.; Davari, M. D.; Zhu, L.; Bocola, M.; Kato, S.; Onoda, A.; Hayashi, T.; Okuda, J.; Schwaneberg, U. *ACS Catal.* **2018**, *8*, 3358–3364. doi:10.1021/acscatal.7b03652

73. Sauer, D. F.; Bocola, M.; Broglia, C.; Arlt, M.; Zhu, L.-L.; Brocker, M.; Schwaneberg, U.; Okuda, J. *Chem. – Asian J.* **2015**, *10*, 177–182. doi:10.1002/asia.201403005

74. Philippart, F.; Arlt, M.; Gotzen, S.; Tenne, S.-J.; Bocola, M.; Chen, H.-H.; Zhu, L.; Schwaneberg, U.; Okuda, J. *Chem. – Eur. J.* **2013**, *19*, 13865–13871. doi:10.1002/chem.201301515

75. Basauri-Molina, M.; Verhoeven, D. G. A.; van Schaik, A. J.; Klein, H.; Klein Gebbink, R. J. M. *Chem. – Eur. J.* **2015**, *21*, 15676–15685. doi:10.1002/chem.201502381

76. Prescher, J. A.; Bertozzi, C. R. *Nat. Chem. Biol.* **2005**, *1*, 13–21. doi:10.1038/nchembio0605-13

77. Rossi, R. *Chim. Ind. (Milan)* **1975**, *57*, 242–243.

78. Kuepper, F. W.; Streck, R. *Chem.-Ztg.* **1975**, *99*, 464–465.

79. Isarov, S. A.; Pokorski, J. K. *ACS Macro Lett.* **2015**, *4*, 969–973. doi:10.1021/acsmacrollett.5b00497

80. Kiessling, L. L.; Strong, L. E. *Bioactive Polymers*. In *Alkene Metathesis in Organic Synthesis*; Fuerstner, A., Ed.; *Topics in Organometallic Chemistry*, Vol. 1; Springer: Berlin, 1998; pp 199–231. doi:10.1007/3-540-69708-x_8

81. Kiessling, L. L.; Gestwicki, J. E.; Strong, L. E. *Angew. Chem., Int. Ed.* **2006**, *45*, 2348–2368. doi:10.1002/anie.200502794

82. Puffer, E. B.; Pontrello, J. K.; Hollenbeck, J. J.; Kink, J. A.; Kiessling, L. L. *ACS Chem. Biol.* **2007**, *2*, 252–262. doi:10.1021/cb600489g

83. Lin, Y. A.; Chalker, J. M.; Floyd, N.; Bernardes, G. J. L.; Davis, B. G. *J. Am. Chem. Soc.* **2008**, *130*, 9642–9643. doi:10.1021/ja8026168

84. Kodama, K.; Fukuzawa, S.; Nakayama, H.; Kigawa, T.; Sakamoto, K.; Yabuki, T.; Matsuda, N.; Shirouzu, M.; Takio, K.; Tachibana, K.; Yokoyama, S. *ChemBioChem* **2006**, *7*, 134–139. doi:10.1002/cbic.200500290

85. Kodama, K.; Fukuzawa, S.; Nakayama, H.; Sakamoto, K.; Kigawa, T.; Yabuki, T.; Matsuda, N.; Shirouzu, M.; Takio, K.; Yokoyama, S.; Tachibana, K. *ChemBioChem* **2007**, *8*, 232–238. doi:10.1002/cbic.200600432

86. Li, N.; Lim, R. K. V.; Edwardraja, S.; Lin, Q. *J. Am. Chem. Soc.* **2011**, *133*, 15316–15319. doi:10.1021/ja2066913

87. Brustad, E.; Bushey, M. L.; Lee, J. W.; Groff, D.; Liu, W.; Schultz, P. G. *Angew. Chem., Int. Ed.* **2008**, *47*, 8220–8223. doi:10.1002/anie.200803240

88. Hunter, L.; Condie, G. C.; Harding, M. M. *Tetrahedron Lett.* **2010**, *51*, 5064–5067. doi:10.1016/j.tetlet.2010.07.105

89. Bhushan, B.; Lin, Y. A.; Bak, M.; Phanumartwiwath, A.; Yang, N.; Bilyard, M. K.; Tanaka, T.; Hudson, K. L.; Lercher, L.; Stegmann, M.; Mohammed, S.; Davis, B. G. *J. Am. Chem. Soc.* **2018**, *140*, 14599–14603. doi:10.1021/jacs.8b09433

90. Lu, X.; Fan, L.; Phelps, C. B.; Davie, C. P.; Donahue, C. P. *Bioconjugate Chem.* **2017**, *28*, 1625–1629. doi:10.1021/acs.bioconjchem.7b00292

91. Toussaint, S. N. W.; Calkins, R. T.; Lee, S.; Michel, B. W. *J. Am. Chem. Soc.* **2018**, *140*, 13151–13155. doi:10.1021/jacs.8b05191

92. Verdine, G. L.; Hilinski, G. J. *Methods Enzymol.* **2012**, *503*, 3–33. doi:10.1016/b978-0-12-396962-0.00001-x

93. Blackwell, H. E.; Grubbs, R. H. *Angew. Chem., Int. Ed.* **1998**, *37*, 3281–3284. doi:10.1002/(sici)1521-3773(19981217)37:23<3281::aid-anie3281>3.0.co;2-v

94. Walensky, L. D.; Kung, A. L.; Escher, I.; Malia, T. J.; Barbuto, S.; Wright, R. D.; Wagner, G.; Verdine, G. L.; Korsmeyer, S. J. *Science* **2004**, *305*, 1466–1470. doi:10.1126/science.1099191

95. Moellering, R. E.; Cornejo, M.; Davis, T. N.; Del Bianco, C.; Aster, J. C.; Blacklow, S. C.; Kung, A. L.; Gilliland, D. G.; Verdine, G. L.; Bradner, J. E. *Nature* **2009**, *462*, 182–188. doi:10.1038/nature08543

96. Bernal, F.; Wade, M.; Godes, M.; Davis, T. N.; Whitehead, D. G.; Kung, A. L.; Wahl, G. M.; Walensky, L. D. *Cancer Cell* **2010**, *18*, 411–422. doi:10.1016/j.ccr.2010.10.024

97. Meric-Bernstam, F.; Saleh, M. N.; Infante, J. R.; Goel, S.; Falchook, G. S.; Shapiro, G.; Chung, K. Y.; Conry, R. M.; Hong, D. S.; Wang, J. S.-Z.; Steidl, U.; Walensky, L. D.; Guerlavais, V.; Payton, M.; Annis, D. A.; Aivado, M.; Patel, M. R. J. *Clin. Oncol.* **2017**, *35* (Suppl. 15), 2505. doi:10.1200/jco.2017.35.15_suppl.2505

License and Terms

This is an Open Access article under the terms of the Creative Commons Attribution License (<http://creativecommons.org/licenses/by/4.0>). Please note that the reuse, redistribution and reproduction in particular requires that the authors and source are credited.

The license is subject to the *Beilstein Journal of Organic Chemistry* terms and conditions: (<https://www.beilstein-journals.org/bjoc>)

The definitive version of this article is the electronic one which can be found at:
[doi:10.3762/bjoc.15.39](https://doi.org/10.3762/bjoc.15.39)



Synthesis of polydicyclopentadiene using the $\text{Cp}_2\text{TiCl}_2/\text{Et}_2\text{AlCl}$ catalytic system and thin-layer oxidation of the polymer in air

Zhargolma B. Bazarova¹, Ludmila S. Soroka¹, Alex A. Lyapkov¹, Mekhman S. Yusubov¹ and Francis Verpoort^{*1,2,3,4}

Full Research Paper

Open Access

Address:

¹National Research Tomsk Polytechnic University, Tomsk, 634050, Russian Federation, ²Laboratory of Organometallics, Catalysis and Ordered Materials, State Key Laboratory of Advanced Technology for Materials Synthesis and Processing, Wuhan University of Technology, Wuhan, 430070, China, ³College of Arts and Sciences, Khalifa University of Science and Technology, PO Box 127788, Abu Dhabi, UAE and ⁴Ghent University, Global Campus Songdo, 119 Songdomunhwa-Ro, Yeonsu-Gu, Incheon 406-840, South Korea

Email:

Francis Verpoort* - Francis.verpoort@ugent.be

* Corresponding author

Keywords:

bis(cyclopentadienyl)titanium dichloride; cationic polymerization; oxidation; polydicyclopentadiene; thin layers

Beilstein J. Org. Chem. **2019**, *15*, 733–745.

doi:10.3762/bjoc.15.69

Received: 13 September 2018

Accepted: 04 March 2019

Published: 20 March 2019

This article is part of the thematic issue "Progress in metathesis chemistry III".

Guest Editors: K. Grela and A. Kajetanowicz

© 2019 Bazarova et al.; licensee Beilstein-Institut.

License and terms: see end of document.

Abstract

The polymerization process of dicyclopentadiene using a multicomponent catalytic system based on bis(cyclopentadienyl)titanium dichloride and diethylaluminum chloride was studied. It was demonstrated that the application of an excess of the aluminum component leads to the formation of stable charged complexes of blue discoloration, which initiate cationic polymerization of dicyclopentadiene. Unstabilized thin layers of obtained polydicyclopentadiene undergo oxidation and structuring under atmospheric oxygen. Oxidation of polydicyclopentadiene films in air occurs slowly during several weeks and can be determined by the increase of carbonyl and hydroxyl adsorption bands in infrared spectra. Along with oxidation, cross-linking processes occur in polymers, which lead to a change in physical parameters of the layers, and more precisely to a decrease in the permeability of atmospheric oxygen through the layers. Consequently, this leads to the transition of the oxidation from a kinetic mode into a diffusive mode. Such structural changes do not occur in a polymer that was stabilized by adding an antioxidant.

Introduction

Currently, polymerization of dicyclopentadiene and norbornene derivatives applying various catalyst systems is of great interest [1–7]. Dicyclopentadiene (DCPD) is a secondary product of the

ethylene and propylene production and is used as a monomer to obtain a polymer with particular properties – polydicyclopentadiene (PDCPD) [8,9]. Cationic polymerization of DCPD takes

place with metal-halide-based catalyst systems and organometallic compounds. A number of scientific reports were dedicated to the investigation of DCPD polymerization based on these systems [10,11]. One of the drawbacks of these catalyst systems is the “excessive hardness” of the system viz. HSAB theory leading to the formation of cross-linked structures and gelation of the system. Substitution of chlorine atoms in the catalyst structure with organic ligands allows reducing of the hardness of the systems and contributes to the generation of products having a linear structure. To realize this, the usage of a catalyst component bearing already organic ligands in its structure – bis(cyclopentadienyl)titanium dichloride (Cp_2TiCl_2) is proposed.

Polymers based on DCPD, obtained by cationic polymerization, are characterized by certain disadvantages. They have a low molecular weight, a fairly rigid structure of the polymer chains due to crosslinking processes occurring during polymerization. In addition, DCPD polymers obtained from “hard” catalytic systems, such as TiCl_4 , SnCl_4 , etc., are easily susceptible to oxidation. Catalytic systems which are less “hard” can overcome these disadvantages to some extent.

The aim of this study is to investigate the interaction between Cp_2TiCl_2 and diethylaluminum chloride (AlEt_2Cl) in toluene which results in the formation of a complex, active for the DCPD polymerization. Additionally, optimization of the ratio between the two compounds of the catalyst system was performed using electron spectroscopy. Furthermore, the DCPD polymerization in toluene was investigated using the optimized catalyst system, and also the dynamics of the structural transformations occurring in thin layers of PDCPD during oxidation in air.

Polymers obtained during the dicyclopentadiene polymerization under these conditions are well soluble in aromatic and chlorinated solvents, and from these solutions, smooth transparent films can be produced. However, the surface of PDCPD loses its transparency and becomes dark as a function of time when stored in air. This is attributed to the formation of cross-linking in the polymer structure and oxidation of unsaturated bonds, which are excessively present in the polymer structure [12-14].

Oxidation of thin PDCPD films in air occurs slowly and is observable by the intensity increase of vibrational bands deriving from carbonyl and hydroxy groups in the infrared spectra of the polymers. More specifically, an intensity increase of the wide band at 3400 cm^{-1} is observed, which is assigned to vibrations of hydroxy groups located near various carbon atoms in the main polymer chain. Apart from this, the intensity of the

bending vibrations of carboxyl groups at 1700 cm^{-1} and of ether groups at $1030\text{--}1080\text{ cm}^{-1}$ increases as well.

Results and Discussion

Study of the complex formation between Cp_2TiCl_2 and AlEt_2Cl

It is known that the catalytic activity of the Cp_2TiCl_2 /organo-aluminum compound is determined by the molar ratio of the components of the catalytic system [15]. The rate of transformation in the system depends both on the Al:Ti molar ratio and on the temperature [16]. UV spectra of toluene solutions of Cp_2TiCl_2 and AlEt_2Cl (Figure 1) in the visible region at ambient temperature clearly demonstrate that during the first minute of the reaction an intermediate compound is formed, which gradually decomposes with formation of the blue complex [15,16].

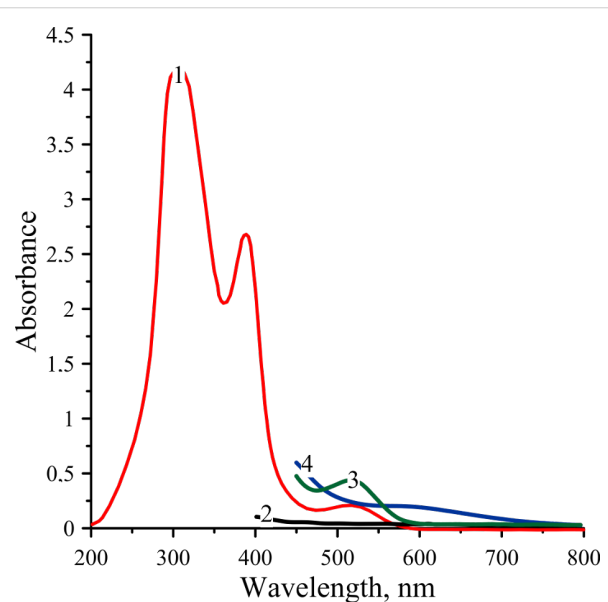


Figure 1: Absorption spectra in the UV and visible spectral region:
 1) bis(cyclopentadienyl)titanium dichloride (*n*-hexane, 0.4 mmol/L);
 2) diethylaluminum chloride (*n*-hexane, 2.5 mmol/L);
 3) $\text{Cp}_2\text{TiCl}_2\text{--AlEt}_2\text{Cl}$ (toluene, 10 mmol/L, Ti/Al ratios is 1:1, immediately after mixing); 4) $\text{Cp}_2\text{TiCl}_2\text{--AlEt}_2\text{Cl}$ (toluene, 10 mmol/L, Ti/Al ratios is 1:1, 10 minutes after mixing).

The complexation between the organoaluminum compound and Cp_2TiCl_2 was further confirmed using ^1H NMR spectroscopy [17,18].

The influence of the Ti/Al ratio was previously discussed [15,19]. Nonetheless, we studied the effect of the Ti/Al ratio on the formation of an absorption band at 700 nm (Figure 2). From the obtained data it follows that the absorption band at 700 nm appears only at Ti/Al ratios above 1:1, therefore, the ratio of Ti/Al equal to 1:1.5 was further used.

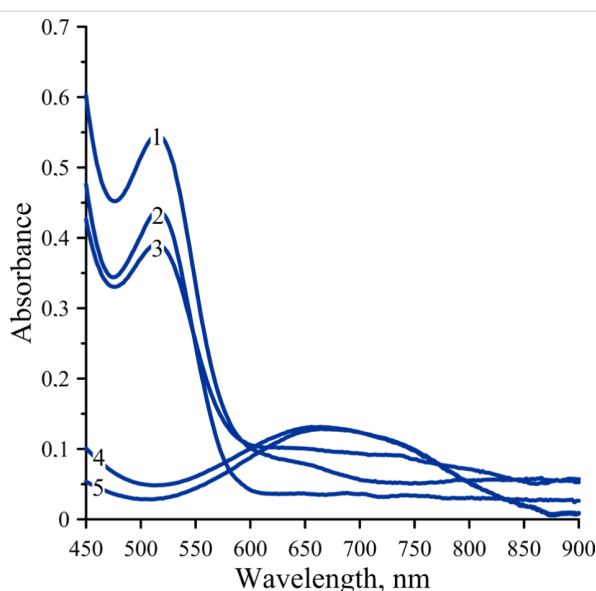


Figure 2: Absorption spectra in the visible spectral region:
 1) $\text{Cp}_2\text{TiCl}_2\text{AlEt}_2\text{Cl}$ (toluene, 10 mmol/L, Ti/Al ratios is 1:0.5);
 2) $\text{Cp}_2\text{TiCl}_2\text{AlEt}_2\text{Cl}$ (toluene, 10 mmol/L, Ti/Al ratios is 1:0.7);
 3) $\text{Cp}_2\text{TiCl}_2\text{AlEt}_2\text{Cl}$ (toluene, 10 mmol/L, Ti/Al ratios is 1:0.9);
 4) $\text{Cp}_2\text{TiCl}_2\text{AlEt}_2\text{Cl}$ (toluene, 10 mmol/L, Ti/Al ratios is 1:1);
 5) $\text{Cp}_2\text{TiCl}_2\text{AlEt}_2\text{Cl}$ (toluene, 10 mmol/L, Ti/Al ratios is 1:1.5).
 All spectra correspond to time 40 minutes after mixing.

During this complex formation, generation of cyclopentadiene (CPD) trimers, resulting from the interaction between the cyclopentadiene ring of bis(cyclopentadienyl)titanium dichloride and dicyclopentadiene, occurs. Figure 3 presents the ^1H NMR spectra of the product formed in the reaction mass during the polymerization of DCPD in hexane (DCPD concentration of 1.5 mol/L, concentration of the catalyst system of 2.5 mmol/L, Ti/Al ratio is 1:1.5). After removing the polymer precipitate from solution, the remaining product is identified as a CPD trimer. The amount of trimer formed is small and amounts to 1–3% of the total DCPD taken per reaction. The appearance of interaction products of DCPD and the catalytic system generating the CPD trimer was unexpected. Typically, the CPD trimer is formed under more severe conditions, for example, at high temperatures $\approx 180\text{ }^\circ\text{C}$, (see Figure 3).

This was confirmed by NMR analyses of the interaction products between the complex of bis(cyclopentadienyl)titanium dichloride and diethylaluminum chloride with dicyclopentadiene (Figure 3b). The NMR spectrum of tricyclopentadiene obtained via condensation of dicyclopentadiene and cyclopentadiene is presented for comparison (Figure 3a).

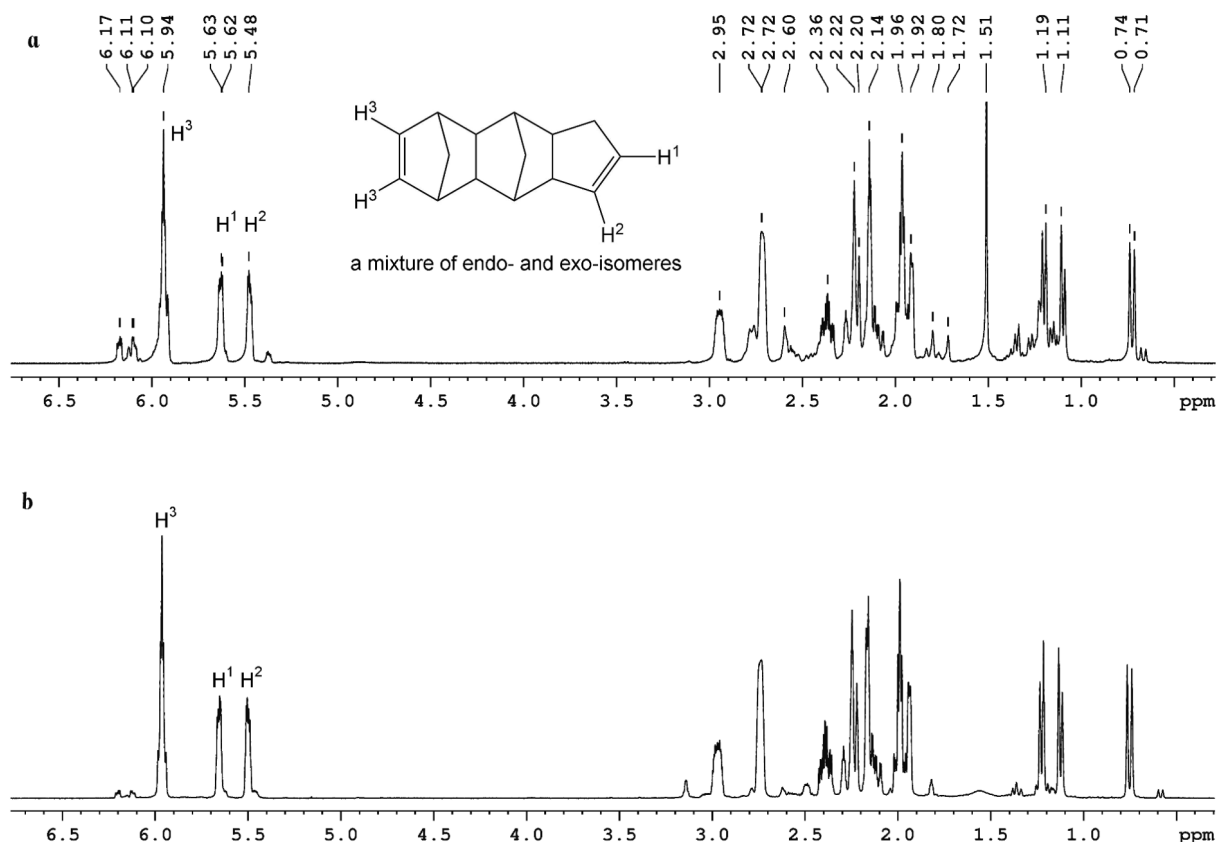
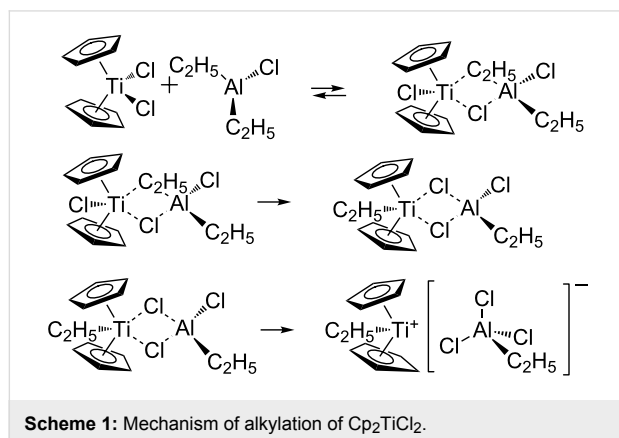


Figure 3: ^1H NMR spectra of tricyclopentadiene (a) and the interaction product between Cp_2TiCl_2 and AlEt_2Cl with dicyclopentadiene (b).

Dialkyl derivatives of aluminum very easily alkylate Cp_2TiCl_2 . Alkylation can occur according to the following mechanism (Scheme 1):



During the interaction of the intermediate complex with cyclo- and dicyclopentadiene, generation of metal carbene species is possible, which can also take part in the formation of polydicyclopentadiene. Already in the work of Grubbs and others [20–23], the possibility was pointed out of the formation of simple structures with a carbene bond via interaction of organometallic transition metal complexes with organic aluminum compounds. The formation of such unstable bis(cyclopentadienyl)titanium dichloride complexes with a $\text{Ti}=\text{CHR}$ fragment is possible as well in this case. The obtained complex is polar-

ized in such a way that the metal has a positive charge, and the carbon atom has a negative charge [23]. It is assumed that after the formation of such complexes, they initiate the metathesis polymerization of dicyclopentadiene.

In the UV–vis spectrum of Cp_2TiCl_2 , two maxima are observed at 388 and 516 nm. It is known that when a solution of AlEt_2Cl is added to a Cp_2TiCl_2 solution, the maxima at 388 and 516 nm will disappear and a new band will appear in the region of 580 nm [15,16].

Mixing of toluene solutions of Cp_2TiCl_2 and AlEt_2Cl demonstrates also a change in the visible region at ambient temperature and with the increase of the AlEt_2Cl content the band at 516 nm, characteristic for Cp_2TiCl_2 , disappears. As a result, a new band appears in the region of 570–610 nm, confirming the formation of an intermediate complex between Cp_2TiCl_2 and AlEt_2Cl , however, this only occurs when an excessive amount of diethylaluminum chloride is present in solution.

Hence, the band with maximum absorption in the region of 580 nm is assigned to the intermediate complex $\text{Cp}_2\text{TiCl}_2\text{AlEt}_2\text{Cl}$, which is formed when solutions of Cp_2TiCl_2 and AlEt_2Cl are mixed.

The stability of the formed complex was investigated using visible spectroscopy and the obtained spectra are depicted in Figure 4.

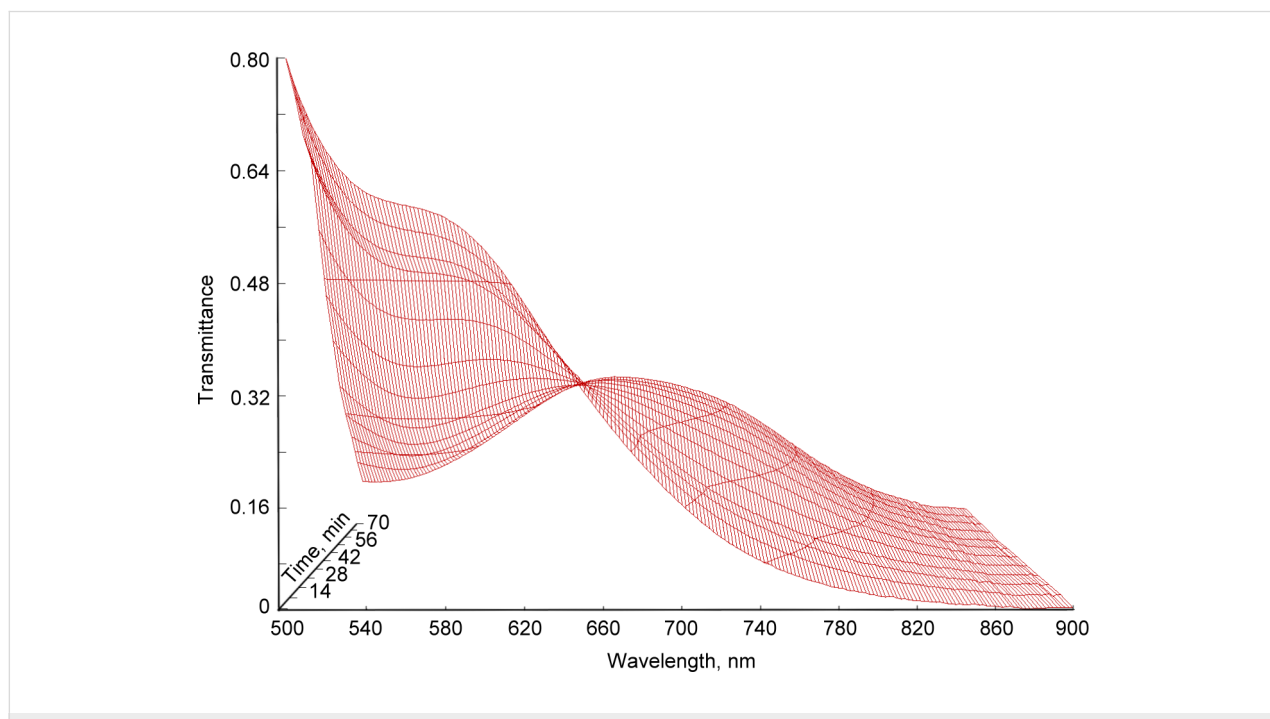


Figure 4: Visible spectra of a mixture of Cp_2TiCl_2 and AlEt_2Cl as function of time.

A clear change as a function of time can be observed by the decrease of the band at 580 nm. Moreover, a shift of the absorption band towards 700 nm and a broadening can be observed. The final visible spectrum (Figure 2, curve 5) corresponds to $[\text{Cp}_2\text{TiEt}]^+ \cdot [\text{AlEtCl}_3]^-$, the blue complex. Indeed, as reported in previously published papers [15,16], the colored blue complex under these conditions is caused by a compound containing Ti(III) or Ti(IV). This compound corresponds to the final $[\text{Cp}_2\text{TiEt}]^+ \cdot [\text{AlEtCl}_3]^-$ complex.

The presence of an isosbestic point at 656 nm indicates the presence of only two absorbing complexes, which transfers one into the other.

Polymerization of DCPD applying the complex based on Cp_2TiCl_2

Polymerization of DCPD, applying the homogeneous catalytic system consisting of Cp_2TiCl_2 and AlEt_2Cl , was performed by adding a fresh solution of the catalytic system to a toluene solution of the monomer. However, before adding the catalytic complex, the monomer solution was placed in an adiabatic mixing reactor until the temperature was stabilized. To limit the development of the polymer chain and as a deactivator of the

catalyst system, propylene oxide was used. The polymerization of DCPD was carried out under the following conditions: ratio of Ti/Al 1:1.5, concentration of the complex $\text{Cp}_2\text{TiCl}_2/\text{AlEt}_2\text{Cl}$ from 2 to 10 mmol/L, and concentration of DCPD 1.5 mol/L.

Figure 5 shows a typical thermometric curve for the polymerization of DCPD (Ti/Al ratio 1:1.5, concentration of $\text{Cp}_2\text{TiCl}_2/\text{AlEt}_2\text{Cl}$ complex 10 mmol/L, concentration of DCPD 1.5 mol/L). Based on the assumption that the stage of chain growth proceeds as a pseudo-first order reaction, for every experiment, we calculated the observed reaction constant using the experimental curve in semi-logarithmic coordinates (Figure 5b) [24]. The value of the observed constant of DCPD polymerization rate in the toluene solution applying the catalyst system amounts to $0.011 \text{ mol}^{-1} \cdot \text{s}^{-1}$.

Furthermore, it is assumed that in this case, cationic polymerization of DCPD proceeds via one of the double bonds. With the participation of the double bond from the norbornene ring of dicyclopentadiene in the double bond reaction, as a result of the rearrangement of the active site, structures of both *exo*- and *endo*-polydicyclopentadiene (**A** and **B**, see Scheme 2) can be formed [1,10].

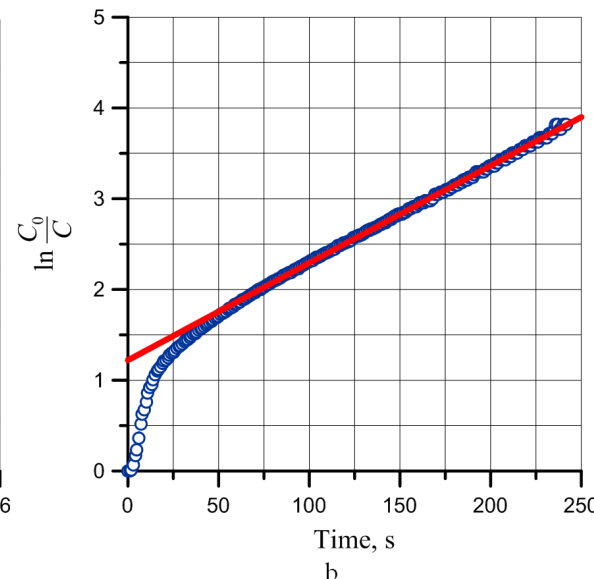
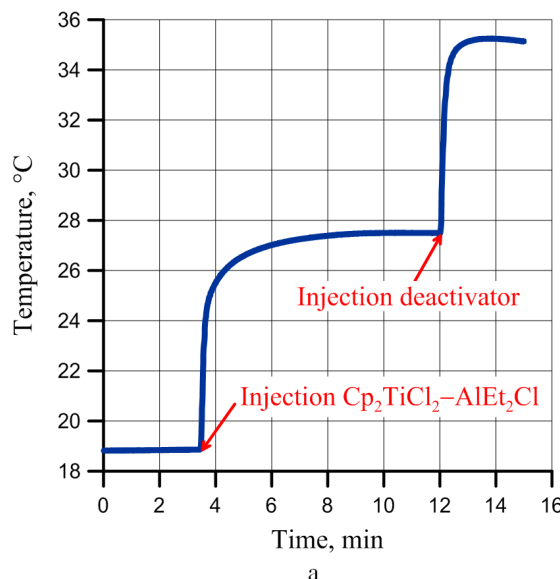
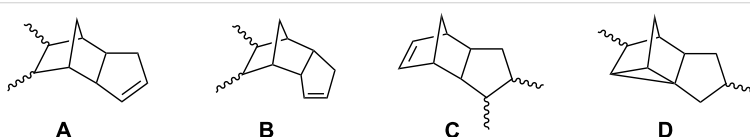


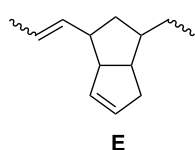
Figure 5: Thermometric curve of DCPD polymerization using the catalyst system based on Cp_2TiCl_2 (a) and its semi-logarithmic plot of $\ln C_0/C$ vs time (b).



Scheme 2: The structures formed as a result of the cationic polymerization of dicyclopentadiene.

At the same time, with participation in the reaction of the cyclopentene double bond, one of the options may be the formation of the **D** units (Scheme 2) as a result of the transannular rearrangement of the growing carbocation [1]. As it was found, **A**-type units (up to 70%) dominate in the structure of polymers formed as a result of cationic polymerization. The number of formed **B**- and **C**-type units is about the same.

In addition, a small amount of polymer **E** units (5–7%) is also formed as a result of the metathesis polymerization of dicyclopentadiene (see Scheme 3). It was reported [20,22,23,25,26] that the Tebbe reagent, as shown, is a precursor of titanium carbene, which reacts with R-olefin and a Lewis base to form stable crystalline titanacyclobutanes. Both titanium carbene and titanacycles are ROMP catalysts (Scheme 4).



Scheme 3: The units resulting from ROMP of dicyclopentadiene.

PDCPD polymers were obtained by precipitation in ethanol, dried and characterized by FTIR, NMR, and GPC.

Figure 6 displays a typical infrared spectrum of PDCPD obtained with the catalyst system based on Cp_2TiCl_2 and AlEt_2Cl .

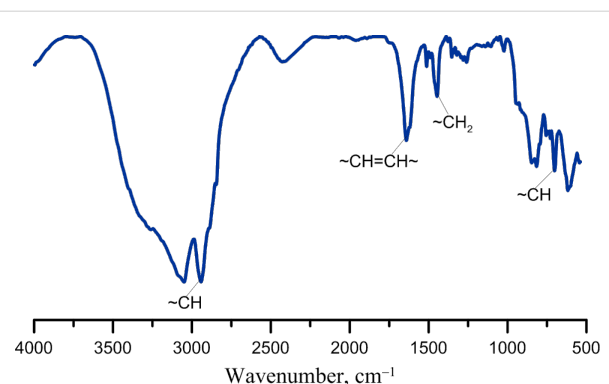
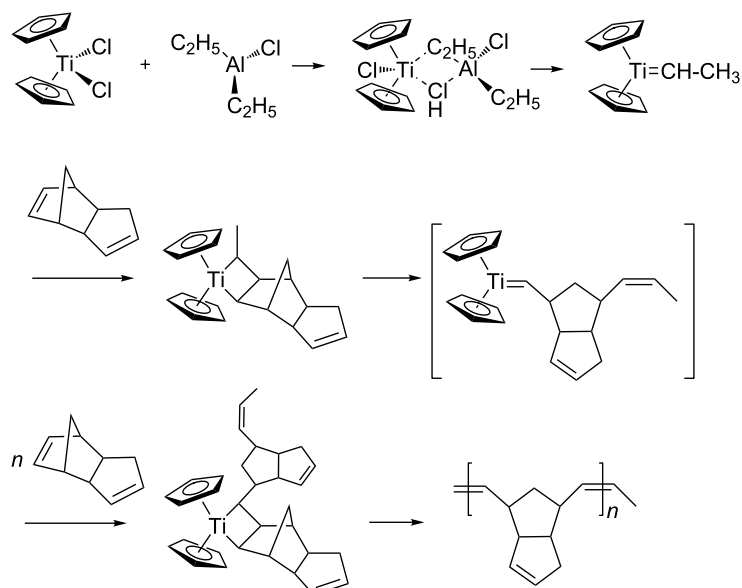


Figure 6: FTIR spectrum of PDCPD obtained in toluene with the catalyst system based on Cp_2TiCl_2 and AlEt_2Cl .

This spectrum displays specific regions, e.g., the regions from 690 to 800 cm^{-1} can be assigned to out-of-plane deformation vibrations of the C–H group. The band at 1440 cm^{-1} points out the presence of CH_2 groups. The bands in the region of 1620 cm^{-1} confirm the presence of $\text{C}=\text{C}$ groups, while the absorption band at 2990 cm^{-1} demonstrates the presence of $\text{CH}-\text{CH}_2$ groups in the ring.

Figure 7 shows the ^1H NMR spectrum of the obtained polymer, in which the region from 0.5 to 3.5 ppm is assigned to aliphatic protons. This region contains a wide signal corresponding to the superposition of resonances of $-\text{CH}$ and $-\text{CH}_2$ groups of cyclopentene and cyclopentane rings. The region from 5.0 to 6.3 ppm contains several wide signals corresponding to reso-



Scheme 4: Mechanism of ROMP dicyclopentadiene.

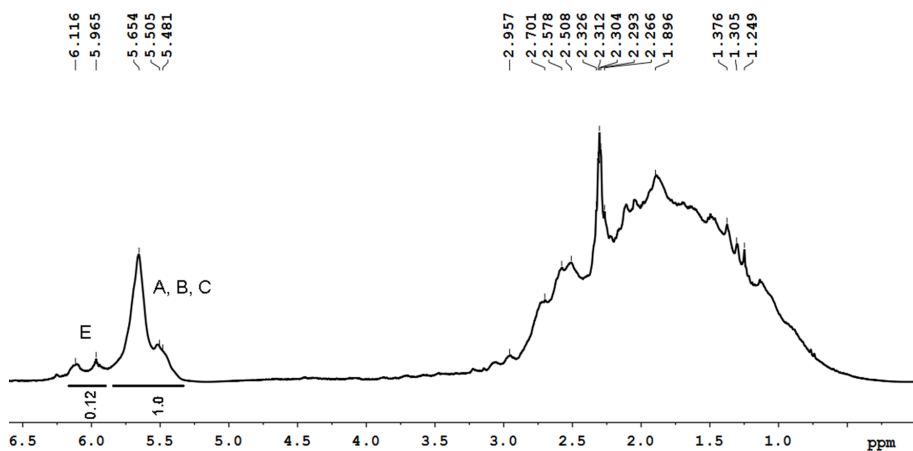


Figure 7: ^1H NMR spectrum of PDCPD obtained with the catalytic system based on Cp_2TiCl_2 and AlEt_2Cl .

nances of protons of double bonds of the polymer chain and the cyclopentene ring (see Scheme 2 and Scheme 3).

According to GPC, the molecular weight of the polymers was in the range of $(10\text{--}50)\cdot 10^3$ with a molecular weight distribution of about 2–3.

Figure 8 displays the GPC traces for two samples of DCPD polymers obtained at a concentration of $\text{Cp}_2\text{TiCl}_2/\text{AlEt}_2\text{Cl}$ complex 2 mmol/L (curve 1) and 10 mmol/L (curve 2). The remaining conditions are the same: Ti/Al ratio 1:1.5, concentra-

tion of DCPD 1.5 mol/L. $M_w(1) = 5.13\cdot 10^4$, $M_n(1) = 2.69\cdot 10^4$, PDI(1) = 1.91; $M_w(2) = 1.32\cdot 10^4$, $M_n(2) = 4.84\cdot 10^3$, PDI(2) = 2.73 of additional monomer.

Oxidizing of thin layers of PDCPD in air

Oxidation in air of olefinic bonds in a thin layer of polydicyclopentadiene is a gradual process and can be observed by the increase of intensity of the vibration band of carbonyl and hydroxy groups in the infrared spectra of the polymers (Figure 9). The wide band at 3400 cm^{-1} belongs to stretch vibrations of hydroxy groups located at various carbon atoms in the main polymer chain. The intensity of the deformation vibration of the carbonyl groups also increases at 1700 cm^{-1} , while the intensity of the deformation vibration of the double bonds decreases at 1620 cm^{-1} .

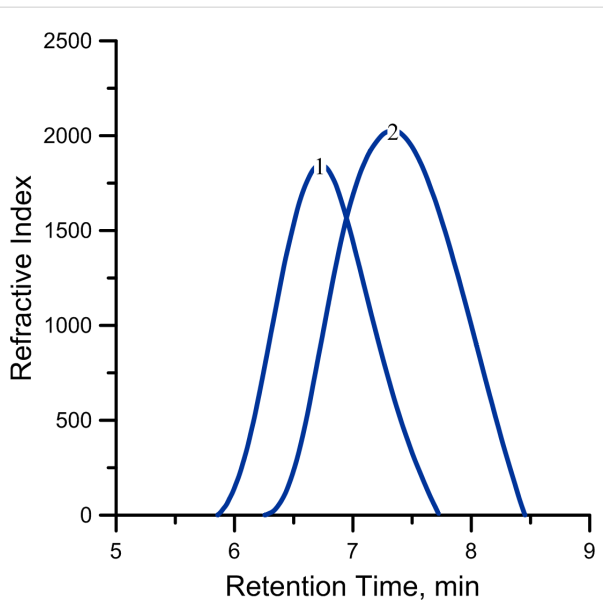


Figure 8: GPC traces for two samples of DCPD polymers obtained at a concentration of $\text{Cp}_2\text{TiCl}_2/\text{AlEt}_2\text{Cl}$ complex 2 mmol/L (curve 1) and 10 mmol/L (curve 2).

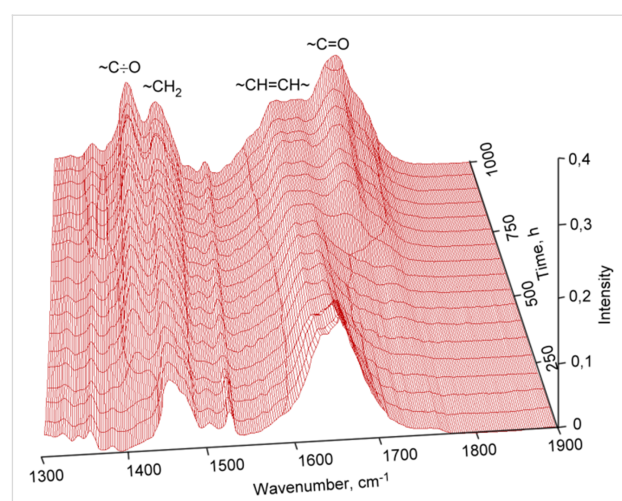


Figure 9: IR spectra of cationic polymerized dicyclopentadiene taken after certain periods of time exposed to air.

Figure 9 reveals that structural changes gradually happen during the exposure time of polydicyclopentadiene thin layers in the air as a result of the oxidation of double bonds. A new vibrational band at 1410 cm^{-1} in the IR spectrum appears which is originating from the primary radicals which are formed alongside the chain initiation.

The kinetics for the oxidation in air at ambient temperature of PDCPD layers was studied applying the changes in intensity of the double bond deformation vibrations. Figure 10 shows the kinetic curve of the PDCPD oxidation obtained from the correlation between the changes of the relative intensity of double bond deformation vibrations and the layer exposure time in air at ambient temperature.

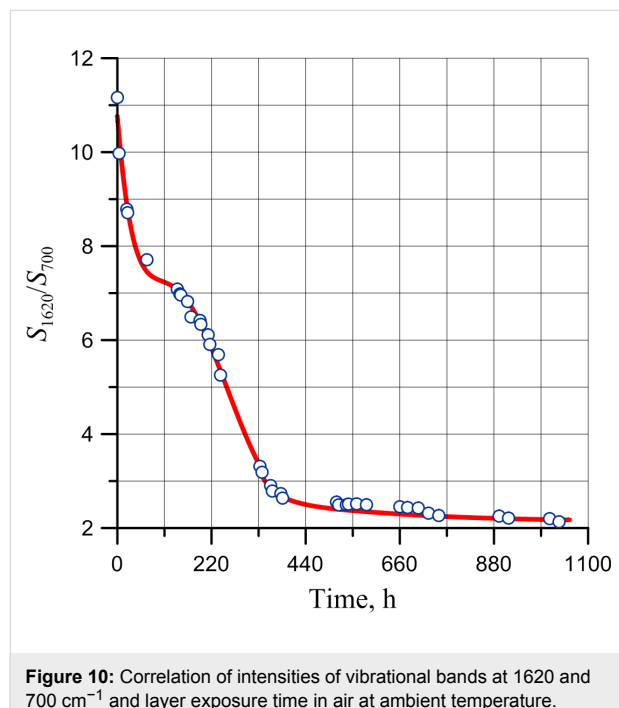
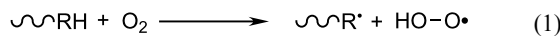


Figure 10: Correlation of intensities of vibrational bands at 1620 and 700 cm^{-1} and layer exposure time in air at ambient temperature.

The correlation presented in Figure 10 demonstrates that the kinetics of double bond consumption during oxidation occurs in two stages. During the first stage, the chain (formation of primary radicals) initiates, and then the chain process of PDCPD oxidation follows.

Various mechanisms of chain initiation are possible, e.g., the formation of primary free radicals initiating the chain reaction of polymer oxidation (Equation 1). More often, the chain initiation step is described as a bimolecular interaction between oxygen and a monomer unit of the polymer:



Accumulation of peroxides in the polymer layer is confirmed by DSC analysis of films subjected to air oxidation for 700 hours (Figure 11).

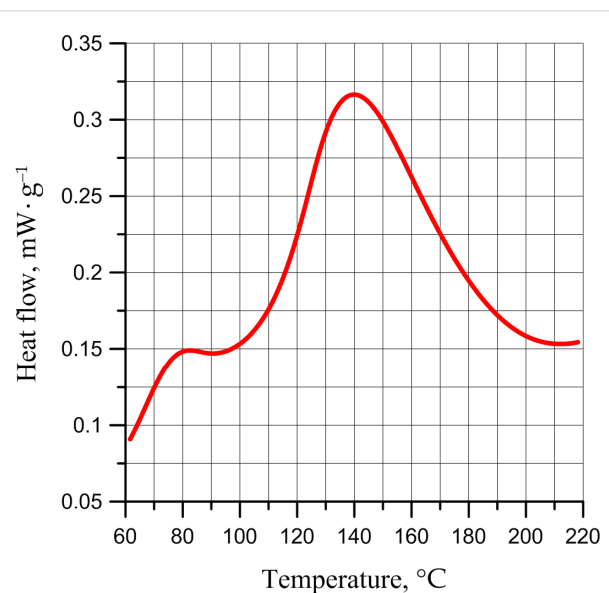


Figure 11: DSC exotherm for PDCPD subjected to air oxidation for 700 hours.

From the DSC curve (Figure 11), at $140\text{ }^\circ\text{C}$ an exothermic peak can be observed corresponding to the decomposition of peroxides accumulated during the oxidation of PDCPD. The peak value of heat flux is slightly lower than that given in [27], which is explained by the slower diffusion of oxygen into the polymer film from air and the lower temperatures of the oxidation of thin PDCPD films in this study.

In our opinion, the peak at $80\text{ }^\circ\text{C}$ can correspond to the processes of oxidation of $-\text{C}=\text{C}-$ bonds in the polymer chain due to adsorbed oxygen. In the DSC of unexposed film, this peak is absent. However, the DSC of unexposed film in air atmosphere (Figure 12) shows that the oxidation and decomposition of peroxides formed during the oxidation of polydicyclopentadiene occur simultaneously.

HO-O^\bullet radicals formed during this process can react with monomer components near them, thus, forming R^\bullet radicals and recombine with primary R^\bullet radicals. Therefore, the theoretical yield of radical formation in the reaction (1) ranges between 0 and 2, and can be conveniently described as the reaction given in Scheme 5.

Impurities remaining in the polymer after its purification can participate in the initiation of the chain oxidation. These impurities can include initiator or catalyst residues, metal impurities

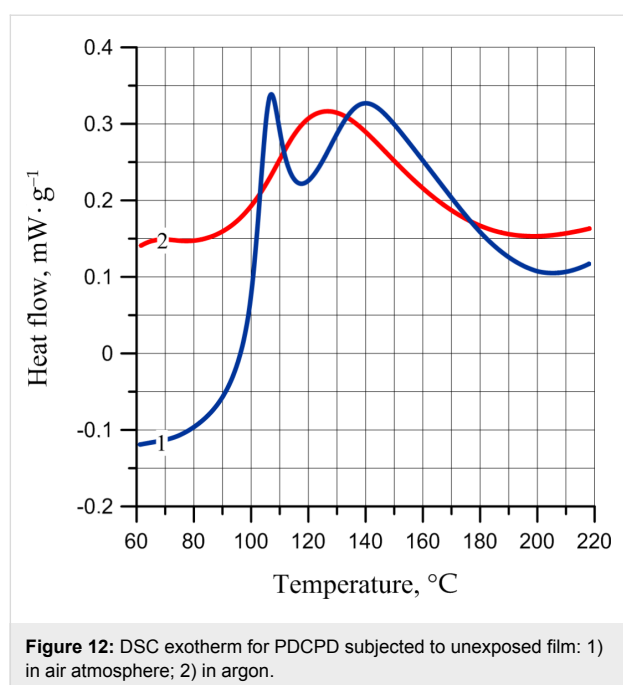


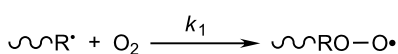
Figure 12: DSC exotherm for PDCPD subjected to unexposed film: 1) in air atmosphere; 2) in argon.



Scheme 5: Possible radical formation in the reaction (1).

with mixed valences, in particular, those of iron and copper, peroxy and carbonyl group-containing compounds.

Unlike the initiation, the steps of chain propagation during polymers oxidation are well studied [28]. The first step of chain propagation consists of the interaction of the free R^\bullet radical with oxygen (Scheme 6) and occurs at an observable rate at low temperatures.



Scheme 6: The first step of the chain propagation.

In a kinetic mode, the polymer oxidation rate is limited by the kinetic steps of the chain process, indicating that oxygen is quickly transferred from the gaseous phase into a polymer (macro-diffusion) and does not limit the process rate. Otherwise, when oxygen is slowly supplied into the sample, the process rate is limited by the diffusion, and the oxidation takes place in a diffusion mode. The reaction kinetics is consecutive and hence, it is characterized by a wide range of rate constants and can be described by the following equation:

$$\frac{dc}{dt} = D \left(\frac{\partial^2 c}{\partial x^2} \right) - kc \quad (2)$$

where the first element on the right defines the oxygen diffusion rate into that element, and the second element defines the rate of its chemical reaction.

The univocal criterion of the diffusion mode is the correlation of the oxidation rate and the sample size (layer thickness, ball or cylinder diameter, etc.). If the sample is plate-shaped and $2l$ thick and its linear size is much bigger than $2l$, then the concentration of oxygen in each element of the sample at time t is determined by following Equation 2.

However, under stationary conditions, when the oxygen supply rate into the sample during diffusion equals its consumption rate in the chemical reaction, then the oxygen concentration in each element is independent of the time, i.e.,

$$\frac{dc}{dt} = 0.$$

Hence, Equation 2 can be reorganized as:

$$D \left(\frac{\partial^2 c}{\partial x^2} \right) - kc = 0$$

Under boundary conditions ($c = c_0$ as $x = 0$ and $dc/dx = 0$ as $x = l$), the solution of this equation gives the oxidation rate as a ratio to a polymer mass unit [28]:

$$r_m = (Dk)^{1/2} \rho^{-1} l^{-1} c_0 \tanh \left[(Dk)^{1/2} l \right]$$

where D is the oxygen diffusion coefficient; ρ is the polymer density and for $l \rightarrow \infty$ $(r_m)_\infty \rightarrow 0$, while $l = 0$ $r_m = kc_0$, i.e., oxidation transfers into a kinetic mode. In this case, the value of k is $1.6 \cdot 10^{-3} \text{ h}^{-1}$.

Equation 2 helps to understand the appearance of the curves of the dwell time of a layer in air at ambient temperature (Figure 13).

According to the classical theory of oxidation of polymers, the formation of primary radicals occurs predominantly, and only when they are formed, further oxidation of the $-\text{C}=\text{C}-$ bonds occurs with the aid of the peroxide radicals formed. However, crosslinking of polymer chains occurs along with oxidation processes, which leads to compaction of the polymer structure and

reduction of the mobility of the polymer chains. This adversely affects the rate of penetration of air oxygen through the layer of the structured polymer. As a result, physical adsorption of oxygen and its transport through the polymer layer becomes the slowest process, which leads to a change in shape of the kinetic curve of the accumulation of peroxide radicals (Figure 13).

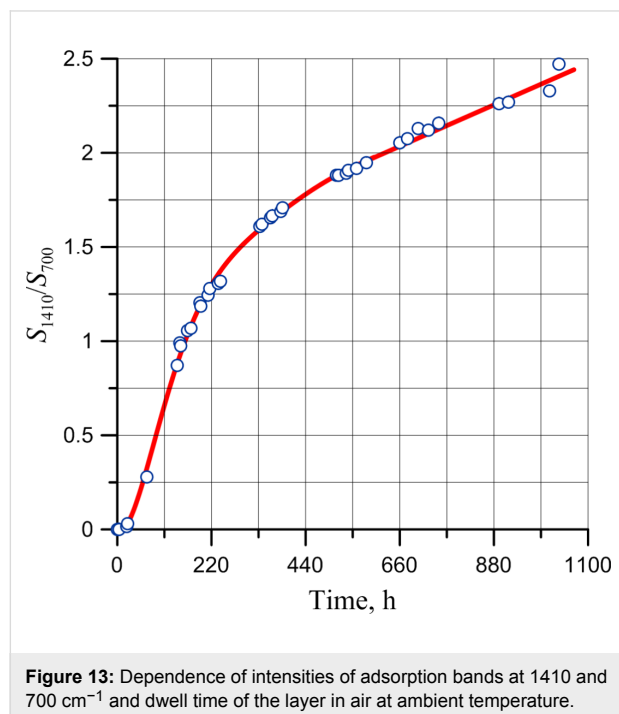


Figure 13: Dependence of intensities of adsorption bands at 1410 and 700 cm^{-1} and dwell time of the layer in air at ambient temperature.

The curve in Figure 13 averages the experimental points of the oxidation process and is a result of two interpolations – a curve in the initial part (up to about 500 hours) and a straight line for the rest of the time interval. In fact, the transition to the diffusion mode occurs much earlier, as can be clearly seen from the semi-logarithmic curve (Figure 14).

A number of PDDCP studies [29] indicate the possibility of the formation of a thin film of a chemically modified polymer, which reduces its permeability to corrosive media. We assume that in case of PDCPD oxidation, the formation of chemically modified polymer layers also occurs, which reduce the permeability of the film to oxygen.

The double bonds located on the surface of the polymer are capable of various addition reactions (bromination, epoxidation, oxidation) forming films of several tens or hundreds of nanometers thick on the surface. However, no further penetration of reactants into the deeper polydicyclopentadiene layers occurs [28]. It is this effect that causes the great chemical inertness of PDCPD in relation to aggressive media. Actually, since the initial part of the curve is exponential, then along with the

increase of the duration of the layer oxidation, and while structuring is in progress, the process gradually transfers into the diffusion mode.

The transfer into the diffusion mode of the oxidation is shown by a semi-logarithmic curve when its slope changes (Figure 14).

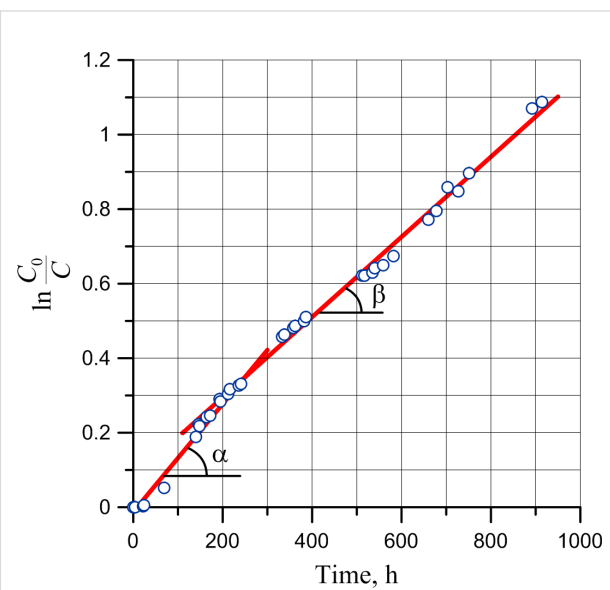


Figure 14: Semi-logarithmic kinetic curve of PDCPD oxidation in air (thin layer on silicon) with respect to intensities of adsorption bands at 1410 and 700 cm^{-1} .

The oxygen concentration is maximal before the polymer layer; therefore, at a small depth of the layer, the rate of oxygen consumption is determined by the proceeding polymer oxidation reactions. However, the resulting film of oxidized cross-linked polydicyclopentadiene prevents further penetration of oxygen into the depth of the polymer layer (Figure 15).

At this stage in general, the oxidation process is limited by the diffusion of oxygen in the thickness of the polymer layer. The rate of oxygen consumption at the initial time point is influenced by many factors, of which the main factors are the formation and growth of the thickness of the oxidized cross-linked polymer layer on the film surface and the change in the rate of oxygen diffusion through the layer due to the changing properties of the polymer film. Later on, when the layer of oxidized cross-linked polymer is formed, the speed of the PDCPD oxidation process is limited only by the rate at which oxygen enters the polymer layer.

At the same time, the accumulation of carbonyl and hydroxy group vibrations in the polymer does not occur immediately when the induction period is finished (Figure 16).

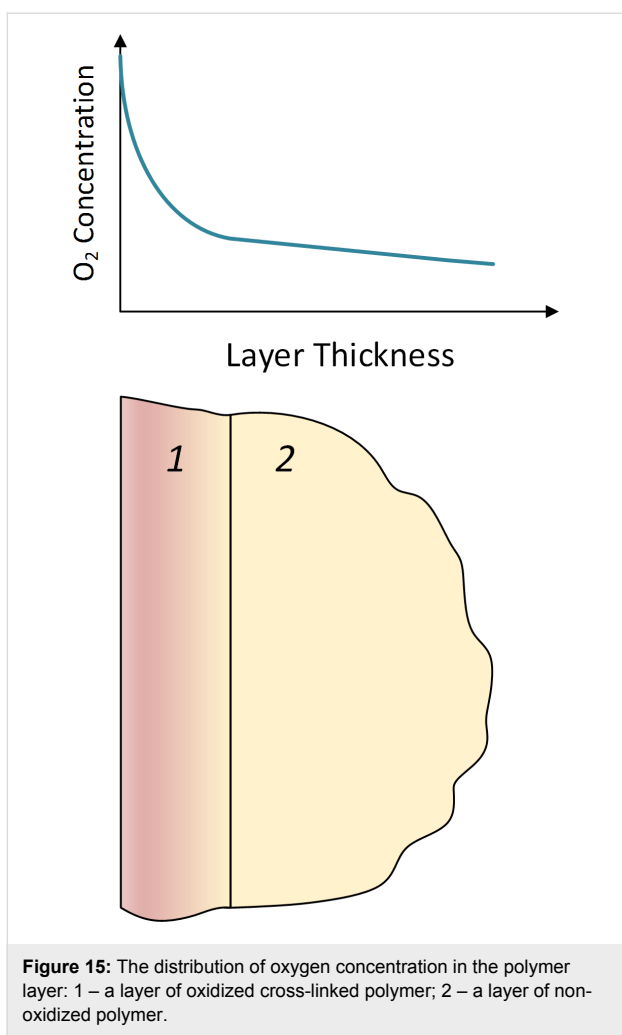


Figure 15: The distribution of oxygen concentration in the polymer layer: 1 – a layer of oxidized cross-linked polymer; 2 – a layer of non-oxidized polymer.

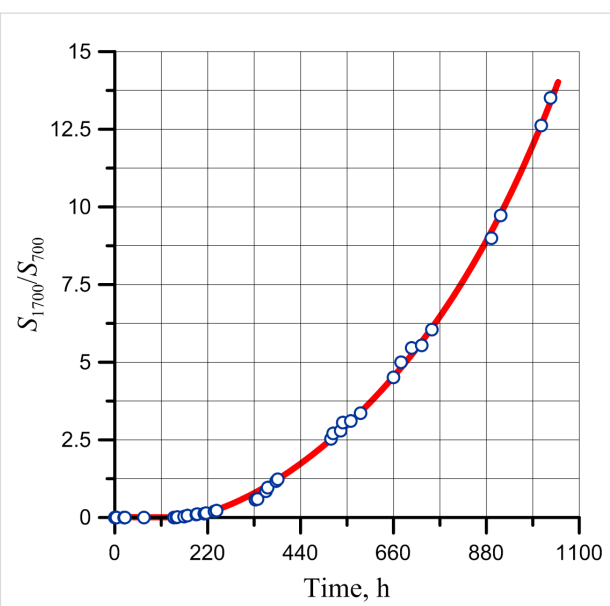


Figure 16: Dependence of the ratio of adsorption bands at 1700 and 700 cm^{-1} on the exposure time of the layer in air at ambient temperature.

It is worth to mention that its induction period coincides with the passing of the first stage of double bond consumption in the polymer (Figure 10).

Finally, the abovementioned structural changes did not occur in the polymer which was stabilized by adding an antioxidant (Agidole-1 in the amount of 0.2% by mass). The infrared spectrum of the thin layer of the stabilized polymer (Figure 17a)

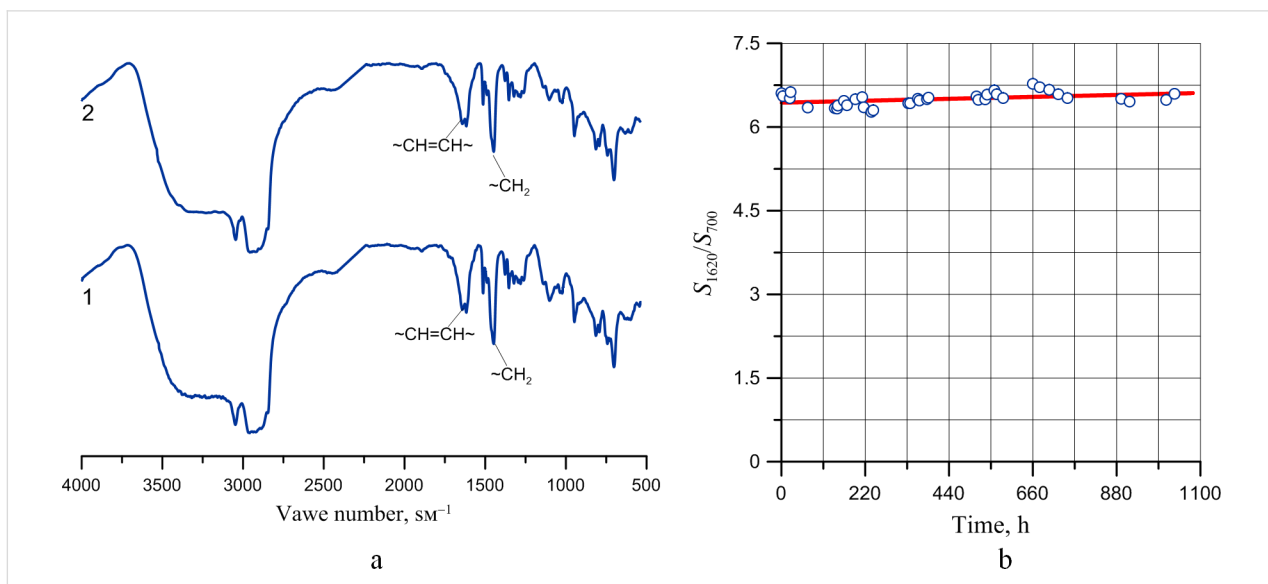


Figure 17: Infrared spectra (a) of products of cationic polymerization of DCPD, stabilized with an antioxidant, after 24 hours (curve 1) and 1030 hours (curve 2) after synthesis (thin layer on silicon wafer) and (b) the correlation of intensity ratios of adsorption bands at 1620 and 700 cm^{-1} vs layer exposure time in air at ambient temperature.

does not change and no consumption of double bonds in the polymer can be detected (Figure 17b).

Conclusion

This study reports regularities of DCPD polymerization in a toluene solution applying a catalytic system consisting of Cp_2TiCl_2 and AlEt_2Cl . It was demonstrated that the use of an excessive amount of organoaluminum leads to the formation of stable charged blue complexes which initiate the cationic polymerization of dicyclopentadiene.

Polymer thin-film coatings of PDCPD obtained via cationic polymerization in air undergo oxidation and transformation. Oxidation in air of unsaturated bonds in layers occurs gradually and takes place during several weeks and comes amid with the growth of carbonyl and hydroxy group vibration bands in the infrared spectra. At the same time, structuring and isomerization occur in layers generating changes in their physical properties, in particular, the decrease of layer permeability for atmospheric air. In its turn, this leads to the transition of the oxidation from a kinetic mode into a diffusion one.

These structural changes do not occur in a polymer stabilized by adding an antioxidant in the studied period of time.

Experimental

Dehydrated toluene, prepared according to a well-known procedure, was used as a solvent [30]. Polymerization of DCPD in toluene was carried out in a 100 mL adiabatic mixing reactor [31]. A thermometric method was used to study the kinetics of the process, which was carried out in adiabatic conditions with minor temperature change; hence, the thermometric curve is at the same time a kinetic plot [24]. The temperature was registered during the process with a digital thermometer, consisting of a platinum thin film resistance thermometer placed on a ceramic substrate and placed in a stainless steel thin-wall case.

The catalyst for cationic DCPD polymerization is a complex that is formed during the interaction of Cp_2TiCl_2 with AlEt_2Cl . The estimated amount of Cp_2TiCl_2 (Sigma-Aldrich, 99% pure) was dissolved in toluene. AlEt_2Cl was used as a solution in toluene with a concentration of 0.232 g/mL. All working solutions were obtained by diluting the stock solutions with dry solvent until the required concentration was obtained.

DCPD (Hangzhou Uniwise International Co., Ltd., 99% pure) was purified from stabilizers by distillation under reduced pressure (≈ 6.6 kPa).

All operations with monomer and catalyst were carried out in a glove box MBraun Labstar provided with an argon atmosphere.

UV-vis spectra of catalyst system solutions were registered by a spectrophotometer Thermo Scientific Evolution 201 using a wavelength range from 200 to 900 nm.

Infrared spectra of the polymer were registered applying an FTIR spectrometer Simeks FT-801 in the range from 500 to 4000 cm^{-1} . A silicon plate with a diameter of 8 mm was applied to support the polymer film and degreased before use. Polymer films were applied by irrigation from 2–5% solutions of PDCPD in toluene, followed by drying at $25\text{ }^\circ\text{C}$ under a nitrogen atmosphere (Binder VDL 23 Vacuum Drying Oven), with a gradual decrease in pressure at the end of the drying process.

The thickness of the polymer film was controlled so that the maximum light absorption in the wavelength range of 500–4000 cm^{-1} did not exceed 1.2 units of absorption (EP) and remained in the preferred range of 0.3–1.0 EP. The optimum thickness of the film of polydicyclopentadiene was 10 μm .

^1H NMR spectra were recorded using an FT-NMR spectrometer Bruker Avance III AV400 (400 MHz) with HMDS as an internal standard. Samples with a mass of 10 mg were dissolved in CDCl_3 . Chemical shifts were determined by the residual non-deuterated chloroform signal.

Analysis of the molecular weight of the polymers was performed using gel-permeation chromatography on the instrument Agilent Technologies 1260 Infinity with a refractive index detector, GPC/SEC – styrogel column, length 300 mm, internal diameter 7.5 mm, eluent (CHCl_3) rate 1 mL/s, calibration according to the polystyrene standards known molecular weight.

Thermal analysis was performed using a DSC 204 F1 Phoenix (NETZSCH) at a heating rate $10\text{ }^\circ\text{C}/\text{min}$ with aluminum pans (the lid was manually drilled to ensure the access of argon). The DSC instrument was first calibrated with an indium standard. Measurements were carried out under an inert argon (or air) atmosphere at a flow rate of 50 mL/min. Approximately 1 mg of virgin or oxidized sample was heated from $25\text{ }^\circ\text{C}$ up to $250\text{ }^\circ\text{C}$.

Acknowledgements

The authors acknowledge the support from Tomsk Polytechnic University Competitiveness Enhancement Program grant (VIU-2019). F.V. would like to express his deep accolade to the “State Key Laboratory of Advanced Technology for Materials Synthesis and Processing” Wuhan University of Technology for financial support.

ORCID® IDs

Ludmila S. Soroka - <https://orcid.org/0000-0002-5401-0701>
 Alex A. Lyapkova - <https://orcid.org/0000-0002-2072-4239>
 Mekhman S. Yusubov - <https://orcid.org/0000-0001-9233-1824>
 Francis Verpoort - <https://orcid.org/0000-0002-5184-5500>

References

- Peng, Y. X.; Liu, J. L.; Cun, L. F. *J. Polym. Sci., Part A: Polym. Chem.* **1996**, *34*, 3527–3530. doi:10.1002/(sici)1099-0518(199612)34:17<3527::aid-pola6>3.0.co;2-r
- Pacreau, A.; Fontanille, M. *Makromol. Chem.* **1987**, *188*, 2585–2595. doi:10.1002/macp.1987.021881110
- Hilil, A. R.; Balogh, J.; Moncho, S.; Su, H.-L.; Tuba, R.; Brothers, E. N.; Al-Hashimi, M.; Bazzi, H. S. *J. Polym. Sci., Part A: Polym. Chem.* **2017**, *55*, 3137–3145. doi:10.1002/pola.28695
- Hayano, S.; Tsunogae, Y. *Macromolecules* **2006**, *39*, 30–38. doi:10.1021/ma052088c
- Rule, J. D.; Moore, J. S. *Macromolecules* **2002**, *35*, 7878–7882. doi:10.1021/ma0209489
- Ashirov, R. V.; Zemlyakov, D. I.; Lyapkova, A. A.; Kiselev, S. A. *Kinet. Catal.* **2013**, *54*, 469–474. doi:10.1134/s0023158413040010
- Ashirov, R. V.; Zemlyakov, D. I.; Lyapkova, A. A.; Kiselev, S. A.; Vervacke, D. J. *Appl. Polym. Sci.* **2014**, *131*, 40130. doi:10.1002/app.40130
- Ivin, K. J. *J. Mol. Catal. A: Chem.* **1998**, *133*, 1–16. doi:10.1016/s1381-1169(97)00249-5
- Vervacke, D. *An introduction to PDCPD*, Waarschoot-Belgium, Product Rescue, 2008.
- Davidson, T. A.; Wagener, K. B.; Priddy, D. B. *Macromolecules* **1996**, *29*, 786–788. doi:10.1021/ma950852x
- Qian, Y.; Dono, K.; Huang, J.; Ma, H. *J. Appl. Polym. Sci.* **2001**, *81*, 662–666. doi:10.1002/app.1482
- Le Gac, P. Y.; Choqueuse, D.; Paris, M.; Recher, G.; Zimmer, C.; Melot, D. *Polym. Degrad. Stab.* **2013**, *98*, 809–817. doi:10.1016/j.polymdegradstab.2012.12.023
- Richaud, E.; Le Gac, P. Y.; Verdu, J. *Polym. Degrad. Stab.* **2014**, *102*, 95–104. doi:10.1016/j.polymdegradstab.2014.01.036
- Lyapkova, A. A.; Gvozdikov, E. L.; Tarakanovskaya, A. N.; Tarnovskaya, O. D.; Yakovleva, Y. S. *Procedia Chem.* **2014**, *10*, 223–228. doi:10.1016/j.proche.2014.10.038
- Breslow, D. S.; Newburg, N. R. *J. Am. Chem. Soc.* **1959**, *81*, 81–86. doi:10.1021/ja01510a018
- Long, W. P.; Breslow, D. S. *J. Am. Chem. Soc.* **1960**, *82*, 1953–1957. doi:10.1021/ja01493a029
- Adema, E. H.; Bos, H.; Vrinssen, C. H. *Recl. Trav. Chim. Pays-Bas* **1960**, *79*, 1282–1288. doi:10.1002/recl.19600791207
- Bryliakov, K. P.; Talsi, E. P.; Bochmann, M. *Organometallics* **2004**, *23*, 149–152. doi:10.1021/om0340261
- Chien, J. C. W. *J. Am. Chem. Soc.* **1959**, *81*, 86–92. doi:10.1021/ja01510a019
- Howard, T. R.; Lee, J. B.; Grubbs, R. H. *J. Am. Chem. Soc.* **1980**, *102*, 6876–6878. doi:10.1021/ja00542a050
- Gilliom, L. R.; Grubbs, R. H. *J. Am. Chem. Soc.* **1986**, *108*, 733–742. doi:10.1021/ja00264a027
- Petasis, N. A.; Fu, D.-K. *J. Am. Chem. Soc.* **1993**, *115*, 7208–7214. doi:10.1021/ja00069a018
- Zhang, D.; Huang, J.; Qian, Y.; Chan, A. S. C. *J. Mol. Catal. A: Chem.* **1998**, *133*, 131–133. doi:10.1016/s1381-1169(98)00087-9
- Phansi, P.; Danchana, K.; Cerdà, V. *TrAC, Trends Anal. Chem.* **2017**, *97*, 316–325. doi:10.1016/j.trac.2017.09.019
- Tebbe, F. N.; Parshall, G. W.; Reddy, G. S. *J. Am. Chem. Soc.* **1978**, *100*, 3611–3613. doi:10.1021/ja00479a061
- Qian, Y.; Huang, J.; Bala, M. D.; Lian, B.; Zhang, H.; Zhang, H. *Chem. Rev.* **2003**, *103*, 2633–2690. doi:10.1021/cr020002x
- Defauchy, V.; Le Gac, P. Y.; Guinault, A.; Verdu, J.; Recher, G.; Drozdak, R.; Richaud, E. *Polym. Degrad. Stab.* **2017**, *142*, 169–177. doi:10.1016/j.polymdegradstab.2017.06.005
- Voigt, J. *Die Stabilisierung der Kunststoffe gegen Licht und Wärme*; Springer Verlag: Berlin, Germany, 1966. doi:10.1007/978-3-642-52097-6
- Perring, M.; Long, T. R.; Bowden, N. B. *J. Mater. Chem.* **2010**, *20*, 8679–8685. doi:10.1039/c0jm01999b
- Weissberger, A.; Proskauer, E. S.; Riddick, J. A.; Toops, E. E. *Organic Solvents. Physical Properties and Methods of Purification*; Interscience Publishers: New York, 1955.
- Ionova, E. I.; Lyapkova, A. A.; Bondaletova, V. G.; Bondaletova, L. I.; Petrenko, T. V. *Coke Chem.* **2009**, *52*, 496–500. doi:10.3103/s1068364x09110076

License and Terms

This is an Open Access article under the terms of the Creative Commons Attribution License (<http://creativecommons.org/licenses/by/4.0>). Please note that the reuse, redistribution and reproduction in particular requires that the authors and source are credited.

The license is subject to the *Beilstein Journal of Organic Chemistry* terms and conditions: (<https://www.beilstein-journals.org/bjoc>)

The definitive version of this article is the electronic one which can be found at:
[doi:10.3762/bjoc.15.69](https://doi.org/10.3762/bjoc.15.69)



Hoveyda–Grubbs catalysts with an N→Ru coordinate bond in a six-membered ring. Synthesis of stable, industrially scalable, highly efficient ruthenium metathesis catalysts and 2-vinylbenzylamine ligands as their precursors

Kirill B. Polyanskii¹, Kseniia A. Alekseeva¹, Pavel V. Raspertov¹, Pavel A. Kumandin¹, Eugeniya V. Nikitina¹, Atash V. Gurbanov^{2,3} and Fedor I. Zubkov^{*1}

Full Research Paper

Open Access

Address:

¹Organic Chemistry Department, Faculty of Science, Peoples' Friendship University of Russia (RUDN University), 6 Miklukho-Maklaya St., Moscow 117198, Russian Federation, ²Centro de Química Estrutural, Instituto Superior Técnico, Universidade de Lisboa, Av. Rovisco Pais, 1049-001 Lisbon, Portugal and ³Organic Chemistry Department, Baku State University, Z. Xalilov Str. 23, Az 1148 Baku, Azerbaijan

Email:

Fedor I. Zubkov^{*} - fzubkov@sci.pfu.edu.ru

* Corresponding author

Keywords:

CM; cross metathesis; Hoveyda–Grubbs catalyst; olefin metathesis; RCM; ring-closing metathesis; ring-opening cross metathesis; ROCM; ruthenium metathesis catalyst; styrene; 2-vinylbenzylamine

Beilstein J. Org. Chem. **2019**, *15*, 769–779.

doi:10.3762/bjoc.15.73

Received: 23 October 2018

Accepted: 25 February 2019

Published: 22 March 2019

This article is part of the thematic issue "Progress in metathesis chemistry III".

Guest Editors: K. Grela and A. Kajetanowicz

© 2019 Polyanskii et al.; licensee Beilstein-Institut.

License and terms: see end of document.

Abstract

A novel and efficient approach to the synthesis of 2-vinylbenzylamines is reported. This involves obtaining 2-vinylbenzylamine ligands from tetrahydroisoquinoline by alkylation and reduction followed by the Hofmann cleavage. The resultant 2-vinylbenzylamines allowed us to obtain new Hoveyda–Grubbs catalysts, which were thoroughly characterised by NMR, ESIMS, and X-ray crystallography. The utility of this chemistry is further demonstrated by the tests of the novel catalysts (up to 10⁻² mol %) in different metathesis reactions such as cross metathesis (CM), ring-closing metathesis (RCM) and ring-opening cross metathesis (ROCM).

Introduction

Ruthenium-catalysed olefin metathesis reactions have been playing an important role in various fields of organic synthesis in the past three decades. The significance of this transforma-

tion is confirmed by more than 20 reviews devoted to various aspects of metathesis reactions, which were published in last three years (2016–2018). In this paper, we mention only a few

of them [1-12], including most popular recent books [13,14]. Obviously, the application of various catalysts is required to achieve the best results in each of the many directions of metathesis reactions such as cross metathesis – CM, ring-opening metathesis – ROM, ring-closing metathesis – RCM, ring-opening metathesis polymerization – ROMP and acyclic diene metathesis – ADMET. This motivates the investigations into the development of new, efficient, stable, and highly selective catalytic systems based on ruthenium complexes. However, in reality, a limited set of commercially available catalysts is used for the whole range of metathesis reactions most probably due to economical reasons. For example, in 2018, Merck offered more than 20 ruthenium metathesis catalysts. The most popular of them are shown in Figure 1.

The framework of these catalysts consists of two main parts that surround the ruthenium centre – “the upper” one is the N-heterocyclic carbene (NHC) ligand and “the lower” one is the 2-alkoxybenzylidene ligand. These determine the principal catalytic properties of the ruthenium complexes. Many ligands were tested as the upper part in various publications, which concluded that NHCs groups, in particular, 1,3-bis(2,4,6-trimethylphenyl)imidazolidine are superior in terms of price/quality ratio. We suppose that further advances should be rather aimed at the lower part of the ruthenium complex [15-17]. This trend is confirmed partly by the Grubbs catalysts with a pyridine group (Figure 1) recently released to the market.

It has been experimentally established that the catalysts with an *O*-isopropyl group in their structure usually show the best combination of stability and activity. However, the oxygen atom having only one site for modification (i.e., the alkyl substituent) reduces the potential diversity of the chemical environment of the catalytic centre [18-21]. In our opinion, replacing the oxygen atom by the nitrogen atom in the lower part of the catalyst would enhance the variability for both steric and electronic effects of the substituents (Figure 1). This would enable a rational selection of the optimal catalysts for specific metathesis reactions.

It should be mentioned here that the idea of replacing the oxygen atom with nitrogen in the Grubbs catalyst is not new but only a limited number of examples are available in the literature [22-38]. Moreover, a small number of patents, which describe the applications of such type of catalysts in ROMP reactions, were published [25-28]. Among all these applications, the use of the catalysts for the polymerization of dicyclopentadiene has the greatest industrial importance [3,9,29-31]. Noteworthy, there are only rare and sporadic publications describing the synthesis and properties of the Grubbs catalysts with an *N*–Ru coordinate bond in a six-membered ring [32-38].

Thus, the present work opens a series of studies by our group, which will be devoted to the synthesis and reactivity of

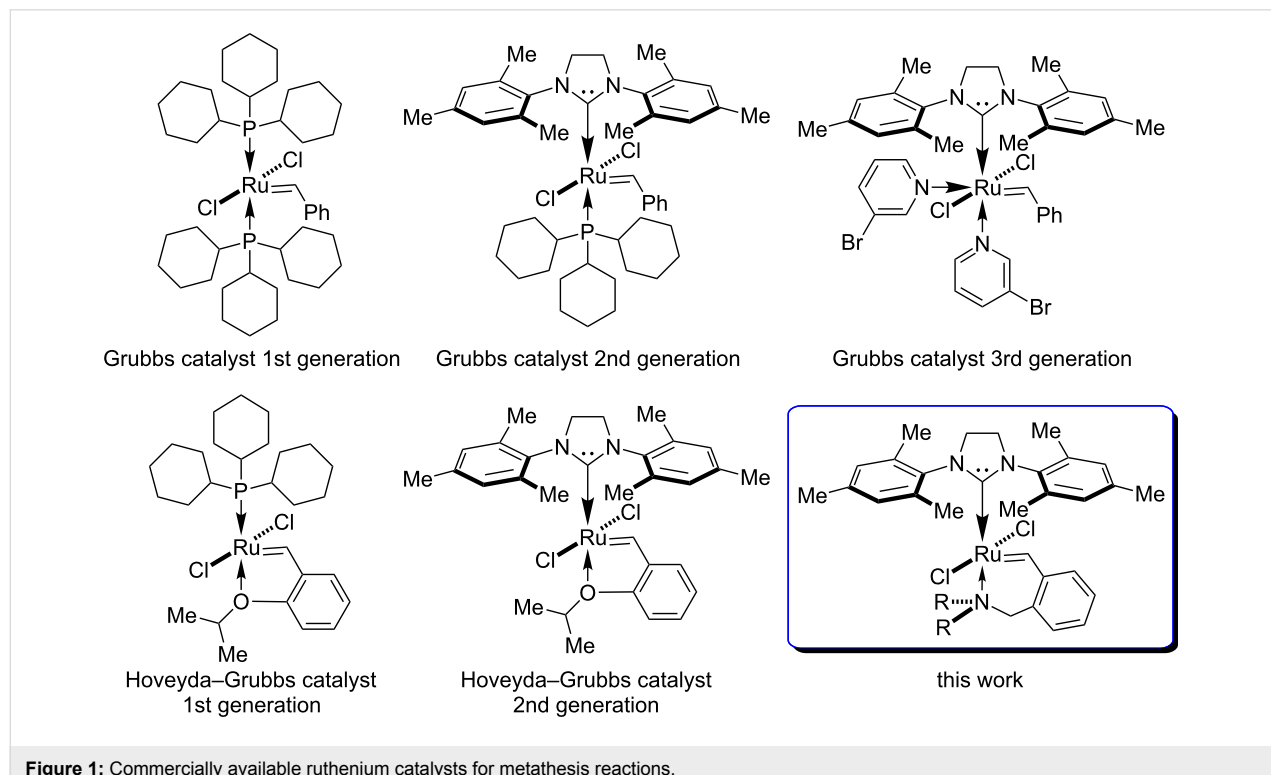


Figure 1: Commercially available ruthenium catalysts for metathesis reactions.

Hoveyda–Grubbs-type catalysts possessing a six-membered ruthenium-containing ring with the $\text{N}\rightarrow\text{Ru}$, $\text{S}\rightarrow\text{Ru}$, and $\text{Se}(\text{Te})\rightarrow\text{Ru}$ coordinate bonds.

Results and Discussion

2-Vinylbenzylamine synthesis

The assembly of the nitrogen-containing ruthenium catalysts required preliminary synthesis of the imidazolium ligand and *o*-vinylbenzylamines (Figure 2). Whereas numerous methods for the preparation of the carbene precursor are known, no satisfactory suitable approach for the synthesis of *ortho*-substituted styrenes was found.

Several methods have been reported for the synthesis of 2-(*N,N*-dialkylaminomethyl)styrenes [39–46] relying on different approaches: i) from *o*-vinylbenzyl chloride [43], ii) by the Hofmann cleavage of quaternary tetrahydroisoquinoline salts under the action of silver oxide [39,42] and iii) by a reaction of 2-(2-bromoethyl)benzyl bromide with secondary amines under microwave irradiation followed by the decomposition of the products under the action of potassium *tert*-butoxide [46]. All of the above routes offer some advantages but they all are rather expensive.

Thus, the initial stage of this work included the development of a preparative scalable method for the synthesis of vinylbenzenes, which provided a wide range of *o*-aminomethylstyrenes

from readily accessible reagents in good yields avoiding formation of byproducts. In this process, the synthesis of 2-vinylbenzylamines from isoquinolines (Scheme 1) involved the following steps: alkylation of isoquinolines to afford isoquinolinium salts **1**, its reduction with formic acid giving rise to tetrahydroisoquinolines **2** in a nearly quantitative yield, which upon alkylation gave quaternary salts **3**, finally these salts underwent the Hofmann elimination to form *N,N*-dialkylaminomethylstyrenes **4** in yields higher than 60% (Table 1). Our attempts to synthesise highly sterically hindered 2-vinyl-*N,N*-diisopropylbenzylamine by an analogous method failed at the stage of the quaternary salt **3**.

Table 1: Yields of target 2-vinylbenzylamines **4** after four steps.

entry	compound	R ¹	R ²	R ² X	yield, % ^a
1	4a	Me	Me	Me ₂ SO ₄	87
2	4b	Me	Et	Et ₂ SO ₄	88
3	4c	Me	Bn	BnCl	78
4	4d	Me	iPr	iPrI	80
5	4e	Et	Et	Et ₂ SO ₄	76
6	4f	Et	iPr	iPrI	72
7	4g	Bn	Bn	BnCl	60

^aAll yields are given after flash column chromatography or vacuum distillation.

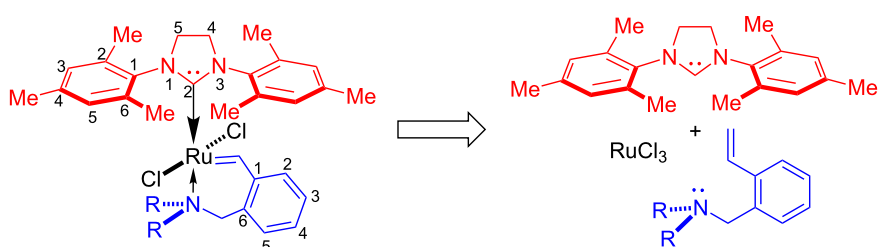
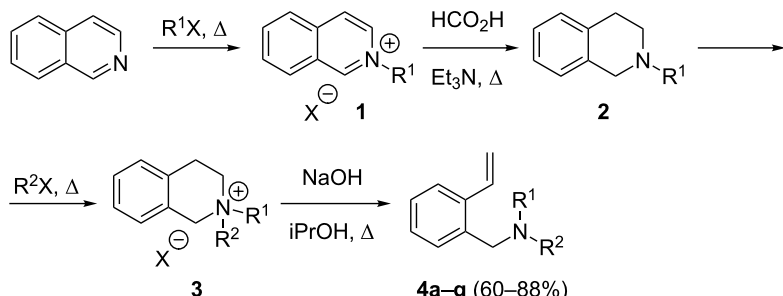
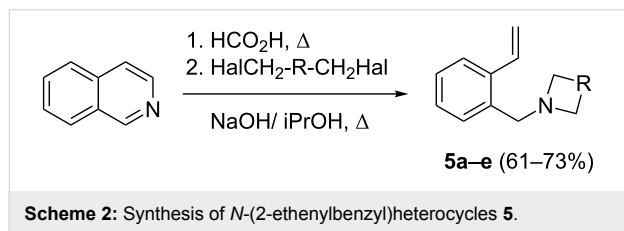


Figure 2: Retrosynthesis of the ruthenium catalysts.



Scheme 1: Efficient multistep synthesis of *N,N*-dialkyl-2-vinylbenzylamines **4** ($\text{R}^1\text{X} = \text{Me}_2\text{SO}_4$, Et_2SO_4 or BnCl , see Experimental part, Supporting Information File 1 and Table 1).

The application of terminal dihalogen derivatives afforded styrenes **5** with a cyclic tertiary amino group from 1,2,3,4-tetrahydroisoquinoline (Scheme 2). In this case, the initial isoquinoline was reduced in the presence of formic acid and then converted into the desired products **5** by a one-pot solvent-free reaction under the action of the corresponding dihalide in alkaline media in a total yield of 61–73% (Table 2).



It should be noted that the above-described method was useful for the synthesis of styrenes in quantities of up to 100 g (or even more, if necessary). This scalability was purposefully demon-

strated by the multigram synthesis of **5e** (see Experimental part in Supporting Information File 1).

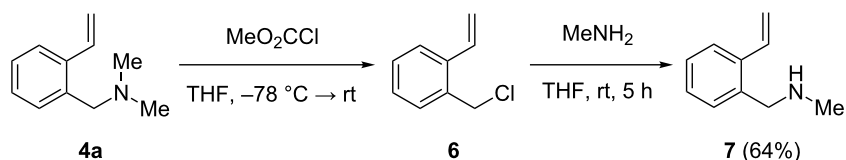
Despite a considerable scope for varying substituents at the nitrogen atom in styrenes **4** and **5**, the developed procedures (Scheme 1 and Scheme 2) do not allow one to obtain benzylamines with a secondary nitrogen atom. The approach outlined in Scheme 3 makes it possible to overcome this problem [44].

Thus, the pathways described in Schemes 1–3 permit one to vary the steric volume of substituents at the nitrogen atom in a wide range enabling synthesis of selective Grubbs catalysts with different catalytic activity. These styrenes were used in the preparation of the target ruthenium complexes shown in Scheme 4. This transformation was carried out using known standard methods including the interaction of the indenylidene derivative **8** with 1,3-dimesityl-2-(trichloromethyl)imidazolidine (**9**) [47–50].

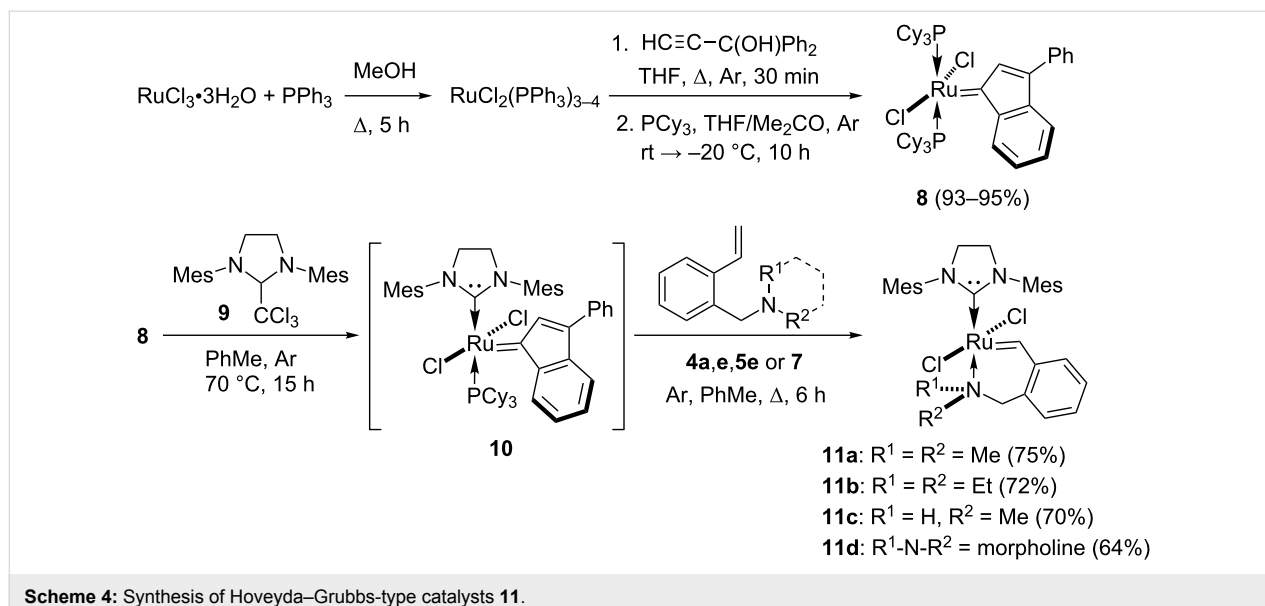
Table 2: Structure and yields of *N*-(2-vinylbenzyl)heterocycles **5**.

entry	compound	structure	initial alkyl halide (HalCH ₂ -R-CH ₂ Hal)	yield, % ^a
1	5a		Br(CH ₂) ₄ Br	61
2	5b		Br(CH ₂) ₅ Br	73
3	5c		ClCH ₂ CH ₂ Cl	72
4	5d		BrCH ₂ CH ₂ Br	70
5	5e		(ClCH ₂ CH ₂) ₂ O	72

^aAll yields are given after column chromatography or vacuum distillation.



Scheme 3: Synthesis of *N*-monoalkyl-2-vinylbenzylamine **7**.

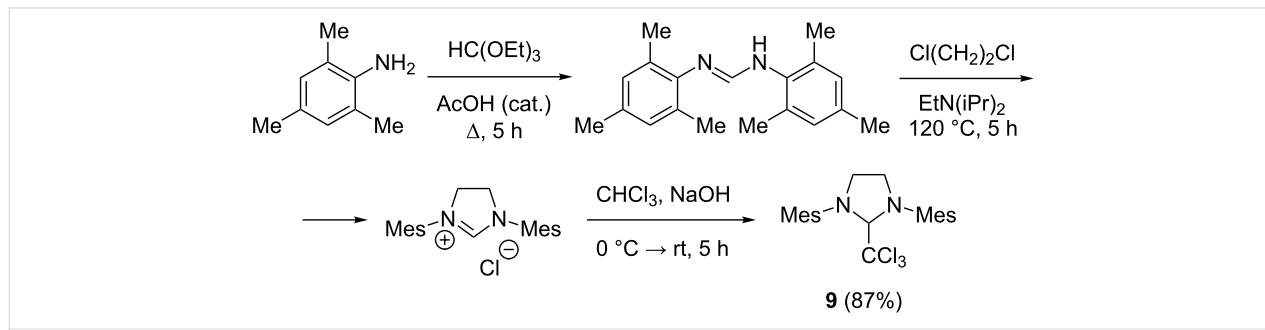
**Scheme 4:** Synthesis of Hoveyda–Grubbs-type catalysts 11.

Several approaches have been described earlier for the preparation of the “chloroform adduct” (**9**) [51–55]. Even though these approaches provide good yields they have some drawbacks such as the use of expensive reagents, difficulties in the purification process, and data analysis. Here we propose an alternative reliable procedure for the synthesis of 2-(trichloromethyl)-1,3-bis(2,4,6-trimethylphenyl)imidazolidine (**9**), which was successfully scaled up to 15 g and 30 g (Scheme 5, see Experimental part in Supporting Information File 1). In this process, the key differences are the use of the Hung’s base at the cyclization stage and of granulated alkali in the last step, which provides the target high-purity imidazolidine in 85–87% yield. We stress that there is no need for the isolation and purification of intermediate substances.

The introduction of Ru-indenylidene complex **8** in one-pot reaction with adduct **9** followed by reaction with styrenes **4a**, **4e**, **5e** or **7** gave target Hoveyda–Grubbs-type catalysts **11** in moderate yields (Scheme 4). The products were light-green powders. The synthesised catalysts demonstrated prominent stability in

air at room temperature for at least 4 years, which was proved by ^1H NMR spectra. The simple spectrum recorded in 2014 and at the end of 2018 were identical, they did not show new signals. The catalysts have good solubility in CH_2Cl_2 , CHCl_3 and moderate solubility in benzene and toluene. Therefore, they can be used for almost any purpose.

Among all of the synthesised catalysts, only three catalysts **11a–c** were obtained as good crystals suitable for X-ray diffraction analysis. Unfortunately, we were not able to obtain single crystals of satisfactory quality for the morpholino-containing catalyst **11d**. Still, the accessible X-ray structural information is sufficient to correlate structure with catalytic activity as presented in the following section (Figure 3). According to the X-ray data, the molecules **11a–c** comprise a heterocyclic system with a five-coordinated ruthenium atom having similar general geometrical features. Two chlorine atoms occupy an ordinary *trans*-position relative to the central ruthenium atom. The ruthenium-containing six-membered ring has a slightly distorted envelope conformation with a ca. 51° to 54° deviation of the

**Scheme 5:** Synthesis of the “chloroform adduct” **9**.

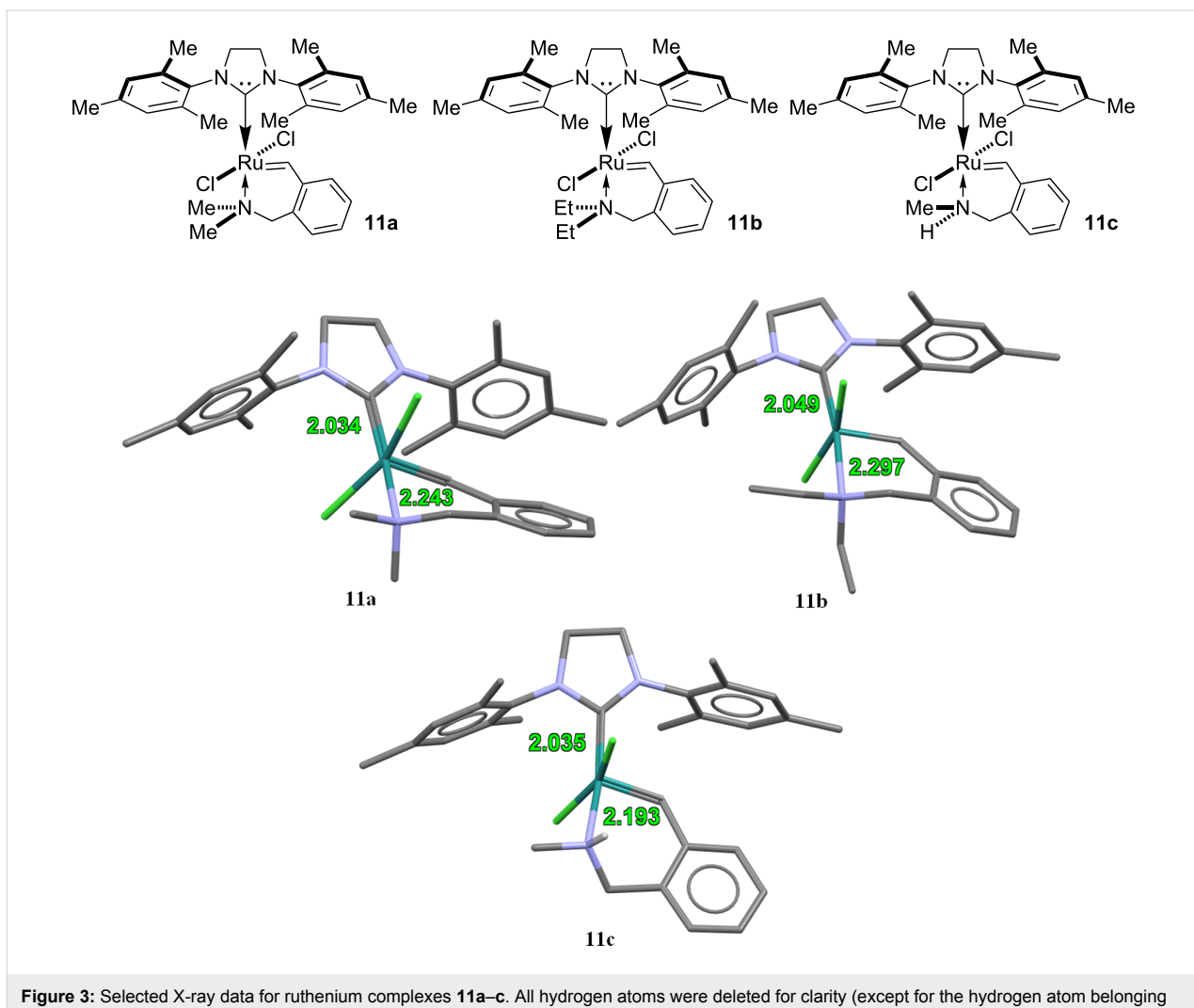


Figure 3: Selected X-ray data for ruthenium complexes **11a–c**. All hydrogen atoms were deleted for clarity (except for the hydrogen atom belonging to the NH group in compound **11c**).

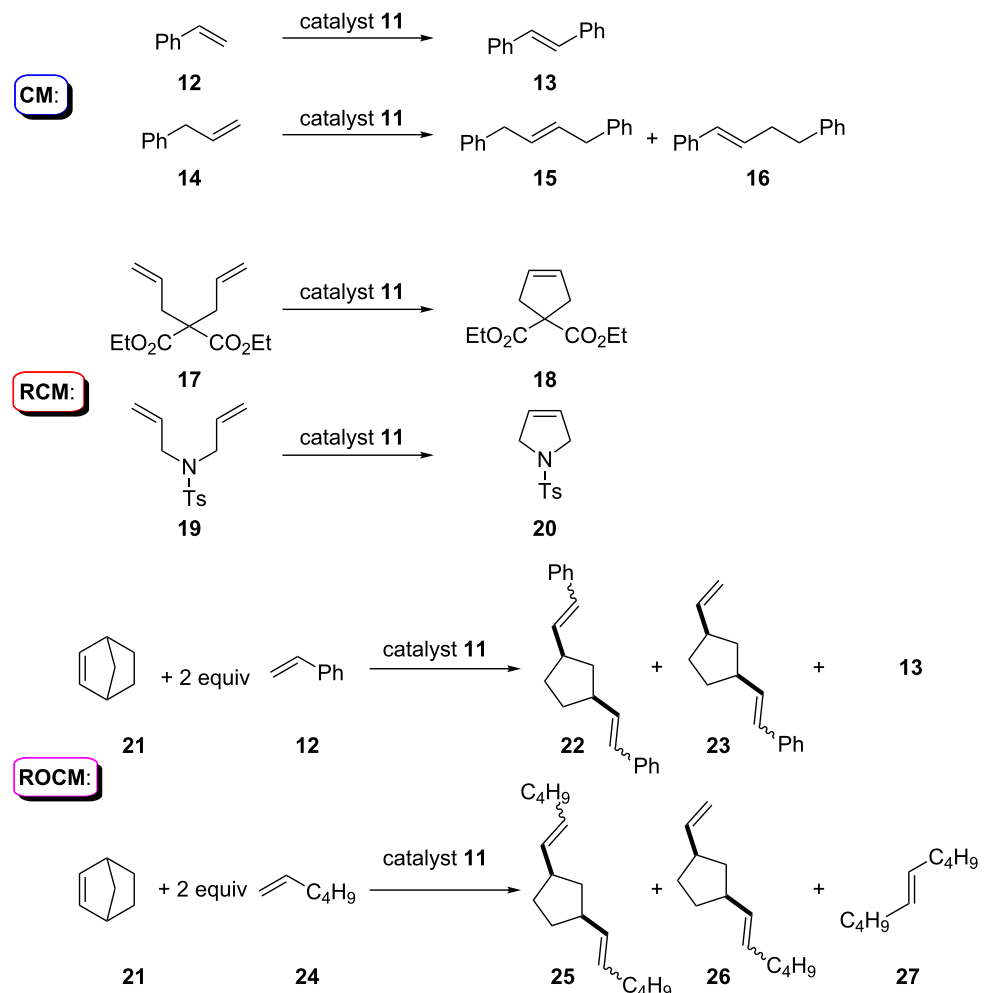
nitrogen atom from the mean plane of other five atoms. The most important feature of the catalyst structure is the length of the ruthenium–nitrogen bond, which should have the strongest effect on the catalytic activity. With the increase of the steric volume of substituents at the nitrogen atom, the ruthenium–nitrogen coordinate bond is extended, which makes it weaker. That should, obviously, increase the activity of the catalyst towards metathesis reactions. An increase in the $\text{N} \rightarrow \text{Ru}$ bond length along the series **11c** (2.193 Å) – **11a** (2.243 Å) – **11b** (2.297 Å) suggests that compound **11b** (with the NEt_2 substituent) is expected to be the most active as a catalyst.

It should be mentioned that some of catalysts **11** have been synthesized recently in a more complex way in lower yields [32].

The third part of this study was devoted to the demonstration of catalytic properties of metallo-complexes **11** in “standard” me-

tathesis reactions (Scheme 6, Table 3). As a model substrate we chose easily available alkenes and dienes, such as i) styrene (**12**) and allylbenzene (**14**) for CM reactions, ii) diethyl diallylmalonate (**17**) and diallyltosylamide (**19**) for RCM reactions, iii) norbornene (**21**) and styrene/hex-1-ene for ROCM metathesis reactions. This selection of model subtests for metathesis is also explained by the possibility to control the course of metathesis and the composition of the reaction mixtures by the GC–MS technique only (GC–MS was carried out using external calibration for CM and RCM reactions). The validity of quantitative GC–MS analysis was confirmed by additional LC–MS and ^1H NMR analysis of selected reaction mixtures.

At the beginning of this part, we tested the stability of catalysts **11** in different solvents at different temperatures and conditions (10 mg of **11** in 10 mL of solvent). From this study, we concluded that all catalysts were stable in boiling dry toluene or benzene under argon atmosphere. The catalysts retained their



Scheme 6: Catalytic activity of compounds **11** in the metathesis reactions.

green color for at least a week, which confirms the absence of decomposition. In more polar solvents like dichloromethane and chloroform (bp 40 and 61 °C) boiling under argon also does not cause visible decoloration. On the other hand, the catalysts readily decompose within 0.5–1 h upon boiling in CH_2Cl_2 or CHCl_3 in the presence of air. Boiling in tetrahydrofuran or acetonitrile even under an argon atmosphere leads to a rapid decomposition of the catalysts within 5–10 minutes (the solutions turn black). Therefore, THF and MeCN were excluded from further studies.

In the test reactions, three concentrations of the catalysts (1.0, 0.1 and 0.01 mol %) were applied for the transformation of styrene (**12**) to *trans*-stilbene (**13**) by cross-metathesis reaction (Scheme 6). First experiments (entries 1–4, Table 3) revealed that the nonpolar solvents (PhH and PhMe) are not suitable for the CM reactions. Using of 1 mol % of catalyst **11a** even under

an argon atmosphere produced only traces of the target stilbene (**13**). In these conditions, catalyst **11b** was more active than **11a**, but also gave insufficient results. Thereupon, these two solvents were also abandoned in the course of the following investigations.

In this process, temperature also exerts a strong influence on the catalytic activity of metallo complexes **11**. None of catalysts **11** were active at room temperature (19–23 °C) towards the styrene cross metathesis, meaning that all reactions required temperatures higher than 30–35 °C. After all observations, we concluded that dichloromethane is the best solvent for this reaction. At 40 °C, concentrations from 1.0 to 0.1 mol % of the morpholine-based complex **11d** showed the best catalytic activity by providing styrene in 91–97% yields (entries 12 and 13 of Table 3). The somewhat less sterically loaded *N,N*-diethyl catalyst **11b** also gave acceptable yields for concentrations from 1.0

Table 3: Reaction conditions and yields of the metathesis products.

entry	starting compound	catalyst	catalyst concentration (mol %)	solvent ^a (conditions)	yield (%), ratio ^b of the products
1	12	11a	1	PhMe (Ar)	13 (traces) ^c
2	12	11b	1	PhMe (Ar)	12/13 (43%), 51:49
3	12	11a	1	PhH (Ar)	13 (traces) ^c
4	12	11b	1	PhH (Ar)	12/13 (52%), 40:60
5	12	11a	1	MeCN (Ar)	no product ^c
6	12	11a	1	THF (Ar)	no product ^c
7	12	11a	1	CH ₂ Cl ₂ (Ar)	13 (17%) ^d
8	12	11a	0.1	CH ₂ Cl ₂ (Ar)	13 (traces) ^c
9	12	11b	1	CH ₂ Cl ₂ (Ar)	13 (49%) ^d
10	12	11b	0.1	CH ₂ Cl ₂ (Ar)	13 (79%) ^d
11	12	11c	1	CH ₂ Cl ₂ (Ar)	12/13 (51%), 44:56
12	12	11d	1	CH ₂ Cl ₂ (Ar)	13 (91%) ^d
13	12	11d	0.1	CH ₂ Cl ₂ (Ar)	13 (97%) ^d
14	12	11d	0.01	CH ₂ Cl ₂ (Ar)	12/13 (93%), 69:31
15	12	11a	1	CHCl ₃ (Ar)	13 (86%) ^d
16	12	11a	0.1	CHCl ₃ (Ar)	13 (95%) ^d
17	12	11b	1	CHCl ₃ (Ar)	13 (96%) ^d
18	12	11b	0.1	CHCl ₃ (Ar)	13 (97%) ^d
19	12	11b	0.01	CHCl ₃ (Ar)	13 (81%) ^d
20	12	11b	0.1	CHCl ₃ (air)	13 (89%) ^d
21	12	11d	1	CHCl ₃ (Ar)	13 (95%) ^d
22	12	11d	0.1	CHCl ₃ (Ar)	13 (99%) ^d
23	12	11d	0.01	CHCl ₃ (Ar)	12/13 (98%), 64:36
24	14	11b	0.1	CHCl ₃ (Ar)	15/16 (93%), 64:36
25	17	11a	0.1	CHCl ₃ (air)	17/18 (46%), 44:56
26	17	11b	0.1	CHCl ₃ (air)	17/18 (58%), 42:58
27	17	11b	0.01	CHCl ₃ (Ar)	18 (traces) ^e
28	17	11b	0.1	CHCl ₃ (Ar)	17/18 (98%), 2:98
29	17	11d	0.1	CHCl ₃ (air)	17/18 (63%), 42:58
30	17	11d	0.1	CHCl ₃ (Ar)	17/18 (96%), 4:96
31	17	11d	0.01	CHCl ₃ (air)	18 (traces)
32	19	11d	0.1	CHCl ₃ (Ar)	19/20 (99%), 5:95
33	19	11d	0.01	CHCl ₃ (Ar)	19/20 (75%), 23/77
34	21 + 2 equiv 12	11a	0.1	CHCl ₃ (Ar)	13/22/23 (71%), ≈77/20/3 ^f
35	21 + 2 equiv 12	11d	0.1	CHCl ₃ (Ar)	13/22/23 (78%), ≈81/18/1 ^f
36	21 + 2 equiv 24	11a	0.1	CHCl ₃ (Ar)	25/26/27 (40%), ≈3/76/21 ^f
37	21 + 2 equiv 24	11b	0.1	CHCl ₃ (Ar)	25/26/27 (52%), ≈2/72/26 ^f

^aAll experiments were performed in boiling solvents (10 mL) for 4 h at stirring. ^bAccording to GC–MS analysis with external calibration. ^cOnly the starting styrene (**12**) was detected by GC–MS. Term “traces” was used if the product content in the resulting mixture was less than 1%. ^dIsolated yields are given. ^eThe starting diallyl diethyl malonate **17** was detected by GC–MS. ^fThe compositions of the reaction mixtures were determined by GC–MS without external calibration.

to 0.1 mol % (Table 3, entries 9 and 10). Under the same conditions the *N,N*-dimethyl catalyst **11a** provided lower yields (Table 3, entries 7 and 8). Similarly, the least sterically loaded *N*-methyl complex **11c** gave a mixture of products **12/13** (Table 3, entry 11) in low yields. The metathesis reaction did

not proceed completely, even in the presence of 2 mol % of the catalyst. As a result, we did not explore the catalytic activity of **11c** hereinafter. These experimental observations are consistent with the X-ray data obtained for catalysts **11a–c** (Figure 3). In spite of the fact that we do not have the X-ray analysis for cata-

lyst **11d**, it is possible to assume that this complex should exhibit the longest coordination N→Ru bond (at least more than 2.30 Å). Interestingly, lower yields of stilbene from styrene in CH_2Cl_2 were obtained in the presence of 1.0 mol % of catalyst **11a,c,d** as compared with 0.1 mol % of catalyst (cf. Table 3, entries 9/10, 12/13). Obviously, a high concentration of the catalysts accelerates the formation of undesirable products (oligomers and polymers of styrene). At 40 °C in dichloromethane, excellent yields of stilbene were obtained only under the action of metallo complex **11d**. For this reason, we explored elevated temperatures for the metathesis reactions.

The following series of experiments was performed in CHCl_3 (entries 15–23, Table 3) at 60–61 °C with different concentrations of catalysts. Ruthenium complex **11b** was efficient in the 0.01 mol % concentration under argon atmosphere and in the 0.1 mol % concentration in air. In case of allylbenzene (**14**), the action of catalyst **11b** (0.1 mol %) gave the mixture of isomeric 1,4-diphenylbutenes **15** and **16** in the ratio of 64:36 in 93% yield. Only a small amount of the starting compound **14** underwent polymerisation.

The utility of the catalyst for the RCM reaction was demonstrated by the cyclization of dienes **17** and **19** (Table 3, entries 25–33) in both air and argon atmosphere. The complexes **11a**, **11b** and **11d** in the air atmosphere provided cyclic alkenes **18**, **20** with a strong admixture of initial dienes (Table 3, entries 25, 26, 29). Under argon atmosphere, the same transformations provided good results in the presence of 0.1–0.01 mol % of catalysts **11b,d** (Table 3, entries 28, 30–32).

Similarly, in the case of the ROCM reactions (Scheme 6), catalysts **11a,b** did not provide high selectivity (Table 3, entries 34–37). Interactions of norbornene (**21**) with a two-fold excess of styrene (**12**) or hex-1-ene (**24**) was accompanied by the CM reaction, which provided products of the ring opening (**22**, **23**, **25**, **26**) and significant amounts of byproducts due to the side cross metathesis (**13** and **27**). Moreover, sparingly soluble high molecular weight products were isolated from all reactions; according to gel permeation chromatography data, these solids are, presumably, norbornene oligomers (see, for example data for entry 35, Supporting Information File 1 and Supporting Information File 2). These four examples demonstrate the principal possibility of application of catalysts **11** in ROCM reactions.

It is known that metathesis reactions carried out in chloroform medium under similar conditions (see Table 3) can give products of the Kharasch radical addition of CHCl_3 across olefins [56,57]. It is worth to note in the end of this part, that we did not

detect formation of chlorine-containing products (molecular peaks with the isotopic distribution characteristic for chlorine were absent in GC–MS spectra).

Conclusion

The present work reports an efficient method for the synthesis of 2-(*N,N*-dialkylaminomethyl)styrenes. The resultant vinyl benzenes are excellent precursors for the synthesis of a new type of Hoveyda–Grubbs catalysts bearing an N→Ru coordinate bond in a six-membered ring. This process does not require the use of complex equipment, extremely expensive or toxic reagents. The structure of the catalysts were elucidated in detail by 2D NMR and X-ray crystallography. The high catalytic activity of the metallo complexes was demonstrated by several examples of cross metathesis (CM), ring-closing (RCM) and ring-opening cross metathesis (ROCM) reactions.

Furthermore, almost all steps of ligands' and catalysts' synthesis were accomplished in preparative and multigram scales.

Supporting Information

Supporting Information File 1

Experimental and analytical data.

[<https://www.beilstein-journals.org/bjoc/content/supplementary/1860-5397-15-73-S1.pdf>]

Supporting Information File 2

Copies of NMR spectra of synthesised compounds and selected GC–MS data of the metathesis products. Check-cif reports for compounds **11a–c**.

[<https://www.beilstein-journals.org/bjoc/content/supplementary/1860-5397-15-73-S2.pdf>]

Acknowledgements

Funding for this research was provided by the Russian Science Foundation (RSF) (project No. 18-13-00456)

ORCID® IDs

Fedor I. Zubkov - <https://orcid.org/0000-0002-0289-0831>

References

1. Yu, M.; Lou, S.; Gonzalez-Bobes, F. *Org. Process Res. Dev.* **2018**, *22*, 918–946. doi:10.1021/acs.oprd.8b00093
2. Ogba, O. M.; Warner, N. C.; O'Leary, D. J.; Grubbs, R. H. *Chem. Soc. Rev.* **2018**, *47*, 4510–4544. doi:10.1039/c8cs00027a
3. Chen, Y.; Abdellatif, M. M.; Nomura, K. *Tetrahedron* **2018**, *74*, 619–643. doi:10.1016/j.tet.2017.12.041
4. Mukherjee, N.; Planer, S.; Grela, K. *Org. Chem. Front.* **2018**, *5*, 494–516. doi:10.1039/c7qo00800g

5. Lecourt, C.; Dhambri, S.; Allievi, L.; Sanogo, Y.; Zeghbib, N.; Ben Othman, R.; Lannou, M.-I.; Sorin, G.; Ardisson, J. *Nat. Prod. Rep.* **2018**, *35*, 105–124. doi:10.1039/c7np00048k
6. Biffis, A.; Centomo, P.; Del Zotto, A.; Zecca, M. *Chem. Rev.* **2018**, *118*, 2249–2295. doi:10.1021/acs.chemrev.7b00443
7. Montgomery, T. P.; Johns, A. M.; Grubbs, R. H. *Catalysts* **2017**, *7*, 87. doi:10.3390/catal7030087
8. Hughes, D.; Wheeler, P.; Ene, D. *Org. Process Res. Dev.* **2017**, *21*, 1938–1962. doi:10.1021/acs.oprd.7b00319
9. Sinclair, F.; Alkattan, M.; Prunet, J.; Shaver, M. P. *Polym. Chem.* **2017**, *8*, 3385–3398. doi:10.1039/c7py00340d
10. Montgomery, T. P.; Ahmed, T. S.; Grubbs, R. H. *Angew. Chem., Int. Ed.* **2017**, *56*, 11024–11036. doi:10.1002/anie.201704686
11. Paradiso, V.; Costabile, C.; Grisi, F. *Molecules* **2016**, *21*, No. 117. doi:10.3390/molecules21010117
12. Higman, C. S.; Lummiss, J. A. M.; Fogg, D. E. *Angew. Chem., Int. Ed.* **2016**, *55*, 3552–3565. doi:10.1002/anie.201506846
13. Grubbs, R. H.; Wenzel, A. G.; O'Leary, D. J.; Khosravi, E. *Handbook of Metathesis*, 2nd ed.; Wiley-VCH: Weinheim, Germany, 2015.
14. van Lierop, B. J.; Lummiss, J. A. M.; Fogg, D. E. Ring-Closing Metathesis. *Olefin Metathesis*; John Wiley & Sons, Inc.: Hoboken, NJ, U.S.A., 2014; pp 85–152. doi:10.1002/9781118711613.ch3
15. Scholl, M.; Trnka, T. M.; Morgan, J. P.; Grubbs, R. H. *Tetrahedron Lett.* **1999**, *40*, 2247–2250. doi:10.1016/s0040-4039(99)00217-8
16. Scholl, M.; Ding, S.; Lee, C. W.; Grubbs, R. H. *Org. Lett.* **1999**, *1*, 953–956. doi:10.1021/o1990909q
17. Fürstner, A.; Ackermann, L.; Gabor, B.; Goddard, R.; Lehmann, C. W.; Mynott, R.; Stelzer, F.; Thiel, O. R. *Chem. – Eur. J.* **2001**, *7*, 3236–3253. doi:10.1002/1521-3765(20010803)7:15<3236::aid-chem3236>3.0.co;2-s
18. Michrowska, A.; Bujok, R.; Harutyunyan, S.; Sashuk, V.; Dolgonos, G.; Grela, K. *J. Am. Chem. Soc.* **2004**, *126*, 9318–9325. doi:10.1021/ja048794v
19. Barbasiewicz, M.; Bieniek, M.; Michrowska, A.; Szadkowska, A.; Makal, A.; Woźniak, K.; Grela, K. *Adv. Synth. Catal.* **2007**, *349*, 193–203. doi:10.1002/adsc.200600478
20. Kos, P.; Savka, R.; Plenio, H. *Adv. Synth. Catal.* **2013**, *355*, 439–447. doi:10.1002/adsc.201200956
21. Engle, K. M.; Lu, G.; Luo, S.-X.; Henling, L. M.; Takase, M. K.; Liu, P.; Houk, K. N.; Grubbs, R. H. *J. Am. Chem. Soc.* **2015**, *137*, 5782–5792. doi:10.1021/jacs.5b01144
22. Duan, Y.; Wang, T.; Xie, Q.; Yu, X.; Guo, W.; Wang, J.; Liu, G. *Dalton Trans.* **2016**, *45*, 19441–19448. doi:10.1039/c6dt03899a
23. Occhipinti, G.; Bjørsvik, H.-R.; Törnroos, W. K.; Jensen, V. R. *Organometallics* **2007**, *26*, 5803–5814. doi:10.1021/om070219n
24. Tzur, E.; Szadkowska, A.; Ben-Asuly, A.; Makal, A.; Goldberg, I.; Woźniak, K.; Grela, K.; Lemcoff, N. G. *Chem. – Eur. J.* **2010**, *16*, 8726–8737. doi:10.1002/chem.200903457
25. Zannan Science and Technology (Shanghai) Co., Ltd.; Zheng-Yun, Z. Metal complex ligand, metal complex, preparation method and use of metal complex, polymers and preparation method and use of polymers. CN Patent 104262403A, Sept 27, 2008.
26. Francis Walter Cornelius Verpoort; Xia, L. Group 8 transition metal catalysts and method for making same and process for use of same in olefin disproportionation reactions. WO Patent WO2017185324 A1, April 29, 2016.
27. Zannan Scitech Co., Ltd.; Zhan, J. Z.-Y. Highly active metathesis catalysts selective for ROMP and RCM reactions. WO Patent WO201179439 A1, Dec 30, 2009.
28. PJSC Rosneft Oil Co.; Polyanskii, K. B.; Afanas'ev, V. V.; Bespalova, N. B. Dicyclopentadiene metathesis polymerization catalyst in the form of a ruthenium complex and method for producing same. WO Patent WO2015115937 A1, Jan 29, 2014.
29. PJSC Rosneft Oil Co.; Polyanskii, K. B.; Afanasev, V. V.; Zemtsov, D. B.; Panov, D. M.; Bespalova, N. B. Method of producing catalyst for metathesis polymerisation of dicyclopentadiene. RU Patent RU2577252 C1, Feb 26, 2015.
30. PJSC Rosneft Oil Co.; Polyanskii, K. B.; Afanas'ev, V. V.; Zemtsov, D. B.; Panov, D. M.; Bespalova, N. B. Catalyst of metathesis polymerisation of dicyclopentadiene in form of ruthenium complex and method of obtaining thereof. RU Patent RU2545179 C1, Jan 29, 2014.
31. Ivin, K. J.; Mol, J. C. *Olefin metathesis and metathesis polymerization*; Academic Press: London, 1997; p 204.
32. Shcheglova, N. M.; Kolesnik, V. D.; Ashirov, R. V.; Krasnokutskaya, E. A. *Russ. Chem. Bull.* **2016**, *65*, 490–497. doi:10.1007/s11172-016-1327-x
33. Kiselev, S. A.; Lenev, D. A.; Lyapkov, A. A.; Semakin, S. V.; Bozhenkova, G.; Verpoort, F.; Ashirov, R. V. *RSC Adv.* **2016**, *6*, 5177–5183. doi:10.1039/c5ra25197d
34. Pump, E.; Leitgeb, A.; Kozłowska, A.; Torvisco, A.; Falivene, L.; Cavallo, L.; Grela, K.; Slugovc, C. *Organometallics* **2015**, *34*, 5383–5392. doi:10.1021/acs.organomet.5b00715
35. Shcheglova, N. M.; Kolesnik, V. D.; Ashirov, R. V.; Krasnokutskaya, E. A. *Russ. J. Org. Chem.* **2015**, *51*, 907–909. doi:10.1134/s1070428015070015
36. Grudzień, K.; Żukowska, K.; Malinśka, M.; Woźniak, K.; Barbasiewicz, M. *Chem. – Eur. J.* **2014**, *20*, 2819–2828. doi:10.1002/chem.201303826
37. Ashirov, R. V.; Zemlyakov, D. I.; Lyapkov, A. A.; Kiselev, S. A. *Kinet. Catal.* **2013**, *54*, 469–474. doi:10.1134/s0023158413040010
38. Szadkowska, A.; Gstrein, X.; Burtscher, D.; Jarzembska, K.; Woźniak, K.; Slugovc, C.; Grela, K. *Organometallics* **2010**, *29*, 117–124. doi:10.1021/om900857w
39. Rheiner, A., Jr.; Brossi, A. *Helv. Chim. Acta* **1962**, *45*, 2590–2600. doi:10.1002/hlca.19620450728
40. Ito, Y.; Nakatsuka, M.; Saegusa, T. *J. Am. Chem. Soc.* **1982**, *104*, 7609–7622. doi:10.1021/ja00390a036
41. Suzuki, T.; Takamoto, M.; Okamoto, T.; Takayama, H. *Chem. Pharm. Bull.* **1986**, *34*, 1888–1900. doi:10.1248/cpb.34.1888
42. Kafka, S.; Trška, P.; Kytner, J.; Taufmann, P.; Ferles, M. *Collect. Czech. Chem. Commun.* **1987**, *52*, 2047–2056. doi:10.1135/cccc19872047
43. Padwa, A.; Dent, W. *J. Org. Chem.* **1987**, *52*, 235–244. doi:10.1021/jo00378a013
44. Molander, G. A.; Pack, S. K. *Tetrahedron* **2003**, *59*, 10581–10591. doi:10.1016/j.tet.2003.08.071
45. Segal, I.; Zablotskaya, A.; Lukevics, E. *Chem. Heterocycl. Compd.* **2005**, *41*, 613–624. doi:10.1007/s10593-005-0192-6
46. Shcheglova, N. M.; Kolesnik, V. D.; Ashirov, R. V. *Russ. J. Org. Chem.* **2013**, *49*, 1329–1334. doi:10.1134/s1070428013090145
47. Dorta, R.; Kelly, R. A., III; Nolan, S. P. *Adv. Synth. Catal.* **2004**, *346*, 917–920. doi:10.1002/adsc.200404047
48. Fürstner, A.; Guth, O.; Düffels, A.; Seidel, G.; Liebl, M.; Gabor, B.; Mynott, R. *Chem. – Eur. J.* **2001**, *7*, 4811–4820. doi:10.1002/1521-3765(20011119)7:22<4811::aid-chem4811>3.0.co;2-p

49. Jimenez, L. R.; Tolentino, D. R.; Gallon, B. J.; Schrödi, Y. *Molecules* **2012**, *17*, 5675–5689. doi:10.3390/molecules17055675

50. Pump, E.; Slugovc, C.; Cavallo, L.; Poater, A. *Organometallics* **2015**, *34*, 3107–3111. doi:10.1021/om501246q

51. Musengimana, E.; Fatakanwa, C. *Orient. J. Chem.* **2013**, *29*, 1489–1496. doi:10.13005/ojc/290426

52. Trnka, T. M.; Morgan, J. P.; Sanford, M. S.; Wilhelm, T. E.; Scholl, M.; Choi, T.-L.; Ding, S.; Day, M. W.; Grubbs, R. H. *J. Am. Chem. Soc.* **2003**, *125*, 2546–2558. doi:10.1021/ja021146w

53. Nyce, G. W.; Csihony, S.; Waymouth, R. M.; Hedrick, J. L. *Chem. – Eur. J.* **2004**, *10*, 4073–4079. doi:10.1002/chem.200400196

54. Bell, A.; Grubbs, R. H.; Morgan, J. P.; Moore, J. L. High activity metal carbene metathesis catalysts generated using a thermally activated N-heterocyclic carbene precursor. US Patent US6838489 B2, March 23, 2001.

55. Arduengo, A. J., III; Calabrese, J. C.; Davidson, F.; Rasika Dias, H. V.; Goerlich, J. R.; Krafczyk, R.; Marshall, W. J.; Tamm, M.; Schmutzler, R. *Helv. Chim. Acta* **1999**, *82*, 2348–2364. doi:10.1002/(sici)1522-2675(19991215)82:12<2348::aid-hlca2348>3.0.co;2-m

56. Tallarico, J. A.; Malnick, L. M.; Snapper, M. L. *J. Org. Chem.* **1999**, *64*, 344–345. doi:10.1021/jo982349z

57. Alcaide, B.; Almendros, P.; Luna, A. *Chem. Rev.* **2009**, *109*, 3817–3858. doi:10.1021/cr9001512

License and Terms

This is an Open Access article under the terms of the Creative Commons Attribution License (<http://creativecommons.org/licenses/by/4.0>). Please note that the reuse, redistribution and reproduction in particular requires that the authors and source are credited.

The license is subject to the *Beilstein Journal of Organic Chemistry* terms and conditions: (<https://www.beilstein-journals.org/bjoc>)

The definitive version of this article is the electronic one which can be found at:
[doi:10.3762/bjoc.15.73](https://doi.org/10.3762/bjoc.15.73)